



UNIVERSIDAD NACIONAL AUTÓNOMA DE MÉXICO
POSGRADO EN CIENCIAS DE LA TIERRA
CENTRO DE GEOCIENCIAS

Contribuciones a la variación secular en México y su aplicación en fechamientos paleomagnéticos

Tesis con base en artículos científicos que para optar el grado de:

Doctor en ciencias de la tierra

PRESENTA:

Ahmed Nasser Mahgoub Ahmed

Director de Tesis

Dr. Harald Böhnel

CENTRO DE GEOCIENCIAS

Comité Tutorial

Dr. John Shaw University of Liverpool (UK)

Dr. Peter Schaaf Instituto de Geofísica (UNAM)

JURIQUILLA, QRO., MÉXICO. Junio, 2018



Universidad Nacional
Autónoma de México



UNAM – Dirección General de Bibliotecas
Tesis Digitales
Restricciones de uso

DERECHOS RESERVADOS ©
PROHIBIDA SU REPRODUCCIÓN TOTAL O PARCIAL

Todo el material contenido en esta tesis esta protegido por la Ley Federal del Derecho de Autor (LFDA) de los Estados Unidos Mexicanos (México).

El uso de imágenes, fragmentos de videos, y demás material que sea objeto de protección de los derechos de autor, será exclusivamente para fines educativos e informativos y deberá citar la fuente donde la obtuvo mencionando el autor o autores. Cualquier uso distinto como el lucro, reproducción, edición o modificación, será perseguido y sancionado por el respectivo titular de los Derechos de Autor.



UNIVERSIDAD NACIONAL AUTÓNOMA DE MÉXICO
POSGRADO EN CIENCIAS DE LA TIERRA
CENTRO DE GEOCIENCIAS

Contributions to secular variation in Mexico and its application in paleomagnetic dating

Thesis based on scientific articles that to obtain the degree of:
Doctor in Earth Sciences

PRESENT:

Ahmed Nasser Mahgoub Ahmed

Thesis Director

Dr. Harald Böhnel

CENTRO DE GEOCIENCIAS

Tutorial Committee

Dr. John Shaw University of Liverpool (UK)

Dr. Peter Schaaf Instituto de Geofísica (UNAM)

JURIQUILLA, QRO., MÉXICO. June, 2018

Declaratoria ética

Declaro conocer el Código de Ética de la Universidad Nacional Autónoma de México, plasmado en la Legislación Universitaria. Con base en las definiciones de integridad y honestidad ahí especificadas, aseguro mediante mi firma al calce que el presente trabajo es original y enteramente de mi autoría. Todas las citas de, o referencias a, la obra de otros autores aparecen debida y adecuadamente señaladas, así como acreditadas mediante los recursos editoriales convencionales.

Ethical declaration

I declare to know the Code of Ethics of the National Autonomous University of Mexico, embodied in the University Legislation. Based on the definitions of integrity and honesty specified there, I assure you by my signature that this work is original and entirely my responsibility. All citations of, or references to, the work of other authors appear duly and adequately indicated, as well as accredited through conventional editorial resources.

Thanks and gratitude to

Allah. I bow to **Allah** thanking His Majesty for his help in the production of this work.

My parents. Wish for both of you health and happiness, and may Allah bless you.

Mohamed, Mahmoud, Mahgoub, Nermeen, Salah. My dear brothers, I wish you success and happiness.

Nassercito. My son, every time I look at you I see in you the hope of the present and the promise of my future.

Amal. My beautiful wife: Allah sustains love and perpetuates your love for us and we become the sweetest of the three:

Love, you and me..

Resumen

El campo magnético de la Tierra (CMT), también conocido como campo geomagnético, se genera en el núcleo externo líquido de nuestro planeta. El CMT nos ayuda entre varias cosas para la navegación, y como escudo para desviar la mayor parte del viento solar vital para proteger la vida en la Tierra. La dirección y la intensidad del CMT cambian intermitentemente en diferentes escalas de tiempo: de decenas a miles de años, de un lugar a otro en todo el mundo, este fenómeno es llamado variación secular. Obtener datos del CMT para los períodos anteriores a las mediciones históricas podría lograrse mediante el uso de artefactos arqueológicos y materiales geológicos. Descifrar la variación secular del CMT tiene una amplia aplicación en muchas disciplinas; la más notable de todas es su uso para comprender el comportamiento del geodinamo en el interior profundo de la Tierra, y recientemente en el campo del fechamiento paleomagnético de materiales arqueológicos y geológicos. Sin embargo, el uso de estas aplicaciones está limitado por factores tales como: (i) inexactitud en los datos de edad de los materiales analizados (lavas, artefactos arqueológicos y especialmente sedimentos), (ii) si bien es sencillo determinar la dirección del campo paleomagnético, la paleointensidad se considera difícil de obtener, y (iii) la distribución desigual de los datos de variación secular en el tiempo y el espacio. Desafortunadamente, México es un país que cuenta con escasos datos de variación secular. Por lo tanto, el presente proyecto se ha centrado principalmente en mejorar nuestra comprensión global y regional de la variación del campo magnético de la Tierra durante el Cuaternario tardío. Esto se logró mediante la construcción de curvas vectoriales SV completas para el centro de México, lo que podría aplicarse notablemente a la datación paleomagnética. Para este propósito, hemos muestreado decenas de rocas volcánicas independientes y objetos arqueológicos distribuidos principalmente a lo largo del cinturón volcánico Transmexicano (TMVB). El segundo enfoque principal de la tesis se centró en la datación paleomagnética de dos grupos de erupciones monogenéticas del Holoceno ubicadas en el campo volcánico Michoacán-Guanajuato (MGVF) y también en dos flujos de lava muestreados del volcán Ceboruco en el centro-oeste de México. En total, se tomaron muestras de 10 flujos en 50 sitios paleomagnéticos con el fin de

recuperar las direcciones e intensidades paleomagnéticas de ellos. Además, la aplicabilidad del paleomagnetismo como método alternativo para descifrar la evolución de la erupción de un determinado volcán fue otro tema durante mi proyecto de doctorado. La tesis se compone de cuatro artículos aceptados y otros dos artículos: uno ha sido enviado y otro que se presentará para su publicación en revistas ISI revisadas por pares:

Artículo 1, "El estudio paleomagnético del volcán escudo El Metate (Michoacán, México) confirma su naturaleza monogenética y su corta edad (~ 1250 dc)". Es un análisis paleomagnético clásico para varios flujos de lava emitidos por un reciente volcán (1250 dc) llamado El Metate, ubicado en Michoacán (México). Se ha propuesto recientemente que este gran volcán (~ 9.2 km³) con trece flujos de lava tiene un origen monogenético, basado en observaciones de campo y petrología. Sin embargo, no se pudo realizar una datación por edad directa del 14C para los flujos de lava más jóvenes para probar esta hipótesis debido a la ausencia de material documentable (paleosuelos). Por esta razón, se llevaron a cabo análisis paleomagnéticos en varios flujos de lava y se obtuvieron direcciones e intensidades indistinguibles de forma interesante, aprobando que todos se formaran en 100 años o menos. Por lo tanto, nuestros resultados confirman y respaldan la hipótesis de la naturaleza monogenética de la erupción de El Metate.

Artículo 2, "Edades inferidas paleomagnéticamente de un grupo de erupciones monogenéticas del Holoceno en el área de Tacámbaro-Puruarán (Michoacán, México): Implicaciones para riesgos volcánicos", proporciona nuevos datos de edad paleomagnéticos para cuatro respiraderos del Holoceno monogenéticos, es decir, La Tinaja, La Palma, Mesa La Muerta y Malpaís de Cutzaróndiro (en orden cronológico según las relaciones estratigráficas) que forman un pequeño grupo ubicado dentro del área de Tacámbaro-Puruarán en Michoacán. Nuestros nuevos datos paleomagnéticos indican que sus erupciones se produjeron por separado en el tiempo con intervalos de recurrencia variables que oscilan entre ~ 300 y ~ 2300 años, aunque están muy agrupados en el espacio. La identificación de pequeños grupos con varios volcanes jóvenes que estallaron

en períodos de cientos a miles de años abre varios aspectos clave con respecto a las futuras evaluaciones de riesgo volcánico en el volcánicamente activo campo volcánico de Michoacán-Guanajuato, y también debe considerarse cuando restringe la naturaleza del sistema de tuberías magmáticas.

Artículo 3, "Restricciones paleomagnéticas en las edades del Holoceno Malpaís de Zacapu erupciones de flujo de lava, Michoacán (México): Implicaciones para la arqueología y los peligros volcánicos". Presenta una investigación interdisciplinaria donde la información vulcanológica y arqueológica se ha relacionado con los procedimientos de datación paleomagnéticos. Cabe destacar que este trabajo muestra que los futuros esfuerzos de mitigación de peligros volcánicos podrían beneficiar la combinación de estudios geofísicos, vulcanológicos y arqueológicos.

Artículo 4, "datación paleomagnética de dos flujos recientes de lava del volcán Ceboruco, oeste de México", donde el procedimiento de datación paleomagnética fue probado por primera vez en México en dos flujos de lava muestreados desde Ceboruco, en el oeste de México. Un flujo histórico entró en erupción en el año 1870, y nuestro procedimiento de datación da un rango de edad entre 1755 y 1871. El segundo flujo, concretamente Ceboruco, data del año 1000 y 1134, lo que implica que el volcán Ceboruco estuvo inactivo durante al menos 736 años hasta que 1870 erupción. Este período es mucho más largo de lo que se sugirió anteriormente y, por lo tanto, se debe considerar al modelar la evolución del magma en esta área, las estimaciones del riesgo volcánico.

Artículo 5, "Una curva de variación secular de la paleointensidad de 3600 años para México". Presenta nuevos datos de paleointensidad que cubren los últimos 3600 años que se utilizan junto con datos seleccionados previamente publicados para México con el fin de construir una curva de variación secular de paleointensidad para México Central. Las características importantes de los altos y bajos de la intensidad del campo magnético de la Tierra podrían capturarse a partir de la nueva curva. Entre estas características se encuentra un pico de gran intensidad documentado por primera vez en México alrededor del año 250 aC, que es comparable al pico de paleointensidad de Levante. La comparación de estos hallazgos con los datos de otras regiones indica que en los últimos 3600 años, el

campo magnético de la Tierra fue impulsado por la aparición de componentes no dipolos fuertes y rápidamente fluctuantes que superponían el campo dipolar dominante.

Artículo 6, "Datos de variación secular tardía-cuaternaria de los volcanes mexicanos", proporciona nuevas 32 direcciones paleomagnéticas robustas y 21 intensidades de alta calidad obtenidas de 33 flujos de lava del Cinturón Volcánico Transmexicano, que se utilizan para construir vectores completos seculares curva de variación para México Central. Los nuevos datos son esenciales para mejorar los modelos de campo geomagnético global, lo que a su vez mejorará el enfoque de datación paleomagnética para México. Las nuevas curvas se calcularon para dos períodos: DC 2,000-2,200 AC y 2,200-45,000 AC, debido a la distribución desigual de los datos. Durante todo el período, se observan numerosas características del campo magnético de la Tierra donde las direcciones cambian abruptamente acompañadas de intensidades extremadamente altas o caídas repentinas de intensidad. Además, se observaron inclinaciones anormales bajas acompañadas de marcadas declinaciones del oeste y muy bajas intensidades entre 26,000 y 24,000 AC. Estos comportamientos anómalos podrían atribuirse a sacudidas geomagnéticas y / o una excursión documentada en primer lugar para México para el Cuaternario tardío. Comparando con otras regiones, esta excursión puede estar relacionada con la excursión Mono Lake.

Abstract

The Earth's magnetic field (EMF), also known as the geomagnetic field, is believed to be generated in the electrically conducting liquid outer core of our planet. The EMF helps us among several other aspects for navigation, and as a shield to deflect most of the solar wind to protect life on Earth. Outstandingly, the EMF direction and intensity change on different time scales from about a year to several thousand years, and also from place to place over the globe, a phenomena called "secular variation (SV)". Getting insight into the SV data of the Earth's magnetic field for periods preceding the historical measurements could be achieved by the use of archeological artefacts and geological materials. Deciphering the SV of the EMF has extensive application in many more disciplines; most notably of all is its use in understanding the behavior of the geodynamo in the earth's deep interior, and recently in the field of paleomagnetic dating of archeological and geological materials. However, the use of these application is limited by factors such as: (i) unavailable or inaccurate age data of the analyzed materials (lavas, archeological artifacts, and especially sediments); (ii) while it is straightforward to determine the past magnetic field direction, the paleointensity is often difficult to obtain; (iii) the uneven distribution of the SV data in time and space. Unfortunately, Mexico is one of the regions with few SV data. Therefore, the present project has focused mainly on enhancing our global and regional understanding of the Earth's magnetic field variation during the Late Quaternary. This was achieved through constructing full vector SV curves for central Mexico which remarkably could be applied for paleomagnetic dating. For this purpose, we have sampled tens of independent volcanic rocks and archeological objects distributed mainly along the Trans-Mexican volcanic belt (TMVB). The second main focus of the thesis was set on paleomagnetic dating of two clusters of Holocene monogenetic eruptions located in the Michoacán-Guanajuato volcanic field (MGVF) and also on two lava flows sampled from the Ceboruco volcano in west-central Mexico. In total, 10 flows were sampled in 50 paleomagnetic sites in order to recover the paleomagnetic directions and intensities from them. Moreover, the applicability of paleomagnetism as an alternative method in deciphering the eruption evolution of a certain volcano was another topic during my PhD

project. The thesis is composed of four accepted articles and another two articles: one has been submitted and another one to be submitted for publication in peer-reviewed ISI journals:

Paper 1, “Paleomagnetic study of El Metate shield volcano (Michoacán, Mexico) confirms its monogenetic nature and young age (~1250 CE)”. It is a classical paleomagnetic analyses for several lava flows emitted from a recent (1250 AD) shield volcano named El Metate, located in Michoacán (Mexico). This large volcano (~ 9.2 km³) with thirteen lava flows has been recently proposed to be of monogenetic origin, based on field and petrology observations. However, no direct ¹⁴C age dating could be performed for the younger lava flows to prove this hypothesis because of the absence of datable material (paleosols). For this reason, paleomagnetic analyses were carried out on several lava flows and interestingly indistinguishable directions and intensities were obtained approving that all they were formed within 100 years or less. Thus, our results confirm and support the hypothesis of the monogenetic nature of El Metate eruption.

Paper 2, “Paleomagnetically inferred ages of a cluster of Holocene monogenetic eruptions in the Tacámbaro-Puruarán area (Michoacán, México): Implications for volcanic hazards”, provides new paleomagnetic age data for four monogenetic Holocene vents namely La Tinaja, La Palma, Mesa La Muerta, and Malpaís de Cutzaróndiro (in chronological order according to stratigraphic relations) that form a small cluster located within the Tacámbaro-Puruarán area in Michoacán. Our new paleomagnetic data indicate that their eruptions occurred separately in time with varying recurrence intervals ranging between ~300 and ~2300 years, although they are closely clustered in space. The identification of such small clusters with several young volcanoes that erupted in periods of hundreds to thousands of years opens several key aspects regarding to future volcanic hazard assessments in the volcanically active Michoacán-Guanajuato volcanic field, and also should be considered when constraining the nature of the magmatic plumbing system.

Paper 3, “Paleomagnetic constraints on the ages of the Holocene Malpaís de Zacapu lava flow eruptions, Michoacán (México): Implications for archeology and volcanic hazards”. It presents an interdisciplinary research where the volcanological and archeological

information has been linked to the paleomagnetic dating procedures. Noteworthy, this work shows that future volcanic hazard mitigation efforts could benefit combining geophysical, volcanological and archeological studies.

Paper 4, “Palaeomagnetic dating of two recent lava flows from Ceboruco volcano, western Mexico”, where the paleomagnetic dating procedure was tested for the first time in Mexico on two lava flows sampled from Ceboruco, western Mexico. One historical flow was erupted in AD 1870, and our dating procedure gives an age range between AD 1755 and 1871. The second flow, namely Ceboruco, was date between AD 1000 and 1134 implying that Ceboruco volcano was inactive for at least 736 years until the 1870 eruption. This period is much longer than was previously suggested and thus should be considered in modeling the magma evolution in this area the estimations of volcanic risk.

Paper 5, “A 3600 years paleointensity secular variation curve for Mexico”. It presents new paleointensity data covering the past 3600 years which are used together with selected previously published data for Mexico in order to construct a paleointensity secular variation curve for Central Mexico. Important features of the Earth’s magnetic field intensity highs and lows could be captured from the new curve. Among these features is a large intensity peak documented for the first time for Mexico at around 250 BC, which is comparable to the Levant paleointensity spike. Comparing these findings with the data from other regions indicates that over the last 3600 years the Earth’s magnetic field was driven by the emergence of strong and rapidly fluctuating nondipole components superimposing the dominating dipole field.

Paper 6, “Late-Quaternary secular variation data from Mexican volcanoes”, provides new robust 32 paleomagnetic directions and 21 high-quality intensities obtained from 33 lava flows from the Trans-Mexican Volcanic Belt, which are used to construct full vector secular variation curve for Central Mexico. The new data are essential for enhancing the global geomagnetic field models which in turn will enhance the paleomagnetic dating approach for Mexico. The new curves were calculated for two periods: AD 2,000–2,200 BC and 2,200–45,000 BC, due to the uneven distribution of the data. During the entire period, numerous features of the Earth’s magnetic field are noted where the directions abruptly

changed accompanied by extremely high intensities or sudden intensity drops. Moreover, abnormal inclinations low accompanied by marked westerly declinations and very low intensities were observed between 26,000 and 24,000 BC. These anomalous behaviors could be attributed to geomagnetic jerks and/or an excursion firstly documented for Mexico for the Late Quaternary. Comparing with other regions, this excursion may be related to the Mono Lake excursion.

INSTITUTIONAL ACKNOWLEDGMENTS

I thank the Universidad Nacional Autónoma de México (UNAM) for giving me the opportunity to do the Doctorate in the Postgraduate of Earth Sciences.

To the Centro de Geociencias (CGEO) of the Universidad Nacional Autónoma de México (UNAM) campus Juriquilla, Querétaro, for allowing me to use its facilities and equipment in the Laboratory of Paleomagnetism, which made possible the realization of this work.

This thesis would not have been possible without the financial support granted to the research projects of the National Council of Science and Technology (CONACYT-180032) and UNAM-DGAPA-PAPIIT (IN-111915).

ACKNOWLEDGMENTS

As I come from a distant place, I always say that the four years I spent in Mexico, where I finished my doctorate, would not have been possible without the presence of people who helped me in the academic level and also in the personal level.

First of all, I would like to express my sincere gratitude to my advisor **Dr. Harald Böhnel** for the continued support of my PhD and related research, motivation and great knowledge. The door of Harald's office was always open whenever I was in a trouble place or had a question about my research or writing. He always allowed this thesis to be my own work, but he guided me in the right direction when I thought I needed him, **Thanks Harald**.

I would like to acknowledge and thank deeply my tutored committee: **Dr. John Shaw and Dr. Peter Schaff** for supervising my academic performance during these four years. To the members of my pre-doctoral examination: **Dr. Roberto S. Molina, Dr. Luis Alva Valdivia, Dr. Gerardo Carrasco, and Dr. Edgardo Cañón** for their useful comments and advice. My sincere thanks go also to **Dr. Claus Siebe** for his advice and comments in the field work that definitely made my work more interesting.

My sincere thanks to all the administrative staff of CGEO for the support received during my stay. In Special, I want to thank **Dr. Mariano Cerca**, the postgraduate coordinator, for always being willing to provide assistance in the procedures related to the graduate and also related to the immigration office. I also thank **Mrs. Marta Pereda Miranda** for her valuable assistance to me (since I arrived in Mexico) and for being fully aware of what we need and for her dedication to work. I would also like to express my sincere thanks to **Mr. Armando Ramirez Morán** for the assistance in the graduation processes.

I want to thank the **M.Sc. Erick Juárez-Arriaga and Kurt Wogau** "the paleomagots" and **M.Sc. Sergio Salinas** "the geomorphologist" for their accompanying me in the field trips where we have had a good time together. **Ing. Jorge Escalante** thanks for all the technical support, especially for the Curie balance. I am pleased to thank the laboratory technician of paleomagnetism **Mr. Marcos Ortega Yurjar** for all his collaboration and his good spirit always.

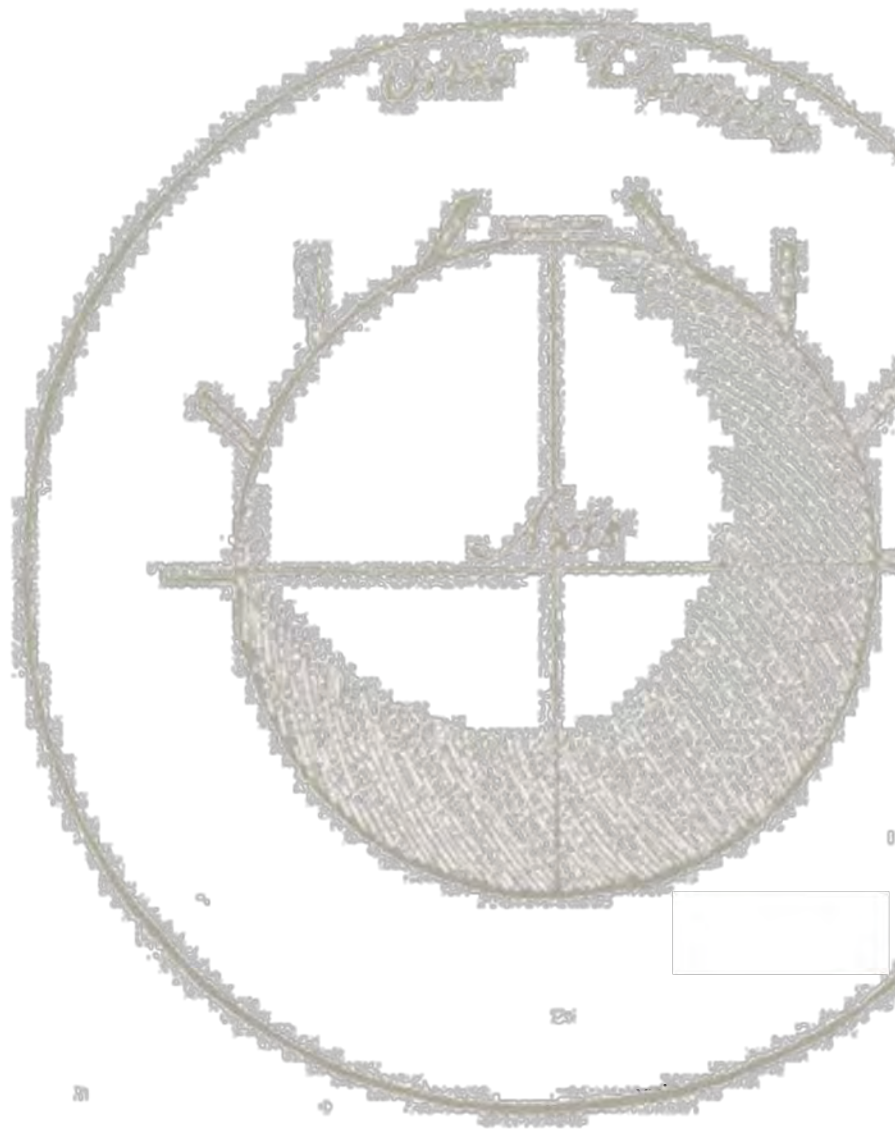
A special recognition goes to **Mrs. Regina Nava-Böhnel**, a wonderful woman with her generous and unconditional support; the words of praise do not break her right thanks for everything Regina. To **Miss. Astrid Böhnel**, I am grateful for what you did with my wife, especially during her pregnancy. Being with us on the day of Nassercito birth and your generous help cannot be forgotten. **Mr. Mohamed Zabady**, I met you recently, but I learned a lot from you; Thanks for helping me without charge it is a feeling that cannot be expressed. To **Dr. Khaled Abouelezz**, your advice to me and your academic guidance since even before I came to Mexico helped me a lot, I am grateful to you and I hope that Allah gives you and your family the happiness in this world and in the rest.

Finally, a message of thanks and gratitude to all my friends who had fun with them here at the Centro de Geociencias, especially, ***Gonzalo Cid, Melisa Ramos, Luis Rocha, Erick Medina, Lisel Duran, Daniel Serrano and his family, Edgar Juárez, Diego Garcia and Myrna Lorena.*** Also, I would like to thank my friends who have spent a good time with them in the laboratory of paleomagnetism: ***Héctor, Rosario, Alberto, Karina, Emiliano, Sergio, Jean.***

To all my friends, Muchas Gracias!!!

... Now must we consider separately the globe itself of the earth. Those experiments which have been proved by means of the terrella, how magnetick things conform themselves to the terrella, are all or at least the principal and most important of them, displayed by means of the earth's Body: And to the earth things magnetical are in all respects associate....

William Gilbert, London, 1600



Contents

Resumen / Summary	v
1. INTRODUCTION	1
1.1. Earth's magnetic field	1
1.2. Full vector Late Quaternary paleomagnetic secular variation	2
1.3. Thesis Hypothesis	5
1.4. Objectives	5
1.5. Thesis structure	7
1.6. Study Area and field sampling	8
1.6. Methodological strategy	11
2. MANUSCRIPT 1	
Paleomagnetic study of El Metate shield volcano (Michoacán, Mexico) confirms its monogenetic nature and young age (~1250 CE).	25
3. MANUSCRIPT 2	
Paleomagnetically inferred ages of a cluster of Holocene monogenetic eruptions in the Tacámbaro-Puruarán area (Michoacán, México): Implications for volcanic hazards	36
4. MANUSCRIPT 3	
Paleomagnetic constraints on the ages of the Holocene Malpaís de Zacapu lava flow eruptions, Michoacán (México): Implications for archeology and volcanic hazards	48
5. MANUSCRIPT 4	
Palaeomagnetic dating of two recent lava flows from Ceboruco volcano, western Mexico	66
6. CONCLUSIONS	80
REFERENCES	84
SUPPLEMENTARY MATERIALS	92
I. Manuscript 5: A 3600 years paleointensity secular variation curve for Mexico	93
II. Manuscript 6: Late-Quaternary secular variation data from Mexican volcanoes	168
III. Supplementary material for manuscript 2	281
IV. Supplementary material for manuscript 4	291

1. Introduction

1.1. Earth's magnetic field

The Earth's magnetic field (EMF) or the geomagnetic field is generated within the fluid outer core of the Earth by some form of magnetohydrodynamic dynamo, referred to as geodynamo (e.g., Merrill et al., 1996). Studying the record of the direction and intensity of the geomagnetic field over the geological times (Paleomagnetism) provides us a conclusive knowledge of the Earth's history and provides crucial data that is used to reconstruct the continents to their original position (plate tectonics). The EMF at the Earth's surface resemble the field of a magnetic dipole located at the center of the Earth and inclined by around 12° relative to the Earth's rotation axis (Fig. 1.1); the tilted geocentric axial dipole (GAD) hypothesis.

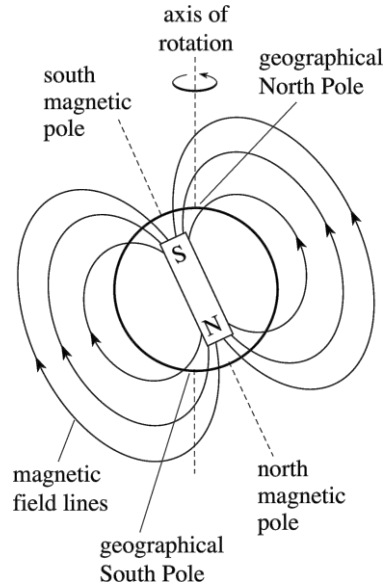


Figure 1.1 The Earth's magnetic field resemble the field produced by a simple bar magnet and could be approximated to a dipole field with a north and south Pole. Also demonstrated the geographic pole where the magnetic pole makes angle of $\sim 12^\circ$ with it.

Based on this hypothesis, the magnetic inclination attains values equal to $+90^\circ$ or -90° at the magnetic poles where the EMF intensity is twice as large as along the equator. Approximately 90% of the present geomagnetic field can be described by the tilted GAD model while the remaining is attributed to non-dipolar origin. Unlike the long-term variation of the dipolar field, the non-dipole component implies shorter period of the EMF fluctuations, commonly between a year and $\sim 10^5$ years. These short-term variations are referred to as secular variation (SV). Currently, the present geomagnetic field is continuously measured in magnetic observatories, and also via orbiting satellites. Direct instrumental measurements for the magnetic declination date back to the 16th century while the magnetic inclination measurements were started in the 17th century. The first survey of

the magnetic field intensity was done in the 19th century. For the last 400 years, Jackson et al. (2000) have built a high resolution geomagnetic field model (GUFM1) based on the aforementioned historical data. Going back in time, even just for the last few thousands of years, no direct measurements are available anymore and the workaround solution lies in deciphering the magnetic field retained by geological and archeological materials.

Remanent magnetization in rocks is acquired by different mechanisms, most notably is the thermal remanent magnetization (TRM) acquired through cooling from high temperature at $\sim 700^{\circ}\text{C}$ or more (above the Curie temperature, T_c) in the presence of an ambient field, and the other is the remanence acquired by a sediment during or closely after deposition of the ferromagnetic grains, called depositional (or post depositional) remanent magnetization (DRM or pDRM). Volcanic rocks and fired archeological objects possess TRM where spot information of the paleofield direction and intensity are faithfully preserved, while marine and lacustrine sediments acquire a DRM which provides a semi-continuous record of the EMF variation. However, it should be mentioned that most likely the remanence acquisition processes in marine sediments is followed by several other factors which undesirably disturb the paleomagnetic record, such as flattening, compaction, and diagenesis (see Kok and Tauxe, 1996). Further on, the magnetic field intensity can only be determined relatively (see Tauxe, 1993) as will be presented in section 1.6.3 The TRM, on the other hand, is stable over geological times and resistant to the recent magnetic fields, and absolute estimates of the paleofield intensity can be obtained (see section 1.6.3). Altogether, this points to the superiority of the TRM over DRM in reconstructing the SV changes.

1.2. Full vector Late Quaternary paleomagnetic secular variation

Paleomagnetic secular variation (PSV) refers to temporal and spatial variations of the Earth's magnetic field (EMF) due to internal processes (flow of liquid in the Earth's outer core), over periods of a year to millions of years. Understanding the full vector evolution of the EMF can be used in different geophysical disciplines, such as: the evolution of the Earth's core (Elsasser, 1956); variations in heat flow across the core-mantle-boundary (Glatzmaier et al., 1999); the effect of the nucleation and growth of the solid inner core on the EMF (Smirnov et al., 2003). Also, for the recent years it was applied to date recent volcanic eruptions and archeological artefacts (e.g. Tanguy et al., 2003; Arrighi et al., 2006;

Speranza et al., 2006, 2008; Hagstrum & Blinman 2010; Roperch et al. 2015). Moreover, determining the EMF intensity changes in the past helps in realizing how stable it was, which could be used to investigate whether the present day field is approaching a polarity change or reversal (Hulot et al., 2002). In this context, it must be mentioned that over the geological timescales the EMF has been frequently *reversed* where the positions of the magnetic north and magnetic south are interchanged. The Earth's field has alternated periods of normal and reverse polarity. These periods are referred to as *chrons*. The last full polarity reversal, the Matuyama/Brunhes reversal, has occurred around 780,000 years ago. Then after, the EMF is of the present normal polarity state. Polarity chrons could be interrupted by *geomagnetic excursions* which are defined as abnormal fast directional change in the EMF where the virtual geomagnetic poles (VGPs) lie at latitude between + and - 45° from the VGP. Unlike reversal, many proposed excursions were not recorded around the entire globe, possibly due to their short duration of generally <3,000 years and only rarely up to 10,000 years. Within the Late Quaternary two globally observed excursions named Laschamp and Mono Lake have been identified, which have been recently dated by Laj and Kissel (2014) at ~ 41.2±1.6 kyr and 34.2±1.2 kyr, respectively. The EMF intensity during the excursion is reduced to its lowest value (Ferk and Leonhardt, 2009). Moreover, during the recent few thousand years extreme variations of the geomagnetic field were observed, which are called archeomagnetic jerks (Genevey and Gallet, 2002; Gallet et al., 2003) where directions and/or intensities of the EMF changed abruptly, and geomagnetic spikes (Ben-Yosef et al., 2009) which involve intensity maxima. From the above mentioned features it is obvious that determining the paleofield intensity beside the directions has prime importance.

Globally, Late Quaternary SV data distribution is uneven where the data are largely concentrated in the northern hemisphere and most specifically in Europe. In fact, since the 1990's, enormous efforts have been devoted for enhancing the SV data (e.g. Böhnell and Molina, 2002; Hagstrum and Champion, 2002; Schnepf et al., 2005; Schnepf et al., 2006; Tema et al., 2006; Gomez-Paccard et al., 2006; Di Chiara et al., 2012, 2014; Michalk et al., 2010; Kovacheva et al., 2014; Kissel et al., 2015a, b; Tema et al., 2017; Cai et al., 2017). Currently, there are several global datasets, for example the GEOMAGIA50 (Brown et al., 2015); the HISTMAG (Arneitz et al., 2017); and the MAGIC (<https://www2.earthref.org/MagIC>). We use here the GEOMAGIA50 global dataset to

recover directions and intensities published for a specific region and for a certain period of time within the last 50,000 years. It should be mentioned here that a number of global and regional models have been recently constructed through the use of such global datasets. These models are different in terms of the type of the geological materials included and also of the mathematical approach used for constructing the model curves. The most recent global field models are: ARCH10k.1 (Constable et al., 2016) for the last 10,000 years; CALS10k.1b (Korte et al., 2011) for the last 10,000 years; SHA.DIF.14k (Pavón-Carrasco et al., 2014) covers the entire Holocene. Both ARCH10k.1 and SHA.DIF.14k use a combination of archeomagnetic and lava flow data, while CALS10k.1b apart from archeomagnetic and lava flow data also includes numerous sedimentary data. Therefore, in comparison to ARCH10k.1 and SHA.DIF.14k, CALS10k.1b is strongly smoothed. All these models are constrained by the historical GUFM1 model (Jackson et al., 2000) for the past four centuries.

In order to illustrate how the SV intensity data is distributed during the Late Quaternary, Fig. 1.2 shows the global and temporal distribution of the EMF intensity given as virtual axial dipole moments (VADM) (black dots), together with the Mexican data as red

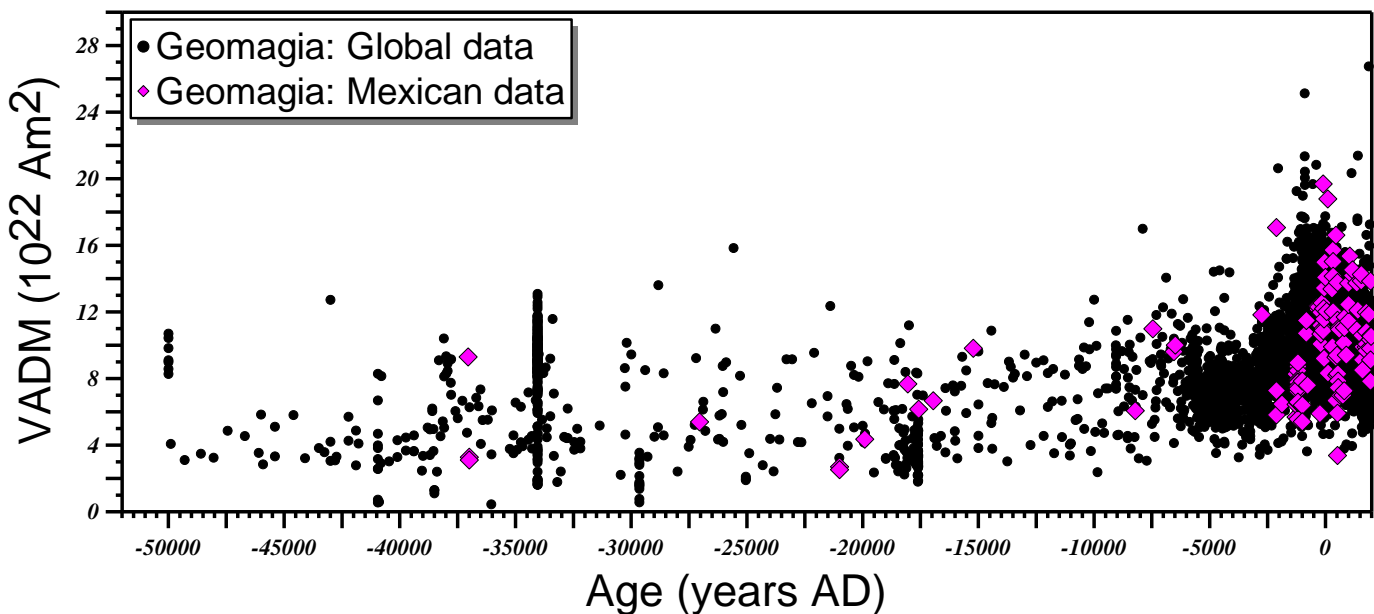


Figure 1.2 Late Quaternary secular variation intensity data (expressed as the virtual axial dipole moment; VADM) for the entire globe (black dots) and also for Mexico (red diamonds) compiled from the Geomagia50.v3 data base (Brown et al., 2015). From the figure it is evident that both global and Mexican data are concentrated for the last 10,000 years, and also it is clear that the Mexican and the global data are scattered.

diamonds. It is evident from Fig. 1.2 that the number of data is decreasing strongly with increasing age, with Holocene SV data representing $\approx 88\%$ of the total (4523/5115). The same applies for the Mexican data where 108 of 119 ($\approx 90\%$) intensity data correspond to the Holocene. This indicates that global SV data for periods between 10,000-50,000 years are scarce. In this context, regions of high volcanic activity such as Mexico, Japan, and Hawaii are ideal locations to densify SV data and construct high-resolution curves for the aforementioned time span. Moreover, for the last 10,000 years the VADM_s for Mexico are strongly scattered which suggests that these data are affected by experimental problems and/or wrong age determinations. Noteworthy, these simple remarks reflected the importance of performing further studies in such interesting topic and pave the way to list the main objectives of the present thesis.

1.3. Thesis hypothesis

Understanding the origin of the earth's magnetic field needs an accurate knowledge of its variation through the geological timescales. Full-vector paleomagnetic field is determined through separating the desired TRM component that instantaneously locked in volcanic or archeological materials from un-wanted other components and calculating the paleofield intensity. It should be noted that magnetic field directions are fairly easy to be determined while measuring its intensity proves to be frequently difficult because required conditions in the analyzed natural rock sample are not always encountered. Constructing a detailed full-vector field over a certain time can be used in enhancing the recently constructed global geomagnetic curve models (Constable et al., 2016; Korte et al., 2011; Pavón-Carrasco et al., 2014) and also in the dating applications (paleomagnetic dating). In this latter, the magnetic field direction and intensity registered locally by a suitable material of unknown age are compared with local secular variation curve model and/or with the global curves. Paleomagnetic dating can be used as an alternative of the radiocarbon dating (^{14}C) because sometimes it becomes difficult to get a datable organic material necessary for the ^{14}C dating procedure.

1.4. Objectives

Mexico is an ideal place for reconstructing the past variation of the EMF due to the availability of splendid archeological sites and also its high prevalence of volcanic rocks

which mainly spread along the Trans-Mexican volcanic belt (TMVB). On the other hand, during the Holocene, dozens of volcanic eruptions have occurred in the TMVB which certainly impacted the human populations. Age dating of such eruptions is important for assessing future volcanic hazards. My PhD project therefore was designed to:

1. Enrich the Late-Quaternary paleomagnetic secular variation database for Mexico.

Recently, the construction of full vector PSV curves received considerable attention in several regions of the world including Bulgaria (Kovacheva et al., 2014) for the last 8 ka, Canary and Azores Islands (Kissel et al., 2015) and Hawaii Islands (Tema et al., 2017) for the Holocene, and China for the last 6 ka (Cai et al., 2017). In addition, numerous PSV declination and inclination curves with reasonable resolution, but often for shorter periods, have been constructed for Europe (e.g. Schnepf et al., 2005; 2006; Tema et al., 2006; Gomez-Paccard et al., 2006; Batt et al., 2017), and also for Western North America (Hagstrum and Champion, 2002). Unfortunately, no comparable curves have so far been established for Mexico in spite of the large number of Quaternary volcanoes concentrated along the Trans-Mexican volcanic belt (TMVB). Therefore, the thesis aims mainly to enrich the Late-Quaternary Mexican PSV database by providing new directions and intensities by sampling tens of independent volcanic rocks and archeological objects. Also, the previous published data was evaluated in order to take a decision to reject the unreliable ones, due to ages and paleomagnetic errors. The present study provides a paleointensity secular variation curve for the last 3600 years with convenient resolution, which is compared to the global data in order to get insight into non-dipole nature in this period. Moreover, we have constructed full-vector secular variation curves for Mexico for the last 47 ka years which could enhance our perception of the nature of Earth's magnetic field in the past. Besides that, we also stress the danger of using published paleomagnetic data blindly without performing careful assessment. This generally is achieved by studying multiple sites per lava flow.

2. Date Holocene volcanic clusters by means of 'paleomagnetic dating'.

Part of thesis project has been devoted to check validity of the paleomagnetic dating technique and also to provide new paleomagnetic ages for some Holocene erupted volcanoes. The impact of volcanic eruptions on the human communities have been investigated in this context. This was accomplished in three different areas and interesting conclusions were obtained which should be considered for hazard assessment.

3. Deciphering the eruption evolution of a large volcanic centre in Mexico ‘El Metate’.

Herein, we have applied paleomagnetism as an alternative technique to investigate whether the eruption nature of a certain volcano was monogenetic or in a various distinct events. We have, paleomagnetically, analysed several lavas flows emitted from El Metate volcano (Michoacán) and dated each of them based on the outgoing directions and intensities. This study could contribute in volcanic hazard assessments, where the period of eruptions of these lava can be identified.

1.5. Thesis structure

This thesis is composed of six articles: four accepted (paper 1-4) and two more articles (Supplementary materials I and II; papers 5 and 6): one has been submitted and another one to be submitted for publication in peer-reviewed ISI journals:

Paper 1, *“Paleomagnetic study of El Metate shield volcano (Michoacán, Mexico) confirms its monogenetic nature and young age (~1250 CE)”*: this is a classical paleomagnetic analyses for several lava flows emitted from this volcano in order to check whether it is a monogenetic as recently proposed by Chevrel et al., (2016a, b). The idea was to sample this huge shield volcano from the oldest to the youngest lavas and to compare their directions and intensities.

Paper 2, *“Paleomagnetically inferred ages of a cluster of Holocene monogenetic eruptions in the Tacámbaro-Puruarán area (Michoacán, México): Implications for volcanic hazards”*, provides new paleomagnetic age data for three flows that could not be dated by ¹⁴C (Guilbaud et al., 2012). The ages can be used in developing a strategy that aimed at reducing risk in the active Michoacán-Guanajuato volcanic field.

Paper 3, *“Paleomagnetic constraints on the ages of the Holocene Malpaís de Zacapu lava flow eruptions, Michoacán (México): Implications for archeology and volcanic hazards”*, presents an interdisciplinary research where the volcanological and archeological information has been linked to the paleomagnetic dating results in order to investigate the impact of the Holocene volcanic eruption on the Pre-Hispanic civilization on this area: the Tarascan culture.

Paper 4, *“Palaeomagnetic dating of two recent lava flows from Ceboruco volcano, western Mexico”*, this was the first time the paleomagnetic dating technique was applied in Mexico . Two lavas were sampled where one of them has an historic age of 1870 AD and is

re-dated by paleomagnetic means for validation of the method, while the other could not be dated as no datable material could be found for ^{14}C analyses.

Paper 5 {in supplementary I}, ‘*A 3600 years paleointensity secular variation curve for Mexico*’, presents new paleointensity data covering the past 3600 years which are used together with selected previously published data for Mexico in order to construct a paleointensity secular variation curve for Central Mexico.

Paper 6 {in supplementary II}, ‘*Late-Quaternary secular variation data from Mexican volcanoes*’, presents new robust 32 paleomagnetic directions and 21 high-quality intensities obtained from 33 lava flows from the Trans-Mexican Volcanic Belt, which are used to construct full vector secular variation curve for Central Mexico.

1.6. Study area and field sampling

1.6.1. The volcanic rocks

The volcanic rocks were broadly sampled from the Trans-Mexican volcanic belt (TMVB; Fig. 1.3) which is an active E-W volcanic arc crossing central Mexico for 1200 km and originated as a result of the subduction of the oceanic Cocos and Rivera Plates underneath the continental North American Plate (e.g. Blatter and Hammersley, 2010; Gómez-Tuena et al., 2003; Kim et al., 2012; Pardo and Suárez, 1995). This volcanic arc consists of a large number of Late Tertiary to Quaternary maars, scoria cones, domes, calderas, and strato-volcanoes, mostly with a calc-alkaline composition (e.g. Carmichael, 2002; Ferrari et al., 2012). One notable feature of the TMVB is its oblique position with respect to the Middle American trench. It could be classified into four main sectors (Fig.1.3) each with distinct geologic and tectonic features (Demant, 1978; Pasquaré et al., 1991): (1) the western sector that is located between the Pacific coast and the triple junction including the Ceboruco and Tequila volcanic field; (2) the western-central segment include the Michoacán-Guanajuato volcanic field (MGVF) with an area of $\approx 40,000 \text{ km}^2$, which among the other sectors contains the highest concentration of monogenetic volcanoes (Guilbaud et al., 2012); (3) the central sector is hosting the Sierra del Chichinautzin Volcanic Field (SCVF) located south of Mexico City and extending from Popocatepétel to Toluca; (4) Eastern-TMVB includes the Pico de Orizaba (PDO), Xalapa volcanic field (XVF) and the Tuxtla Volcanic Field (TVF) located at the Mexico’s Gulf Coastal Plain.

Paleomagnetic field sampling was carried out in several field trips which began in March,

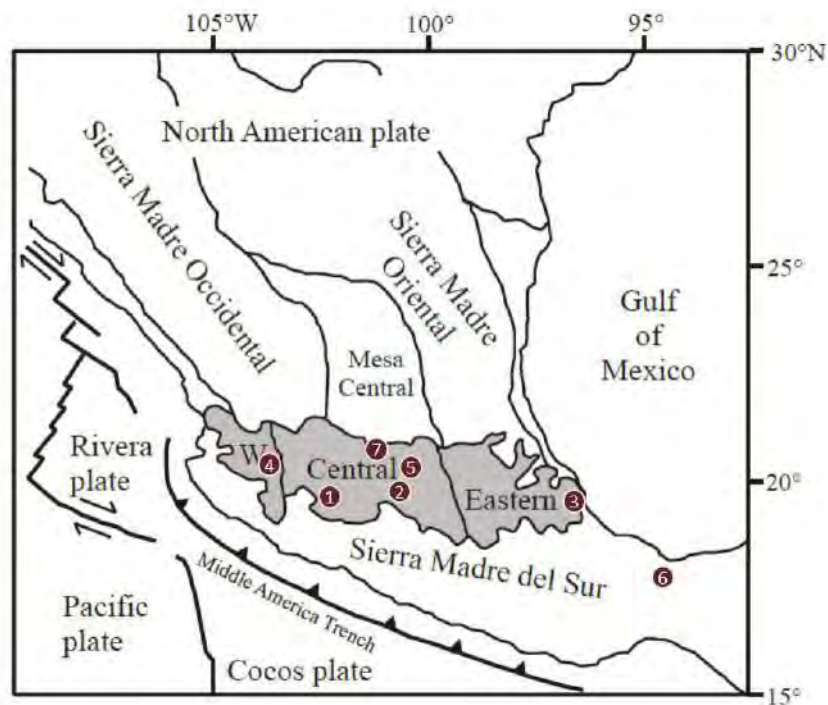


Figure 1.3 Location of the Trans-Mexican Volcanic Belt (grey area) and its three main sectors the Western, Central, and the eastern part (modified from Gómez-Tuena et al., 2005). Also demonstrated the locations of the studied volcanic samples and the archeological locations as plotted in red squares. Numbers represent the location name as follows: (1) the Michoacán-Guanajuato volcanic field (MGVF); (2) the Sierra del Chichinautzin Volcanic Field (SCVF); (3) Eastern-TMVB including the Tuxtla Volcanic Field (TVF) located at the Mexico's Gulf Coastal Plain; (4) the western sector that includes the Ceboruco volcanic field; (5) the Teotihuacán and Xitle heated pottery fragments; (6) the Olmecs; (7) the Santa Rosa de Viterbo historical temple.

2015 and ended in July 2017. For the volcanic rocks, 43 cooling units of lavas and bombs were sampled in 161 paleomagnetic sites located along the TMVB distributed as follows: 23 from the MGVF; 10 from the SCVF; 8 were sampled from the E-TMVB; and 2 lava flows have been sampled from Ceboruco. As mentioned in the objectives, for the purpose of enhancing the Late Quaternary SV data in Mexico a high-quality age data is one of the intrinsic issues. Therefore, the ages were determined mostly by the radiocarbon dated (^{14}C) which so far is considered the most reliable dating technique applied on Late-Quaternary erupted volcanic materials. In some others, the thermoluminescence (TL) method was applied for dating, and finally there is one historical lava flow.

1.6.2. The archeological artefacts

For the archeological materials, a number of 60 pieces of potteries, ceramics, and bricks were collected in four locations within Central Mexico (Fig. 1.3). A brief description of each location is listed here:

1. San Lorenzo Tenochtitlán, Veracruz, and satellite centers (Olmec culture). San Lorenzo is the earliest Olmec capital which is located in the coastal plains of the southeast portion of the Mexican state of Veracruz (17.75°N, 94.76°W). The secondary center of Loma del Zapote is located immediately south of the capital, and the site complex of El Bajío-El Remolino is located 3-4 km to the north. San Lorenzo is well-known for the 10 majestic colossal stone heads unearthed there and many other magnificent stone sculptures. Since 1990 the San Lorenzo Tenochtitlán Archaeological Project has concentrated on investigating the ancient environment and subsistence as well as documenting and explaining diachronic settlement patterns at the site and regional level. Its objectives include the excavation of diverse areas within the capital of San Lorenzo in order to understand the differential use of space over time. The samples used in the present study come from whole and partial vessels found on occupation floors within sealed excavation contexts at the capital and satellite centers. These contexts vary in function with the representation of domestic, ceremonial and administrative areas. Their temporal placement is supported by ¹⁴C dates and relative dating by ceramic attributes.

2. Teotihuacán. Teotihuacán (19.69°N, 98.84°W) is an ancient Mesoamerican city located in a sub-valley of the Valley of Mexico, located in the State of Mexico 40 kilometers northeast of modern-day Mexico City, known today as the site of many of the architecturally most significant Mesoamerican pyramids built in the pre-Columbian Americas. The pottery sherds from Cuanalan, Teopancazco, Cueva del Pirul, and Cueva de las Varillas come from extensive excavations headed by Linda R. Manzanilla: Cuanalan is a Late and Terminal Formative village located to the south of the Teotihuacan Valley; Teopancazco is a multiethnic neighborhood center of the Classic period in Teotihuacan; Cueva del Pirul and Cueva de las Varillas are two quarry tunnels located to the east of the Pyramid of the Sun in Teotihuacan, with post-Teotihuacan occupations (Epiclassic and Late Postclassic). All of the studied sherds were dated by ¹⁴C dates.

3. Santa Rosa de Viterbo bricks. The Temple and Convent of Saint Rose of Viterbo (Santa Rosa de Viterbo) is located in the city of Queretaro, Mexico, representing the greatest expression of Queretaro Baroque in the eighteenth century and one of the most

representative buildings with its architecture and elaborate altar pieces. The bricks come from the foundation walls of the constructions started in 1798 AD.

4. Xitle heated pottery fragments. Xitle monogenetic volcano (19.32°N, 99.18°W) is one of the youngest of the Chichinautzin monogenetic volcanic field with a ^{14}C age of $\approx 1530\text{--}1630$ BP (cal 373 \pm 56 AD; Siebe, 2000; Gonzales et al., 2000). Large discrepancies in the paleointensities led Böhnel et al. (2003) to perform paleointensity experiments using the microwave method on baked sediments and pottery fragments proved to be reheated during the Xitle eruption. Accordingly, in these materials, their newly acquired TRM have the same age as those of Xitle (373 AD). In the present study, several additional pottery fragments were collected directly beneath the Xitle lava flow. Four pottery fragments were subdivided into 17 specimens and used for the PI experiments. The main purpose was to enhance the available PI data published for Xitle through performing the IZZI-Thellier experiments on these potteries and applying a strict set of selection criteria.

1.7. Methodological Strategy

The main approach to be followed in the present project is to provide Mexico with new reliable paleomagnetic directions and intensities and applying paleomagnetic dating. As the credibility of the results is largely depend on the magnetic properties of the analyzed material, some of the routinely performed rock magnetic experiments were applied in order to define the magneto-mineralogy and thermal stability, and also to characterize the domain size of the enclosed magnetic minerals. The relation between the rock magnetic properties and the paleointensity success rate were partly discussed in the thesis. Below is a brief description of the experiments that have been carried out.

1.7.1 Rock magnetic properties

Hysteresis loops with a maximum field of 1.0 T were done on small pieces weighting no more than 0.05 grams using the alternating gradient force magnetometer (MicroMag 2900) located in the Paleomagnetic Laboratory of Centro de Geociencias (Querétaro, Mexico). For these loops, 5 mT field steps were taken with 100 ms averaging time. Back field curves were measured for each hysteresis loop by applying a maximum field of 1.0 T followed by a succession of increasing back field values (5 mT steps). The hysteresis parameters saturation magnetization M_s , remanent saturation M_{rs} , and coercive force H_c were calculated from the hysteresis loops data after subtracting the paramagnetic contribution.

The remanent coercive force (H_{cr}) was determined from the backfield demagnetization curves. Hysteresis data allowed determining the bulk magnetic granulometry of a sample, which was deduced from a Day diagram (Day et al., 1977). The high-field induced magnetization of samples was measured as function of temperature for Curie temperature determination, by means of a modified horizontal translation Curie balance built in the laboratory. Samples were milled into powder so as to be inserted into the oven of the horizontal translation Curie balance in a field of 500 mT with $T_{max}=600^{\circ}C$. The experiments were done in air in order to give information about magneto-mineralogical changes.

1.7.2 Paleomagnetic analyses

Reliable information of the past geomagnetic field direction could be obtained unequivocally. As mentioned above, the natural remanent magnetization (NRM) of volcanic rocks is of thermal origin (TRM). In some cases, the primarily acquired TRM component could be overprinted by secondary magnetization components such as the viscous (VRM) or the isothermal remanent magnetization (IRM). The main goal of paleomagnetic analyses is to separate the desired TRM component from the un-wanted other components. To start with, paleomagnetic sampling of several samples from a certain site must be performed. Choosing a convenient site is of great importance as we must be fairly sure that it has not been moved anymore after possessing the TRM.

Paleomagnetic core samples were recovered by using a portable gasoline-powered drill with a diamond-tipped (Fig. 1.4a). From each site, 8 to 18 cores with a diameter of 25 mm and a length of 6-15 cm were collected and oriented directly after drilling while they were still attached to the rock outcrop (Fig. 1.4b). In-situ orientation was done by using magnetic and sun compasses and an inclinometer (Fig. 1.4c). The gathered samples are marked and numbered, and the azimuth and dip are noted in the field notebook together with the sun shadow angle and the time for correcting the magnetic declination. The samples are further cut in the laboratory into specimens (at least 3) of 22 mm length (Fig. 1.4d). The NRM was measured with Agico JR5 or JR6 spinner magnetometers which automatically convert the specimen coordinate to geographic coordinate system based on the field orientation parameters. The paleomagnetic directions are obtained by alternating field (AF) demagnetization which was accomplished by an Agico LDA-3 equipment in 10-12 steps ranging from 3 to 80 mT. Demagnetization data are graphically displayed on orthogonal

vector plots (Zijderveld, 1967) and on equal-area projections (Fig. 1.5a). For each sample, the characteristic remanent magnetization direction (ChRM) was determined applying the principal components analysis (PCA; Kirschvink, 1980). Mean direction was computed using Fisher statistics (Fisher, 1953) (Fig. 1.5b).

Software used in this context is the PMGSC 4.2 (Enkin, 2005) and PMag Tool 4.2b (Hounslow, [https:// www.lancaster.ac.uk/staff/hounslow/resources/software/pmagtool.htm](https://www.lancaster.ac.uk/staff/hounslow/resources/software/pmagtool.htm)).

Finally, reliability of the mean paleomagnetic direction can be checked by two parameters; the α_{95} which is defined as the confidence limit for the calculated mean direction at 95% probability level; and the precision parameter (k). For further details, *see Tauxe (2010)*.



Figure 1.4 (a) Field sampling image showing how we drill the lava flow using portable gasoline-powered drill; (b) Another image demonstrate how we orient the samples before taking out from the attached rock outcrop; (c) Overall view of the orienting device used in the present thesis with digital inclinometer and sun to magnetic compass with ocular reading; (d) Paleomagnetic core samples with the orientation arrows, and also showed some specimens.

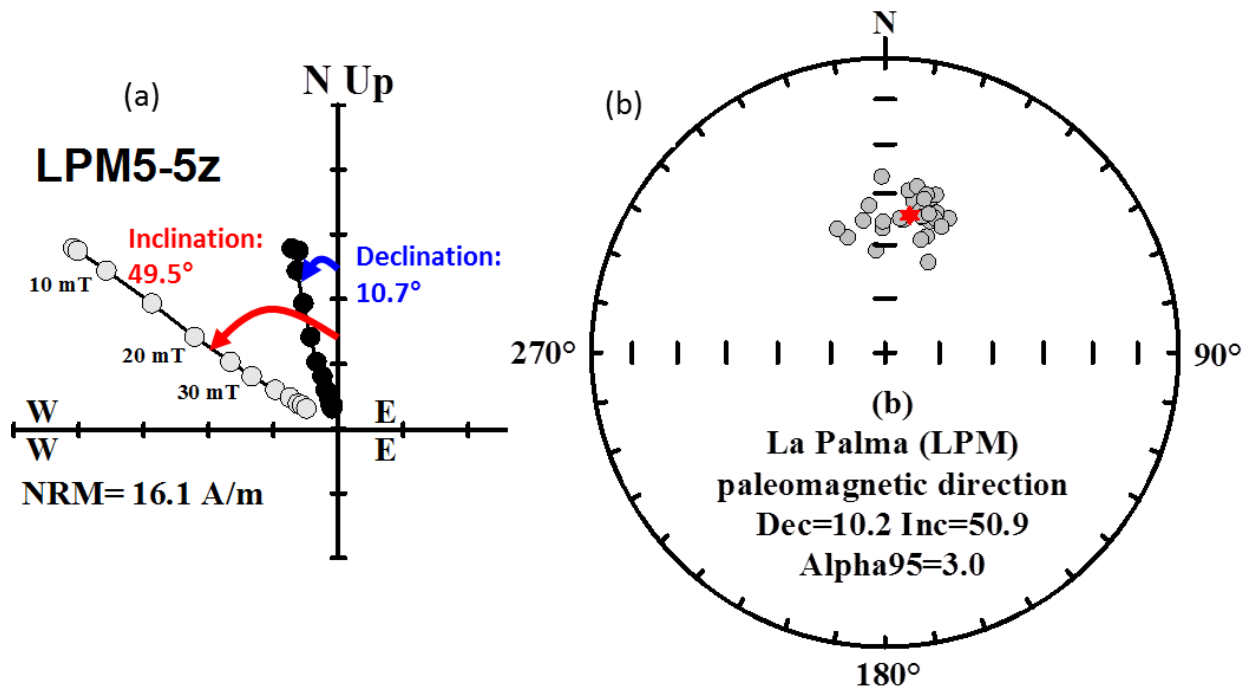


Figure 1.5 (a) Representative example of Zijderveld diagram showing the horizontal (declination, black dots) and vertical magnetization components (grey dots). The characteristic remanent magnetization direction of this specimen (LPM5-5z) was determined by applying the principal component analysis which gave values of 10.7° and 49.5° for declination and inclination, respectively. (b) Example of equal area projection of specimen and site means direction calculated for lava flow named La Palma. The mean direction is illustrated in red star.

1.7.3. Paleointensities

Unlike paleodirections, determining a paleofield intensity (hereinafter, Paleointensity: PI) is not straightforward because several conditions must be met for the analyzed material. For this reason, this area of research has witnessed systematic revolution since it was applied in the 1950s. Historically, the idea of recovering the intensity from materials that acquire a remanent magnetization by cooling in the paleofield goes back to Folgheraiter (1899) and (Dunlop, 2011). He hypothesized that it may be possible to reconstruct the paleofield if these materials are heated and cooled in the laboratory in a known magnetic field, and their natural remanent magnetization is compared to the magnetization imparted in the laboratory (Folgheraiter, 1899). Later, Koenigsberger (1938) predicted the complication of

obtaining such paleointensity estimate. He summarized what was then known about how minerals alter when heated; recognizing that changes in grain size and texture can have important effect on magnetization as chemical changes in mineral species. Practically every rock he measured altered its magnetic character during heating. Precise ancient field estimates were unattainable with his data. Based on the retained NRM origin, there are two types of paleointensity data; *absolute and relative PI*.

The absolute PI are obtained from those materials that acquired a TRM as igneous rocks and archeological artefacts, while the paleointensity value in sedimentary materials can only be determined relatively, as they acquire a depositional remanent magnetization (DRM). As the present thesis deals with volcanic and archeological materials, we will focus only on the absolute PI methods.

(1) Thellier-type paleointensity experiments

The Thellier-technique (Thellier and Thellier, 1959) is the most widely used method for the determination of the absolute PI. It is named after Emile and Odette Thellier as they have developed a sophisticated technique for determining paleointensities from thermoremanent magnetization through a series of double heating steps in the laboratory. Their assumption was that determining the intensity of the ancient magnetic field (PI) relies on the fact that TRM acquired by rocks or fired objects are linearly related to the ambient field for low fields such as the Earth's (Fig. 1.6); *the linearity law*. However, it should be mentioned that this law is valid only for single and pseudo-single domain particles (Neel, 1949; 1955) and the larger the size the increasing complexity of the domain state (flower, vortex, multidomain MD) may violate the law of linearity (Tauxe, 2010). Empirical studies have shown that TRM acquisition is significantly non-linear even at rather low field strengths and that the departure from non-linearity is grain size dependent (see Dunlop and Argyle, 1997). Nonetheless, the Earth's today field is within the linear region (Tauxe, 2010). Beside the linearity law, Thellier and Thellier (1959) have assumed three more laws for the acquisition of TRM in non-interacting single domain particles:

(i) The law of reciprocity states that the blocking- (T_b ; heating and cooling in-field) and unblocking (T_{ub} ; heating and cooling without field) temperatures of the magnetic grains are equal, and thus a partial thermal remanences (pTRM) that is acquired between two

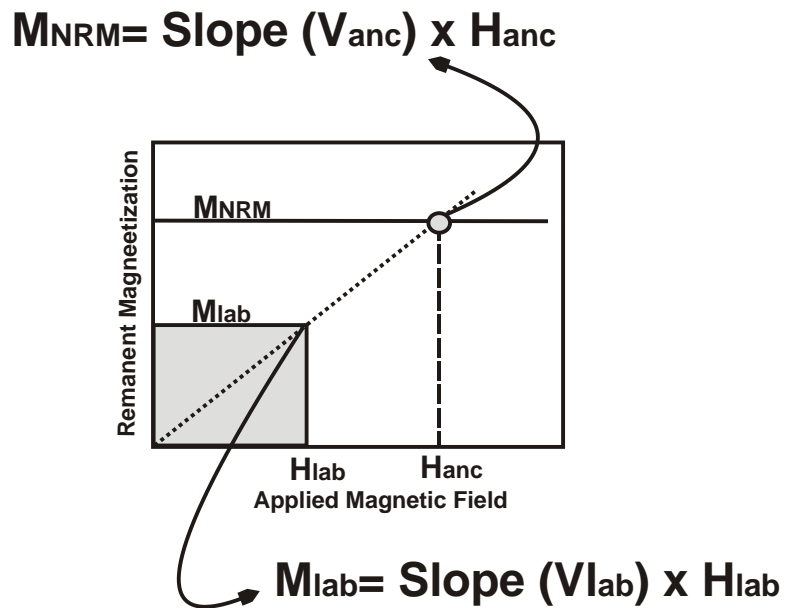


Figure 1.6 The main principal of paleointensity estimation. Determining the intensity of the ancient magnetic field B_{anc} relies on the fact that remanent magnetization (M_{NRM}) acquired by rocks are frequently approximately linearly related to the ambient field for low fields such as the Earth's $\{M_{NRM} = V_{anc} \cdot B_{anc} \text{ (1); } V_{anc} \text{ constant of proportionality}\}$. The idea here is to give the rock a laboratory remanence (M_{lab}) in a known laboratory magnetic field (B_{lab}) in order to get the relation $\{M_{lab} = V_{lab} \cdot B_{lab} \text{ (2)}\}$. From (2) we can determine the proportionality constant $\{V_{lab} = V_{anc} \text{ (3)}\}$ and subsequently the desired B_{anc} could be defined. (Redrawn after Tauxe, 2010).

temperatures T_1 and T_2 will be demagnetized completely by a zero-field heating in the same interval;

(ii) The law of independence: The pTRMs acquired by cooling between any two temperature steps are independent of those acquired between any other two temperature steps.

(iii) The law of additivity: The total TRM is the sum of all the independent pTRMs.

The classical Thellier method involves heating the samples twice in the presence of a laboratory field (infield-infield protocol; II). After the first heating step, the remanence (M_1) will be: $M_{NRM} + M_{pTRM}$. After that the same sample are heated and cooled again in an opposite laboratory field, so the second remanence (M_2) is: $M_{NRM} - M_{pTRM}$. By vector addition and subtraction, the NRM remaining and the pTRM the sample gained during each step can be determined. Analysis of the data are performed using the Arai plots (Nagata et al., 1963) (Fig.1.7a) where the NRM remaining in the sample is plotted (as the

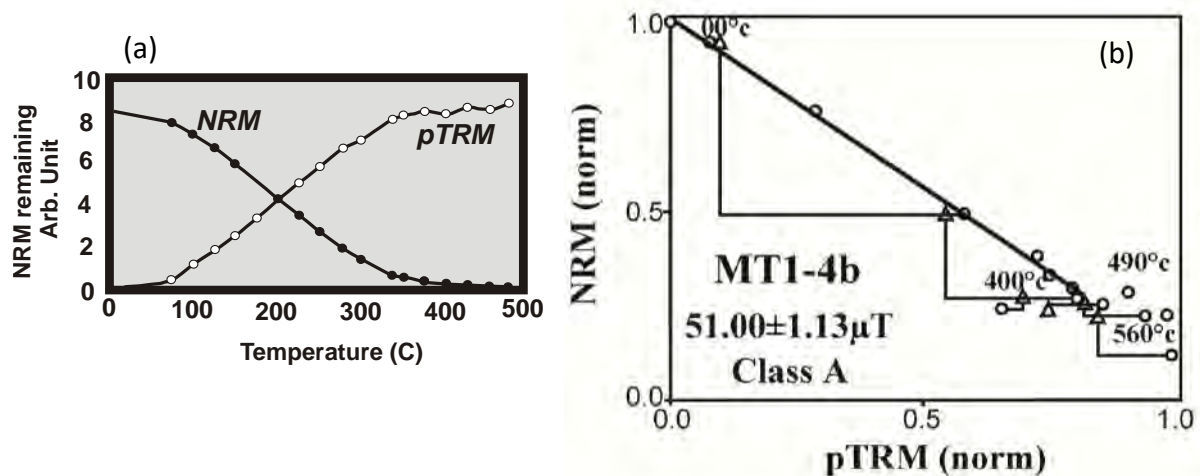


Figure 1.7 Illustration of stepwise heating method for determining absolute paleointensity. (a) Nagata plot showing the how the sample is step wisely demagnetized (filled circles) and remagnetized (open circles) during the Thellier experiment. (b) Representative example of an Arai-Plot showing the NRM component remaining versus pTRM gained at each temperature step. This experiment was done by the IZZI protocol and the triangles represent the pTRM checks.

ordinate) against the laboratory pTRM acquired at different stages of the experiment (on the abscissa). The value of the paleointensity is obtained by multiplying the slope (V) of the best fit line to these data in the Arai plot with the laboratory magnetic field (B_{lab}) applied to the sample. Later, three protocols have been proposed which differ from the original method in the way the laboratory field is set during the double heating step. These protocols are:

- (i) *The Coe's protocol* (Coe, 1967) in which the field is switched off during the first treatment (the sample is in a magnetic vacuum) and switched on in the second (zero-field/in-field; ZI).
- (ii) *The Aitken's protocol* (Aitken et al., 1988) inverted the previous (ZI) into in-field/zero-field (IZ) protocol. Herein, the field is switched on during the first treatment and off during the second.
- (iii) *The IZZI protocol* (Tauxe and Staudigel, 2004) implies that both of the Aitken's and the Coe's protocols are applied consecutively, where the IZ is applied first and then alternated with the ZI for the next heating step (Fig. 1.7b).

It is worth mentioning that these protocols should be supplemented by extra treatments in order to detect magneto mineralogical changes and the presence of biasing MD effects. These treatments are: (i) *pTRM checks* (Coe, 1967) which repeats one or several lower temperature steps and is carried out in-field, and allows determining whether the remanence carrying capacity of the specimen has changed (Triangles in Fig. 1.7b); (ii) *pTRM tail checks* (Riisager and Riisager, 2001) repeat demagnetization steps carried out to assess whether the partial thermal remanence gained in the laboratory at a given temperature is removed completely by re-heating to the same temperature in a zero-field; (iii) *Additivity checks* (Krása et al., 2003) are designed to detect multidomain behavior.

While the double-heating Thellier PI is widely used, it has some drawbacks:

- The multiple heating steps required for the experiments ‘often’ induce thermally induced alteration,
- Carrying multidomain or even pseudo-single magnetic grains in the original TRM make the treated samples non-obedient to the above mentioned Thellier laws particularly the reciprocity law.

Analyses of the PI data can be performed automatically by some software, for example the ThellierTool4.22 software (Leonhardt et al., 2004) or the Thellier-GUI (Shaar and Tauxe, 2013). Several parameters have been proposed in order to check the quality of the paleointensity data. These parameters take into account: the alteration; the NRM stability during the experiment; the statistics of the best-fit line itself used for calculating the PI, for more details see “Standard Paleointensity Definitions” of Paterson et al. (2014). Besides the time and effort required, the common success rate in lava samples is ~40%. The success rate is larger in the archeological artefacts as predominantly the grain size is much smaller due to the clays used for the production and the relatively fast cooling rate (~ 12 hours).

An alternative way of demagnetizing and remagnetizing the sample is to subject it to a high-frequency electromagnetic field in the microwave system ‘**the Microwave method**’ (Walton et al., 1996; Hill and Shaw, 1999). This method was proposed to reduce the alteration because it heats only the magnetic grain by affecting directly the magnetic spin system using ferromagnetic resonance. Also, it is only applied during ~ 10 seconds which compared to the ~ one hour single heating step required in an oven reduces significantly the danger of thermal alterations. A microwave system is fairly complex and thus is available

in only two places: the University of Liverpool's Geomagnetism Laboratory and in the Paleomagnetic Laboratory of Centro de Geociencias (Querétaro, Mexico).

(2) Shaw method

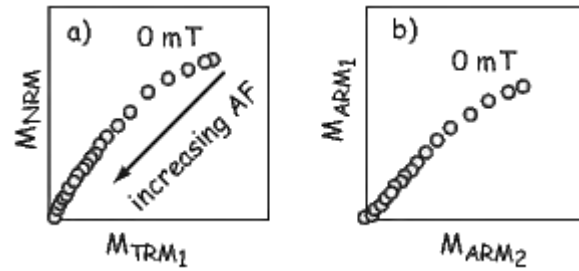
The Shaw method (Shaw, 1974) is an alternative method designed for avoiding the numerous heating steps needed in the Thellier-type experiment. In this method, the sample (NRM) is heated up once to a temperature higher than its Curie temperature (T_c) in the presence of an ambient magnetic field (H_{lab}). Therefore, the sample acquires a full TRM. The basic notion of Shaw's method is to compare the coercivity spectra of the NRM and the acquired TRM, given by their stepwise alternating field (AF) demagnetization data. Equality in the coercivity ratio indicates that ratio TRM/NRM is equal to unity and hence one can apply the linearity law $\{TRM/NRM = Blab/Banc; TRM/NRM = V\}$ to obtain the ancient field intensity Banc $\{Banc = V \cdot Blab\}$. The following steps are taken to implement this method (Fig. 1.8):

1. After measuring the NRM of a sample, progressively demagnetize it with alternating fields (AF) to establish the coercivity spectrum of the sample prior to heating.
2. Induce an anhysteretic remanent magnetization (M_{ARM1}) in your sample. Note that ARM is a type of magnetization in which you need equipment consisting of coils capable of producing simultaneously a direct and alternating field. It has been agreed that ARM has characteristics somewhat analogous to an TRM (Dunlop and Özdemir, 1997).
3. Progressively AF demagnetization of the M_{ARM1} to establish the relationship between the coercivity spectrum of M_{NRM} and M_{ARM1} prior to any laboratory heating.

Acquire a full TRM in the sample (single heating) which is subsequently AF demagnetized (M_{TRM1}) as well and finally the specimen is given a second ARM (M_{ARM2}) and AF demagnetized again. If the first and second ARMs do not have the same coercivity spectrum as in Figure 1.8b, the coercivity of the specimen has changed and the NRM/TRM ratio is suspect (Tauxe, 2010).

Some modifications have been done on this method, for example Tsunakawa and Shaw

Figure 1.8 the Shaw method. a) Plot of pairs of NRM and the first TRM for each AF demagnetization step. b) Plot of pairs of the first ARM and the second ARM for each AF demagnetization step (Tauxe, 2010).



(1994) proposed imparting a double-heating technique (DHT Shaw method) to check for alteration. Also, Yamamoto et al., (2003) and Mochizuki et al., (2004) applied the double heating technique of the Shaw method with low-temperature demagnetization (LTD-DHT Shaw method; Tsunakawa et al., 1997; Yamamoto et al., 2003; Oishi et al., 2005). LTD-DHT is an improved version of the Shaw method, utilizing the low temperature demagnetization as an effective technique for demagnetizing exclusively the multidomain like components (Ozima et al., 1964, Heider et al., 1992, and Yamamoto et al., 2003).

The most important advantage of Shaw method lies in its speed as well as potentially avoiding alterations because the sample is only heated once. Furthermore, one can easily remove secondary components of magnetization as the high-coercive-force region is generally least affected by thermal alteration (Tsunakawa and Shaw, 1994). However, it suffers from the higher risk of thermo-chemical alteration as the samples have to be heated above their highest Curie temperature.

(3) Multispecimen Method (MSP)

Dekkers and Böhnelt (2006) proposed a new method designed specially to avoid the undesirable multidomain effects and also to reduce the risk of alteration. It is called ‘multispecimen parallel differential pTRM method (MSP-DB)’. Instead of step-wise increasing the temperature and applying a constant magnetic field to one specimen in the furnace as in Thellier-style experiments, they proposed to use multiple specimens each heated in a different applied magnetic field in the furnace but all heated to the same temperature, which can be much lower than the Curie temperature. This method ideally requires that the NRM is composed uniquely by the original TRM. The basic idea here is that if a pTRM is induced parallel to the original TRM in a smaller laboratory field than the paleofield, the result will be a lower magnetization than the original TRM. If the pTRM is induced in a stronger field, the result will be a higher magnetization than the original TRM.

If induced in the same field as the paleofield, no change in remanence will occur. So, the paleofield (PI) is the field strength at which the difference between pTRM and TRM (this is the composite remanence after pTRM acquisition) and the original TRM is zero (Fig. 1.9). Two steps are needed to perform the MSP-DB experiment: (1) measure the NRM of each specimen (m_0), (2) acquire partial thermoremanence pTRM (m_1) parallel to the sample NRM (TRM) by heating them in a laboratory field H_{lab} to the set temperature. Now, calculate the DB ratio ($QDB = m_1 - m_0 / m_0$) and plot this ratio against the lab field H_{lab} (Fig. 1.9). According to what has been explained, the QDB ratio should be zero if the laboratory field is equal to the desired ancient field B_{anc} . Fabian and Leonhardt (2010) demonstrated that the original claim of domain-state independence by Dekkers and Böhnell (2006) was not entirely correct. Furthermore, the classical MSP-DB protocol suffers from tail-effects associated with imparting a pTRM. These effects give rise to an overestimation of the paleointensity values calculated from the MSP-DB protocol. Based on experiments on magnetic minerals of well controlled grain sizes, Fabian and Leonhardt (2010) proposed the MSP-DSC protocol, where DSC is an abbreviation of “domain-state corrected”. This modification requires three additional steps to the original MSP protocol (m_0 and m_1 represent the NRM and original single-step MSP-DB protocol); Step 2 (m_2) involves heating and cooling in a field antiparallel to the NRM; in Step 3 (m_3) we heat in zero field and then the cooling is performed in a parallel oven field; finally Step 4 (m_4) is a repetition of step 1. Analyzing the MSP-DB&DSC data can be done through using the recently provided MSP-Tool (Monster et al., 2015). In this software a number of decisive parameters are included through which we can inspect the reliability of the results. There are three reliability criteria that must be considered through analyzing the data: the alteration criterion $|\epsilon_{alt}|$; the thermal-induced alteration during the experiment (Fabian & Leonhardt 2010; Monster et al. 2015) m_{ust} ; the directional criterion which is the angle between the isolated NRM and induced pTRM (Monster et al. 2015); the intersection criterion (Δb) (Monster et al., 2015) tests whether the linear fit regression line intersects the y-axis at the theoretically predicted value (-1).

1.7.3 Paleomagnetic dating

Paleomagnetic dating is a new method which has been increasingly used over the past decades to date Holocene volcanic eruptions or archeological artefacts (e.g., Tanguy et al., 2003; Speranza et al., 2008). The method is based on the comparison of the EMF elements

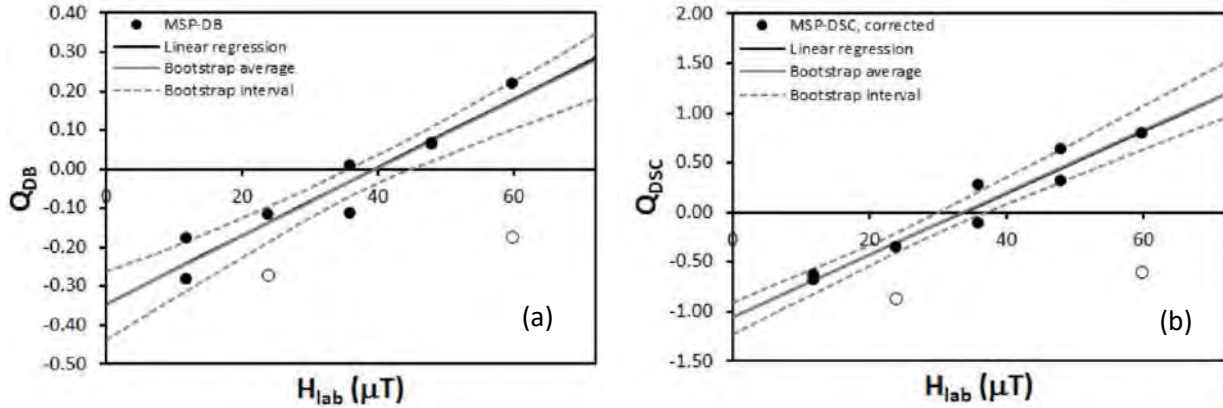


Figure 1.9 multispecimen plots for the (a) MSP-DB and (b) MSP-DSC. Closed and open dots represent the used and discarded data, respectively. The grey shaded areas represent the 95% confidence interval. The figure from Monster et al (2015).

(declination, inclination, and intensity) registered locally by a suitable material (e.g. lava rock or archaeological pottery) of unknown age with secular variation "master curves" established for the same geographical region" [e.g. by ARCH10k.1 (Constable et al., 2016); CALS10k.1b (Korte et al., 2011); SHA.DIF.14k (Pavón-Carrasco et al. (2014))] The methodology of paleomagnetic dating was proposed by Lanos (2004) and application of this method can be implemented using the freely available Matlab software `archaeo_dating` (Pavón-Carrasco et al., 2011). The Lanos (2004) approach uses the probability density functions (PDF) of the three geomagnetic field elements: declination (D), inclination (I) and intensity (F). The undated paleomagnetic field element D is considered normally distributed at a fixed time t , with a mean value $G_D(t)$ and standard deviation error σ_D . Also, the geomagnetic field element provided by the master curve $G_D(t)$ at the same fixed time is supposed normally distributed with mean and standard deviation given by:

$$\bar{G}_D(t) \text{ and } \sigma_G : G_D(t) \sim N(\bar{G}_D(t), \sigma_G^2(t)).$$

At time t , the conditional probability density (or likelihood) of the observation (non-dated palaeomagnetic element) is given by:

$$\begin{aligned} PDF_D(t) &= p(D|G, t) \\ &= \int_{-\infty}^{+\infty} p(D|G, D, t) \cdot p(D|G, t) \cdot dD. \end{aligned}$$

For more clarification, Figure 1.10 shows a graphical example (Pavón-Carrasco et al., 2011). The probability density map of the undated paleomagnetic element ($D=20^\circ$ in this example) is shown in the upper left panel. The probability density map of the master curve (in the example SHA.DIF.3K) at a specific latitude and longitude (here 40°N ; 4°W) is plotted in the upper right panel. Combining both maps leads to obtain the final probability density map (Fig. 1.10c). The integration, over the declination values of the final map, gives the Probability Density Function (PDF) of the undated declination (Fig. 1.10d). In order to obtain the most probable age, we have to combine the probability density functions (PDFs) of the geomagnetic field elements. Currently available geomagnetic field models go back to an maximum age of 14000 years (the Holocene) for performing paleomagnetic dating (SHA.DIF.14k, Pavón-Carrasco et al, 2014). However, as mentioned by Pavón-Carrasco et al (2014), for ages older than 6000 BC the applicability of the model becomes increasingly limited because the non-dipole components of the EMF are less resolved, and also due to the fact that going back in time the uncertainties generally increase. From the above, the validity of the age data obtained by this method substantially depends on several factors, including the credibility of the given age of the input data upon which the model has been constrained and the approach being followed by the EMF fluctuations in space and time. Since EMF elements (declination, inclination, and intensity) vary in a semi-cyclic pattern, the method frequently provides several possible age ranges for a single eruptive volcanic material (e.g. lava). Periods of rapid SV changes on the other hand would provide unique solution and thus give more precise age data. Furthermore, while the EMF directions are fairly easy to determine, measuring its paleointensity proves to be frequently difficult. Finally, it should be noted that a common shortcoming of all these paleomagnetic curve models arises from the uneven distribution of the global paleomagnetic secular variation (PSV) data, especially because most of the data have been sourced from localities in the northern hemisphere, particularly from Europe.

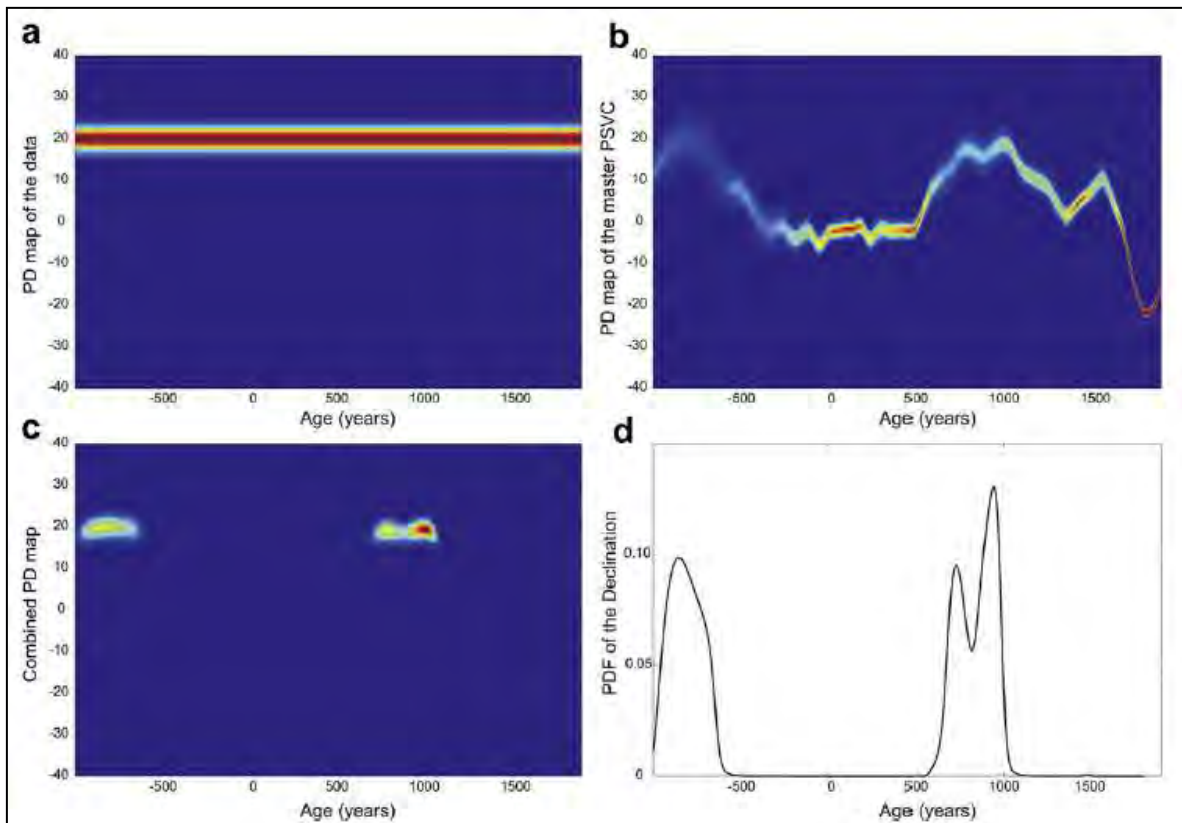


Figure 1.10 Probability density (PD) maps of the undated paleomagnetic data (a) and of the master PSVC (b). (c) Combined PD map and (d) final Probability Density Function (PDF) for the data. Dark blue represent zero probability ($p=0$) while dark red represent maximum probability ($p=1$). The figure from Pavón-Carrasco et al (2011).

2. Paleomagnetic study of El Metate shield volcano (Michoacán, Mexico) confirms its monogenetic nature and young age (~1250 CE).

Ahmed Nasser Mahgoub^{a*}, Harald Böhnel^a, Claus Siebe^b, Magdalena Oryaëlle Chevrel^c

^a Centro de Geociencias, Universidad Nacional Autónoma de México (UNAM), Blvd. Juriquilla No. 3001, Querétaro C.P. 76230, Mexico

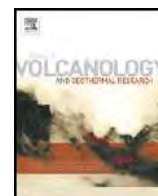
^b Departamento de Vulcanología, Instituto de Geofísica, Universidad Nacional Autónoma de México, Coyoacán, C.P. 04510 Ciudad de Mexico, Mexico

^c Facultad de Ingeniería, División de Ciencias de la Tierra, Universidad Nacional Autónoma de México, Mexico

Accepted: Journal of Volcanology and Geothermal Research, 336:209-218 (2017).

Individual contributions of the authors:

- i. **Ahmed Nasser Mahgoub:** conception and design of the study, fieldwork, sampling, conducting paleomagnetic and paleointensity experiments, processing, analysis and interpretation of data, writing the article.
- ii. **Harald Böhnel:** design the research study, fieldwork, participating in the interpretation of data and revising the article, financing for the project.
- iii. **Claus Siebe:** design the research study, participating in the interpretation of data and revising the article, financing for the project.
- iv. **Magdalena Oryaëlle Chevrel:** designing the geological map, revising the article.



Paleomagnetic study of El Metate shield volcano (Michoacán, Mexico) confirms its monogenetic nature and young age (~1250 CE)



Ahmed Nasser Mahgoub^{a,*}, Harald Böhnell^a, Claus Siebe^b, Magdalena Oryaëlle Chevrel^c

^a Centro de Geociencias, Universidad Nacional Autónoma de México (UNAM), Blvd. Juriquilla No. 3001, Querétaro 76230, Mexico

^b Departamento de Vulcanología, Instituto de Geofísica, Universidad Nacional Autónoma de México, Coyoacán, C.P. 04510 Ciudad de México, Mexico

^c Laboratoire Magmas et Volcans, Université Blaise Pascal CNRS, 6 av. Blaise Pascal, 63178 Aubière, France

ARTICLE INFO

Article history:

Received 5 December 2016

Received in revised form 10 February 2017

Accepted 26 February 2017

Available online 1 March 2017

Keywords:

Paleomagnetism

El Metate

Michoacán-Guanajuato Volcanic Field

Holocene secular variation

Paleointensity

Paleomagnetic dating

Monogenetic volcano

ABSTRACT

In a recent study, Chevrel et al. (2016a, b) radiocarbon-dated the oldest lava flow of the voluminous (~9.2 km³) El Metate shield volcano (Michoacán, Mexico) at cal 1250–1260 CE and proposed that its eruption was monogenetic in origin, with twelve younger lava flows emplaced during a short period of only ~35 years, but certainly <275 years. In order to test this hypothesis, we undertook a detailed paleomagnetic study of five lava flows from El Metate to check the consistency of their paleomagnetic directions. Additionally, a group of representative specimens was treated with the double-heating Thellier experiment using the IZZI protocol for paleointensity determination. Flow mean paleomagnetic directions obtained for four of the flows are indistinguishable, and discordant directions were obtained from the site of the 5th flow measured, probably due to the tilting of the sampled block after remanence acquisition. Mean paleodirections and intensities were used for paleomagnetic dating applying the global paleosecular variation model SHA.DIF.14k. The resulting age range for the eruption is 1150–1290 CE, which overlaps with the range previously determined by the ¹⁴C method by Chevrel et al. (2016a). Accepting the ¹⁴C age of the oldest flow as the maximum age, the age range would be reduced to 1250–1290 CE, which strongly supports the hypothesis of a monogenetic nature of the El Metate eruption.

© 2017 Elsevier B.V. All rights reserved.

1. Introduction and geological background

El Metate is a shield volcano located in the southern sector of the Michoacán-Guanajuato Volcanic Field (MGVF) and only 14 km NNE of the city of Uruapan in Michoacán, Mexico (Fig. 1). The MGVF forms the western-central section of the Trans-Mexican Volcanic Belt (TMVB), a continental arc that crosses Mexico in an east-west direction between 19° and 21° of northern latitude. The TMVB consists of monogenetic fields, stratovolcanoes, and volcanic plateaus whose distribution is controlled by regional tectonics (e.g. Thorpe, 1977; Ferrari et al., 2012; Johnson and Harrison, 1989; Suter et al., 1999). Its origin is related to the subduction of the Rivera and Cocos plates underneath the North America plate (Pardo and Suárez, 1995). The MGVF contains the largest concentration of monogenetic volcanoes within the TMVB and probably also within a subduction-related volcanic arc in the entire world (Hasenaka and Carmichael, 1985b; Valentine and Connor, 2015). It encloses >1000 monogenetic cinder cones, ~400 medium-sized shields and domes, ~100 isolated viscous flows and lava domes, 22 rare phreatomagmatic structures, and two strato-volcanoes (Hasenaka and Carmichael, 1985a, 1985b, 1987; Hasenaka et al., 1994). The impact of

its two historic monogenetic eruptions of Paricutin (1943–1952) and Jorullo (1759–1774) on human settlements is well documented (Fries, 1953; Luhr and Simkin, 1993; Guilbaud et al., 2011; Rasoazanamparany et al., 2016).

Morphologically, El Metate is characterized by a small roughly symmetrical central dome, which is surrounded by a broad shield of well-preserved young lava flows (Siebe et al., 2014; Chevrel et al., 2016a). It has a basal diameter of ~10 km and a height of ~600 m. Chevrel et al. (2016a, 2016b) proposed that El Metate is composed of thirteen flow units (in stratigraphic order from MT1 to MT13; Fig. 1) and has a total dense rock equivalent volume of 9.2 km³.

The first radiocarbon age thought to date El Metate was provided by Hasenaka and Carmichael (1985a) and yielded a conventional date of 4700 ± 200 yr BP. At the same location, Chevrel et al. (2016a) dated the same paleosol and obtained a younger age of 3775 ± 50 yr BP. Through additional field work and with the aid of chemical analyses of the dated ash layer, Chevrel et al. (2016a) discovered that this fallout layer did not stem from El Metate but from the nearby Hoya Urutzen scoria cone. Subsequently, they obtained two new radiocarbon dates on different paleosol samples below the oldest El Metate flow (at site MT1 and 500 m to its east, see Fig. 1), which yielded a combined calibrated age of cal 1250–1260 CE as defined by the overlap at the 95% probability level. They proposed that El Metate was built during one

* Corresponding author.

E-mail address: ahmednasser@geociencias.unam.mx (A.N. Mahgoub).

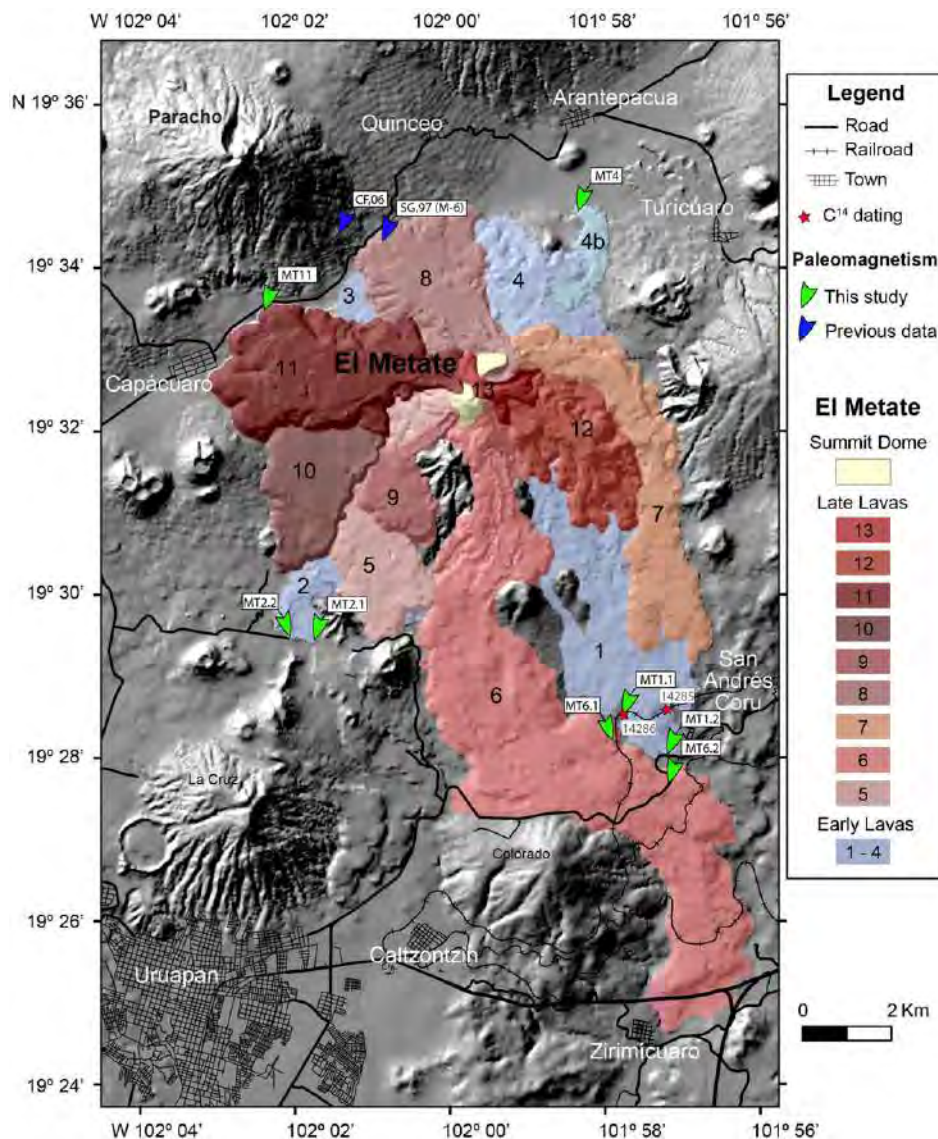


Fig. 1. Digital elevation model of El Metate volcano and surroundings with sampling locations (after Chevrel et al., 2016a, 2016b). Thirteen identified lava flows are indicated in colors according to their stratigraphic position. Blue arrows represent the previous paleomagnetic samples SG, 97 (M-6) of Gonzalez et al. (1997), and CF, 06 of Conte-Fasano et al. (2006). Green arrows indicate sampling points of the present paleomagnetic study. Red stars represent the paleosol location for C^{14} analysis provided in Chevrel et al. (2016a).

single eruption and should hence be considered as monogenetic: all thirteen flow units of El Metate (Fig. 1) were erupted during a short time period of possibly ~35 years based on viscosity-based flow velocity estimates, and certainly not longer than 275 years based on historic considerations (the eruption must have ended well before 1530 CE when the Spaniards arrived in this area since the eruption is not mentioned in their chronicles). Unfortunately, no datable material (e.g. paleosol) could be found underneath the stratigraphically youngest lava flows to constrain the duration of the eruption.

The Holocene paleomagnetic secular variation (PSV) database has grown over the recent periods and been used to develop geomagnetic field models like CALS3k.4 (Korte and Constable, 2011), ARCH3k (Korte et al., 2009), and SHA.DIF.14k (Pavón-Carrasco et al., 2014). For such models, data obtained from both heated archeological artifacts and volcanic products certainly are preferred because of their fidelity. During the Holocene, numerous monogenetic eruptions occurred in the MGVF (Hasenaka and Carmichael, 1985a, 1985b; Guilbaud et al., 2012; Siebe et al., 2014; Kshirsagar et al., 2015, 2016; Chevrel et al., 2016a, 2016b) potentially providing a prime source for contributing to the Mexican Holocene PSV database. The last review of PSV data was

published by Böhnel and Molina-Garza (2002), but according to recent, yet unpublished C^{14} ages (Siebe, personal information) many of the ages cited in that work are too old, sometimes by several thousands of years. Additionally, sometimes the paleomagnetic data cited there could not be reproduced and thus may be affected by sampling errors, e.g. by selecting unsuitable sites where rocks were moved after cooling or sampling a site that corresponds to a different, undated volcano. Paleointensity data, in particular those obtained several decades ago, might also be unreliable because of the less developed experimental methods used then. We are preparing an update of the PSV data base for Mexico, and in the present work we mention these problems, because they also affected previously published paleomagnetic data for El Metate. During their early attempts in defining the PSV for Mexico, Gonzalez et al. (1997) and Conte-Fasano et al. (2006) conducted paleomagnetic studies on El Metate using the now known to be incorrect age of Hasenaka and Carmichael (1985a, 1985b). Their sampling locations are plotted in Fig. 1, but we note here that the reported coordinates lack precision (reported with only 0.01° or ≈ 1 km resolution). Accordingly, the site of Conte-Fasano et al. (2006) (site CF, 06) plots outside of the area occupied by El Metate lava flows, and site SG, 97 sampled by

Gonzalez et al. (1997) seems to be on top of flow 8, an unlikely location since access to this part is particularly difficult. While both paleomagnetic directions probably correspond to the same El Metate flow (flow 8), as no other lava rocks are exposed within the area around of their reported coordinates, they are discordant between themselves, and also with respect to the directions obtained in this study, obtained from carefully selected sites (Table 1). Altogether this suggests that the paleodirection data published earlier are unreliable, and possibly samples were taken from blocks that were moved after remanence acquisition, which indeed is a serious danger in this blocky lava flow with limited exposures. Only the study of multiple, independent sites as carried out in the present work, may provide reliable paleomagnetic data under such conditions. Gonzalez et al. (1997) also provided a PI of $52.9 \pm 4.2 \mu\text{T}$, based on a number of six samples, which still may be reliable as it would at least not be affected by post-cooling movements (see below).

Because of the problems mentioned above we undertook the present study with the goal of determining reliable paleodirections and paleointensities for El Metate lava flows in order to contribute to the PSV data base for Mexico, but also to obtain a paleomagnetic age and compare this with the radiocarbon age of cal 1250–1260 CE provided by Chevrel et al. (2016a). As these authors only could obtain datable material related to the oldest El Metate lava flow, we will test in this work their hypothesis of the monogenetic origin of El Metate and its important consequences for the evolution of this volcano (Chevrel et al., 2016a, 2016b), by studying five lava flows that cover almost the entire stratigraphic section, from the initial to the final stages of the eruption.

2. Sampling procedures

Our sampling strategy was designed to define whether El Metate's lava flows were emplaced within a relatively short period (<275 years and possibly only about 35 years) as suggested by Chevrel et al. (2016a), or over a longer time span by several discrete eruptions. Accordingly, during several fieldwork campaigns during the last 12 years, samples were collected from the two oldest lava flows (sites MT1.1 and MT 1.2 for flow 1 and MT2.1 and MT2.2 for flow 2), from two stratigraphically intermediate flows (sites MT4 for flow 4b, and MT6.1 and MT6.2 for flow 6), and from flow 11 (site MT11), which corresponds to the third youngest flow (Fig. 1). The two youngest flows were not sampled because of their difficult access and outcrop

conditions. In MT1, MT2, and MT6, two independent sites were sampled at locations as far as possible from each other (Fig. 1). Within each site, 8 to 16 cores were drilled by using a portable gasoline powered drill with a 25 mm diamond barrel. Cores were between ~8 and 15 cm long and oriented using both magnetic and sun compasses in order to check for local magnetic anomalies (such as produced by lightning strikes). The difference between the magnetic and sun compass readings was on average ~3° and did not exceed 6°. Sampling within each site was distributed laterally as far as possible and aimed at covering a well-averaged area of the flow. Care was taken to ensure that sampling was done on unmoved blocks of rock, as far as this could be assessed in the field; only site MT11 was already suspected during the sampling to be tilted, but since this was the best outcrop that we could find at this flow, we nonetheless decided to give it a try (Fig. 2). Most outcrops were large natural or man-made outcrops, where the interior of the flow could be observed over several tens of meters distance and where no major relative movement of block was apparent. No tilt correction was applied, as all lava flows are unaffected by tectonic movements and unfolded.

In total, 95 cores from five different lava flows were collected. In the laboratory each drill core was cut into specimens of 22 mm length providing at least 3 specimens.

3. Rock magnetic properties

Rock magnetic measurements were carried out in samples from each lava flow to define the magneto-mineralogy and thermal stability. Accordingly, on a number of representative specimens, we determined thermomagnetic curves ($T_{\text{max}} = 600 \text{ }^\circ\text{C}$) with a horizontal translation Curie balance in a field of 500 mT, and isothermal remanent magnetization (IRM) acquisition curves.

Thermomagnetic analyses were performed on three cores per lava flow (total 15 samples). Based on the Curie temperatures (T_c) defined by the heating curves, the examined samples were categorized into three main groups (Fig. 3). Thereafter, according to the degree of reversibility between the heating and cooling curves, group 1 was split in two subgroups (1a and 1b, Fig. 3). Samples of group 1a (5 cores) are characterized by a single and high Curie temperature T_c of 530–560 °C with a <10% decrease in magnetization upon cooling to room temperature (Fig. 3a), reflecting the presence of Ti-poor titanomagnetite. All samples of MT11 belong to this group. Group 1b with 3 samples from site MT6 shows a similar behavior (Fig. 3b), but with a stronger decrease of

Table 1

(a) Previous and (b) present paleomagnetic site mean directions for El Metate lava flows: SG, 97 of Gonzalez et al. (1997), and CF, 06 of Conte-Fasano et al. (2006), latitude and longitude of the sampling coordinates; n, number of samples used in the calculation of the site-mean direction; N, total number of samples measured; R, unit vector sum; k, precision parameter; α_{95} , 95% confidence angle; Dec, declination; Inc, inclination. Shaded rows mark rejected sites (see text for details).

Site	Latitude (N)	Longitude (W)	n	N	R	k	α_{95}	Dec	Inc
a) Previous studies									
SG, 97	19.57	102.01	5	5	4.98672	301.1	4.4	82.0	41.5
CF, 06	19.57	102.02	8	11	7.99142	816	1.9	16.1	24.6
b) Present study									
Metate 1									
MT1.1	19°28'27.50"	101°57'39.50"	10	12	9.96522	258.80	3.0	355.6	38.5
MT1.2	19°27'57.13"	101°57'8.51"	6	12	5.96926	162.67	5.3	348.7	32.4
Mean			16	24	15.89517	143.09	3.1	352.9	36.2
Metate 2									
MT2.1	19°29'22.01"	102° 1'40.90"	9	12	8.91676	72.20	6.1	349.6	36.0
MT2.2	19°29'26.15"	102° 1'54.88"	6	8	5.92334	65.22	8.4	346.5	32.3
Mean			15	20	14.80145	70.51	4.6	348.4	34.5
Metate 4									
MT4	19°34'39.20"	101°58'12.12"	10	12	9.95519	200.83	3.4	348.5	38.5
Metate 6									
MT6.1	19°28'6.60"	101°57'46.80"	9	12	8.95700	186.05	3.8	348.4	33.8
Met6.2	19°27'39.24"	101°57'5.40"	9	11	8.76939	34.69	8.9	322.3	60.5
Metate 11									
MT11	19°33'30.61"	102° 2'5.20"	13	16	12.89616	115.56	3.9	323.6	71.7
El Metate mean (all samples)			50	95	49.55676	113.10	1.9	349.9	35.7
El Metate mean (site means)			6	8	5.98896	452.95	3.2	349.5	35.3

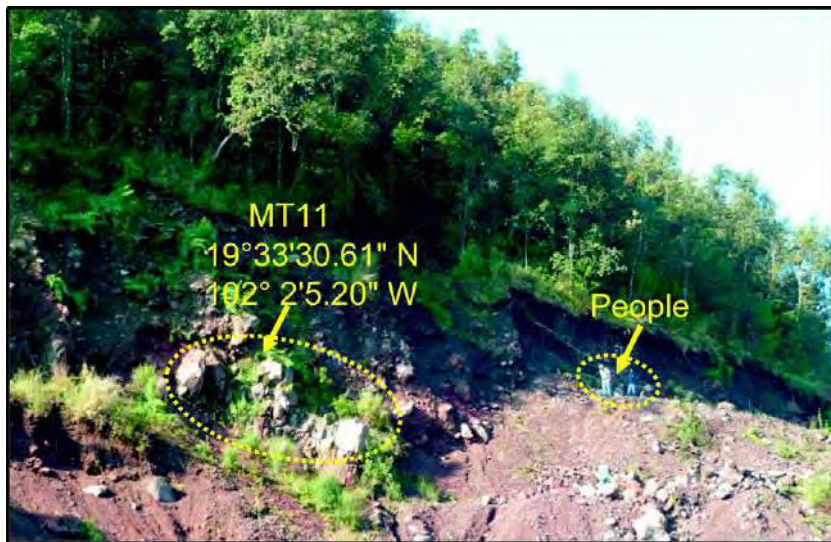


Fig. 2. Photograph of sampling site MT11, which is a small quarry excavated into the steep 150-m-high flow front of El Metate's lava flow 11. This was the only outcrop of this flow displaying large blocks (large dashed circle). Unfortunately, we suspect that all blocks at the flow front were moved after cooling, hence useless for our purposes. People (small dashed circle) for scale. The photo was taken facing south.

magnetization after cooling of 10–30%, suggesting an oxidation of the titanomagnetite minerals during heating. Thermomagnetic curves of group 2 (6 samples) show the presence of two magnetic phases with Curie temperatures around 300–330 °C and 500–540 °C interpreted to be both Ti-rich and Ti-poor titanomagnetite minerals, respectively

(Fig. 3c). The cooling curves match with the heating curves reflecting the stability of these minerals against thermal alteration. The three samples of MT2 belong to this group. Finally, group 3 defined by only one sample of MT1 exhibits a similar heating curve (Fig. 3d), but the cooling curve is characterized by the suppression of the low- T_c component and

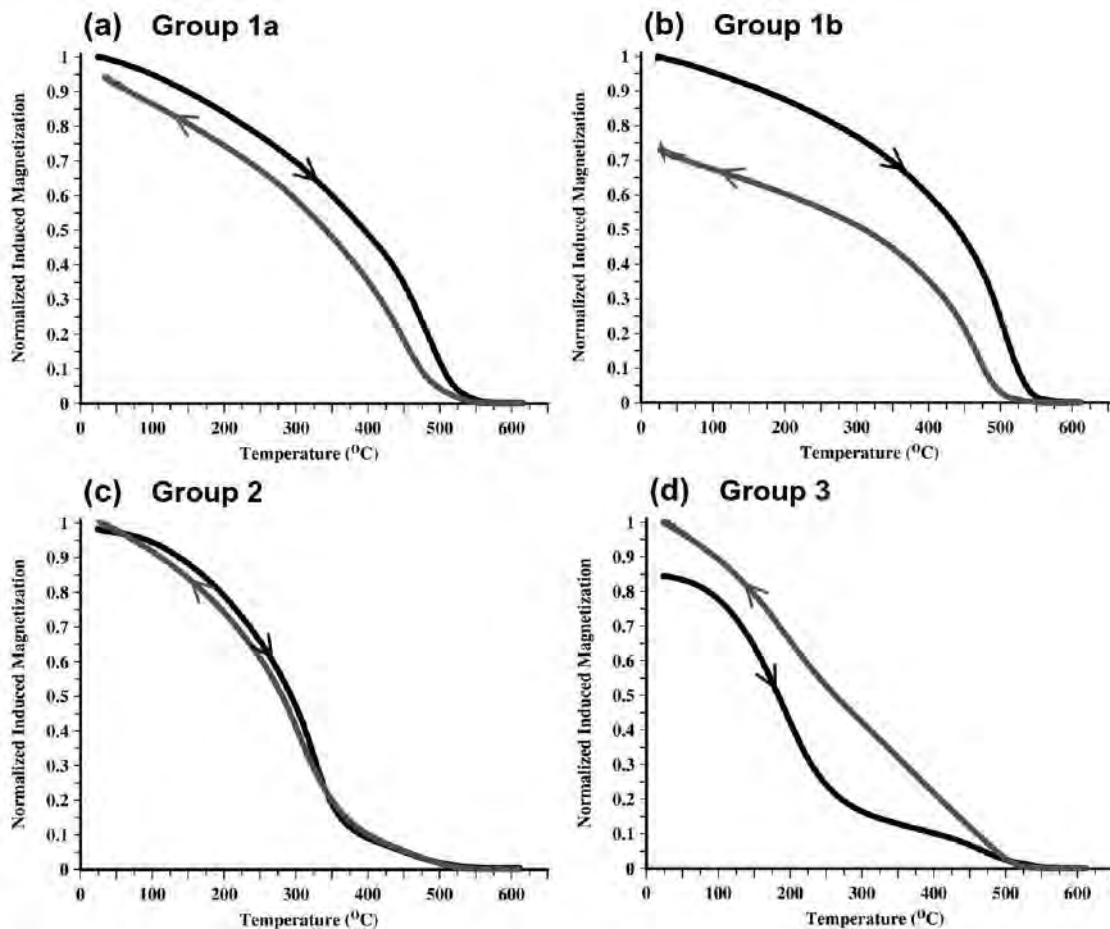


Fig. 3. Variation of high-field induced magnetization with temperature showing three groups of thermomagnetic curves, with group 1 subdivided into two subgroups 1a and 1b. Heating and cooling curves are indicated by arrows and black and grey colors, respectively.

is clearly irreversible with a ~ 15% increase in magnetization after cooling. This was possibly caused by the exsolution of homogeneous low- T_c titanomagnetite phases to a single phase of Ti-poor titanomagnetite.

Progressive acquisition of IRM in an increasing magnetic field (starting at 10 mT and up to 1000 mT) was done on five cores per flow (total 25). On the basis of their IRM curves, investigated samples were divided into three groups (Fig. 4). Group A was observed in samples from MT1 and MT6 and acquire 90% of their maximum IRM in fields of 0.13–0.16 T, revealing the presence of soft magnetic minerals like magnetite or Ti-poor titanomagnetite probably of pseudo-single domain (PSD) and/or multidomain (MD) grain-sizes. Group B was recognized in both MT2 and MT4 where their IRM saturates at ~0.3 T, pointing to the dominance of somewhat higher coercivity (titano-) magnetite minerals of single domain (SD) and/or PSD grain size. MT11 samples belong to group C where IRM reached only 60% of the maximum IRM in fields around 0.2 T and still did not saturate at 0.5 T, thus indicating a contribution of high-coercivity minerals, like SD magnetite or hematite.

4. Paleomagnetic directions

All natural remanent magnetization (NRM) measurements were carried out with an AGICO JR-5 spinner magnetometer (noise level $\sim 5 \times 10^{-6} \text{ Am}^{-1}$). Characteristic remanent magnetization (ChRM) directions were determined by means of stepwise alternating field (AF) demagnetization. For AF demagnetization, an AGICO LDA-3 equipment was used and the samples were demagnetized in 12 steps from 5 to 90 mT. Demagnetization data were analyzed by the program PMGSC 4.2 (Enkin, 2005). From orthogonal vector plots (Fig. 5a, b, c) predominantly univectorial magnetization trends towards the origin of the diagram were observed, sometimes with a small viscous component overprinting the primary one, but this was easily removed at the first steps of AF demagnetization (Fig. 5d, e, f). The median destructive fields (MDFs) for lava flow units 1 and 6 were intermediate (25–30 mT), whereas higher MDFs (40–55 mT) were found in the cooling units 2, 4, and 11. Notably, varying values of MDFs between different cooling units of El Metate reflect their differing magnetic grain sizes. The direction of the ChRM was calculated using principal component analysis (PCA; Kirschvink, 1980). In almost all cases, the ChRM directions for each sample were calculated by 6–10 vector end points and are characterized by maximum angular deviation (MAD) values of $\sim 1.5^\circ$ on average. Site mean directions were calculated using Fisher statistics (Fisher, 1953, using PMag Tools Version 4.2), after testing for outliers at the 95% confidence level, and are presented in Table 1 and Fig. 6. For lava flows 1

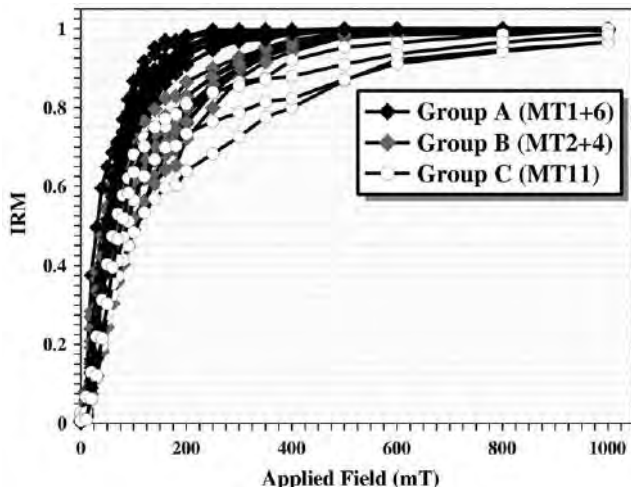


Fig. 4. Normalized IRM acquisition curves for three groups of samples.

and 2, two sites from each were available to calculate the flow mean directions (Table 1 and Fig. 6a and b). In these flows within-site dispersion was relatively high with a confidence angle α_{95} between 6.1 and 8.4° (except for site MT1.1 which has an $\alpha_{95} = 3.0^\circ$). These sites were taken from railroad cuts and the dispersion may be attributed to small and random movement of blocks along the outcrops. However, it is important to note that all used 31 data points of MT1 and MT2 satisfy the Fisher distribution, as checked applying the appropriate test in the PmagTool program. For MT4, ten samples out of 12 yielded a similar site-mean direction with a low dispersion (Table 1 and Fig. 6c). In regard to cooling unit 6 (MT6), the two sites yielded dissimilar results. For MT6.1, we obtained a well defined site-mean direction with an $\alpha_{95} = 3.8^\circ$ (Table 1 and Fig. 6d) that is also consistent with the values obtained on the other flows mentioned above. On the other hand, the site mean direction calculated for MT6.2 displays a steep inclination of $I = 60.5^\circ$ with $\alpha_{95} = 8.9^\circ$ (Table 1; Fig. 6d), which is different from site MT6.1. This inclination is also inconsistent with the paleosecular variation patterns for central Mexico over the past 4000 years. The reason for this different direction could be undetected block movements, and additionally the inferior rock magnetic properties of these samples, producing the large dispersion. Based on the above, we are confident that MT6.1 represents the El Metate flow MT6 mean direction. Finally, the site-mean direction of MT11 is characterized by a small $\alpha_{95} = 3.9^\circ$ (Table 1 and Fig. 6e), with a much steeper inclination of 71.7° than the other sites (24.6° to 41.5°). As already mentioned above, this result corresponds to one big block exposed at the upper part of the front of flow MT11 (see Fig. 2), which we suspected already during fieldwork to have moved after cooling. Under the reasonable assumption that the block slumped approximately towards the north, this would have produced the inclination difference of about 35° . Site MT11 was therefore not used for further interpretations of paleodirections.

The obtained flow mean directions from lava flows MT1, MT2, MT4, and MT6 were used to evaluate their directional independence by means of the F-distribution test (McFadden and Lowes, 1981). This test shows whether two mean directions are significantly different at a chosen confidence level (in this case 95%). If these directions are indistinguishable they recorded the same field and thus probably represent the same instance in time, in particular for the case of the short age range represented by a volcano such as El Metate. The F-test applied to MT1 and MT6 results in a value of 0.103 which is smaller than the F table value (at 95% significance level) of 0.139, which means that it is positive. Also, the F-test applied to all other flow combinations was positive which indicates that the four flow mean directions of El Metate are undistinguishable at the 95% significance level. Accordingly, an overall El Metate paleodirection was calculated for four flows MT1, MT2, MT4, and MT6 using all individual ChRM directions: Dec = 349.9 , Inc = 35.7 , $n = 50$, and $\alpha_{95} = 1.9^\circ$ (Table 1 and Fig. 7a). The mean direction based on six site means is indistinguishable but has a slightly larger confidence angle: Dec = 349.5 , Inc. = 35.3 , $n = 6$, and $\alpha_{95} = 3.2^\circ$ (Table 1 and Fig. 7b).

5. Paleointensities

A total of 52 samples were subjected to the double heating Thellier PI experiments (Thellier and Thellier, 1959) applying the IZZI protocol (Tauxe and Staudigel, 2004). In this protocol the Aitkin in-field/zero-field (Aitken et al., 1988; IZ) and the Coe zero-field/in-field (Coe, 1967; ZI) protocols are applied consecutively, which allows to detect the effect of high temperature pTRM tails (Yu and Tauxe, 2005; Yu et al., 2004). Both pTRM (Coe, 1967) and pTRM-tail checks (Riisager and Riisager, 2001) were used to check for alteration of magnetic minerals. For the experiments we used an ASC Scientific TD48 furnace, with heating steps of 100, 200, 250, 300, 340, 370, 400, 430, 460, 490, 510, 530, 560, and 580 $^\circ\text{C}$. pTRM checks were done at 100, 250, 340, 400, 460, and 510 $^\circ\text{C}$ while pTRM-tail checks at 250, 340, 400, 460, 510, and 560 $^\circ\text{C}$. For 25 cylindrical samples (group 1) the laboratory field of

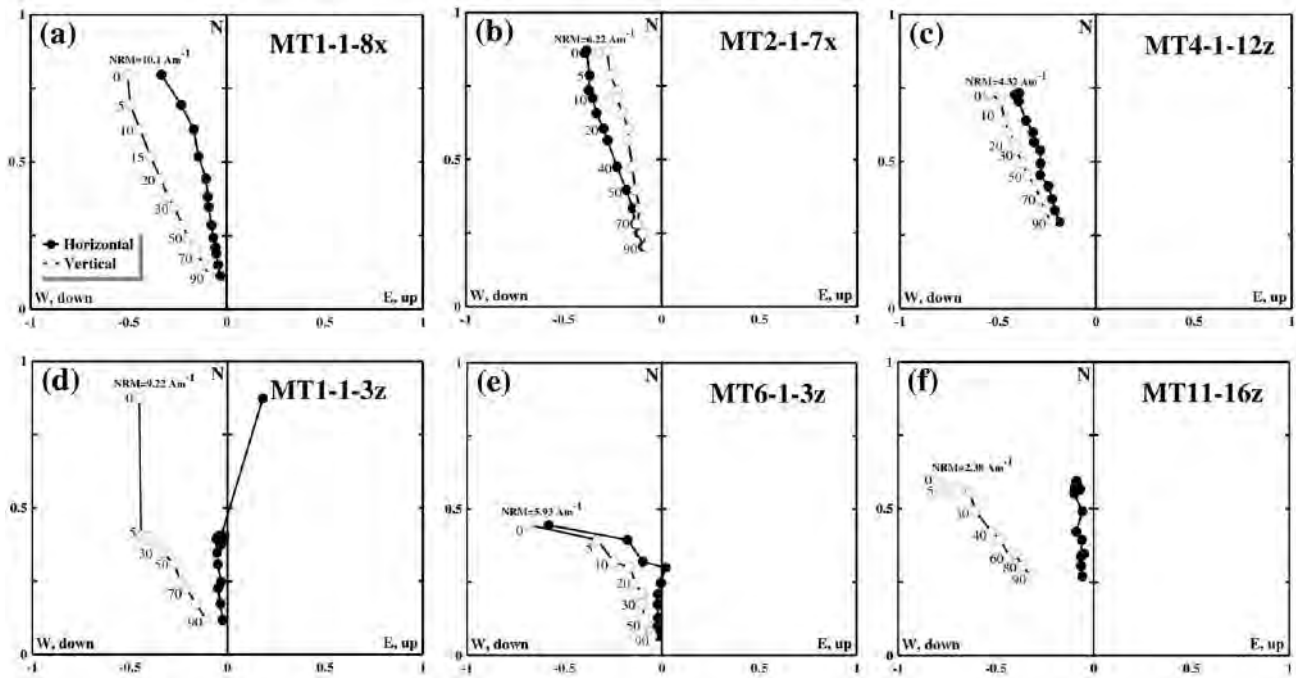


Fig. 5. Orthogonal vector plots of AF demagnetized samples from the five studied lava flows. Labels along curves denote the maximum AF amplitude applied during the demagnetization steps.

60 μT was applied parallel to their z-axis, while for a second group (group 2) of 27 samples their NRM directions were oriented parallel to the applied field (60 μT) with a precision better than 5° . For PI experiments only samples with a single-component NRM were selected.

Data were analyzed with the ThellierTool4.11 software (Leonhardt et al., 2004), and in order to evaluate our PI estimates the acceptance criteria sets A and B as given in the Thellier tool (Leonhardt et al., 2004) and with the modifications of Paterson et al. (2014; TTA and TTB) were used (for more details see <http://www.paleomag.net/SPD/home.html>). Furthermore, at the flow level, at least three specimens should be available to calculate the flow mean intensity with a standard deviation (σ) either $<20\%$ or smaller than 10 μT .

Paleointensity results for each studied flow are listed in Table 2 together with different quality parameters, and representative PI or Arai plots are shown in Fig. 8a. In total, 27 specimens passed the Thellier Tool A or B acceptance criteria resulting in an overall success rate of 52%. We note that the success rate varies for the samples according to

their orientation with respect to the applied field, with $\sim 40\%$ for group 1 (with the applied field parallel to the sample's z-axis) and $\sim 63\%$ for group 2 (with the field direction parallel to the sample's NRM). Predominantly, failure was due to multi-domain effects, which is clearly visible in the Arai plots as 'zigzagging' or 'sagging' (Fig. 8b). In regard to flow MT4, six specimens gave a mean PI of 43.44 ± 14.02 with a standard deviation that is larger than the maximum allowed value of 10 μT and thus this PI estimate was excluded from further discussion. For the remaining flows, three to seven specimens passed the acceptance criteria and their PI were used to calculate the flow mean PI (Table 2), with standard deviations ranging between 8.51 and 4.38 μT .

In order to ascertain whether the mean-PI values for El Metate lava flows are similar, a two-sample Student's *t*-test assuming equal variance and using a pooled estimate of the variance μ was performed. In this test the null hypothesis stating that the two means are equal ($H_0: \mu_1 = \mu_2$) is checked against the alternative hypothesis that the two means are different ($H_a: \mu_1 \neq \mu_2$). Our analyses confirm the null hypothesis, since

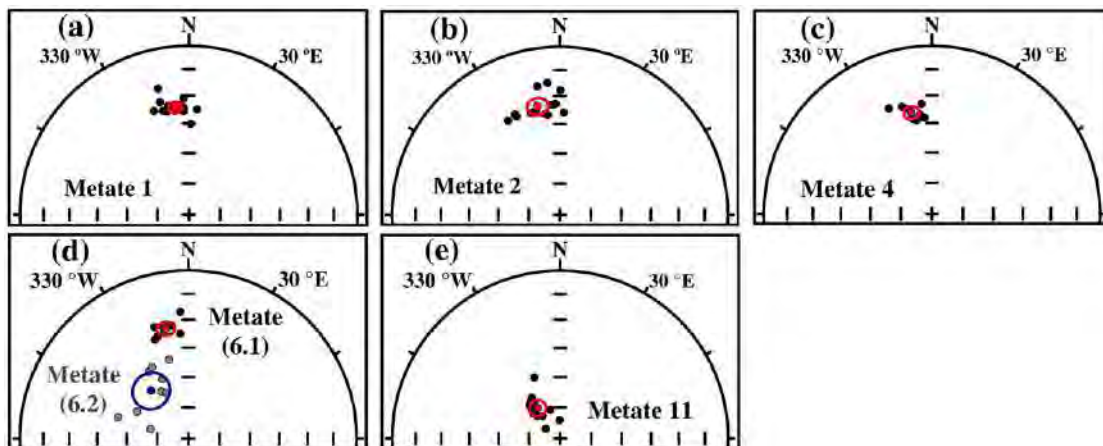


Fig. 6. Characteristic remanent magnetization directions for the five lava flows. Flow mean directions are shown by larger red dots and their 95% confidence angles. Metate site 6.2 directions are distinguished from site 6.1 by grey colour and its mean by blue colour (for more information see text).

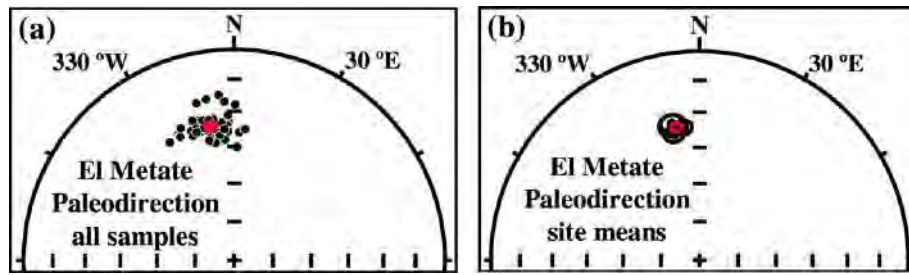


Fig. 7. (a) Overall mean direction for El Metate based on all individual samples, shown by the red dot and red 95% confidence angle. (b) Site mean directions of four El Metate lava flows with 95% confidence angles and the resulting mean direction shown in red colour.

the *t*-value of 0.377 is less than the 95% confidence level of 2.228, when comparing MT1 with MT11. Similarly, comparing MT1 with MT2 and MT1 with MT6 provides comparable *t*-test results, showing that these flow mean PI are concordant as well. Thus, 21 accepted PI data from flows MT1, MT2, MT6, and MT11 were used to calculate an overall mean paleointensity of $55.58 \pm 6.64 \mu\text{T}$ (Table 2) for El Metate volcano.

6. Paleomagnetic dating

Using the full vector paleomagnetic result for El Metate, we applied the paleomagnetic dating method to this volcano by means of the

Matlab tool *archaeo_dating* (Pavón-Carrasco et al., 2011). The global field model SHA.DIF.14k (Pavón-Carrasco et al., 2014) was used to accomplish this task. Recently, this model was successfully applied on two lava flows from Ceboruco volcano in western Mexico (Böhnel et al., 2016), which is of a similar age as El Metate. As input data for the paleomagnetic dating, we may use the overall mean of the six accepted site mean directions (Table 1). These directions are characterized by variable sample numbers and dispersion, as reflected by precision parameters *k* with values between 65.22 and 258.80. To avoid a bias of the overall mean direction by data of lower precision, a weighting of these site mean directions would be necessary, which is not commonly done. Therefore, we used the overall mean based on the listed site mean

Table 2

The Thellier–IZZI paleointensity results and associated statistics: Field direction, arb/par, arbitrary along z-axis, parallel to the sample NRM; N, number of points included in the linear best-fit; *f*, fraction of the NRM used for best-fit; *g*, the gab factor; *q*, quality factor; MAD_{anc}, anchored maximum angular deviation; α , angular difference between anchored and non-anchored best solution; δCK , relative check error; δpal , cumulative check difference; δTR , tail check; δt^* , normalized tail of pTRM; PI, paleointensity; σ (μT), standard deviation.

Sample	Field direction	N	T (°C)	f	g	q	MAD _{anc}	α	δCK	δpal	δTR	δt^*	Class	PI	σ (μT)
Metate 1 (MT1)															
2b	arb	6	0–340	0.82	0.74	6.31	3.14	1.89	5.37	10.85	5.92	6.26	B	53.04	5.23
3z	par	12	200–560	0.47	0.87	6.89	4.25	14.7	3.51	1.41	1.89	1.75	A	48.58	2.86
4b	par	6	0–340	0.72	0.75	24.4	2.30	2.32	3.41	2.98	5.21	7.54	A	51.00	1.13
5z	par	6	100–370	0.62	0.67	26.8	2.22	2.98	6.28	6.67	3.23	4.25	A	50.88	0.79
6b	par	12	0–510	0.72	0.88	23.3	2.91	6.21	8.87	3.54	3.91	2.54	B	63.11	1.72
7b	par	13	0–530	0.86	0.85	13.0	5.09	6.91	8.57	4.21	3.12	1.54	B	50.42	2.83
10z	arb	6	0–340	0.76	0.77	7.30	2.00	1.65	2.63	1.16	7.04	4.62	A	58.10	4.64
Mean														53.59	5.17
Metate 2 (MT2)															
2z	arb	12	0–510	0.81	0.80	11.0	3.22	2.87	3.60	9.10	2.08	3.97	A	68.50	4.05
7z	par	13	0–530	0.40	0.75	2.62	2.57	10.8	4.99	5.97	7.96	4.43	B	58.44	6.45
12a	par	9	0–430	0.47	0.77	4.90	2.73	7.55	1.80	3.07	1.43	1.90	B	54.98	4.12
Mean														60.64	7.02
Metate 4 (MT4)															
4a	par	10	0–460	0.44	0.87	4.51	3.62	8.74	3.85	11.7	4.82	3.62	B	32.59	2.79
6z	arb	9	0–430	0.40	0.79	2.71	3.31	9.06	6.52	0.94	0.67	13.8	B	41.81	4.81
7z	arb	9	0–430	0.48	0.83	4.84	3.72	8.80	2.68	2.37	4.44	5.51	B	31.93	2.62
10a	par	12	0–510	0.55	0.82	5.30	2.05	3.37	2.25	2.68	2.18	2.87	A	54.99	4.70
11z	arb	7	0–370	0.47	0.78	5.30	3.60	6.13	3.65	5.45	3.14	2.46	A	33.56	2.30
12z	arb	12	0–510	0.69	0.79	8.71	1.73	1.71	2.02	5.73	3.29	1.41	A	65.78	4.13
Mean														43.44	14.02
Metate 6 (MT6)															
1a	par	12	0–510	0.71	0.78	7.77	1.59	0.31	3.45	1.48	3.24	4.41	A	68.53	4.88
3a	arb	6	100–370	0.42	0.77	3.43	5.0	6.84	8.21	9.14	4.02	5.31	B	42.37	4.00
7b	par	12	0–510	0.79	0.86	10.7	4.89	6.97	6.92	0.66	7.78	1.26	A	50.53	3.20
8z	arb	8	0–400	0.40	0.75	2.36	1.93	4.50	5.96	11.75	3.0	0.30	B	60.50	7.70
9a	par	6	0–340	0.42	0.77	3.73	2.52	0.92	5.05	0.36	2.57	5.60	B	61.85	5.41
10z	par	13	100–560	0.88	0.82	11.2	2.11	1.86	4.91	3.21	4.53	1.56	A	53.20	3.41
Mean														56.16	8.51
Metate 11 (MT11)															
2b	par	14	0–560	0.37	0.87	4.22	1.65	2.67	6.35	4.24	4.38	6.07	B	61.39	4.36
5z	par	10	300–560	0.41	0.76	7.35	1.98	3.0	3.87	7.59	2.10	3.97	B	56.23	2.41
7z	Arb	12	200–560	0.91	0.83	28.2	3.74	2.92	4.83	6.13	3.14	2.39	A	53.53	1.42
14b	par	9	100–460	0.55	0.75	10.6	5.04	14.5	6.09	6.05	2.99	1.56	A	51.79	2.04
16b	par	14	0–560	0.82	0.91	41.3	5.89	7.26	4.76	5.42	1.39	0.26	A	50.23	0.91
Mean														54.63	4.38

El Metate Paleointensity: PI = 55.58; σ = 6.64; n = 21.

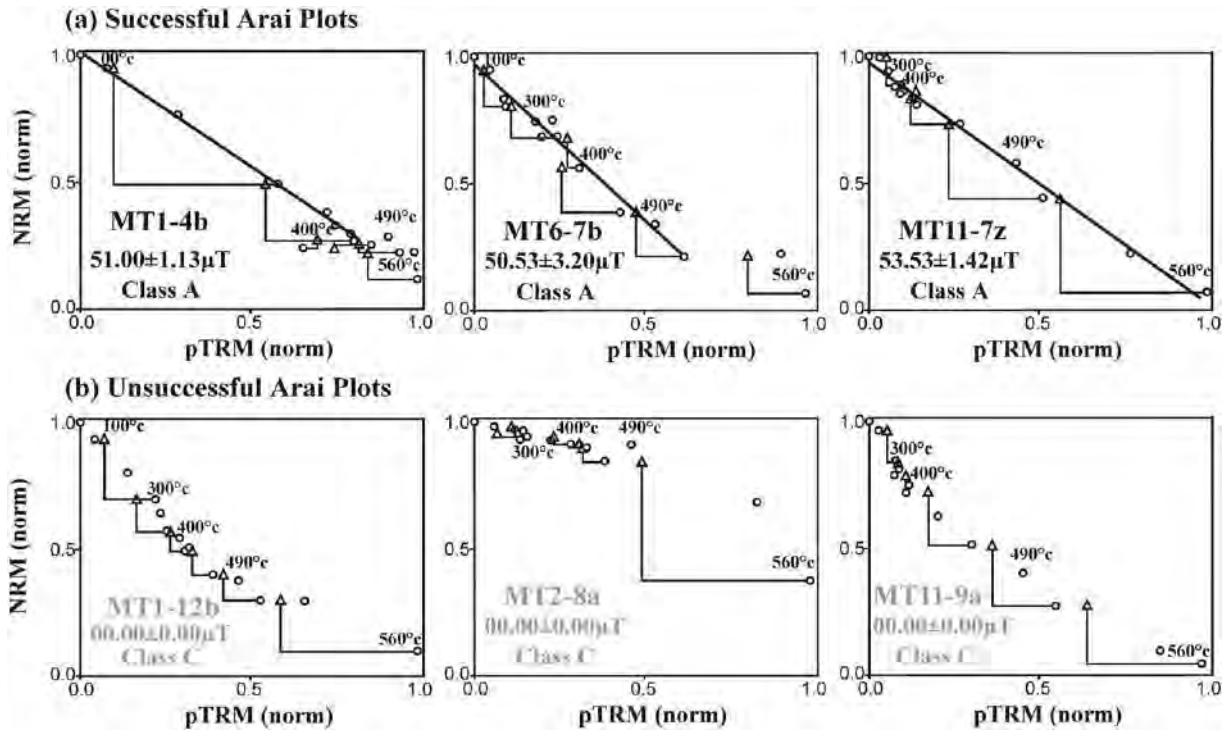


Fig. 8. IZZI-Thellier results. (a) Three examples of typical IZZI-Thellier results passing the two defined sets of selection criteria: A and B class. (b) Three examples of rejected IZZI-Thellier results which accordingly affiliated to C class. NRM and pTRM are normalized. NRM vs. pTRM data are shown as circles, with the black best-fit lines. pTRM checks are shown as triangles. Some temperature steps also indicated. The analyses were done using TellierTool.

directions. On the other hand, we have shown above that all site mean directions are indistinguishable, suggesting a very similar age. We therefore will use the overall mean direction calculated from 52 ChRM directions from all accepted sites as our main choice for dating.

As the oldest El Metate lava flow MT1 has a maximum radiocarbon age of about cal 1150 CE (see [Chevrel et al., 2016a](#)) and could not be

younger than the arrival of the Spaniards around 1550 CE, we restricted the time interval to this period 1150–1550 CE. This provides a well constrained paleomagnetic age range of 1150–1290 CE ([Fig. 9](#)), which coincides well with the calibrated radiocarbon age. Using the paleodirection based on the site mean directions, this age range would only increase by nine years to 1150–1299 CE.

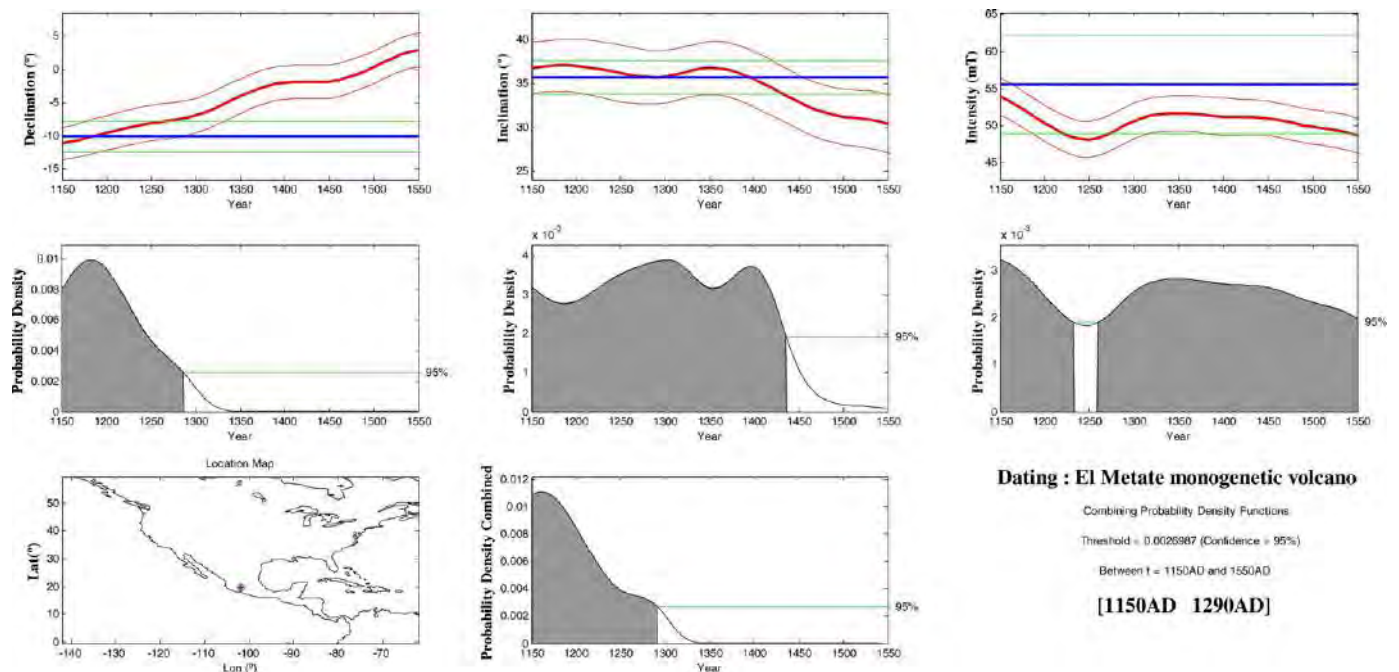


Fig. 9. Paleomagnetic dating of El Metate monogenetic shield volcano. Red curves show the variation in time of the components of the paleomagnetic field as determined from the SHA.DIF.14k model, and blue horizontal lines are the components of the full vector direction determined for El Metate volcano; all curves and lines are shown with their respective 95% confidence intervals. The combined probability density derived from the declination, inclination, and paleointensity data is shown as shaded peaks and the minimum 95% confidence level by horizontal green lines.

Dating : El Metate monogenetic volcano

Combining Probability Density Functions:
 Threshold = 0.0026987 (Confidence = 95%)
 Between t = 1150AD and 1550AD
[1150AD 1290AD]

7. Discussion: are the El Metate lava flows the result of one single or several independent eruptions?

Rock magnetic properties obtained from thermomagnetic analyses and IRM acquisition curves revealed differences between the five lava flows of El Metate shield volcano pointing to variations in the composition and size of magnetic particles in these flows. Such variations are to be expected, since El Metate erupted two compositionally different types of magma (Chevrel et al., 2016b). This magma variability together with different cooling histories of the sampling sites of the El Metate flows, as well as their sampling at certainly different levels within these flows may explain the variations in magnetic mineralogy and grain sizes.

Our study covered the entire stratigraphy of lava flows accessible in the field (MT1 to MT11), and wherever possible, two or more independent sites were sampled in order to check the within-flow paleomagnetic consistency (e.g. Hagstrum and Champion, 1994; Speranza et al., 2006; Böhnell et al., 2016). Good quality site mean directions were obtained from the eight studied sites, but MT6.2 and MT11 had to be rejected because their mean direction differed strongly from other sites of the same flow. The remaining paleodirections from flows MT1, MT2, MT4, and MT6 are very consistent and indistinguishable at the 95% confidence level, allowing to combine all ChRM directions into one overall mean direction. This direction is interpreted to represent the geomagnetic field during the buildup of El Metate volcano, and the indistinguishable directions of the different flows suggest that they were all erupted during a short time period of probably <50–100 years, as otherwise the secular variation would have resulted in the acquisition of significantly different directions (for typical secular variation changes during the last 21 centuries, see for example Bucur, 1994).

Concordant and reliable IZZI-Thellier results were obtained from four out of five lava flows, and the success rate at the sample level was 52% and thus relatively high. Our PI results support the suggestion of Paterson et al. (2015) and De Groot et al. (2016) that choosing a small angle between the applied field direction and the sample NRM during paleointensity experiments reduces the multi-domain effect and thus enhances the technical quality of the PI results. This is clearly shown by our samples, with a success rate of 63% for the group where the field was parallel to the NRM direction vs. 40% for the group with a random angular orientation.

The concordant paleodirections and paleointensities of the studied lava flows indicate that they were emplaced during a period of <50–100 years, which thus supports the monogenetic origin of El Metate shield volcano as proposed by Chevrel et al. (2016a, 2016b). It must be noted however that the paleomagnetic dating method can inherently not determine a shorter emplacement period than 100–200 years for El Metate, due to the uncertainty of the used field model SHA.DIF.14k and the uncertainty of the paleomagnetic results. Even so, the youngest possible age defined by the arrival of the Spanish conquerors to the El Metate area in 1530 CE can be excluded by the paleomagnetic age range of 1150–1290 CE. This range overlaps entirely the ¹⁴C age range as defined by its error limits. If we use the age proposed by Chevrel et al. (2016a) as the most probable for flow MT1 (cal 1250–1260 CE) as a limit for the paleomagnetic age range, only a short period of 40 years would remain for the emplacement of the younger lava flows. This is in very good agreement with the eruption time of about 35 years proposed by Chevrel et al. (2016a), based on a total emitted lava volume of 10.8 km³ and a continuous extrusion rate of 10 m³/s.

Our results are derived from a completely independent dating method, which also applies to the previous undated younger El Metate flows. They strongly support the hypothesis of Chevrel et al. (2016a, 2016b) that this huge volcano indeed is not a common shield or composite volcano with a prolonged eruption history. For the consequences of such a short eruption time representing in terms of magma composition and evolution, eruption style, and magma viscosity, we refer to their original publications.

8. Conclusions

The present study supports that El Metate is the youngest (cal 1250–1260 CE) monogenetic shield volcano of the Michoacán–Guanajuato Volcanic Field, and with a total volume of ~9.2 km³ the most voluminous Holocene eruption in Mexico and the most voluminous andesitic effusive eruption worldwide so far reported as proposed by Chevrel et al. (2016a, 2016b). Five of thirteen lava flows from this shield volcano were studied by rock-magnetic, paleomagnetic, and paleointensity methods in order to test its monogenetic origin, as only the oldest flow could be ¹⁴C dated. Flow-mean paleomagnetic directions obtained from four flows (MT1, MT2, MT4, and MT6) are indistinguishable, and the only discordant mean direction available for site MT11 is certainly due to block movement after remanence acquisition. Similar problems were also found in a few sites from other flows. Such discordant results show that it is mandatory to ensure that the sampled lava blocks are in place, and if possible to core multiple sites along each of the lava flows, especially when these are of such great thickness and extremely blocky in nature as it is the case of El Metate. Flow mean directions are indistinguishable at the 95% confidence level and suggest that these flows were emplaced in a time span of probably <50–100 years, which is further supported by concordant flow-mean paleointensity values obtained from four flows. Paleomagnetic dating of El Metate volcano indicates an age range between 1150–1290 CE (95% probability level) and thus confirms its ¹⁴C age of 1250–1260 CE. Using this most probable ¹⁴C age as a limit for the paleomagnetic dating, this restricts the duration of the eruption to only 40 years, ending much before the first arrival of the Spanish conquerors around 1530 CE. Thus we conclude that the paleomagnetic data are fully compatible with a monogenetic origin of El Metate volcano. Interestingly, if small scoria cone eruptions are known to have important repercussions (e.g. Paricutin), much more voluminous shield volcanoes such as El Metate should have an even larger impact on the local population and environment, possibly triggering human migrations (Chevrel et al., 2016a). Unfortunately, El Metate's impact is still difficult to evaluate in the absence of written sources from archeological sites (Pereira et al., 2013).

Acknowledgments

Ing. J. Escalante supported studies with the Curie balance and Ing. Emilio Nava the maintenance of the computers and network in the laboratory. Field and laboratory costs of A.N.M. and H.B. were covered by Consejo Nacional de Ciencia y Tecnología funds (CONACyT-180032) and those of O.C. and C.S. were defrayed from projects CONACyT-167231 and the Dirección General de Asuntos del Personal Académico (DGAPA, UNAM IN-101915) granted to C. Siebe. We thank Américo González-Esparza, Adriana Briseño, and Ernesto Andrade at UNAM Campus Morelia for providing lodging facilities at the Mexican Array Radio Telescope (MEXART) near Coeneo during field campaigns.

References

- Aitken, M.J., Allsop, A.L., Bussell, G.D., Winter, M.B., 1988. Determination of the intensity of the Earth's magnetic field during archaeological times—reliability of the Thellier technique. *Rev. Geophys.* 26, 3–12.
- Böhnell, H., Molina-Garza, R., 2002. Secular variation in Mexico during the last 40,000 years. *Phys. Earth Planet. Inter.* 133 (1), 99–109.
- Böhnell, H., Pavón-Carrasco, F.J., Sieron, K., Mahgoub, A.N., 2016. Palaeomagnetic dating of two recent lava flows from Ceboruco volcano, western Mexico. *Geophys. J. Int.* 207 (2), 1203–1215.
- Bucur, I., 1994. The direction of the terrestrial magnetic field in France during the last 21 centuries. *Phys. Earth Planet. Inter.* 87, 95–109.
- Chevrel, M.O., Siebe, C., Guilbaud, M.N., Salinas, S., 2016a. The 1250 CE El Metate shield (Michoacán): Mexico's most voluminous Holocene eruption and its significance for archaeology and hazards. *The Holocene* 26 (3):471–488. <http://dx.doi.org/10.1177/0959683615609757>.
- Chevrel, M.O., Guilbaud, M.N., Siebe, C., 2016b. The AD 1250 effusive eruption of El Metate shield volcano (Michoacán, Mexico): magma source, crustal storage, eruptive dynamics, and lava rheology. *Bull. Volcanol.* 78 (4):32. <http://dx.doi.org/10.1007/s00445-016-1020-9>.

- Coe, R.S., 1967. Paleo-intensities of the Earth's magnetic field determined from Tertiary and Quaternary rocks. *J. Geophys. Res.* 72 (12), 3247–3262.
- Conte-Fasano, G., Urrutia-Fucugauchi, J., Goguitchaichvili, A., Morales-Contreras, J., 2006. Low-latitude paleosecular variation and the time-averaged field during the late Pliocene and Quaternary—paleomagnetic study of the Michoacán-Guanajuato volcanic field, Central Mexico. *Earth Planets Space* 58 (10), 1359–1371.
- Enkin, R., 2005. PMGSC 4.2, Geological Survey of Canada, Sidney, British Columbia, Canada.
- Ferrari, L., Orozco-Esquivel, T., Manea, V., Manea, M., 2012. The dynamic history of the Trans-Mexican Volcanic Belt and the Mexico subduction zone. *Tectonophysics* 522, 122–149.
- Fisher, R.A., 1953. Dispersion on a sphere. *Proc. R. Soc. Lond. A* 127, 205–305.
- Fries, C., 1953. Volumes and weights of pyroclastic material, lava and water erupted by Parícutin Volcano, Michoacán, Mexico. *Trans. Am. Geophys. Union* 34, 603–616.
- Gonzalez, S., Sherwood, G., Böhnell, H., Schnepf, E., 1997. Paleosecular variation in Central Mexico over last 30,000 years: the record from lavas. *Geophys. J. Int.* 130, 201–219.
- de Groot, L.V., Pimentel, A., Di Chiara, A., 2016. The multimethod palaeointensity approach applied to volcanics from Terceira: full-vector geomagnetic data for the past 50 kyr. *Geophys. J. Int.* 206 (1), 590–604.
- Guilbaud, M.N., Siebe, C., Layer, P., Salinas, S., Castro-Govea, R., Garduño-Monroy, V.H., Le Corvec, N., 2011. Geology, geochronology, and tectonic setting of the Jorullo Volcano region, Michoacán, México. *J. Volcanol. Geotherm. Res.* 201:97–112. <http://dx.doi.org/10.1016/j.jvolgeores.2010.09.005>.
- Guilbaud, M.N., Siebe, C., Layer, P., Salinas, S., 2012. Reconstruction of the volcanic history of the Tacámbaro-Puruarán area (Michoacán, México) reveals high frequency of Holocene monogenetic eruptions. *Bull. Volcanol.* 74, 1187–1211.
- Hagstrum, J.T., Champion, D.E., 1994. Paleomagnetic correlation of Late Quaternary lava flows in the lower east rift zone of Kilauea Volcano, Hawaii. *J. Geophys. Res.* 99, 21679–21690.
- Hasenaka, T., Carmichael, I.S.E., 1985a. The cinder cones of Michoacán-Guanajuato, central Mexico: their age, volume and distribution, and magma discharge rate. *J. Volcanol. Geotherm. Res.* 25, 105–124.
- Hasenaka, T., Carmichael, I.S.E., 1985b. Compilation of location, size, and geomorphological parameters of volcanoes of the Michoacán-Guanajuato volcanic field, central Mexico. *Geophys. Int.* 24 (4), 577–607.
- Hasenaka, T., Carmichael, I.S.E., 1987. The cinder cones of Michoacán-Guanajuato, central Mexico: petrology and chemistry. *J. Petrol.* 28, 241–269.
- Hasenaka, T., Ban, M., Delgado-Granados, H., 1994. Contrasting volcanism in the Michoacán-Guanajuato volcanic field, central Mexico: shield volcanoes vs. cinder cones. *Geophys. Int.* 33 (1), 125–138.
- Johnson, C.A., Harrison, C.G.A., 1989. Tectonics and volcanism in central Mexico: a Landsat thematic mapper perspective. *Remote Sens. Environ.* 28, 273–286.
- Kirschvink, J.L., 1980. The least-squares line and plane and analysis of palaeomagnetic data. *Geophys. J. R. Astron. Soc.* 62, 699–718.
- Korte, M., Constable, C., 2011. Improving geomagnetic field reconstructions for 0–3 ka. *Phys. Earth Planet. Inter.* 188 (3), 247–259.
- Korte, M., Donadini, F., Constable, C.G., 2009. Geomagnetic field for 0–3 ka: 2. A new series of time-varying global models. *Geochim. Geophys. Geosyst.* 10.
- Kshirsagar, P., Siebe, C., Guilbaud, M.N., Salinas, S., Layer, P., 2015. Late Pleistocene Alberca de Guadalupe maar volcano (Zacapu basin, Michoacán): stratigraphy, tectonic setting, and paleo-hydrogeological environment. *J. Volcanol. Geotherm. Res.* 304: 214–236. <http://dx.doi.org/10.1016/j.jvolgeores.2015.09.003>.
- Kshirsagar, P., Siebe, C., Guilbaud, M.N., Salinas, S., 2016. Geological and environmental controls on the change of eruptive style (phreatomagmatic to Strombolian-effusive) of Late Pleistocene El Caracol tuff cone and its comparison with adjacent volcanoes around the Zacapu basin (Michoacán, México). *J. Volcanol. Geotherm. Res.* 318: 114–133. <http://dx.doi.org/10.1016/j.jvolgeores.2016.03.015>.
- Leonhardt, R., Heunemann, C., Krása, D., 2004. Analyzing absolute paleointensity determinations: acceptance criteria and the software ThellierTool4.0. *Geochim. Geophys. Geosyst.* 5 (12).
- Luhr, J.F., Simkin, T., 1993. Parícutin. The Volcano Born in a Mexican Cornfield. Geoscience Press, Phoenix, Arizona 427 p.
- McFadden, P.L., Lowes, F.J., 1981. The discrimination of mean directions drawn from Fisher distributions. *Geophys. J. R. Astron. Soc.* 67, 19–33.
- Pardo, M., Suárez, G., 1995. Shape of the subducted Rivera and Cocos plates in southern Mexico: seismic and tectonic implications. *J. Geophys. Res.* 100 (12), 12,357–12,373.
- Paterson, G.A., Tauxe, L., Biggin, A.J., Shaar, R., Jonestrask, L.C., 2014. On improving the selection of Thellier-type paleointensity data. *Geochim. Geophys. Geosyst.* 15, 1180–1192.
- Paterson, G.A., Biggin, A.J., Hodgson, E., Hill, M.J., 2015. Thellier-type paleointensity data from multidomain specimens. *Phys. Earth Planet. Inter.* 245:117–133. <http://dx.doi.org/10.1016/j.pepi.2015.06.003>.
- Pavón-Carrasco, F.J., Rodríguez-González, J., Ossete, M.L., Torta, J.M., 2011. A Matlab tool for archaeomagnetic dating. *J. Archaeol. Sci.* 38, 408–419.
- Pavón-Carrasco, F.J., Ossete, M.L., Torta, J.M., De Santis, A., 2014. A geomagnetic field model for the Holocene based on archaeomagnetic and lava flow data. *Earth Planet. Sci. Lett.* 388, 98–109.
- Pereira, G., Michelet, D., Migeon, G., 2013. La migración de los purépecha hacia el norte y su regreso a los lagos. *Arqueol. Mex.* 21 (123), 55–60.
- Rasoazanampanary, C., Widom, E., Siebe, C., Guilbaud, M.N., Spicuzza, M.J., Valley, J.W., Valdez, G., Salinas, S., 2016. Temporal and compositional evolution of Jorullo volcano, Mexico: implications for magmatic processes associated with a monogenetic eruption. *Chem. Geol.* 434:62–80. <http://dx.doi.org/10.1016/j.chemgeo.2016.04.004>.
- Risager, P., Risager, J., 2001. Detecting multidomain magnetic grains in Thellier paleointensity experiments. *Phys. Earth Planet. Inter.* 125 (1), 111–117.
- Siebe, C., Guilbaud, M.N., Salinas, S., Kshirsagar, P., Chevrel, M.O., De la Fuente, J.R., Hernández-Jiménez, A., Godínez, L., 2014. Monogenetic volcanism of the Michoacán-Guanajuato Volcanic Field: Maar craters of the Zacapu basin and domes, shields, and scoria cones of the Tarascan highlands (Paracho-Parícutin region). *Field Guide, Pre-meeting Fieldtrip for the 5th International Maar Conference (5IMC-IAVCEI)*, Querétaro, 13–17 November, México 33 p.
- Speranza, F., Branca, S., Coltelli, M., D'Ajello Caracciolo, F., Vigliotti, L., 2006. How accurate is "paleomagnetic dating"? New evidence from historical lavas from Mount Etna. *J. Geophys. Res.* Solid Earth 111 (B12). <http://dx.doi.org/10.1029/2006JB004496>.
- Suter, M., Contreras, J., Gómez-Tuena, A., Siebe, C., Quintero-Legorreta, O., García-Palomero, A., Macías, J.L., Alaniz-Álvarez, S.A., Nieto-Samaniego, A.F., Ferrari, L., 1999. Effect of strain rate in the distribution of monogenetic and polygenetic volcanism in the Transmexican volcanic belt: comments and reply. *Geology* 27 (6), 571–575 [http://dx.doi.org/10.1130/0091-7613\(1999\)027<0571:EOSRIT>2.3.CO;2](http://dx.doi.org/10.1130/0091-7613(1999)027<0571:EOSRIT>2.3.CO;2).
- Tauxe, L., Staudigel, H., 2004. Strength of the geomagnetic field in the Cretaceous Normal Superchron: new data from submarine basaltic glass of the Troodos Ophiolite. *Geochim. Geophys. Geosyst.* 5, Q02H06.
- Thellier, E., Thellier, O., 1959. Sur l'intensité du champ magnétique terrestre dans le passé historique et géologique. *Ann. Geophys.* 15, 285–378.
- Thorpe, R.S., 1977. Tectonic significance of alkaline volcanism in eastern Mexico. *Tectonophysics* 40 (3–4), T19–T26.
- Valentine, G.A., Connor, C.B., 2015. Basaltic volcanic fields. In: Sigurdsson, H., Houghton, B.F., McNutt, S.R., Rymer, H., Stix, J. (Eds.), *Encyclopedia of Volcanoes*, second ed. Academic Press, London, pp. 423–439.
- Yu, Y., Tauxe, L., 2005. Testing the IZZI protocol of geomagnetic field intensity determination. *Geochim. Geophys. Geosyst.* 6 (5):Q05H17. <http://dx.doi.org/10.1029/2004GC000840>.
- Yu, Y., Tauxe, L., Genevey, A., 2004. Toward an optimal geomagnetic field intensity determination technique. *Geochim. Geophys. Geosyst.* 5 (2):Q02H07. <http://dx.doi.org/10.1029/2003GC000630>.

3. Paleomagnetically inferred ages of a cluster of Holocene monogenetic eruptions in the Tacámbaro-Puruarán area (Michoacán, México): Implications for volcanic hazards

Ahmed Nasser Mahgoub^{a*}, Harald Böhnel^a, Claus Siebe^b, Sergio Salinas^c, Marie-Noëlle Guilbaud^b

^a Centro de Geociencias, Universidad Nacional Autónoma de México (UNAM), Blvd. Juriquilla No. 3001, Querétaro C.P. 76230, Mexico

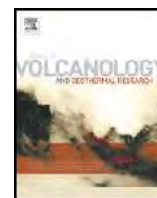
^b Departamento de Vulcanología, Instituto de Geofísica, Universidad Nacional Autónoma de México, Coyoacán, C.P. 04510 Ciudad de Mexico, Mexico

^c Facultad de Ingeniería, División de Ciencias de la Tierra, Universidad Nacional Autónoma de México, Mexico

Accepted: Journal of Volcanology and Geothermal Research, 347:360-370 (2017).

Individual contributions of the authors:

- i. **Ahmed Nasser Mahgoub:** conception of the study, field work, sampling, laboratory measurements, analyzing and interpreting of data, writing the article.
- ii. **Harald Böhnel:** design the research study, fieldwork, participating in the interpretation of data and revising the article, financing for the project.
- iii. **Claus Siebe:** design the research study, fieldwork, participating in the interpretation of data and revising the article, financing for the project.
- iv. **Sergio Salinas:** designing the geological map, fieldwork, revising the article.
 - i. **Marie-Noëlle Guilbaud:** providing the chemical analyses, revising the article.



Paleomagnetically inferred ages of a cluster of Holocene monogenetic eruptions in the Tacámbaro-Puruarán area (Michoacán, México): Implications for volcanic hazards

Ahmed Nasser Mahgoub ^{a,*}, Harald Böhnel ^a, Claus Siebe ^b, Sergio Salinas ^c, Marie-Noëlle Guilbaud ^b

^a Centro de Geociencias, Universidad Nacional Autónoma de México (UNAM), Blvd. Juriquilla No. 3001, Querétaro C.P. 76230, Mexico

^b Departamento de Vulcanología, Instituto de Geofísica, Universidad Nacional Autónoma de México, Coyoacán, C.P. 04510 Ciudad de México, Mexico

^c Facultad de Ingeniería, División de Ciencias de la Tierra, Universidad Nacional Autónoma de México, Mexico

ARTICLE INFO

Article history:

Received 11 July 2017

Received in revised form 2 October 2017

Accepted 8 October 2017

Available online 10 October 2017

Keywords:

Paleomagnetic dating

Monogenetic cluster

Holocene

Lava flows

Michoacán

México

ABSTRACT

The paleomagnetic dating procedure was applied to a cluster of four partly overlapping monogenetic Holocene volcanoes and associated lava flows, namely La Tinaja, La Palma, Mesa La Muerta, and Malpaís de Cutzaróndiro, located in the Tacámbaro-Puruarán area, at the southeastern margin of the Michoacán-Guanajuato volcanic field. For this purpose, 21 sites distributed as far apart as possible from each other were sampled to obtain a well-averaged mean paleomagnetic direction for each single lava flow. For intensity determinations, double-heating Thellier experiments using the IZZI protocol were conducted on 55 selected samples. La Tinaja is the oldest of these flows and was dated by the ¹⁴C method at $\sim 5115 \pm 130$ years BP (cal 4184–3655 BCE). It is stratigraphically underneath the other three flows with Malpaís de Cutzaróndiro lava flow being the youngest. The paleomagnetic dating procedure was applied using the Matlab archaeo-dating tool in couple with the geomagnetic field model SHA.DIF.14k. Accordingly, for La Tinaja several possible age ranges were obtained, of which the range 3650–3480 BCE is closest to the ¹⁴C age. Paleomagnetic dating on La Palma produced a unique age range of 3220–2880 BCE. Two ages ranges of 2240–2070 BCE and 760–630 BCE were obtained for Mesa La Muerta and a well-constrained age of 420–320 BCE for Malpaís de Cutzaróndiro. Although systematic archaeological excavations have so far not been carried out in this area, it is possible that the younger eruptions were contemporary to local human occupation. Our paleomagnetic dates indicate that all four eruptions, although closely clustered in space, occurred separately in time with varying recurrence intervals ranging between ~ 300 and ~ 2300 years. This finding should be considered when constraining the nature of the magmatic plumbing system and developing a strategy aimed at reducing risk in the volcanically active Michoacán-Guanajuato volcanic field, where several young monogenetic volcano clusters have been identified recently. These enigmatic small “flare-ups” (outbursts of small pods of magma in geologically short periods of time within a small area) have also been encountered in other subduction-related volcanic fields around the globe (e.g. Cascades arc in the western U.S.A.) and still require to be investigated by geophysical and petrological means in order to understand their origin.

© 2017 Elsevier B.V. All rights reserved.

1. Introduction

Several thousand Miocene to Quaternary volcanoes form the Trans-Mexican Volcanic Belt (TMVB), which is an E-W trending subduction-related continental arc stretching across central Mexico (e.g. Ferrari et al., 2012). Within the western-central segment of the TMVB is the Michoacán-Guanajuato Volcanic Field (MGVF) with an area of $\sim 40,000$ km² (Fig. 1). This field contains the largest concentration of young monogenetic volcanoes within the TMVB and possibly also in the world (Hasenaka and Carmichael, 1985a, 1985b; Valentine

and Connor, 2015; Kshirsagar et al., 2016). During the Late Pleistocene and Holocene dozens of volcanic eruptions have occurred in the MGVF (e.g. Guilbaud et al., 2012; Kshirsagar et al., 2015, 2016). Of these, several impacted human populations (Chevrel et al., 2016a, 2016b; Mahgoub et al., 2017a), including the historic eruptions of Jorullo (1759–1774 CE; Guilbaud et al., 2011; Rasoazanamparany et al., 2016) and Parícutin (1943–1952 CE; Luhr and Simkin, 1993; Pioli et al., 2008). This makes research topics aimed at assessing future volcanic hazards in such a highly active region mandatory (e.g. Guilbaud et al., 2012). Foremost among the open questions is the one regarding the age of the different eruptions and their recurrence time interval. Although radiocarbon dating (¹⁴C) has proven to be the most reliable method and been widely used to date late Quaternary (<40,000 years

* Corresponding author.

E-mail address: ahmednasser@geociencias.unam.mx (A.N. Mahgoub).

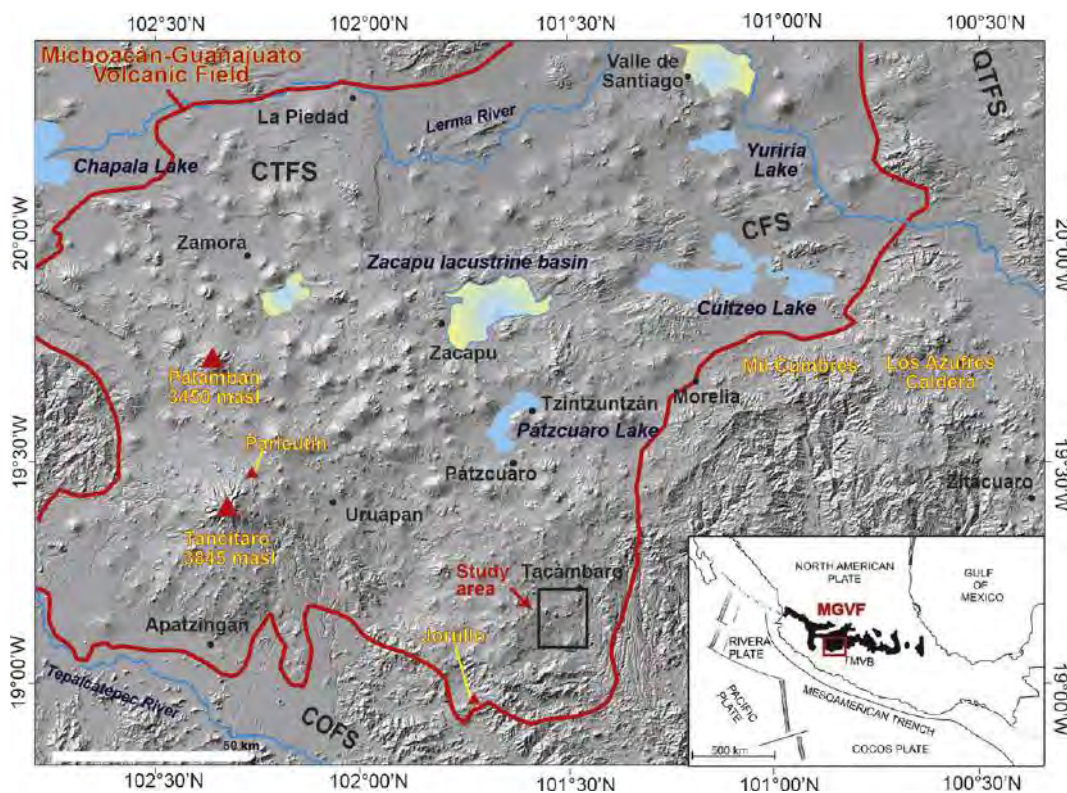


Fig. 1. Digital elevation model of the Michoacán-Guanajuato Volcanic Field (MGVF) showing the location of the Zacapu basin and the study area (black rectangle denotes area covered in Fig. 2). Major fault systems are: CFS = Cuitzeo fault system, CTFS = Chapala-Tula fault system, COFS = Chapala-Oaxaca fault system, QTFS = Querétaro-Taxco fault system. Inset map at lower right corner shows location of the MGVF within the TMVB (modified after Kshirsagar et al., 2015).

BP) volcanic products and archaeological contexts, it cannot be always applied, especially when datable organic material is absent or cannot be found. In order to overcome these difficulties, other methods (e.g. thermal luminescence dating, $^{40}\text{Ar}/^{39}\text{Ar}$, etc.) have been developed (Walker, 2013). Recently, a new method by paleomagnetic means has emerged as an alternative dating technique. Simply, in this method the Earth's magnetic field (EMF) elements (declination, inclination, and intensity) registered locally by a suitable material (e.g. lava rock or archaeological pottery) of unknown age are compared with secular variation curves for the same geographical region (e.g. Korte and Constable, 2003, 2005, 2011; Pavón-Carrasco et al., 2009, 2014). The validity of the age data obtained by this method substantially depends on several factors, including the credibility of the given age of the input data upon which the model has been constrained and the approach being followed by the EMF fluctuations in space and time. Since EMF elements (declination, inclination, intensity) behave in a cyclic pattern, the method frequently provides several possible age ranges for a single eruptive volcanic material (e.g. lava). It should be noted that a common shortcoming of all these paleomagnetic curve models arises from the uneven distribution of the global paleomagnetic secular variation (PSV) data points, especially because most of the data have been sourced from localities in the northern hemisphere, particularly from Europe. Furthermore, while the EMF directions are fairly easy to determine, measuring its paleointensity proves to be frequently difficult because required conditions in the analyzed natural rock sample are not always encountered.

In the present study, four Holocene vents that emitted lava flows and form a small cluster were sampled for the purpose of paleomagnetic dating. As will be discussed in more detail below, Guilbaud et al. (2012) radiocarbon-dated the La Tinaja scoria cone and associated lava flows (Fig. 2), which is stratigraphically below the other flows. Therefore La Tinaja's ^{14}C age represents the maximum possible age for all of the studied lava flows.

2. Geological background

The 690 km² Tacámbaro-Puruarán study area is located at the southeastern margin of the MGVF and ~40 km northeast of the historic Jorullo volcano (Fig. 1). Guilbaud et al. (2012) investigated Late Tertiary to Quaternary volcanism in this area, produced a geologic map based on multiple $^{40}\text{Ar}/^{39}\text{Ar}$ dates, estimated erupted volumes, and also reported radiocarbon ages for several Holocene monogenetic volcanoes. Based on field relations and satellite image analysis, these authors concluded that La Tinaja scoria cone and associated lava field is at the center of a small cluster of four Holocene monogenetic volcanoes that in chronological order also includes La Palma, Mesa La Muerta, and Malpaís de Cutzaróndiro (Fig. 2). The latter are stratigraphically younger than La Tinaja scoria cone, which was dated at 5115 ± 130 years BP (cal 4184–3655 BCE).

The present study was primarily aimed at dating the three younger lava flows. Fieldwork aided by digital elevation model-based morphological observations and geochronological data were integrated to construct a geological map (Fig. 2), which shows the partly overlapping small-volume Holocene lava flows that emanated from different vents at different times (hence, can be individually considered monogenetic) and are underlain by Pleistocene volcanic units. All of these young flows are quite thick (tens of meters) and display surface textures that range from rubbly 'aa' to blocky (as defined by Kilburn, 2000), which are typical for viscous coulées with steep marginal fronts. Furthermore, they are only sparsely covered by an incipient soil that sustains a forest (mostly oak). In strong contrast, the forest in areas adjacent to the lavas has been cleared for agricultural purposes. Today, these surfaces are occupied by avocado orchards and sugar-cane plantations, which grow well on these more developed fertile volcanic soils. The four eruption vents are roughly aligned in a NE-SW direction, suggesting the existence of an inferred fault zone that controlled the final ascent of magmas along dikes. Such a NE-SW alignment of vents is also

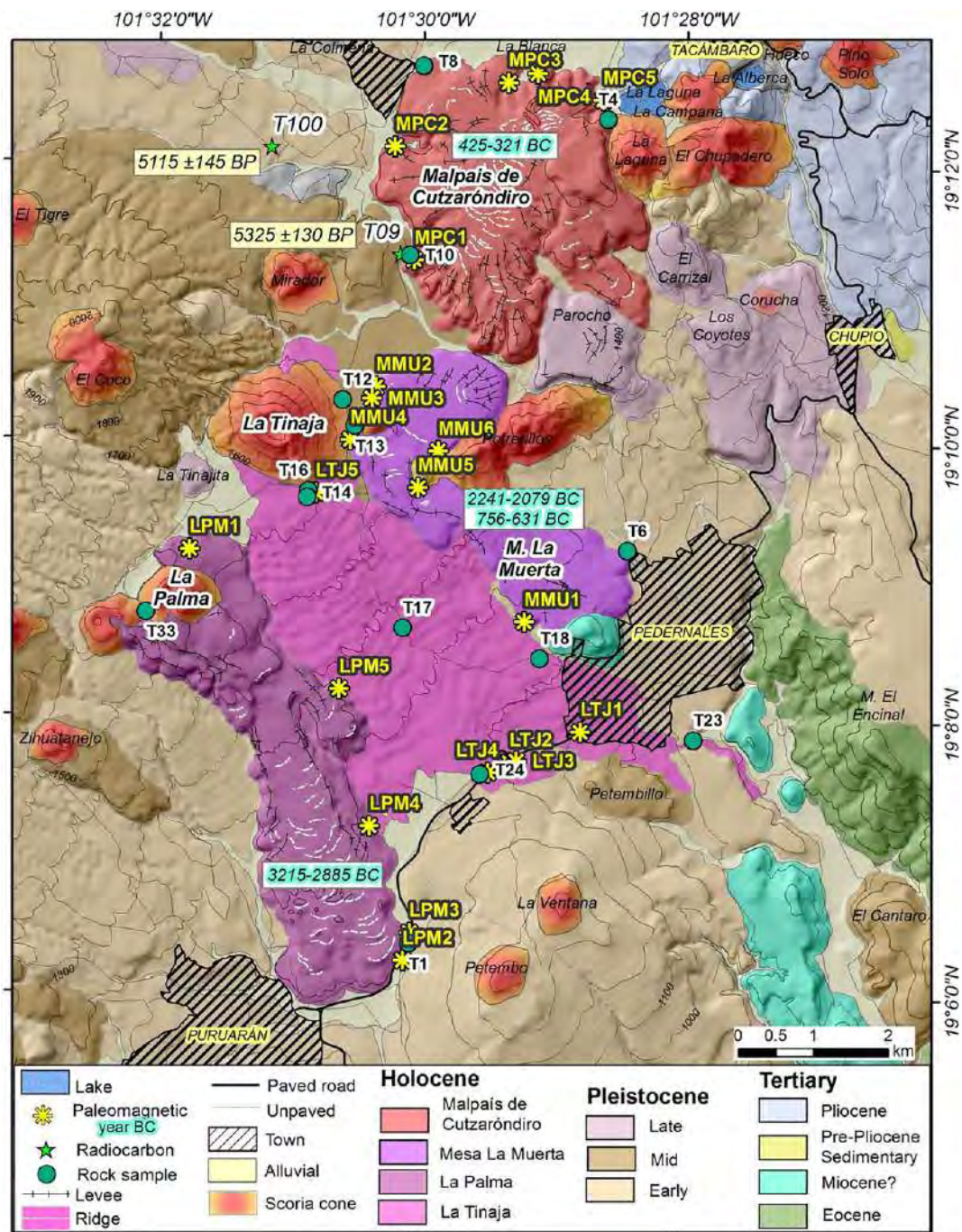


Fig. 2. Geological map showing Holocene monogenetic volcanoes near Tacámbaro (Michoacán), as well as the location of different sampling sites.

observable in the Jorullo area further to the south (Guilbaud et al., 2011), as well as in other regions of the MGVF (Kshirsagar et al., 2016), suggesting a tectonic control of regional dimensions (e.g. Johnson and Harrison, 1990; Guilbaud et al., 2012).

The oldest of the four Holocene flows, La Tinaja, was issued from a small (~397 m high, above surrounding ground) scoria cone (Fig. 3a). Its olivine-bearing basaltic andesite ($\text{SiO}_2 = 54.1\text{--}58.3$ wt%) compound lavas are ~30 m thick, reach as far as ~8 km to the SE of the cone, and cover a minimum surface of 14.7 km² with a volume estimated at 0.44 km³ (dimensions and modal mineralogical analyses of all the different lava flows are listed in Table 1). Mineralogically, La Tinaja lavas are composed of forsteritic olivine and plagioclase phenocrysts in a glassy matrix with microlites of the same crystal phases plus minor augite. Two paleosol samples directly underlying deposits of coarse-ash to

fine-lapilli fallout layers from the La Tinaja scoria cone (locations T09 and T100 indicated in Fig. 2; for more details see Guilbaud et al., 2012) were dated by the conventional radiocarbon method at 5325 ± 130 and 5115 ± 130 years BP, respectively. Since both samples stem from the paleosol, the younger age should be closer to the eruption date. This date (5115 ± 130 years BP) was calibrated to calendar years by applying the Stuiver and Reimer (1993) procedure and with the help of the CALIB computer program (version 7.1, IntCal13 calibration curve), which yielded a 95% probability range (2 sigma) of cal 4184–3655 BCE. These are the only radiocarbon samples that could be found during the course of several field campaigns and their dating turned out to be crucial for carrying out with confidence the paleomagnetic dating of the remaining younger lava flows (see below).

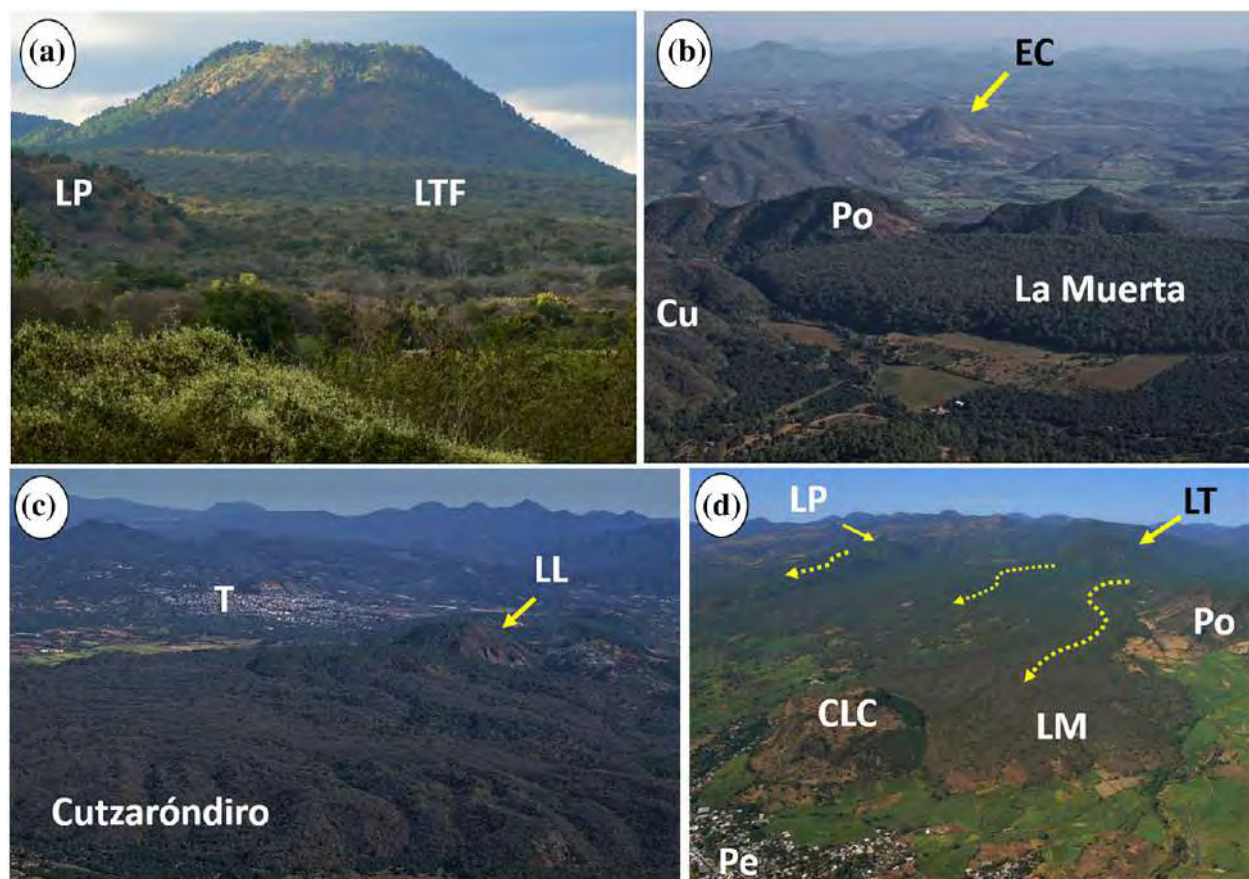


Fig. 3. A. View from the SSE showing La Tinaja scoria cone (dated at ca. 5200 years BP) and its lava flows (LTF) overlain by the younger La Palma lava flow (LP). B. Aerial view of Mesa La Muerta lava flow from the NW. The younger Malpaís de Cutzaróndiro lava flow (Cu) and older Cerro Potrerillos (Po) are also shown. El Cántaro volcano (EC) near the town of Turícuaro is in the background. C. Aerial view from the SW of Malpaís de Cutzaróndiro lava flow. Older Cerro La Laguna scoria cone (LL) and the small city of Tacámbaro (T) are also shown. D. Aerial view of the study area from the SE showing La Palma (LP), La Tinaja (LT), and La Muerta (LM) lava flows (dotted-line arrows). Older volcanic rock-formations Potrerillos (Po) and Cerro La Cruz (CLC), as well as the town of Pedernales (Pe) are also visible. Aerial photos taken Dec. 14, 2008 by Claus Siebe.

To the SW of the La Tinaja cone and stratigraphically above is the smaller La Palma cone (283 m high) and associated lava flow. This flow is much thicker (~60 m) with steep margins attesting to a high

viscosity during emplacement. It covers an area of 8.6 km² with a volume of ~0.5 km³ and is andesitic in composition (SiO₂ = 58.7–61.2 wt%). Observation under the polarizing microscope revealed

Table 1

Dimensions (area, thickness, aspect ratio, volume) and mineralogical modal composition of La Tinaja, La Palma, Mesa La Muerta, and Malpaís de Cutzaróndiro lava flows.

Dimensions of lava fields				Sample	Modal analysis												
Area (km ²)	T (m)	Aspect ratio:T/A	V (km ³)		Pheno ^a					Micropheno and microlites ^a					Matrix ^a	Vesicles	Crystal content
					wt% ^b	Oliv	Plag	Cpx	Opx	Plag	Cpx	Opx	Oliv	Ox			
La Tinaja				T12 T17	54.1	3.3	5.2	0.0	0.0	30.3	0.1	0.0	2.6	0.0	58.5	13.9	41.5
14.7	30	0.002	0.44		58.3	0.8	1.5	0.0	0.5	41.2	0.0	9.8	0.2	0.0	46.0	13.0	54.0
La Palma				T01 T33	58.7	0.8	0.0	0.0	0.0	21.7	0.0	0.0	0.0	4.0	73.4	5.7	26.6
8.6	60	0.007	0.52		61.2	1.2	0.0	0.5	1.9	18.2	0.0	0.2	0.0	3.1	74.9	14.9	25.1
Mesa La Muerta				T06 T13	59.5	0.6	0.0	0.0	0.0	19.0	0.0	0.0	0.0	4.0	76.3	7.4	23.7
5.8	57	0.010	0.33		60.3	0.6	0.0	0.1	0.0	11.1	0.0	0.0	0.0	2.0	86.1	4.0	13.9
Malpaís de Cutzaróndiro				T04 T08	60.9	0.0	0.0	0.0	1.6	12.6	0.0	2.0	0.0	1.1	82.7	11.6	17.3
9.3	80	0.009	0.74		59.9	0.0	0.0	0.4	1.3	6.4	0.0	0.0	0.0	7.8	84.0	8.1	16.0

Area, Thickness (T) and Volume (V) from Guilbaud et al. (2012). Errors are: T = 5 m, A = 3%, V = 0.01–0.02 km³.

Total counts = 1000 (except 500 for T33).

Pheno = phenocrysts > 100 μm; Micropheno = microphenocrysts: 50–100 μm; microlites < 50 μm.

Plag = plagioclase, Oliv = olivine, Cpx = clinopyroxene, Opx = orthopyroxene, Ox: Fe-Ti oxides (granular to square crystals in groundmass).

^a vol% dense.

^b wt%, normalized to a total of 100% (Guilbaud et al. in prep).

olivine, augite, and hypersthene phenocrysts in a glassy matrix with abundant feldspar microlites and opaque oxides. The least voluminous (0.33 km^3 covering an area of 5.8 km^2) of the eruptions corresponds to Mesa La Muerta (Fig. 3b) whose ~57-m-thick lava flows with steep margins was probably issued from a small fissure and did neither form a cone nor a small dome. Mesa La Muerta lavas are also silicic andesites ($\text{SiO}_2 = 59.5\text{--}60.3 \text{ wt}\%$) and cover the northeastern portion of the La Tinaja lavas. Petrographically, they are quite aphyric and characterized by very few olivine and augite phenocrysts in a glassy matrix with feldspar microlites and opaque oxides.

Finally, Malpaís de Cutzaróndiro is not only the youngest, but also the thickest (~80 m) of the studied lava flows. As in the case of Mesa La Muerta, its vent is also covered by lava and difficult to discern, attesting to the purely effusive nature of its eruption, whose silicic lavas must have degassed to a large degree in the upper crust before reaching the surface. It covers an area of 9.3 km^2 with a volume of $\sim 0.74 \text{ km}^3$. As its name implies (*malpaís* means badland in Spanish), its surface is rough and blocky (Fig. 3c). Its andesitic composition ($\text{SiO}_2 = 59.9\text{--}60.9 \text{ wt}\%$) is similar to La Palma and Mesa La Muerta, and its lavas are also quite aphyric with few augite and hypersthene phenocrysts in a glassy matrix with feldspar microlites and opaque oxides.

From the above stratigraphic relations and compositional characteristics, it becomes clear that at least two different magma sources were tapped. La Tinaja erupted first in a gas-rich Strombolian fashion producing a 397 m-high cone and associated ash-fallout blanket, followed by the emission of olivine-bearing basaltic andesite lava flows. After a period of quiescence, La Palma erupted forming first a small cone and then a thick viscous aphyric andesite lava flow. Then, after another period of quiescence, Mesa La Muerta and Malpaís de Cutzaróndiro followed in sequence, both in an entirely effusive style, producing thick andesite flows, whose composition (aphyric andesite) is very similar to La Palma.

3. Paleomagnetic sampling and methodology

Paleomagnetic cores were collected from 21 sites (Fig. 2; latitudes and longitudes for all sites are listed in Supplementary Table S1) distributed as far apart as possible from each other to ensure gathering a well-averaged mean paleomagnetic direction for each lava flow (e.g. Speranza et al., 2006; Böhnell et al., 2016). At each site, 7–18 cores (12 in average) with a diameter of 25 mm and lengths ranging between 6 and 15 cm were recovered with a portable gasoline-powered drill. In situ orientation was determined by both, a magnetic and sun compass, and an inclinometer.

Few road cuts expose the interior of flows and thus most samples (15 sites) were taken from natural outcrops (Fig. 2). Absence of significant soil cover facilitated detecting in situ blocks for drilling. In the case of Malpaís de Cutzaróndiro (MPC), located in the northeast (Fig. 2), the blocky surface of the lava flow talus had been removed at several places by recent quarrying activities, and hence all samples could be taken from the massive interior of the lava flow. Five sites (MPC1–MPC5) were sampled roughly at the same level within the flow and thus should have a similar cooling history and rock magnetic properties. Six different sites were sampled at Mesa La Muerta (MMU) flow, which is characterized by a denser vegetation cover. These sites are distributed all over Mesa La Muerta flow and cores were obtained from different levels within the lava flow. MMU1, MMU2, MMU3, and MMU6 are from the middle part of the flow, while MMU4 and MMU5 were sampled from its lowermost part. In the case of the La Palma flow (LPM) the situation is similar to Mesa La Muerta in terms of lava thickness and site distribution, however the vegetation cover is less dense. Two sites (LPM2 and LPM3) were drilled at a road cut (Fig. 2) while in the case of sites LPM1, LPM4, and LPM5, cores had to be taken over greater distances (40 to 60 m) from each other within each site so that larger block movements could be detected with ease and/or small movements would average out. In the case of La Tinaja (LTJ), four sites were chosen along

road cuts (LTJ1 to LTJ4, see Fig. 2) where the internal flow structure was visible along several meters and up to ~100 m in one stretch. Another site (LTJ5) was drilled near the scoria cone from which the flow was issued (Fig. 2), located ~4400 m from the aforementioned distal La Tinaja lava flow sites.

Drilled cores (total number = 222) were cut into standard cylindrical specimens and their volume magnetic susceptibility (k) measured with SM-150 L/H instruments (ZH Instruments; noise level 10^{-6} SI). Natural remanent magnetization (NRM) vectors were measured with an Agico JR5 spinner magnetometer, while alternating field (AF) demagnetization was accomplished by an Agico LDA-3 equipment and using 10–12 demagnetization steps with a maximum amplitude of 80 mT. At the sample level, principal components analysis (PCA; Kirschvink, 1980) was used to define the characteristic remanent magnetization (ChRM) direction, and the statistical approach proposed by Fisher (1953) was applied to compute the site-mean paleomagnetic direction and its uncertainty. Demagnetization data were displayed on orthogonal vector plots (Zijderveld, 1967) and on equal-area projections. Computer-programs used in this context were: a) PMGSC 4.2 (Enkin, 2005), b) PMag Tool 4.2b (written by Mark W. Hounslow, <https://www.lancaster.ac.uk/staff/hounslow/resources/software/pmagtool.htm>), and c) paleomagnetism.org online package (Koymans et al., 2016).

For paleointensity determinations, double heating IZZI-Thellier experiments (Tauxe and Staudigel, 2004) were conducted on 55 samples with a laboratory field of 50–60 μT , applied parallel to their z-axis. Only samples possessing a single-component NRM and median destructive fields higher than 20 mT were selected. In these experiments, the samples were exposed to temperatures between 100 and 560 °C, and an ASC Scientific TD48 furnace was used for this purpose. pTRM-checks (Coe, 1967) were performed after every other temperature step. Data were analyzed using the ThellierTool4.22 software (Leonhardt et al., 2004), which provides the best fit to data points in a NRM left vs. pTRM gained plot (Arai diagram). To assess the quality of the given IZZI-Thellier results, a fairly strict set of selection criteria was applied. For a sample to be acceptable, the best-fit line should be calculated based on at least 5 data points ($N \geq 5$), and the β -parameter (the ratio of standard error of the slope of the selected segment in the Arai plot to the absolute value of the slope) should be < 0.1 . At least 40% of the total NRM (NRM fraction, f -parameter) should be used, and the quality factor (q) would be acceptable if it is ≥ 5 . For both angles MAD_{anc} , the anchored maximum angular deviation, and α , the angular difference between the anchored and the non-anchored vector, the upper acceptance limit was set to 10° . Sample alteration monitoring was done by the pTRM check criterions: DRAT, the ratio of difference between the pTRM check and relevant TRM value at a specific temperature and the length of the selected NRM-TRM segment, the relative check error $d(\text{CK})$, and the cumulative check difference $d(\text{pal})$. These three criterions were constrained to be $< 10\%$. At lava flow level, at least 3 accepted specimens (N_{min}) should be available to calculate the flow's mean intensity with a standard deviation (σ) smaller than 10 μT .

4. Results

4.1. Paleomagnetic directions

Stepwise AF demagnetization was conducted on a total of 178 samples. Site-mean directions are listed in Table 2 (overall flow-mean directions calculated from individual ChRM directions are listed in Supplementary Table S1).

Specimens from La Tinaja lava flows predominantly possess either a single component of magnetization interpreted as a ChRM direction, or additionally minor secondary magnetization components of probably viscous origin, which could be easily removed by AF demagnetization amplitudes of 5–10 mT (Fig. 4a), but in few specimens stronger secondary components (Fig. 4b) required AF amplitudes of 20–25 mT. Such a

Table 2

Flow mean paleomagnetic directions, paleointensities, paleomagnetic dating ages, and ¹⁴C ages.

Lava flow	Code	Paleomagnetic direction							Paleointensity		Possible Ages	Cal ¹⁴ C age ranges
		n _a /n _t	n/N	R	k	α ₉₅	Dec	Inc	PI	σ (μT)		
La Tinaja	LTJ	4/5	45/48	44.76948	190.87	1.5	3.6	37.4	62.97	21.69	4682–4623 BCE	4400–3935 BCE
											4520–4450 BCE	4450–4420 BCE
											3650–3480 BCE	3870–3810 BCE
											3250–3200 BCE	4260–3640 BCE
La Palma	LPM	3/5	30/34	29.61721	75.76	3.0	10.2	50.9	46.66	6.86	3220–2880 BCE	
Mesa La Muerta	MMU	5/6	40/56	39.57148	91.01	2.4	0.8	15.9	53.91	7.27	2240–2070 BCE	
Malpais de Cutzarondiro	MPC	4/5	35/40	34.56293	77.79	2.8	9.8	33.2	64.76	4.72	760–630 BCE	4308–4305 BCE
											410–320 BCE	

n_a/n_t, is the number of accepted sites/total number of sampled sites; n, number of samples used in the calculation of the site-mean direction; N, total number of samples measured; R, unit vector sum; k, precision parameter; α₉₅, 95% confidence angle; Dec, declination; Inc, inclination; PI, paleointensity; σ (μT), standard deviation of PI.

behavior was typical in specimens from the four sites LT1, LTJ3, LTJ4, and LT5, where the ChRM directions were calculated from 6 to 10 vector end points and the best fit was characterized by maximum angular deviation (MAD) values of 3.4° and often <1°. Three specimens from LTJ1 had MAD values between 9.7° and 4.7°. We note also that these four sites have varying median destructive field (MDF) values, which probably reflects differences in the magnetic mineral grain sizes. Among the four flows, specimens from LTJ3 have the highest MDF values (40–50 mT), while the smallest MDF values (8–25 mT) were found in LTJ5. On the other hand, strong overprints were observed in all 12 specimens from LTJ2 and the ChRM directions were dispersed (Supplement, Fig.

S1) and characterized by large MAD values between 3.7° and 15.2°. Among all La Tinaja sites, LTJ2 specimens have the lowest MDF values. Therefore, no reliable site-mean direction could be calculated for this site. Using all other sites, La Tinaja's paleomagnetic mean direction could be precisely defined: Dec = 3.6°, Inc = 37.4°, α₉₅ = 1.5°, n = 45 (Fig. 5a).

For the La Palma flow, specimens from LPM1, LPM4, and LPM5 retain single components of magnetization (Fig. 4c) or an additional small secondary component that could be removed by AF amplitudes of 5–10 mT. MDF values are on average ~30 mT indicating the presence of a moderate magnetic coercivity related to pseudo single domain (PSD)

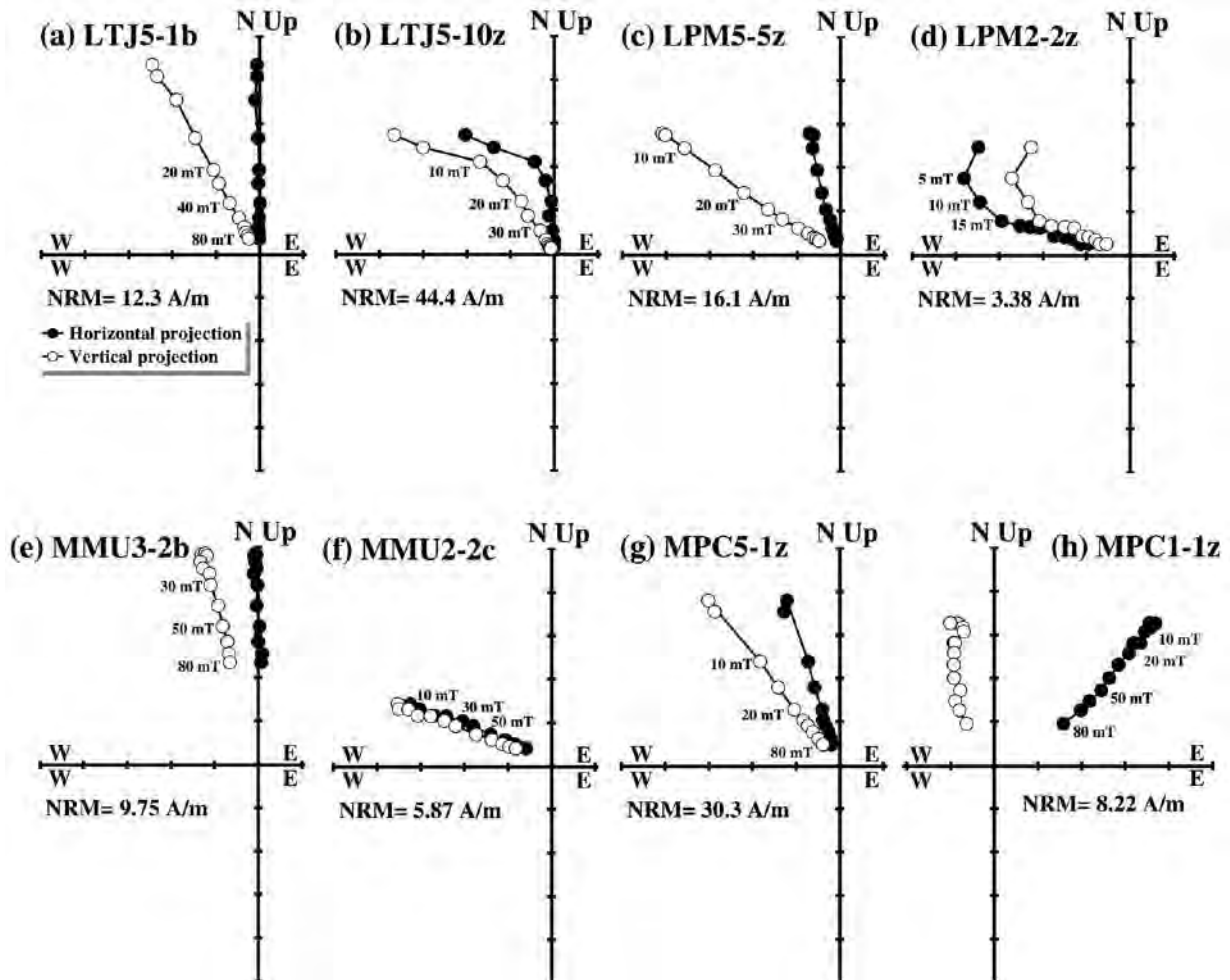


Fig. 4. Representative demagnetization diagrams for the four studied lava flows. Labels along curves denote the maximum AF amplitude applied during the demagnetization steps.

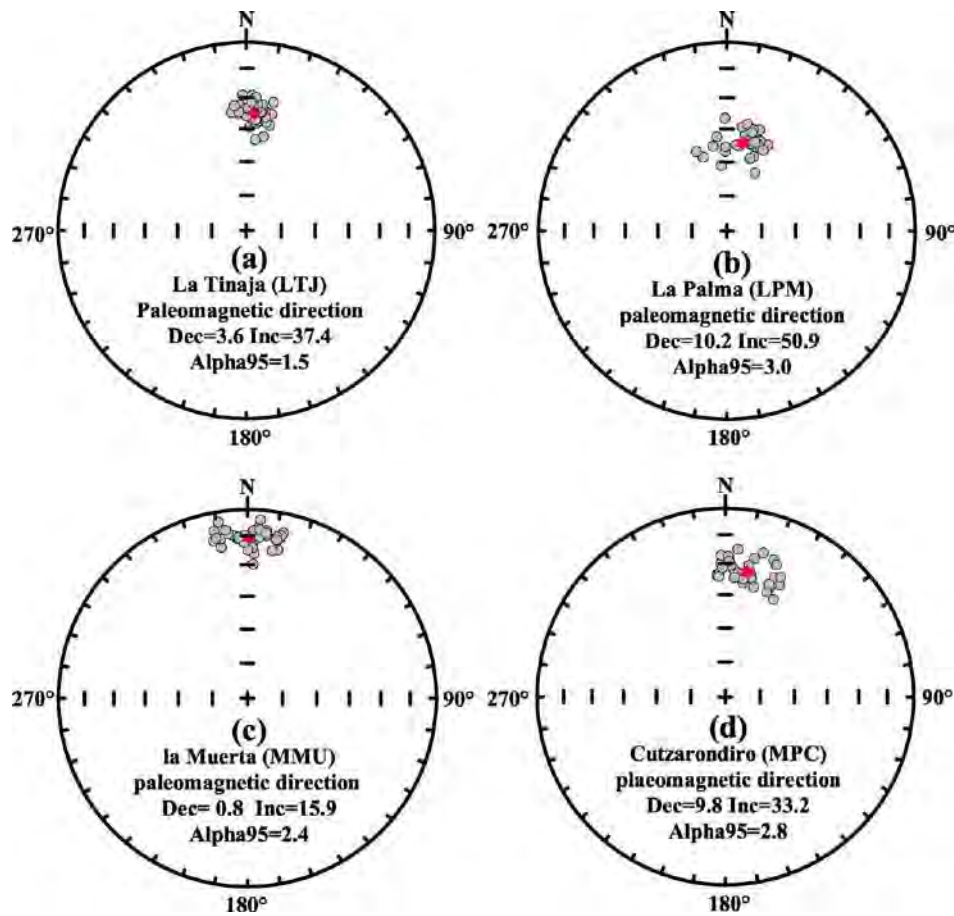


Fig. 5. Equal area projections of the characteristic remanent magnetization directions for the four lava flows under study. Flow-mean directions are shown by large red stars.

grain sizes. LPM2 and LPM3 specimens are characterized by two components of magnetization (Fig. 4d). In all cases, the ChRM directions were calculated from 5 to 12 vector end points and MAD varied between 2.4° and 0.5° . Despite of such acceptable results on the specimen level, ChRM dispersion was large and no site mean direction could be calculated for LPM2 and LPM3, which may be attributed to undetected block movements (Supplement, Fig. S1). On the other hand, consistent site mean directions were obtained from LPM1, LPM4, and LPM5 and thus define the La Palma overall mean direction with a small dispersion (Dec = 10.2, Inc = 50.9, $\alpha_{95} = 3.0^\circ$; see Table 2 and Fig. 5b).

In regard to Mesa La Muerta, most of the demagnetization curves yielded single components of magnetization (Fig. 4e) with a MAD often $< 1.4^\circ$ and characterized by a high MDF of 50–70 mT. Well-defined mean directions were determined from all La Muerta sites (Supplement, Table S1), however, the MMU2 inclination was significantly higher than that of the other five sites (Fig. 4f; see also Supplement, Fig. S1). We thus propose that the steep inclination of MMU2 points to a post-cooling tilt of the whole site, which could not be detected in the field. Excluding site MMU2, a well-defined overall mean direction was determined for the Mesa La Muerta flow: Dec = 0.8, Inc = 15.9, $\alpha_{95} = 2.4^\circ$ (see Table 2 and Fig. 5c).

In the case of Malpaís de Cutzaróniro, demagnetized specimens are characterized by a single-component of NRM, or by small secondary overprints (Fig. 4g and h), and moderate median destructive fields of 15–35 mT. ChRM directions for MPC2, MPC3, MPC4, and MPC5 are very similar and define a flow mean direction with a small confidence circle (Dec = 9.8, Inc = 33.2, $\alpha_{95} = 2.8^\circ$, Table 2 and Fig. 5d). For site MPC1, its calculated site mean direction is characterized by a much more easterly declination of 56.7° , a negative inclination of -8.2° , and a large uncertainty $\alpha_{95} = 10.8^\circ$ (Fig. 4h; see also Supplement Fig. S1

and Table S1). These features lead to the conclusion that this ChRM direction must be the result of the tilting of blocks and therefore was rejected.

4.2. Paleointensity results

Only 22 samples from a total of 55 passed the selection criteria resulting in an overall success rate of 40%. However, the success rate markedly differs between the four flows: It is $\sim 31\%$ (5/16) for La Tinaja samples, $\sim 64\%$ (7/11) for La Palma, $\sim 50\%$ (6/12) for Mesa La Muerta, and $\sim 33\%$ (4/12) for Malpaís de Cutzaróniro. Paleointensity estimates for every accepted sample associated with the selection statistics are listed in the supplementary information (Suppl. Table S2). Paleointensity values for all studied flows are listed in Table 2 and Fig. 6 shows three Arai plots of representative examples of successful intensity determinations, together with their orthogonal vector component plots. The best-fit lines of the accepted specimens are characterized by f-values between 44 and 98%, q-values vary between 5.86 and 51.4, α -angles range from 0.74° to 8.86° , and the alteration monitoring parameters DRAT, d(CK), and d(pal) have values well below 10%. On the other hand, many samples were rejected because of zigzagging or concave PI curves in the Arai plots (Fig. 6d), a feature believed to be caused by multi-domain particles. In such cases no reliable PI could be defined, which is valid for most of the La Tinaja samples. Significant numbers of samples were also rejected because they altered during the experiment, as indicated by pTRM check criterions exceeding the threshold limit (Fig. 6e). A small number of samples failed because only a fraction of NRM could be used due to $f < 10\%$ (Fig. 6f). La Tinaja has a flow mean PI of $62.97 \mu\text{T}$ with a standard deviation of $21.69 \mu\text{T}$ (Table 2), which is much larger than the acceptable value of $10 \mu\text{T}$ and therefore considered

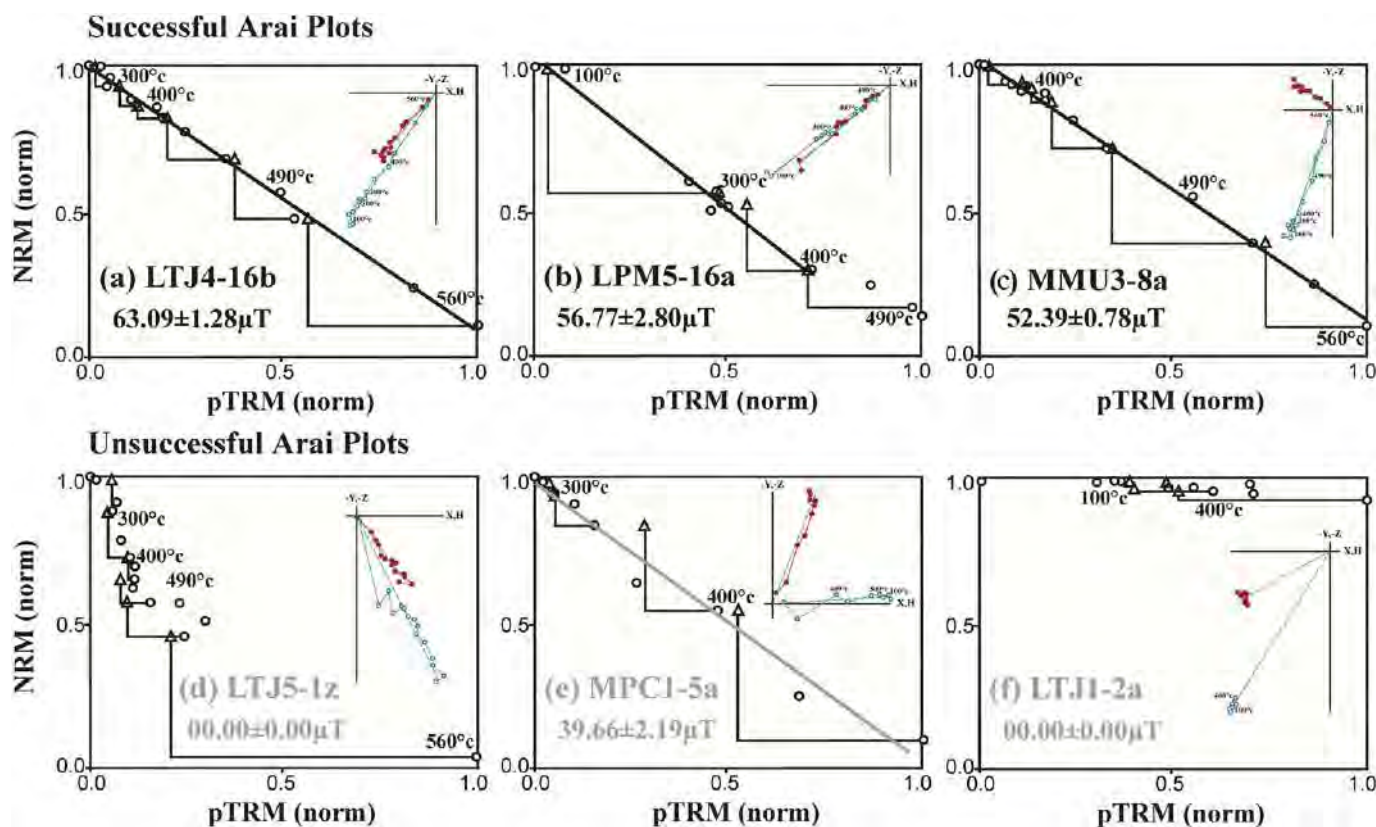


Fig. 6. Examples of typical IZZI-Thellier results and orthogonal vector plots (inset) of accepted (a, b, c) and rejected (d, e, f) specimens. NRM and pTRM data are normalized. NRM vs. pTRM data are shown as circles, with best-fit lines. pTRM checks are shown as triangles. Some temperature steps are also indicated. Paleointensity analyses were done using TellierTool.

unreliable. For the remaining three flows, four to seven samples passed the acceptance criteria and their mean PI (Table 2) have standard deviations between 7.73 and 4.72 μT .

4.3. Paleomagnetic dating

The paleomagnetic dating was executed through the Matlab archaeo-dating tool (Pavón-Carrasco et al., 2011) and by using the global SHA.DIF.14k model (Pavón-Carrasco et al., 2014) to derive local SV reference curves. Lately, the validity of this model for dating the Mexican lavas has been tested with success (Böhnel et al., 2016; Mahgoub et al., 2017a, 2017b). Because a regional SV curve is still not available for Mexico, in the present study the SHA.DIF.14k model was also applied on the four lava flows under consideration in this study. Knowing the ^{14}C -age of the stratigraphically oldest La Tinaja flow allows us to constrain the time interval of archaeomagnetic dating to the period 5000 BCE to 1900 CE. To perform the dating task, we followed the same approach used in previous studies (Böhnel et al., 2016; Mahgoub et al., 2017b), where the flow mean paleomagnetic directions based on the individual ChRM directions were used instead of the unweighted site-mean directions, as the number of sites is small and their site-mean values are characterized by variable statistical parameters.

In the case of La Tinaja, only the flow mean direction based on 45 cores (Table 2) was available, and as shown in Fig. 7a (here only the combined probability density function PDF is shown; for details see Supplementary files), ten possible paleomagnetic ages ranging from 4680 BCE to 1760 CE are produced (considering the accuracy of the method, ages were rounded up to the nearest decade). Paleomagnetic dating of La Palma, which is stratigraphically younger than La Tinaja, yielded only one age range of 3220–2880 BCE (Fig. 7b). This age allows us to consider only those ages provided for La Tinaja which are older than La Palma: 4680–4620 BCE, 4520–4450 BCE, 3650–3480 BCE (Table 2). Two possible age ranges of 2240–2070 BCE and 760–

630 BCE were obtained for Mesa La Muerta (Fig. 7c), and one well-constrained age range of 420–320 BCE for the Malpaís de Cutzaróndiro flow (Fig. 7d).

5. Discussion of dating results and archaeological implications

Well-defined ChRM directions with confidence angles α_{95} between 1.5° and 8.0° were determined for 16 sites and correspondingly the lava flow mean directions were precisely determined with a 95% confidence angle ranging between 1.5° and 3.0° . The McFadden and Lowes (1981) F-distribution test was applied to check whether all accepted ChRM directions of a flow are indistinguishable at the 95% confidence level. Additionally, we applied the McFadden and McElhinny (1990) test in order to evaluate whether two selected site-means from the same flow share a common mean direction. Application of the tests to La Tinaja site-mean directions revealed that they are different at the 95% confidence level, and the same applies for Malpaís de Cutzaróndiro. On the other hand, these tests when applied to the La Palma and Mesa La Muerta sites demonstrate that their site-mean directions are indistinguishable at the 95% confidence level. Significant direction differences have been previously reported elsewhere from independent sites of the same flow (e.g. Hagstrum and Champion, 1994; Speranza et al., 2006), and even within the same site (e.g. Böhnel et al., 2009). These discrepancies could have different sources, including sampling bias due to a small number of data affected by non-random errors caused by local magnetic anomalies and block tilting, among others (Böhnel and Schnepf, 1999). In a similar paleomagnetic dating study of a Late Holocene cluster of lavas in the Zacapu area, located in the north-central part of the MGVF (Mahgoub et al., 2017b), significantly different directions within a single flow were also obtained and related to undetected small movements of the sampled lava blocks after cooling. Although we have no conclusive evidence supporting this explanation in the case of the present study, we consider that the observed within-flow

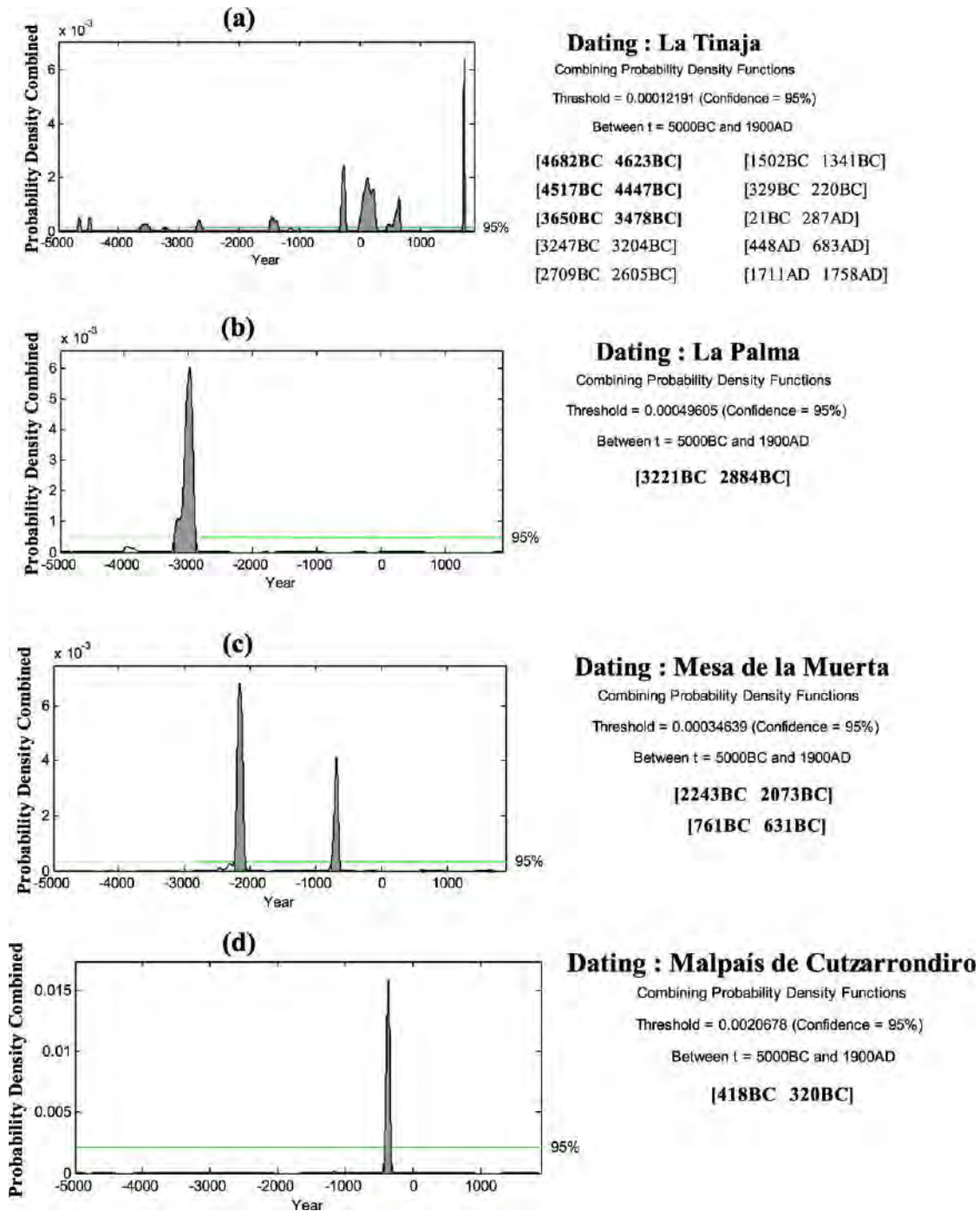


Fig. 7. Paleomagnetic dating of (a) La Tinaja, (b) La Palma, (c) Mesa de la Muerta, and (d) Malpaís de Cutzaróndiro. The combined probability density derived from the declination, inclination and palaeointensity data are shown as shaded peaks with the minimum 95% confidence level by horizontal green lines. For more details, see Supporting Information.

paleomagnetic variations could also be due to such movements, probably affecting the rock along the entire length of the outcrop.

Paleomagnetic dating of La Tinaja provides multiple possible age ranges covering almost the entire time interval considered, which is not surprising since its mean direction ($Dec = 3.6^\circ$ and $Inc = 37.4^\circ$) is close to the axial geocentric dipole direction. Unfortunately, we were not able to obtain a reliable paleointensity measurement, which could have reduced the ambiguity of the paleomagnetic dating. Determining the paleomagnetic ages of the other flows known to be stratigraphically younger than La Tinaja scoria cone and its ^{14}C age of cal 4184–3655 BCE, allowed us to constrain its paleomagnetic age to the range of 3650–3480 BCE. Several hundred years later (3220–2880 BCE), the eruption

of La Palma and its lava flows occurred. In the case of Mesa La Muerta, two paleomagnetically deduced age ranges were obtained (2240–2070 BCE, corresponding to the Early Preclassic (2000–1000 BCE), and 760–630 BCE corresponding to the Middle Preclassic (1000–400 BCE) periods of the Mesoamerican archaeological time scale, respectively). A few hundred years later, the more voluminous and youngest Malpaís de Cutzaróndiro lava flow was erupted at 420–320 BCE during the Late Preclassic (400 BCE–200 CE). The last two eruptions of Mesa La Muerta and Cutzaróndiro probably had an impact on sedentary pre-Hispanic populations, which were by then on the rise all over the wider central Michoacán territory as evidenced by several archaeological sites (e.g. Beekman, 2010). Sedentary human groups were probably also dwelling

in the fertile Tacámbaro–Puruarán area, although we ignore whether specific archaeological studies have been carried out to date in its vicinity. In this context, it is worth mentioning that “Cutzaróndiro” means “abundant coarse ash” in Purépecha, the language spoken by the pre-Hispanic Tarascan people of ancient Michoacán, hinting that some of the eruptions might have been witnessed by early inhabitants of the area.

6. Conclusions and future hazards

Paleomagnetic dating was applied to lava flows emitted from four monogenetic Holocene vents (La Tinaja, La Palma, Mesa La Muerta, and Malpaís de Cutzaróndiro, in chronological eruption order) that form a small cluster located within the wider Tacámbaro–Puruarán area. Stratigraphic relations indicate that La Tinaja is the oldest of these four volcanoes. It was radiocarbon-dated by Guilbaud et al. (2012) at 5115 ± 130 years BP (cal 4184–3655 BCE). A total of 21 paleomagnetic sites from La Tinaja were sampled to evaluate the coherency of the obtained site-mean paleomagnetic directions. Five sites were found to be unacceptable (most probably due to the tilting of blocks), and the remaining 16 sites were used to define the mean directions with small confidence angles $1.5^\circ \leq \alpha_{95} \leq 3.0^\circ$. Except for La Tinaja, where no reliable paleointensity could be determined, flow-mean paleointensities were defined for all flows following the IZZI-Thellier method and applying strict selection criteria. Based on flow-mean directions and intensities paleomagnetic dating of La Tinaja lava flows yielded several possible ages ranges of which the range 3650–3480 BCE is closest to the radiometric date of cal 4184–3655 BCE. Several hundred years later (3220–2880 BCE), the La Palma lava flow was emplaced. Two different paleomagnetic age ranges (2240–2070 BCE and 760–630 BCE) were obtained for Mesa La Muerta, and especially the younger range would imply that the eruption could have been witnessed by pre-Hispanic sedentary populations, which by that time had spread all over central Mexico. This holds even more true for the Malpaís de Cutzaróndiro lava flow, dated by the paleomagnetic method at 420–320 BCE, an age that falls within the Late Pre–Classic period of the Mesoamerican archaeological time scale.

On the other hand, the identification of small clusters comprising several young monogenetic volcanoes that erupted in a sequence of geologically short time intervals (hundreds to few thousands of years) in small areas within the much wider MGVF opens several questions in regard to future volcanic hazard assessments in this region: Will the cluster near Tacámbaro described here “reactivate” again with the emergence of a new vent? How long are such clusters “active”? Will the next monogenetic eruption in the MGVF be a single short-lived isolated eruption, or the beginning of a cluster? Furthermore, is it possible that the historic eruptions of Jorullo and Parícutin represent each the beginning of a cluster and should a new eruption in their close vicinity be expected in the future?

The relevance of clustered monogenetic volcanism is further underscored by the fact that the case near Tacámbaro described here is not unique. Another Holocene cluster was recently reported from the western Zacapu basin (Mahgoub et al., 2017b) in the central-northern part of the MGVF, and in a recent study, Deligne et al. (2016) describe a similar cluster from central Oregon in the subduction-related Cascades volcanic arc of the western USA. In both of these examples, again several different magma sources were tapped within a geologically short period of time. The causes that lead to the formation of multiple magma sources and the local concentration of volcanic activity need to be addressed in order to evaluate the potential impacts of clustered volcanism in the MGVF and other monogenetic fields in different tectonic settings around the world such as the Auckland volcanic field, New Zealand (e.g. Kereszturi et al., 2013), the Newer volcanic province, Australia (e.g. Lesti et al., 2008) or the Harrat Rahat volcanic field, Saudi Arabia (Runge et al., 2014) to name a few. Future work (geophysical and petrological) is needed to address the conditions that allow several

magma sources to be formed and then tapped in close temporal and spatial proximity to each other in order to produce these small “flare ups”.

Acknowledgments

Field and laboratory costs of A.N.M. and H.B. were defrayed by Consejo Nacional de Ciencia y Tecnología (CONACyT-180032) and the Dirección General de Asuntos del Personal Académico, Universidad Nacional Autónoma de México (UNAM-DGAPA IN-111915) granted to H. Böhnel, and costs for C.S., S.S., and M.N.G. were defrayed from projects funded by the Consejo Nacional de Ciencia y Tecnología (CONACyT-167231) and the Dirección General de Asuntos del Personal Académico, Universidad Nacional Autónoma de México (UNAM-DGAPA IN-101915) granted to C. Siebe. Capitán Fernando Valencia is thanked for skillful and safe flights over the study area.

Appendix A. Supplementary data

Supplementary data to this article can be found online at <https://doi.org/10.1016/j.jvolgeores.2017.10.004>.

References

- Beekman, C.R., 2010. Recent research in western Mexican archaeology. *J. Archaeol. Res.* 18, 41–109.
- Böhnel, H., Schnepf, E., 1999. Precision of the paleomagnetic method: An example from the Quaternary Eifel volcanics (Germany). *Earth Planets Space* 51 (6), 403–412.
- Böhnel, H., Michalk, D., Nowaczyk, N., González Naranjo, G., 2009. The use of mini-samples in paleomagnetism. *Geophys. J. Int.* 179, 35–42.
- Böhnel, H., Pavón-Carrasco, F.J., Sieron, K., Mahgoub, A.N., 2016. Palaeomagnetic dating of two recent lava flows from Ceboruco volcano, western Mexico. *Geophys. J. Int.* 207 (2), 1203–1215.
- Chevrel, M.O., Guilbaud, M.N., Siebe, C., 2016a. The AD 1250 effusive eruption of el Metate shield volcano (Michoacán, Mexico): Magma source, crustal storage, eruptive dynamics, and lava rheology. *Bull. Volcanol.* 78 (4):32. <https://doi.org/10.1007/s00445-016-1020-9>.
- Chevrel, M.O., Siebe, C., Guilbaud, M.N., Salinas, S., 2016b. The AD 1250 el Metate shield (Michoacán): Mexico's most voluminous Holocene eruption and its significance for archaeology and hazards. *The Holocene* 26 (3):471–488. <https://doi.org/10.1177/0959683615609757>.
- Coe, R.S., 1967. Paleo-intensities of the Earth's magnetic field determined from Tertiary and Quaternary rocks. *J. Geophys. Res.* 72 (12), 3247–3262.
- Deligne, N.I., Conrey, R.M., Cashman, K.V., Champion, D.E., Amidon, W.H., 2016. Holocene volcanism of the upper McKenzie River catchment, central Oregon Cascades, USA. *Bull. Geol. Soc. Amer.* 128 (11/12), 1618–1635.
- Enkin, R., 2005. PMGSC 4.2. Geological survey of Canada, Sidney, British Columbia, Canada.
- Ferrari, L., Orozco-Esquivel, T., Manea, V., Manea, M., 2012. The dynamic history of the Trans-Mexican Volcanic Belt and the Mexico subduction zone. *Tectonophysics* 522 (523), 122–149.
- Fisher, R.A., 1953. Dispersion on a sphere. *Proc. R. Soc. Lond. A* 127, 295–305.
- Guilbaud, Marie-Noëlle, Siebe, Claus, Widom, Elisabeth, Rasozanamparany, Christine, Salinas, Sergio, Castro Govea, Renato, in prep. Petrography and geochemistry of monogenetic volcanoes and exposed tertiary basement in the Jorullo–Tacámbaro area, trenchward margin of the Michoacán–Guanajuato Volcanic Field: Implications for magma generation and differentiation in the western-central part of the Trans-Mexican Volcanic Belt, in prep.
- Guilbaud, M.N., Siebe, C., Layer, P., Salinas, S., Castro-Govea, R., Garduño-Monroy, V.H., Corvec, N.L., 2011. Geology, geochronology, and tectonic setting of the Jorullo Volcano region, Michoacán, México. *J. Volcanol. Geotherm. Res.* 201, 97–112.
- Guilbaud, M.N., Siebe, C., Layer, P., Salinas, S., 2012. Reconstruction of the volcanic history of the Tacámbaro–Puruarán area (Michoacán, México) reveals high frequency of Holocene monogenetic eruptions. *Bull. Volcanol.* 74, 1187–1211.
- Hagstrum, J.T., Champion, D.E., 1994. Paleomagnetic correlation of Late Quaternary lava flows in the lower east rift zone of Kilauea Volcano, Hawaii. *J. Geophys. Res. Solid Earth* 99 (B11), 21679–21690.
- Hasenaka, T., Carmichael, I.S.E., 1985a. The cinder cones of Michoacán–Guanajuato, central Mexico: their age, volume and distribution, and magma discharge rate. *J. Volcanol. Geotherm. Res.* 25, 105–124.
- Hasenaka, T., Carmichael, I.S.E., 1985b. Compilation of location, size, and geomorphological parameters of volcanoes of the Michoacán–Guanajuato volcanic field, central Mexico. *Geophys. Res. Lett.* 12 (4), 577–607.
- Johnson, C.A., Harrison, C.G.A., 1990. Neotectonics in central Mexico. *Phys. Earth Planet. Inter.* 64, 187–210.
- Kereszturi, G., Nemeth, K., Cronin, S.J., Agustín-Flores, J., Smith, I.E.M., Lindsay, J., 2013. A model for calculating eruptive volumes for monogenetic volcanoes – Implication for the Quaternary Auckland Volcanic Field, New Zealand. *J. Volcanol. Geotherm. Res.* 266, 16–33.

- Kilburn, C., 2000. Lava flows and flow fields. In: Sigurdsson, H., Houghton, B.F., McNutt, S.R., Rymer, H., Stix, J. (Eds.), *Encyclopedia of Volcanoes*. Academic Press, London.
- Kirschvink, J.L., 1980. The least-squares line and plane and analysis of palaeomagnetic data. *Geophys. J. R. Astron. Soc.* 62, 699–718.
- Korte, M., Constable, C.G., 2003. Continuous global geomagnetic field models for the past 3000 years. *Phys. Earth Planet. Inter.* 140 (1), 73–89.
- Korte, M., Constable, C.G., 2005. The geomagnetic dipole moment over the last 7000 years—new results from a global model. *Earth Planet. Sci. Lett.* 236 (1), 348–358.
- Korte, M., Constable, C.G., 2011. Improving geomagnetic field reconstructions for 0–3 ka. *Phys. Earth Planet. Inter.* 188 (3), 247–259.
- Koymans, M.R., Langereis, C.G., Pastor-Galan, D., van Hinsbergen, D.J.J., 2016. *Paleomagnetism.org: an online multi-platform open source environment for paleomagnetic data analysis*. *Comput. Geosci.* 93, 127–137.
- Kshirsagar, P., Siebe, C., Guilbaud, M.N., Salinas, S., Layer, P., 2015. Late Pleistocene Alberca de Guadalupe maar volcano (Zacapu basin, Michoacán): stratigraphy, tectonic setting, and paleo-hydrogeological environment. *J. Volcanol. Geotherm. Res.* 304: 214–236. <https://doi.org/10.1016/j.jvolgeores.2015.09.003>.
- Kshirsagar, P., Siebe, C., Guilbaud, M.N., Salinas, S., 2016. Geological and environmental controls on the change of eruptive style (phreatomagmatic to Strombolian-effusive) of Late Pleistocene el Caracol tuff cone and its comparison with adjacent volcanoes around the Zacapu basin (Michoacán, México). *J. Volcanol. Geotherm. Res.* 318: 114–133. <https://doi.org/10.1016/j.jvolgeores.2016.03.015>.
- Leonhardt, R., Heunemann, C., Krása, D., 2004. Analyzing absolute paleointensity determinations: acceptance criteria and the software ThellierTool4.0. *Geochim. Geophys. Geosyst.* 5 (12).
- Lesti, C., Giordano, G., Salvini, F., Cas, R., 2008. Volcano tectonic setting of the intraplate, Pliocene–Holocene, Newer Volcanic Province (southeast Australia): role of crustal fracture zones. *J. Geophys. Res.* 113 (B07407). <https://doi.org/10.1029/2007JB005110>.
- Luhr, J.F., Simkin, T., 1993. *Paricutin: The Volcano Born in a Mexican Cornfield*. Geoscience Press (427 p).
- Mahgoub, A.N., Böhnel, H., Siebe, C., Chevrel, M.O., 2017a. Paleomagnetic study of el Metate shield volcano (Michoacán, Mexico) confirms its monogenetic nature and young age (~1250 CE). *J. Volcanol. Geotherm. Res.* 336:209–218. <https://doi.org/10.1016/j.jvolgeores.2017.02.024>.
- Mahgoub, A.N., Reyes-Guzman, N., Böhnel, H., Siebe, C., Pereira, G., Dorison, A., 2017b. Paleomagnetic constraints on the ages of the Holocene Malpaís de Zacapu lava flow eruptions, Michoacán (Mexico): Implications for archeology and volcanic hazards. The Holocene <https://doi.org/10.1177/0959683617721323>.
- McFadden, P.L., Lowes, F.J., 1981. The discrimination of mean directions drawn from Fisher distributions. *Geophys. J. R. Astron. Soc.* 67, 19–33.
- McFadden, P.L., McElhinny, M.W., 1990. Classification of the reversal test in palaeomagnetism. *Geophys. J. Int.* 103, 725–729.
- Pavón-Carrasco, F.J., Osete, M.L., Torta, J.M., Gaya-Piqué, L.R., 2009. A regional archeomagnetic model for Europe for the last 3000 years, SCHA. DIF. 3K: applications to archeomagnetic dating. *Geochim. Geophys. Geosyst.* 10 (3).
- Pavón-Carrasco, F.J., Rodríguez-González, J., Osete, M.L., Torta, J.M., 2011. A Matlab tool for archeomagnetic dating. *J. Archaeol. Sci.* 38, 408–419.
- Pavón-Carrasco, F.J., Osete, M.L., Torta, J.M., De Santis, A., 2014. A geomagnetic field model for the Holocene based on archeomagnetic and lava flow data. *Earth Planet. Sci. Lett.* 388, 98–109.
- Pioli, L., Erlund, E., Johnson, E., Cashman, K.V., Wallace, P., Rosi, M., Delgado, H., 2008. Explosive dynamics of violent Strombolian eruptions: the eruption of Paricutin volcano 1943–1952 (Mexico). *Earth Planet. Sci. Lett.* 271 (1–4), 359–368.
- Rasoazanamparany, C., Widom, E., Siebe, C., Guilbaud, M.-N., Spicuzza, M.J., Valley, J.W., Valdez, G., Salinas, S., 2016. Temporal and compositional evolution of Jorullo volcano, Mexico: implications for magmatic processes associated with a monogenetic eruption. *Chem. Geol.* 434, 62–80.
- Runge, M.G., Bebbington, M.S., Cronin, S.J., Lindsay, J.M., Kenedi, C.L., Moufti, M.R.H., 2014. Vents to events: determining an eruption event record from volcanic vent structures for the Harrat Rahat in Saudi Arabia. *Bull. Volcanol.* 76, 804.
- Speranza, F., Branca, S., Coltelli, M., D'Ajello Caracciolo, F., Vigliotti, L., 2006. How accurate is "paleomagnetic dating"? New evidence from historical lavas from Mount Etna. *J. Geophys. Res. Solid Earth* 111 (B12). <https://doi.org/10.1029/2006JB004496>.
- Stuiver, M., Reimer, P.J., 1993. Extended ¹⁴C database and revised CALIB radiocarbon calibration program. *Radiocarbon* 35, 215–230.
- Tauxe, L., Staudigel, H., 2004. Strength of the geomagnetic field in the Cretaceous Normal Superchron: new data from submarine basaltic glass of the Troodos Ophiolite. *Geochim. Geophys. Geosyst.* 5 (Q02H06).
- Valentine, G.A., Connor, C.B., 2015. Basaltic volcanic fields. In: Sigurdsson, H., Houghton, B.F., McNutt, S.R., Rymer, H., Stix, J. (Eds.), *Encyclopedia of Volcanoes*, 2nd edn Academic Press, London, pp. 423–439.
- Walker, M.J.C., 2013. *Quaternary Dating Methods*. John Wiley & Sons, Chichester (304 p).
- Zijderveld, J.D.A., 1967. AC demagnetization of rocks: analysis of results. In: Runcorn, S.K., Creer, K.M., Collinson, D.W. (Eds.), *Methods in Paleomagnetism*. Elsevier, Amsterdam, pp. 254–286.

4. Paleomagnetic constraints on the ages of the Holocene Malpaís de Zacapu lava flow eruptions, Michoacán (México): Implications for archeology and volcanic hazards

Ahmed Nasser Mahgoub^{a*}, Nanci Reyes-Guzmán^b, Harald Böhnel^a, Claus Siebe^b, Gregory Pereira^c, and Antoine Dorison^c

^a Centro de Geociencias, Universidad Nacional Autónoma de México (UNAM), Blvd. Juriquilla No. 3001, Querétaro, 76230, México

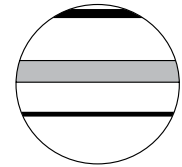
^b Departamento de Vulcanología, Instituto de Geofísica, Universidad Nacional Autónoma de México, Coyoacán, C.P. 04510, México D.F., México

^c UMR 8096 “Archéologie des Amériques” (CNRS and Université Paris 1), Paris, France


Accepted: Journal of The Holocene, doi: org/10.1177/0959683617721323.

Individual contributions of the authors:

- i. **Ahmed Nasser Mahgoub:** visualizing and designing the study, field work, laboratory measurements, analyzing and interpreting of data, writing the article.
- ii. **Nanci Reyes-Guzmán:** providing radiocarbon age data, designing the geological map.
- iii. **Harald Böhnel:** design the research study, fieldwork, participating in the interpretation of data and revising the article, financing for the project.
- iv. **Claus Siebe:** providing radiocarbon age data, fieldwork, revising the article, financing for the project.
 - i. **Gregory Pereira:** providing the archeological and environmental information,
 - ii. **Antoine Dorison:** providing the archeological and environmental information.



Paleomagnetic constraints on the ages of the Holocene Malpaís de Zacapu lava flow eruptions, Michoacán (México): Implications for archeology and volcanic hazards

The Holocene
2018, Vol. 28(2) 229–245
© The Author(s) 2017
Reprints and permissions:
sagepub.co.uk/journalsPermissions.nav
DOI: 10.1177/0959683617721323
journals.sagepub.com/home/hol


Ahmed Nasser Mahgoub,¹ Nanci Reyes-Guzmán,² Harald Böhnel,¹
Claus Siebe,² Gregory Pereira³ and Antoine Dorison³

Abstract

Four monogenetic Holocene lava flows located within the Michoacán-Guanajuato Volcanic Field, Mexico, were sampled for paleomagnetic dating. These flows (namely, El Infiernillo, Malpaís Las Víboras, El Capaxtiro, and Malpaís Prieto) are within the heartland of the pre-Hispanic Tarascan civilization and were inhabited repeatedly since at least 100 BC, but no relation with the volcanic evolution has been proposed so far. The stratigraphically oldest lava flow, El Infiernillo, has a radiocarbon age of 3200 ± 30 yr BP (cal. 1525–1420 BC), and it was used to validate the method. Using full-vector paleomagnetic data from three sites as input for paleomagnetic dating applying the global paleosecular variation model SHA.DIF.14k, an age range of 1500–1370 BC was obtained. Two age ranges of 1340–1230 and 1030–940 BC were obtained for Malpaís Las Víboras. A younger age range of 200–80 BC was obtained for the Capaxtiro lava flow and, finally, the Malpaís Prieto lava flow erupted within the range of AD 830–960. The human occupation history of these flows started around 100 BC during the late Pre-Classic, probably shortly after the Capaxtiro eruption. Archeological records indicate an abandonment of the entire area around AD 900 (late to terminal Classic), which coincides with the paleomagnetic age of the Malpaís Prieto eruption. Interestingly, this area was heavily repopulated again only few hundred years later around AD 1250 and belongs to the core region in which the Tarascan civilization has its roots. The eruption recurrence interval of roughly 1000 years indicates that a new monogenetic eruption should be expected to occur again in the future and that this area deserves to be studied in greater detail with particular emphasis on the impact of past eruptions. This could help to better evaluate volcanic hazards and design preparedness strategies to minimize the impact of a future eruption.

Keywords

archeology, Holocene, lava flows, Michoacán, paleomagnetic dating, Tarascans

Received 7 January 2017; revised manuscript accepted 12 June 2017

Introduction

Paleomagnetic secular variation (PSV) refers to temporal and spatial variations of the Earth's magnetic field (EMF) due to internal processes (flow of liquid in the Earth's outer core) in geologically short timescales ($\ll 1$ Ma). In recent decades, numerical models describing the observed temporal evolution of the geomagnetic field during the past centuries have been developed, for example, GUFM (Jackson et al., 2000) and UFM1 (Blokhin and Jackson, 1992). For longer periods of time, the evolution of the EMF can only be derived from the record in different archives (lake sediments, heated archeological artifacts, and lavas). Data obtained from archeological and volcanic products are the preferred inputs for the regional and global modeling of the EMF variations (Korte and Constable, 2003, 2005, 2011; Korte et al., 2009; Pavón-Carrasco et al., 2009, 2014), as these are based on high fidelity thermoremanent magnetization (TRM). Obtaining high-resolution PSV records in a particular region is of interest because they can be applied in paleomagnetic dating (e.g. Arrighi et al., 2006; Böhnel et al., 2016; Hagstrum and Blinman, 2010; Roperch et al., 2015; Speranza et al., 2006, 2008; Tanguy et al., 2003), among other fields. Paleomagnetic age constraints can be helpful in solving various types of scientific problems. For example, by dating lava flows, it can contribute to assess hazards in active volcanic regions (Cassidy,

2006). But it can also help in dating archeological remains, especially in areas where written historic records are absent. Both of these themes are addressed in this case study in which the Malpaís de Zacapu Holocene lava flows (namely, El Infiernillo, Malpaís Las Víboras, El Capaxtiro, and Malpaís Prieto), located at the W margin of the Zacapu lacustrine basin in the Michoacán-Guanajuato Volcanic Field (MGVF) in central-western Mexico were targeted. This field (Figure 1) has the largest concentration of monogenetic volcanoes in

¹Centro de Geociencias, Universidad Nacional Autónoma de México (UNAM), México

²Departamento de Vulcanología, Instituto de Geofísica, Universidad Nacional Autónoma de México (UNAM), México

³Archéologie des Amériques, UMR 8096 – CNRS and Université Paris 1, France

Corresponding author:

Ahmed Nasser Mahgoub, Centro de Geociencias, Universidad Nacional Autónoma de México (UNAM), Blvd. Juriquilla No. 3001, Querétaro, 76230, México.

Email: ahmednasser@geociencias.unam.mx

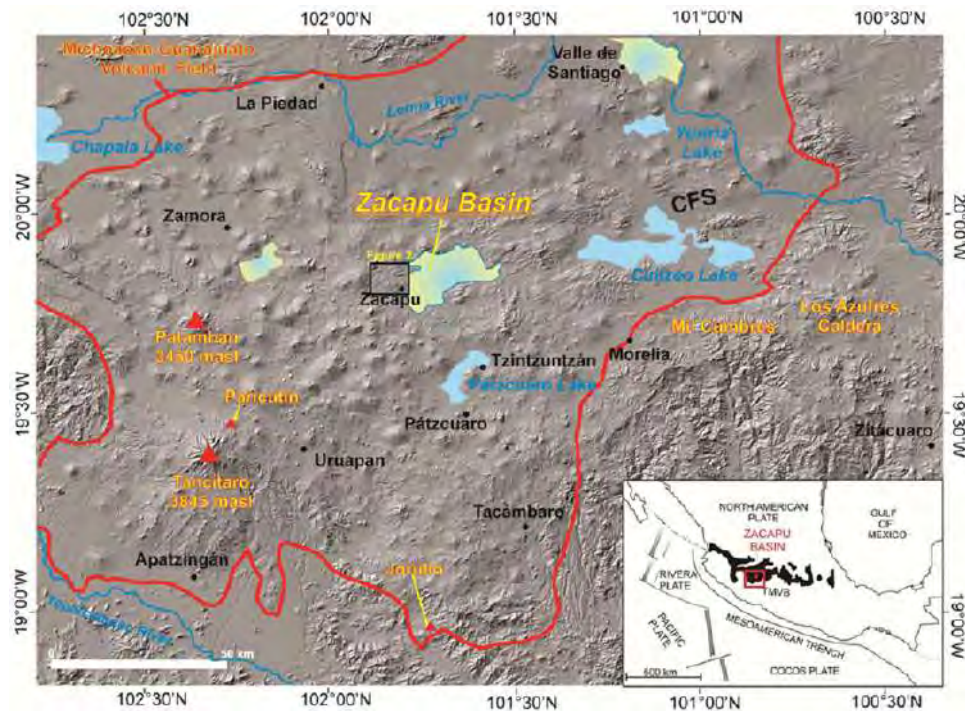


Figure 1. Digital elevation model (modified from Kshirsagar et al., 2015) of the MGVF showing the location of the Malpaís de Zacapu lava flows at the western margin of the Zacapu lacustrine basin. The major fault system is Cuitzeo Fault System (CFS), the most prominent fault system affecting the Zacapu basin. Black rectangle indicates area covered by the geological map shown in Figure 2. Inset map at lower right corner shows location of the MGVF within the TMVB.

the Trans-Mexican Volcanic Belt (TMVB; Siebe et al., 2014) with more than 1000 monogenetic vents. Of these, the majority are scoria cones including the historical Jorullo (1759–1774) and Parícutin (1943–1952) volcanoes. In addition, ~400 medium-sized volcanoes (shields and domes), fewer viscous flows and lava domes, and rare maars occur (Chevrel et al., 2016a, 2016b; Guilbaud et al., 2011, 2012; Hasenaka and Carmichael, 1985, 1987; Kshirsagar et al., 2015, 2016). Notably, pre-Hispanic humans have continuously inhabited the territory of the present State of Michoacán since at least 5000 yr BC (Beekman, 2010; Faugère, 2006; Watts and Bradbury, 1982). Earliest sedentary populations around 2000 BC were succeeded by small-village societies, and from AD 1350 onward, the Tarascan Empire became established around the shores of Lake Pátzcuaro (Pollard, 1993). Considering the abundance of young volcanoes in this region, the impact of volcanism on pre-Hispanic human development and population migrations should not be ruled out. Unfortunately, the absence of written sources from archeological sites complicates evaluating the impact of volcanic eruptions on the pre-Hispanic populations of Michoacán (Pereira et al., 2013), as it can be established only based on archeological findings and their interpretation.

Geological background: The MGVF and the Zacapu basin

The Holocene Malpaís de Zacapu lava flows (*malpaís* means ‘badland’ in Spanish) are located in the MGVF that forms the western-central segment of the TMVB (Figure 1). This continental arc stretches across central Mexico for 1200 km in an East-West direction from the coast at the Gulf of Mexico to the Pacific Ocean. It traverses the *Mexican Altiplano*, a highland characterized by active normal faulting and horst-and-graben structures that result in the formation of basins often occupied by broad (but shallow) lakes, such as the Pátzcuaro and Cuitzeo lakes in Michoacán.

The TMVB is related to the subduction of the oceanic Cocos Plate underneath the continental North American Plate

(e.g. Blatter and Hammersley, 2010; Gómez-Tuena et al., 2003; Kim et al., 2012; Pardo and Suárez, 1995) and consists of a large number of late Tertiary to Quaternary maars, scoria cones, domes, calderas, and strato-volcanoes, the chemical and mineralogical composition of which is largely calc-alkaline (e.g. Carmichael, 2002; Demant, 1978; Ferrari et al., 2012). One notable feature of the TMVB is the abundance (>3000) of scoria cones and other types of small monogenetic volcanoes, which outnumber by several orders of magnitude the few dozens of the much larger strato-volcanoes (Guilbaud et al., 2012; Hasenaka and Carmichael, 1985).

Within the boundaries of the MGVF, which occupies an area of ~40,000 km², the surface topography is dominated by andesitic Plio-Quaternary volcanic landforms. Intense recent volcanic activity conceals most of the older rocks; hence, the underlying basement can only be inferred from outcrops located beyond the limits of the MGVF, which must include plutonic rocks as evidenced by partially fused granodiorite xenoliths found in products of the Parícutin (McBirney et al., 1987; Wilcox, 1954) and Arocútin (Corona-Chávez et al., 2006) scoria cones.

The Holocene Malpaís de Zacapu lava flows are located at the W margin of the ENE-WSW trending Zacapu tectonic basin (Figure 1). The lowest part of the basin (1980 m a.s.l.) is today occupied by a cultivated flat surface of lacustrine origin that is surrounded by Plio-Quaternary volcanoes that are mostly basaltic andesite to andesite in composition (Demant, 1992; Siebe et al., 2013). A few dacites and rhyolites occur forming domes and ignimbrite sheets. The area is characterized by active normal domino-style fault systems that form the western extent of the seismically active Cuitzeo Fault Zone (Johnson and Harrison, 1990) also called the Morelia-Acambay Fault System (Garduño-Monroy et al., 2009; Suter et al., 2001). Faulting around the basin follows a general direction of N65°E to N85°E with dip-directions toward the NNW and SSE. Noticeably, faulting is less evident toward the west of the basin, because of a denser coverage by younger (<40 ka) volcanics (Pasquaré et al., 1991).

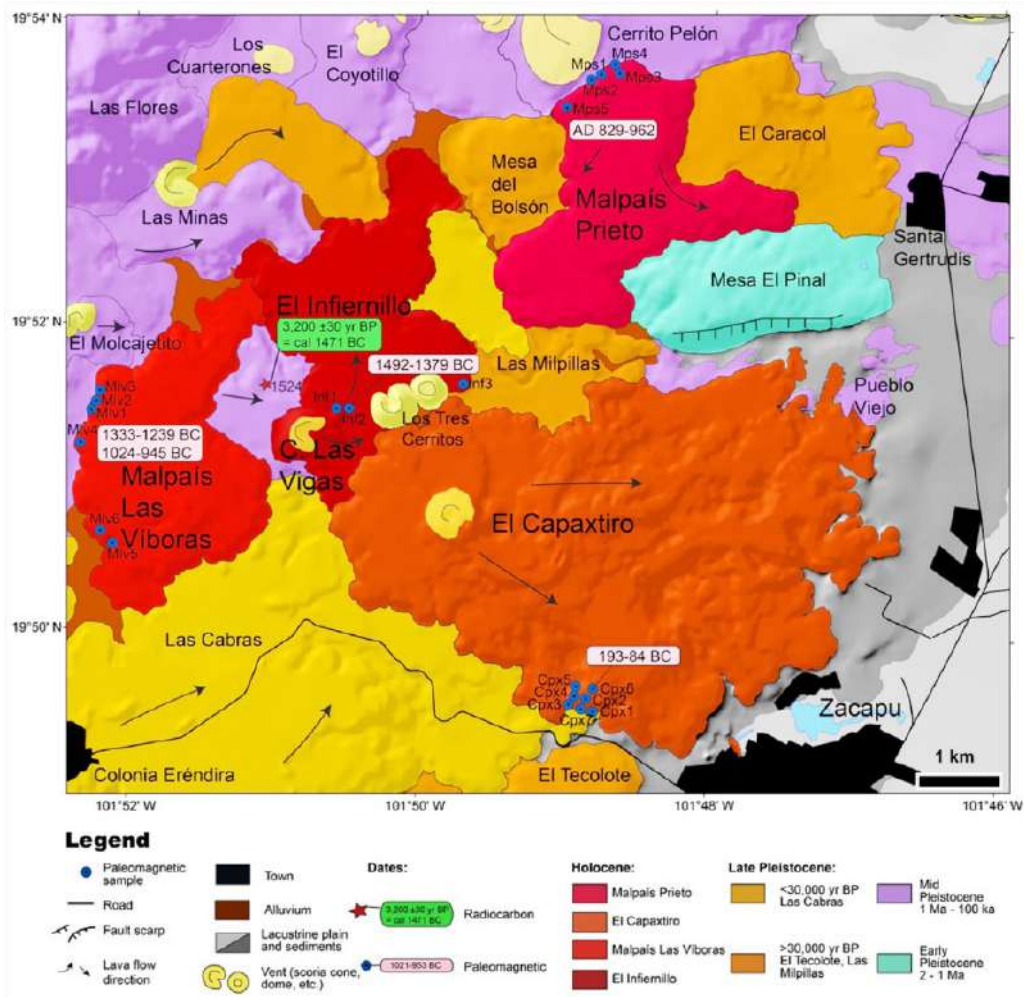


Figure 2. Geological map showing sampling locations of the young lava flows dated in this study.

Hasenaka and Carmichael (1985) and Ban et al. (1992) reported first radiometric ages (^{14}C and K-Ar, respectively) for the MGVF, including a few for volcanoes in the Zacapu basin. New radiometric dates of volcanoes in the eastern and northern parts of the basin (^{14}C and ^{40}Ar - ^{39}Ar) were published by Kshirsagar et al. (2015, 2016).

The only previous work focusing on the Malpaís de Zacapu lava flows was undertaken by Demant (1992) and includes a geologic map with stratigraphic data, as well as chemical and mineralogical analyses of the main lava flows. In his seminal work, the author established that the flows comprising the *malpaís* are andesitic and must be Holocene in age due to their youthful morphology. They were issued from four different eruption sites in the following chronological order: El Infiernillo, Malpaís Las Víboras, El Capaxtiro, and Malpaís Prieto. Our study confirms in essence these findings and was primarily aimed at dating the lava flows. Fieldwork aided by digital elevation model-based morphological observations and geochronological data were integrated to construct a new geological map (Figure 2), which shows the overlapping small-volume Holocene monogenetic lavas underlain by Pleistocene volcanic units. The oldest unit (Mesa El Pinal) is cut by a prominent normal fault and probably not much older than 2 Ma (early Pleistocene).

The oldest of the four Holocene flows, El Infiernillo, was issued from the Las Vigas volcano, a small (~100 m high) scoria cone. Its olivine-bearing basaltic andesite ($\text{SiO}_2 = 56.3\text{--}58.7$ wt.%) lavas are ~50 m thick and cover a minimum surface of 5.8 km² with a volume estimated at 0.3 km³. Mineralogically, they are composed of forsteritic olivine (~1 mm), pargasitic hornblende

(frequently opacitized), augite, and hypersthene phenocrysts in a glassy matrix with feldspar microlites and opaque oxides. One paleosol sample (ZAC-1524A, laboratory no. B-411354, latitude 19°51'36.6", longitude 101°51'08.9", altitude 2192 m a.s.l.) directly underlying a 45-cm-thick deposit of coarse ash to fine lapilli fallout layers from the Las Vigas scoria cone (Figure 3) was dated by the accelerator mass spectrometry (AMS) method at Beta Analytic (Miami, Florida) at 3200 ± 30 yr BP ($\delta^{13}\text{C} = -22.2$). The date was calibrated to calendar years by applying the Stuiver and Reimer (1993) procedure and with the help of the CALIB Computer Program (version 7.1, n.d.; IntCal13 calibration curve), which yielded a 95% probability range (2 σ) of cal. 1525–1420 BC. This is the only radiocarbon sample that could be found during the course of several field campaigns and its dating turned out to be crucial for carrying out with confidence the paleomagnetic dating of the remaining younger lava flows (see below).

To the west of the Las Vigas cone and stratigraphically above is the Malpaís Las Víboras lava flow. This flow is also quite thick (~70 m) with steep margins attesting to a high viscosity during emplacement. It covers an area of 5.9 km² with a volume of ~0.4 km³ and is andesitic in composition ($\text{SiO}_2 = 61.1\text{--}62.5$ wt.%). Observation under the polarizing microscope revealed plagioclase, pargasitic hornblende (mostly opacite), augite, and hypersthene phenocrysts in a glassy matrix with abundant feldspar microlites and opaque oxides.

The most voluminous (3.2 km³ covering an area of 20.9 km²) of the eruptions corresponds to El Capaxtiro whose multiple ~150-m-thick overlapping lava flows were issued from a small cone (El Capaxtiro proper). They reached as far as 6 km to the



Figure 3. Photographs showing the outcrop where paleosol sample ZAC-1524 dated at 3200 ± 30 yr BP was obtained: (a) Roadcut 600 m NW of Las Vigas scoria cone (shown in background). (b) Close-up view of the Las Vigas coarse ash fallout with sampled ochre-brown paleosol directly underneath. Spatula for scale is 25 cm long.

east toward lake Zacapu, where they directly cover lacustrine deposits, as observable in the immediate vicinity of the city of Zacapu. Capaxtiro lavas are the most silicic ($\text{SiO}_2 = 61.1\text{--}64.2$ wt.%) and also cover the southern portion of the Infiernillo lavas. Petrographically, they include plagioclase, pargasitic hornblende (mostly opacite 'ghosts'), augite, and hypersthene phenocrysts in a glassy matrix with abundant feldspar microlites and opaque oxides.

Finally, Malpaís Prieto is not only the youngest but also the smallest of the studied lava flows. It is quite thick (~90 m) and covers an area of 5.7 km^2 with a volume of $\sim 0.5 \text{ km}^3$. As its name implies (*prieto* means dark colored in Spanish), its rough blocky surface is pitch black and resembles a moonscape, being almost devoid of vegetation. Just from its appearance, it can be judged that it must be one of the youngest lava flows in the entirety of Michoacán. Its composition ($\text{SiO}_2 = 61.5\text{--}62.8$ wt.%) is quite similar to Malpaís Las Víboras and El Capaxtiro and also contains plagioclase, pargasitic hornblende (mostly opacite), augite, and hypersthene phenocrysts in a glassy matrix with abundant feldspar microlites and opaque oxides.

Finally, it is worth mentioning that rounded quartz grains (1 mm in size) with reaction coronas of augite, as well as 1- to 2-mm partially resorbed plagioclase crystals displaying polysynthetic twinning are ubiquitous in all lavas. They are in disequilibrium and xenocrystic in origin. We suspect that they either stem from shallow Tertiary plutons or from younger shallow partly crystallized silicic magma chambers from which they were incorporated by ascending mafic magmas as attested by the forsteritic olivines found in the Infiernillo lavas. All of these observations point toward a complex petrologic origin of these monogenetic magmas,

as indicated in various recent studies elsewhere in the MGVF (e.g. Rasoazanamparany et al., 2016).

Environmental and archeological background

The lake basins of Michoacán have been of interest for their archeological records. It seems that favorable aquatic and riparian conditions attracted early nomadic humans and promoted the development of agriculture in this region, which eventually became a major dwelling hub for the Pre-Hispanic Tarascan populations. Also known as *Purépechas*, the Tarascans erected around Lake Pátzcuaro one of the largest Mesoamerican empires during the late Post-Classic period, prior to the conquest by the Spaniards. The Tarascans and their predecessors resided mostly near riverine valleys and lakes (O'Hara et al., 1993; Pollard, 1993, 2012), including the area of the Zacapu basin. In this context, several archeological excavations (e.g. Arnauld et al., 1994; Arnauld and Faugère-Kalfon, 1998; Michelet and Carot, 1998; Michelet et al., 2005; Pereira, 2005) have been undertaken within the basin. At the same time, and in order to define the environmental factors that fostered the rise of human civilization in this region, paleoclimate studies focusing on the analysis of the lake sediments (and particularly on their microfossil contents) have been carried out (e.g. Metcalfe, 1992, 1995; Newton et al., 2005; Pétrequin, 1994; Telford et al., 2004; Xelhuantzi-López, 1994). Although particular attention has been paid to the Holocene, some of these records go back as far as 52,000 yr BP (e.g. Correa-Metrio et al., 2012; Metcalfe and Harrison, 1984; Ortega-Guerrero et al., 2002; Tricart, 1992). These studies indicate that the extent and depth of the lake Zacapu have changed over time and that conditions even turned marshy during the late Pleistocene (Ortega-Guerrero et al., 2002; Tricart, 1992). The lake possessed a natural shallow discharge toward the North (Siebe et al., 2012) until it was artificially drained in the late 19th century to gain fertile land for agricultural purposes (Noriega and Noriega, 1923).

Archeological investigations carried out in the Zacapu area since the early 1980s within the frame of the Michoacán Project (Michelet, 1992; Michelet et al., 1989) have documented a human occupation sequence that starts around 100 BC and continues until the conquest by the Spaniards. Figure 4 shows the ages of ceramics found in 18 excavation sites, which indicates continuous occupation between AD 550 and about AD 1550, with a clear interruption between AD 900 and 1250. These studies as well as more recent investigations that initiated in 2010 under the umbrella of the Uacusecha archeological project show that the Malpaís de Zacapu area was densely populated during the middle/late Pre-Classic (AD 1250–1450). Surface prospection as well as the acquisition of a high-resolution light detection and ranging (LIDAR) image indicates that the Infiernillo, Capaxtiro, and Malpaís Prieto lava flows were occupied by four large urban settlements. The remains of thousands of domestic units as well as 50 ceremonial complexes with pyramidal mounds are still observable (Forest, 2014; Michelet, 1998; Migeon, 1998; Pereira et al., in press). These recent archeological studies also show important demographic fluctuations, which probably correspond to migration events (Arnauld et al., 1993; Arnauld and Faugère-Kalfon, 1998; Pereira et al., 2013). As discussed further on it is possible that some of these ruptures in the history of the pre-Hispanic settlements could be related to episodes of volcanic activity in this area.

Sampling procedures

The four lava flows were sampled at 21 different sites in order to check the within-flow paleomagnetic consistency (e.g. Böhnell

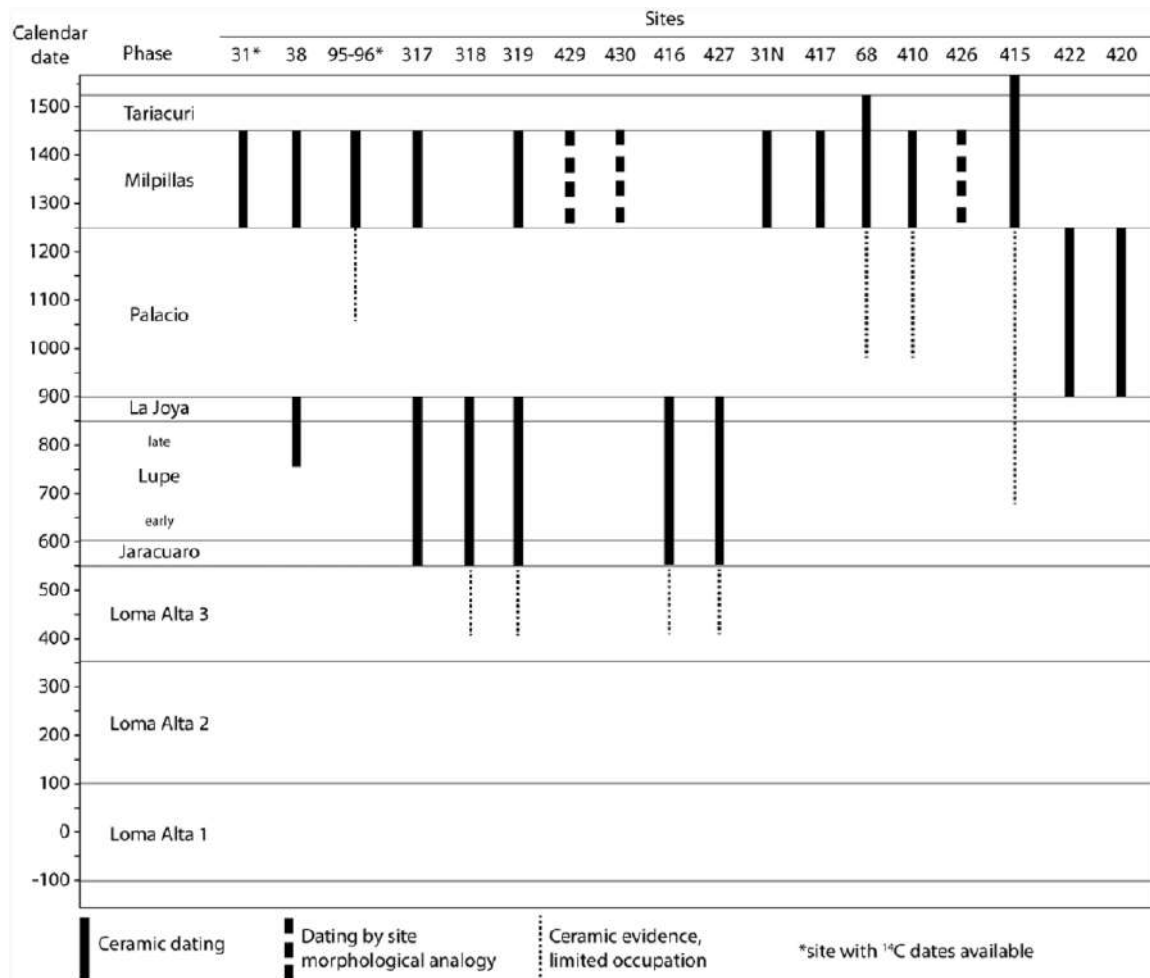


Figure 4. Time-graph showing pre-Hispanic human occupation as revealed by systematic excavations at different sites around the Malpaís de Zacapu area (modified after Michelet, 1992, with new data obtained during the ongoing Uacusecha archeological project). Site 31 is located on the Malpaís Prieto. Note the sudden abandonment of several sites around AD 900, followed by a hiatus that lasted 350 years until AD 1250.

et al., 2016; Hagstrum and Champion, 1994; Speranza et al., 2006). Sites are listed in Table 1, and their distribution is shown in Figure 2. No road cuts exhibiting the interior of the flows were found, and field observations indicate that their thickness ranges from 10 to almost 200 m with blocky surfaces and prominent marginal levées. Finding suitable drilling sites where the lava was in situ since it cooled down was, therefore, not an easy task. In order to avoid erroneous site mean directions due to moved blocks, multiple sites distributed as far as possible from each other were sampled from each flow. Based on the above, sampling was carried out with a gasoline-powered drill with a 25-mm diamond drill bit. Cores were between ~8 and 15 cm long and oriented using both magnetic and sun compasses to check for local magnetic anomalies (e.g. blocks struck by lightning). The difference between the magnetic and sun readings did not exceed 9° with an average of ~4°. From the four flows, a total of 141 cores (21 sites) were sampled representing an average of 7 cores per site with a minimum and maximum of 5 and 14, respectively.

Laboratory experiments

In the laboratory, it is customary to cut each drill core into several specimens 22 mm in length, providing at least three specimens. In order to obtain reliable mean paleomagnetic direction measurements of the lava flows, one specimen from every drill core was utilized. Low-field volume susceptibility (k) was measured for each specimen using a susceptibility meter (MS2B, Bartington Instruments Ltd), and remanence magnetization measurements were made with an AGICO JR-5 spinner magnetometer (noise

level $\sim 5 \times 10^{-6} \text{ A m}^{-1}$). The direction of the characteristic remanence directions (ChRM) was determined by means of stepwise progressive alternating field (AF) demagnetization. For AF demagnetization, an AGICO LDA-3 equipment was used, and the samples were demagnetized in 14 steps: 3, 5, 7, 10, 15, 20, 25, 30, 40, 50, 60, 70, 80, and 90 mT. Demagnetization results were analyzed with the aid of the program PMGSC 4.2 (Enkin, 2005). For statistical analysis and graphical representation of the data, the program PMag Tool 4.2b by Mark W. Hounslow was used. Characteristic remanence directions were calculated applying principal component analysis (PCA) as described by Kirschvink (1980). The site mean directions were determined using statistical procedures delineated by Fisher (1953). Thermomagnetic curves ($T_{\text{max}} = 650^\circ\text{C}$) were done on two cores per flow in order to define their magnetic mineralogy configuration and thermal stability. For paleointensity (PI) determinations, we carried out double-heating Thellier experiments (Thellier and Thellier, 1959), using the IZZI protocol (Tauxe and Staudigel, 2004), which combines the in-field/zero-field (Aitkin et al., 1988) and zero-field/in-field (Coe, 1967) protocols. Both partial TRM (pTRM) checks (Coe, 1967) and pTRM tail checks (Riisager and Riisager, 2001) were executed in order to analyze the reliability of the forthcoming results. PI experiments were conducted with an ASC Scientific TD48 furnace. Temperature steps used were 100°C, 200°C, 250°C, 300°C, 340°C, 370°C, 400°C, 430°C, 460°C, 490°C, 510°C, 530°C, 560°C, and 580°C. pTRM checks were done at 100°C, 250°C, 340°C, 400°C, 460°C, and 510°C, while pTRM tail checks were done at 250°C, 340°C, 400°C, 460°C, 510°C, and 560°C. Results of the IZZI-Thellier data were analyzed using

Table 1. Site mean paleomagnetic directions: latitude and longitude of the sampling coordinates.

Site	Latitude (°N)	Longitude (°W)	<i>n</i>	<i>N</i>	<i>k</i>	α_{95}	Dec	Inc
El Infiernillo (Inf)								
Inf1	19°51'27.5"	101°50'35.1"	10	10	103.39	4.8	359.1	53.6
Inf2	19°51'27.7"	101°50'29.8"	6	7	438.94	3.2	359.6	50
Inf3	19°51'36.4"	101°49'36.5"	5	7	64.25	9.6	348.6	50.7
Mean	Core Level		21	24	102.71	3.2	356.7	52
	Site Level		3	3	350.2	6.6	355.7	51.5
Malpais Las Viboras (Mlv)								
Mlv1	19°51'25.6"	101°52'16.8"	8	10	111.56	5.3	2.7	18.3
Mlv2	19°51'29.0"	101°52'14.8"	3	5	2179.34	2.6	6.5	18
Mlv3	19°51'31.4"	101°52'13.8"	4	5	764.22	4	5.1	18.5
Mlv4	19°50'40.6"	101°52'15.6"						
Mlv5	19°50'32.4"	101°52'07.4"	10	10	227.64	3.2	357.1	18.2
Mlv6	19°50'35.9"	101°52'12.0"						
Mean	Core Level		25	30	157.42	2.3	1.3	18.3
	Site Level		4	4	423.25	4.5	2.9	18.3
Capaxtiro (Cpx)								
Cpx1	19°49'22.8"	101°48'51.8"	6	6	73.08	7.9	317.9	29.7
Cpx2	19°49'20.5"	101°48'55.7"	6	7	103.19	6.6	350.8	29.5
Cpx3	19°49'23.3"	101°48'56.5"	6	7	79.38	7.6	346.5	28.9
Cpx4	19°49'23.8"	101°48'56.2"	3	3	248.29	7.8	2.5	37.3
Cpx5	19°49'24.3"	101°48'56.0"	4	4	184.14	6.8	347.2	27.1
Cpx6	19°49'21.2"	101°48'55.6"	5	5	337.22	4.2	338.5	32.3
Cpx7	19°49'20.2"	101°48'55.7"						
Mean	Core Level		24	26	73.54	3.5	353	30.7
	Site Level		5	5	95.22	7.9	348.9	31.2
Malpais Prieto (Mps)								
Mps1	19°53'40.6"	101°48'47.5"	5	10	334.37	4.2	357.7	25.4
Mps2	19°53'38.4"	101°48'51.6"	6	8	66.3	8.3	38	18.6
Mps3	19°53'41.6"	101°48'43.7"	5	8	211.51	5.3	356.6	26.4
Mps4	19°53'43.0"	101°48'44.6"	11	14	195.96	3.3	356.5	28.1
Mps5	19°53'27.4"	101°49'1.54"						
Mean	Core level		21	32	230.21	2.1	356.8	27
	Site level		3	3	2958.94	2.3	356.9	26.6

n: number of samples used in the calculation of the site mean direction; *N*: total number of samples measured; *k*: precision parameter; α_{95} : 95% confidence level; Dec: declination; Inc: inclination.

Shaded gray rows represent rejected sites or sites where no meaningful site mean could be calculated (for interpretation, see text). Results on site level are shaded in light blue color.

the ThellierTool4.11 software (Leonhardt et al., 2004). In order to judge the credibility of our PI estimates, acceptance criteria sets A and B as given in the Thellier tool (Leonhardt et al., 2004) with the modifications of Paterson et al. (2014) were used in this study.

Results

Rock-magnetic analyses

Figure 5 shows the variation of the natural remanent magnetization (NRM) intensity and magnetic susceptibility for the 21 studied sites, together with lines of constant Königsberger's factor *Q*. From the three sites of El Infiernillo, we observe that both Inf1 and Inf2 have similar NRM intensities and susceptibilities (Figure 5a).

Together they have a geometrical average NRM intensity of 8.80 A m⁻¹ (excluding one specimen with NRM < 1 A m⁻¹) and an average susceptibility of 24.4 × 10⁻³ (SI). For Inf3, we observe that the susceptibility is nearly half of the aforementioned sites but has approximately the same NRM intensities. Most of the Infiernillo specimens have *Q* values between 6 and 28 (Figure 5a). In contrast, Malpaís Las Viboras sites display a large scatter in NRM intensity values, while their susceptibility values are coherent (Figure 5b). Sites Mlv4 and Mlv5 have the highest and lowest NRM intensities, respectively. For all sites, susceptibility values are on geometrical average 10.9 × 10⁻³ (SI). In this context, it is worth noting that sites Mlv1, Mlv2, Mlv3, and Mlv6 were sampled roughly along the same level (middle part of the lava exposures),

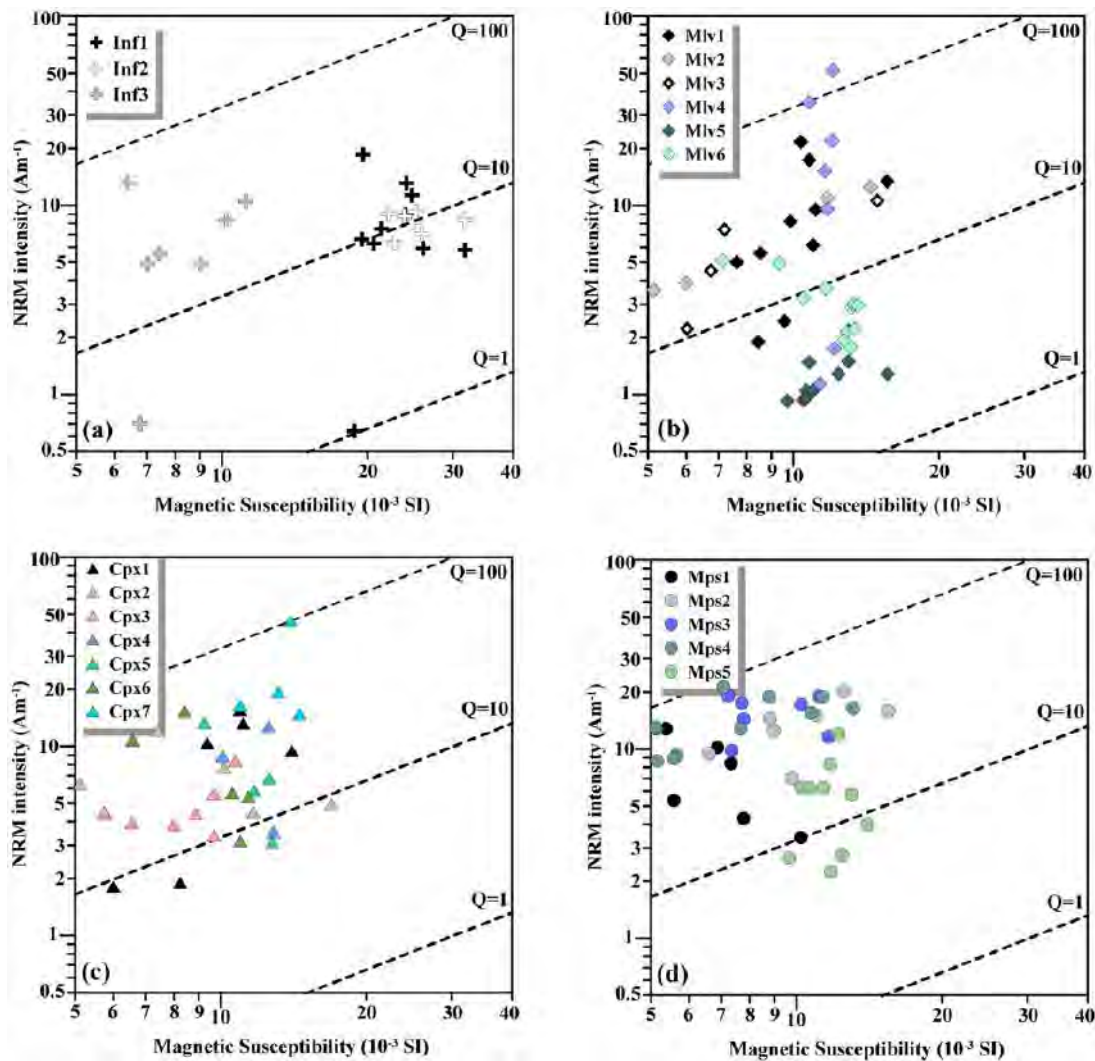


Figure 5. Variation of NRM intensity and magnetic susceptibility for the four studied lava flows. Dashed lines define constant values of Königsberger's factor Q .

Mlv4 was sampled from the uppermost part, while Mlv5 samples were taken from the lowermost part. Therefore, their NRM intensities may have resulted from cooling-rate disparities. The cooling rate was lower in Mlv5 samples and lead to the growth of larger pseudo-single-domain (PSD) to multi-domain (MD) magnetic grains. However, the presence of small PSD to single-domain (SD) grain sizes is expected from Mlv4 samples because of their relatively faster cooling rate. However, near-surface Mlv4 samples might have also been affected by lightning strikes, which produce strong isothermal remanence magnetizations (IRMs), which may account for rather high Q values. In comparison with Malpaís Las Víboras, much smaller scatter in the NRM intensities is noticeable in the Capaxtiro sites, in particular considering that samples were obtained at different levels within the lava exposures (Figure 5c). Average values for the NRM intensity and susceptibility are 9.0 A m^{-1} and $10.2 \times 10^{-3} \text{ (SI)}$. Both properties together define Q values between 10 and 100 (Figure 5c), with the possibility of lightning strikes affecting sample Cpx7. Finally, convergent values were observed in Malpaís Prieto samples (Figure 5d) with average NRM intensity and susceptibility values of 11.2 A m^{-1} and $9.3 \times 10^{-3} \text{ (SI)}$, respectively. Most Malpaís Prieto specimens have Q values ranging between 10 and 100 (Figure 5d).

Thermomagnetic analyses indicate the presence of two types of behaviors with characteristic Curie temperatures (T_c) and distinctive degree of reversibility between the heating and cooling curves (Figure 6). Samples of type A were characterized by single, high Curie temperature ($T_c \sim 530\text{--}560^\circ\text{C}$) and with a decrease

<10% in magnetization upon cooling to room temperature (Figure 6a). This behavior is typical for Ti-poor titanomagnetite, which partially oxidized during heating. We note that type A was observed in seven out of eight cores. Thermomagnetic curve of type B (I core) points to the presence of both Ti-rich ($T_c \sim 300\text{--}330^\circ\text{C}$) and Ti-poor ($T_c \sim 500\text{--}540^\circ\text{C}$) titanomagnetite minerals (Figure 6b). During cooling, the low- T_c component was largely suppressed, probably by exsolution of this mineral, which produced low-Ti titanomagnetite, with a slight increase in the room temperature magnetization.

Paleomagnetic directions

In order to obtain reliable information on the flow mean directions, one specimen of every drill core (total of 141) was utilized. The direction of the ChRM was defined for each sample using PCA (Kirschvink, 1980; program PMGSC 4.2). Predominantly, the ChRM directions have been calculated by 7–10 vector end points and are characterized by maximum angular deviation (MAD) values between 3.2° (few specimens from El Infiernillo and Capaxtiro) and 0.5° and often $<1^\circ$. Flow mean directions on core level and site level were calculated using Fisher statistics (Fisher, 1953, using PMag Tools Version 4.2) and are listed in Table 1.

For El Infiernillo, we point out that single components of magnetization were recorded in most of the investigated cores (Figure 7a, Inf2-5z). Samples displaying this behavior have relatively high

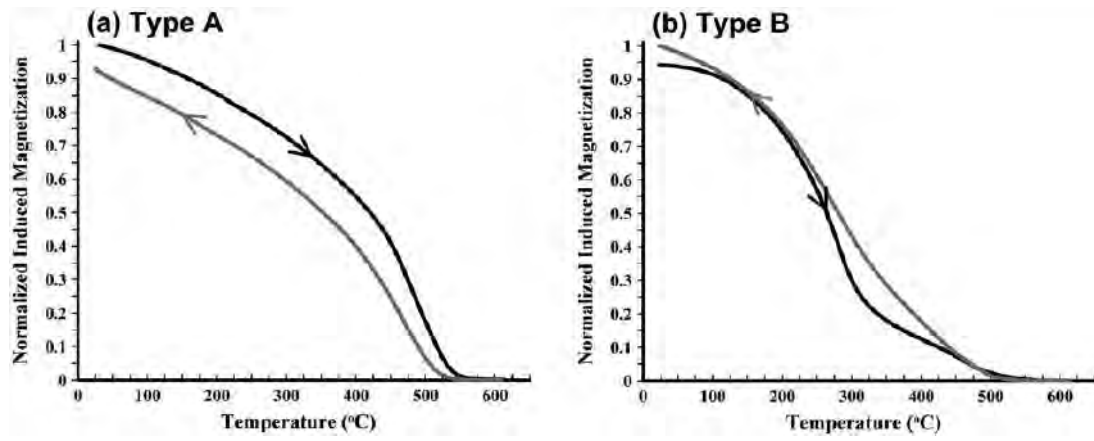


Figure 6. Two types of thermomagnetic curves: (a) type A and (b) type B. Black and gray curves indicate heating and cooling curves, respectively.

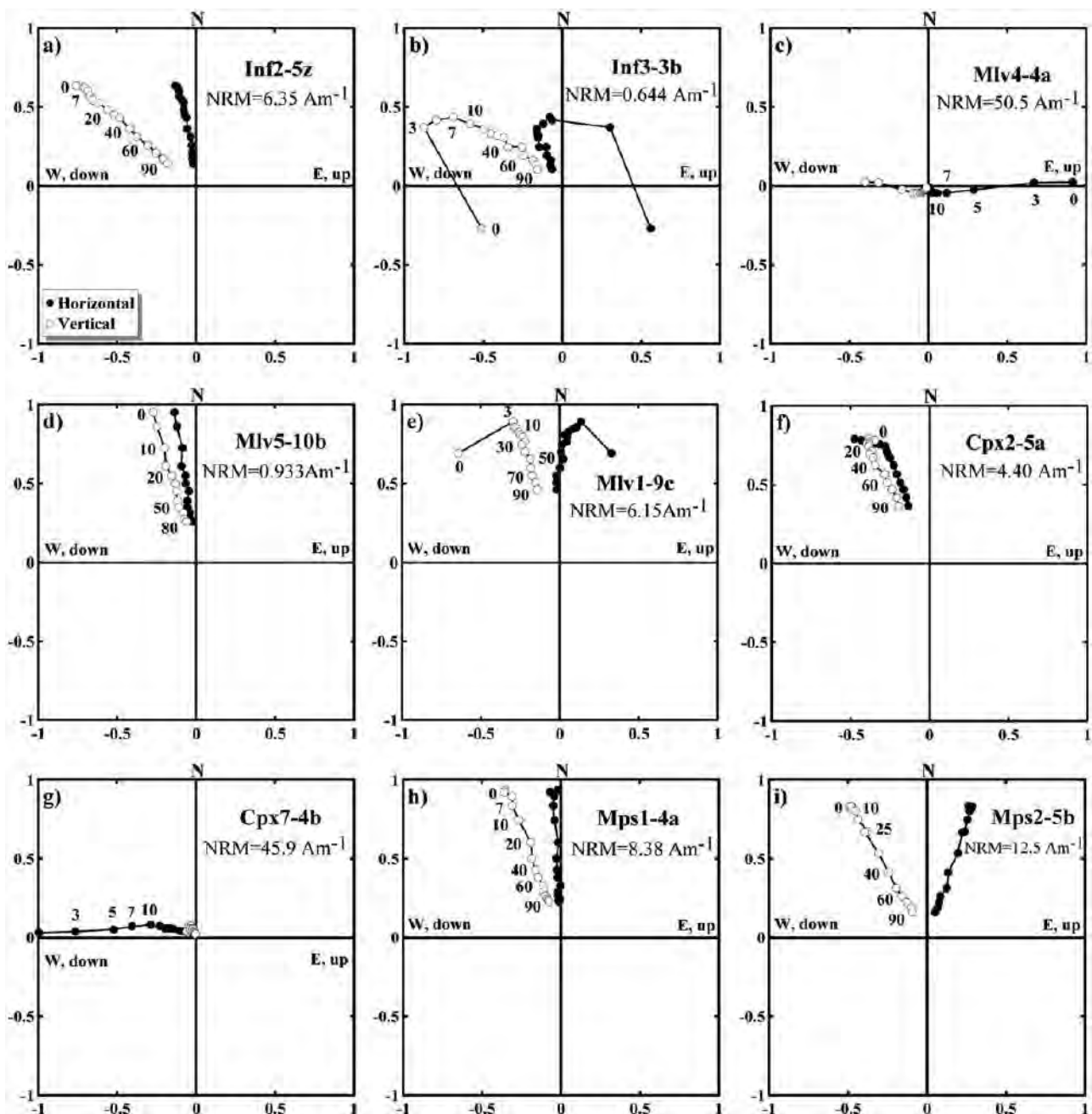


Figure 7. Orthogonal vector plots of AF demagnetized samples from the four studied lava flows. Labels along curves denote the maximum AF amplitude applied during the demagnetization steps. (a, b) El Infiernillo, (c, d, e) Malpaís Las Viboras, (f, g) Capaxitiro, and (h, i) Malpaís Prieto.

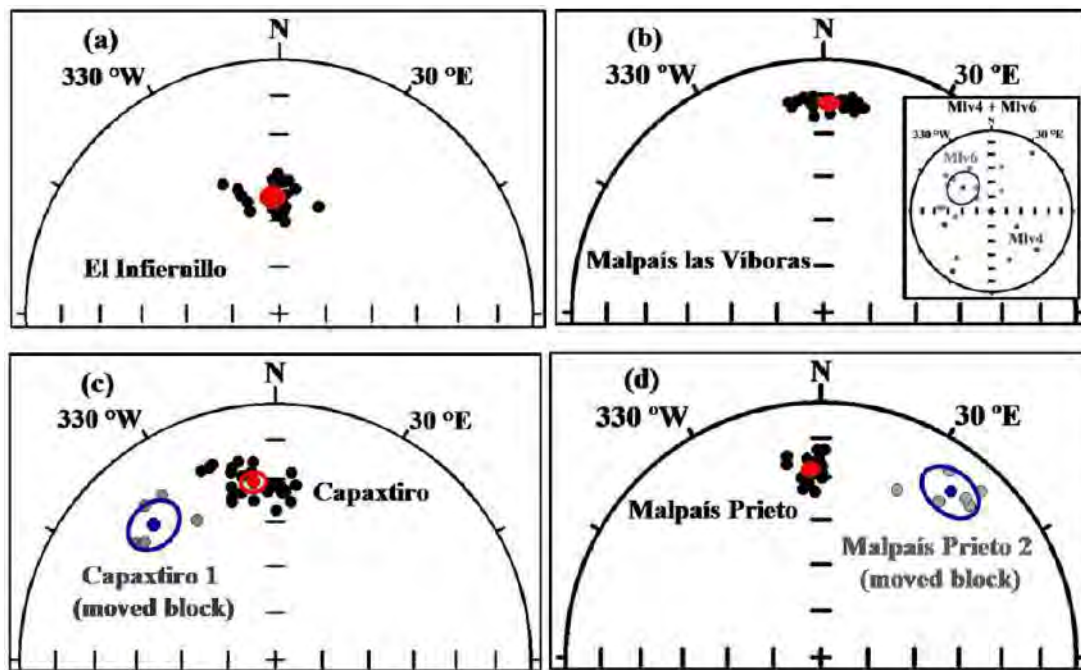


Figure 8. Characteristic remanent magnetization directions for the four lava flows. Inset in (b) shows the dispersed ChRM directions of Mlv4 (green) and Mlv6 (gray; for interpretation, see text). (a) El Infiernillo, (b) Malpaís Las Víboras, (c) Capaxtiro, and (d) Malpaís Prieto.

median destructive fields (MDFs) of 40–55 mT. Few specimens of Inf3 showed minor secondary magnetization components that are probably of viscous origin and were removed by AF amplitudes of 5–10 mT (see Inf3-3b in Figure 7b). An overall flow mean direction was determined from all three sites of the El Infiernillo flow: Dec = 356.7°, Inc = 52.0°, and α_{95} = 3.2° (Table 1 and Figure 8a).

In regard to the Malpaís Las Víboras flow, no results were obtainable from site Mlv4 where we note that all seven specimens show large secondary components during the demagnetization. It is important to mention that some specimens of this site were also characterized by high Q values indicating lightning strike effects (see strong magnetic overprint in Figure 7c). Although individual demagnetization diagrams were stable and of high quality (small MAD values for the best fits), we could not obtain a site mean direction as the ChRM were strongly scattered (see inset in Figure 8b). At site Mlv6, all 11 specimens yielded dispersed ChRM directions (which probably was related to moved blocks) with a site mean direction of high α_{95} = 16.5° (Table 1 and inset in Figure 8b). Thus, it is clear that directions provided by both sites are not reliable and were not included in the calculation of the flow mean direction. Univectorial magnetization trends toward the origin were observed in most samples from Mlv2, Mlv3, and Mlv5 (see Mlv5-10b in Figure 7c). Their MDFs range from 45 to 60 mT. In most cases, samples from Mlv1 have a small viscous component that was easily removed by AF amplitudes of 3–7 mT (Mlv1-9c in Figure 7d). Varying MDF values displayed by samples from this site point toward the simultaneous presence of soft and hard magnetic minerals. These four sites have similar ChRM directions (Table 1) and define an overall flow mean direction with a low dispersion: Dec = 1.3°, Inc = 18.3°, and α_{95} = 2.3° (Figure 8b).

In the case of Capaxtiro, five sites (Cpx2, Cpx3, Cpx4, Cpx5, and Cpx6) were used to calculate the flow mean direction (Table 1). At these sites, a small percentage of samples show low-stability secondary components probably of recent origin that were easily removed by AF amplitudes of 5–15 mT (Cpx2-5a in Figure 7e). These samples have relatively high MDF of 50–70 mT. No site mean direction could be calculated for Cpx7 because it was probably affected by lightning strike and/or moved blocks (see Cpx7-4b in Figure 7g). Cpx1 gave a site mean direction with a relatively large uncertainty of α_{95} = 7.9° (Table 1), which is also

significantly different from the site mean directions calculated from the aforementioned sites. After excluding Cpx1 (shaded row in Table 1, gray dots in Figure 8c), we were able to obtain a well-defined flow mean direction for Capaxtiro (Dec = 353.0°, Inc = 30.7°, and α_{95} = 3.5°).

Most sites of Malpaís Prieto are characterized by a single-component NRM (Figure 7g and h). Samples from these sites show similar NRM intensities, susceptibilities (Figure 4d), and MDFs of 30–45 mT during AF demagnetization. ChRM directions calculated for sites Mps1, Mps3, and Mps4 are very similar and define a flow mean direction with a lower dispersion (Dec = 356.8, Inc = 27, and α_{95} = 2.1°; see Table 1 and Figure 8d). However, site Mps2 displays a more easterly and dispersed mean direction (Dec = 38, Inc = 18.6, and α_{95} = 8.3°; gray dots in Figure 8d). Hence, we deduce that Mps2 samples were obtained from moved blocks and that, therefore, their ChRM directions are not reliable and were thus rejected. Because of the dense vegetation, it was difficult to determine during fieldwork whether this site contained displaced blocks. For Mps5, no site mean direction was obtained, as all ChRM directions were highly dispersed.

Paleointensities

IZZI-Thellier PI experiments were conducted on 40 samples obtained from the four lava flows. Pre-selection of specimens was done based on two criteria: (1) specimens from the same drill core must possess a single-component NRM during demagnetization, and (2) specimens must show a relatively high MDF of >20 mT. Laboratory fields of 50 or 60 μ T were applied during heating and cooling of infield steps. According to Biggin (2010) and Paterson et al. (2015), the greater the angle between the laboratory field and the primary NRM, the greater the influence of MD grain size. Therefore, inside the oven, selected specimens for PI measurements were oriented so that their NRM directions would be parallel to the applied field with a precision better than 5°. Representative examples of successful Arai plots are shown in Figure 9a and b. PI results for each flow are listed in Table 2 together with different quality parameters. The Arai plots of accepted specimens yielded well-constrained straight lines with 6–14 data points (N), the fractions factor (f) ranges from 39% to

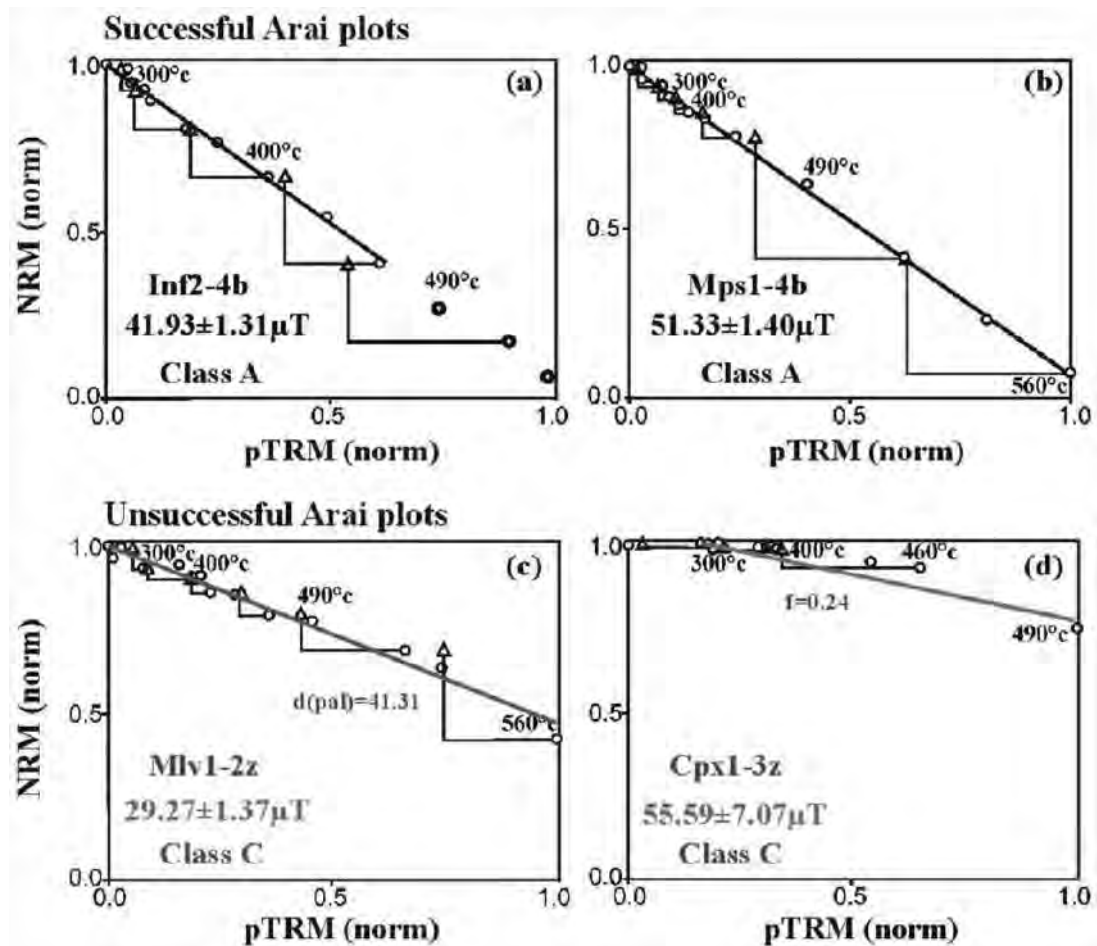


Figure 9. Examples of (a, b) successful and (c, d) unsuccessful paleointensity (Arai) plots for the four lava flows obtained by the IZZI version of the Thellier method. NRM and pTRM are normalized. NRM versus pTRM data are shown as circles, with the black best-fit line. pTRM checks are shown as triangles. The analyses were carried out using ThellierTool.

96%, and the quality parameter (q) varies between 6.50 and 76.9. In regard to the directional variations during the PI experiments, the ChRM produced MADs (MADanc; anc = anchored to the origin) between 4.1° (Inf1-8b) and 1.5° (Mlv2-4z; Table 2). This range is only slightly higher than the MAD range obtained during the AF demagnetization. In total, 20 specimens passed the Thellier tool A or B acceptance criteria resulting in an overall success rate of 50%. But when compared for the different flows, samples from Malpaís Las Víboras have the highest success rate (70%) while those from Capaxtiro have the lowest (40%) success rate. In most cases, failure of the test was due to alteration that resulted from the repeated heating steps as indicated by the pTRM cumulative check difference (dpal) criterion (Figure 9c). A few samples from Capaxtiro failed the test because the fraction of unblocked NRM was too small as indicated by the fraction (f) factor (Figure 9d). More importantly, our investigated samples did not show sagging in the Arai plots, which in turn mean that the MD effect was absent or has been suppressed, as suggested by Biggin (2010) and Paterson et al. (2015).

Paleomagnetic dating

To date, a well-constrained regional paleosecular variation curve for central Mexico for the last few millennia, suitable for paleomagnetic dating, does not exist. For this reason, we used the global model SHA.DIF.14k (Pavón-Carrasco et al., 2014), which was developed by using archeomagnetic and lava flow data obtained from sites around the globe, including Central America, Mexico, and the United States, covering the last 14 millennia. Paleomagnetic dating was carried out with the help of the MATLAB tool

archaeo_dating (Pavón-Carrasco et al., 2011). In a recent paleomagnetic dating study (Böhnel et al., 2016), this model was successfully applied on two lava flows from Ceboruco volcano in western Mexico. This motivated us to use this dating technique on the four lava flows under consideration in this study. Knowledge of the age of El Infiernillo (1525–1420 cal. BC, see above) together with the paleo-direction and intensity data listed in Tables 1 and 2 allows constraining the time interval of archeomagnetic dating to the period 2000 BC to AD 1900. For the paleomagnetic dating, flow mean directions on the core level were used, as individual sites were sampled with variable numbers of cores and also showed large variations of within site dispersion: in the case of the El Infiernillo flow the number of ChRM directions varied between 5 and 10, and precision parameters k between 64.25 and 438.94. For the other flows, similar variations were observed. The use of unweighted site mean directions would overestimate those sites with small number of ChRM directions and/or large dispersion. Finally, the number of sites per flow is small for all flows (three or four sites), and only for Capaxtiro, five site means are available. As all sites could be assigned beyond any doubt to the corresponding lava flow, the dispersion of the individual ChRM directions should be caused by random processes (e.g. Böhnel and Schnepf, 1999), and the overall mean then may also average out minor block movements that may have occurred along the lava flow. Thus, we argue that the use of individual ChRM directions for calculating a flow mean direction is justified in this specific situation. Nevertheless, in Table 1, we list both flow mean directions, and it is evident that in most cases, the uncertainty σ_5 based on site mean directions is about twice compared with that based on individual ChRM directions. The exception is Malpaís Prieto, where both

Table 2. The Thellier-IZZI paleointensity results and associated statistics.

Site	<i>N</i>	<i>T</i>	<i>f</i>	<i>g</i>	<i>q</i>	MAD _{anc}	α	δ CK	δ pal	δ TR	δt^*	Class	PI	σ (μ T)
El Infiernillo (Inf)														
1-3b	8	0–400	0.82	0.75	7.77	1.93	3.38	6.41	7.36	3.73	2.18	A	35.31	2.80
1-8b	10	0–460	0.58	0.87	6.50	4.06	10.5	2.31	1.65	2.93	1.64	A	51.56	4.04
2-1b	13	0–530	0.94	0.89	53.9	1.99	0.17	6.53	3.02	1.92	4.07	A	38.70	0.60
2-4b	10	0–460	0.39	0.85	10.8	1.64	2.76	3.63	0.63	2.80	4.91	A	41.93	1.31
Mean													41.87	6.99
Malpaís Las Viboras (Mlv)														
2-2z	13	100–560	0.79	0.54	10.1	2.95	4.77	1.74	2.56	3.70	1.43	A	30.45	1.30
2-4z	6	430–560	0.63	0.77	11.4	1.52	1.31	5.43	6.20	3.99	0.32	A	28.08	1.20
5-6z	11	0–490	0.52	0.85	9.77	1.44	2.90	6.03	8.07	4.35	1.18	A	31.32	1.54
5-8a	12	0–510	0.59	0.86	8.97	1.67	2.06	3.46	0.34	5.29	0.19	A	24.61	1.39
5-9a	14	0–560	0.91	0.84	12.9	2.71	2.02	4.06	1.59	14.2	2.08	B	19.14	1.14
5-10a	14	0–560	0.94	0.83	12.3	1.57	1.67	3.21	3.71	6.09	1.05	A	18.86	1.20
5-11z	14	0–560	0.94	0.79	9.88	2.01	1.11	4.85	0.96	14.3	0.39	B	18.02	1.35
Mean													24.35	5.73
Capaxtiro (Cpx)														
2-3a	11	0–490	0.72	0.81	21.5	2.43	3.82	3.65	3.01	14.2	2.36	B	50.50	1.8
2-5b	11	0–490	0.77	0.84	25.4	2.51	4.21	4.21	2.57	15.6	1.47	B	48.50	1.20
5-3a	11	0–490	0.75	0.80	29.5	1.98	3.31	3.76	2.48	6.49	1.37	A	44.20	0.90
6-2b	11	0–490	0.76	0.78	22.3	3.64	4.91	2.61	2.98	2.92	0	A	41.00	1.09
Mean													46.05	4.27
Malpaís Prieto (Mps)														
1-4b	14	0–560	0.77	0.79	22.5	2.45	0.86	2.06	1.57	8.79	7.0	A	51.33	1.40
1-7b	9	340–560	0.89	0.75	30.4	1.72	1.94	4.18	7.05	10.6	2.35	B	48.22	1.06
1-8a	9	340–560	0.67	0.86	24.1	2.43	4.29	4.24	9.43	6.43	3.36	A	48.01	1.14
3-2a	14	0–560	0.96	0.82	35.6	2.27	0.71	3.25	4.72	8.35	1.78	A	50.85	1.12
3-4b	14	0–560	0.93	0.84	76.9	2.07	1.37	4.18	9.13	8.60	9.77	B	49.64	0.51
Mean													49.61	1.50

N: number of points included in the linear best fit; *T*: the temperature ranges used for the best fit; *f*: fraction of the natural remanent magnetization (NRM); *g*: the *gab* factor; *q*: quality factor; MAD_{anc}: anchored maximum angular deviation; α : angular difference between anchored and nonanchored best solution; δ CK: relative check error; δ pal: cumulative check difference; δ TR: tail check; δt^* : normalized tail of pTRM; PI: paleointensity; σ (μ T): standard deviation.

overall mean directions have a very similar α_{95} . Moreover, in each flow, the site mean directions were statistically evaluated using the *F*-distribution test (McFadden and Lowes, 1981) in order to analyze their directional independence at the 95% confidence level. Applying the *F*-test on El Infiernillo sites proved that the site mean directions are indistinguishable at the 95% confidence, which is also valid for the Malpaís Prieto sites. In contrast, the *F*-test applied to Malpaís Las Viboras mean directions shows that they are different at the 95% confidence. It is likely that the difference in declination values of Mlv5 is the main cause of this negative outcome, but we also note that some specimens of Mlv1 have similar declinations as Mlv5. Applying the *F*-test on the Capaxtiro also reveals that the site mean directions are different at the 95% probability level. Previous studies (e.g. Hagstrum and Champion, 1994) have shown that such differences between site mean directions of the same lava flow may occur, due to a number of possibly contributing factors. In case of this study, these are most likely due to undetected relative movements between different sites. Therefore, we attribute these within-flow paleomagnetic variations to the natural dispersion (see Böhnell and Schnepp, 1999). As no information is available regarding the most reliable site mean direction, we assume that the overall mean directions calculated from all individual directions may best correspond to the accurate paleomagnetic direction of that particular flow. The flow mean direction calculated this way has a larger uncertainty, which thus will only increase the range of the resulting paleomagnetic dating age. In conclusion, we consider the flow mean paleomagnetic directions calculated for Malpaís Las Viboras and Capaxtiro to be reliable within the obtained confidence limits and to be acceptable input data for the paleomagnetic dating procedure which will provide an age range on the safe side.

Paleomagnetic dating provided for El Infiernillo a well-constrained age range of 1500–1370 BC (Figure 10a; to take into account the limitations of this dating method, here we will round up the ages to the nearest 10 years). This age range matches well the calibrated radiocarbon age range and lends further credibility to the paleomagnetic dating method. Using the mean direction based on site means (Table 1) would increase the age range to 1590–1360 BC, and additional possible age ranges of 1800–1700 BC, AD 10–60, AD 300–650, and AD 1890–1900 would result. Even then, there would be an agreement between the C-14 age and one of the possible paleomagnetic ages. Based on the stratigraphy, the three other lava flows are younger than El Infiernillo, and for their paleomagnetic dating, we constrained the time interval of their emplacement to the period 1500 BC to AD 1900. Two narrow age ranges of 1340–1230 BC and 1030–940 BC (Figure 10b) were obtained for the Malpaís Las Viboras. This means that it erupted shortly after or up to 600 years after El Infiernillo. For Capaxtiro and Malpaís Prieto, two ages were obtained in both cases. Based on the stratigraphic relationships between these flows, it can be proposed that Capaxtiro erupted within the period 200–80 BC (Figure 11a), followed by Malpaís Prieto during the interval AD 830–960 (Figure 11b). The age range of this youngest flow would remain almost unchanged when using the mean direction based on site means for the dating.

Discussion

Rock-magnetic studies were carried out on the four flows under study in order to demonstrate the NRM stability and also to define the magnetic carriers and thermal stability, which is crucial for the PI experiments. These studies revealed significant differences

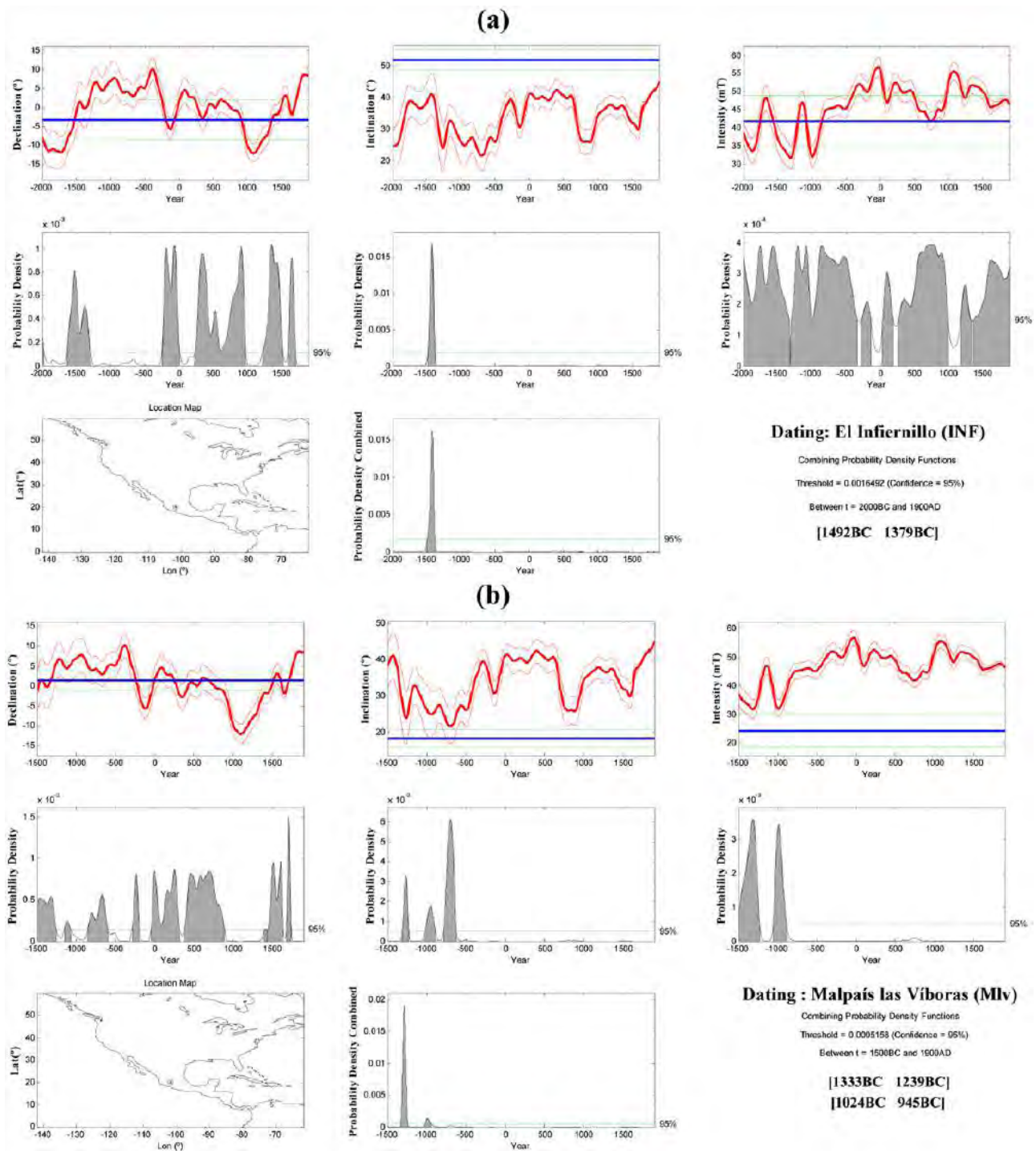


Figure 10. Paleomagnetic dating of (a) El Infiernillo and (b) Malpaís Las Víboras. The combined probability density derived from the declination, inclination, and PI data is shown as shaded peaks and the minimum (95%) confidence level by horizontal green lines.

between the studied lavas in terms of their bulk magnetic properties (NRM intensities and susceptibilities). It was also observed that each studied flow showed variations of these properties to different degrees. Malpaís Las Víboras shows the largest disparities in its values, whereas Capaxtiro and Malpaís Prieto display a greater coherency. This is probably due to differences in composition and crystal size and to processes such as lightning strikes affecting the TRM. As a whole, their Königsberger's factors were located within the $100 > Q > 10$ domain, which indicates the high NRM stability over geological time periods and its suitability for paleomagnetic dating. Thermomagnetic analyses showed that stable Ti-poor titanomagnetite is the predominant magnetic mineral in these lavas. This conclusion is admittedly based on a limited number of samples, but a more detailed rock-magnetic study was beyond the main goal of this study.

As mentioned above, for most sites, ChRM directions could be determined. Nevertheless, some sites had to be eliminated because either these directions were dispersed, or they differed strongly from other sites of the same flow. Mean directions of accepted sites correlate well within their confidence limits. The mean directions for the four lava flows used for paleomagnetic dating are always based on the ChRM directions of all accepted samples from that flow, but in Table 1, we also indicate for comparison mean directions based on the site mean directions, which are very similar but have a larger σ_{95} . We always used individual directions, as there was no doubt that the corresponding sites belong to one single lava flow.

In the case of El Infiernillo lava flow, site Inf3 has a more westerly mean direction than Inf1 and Inf3, but this site also has a larger dispersion with a σ_{95} of 9.6° , which makes this difference

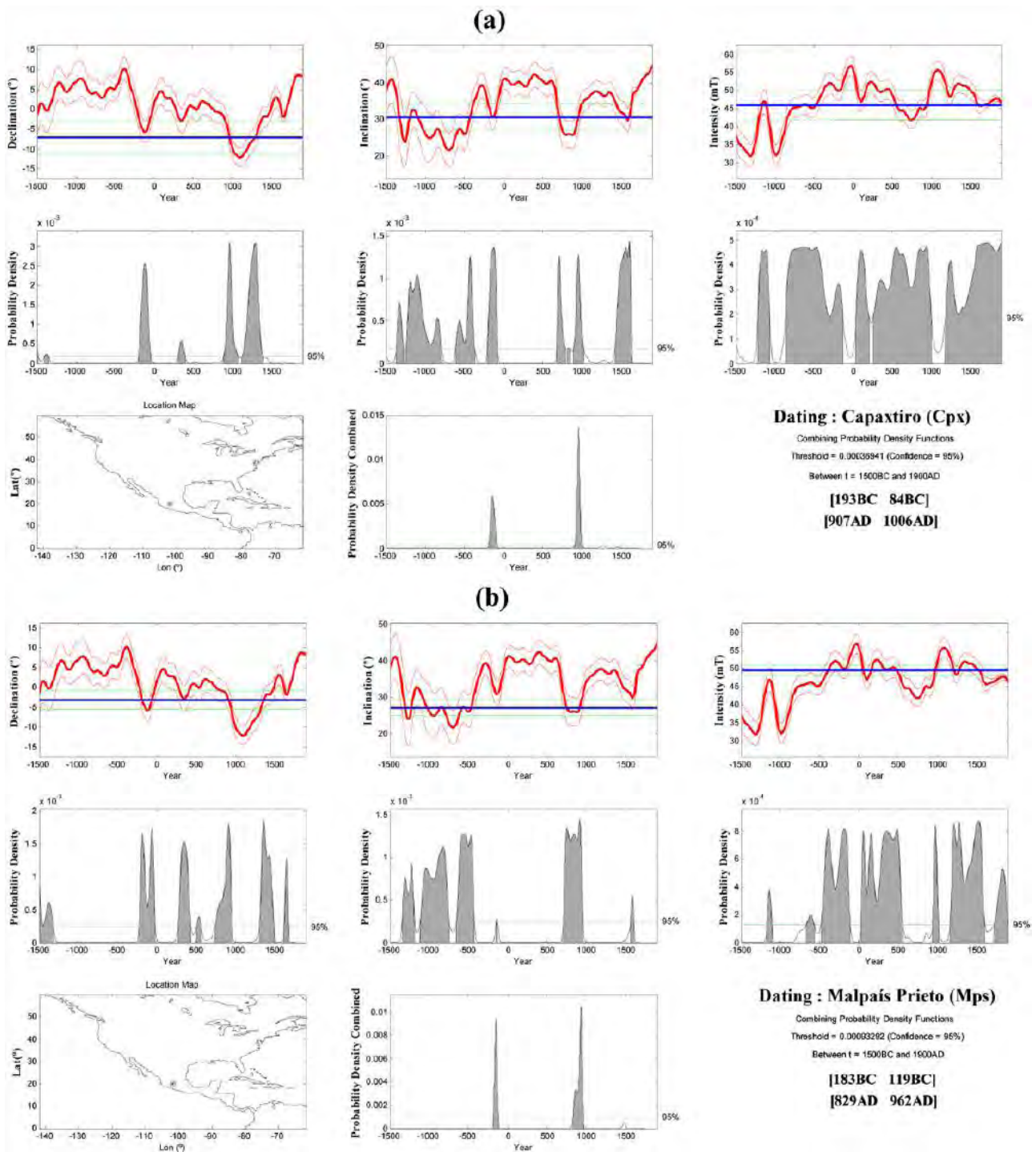


Figure 11. Paleomagnetic dating of (a) Capaxtiro and (b) Malpaís Prieto. For further details, see caption of Figure 9.

insignificant. Site Mlv4 from Malpaís Las Víboras seems to have been affected by lightning strike, as indicated by high Q values, and ChRM directions were dispersed, and no site mean was determined. Partly, this dispersion may be also the effect of moved blocks, which is also suspected for site Mlv6. Both sites were rejected for further analysis. Hence, the overall mean direction for Malpaís Las Víboras is based on four sites, which are distributed over a distance of more than 2 km. For the Capaxtiro lava flow, six out of seven sites yielded well-defined ChRM directions (Table 1). Five sites (Cpx2 to Cpx6) distributed over a distance of ~120 m gave consistent site mean directions, whereas nearby site Cpx1 (less than 10 m away) has a significantly different direction, most probably representing a moved block. Cpx7 has large Q values and seems to be affected by lightning strike, and hence, its site mean direction was not determined. The overall flow mean direction is, therefore, based on five sites distributed over a distance of

about 120 m. From the above, it seems that Cpx1 could represent a moved block and, therefore, was excluded from the overall flow mean calculations. Similarly, for Malpaís Prieto, two of five sites had to be rejected: Mps5 had dispersed ChRM directions and was sampled from several apparently moved blocks. Mps2 directions are less dispersed but define a significantly divergent mean direction compared to the rest of the flows. ChRM directions calculated from Mps1, Mps3, and Mps4 are concordant and best represent the Malpaís Prieto lava flow mean direction. These experiences lead us again to emphasize the utmost importance of sampling lava flow units at multiple sites and over the largest possible distance, as already suggested by Böhnel et al. (2016).

El Infiernillo was studied in this work in order to validate the archeomagnetic dating method by using the global model SHA. DIF.14k. Among the four studied lava flows, this flow is stratigraphically the oldest with a ^{14}C age of cal. 1525–1420 BC. The

concordant paleomagnetic age of 1500–1370 BC thus suggests that this volcano erupted during the early Pre-Classic, and its birth was certainly observed by early settlers in this region. Malpaís Las Víboras erupted shortly or up to 560 years after El Infiernillo, incrementing the volcanic impact on the Middle Pre-Classic local societies. The voluminous Capaxtiro lava flows were emplaced about 740–1260 years after the Malpaís Las Víboras, during the late Pre-Classic. This would imply a large disruption for the more evolved human communities inhabiting these lands. Approximately 910–1160 years later, between AD 830 and 960 (during the late Classic period), the Malpaís Prieto flow erupted. Then, extended settlements were distributed all over central Mexico, and while this lava flow covered a much smaller area than the previous volcanoes, it must have had an important impact on these more developed and extended societies. Regarding recurrence rates of volcanic eruptions, these varied around 1000 years, with the exception of Malpaís Las Víboras, which erupted much sooner after El Infiernillo. If these recurrence rates are valid, another eruption could happen soon.

The different eruptions that formed the Malpaís de Zacapu probably had an impact on the settlement process, provoking displacements within the Zacapu basin area. In regard to the Infiernillo and Las Víboras eruptions, it is difficult to assess their repercussions on early/middle Pre-Classic populations because archeological evidence for that time is still lacking. But with respect to the Capaxtiro eruption (dated here at 200–80 BC), it is interesting to note that it coincides with the earliest archeological sequence in the Zacapu basin, the Loma Alta phase, dated at 100 BC to AD 400. During this phase, a series of islets known as Las Lomas just east of the Capaxtiro lavas were densely inhabited (Arnauld et al., 1993). So far, we can only guess that a direct relation may exist between the Capaxtiro eruption and the rise of the important site of Loma Alta.

Finally, in the case of the Malpaís Prieto eruption, more consistent data are available in regard to its possible impact on local populations. Recent excavations and surveys around this lava flow show that the area was densely populated between AD 500–800/900 (six important sites have been reported so far). All of these sites were abandoned abruptly at the end of this period, which was then followed by a hiatus that lasted from AD 900–1250. Hence, a close relationship between this eruption and the abandonment of the area is quite likely. Around AD 1250, the Malpaís de Zacapu becomes again an important population hub. We note here that many population centers in Mesoamerica collapsed around AD 900–1000, a phenomenon that has been explained by famine due to the effects of long-term regional droughts (e.g. Bhattacharya et al., 2015; Hodell et al., 2005). In the case of Malpaís de Zacapu such a climate-related impact on ancient societies remains to be proven, while the possible volcanic impact is hard to deny in light of the above-mentioned evidence.

Conclusion

Lava flows from four different Holocene monogenetic eruptions collectively known as Malpaís de Zacapu (El Infiernillo, Malpaís Las Víboras, Capaxtiro, and Malpaís Prieto, in stratigraphic succession) located at the western margin of the Zacapu lacustrine basin in Michoacán were subjected to paleomagnetic dating. Because this region (including the surface of the lava flows) was inhabited since at least the Pre-Classic and eventually became part of the heartland of the Tarascan Empire during the Post-Classic, it was desirable to determine the timing of these eruptions and whether they could have impacted human development, that is, by triggering population migrations. Only the oldest eruption, El Infiernillo, could be dated by the radiocarbon method, which yielded an age of cal. 1525–1420 BC. A total of 21 sites distributed as far as possible were sampled from four lava flows in order to provide

reliable paleomagnetic site mean directions which are not affected by blocks that moved after they acquired their remanence or by lightning strike-induced remagnetizations. Flow mean directions are of small dispersion with $2.1 \leq \alpha_{95} \leq 3.5$. Robust estimates of flow mean PIs were obtained by using the IZZI-Thellier method. Full-vector paleomagnetic results were used for paleomagnetic dating applying the MATLAB tool `archaeo_dating` and the global paleosecular variation model SHA.DIF.14k. For El Infiernillo, the dating resulted in an age ranging 1500–1370 BC (95% probability level) which coincides well with the radiocarbon age data, and both correspond to the early Pre-Classic period. For the next younger lava flow of Malpaís Las Víboras, a possible age between 1340 and 940 BC was obtained, corresponding to the Middle Pre-Classic, and reflecting the sustained volcanic activity in this region, which may have affected the ancient population. After 740–1260 years of quiescence, the voluminous lava flows of Capaxtiro were emplaced between 200 and 80 BC during the late Pre-Classic, implying a disaster for communities living nearby. This period coincides with the rise of the important site of Loma Alta in the lowlands east of Capaxtiro. Finally, between AD 830 and 960 and during the late Classic period, Malpaís Prieto erupted, which apparently led to the abandonment of the heavily populated surrounding lava flows as observed in archeological profiles which indicate that this happened around AD 800–900. Long drought periods as observed in eastern Mexico and the Yucatán peninsula might have amplified the volcanic impact. Finally, recurrence periods center around 1000 years in this area and thus indicate that another monogenetic eruption might occur in the near future. This work shows that future volcanic hazard mitigation efforts could benefit from results obtained from interdisciplinary studies that include archeological research.

Funding

Ing. J. Escalante supported studies with the Curie balance. Field and laboratory costs of ANM and HB were covered by Consejo Nacional de Ciencia y Tecnología (CONACyT-180032) and the Dirección General de Asuntos del Personal Académico (UNAM-DGAPA IN-111915) granted to HB and for NR-G and CS were defrayed from projects funded by the Consejo Nacional de Ciencia y Tecnología (CONACyT-167231) and the Dirección General de Asuntos del Personal Académico (UNAM-DGAPA IN-101915) granted to CS. We thank Américo González-Esparza, Adriana Briseño, and Ernesto Andrade at UNAM Campus Morelia for providing lodging facilities at the Mexican Array Radio Telescope (MEXART) near Coeneo during field campaigns. The archaeological investigations carried out in the Zacapu region were funded by the French Ministère des Affaires Étrangères et du Développement International (Mission Archéologique Uacusecha) as well as by the Agence Nationale de la Recherche (Programme Mesomobile).

References

- Aitken MJ, Allsop AL, Bussell GD et al. (1988) Determination of the intensity of the Earth's magnetic-field during archaeological times – Reliability of the Thellier technique. *Reviews of Geophysics* 26(1): 3–12.
- Arnauld C and Faugère-Kalfon B (1998) Evolución de la ocupación humana en el Centro-Norte de Michoacán (Proyecto Michoacán, CEMCA) y la emergencia del Estado Tarasco. In: Darras V (ed.) *Génesis, culturas y espacios en Michoacán*. México: CEMCA, pp. 13–34.
- Arnauld C, Carot P and Fauvet-Berthelot MF (1993) *Arqueología de Las Lomas en la cuenca lacustre de Zacapu, Michoacán, México*. Cuaderno de Estudios Michoacanos 5. México: CEMCA.
- Arnauld C, Carot P and Fauvet-Berthelot MF (1994) Introducción. In: Pétrequin P (ed.) *8000 años de la Cuenca de Zacapu*.

- Evolución de los paisajes y primeros desmontes* (Collection Etudes Méso-américaines II-14). México: CEMCA, pp. 9–28.
- Arrighi S, Tanguy JC and Rosi M (2006) Eruptions of the last 2200 years at Vulcano and Vulcanello (Aeolian Islands, Italy) dated by high-accuracy archaeomagnetism. *Physics of the Earth and Planetary Interiors* 159(3): 225–233.
- Ban M, Hasenaka T, Delgado-Granados H et al. (1992) K-Ar ages of lavas from shield volcanoes in the Michoacán-Guanajuato volcanic field, México. *Geofísica Internacional* 31(4): 467–473.
- Beekman CR (2010) Recent research in western Mexican archaeology. *Journal of Archaeological Research* 18(1): 41–109.
- Bhattacharya T, Byrne R, Böhnell H et al. (2015) Cultural implications of Late-Holocene climate change in the Cuenca Oriental, Mexico. *Proceedings of the National Academy of Sciences* 112(6): 1693–1698.
- Biggin AJ (2010) Are systematic differences between thermal and microwave Thellier-type palaeointensity estimates a consequence of multidomain bias in the thermal results? *Physics of the Earth and Planetary Interiors* 180(1): 16–40.
- Blatter DL and Hammersley L (2010) Impact of the Orozco fracture zone on the central Mexican Volcanic Belt. *Journal of Volcanology and Geothermal Research* 197(1): 67–84.
- Bloxham J and Jackson A (1992) Time-dependent mapping of the magnetic field at the core-mantle boundary. *Journal of Geophysical Research: Solid Earth* 97(B13): 19537–19563.
- Böhnell H and Schnepf E (1999) Precision of the paleomagnetic method: An example from the Quaternary Eifel volcanics (Germany). *Earth, Planets and Space* 51(6): 403–412.
- Böhnell H, Pavón-Carrasco FJ, Sieron K et al. (2016) Palaeomagnetic dating of two recent lava flows from Ceboruco volcano, western Mexico. *Geophysical Journal International* 207(2): 1203–1215.
- CALIB Computer Program (version 7.1) (n.d.) Available at: <http://radiocarbon.pa.qub.ac.uk/calib/calib.html>.
- Carmichael ISE (2002) The andesite aqueduct: Perspectives on the evolution of intermediate magmatism in west-central (105–99° W) Mexico. *Contributions to Mineralogy and Petrology* 143(6): 641–663.
- Cassidy J (2006) Geomagnetic excursion captured by multiple volcanoes in a monogenetic field. *Geophysical Research Letters* 33: L21310.
- Chevrel MO, Guilbaud M-N and Siebe C (2016a) The AD 1250 effusive eruption of El Metate shield volcano (Michoacán, Mexico): Magma source, crustal storage, eruptive dynamics, and lava rheology. *Bulletin of Volcanology* 78(4): 1–28.
- Chevrel MO, Siebe C, Guilbaud M-N et al. (2016b) The AD 1250 El Metate shield (Michoacán): Mexico's most voluminous Holocene eruption and its significance for archaeology and hazards. *The Holocene* 26(3): 471–488.
- Coe RS (1967) Paleo-intensities of the Earth's magnetic field determined from Tertiary and Quaternary rocks. *Journal of Geophysical Research* 72(12): 3247–3262.
- Corona-Chávez P, Reyes-Salas M, Garduño-Monroy VH et al. (2006) Asimilación de xenolitos graníticos en el Campo Volcánico Michoacán-Guanajuato: el caso de Arócutin Michoacán, México. *Revista Mexicana de Ciencias Geológicas* 23(2): 233–245.
- Correa-Metrio A, Lozano-García S, Xelhuantzi-López S et al. (2012) Vegetation in western Mexico during the last 50,000 years: Modern analogs and climate in the Zacapu basin. *Journal of Quaternary Science* 27(5): 509–518.
- Demant A (1978) Características del Eje Neovolcánico Transmexicano y sus problemas de interpretación. *Revista Mexicana de Ciencias Geológicas* 2(2): 172–187.
- Demant A (1992) Marco geológico regional de la laguna de Zacapu, Michoacán, México. In: Demant D, Labat J-N, Michelet D et al. (eds) *El Proyecto Michoacán 1983–1987. Medio ambiente e introducción a los trabajos arqueológicos* (Collection Etudes Mésoaméricaines II-11). México: CEMCA, pp. 53–72.
- Enkin R (2005) *PMGSC 4.2*. Sidney: Geological Survey of Canada.
- Faugère B (ed.) (2006) *Cueva de los Portales. Un sitio arcaico del norte de Michoacán, México* (Colección Científica). México: INAH/CEMCA.
- Ferrari L, Orozco-Esquivel T, Manea V et al. (2012) The dynamic history of the Trans-Mexican Volcanic Belt and the Mexico subduction zone. *Tectonophysics* 522: 122–149.
- Fisher RA (1953) Dispersion on a sphere. *Proceedings of the Royal Society of London, Series A: Mathematical, Physical and Engineering Sciences* 127: 295–305.
- Forest M (2014) *Approches spatio-archéologiques de la structure sociale des sites urbains du Malpaís de Zacapu*. PhD Dissertation, Université de Paris 1 – Panthéon/Sorbonne.
- Garduño-Monroy VH, Pérez-López R, Israde-Alcantara I et al. (2009) Paleoseismology of the southwestern Morelia–Acambay fault system, central Mexico. *Geofísica Internacional* 48(3): 319–335.
- Gómez-Tuena A, LaGatta AB, Langmuir CH et al. (2003) Temporal control of subduction magmatism in the eastern Trans-Mexican Volcanic Belt: Mantle sources, slab contributions, and crustal contamination. *Geochemistry, Geophysics, Geosystems* 4(8). DOI: 10.1029/2003GC000524.
- Guilbaud M-N, Siebe C, Layer P et al. (2011) Geology, geochronology, and tectonic setting of the Jorullo Volcano region, Michoacán, México. *Journal of Volcanology and Geothermal Research* 201(1): 97–112.
- Guilbaud M-N, Siebe C, Layer P et al. (2012) Reconstruction of the volcanic history of the Tacámbaro-Puruarán area (Michoacán, México) reveals high frequency of Holocene monogenetic eruptions. *Bulletin of Volcanology* 74(5): 1187–1211.
- Hagstrum JT and Blinman E (2010) Archeomagnetic dating in western North America: An updated reference curve based on paleomagnetic and archeomagnetic data sets. *Geochemistry, Geophysics, Geosystems* 11(6). DOI: 10.1029/2009GC002979.
- Hagstrum JT and Champion DE (1994) Paleomagnetic correlation of Late Quaternary lava flows in the lower east rift zone of Kilauea Volcano, Hawaii. *Journal of Geophysical Research: Solid Earth* 99(B11): 21679–21690.
- Hasenaka T and Carmichael ISE (1985) The cinder cones of Michoacán-Guanajuato, central Mexico: Their age, volume and distribution, and magma discharge rate. *Journal of Volcanology and Geothermal Research* 25(1): 105–124.
- Hasenaka T and Carmichael ISE (1987) The cinder cones of Michoacán-Guanajuato, central Mexico: Petrology and chemistry. *Journal of Petrology* 28(2): 241–269.
- Hodell DA, Brenner M and Curtis JH (2005) Terminal Classic drought in the northern Maya lowlands inferred from multiple sediment cores in Lake Chichancanab (Mexico). *Quaternary Science Reviews* 24(12): 1413–1427.
- Jackson A, Jonkers AR and Walker MR (2000) Four centuries of geomagnetic secular variation from historical records. *Philosophical Transactions of the Royal Society of London, Series A: Mathematical, Physical and Engineering Sciences* 358(1768): 957–990.
- Johnson CA and Harrison CGA (1990) Neotectonics in Central Mexico. *Physics of the Earth and Planetary Interiors* 64(2–4): 187–210.
- Kim Y, Miller MS, Pearce F et al. (2012) Seismic imaging of the Cocos plate subduction zone system in central Mexico. *Geochemistry, Geophysics, Geosystems* 13(7). DOI: 10.1029/2012GC004033.

- Kirschvink JL (1980) The least-squares line and plane and analysis of palaeomagnetic data. *Geophysical Journal of the Royal Astronomical Society* 62(3): 699–718.
- Korte M and Constable CG (2003) Continuous global geomagnetic field models for the past 3000 years. *Physics of the Earth and Planetary Interiors* 140(1): 73–89.
- Korte M and Constable CG (2005) The geomagnetic dipole moment over the last 7000 years – New results from a global model. *Earth and Planetary Science Letters* 236(1): 348–358.
- Korte M and Constable CG (2011) Improving geomagnetic field reconstructions for 0–3ka. *Physics of the Earth and Planetary Interiors* 188(3): 247–259.
- Korte M, Donadini F and Constable CG (2009) Geomagnetic field for 0–3 ka: 2. A new series of time-varying global models. *Geochemistry, Geophysics, Geosystems* 10(6): Q06008. Available at: <http://dx.doi.org/10.1029/2008GC002297>.
- Kshirsagar P, Siebe C, Guilbaud M-N et al. (2015) Late Pleistocene Alberca de Guadalupe maar volcano (Zacapu basin, Michoacán): Stratigraphy, tectonic setting, and paleo-hydrogeological environment. *Journal of Volcanology and Geothermal Research* 304: 214–236.
- Kshirsagar P, Siebe C, Guilbaud M-N et al. (2016) Geological and environmental controls on the change of eruptive style (phreatomagmatic to Strombolian-effusive) of Late Pleistocene El Caracol tuff cone and its comparison with adjacent volcanoes around the Zacapu basin (Michoacán, México). *Journal of Volcanology and Geothermal Research* 318: 114–133.
- Leonhardt R, Heunemann C and Krása D (2004) Analyzing absolute paleointensity determinations: Acceptance criteria and the software ThellierTool4.0. *Geochemistry, Geophysics, Geosystems* 5(12): Q12016.
- McBirney AR, Taylor HP and Armstrong RL (1987) Paricutin re-examined: A classic example of crustal assimilation in calc-alkaline magma. *Contributions to Mineralogy and Petrology* 95(1): 4–20.
- McFadden PL and Lowes FJ (1981) The discrimination of mean directions drawn from Fisher distributions. *Geophysical Journal of the Royal Astronomical Society* 67: 19–33.
- Metcalfe SE (1992) *Changing Environments of the Zacapu Basin, Central Mexico: A Diatom-Based History Spanning the Last 30,000 Years*. Research Paper No. 48. Oxford: School of Geography, University of Oxford, 38 pp.
- Metcalfe SE (1995) Holocene environmental change in the Zacapu Basin, Mexico: A diatom based record. *The Holocene* 5(2): 196–208.
- Metcalfe SE and Harrison SP (1984) *Cambio ambiental del Cuaternario Tardío en depósitos lacustres en la cuenca de Zacapu, Michoacán. Reconstrucción Preliminar* (Boletín del Instituto de Geografía, vol. 14). México: UNAM, pp. 127–151.
- Michelet D (1992) El Centro-Norte de Michoacán: características generales de su estudio regional. In: Demant D, Labat J-N, Michelet D and et al. (eds) *El Proyecto Michoacán 1983–1987. Medio ambiente e introducción a los trabajos arqueológicos*. México: CEMCA, pp. 9–52.
- Michelet D (1998) Topografía y prospección sistemática de los grandes asentamientos del Malpaís de Zacapu: claves para un acercamiento a las realidades sociopolíticas. In: Darras V (ed.) *Génesis, culturas y espacios en Michoacán*. México: CEMCA, pp. 47–59.
- Michelet D and Carot P (1998) Arqueología de la región de las cuencas lacustres de Michoacán (1946–1996). In: *XXIV Mesa Redonda sobre Antropología e Historia del Occidente de México*. México: Sociedad Mexicana de Antropología, pp. 497–537.
- Michelet D, Arnauld MC and Fauvet-Berthelot MF (1989) El proyecto del CEMCA en Michoacán. Etapa I: un Balance. *TRACE* 16: 70–87.
- Michelet D, Pereira G and Migeon G (2005) La llegada de los uacúsechas a la región de Zacapu, Michoacán: datos arqueológicos y discusión. In: Manzanilla L (ed.) *Reacomodos demográficos del Clásico al Posclásico en el centro de México*. México: IIA, UNAM, pp. 137–153.
- Migeon G (1998) El poblamiento del Malpaís de Zacapu y de sus alrededores del Clásico al Posclásico. In: Darras V (ed.) *Génesis, culturas y espacios en Michoacán*. México: CEMCA, pp. 36–45.
- Newton AJ, Metcalfe SE, Davies SJ et al. (2005) Late Quaternary volcanic record from lakes of Michoacán, central México. *Quaternary Science Reviews* 24(1): 91–104.
- Noriega E and Noriega A (1923) *La desecación de la ciénega de Zacapu y las leyes agrarias. Caso especial, único en el país*. México.
- O'Hara SI, Street-Perrott FA and Burt TP (1993) Accelerated soil erosion around a Mexican highland lake caused by Pre-Hispanic agriculture. *Nature* 362(6415): 48–51.
- Ortega-Guerrero B, Caballero C, Lozano-García S et al. (2002) 2,000 years of environmental history in Zacapu basin, Michoacán, Mexico: The magnetic record. *Earth and Planetary Science Letters* 202(3): 663–675.
- Pardo M and Suárez G (1995) Shape of the subducted Rivera and Cocos plates in southern Mexico: Seismic and tectonic implications. *Journal of Geophysical Research* 100(B7): 12357–12373.
- Pasquaré G, Ferrari L, Garduño VH et al. (1991) *Geology of the Central Sector of the Mexican Volcanic Belt, States of Guanajuato and Michoacán* (Maps and chart series MCH072, scale 1:300000, 1 sheet). Boulder, CO: Geological Society of America, 22 pp.
- Paterson GA, Biggin AJ, Hodgson E et al. (2015) Thellier-type paleointensity data from multidomain specimens. *Physics of the Earth and Planetary Interiors* 245: 117–133.
- Paterson GA, Tauxe L, Biggin AJ et al. (2014) On improving the selection of Thellier-type paleointensity data. *Geochemistry, Geophysics, Geosystems* 15(4): 1180–1192.
- Pavón-Carrasco FJ, Osete ML, Torta JM et al. (2009) A regional archeomagnetic model for Europe for the last 3000 years, SCHA.DIF.3K: Applications to archeomagnetic dating. *Geochemistry, Geophysics, Geosystems* 10(3): Q03013.
- Pavón-Carrasco FJ, Osete ML, Torta JM et al. (2014) A geomagnetic field model for the Holocene based on archaeomagnetic and lava flow data. *Earth and Planetary Science Letters* 388: 98–109.
- Pavón-Carrasco FJ, Rodríguez-González J, Osete ML et al. (2011) A Matlab tool for archaeomagnetic dating. *Journal of Archaeological Science* 38(2): 408–419.
- Pereira G (2005) The utilization of grooved human bones: A reanalysis of artificially modified human bones excavated by Carl Lumholtz at Zacapu, Michoacán, Mexico. *Latin American Antiquity* 16(3): 293–312.
- Pereira G, Michelet D and Migeon G (2013) La migración de los purépecha hacia el norte y su regreso a los lagos. *Arqueología Mexicana* 21(123): 55–60.
- Pereira G, Forest M, Jadot E et al. (in press) Ephemeral cities? The longevity of the Postclassic Tarascan urban sites of Zacapu Malpaís and its consequences on the migration process. In: Arnauld M-C, Beekman C and Pereira G (eds) *Ancient Mesoamerican Cities: Populations on the Move*. Boulder, CO: University Press of Colorado.
- Pétriquin P (1994) *8000 años de la cuenca de Zacapu* (Cuadernos De Estudios Michoacanos, vol. 6). México: Centre de Etudes Mexicaines et Centroaméricaines, 144 pp.
- Pollard HP (1993) *Tariácuri's Legacy: The Prehispanic Tarascan State*. Norman, OK: University of Oklahoma Press, 266 pp.
- Pollard HP (2012) The Tarascan empire. Postclassic social complexity in western Mexico. In: Nichols DL and Pool CA

- (eds) *The Oxford Handbook of Mesoamerican Archaeology*. Oxford: Oxford University Press, pp. 434–448.
- Rasoazanamparany C, Widom E, Siebe C et al. (2016) Temporal and compositional evolution of Jorullo volcano, Mexico: Implications for magmatic processes associated with a monogenetic eruption. *Chemical Geology* 434: 62–80.
- Riisager P and Riisager J (2001) Detecting multidomain magnetic grains in Thellier palaeointensity experiments. *Physics of the Earth and Planetary Interiors* 125(1): 111–117.
- Roperch P, Chauvin A, Lara LE et al. (2015) Secular variation of the Earth's magnetic field and application to paleomagnetic dating of historical lava flows in Chile. *Physics of the Earth and Planetary Interiors* 242: 65–78.
- Siebe C, Guilbaud M-N, Salinas S et al. (2012) Eruption of Alberca de los Espinos tuff cone causes transgression of Zacapu lake ca. 25,000 yr BP in Michoacán, Mexico. In: *4IMC Conference*, Auckland, New Zealand (20–24 February, 2012), Geoscience Society of New Zealand Miscellaneous Publication 131A, pp. 74–75 (Abstract volume).
- Siebe C, Guilbaud M-N, Salinas S et al. (2013) Comparison of the volcanic geology of the Tacámbaro-Puruarán (arc front) and the Zacapu (arc inland) areas in the Michoacán-Guanajuato volcanic field, Mexico. In: *IAVCEI 2013 Scientific Assembly*, Kagoshima, 20–24 July (Abstract volume).
- Siebe C, Guilbaud M-N, Salinas S et al. (2014) Monogenetic volcanism of the Michoacán-Guanajuato Volcanic Field: Maar craters of the Zacapu basin and domes, shields, and scoria cones of the Tarascan highlands (Paracho-Paricutin region). In: *Field Guide, Pre-Meeting Fieldtrip for the 5th International Maar Conference (5IMC-IAVCEI)*, Santiago de Querétaro, 13–17 November, 33 pp. Mexico DF: Instituto de Geofísica, Universidad Nacional Autónoma de México.
- Speranza F, Branca S, Coltelli M et al. (2006) How accurate is 'paleomagnetic dating'? New evidence from historical lavas from Mount Etna. *Journal of Geophysical Research: Solid Earth* 111(B12). DOI: 10.1029/2006JB004496.
- Speranza F, Pompilio M, D' Ajello Caracciolo F et al. (2008) Holocene eruptive history of the Stromboli volcano: Constraints from paleomagnetic dating. *Journal of Geophysical Research: Solid Earth* 113(B9). DOI: 10.1029/2007JB005139.
- Stuiver M and Reimer PJ (1993) Extended ¹⁴C database and revised CALIB radiocarbon calibration program. *Radiocarbon* 35: 215–230.
- Suter M, López-Martínez M, Quintero-Legorreta O et al. (2001) Quaternary intra-arc extension in the central Trans-Mexican volcanic belt. *Geological Society of America Bulletin* 113: 693–703.
- Tanguy JC, Le Goff M, Principe C et al. (2003) Archeomagnetic dating of Mediterranean volcanics of the last 2100 years: Validity and limits. *Earth and Planetary Science Letters* 211: 111–124.
- Tauxe L and Staudigel H (2004) Strength of the geomagnetic field in the Cretaceous Normal Superchron: New data from submarine basaltic glass of the Troodos Ophiolite. *Geochemistry, Geophysics, Geosystems* 5: Q02H06.
- Telford JT, Barker P, Metcalfe SE et al. (2004) Lacustrine responses to tephra deposition: Examples from Mexico. *Quaternary Science Reviews* 23(23–24): 2341–2357.
- Thellier E and Thellier O (1959) Sur l'intensité du champ magnétique terrestre dans le passé historique et géologique. *Annales de Geophysique* 15: 285–378.
- Tricart J (1992) La cuenca lacustre de Zacapu: Un acercamiento geomorfológico. In: Demant D, Labat J-N, Michelet D and et al. (eds) *El Proyecto Michoacán 1983–1987. Medio ambiente e introducción a los trabajos arqueológicos* (Collection Etudes Mésoaméricaines II-11). México: CEMCA, pp. 113–197.
- Watts WA and Bradbury JP (1982) Paleocological studies at Lake Patzcuaro on the west-central Mexican Plateau and at Chalco in the Basin of Mexico. *Quaternary Research* 17(1): 56–70.
- Wilcox RE (1954) Petrology of Paricutin volcano, Mexico. *United States Geological Survey Bulletin* 965C: 281–353.
- Xelhuantzi-López MS (1994) Estudio palinológico de cuatro sitios ubicados en la cuenca de Zacapu: fondo de la ciénega, contacto loma-ciénega, pantano interno y loma alta. *Cuadernos de Estudios Michoacanos* 6: 81–93.

5. Palaeomagnetic dating of two recent lava flows from Ceboruco volcano, western Mexico

Harald Böhnel,¹ Francisco Javier Pavon-Carrasco,¹ Katrin Sieron² and Ahmed Nasser Mahgoub¹

¹Centro de Geociencias, Universidad Nacional Autónoma de México (UNAM), Blvd. Juriquilla No. 3001, Querétaro, 76230, México

²Centro de Ciencias de la Tierra, Universidad Veracruzana, Francisco J. Moreno # 207, Col. Emiliano Zapata, C.P. 91090 Xalapa, Mexico

Accepted: Journal of the Geophysical Journal International, 207: 1203-1215(2016)

Individual contributions of the authors:

- i. **Harald Böhnel:** designing the study, field work, analyzing and interpreting of data, writing the article, financing for the project
- ii. **Francisco Javier Pavón-Carrasco:** field work, participating in the interpretation of data and revising the article
- iii. **Katrin Sieron:** designing the geological map, fieldwork, revising the article.
- iv. **Ahmed Nasser Mahgoub:** conducting paleointensity experiments, participating in the interpretation of data.

Palaeomagnetic dating of two recent lava flows from Ceboruco volcano, western Mexico

Harald Böhnell,¹ Francisco Javier Pavón-Carrasco,^{1,*} Katrin Sieron²
and Ahmed Nasser Mahgoub¹

¹Centro de Geociencias, Universidad Nacional Autónoma de México (UNAM), Blvd. Juriquilla No. 3001, Querétaro 76230, Mexico.

E-mail: hboehnel@geociencias.unam.mx

²Centro de Ciencias de la Tierra, Universidad Veracruzana, Francisco J. Moreno # 207, Col. Emiliano Zapata, C.P. 91090 Xalapa, Mexico

Accepted 2016 August 12. Received 2016 August 11; in original form 2015 December 7

SUMMARY

Two lava flows from the Ceboruco volcano in west-central Mexico were sampled for palaeomagnetic dating. The younger one was emitted in 1870 and used to validate the method, while the older one known as Ceboruco flow is of unknown age but probably younger than ~1005 AD and older than 1528 AD. Each flow was sampled in at least four sites, in order to unravel between site variations. For the 1870 flow, between site differences were notable and additionally post-cooling block movements were important; therefore, two sites had to be rejected. Three sites from the vent area and one at the tip of the 1870 flow provided well-constrained directions. This is also true for Ceboruco lava flow, and overall mean directions and palaeointensities were then used for palaeomagnetic dating applying the Matlab tool *archaeo_dating* and the global palaeosecular variation model SHA.DIF.14k. For the 1870 lava flow, the dating resulted in an age ranging between 1755 and 1871 AD (95 per cent probability level), which includes the real emplacement age. In addition, the Ceboruco lava flow was dated between 1000 and 1134 AD, which is close to the large plinian Jala eruption producing the crater of Ceboruco volcano around 1005 AD. This age is older than previously assumed and suggests an emplacement only shortly after the Jala eruption. As this lava flow is considered to be the youngest one of seven post-Jala lava flows, the age also defines a period of inactivity of Ceboruco volcano of about 730–860 yr before the historic 1870 eruption. Future volcanic hazard analysis will have to take into account this result. Our work also shows that multiple sampling of single lava flows is important to obtain a reliable mean direction. Sampling sites have to be carefully selected so that they represent un-tilted parts of the flows. We interpret this to be the case for the Ceboruco lava flow, while three of the six sites of the 1870 lava flow may have been partly or completely affected by movements after thermoremanent magnetization acquisition. Unfortunately, no better sites were found for this flow.

Key words: Palaeointensity; Palaeomagnetic secular variation; Palaeomagnetism applied to geologic processes; Volcanic hazards and risks.

1 INTRODUCTION

Palaeomagnetic dating is based on the comparison of the geomagnetic field recorded in suitable material of unknown age with a set of reference data of known age, established for the same geographical region, which are used to constrain the classical palaeosecular variation (PSV) master curves. During the last few decades, this method has been used increasingly for palaeomagnetic dating, using the

thermoremanent magnetization (TRM) produced in pottery or kilns during the last firing. The availability of detailed SV master curves for the last millennia (e.g. Gallet *et al.* 2002; Gómez-Paccard *et al.* 2006; Kovacheva *et al.* 2009; Hagstrum & Blinman 2010) has also allowed applying the same methodology for the dating of young lava flows that have been emplaced during the last few thousand years (e.g. Tanguy *et al.* 2003; Arrighi *et al.* 2006; Speranza *et al.* 2006, 2008; Hagstrum & Blinman 2010; Roperch *et al.* 2015). However, the palaeomagnetic dating presents some limitations (e.g. McIntosh & Catanzariti 2006; Pavón-Carrasco *et al.* 2011). The method strongly depends on the PSV master curve used for dating and how this curve has been constrained by well-dated

* Now at: Grupo de Paleomagnetismo, Universidad Complutense de Madrid, Avda. Complutense, s/n. E-28040 Madrid, Spain.

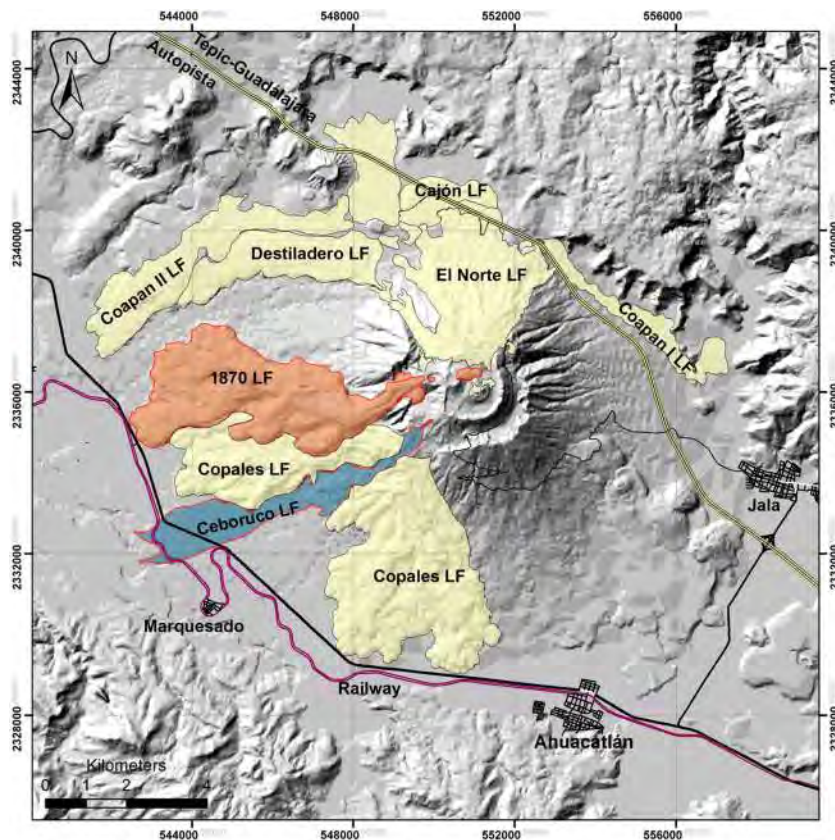


Figure 1. Digital elevation model of Ceboruco volcano, showing the pre-plinian Destiladero lava flow and the seven post-plinian lava flows, including the two dated lava flows (Ceboruco and 1870). Railway (pink), highway (yellow) from Guadalajara to Tepic to the N of Ceboruco and main toll-free roads (black) area also shown, as well as the most important villages.

palaeomagnetic data. In addition, the behaviour of the Earth's magnetic field itself, with cyclical values of declinations and inclinations, can provide several ages for the same volcanic event. These limitations clearly affect our results since, currently, no well-constrained PSV master curve for Mexico is available covering the last millennia. To solve this problem, we need to use a synthetic PSV curve calculated from a global palaeomagnetic model that has been developed by using all the palaeomagnetic data available all around the world.

Such dating is of interest for evaluating the volcanic hazard in active volcanic regions, which often are densely populated (e.g. Italy, Japan, Mexico, Central and South America, Hawaii, Azores and New Zealand). To be able to determine the actual volcanic hazard for a certain region, the eruptive history of the volcanoes must be completely known in order to permit calculating exact recurrence intervals of eruptions and hence the probability of occurrence. Dating lava flows by traditional methods often fails: for applying the ^{14}C dating method, charred organic material is required that unambiguously was produced by the emplacement of the lava flow. Searching for such carbon source has often been unsuccessful or leads to multiple ages that are younger or older than the lava emplacement and thus may be misinterpreted (e.g. Siebe *et al.* 2004).

Here, we report results from two lava flows from the Ceboruco volcano, western Mexico. One flow was emplaced shortly after the historic eruption in 1870, and the so-called Ceboruco flow is probably younger than 1005 AD and thus also of historic age, but older than the first arrival of Spanish conquerors at the region in 1528. No clear evidence was found about any pre-

Spanish historic records (Sieron & Siebe 2008). In this work, we use the 1870 lava to see how works the palaeomagnetic dating method in this region and then apply it to the Ceboruco flow with unknown age.

2 GEOLOGICAL HISTORY OF CEBORUCO VOLCANO

Ceboruco volcano is active since late Quaternary and has an andesitic cone built up mainly by effusive activity which is truncated by two summit craters. This first cone-constructing phase (Nelson 1980) ended approximately 45 ± 8 ka ago (Frey *et al.* 2004), as the age of a lava dyke inside the outer crater walls indicates, representing one of the youngest structures of the andesitic cone. After a longer phase of quiescence, Ceboruco volcano erupted violently (VEI 6) at 1005 ± 15 AD (details of this dating are found in Sieron & Siebe 2008; all ages denoted as AD are calibrated and calculated from ^{14}C ages), emitting $3\text{--}4$ km³ of magma (Gardner & Tait 2000) during the so-called plinian Jala eruption (Nelson 1980). This eruption included major changes in eruptive style and magma composition, compared to the first cone-constructing phase. During this catastrophic eruption, pumice fall-out was deposited mainly to the NE and associated pyroclastic flow and surge deposits were predominantly emplaced to the SW. The plinian Jala eruption produced the outer summit crater, while the inner crater was formed by the drainage of the voluminous Copales lava flow (Fig. 1) and subsequent collapse of the Dos Equis lava

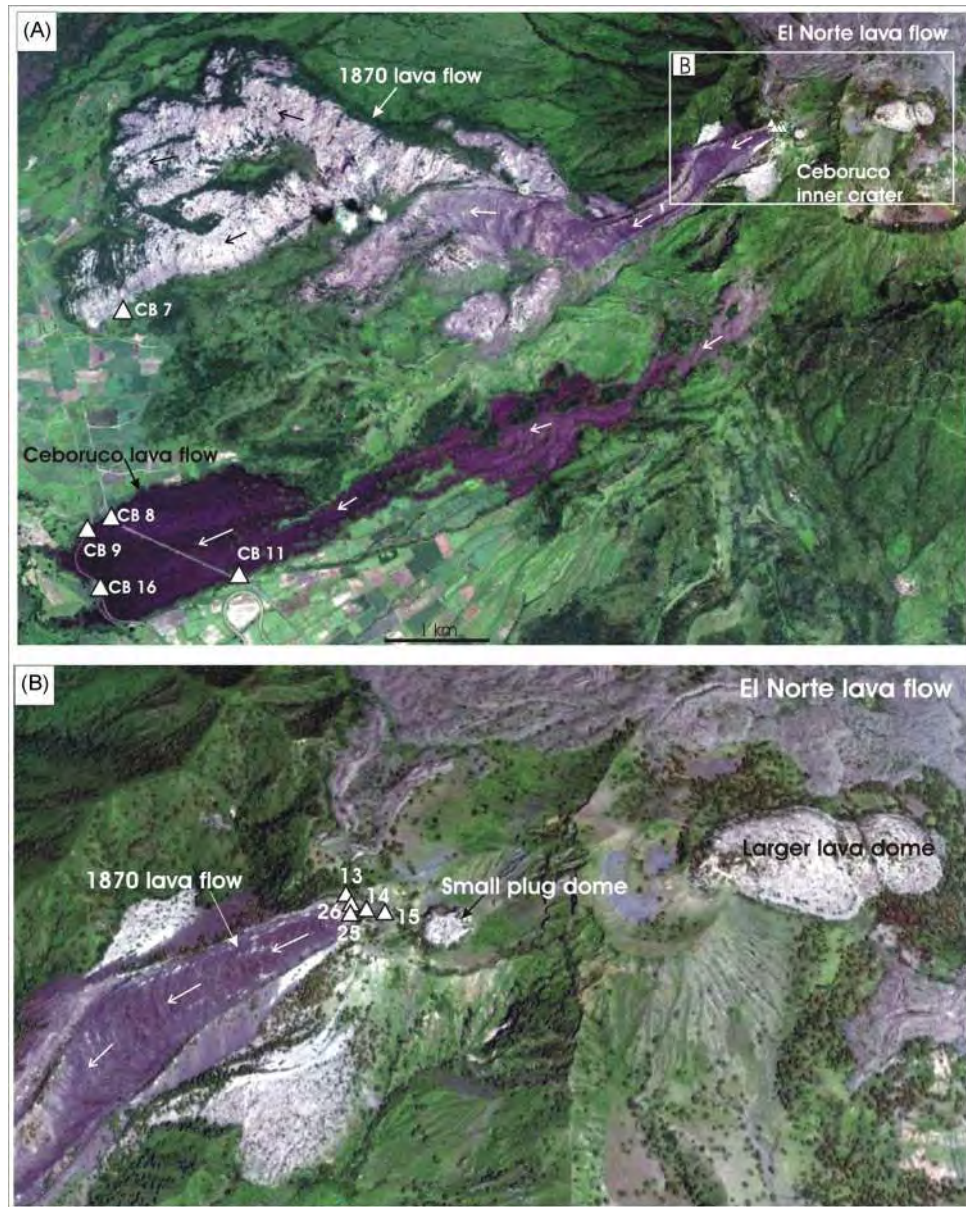


Figure 2. (A) Overview Google Earth image of the 1870 and Ceboruco lava flows, with sampling sites marked as white triangles. (B) Closeup of the Ceboruco crater with the 1870–75 eruption products and sampling sites. Flow directions are indicated by white and black arrows.

dome which grew inside the outer crater probably shortly after the plinian Jala eruption (Nelson 1980). The widespread Jala pumice can be used as a marker horizon, assigning pre-Jala and post-Jala relative ages to the several morphologically young looking lava flows covering the main cone's flanks.

Consequently, the rhyodacitic Destiladero lava flow (W-flank) was emplaced before the plinian Jala eruption, while at least seven other lava flows (from old to young: Copales, Cajón, Coapan I, Coapan II, El Norte, Ceboruco and the historical 1870 lava flow) descended the flanks after the Plinian eruption (Fig. 1). These very recent eruptions with a total volume of about 4 km^3 , occurring after 1005 AD, are difficult to date by the radiocarbon method, mainly because of the short between eruption intervals not permitting any soil formation.

Except for the historical 1870 lava flow, none of the others eruptions has been described in historical documents, although legends are referring to past activity of Ceboruco volcano but without any

time reference. This means that all post-plinian lava flows had already been emplaced by the arrival of the Spanish conquerors in 1528.

Apart of the lava flow emission, several smaller lava domes and pyroclastic cones were emplaced inside the inner summit crater (Fig. 2), which might have been source of historic references to volcanic activity without lava flow emission (see Sieron & Siebe 2008 and Sieron 2009, for more detail).

2.1 CEBORUCO lava flow

Stratigraphically, El Norte lava flow is the youngest lava flow on the northern side and Ceboruco lava flow on the southern flank (Fig. 1), not taking into account the historical 1870 eruption. Only legends exist about eruptions before 1528, which were passed on orally from one generation to the next and were eventually written down

by Spanish chroniclers, but therefore caressing specific eruption dates. One of these, repeatedly quoted by different authors (e.g. Tello 1968; Mota y Padilla 1973; de Ciudad Real 1976) tells a story about a village at the volcano flank which was buried by a lava flow because the inhabitants had sinned.

While Nelson (1980) described the Ceboruco flow as a blocky lava flow, we characterize it rather as an Aa-type lava flow, because of the surface morphology, thickness and the presence of basal and top breccias and a massive, dense, central part.

For its characteristics, including almost no vegetation cover, black colour and the rugged surface of the lava blocks, the Ceboruco lava flow often has been confounded with the historical 1870 lava flow (e.g. Thorpe & Francis 1975; Michalk *et al.* 2008), which indeed is characterized by more vegetation. Ceboruco lava flow is andesitic and has a porphyritic texture, showing larger plagioclase phenocrysts and abundant vesicles in the upper parts of the flow.

2.2 1870–75 eruption

The only historical eruption documented in detail started the 1870 February 23 and lasted until 1875, although the associated dacitic lava flow stopped moving laterally in 1872 already (García 1875; Iglesias *et al.* 1877). The eruption was preceded by precursors like noise, seismic activity and vapour emission and was characterized by intense ash fallout, lava extrusion and probably small pyroclastic flows. The products involve the lava flow and two smaller domes, one sealing the 1870 vent (recognized by 19th century observers) and the other larger one to the E on the flank of the pyroclastic cone (Fig. 2).

The 1870–72 lava is light to medium grey, glassy to vesicular, also showing a porphyritic texture with plagioclase phenocrysts, typical of Ceboruco's post-plinian andesites and dacites. Due to the great thickness and the presence of dense blocks on the surface with few vesicles, we describe the 1870 flow as an authentic block lava flow. Emplacement probably took part by flow inflation, as already proposed by Iglesias *et al.* (1877).

3 FIELD WORK

For palaeomagnetic studies, we collected 25 mm cores in the field with a portable gasoline powered drill. Cores were between about 5 and 12 cm long and oriented *in situ* with a new device equipped with a digital inclinometer (0.1° resolution and 0.2 *in situ* precision), a magnetic compass (0.5 *in situ* divisions, readable through an ocular) and a sun compass with 0.5 *in situ* divisions (for more details on the orienting device see Supporting Information).

To find out about the internal consistency of the palaeomagnetic data within a particular flow, multiple sites were sampled. It has been previously reported (e.g. Hagstrum & Champion 1994; Speranza *et al.* 2006) that mean directions may be significantly different along the same lava flow, which can pose a problem for the application in palaeomagnetic dating. Similarly, Lanza *et al.* (2005) found that individual and well-defined site-mean directions may be significantly different from observatory directions. Finding suitable sites sometimes was a difficult task at Ceboruco volcano, as the two lava flows are very thick and/or characterized blocky surfaces which probably still moved long after cooling below the remanence acquisition temperature, possibly related to inflation-type emplacement mechanism, especially in the case of the very thick dacitic lava flows (1870 and Copales flows). In the case of the Ceboruco flow, four sites produced by road and rail-road cuts (Fig. 2) were selected, where the internal structure of the lava was visible over

dozens of metres and seen unaffected by any important fractures pointing to post-cooling movements of the rock. The 1870 flow is not cut by any kind of road, and thus only natural outcrops could be sampled. Close to the end of the lava flow tongue very large blocks were visible at an intermediate elevation of the flow, where part of the rock had been removed and potentially the massive interior of the flow was accessible. As dictated by the steep topography and dense vegetation, three patches were sampled over a total distance of about 50 m. Two patches included exposures of 3 m or less, and the continuity of rock could not be established between them. The third part was much larger and here the undisrupted lava rock could be observed for more than 30 m. Additionally, we sampled other sites close to the vent area (Fig. 2): CB13 was taken from a levee of the 1870 flow at the top of the outer crater rim. CB15 is the remnant of a plug or a dyke of the 1870 vent, and four drill cores were also taken from the nearby dome or main plug. CB14 is located along the massive inner walls of the vent, and CB25 and CB26 on the massive outside wall of the vent.

4 LABORATORY PROCEDURES

Drill cores were cut in the laboratory into 22 mm long specimens and their magnetic susceptibility measured with an AGICO KLY-3 instrument. Natural remanent magnetization (NRM) vectors were determined with an AGICO JR-5 spinner magnetometer, and stepwise alternating field (AF) demagnetization was carried out with the AGICO LDA-3 equipment, in maximum field amplitudes of 100 mT. Demagnetization data were analysed by the program PMGSC 4.2 (Randy Enkin, Geological Survey of Canada). For statistical analysis and graphical representation of data, the program PMag Tool 4.2b by Mark W. Hounslow was used. Site-mean directions were calculated from averaged directions on core level, when several specimens were measured. Overall mean directions for the two lava flows were determined based on site-mean directions, as well as averaging all cores from the selected sites.

Rock magnetic measurements include the determination of magnetic hysteresis curves with a Princeton Measurement Corp. model MicroMag 2900 instrument, and thermomagnetic analysis of high-field-induced magnetization with a horizontal Curie balance built in the laboratory. For thermal demagnetization and palaeointensity (PI) experiments, an ASC Scientific TD48 furnace was used. PI were determined by the Thellier (1959) method with the modification proposed by Coe (1967) (TTC method). pTRM checks (Coe 1967), pTRM-tail check (Riisager & Riisager 2001) and additivity checks (Krása *et al.* 2003) were performed to obtain criteria regarding the reliability of the results. Data were analysed with the Thellier Tool software (Leonhardt *et al.* 2004). Additionally, PI were determined by the multispecimen method of Dekkers & Böhnel (2006) (MSP-DB), and with the modified protocol proposed by Fabian & Leonhardt (2010) (MSP-DSC) to include a domain state correction and alteration test. In the analysis of these data, we used a domain state proxy (α -parameter) of 0.5 as suggested by Fabian & Leonhardt (2010). The MSP-DSC data were analysed using MSP-Tool (Monster *et al.* 2015). Three reliability criteria have been considered in this study. Thermal-induced alteration $|\varepsilon_{\text{alt}}|$ (Fabian & Leonhardt 2010; Monster *et al.* 2015) during the experiment must be the lowest possible (the alteration criterion): specimens with $|\varepsilon_{\text{alt}}| > 4$ per cent will be rejected from the analyses. The maximum allowed angle between the isolated NRM and pTRM was set to 10°, defining the directional criterion (Monster *et al.* 2015).

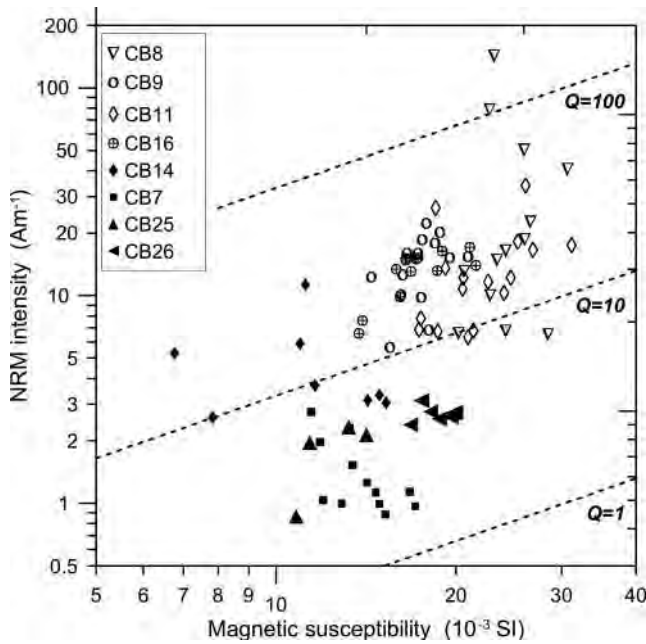


Figure 3. Variation of NRM intensity and magnetic susceptibility for Ceboruco (white symbols) and 1870 (black symbols) lava flows. Interrupted lines define constant values of Königsberger's factor Q .

Furthermore, the third, intersection criterion (Δb) (Monster *et al.* 2015) tests whether the linear fit regression line intersects the y -axis at the theoretically predicted value of -1 . A threshold value of (Δb) is ± 0.1 : the interpreted MSP-DSC linear best fit should intersect the y -axis between -0.9 and -1.1 .

5 RESULTS

The magnetic declination in our sampling area was found to be quite variable, showing site average values between about 4°W and 13°E , over distances of a few hundred metres to several kilometres.

5.1 Magnetic properties

Fig. 4 shows the variation of the NRM intensity and magnetic susceptibility for the eight studied sites, together with lines of constant Königsberger's factor Q , which is the ratio between remanent and induced magnetization, $Q = \text{NRM}/\kappa \cdot H$, where κ is the initial magnetic susceptibility and $H = 33 \text{ Am}^{-1}$ the magnetic field intensity. The Ceboruco flow has a geometrical average NRM intensity of 12.04 Am^{-1} , calculated without the five highest values of NRM $> 33 \text{ Am}^{-1}$, which are suspect of being produced by nearby lightning strikes. Susceptibility values are on geometrical average $19.5 \times 10^{-3} \text{ (SI)}$. Both properties together define Q values between 10 and 100. Average values for the 1870 lava flows are clearly smaller, NRM = 2.09 Am^{-1} (excluding three values of NRM $> 5 \text{ Am}^{-1}$), and $\kappa = 14.26 \times 10^{-3} \text{ (SI)}$. Most 1870 specimens have Q values between about 2 and 10, and are clearly separated in the NRM versus susceptibility diagram from the Ceboruco flow specimens (Fig. 3).

Magnetic hysteresis curves of rock chips are similar for both lava flows, as visible in Fig. 4. All hysteresis curves close in fields $< 250 \text{ mT}$, indicating the presence of low-coercivity minerals like magnetite or titanomagnetite. Values of coercive force are on average $8.3 \pm 1.9 \text{ mT}$ (Ceboruco flow) and $8.2 \pm 2.3 \text{ mT}$ (1870 flow) and thus indistinguishable. Saturation magnetization M_s is higher for

Ceboruco flow ($7.7 \pm 1.9 \times 10^{-4} \text{ Am}^2 \text{ kg}^{-1}$) than for the 1870 flow ($6.0 \pm 2.3 \times 10^{-4} \text{ Am}^2 \text{ kg}^{-1}$). The difference is larger for the remanent saturation magnetization M_{rs} , $1.4 \pm 0.3 \times 10^{-4}$ and $0.82 \pm 0.23 \times 10^{-4} \text{ Am}^2 \text{ kg}^{-1}$, respectively. Magnetization ratios M_{rs}/M_s and coercivity ratios H_{cr}/H_c are plotted in a Day *et al.* (1977) plot (Fig. 5) and indicate slightly smaller magnetic grain sizes for Ceboruco flow than for 1870 flow. In the Day plot, the data points are located slightly to the right of the theoretical SD-MD mixing lines given by Dunlop (2002).

Median destructive fields (MDF) are 20–40 mT for Ceboruco flow and 10–20 mT for 1870 flow, confirming the presence of more multidomain-like particles in the historic lava flow.

Results of thermomagnetic analysis are shown in Fig. 5, often indicating the presence of two minerals with Curie temperatures T_c around 250–300 °C and 500–550 °C (Fig. 5). These Curie temperatures suggest the simultaneous occurrence of Ti-rich and Ti-poor titanomagnetite minerals. The relative concentration of these minerals is variable as indicated by the drop of the magnetization around 300 °C, and only in specimen CB14-1 (Fig. 5a) from the 1870 lava flow the low-Ti titanomagnetite seems to be largely dominating. Cooling curves are very similar to the heating curves, often with a slightly smaller magnetization and thus indicating partial oxidation of the magnetic minerals. The Curie curves from both lava flows show similar variability of low-Ti and high-Ti titanomagnetites.

5.2 Characteristic remanence and flow-mean directions

One specimen of every drill core was demagnetized in up to 10 steps, using AF amplitudes of up to 100 mT, and all demagnetization curves were analysed with the principal component method (Kirschvink 1980; program PMGSC 4.2). Mostly, between five and nine demagnetization steps were used to obtain the characteristic remanence direction (ChRM), with a maximum angular deviation (MAD) less than 2° and often $< 1^\circ$. Most of the specimens showed only minor secondary magnetization components of probably viscous origin, which were removed in AF amplitudes of 20 mT or less (Figs 6a and b). Specimens with stronger secondary components (Figs 6c and d) were probably affected by lightning strikes, and AF amplitudes to remove the overprint were higher, up to 50 mT. Nevertheless, in all such cases, we still obtained a stable end direction, which is similar to that of other specimens from the same site unaffected by such overprints.

Site-mean directions were calculated assuming a Fisher distribution (using PMag Tools Version 4.2), and after testing for outliers at the 95 per cent confidence level. Tables 1 and 2 list these data for the 1870 lava and Ceboruco flow sites, respectively. Also indicated are overall flow-mean directions calculated from all ChRM directions, as well as calculated from the site-mean directions. We note here that of course the confidence limits α_{95} are smaller for the first case, due to the much larger number of individual directions.

Sites CB13 (dyke or plug remnant) and CB15 (levee) and specimens from the central dome of the 1870 lava flow showed highly dispersed ChRM directions and no site mean was calculated. Individual demagnetization diagrams are of high quality, similar to other sites and best fits have small MAD values. Therefore, the dispersion probably reflects post-cooling movement of the rocks, although this was not detected in the field. ChRM directions for site CB7 of the 1870 lava flow are less but also dispersed. Here, the specimens recovered from the two small parts produced most of the dispersion, while specimens from the extended and undisrupted part showed coherent directions which resemble those of the other

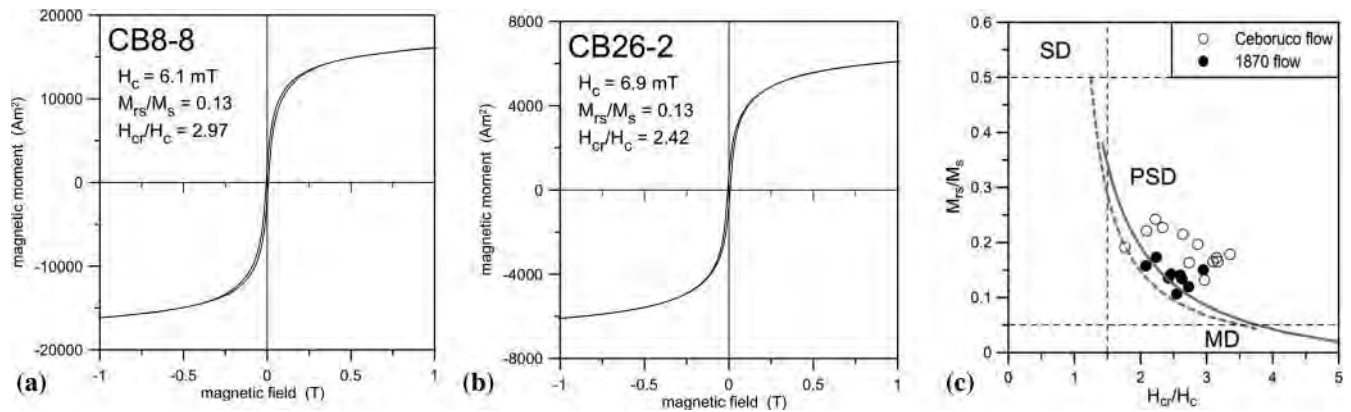


Figure 4. Examples of magnetic hysteresis curves for selected samples from (a) Ceboruco lava flow, (b) 1870 lava flow and Day plot. Interrupted straight lines distinguish magnetic grain sizes: SD: single-domain range, PSD: pseudo-single-domain range, MD: multidomain range. Continuous and interrupted curves represent theoretical mixing curves for SD and MD mixtures according to Dunlop (2002).

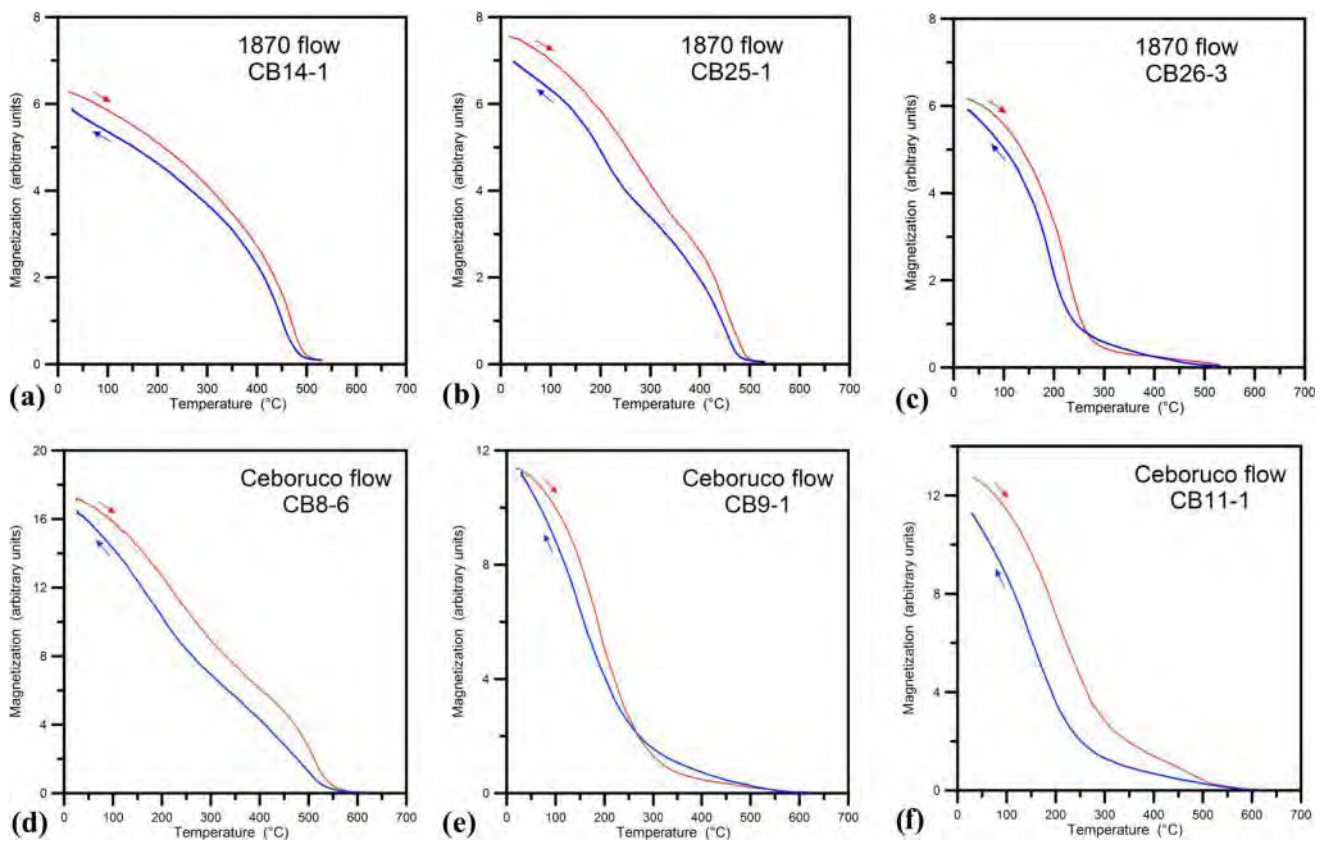


Figure 5. Variation of high-field-induced magnetization with temperature for samples from (a)–(c) 1870 lava flow and (d)–(f) Ceboruco lava flow. Heating and cooling curves are indicated by arrows and red and blue colours, respectively.

sites. Only these specimens were used to calculate the mean direction indicated in Table 1. Sites CB14, 25 and 26, all from locations close to the 1870 vent, have similar ChRM directions and define site-mean directions with a lower dispersion (Table 1 and Fig. 7). When calculating an overall mean based on site-mean directions, a relatively large uncertainty of $\alpha_{95} = 8.6^\circ$ is obtained, due to the small number $n = 4$ of sites. On the other hand, the overall mean direction based on the total number $n = 25$ of ChRM data is very well defined: $D = 7.5^\circ\text{E}$, $I = 42.3^\circ$, $\alpha_{95} = 3.1^\circ$, although it is not significantly different from the mean direction mentioned before. We would like to note that the obtained declination is indistinguish-

able within the uncertainty from the magnetic declination of 9.6° reported by Iglesias *et al.* (1877) for the year 1875. This historical declination was marked in a geological map of that work, although the location where this value was determined is unknown (see fig. 5 in Sieron & Siebe 2008).

ChRM directions were determined for all four sites from Ceboruco flow (Table 2 and Fig. 8). Again, the confidence circle for the overall mean direction of the Ceboruco flow is larger when calculated from four site means ($\alpha_{95} = 5.8^\circ$), compared to that based on $n = 50$ ChRM data, $D = 347.1^\circ\text{E}$, $I = 36.2^\circ$ and $\alpha_{95} = 2.4^\circ$.

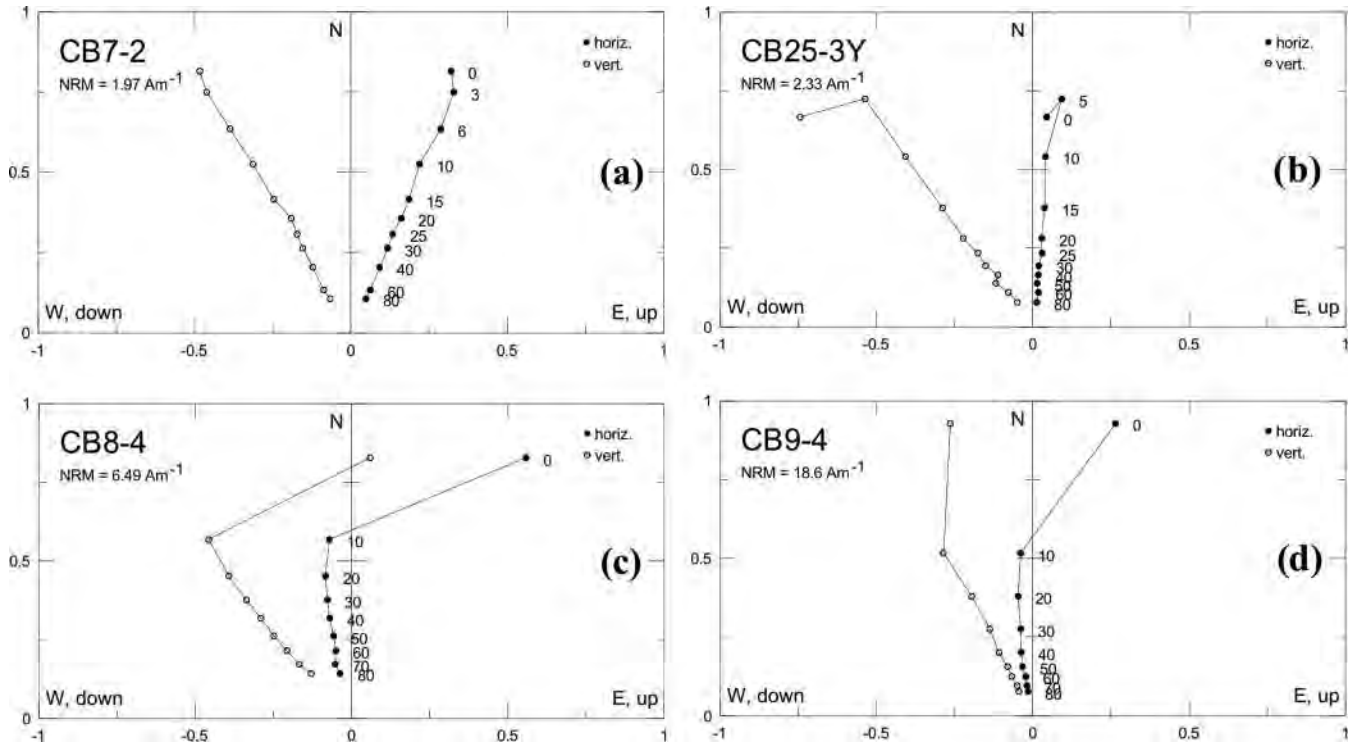


Figure 6. Orthogonal vector plots of AF demagnetized samples from (a) and (b) 1870 lava flow and (c) and (d) Ceboruco lava flow. Labels along curves denote the maximum AF amplitude applied during the demagnetization step.

Table 1. Site-mean directions for four sites of the 1870 lava flow, with sampling coordinates; *N*, number of recovered drill cores; *N'*, number of samples used for calculation of site-mean direction; *R*, unit vector sum; *k*, precision parameter; α_{95} , 95 per cent confidence level; Dec, declination; Inc, inclination.

Site	Latitude	Longitude	<i>N</i>	<i>N'</i>	<i>R</i>	<i>k</i>	α_{95}	Dec	Inc
CB7	21° 6.873'	104° 34.944'	15	6	5.94145	85.4	7.3	358.0	47.2
CB14	21° 7.643'	104° 31.254'	8	8	7.99176	849.7	1.9	10.1	45.9
CB25	21° 7.627'	104° 31.278'	4	4	3.99283	418.5	4.5	13.6	36.2
CB26	21° 7.629'	104° 31.278'	7	7	6.95633	137.4	5.2	8.1	37.1
Mean	Core level		34	25	24.73413	90.3	3.1	7.5	42.3
Mean	Site level		4	4	3.97394	115.1	8.6	7.8	41.7

Table 2. Site-mean directions for four sites of the Ceboruco lava flow, for details see Table 2.

Site	Latitude	Longitude	<i>N</i>	<i>N'</i>	<i>R</i>	<i>k</i>	α_{95}	Dec	Inc
CB8	21° 5.739'	104° 34.897'	12	12	11.84274	69.95	5.2	346.5	40.8
CB9	21° 5.767'	104° 35.100'	13	11	10.86459	73.85	4.9	346.5	36.7
CB11	21° 5.437'	104° 34.214'	14	14	13.90264	133.5	3.5	349.9	36.5
CB16	21° 5.373'	104° 35.009'	9	9	8.85653	55.76	7.0	340.9	28.2
Mean	Core level		51	50	49.34069	74.32	2.4	347.1	36.2
Mean	Site level		4	4	3.98792	248.42	5.8	347.7	35.6

5.3 Palaeointensity results

Michalk *et al.* (2008) reported a PI for the Ceboruco flow, which in their paper was erroneously assigned to the 1870 flow (their site EH). The PI was determined by the MSP-DB method and provides a value of $54 \pm 6 \mu\text{T}$. Here, we report new PI data, in an effort to reduce the uncertainty of this result and applying updated methods. For this PI experiment, specimens were selected from drill cores characterized by only one magnetization component, which is interpreted to be the original TRM.

A total of 30 specimens from the 1870 and Ceboruco lava flows were analysed applying the TTC PI protocol. Laboratory fields were chosen accordingly to the expected PI: 40 μT for the 1870 flow and

60 μT for the Ceboruco flow, and specimens were oriented with their NRM direction parallel to the field in the furnace, with a precision better than 5°. Fifteen specimens passed the Thellier Tool selection criteria of class A or B (Table 3), resulting in an overall success rate of 50 per cent. Fig. 9 shows two representative examples of Arai plots, one for each lava flow and all accepted PI results are listed in Table 4 with their quality parameters. The quality parameter *q* varies between 5.7 and 34.6; only three values of *q* are smaller than 10. Mean PI for the 1870 flow is $45.42 \pm 6.28 \mu\text{T}$ (*n* = 9) and for the Ceboruco flow $58.96 \pm 5.82 \mu\text{T}$ (*n* = 6).

The multispecimen protocol was used only on specimens from Ceboruco lava flow, sites CB11 and CB16, with set temperatures of

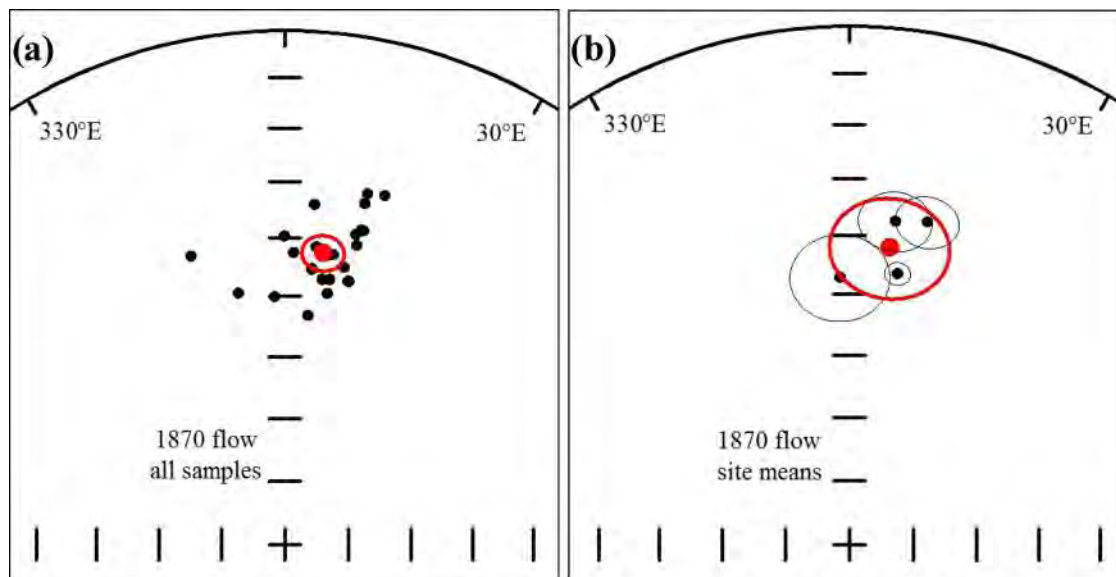


Figure 7. Characteristic remanent magnetization directions for the 1870 lava flow sampled in four sites: (a) individual directions and their overall mean; (b) site-mean directions and their overall mean. Overall mean directions are shown with larger red dots and their 95 per cent confidence angles. Equal area projection.

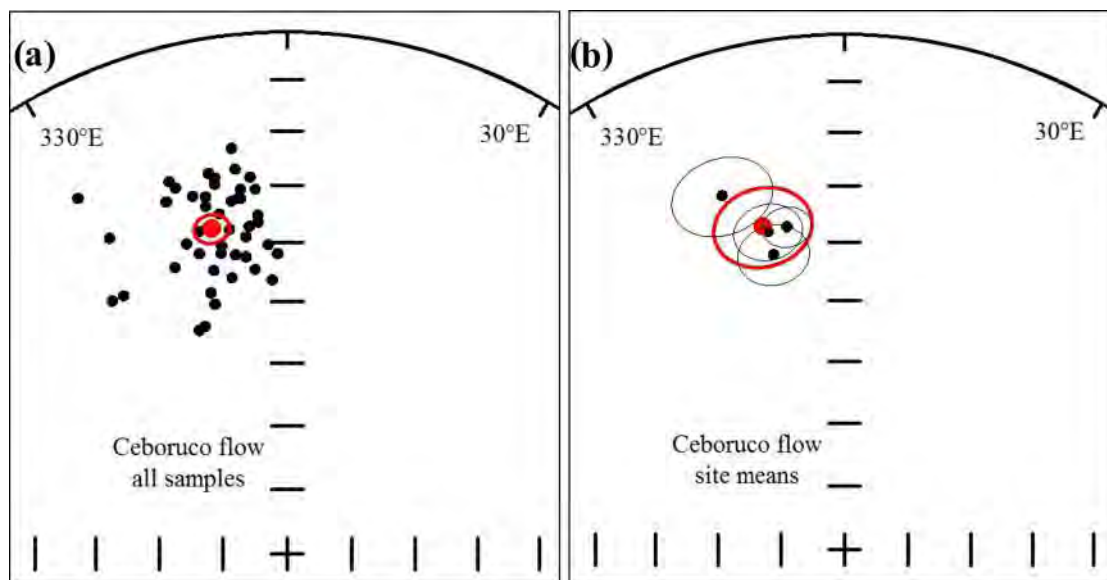


Figure 8. Characteristic remanence directions Ceboruco flow sampled in four sites: (a) individual directions and their overall mean; (b) site-mean directions and their overall mean. Overall mean directions are shown with larger red dots and their 95 per cent confidence angles. Equal area projection.

Table 3. Palaeointensity acceptance criteria: ThellierTool Class A and B (Leonhardt *et al.* 2004) as modified by Paterson *et al.* (2014). N , number of points included in the linear best fit; f , fraction of the NRM used for best fit; β , standard deviation divided by the slope of the best-fit line; q , quality factor, MAD_{ang} , anchored maximum angular deviation; α , angular difference between anchored and non-anchored best solution; δCK , relative check error; δpal , cumulative check difference; δTR , tail check; δr^* , normalised tail of pTRM.

Class	N	f	β	q	MAD_{ang}	α	δCK	δpal	δTR	δr^*
A	≥ 5	≥ 0.35	≤ 0.1	≥ 5	≤ 6	≤ 15	≤ 7	≤ 10	≤ 10	≤ 9
B	≥ 5	≥ 0.35	≤ 0.15	≥ 0	≤ 15	≤ 15	≤ 9	≤ 18	≤ 20	≤ 99

220 °C and 240 °C. Of the 20 specimens from CB11, 9 did not meet the required criteria and were rejected. The data are substantially scattered and the 68 per cent confidence limits for the best-fit line in Fig. 10 are large, resulting in a PI for site CB11 of $67 +15/-8.7 \mu T$. For CB16, 10 specimens out of 15 passed the acceptance criteria, defining a better constrained PI of $60.3 +8.5/-6.9 \mu T$. The best-

fit lines for both sites cross the vertical Q_{DSC} axis very close to the theoretical value of -1 . Both MSP-DSC PI agree within the uncertainty limits with the TTC PI of $58.96 \pm 5.82 \mu T$, but the uncertainty is too large for site CB11 (+22 per cent/-13 per cent) to consider this to be reliable. In the case of site CB16, the uncertainty is similar to the TTC PI result, and the mean values are

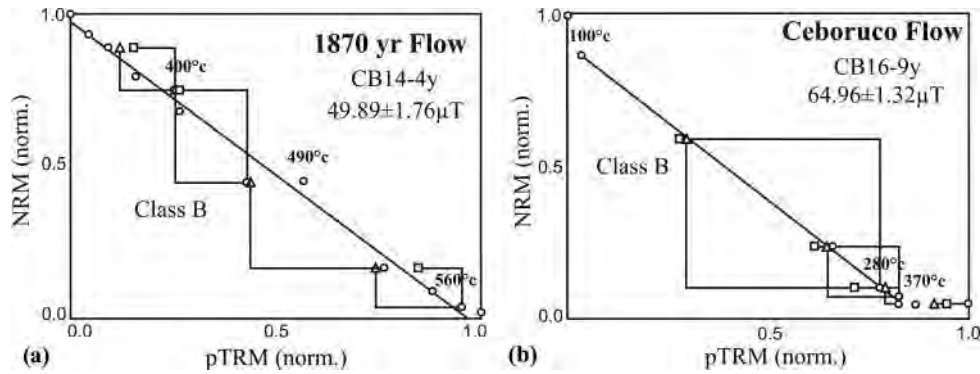


Figure 9. Examples of palaeointensity (Arai) plots for the (a) 1870 and (b) Ceboruco lava flows, obtained by the Coe version of the Thellier method. NRM and pTRM are normalized. NRM versus pTRM data are given as circles, with the black best-fit line. pTRM checks are shown by triangles and additivity checks by square symbols. The analysis was done using ThellierTool.

Table 4. Results of Thellier–Coe palaeointensity experiments for the 1870 and Ceboruco lava flows. Class, quality class according to ThellierTool (Leonhardt *et al.* 2004); PI ± s.d., palaeointensity with standard deviation. Other abbreviations as in Table 3.

Sample	<i>N</i>	<i>f</i>	<i>q</i>	β	MAD _{anc}	α	δ CK	δ pal	δ TR	δ <i>r</i> *	Class	PI ± s.d. (μT)	
1870 lava flow: CB7, 14, 25, 26													
14-3z	12	0.9	25.6	0.03	1.2	1.2	5.3	2.6	3.5	0.5	B	58.22 ± 1.74	
14-4y	12	1.0	24.4	0.04	1.3	0.7	2.7	1.4	0.8	2.3	B	49.89 ± 1.76	
14-5z	10	1.0	7	0.09	0.9	0.1	1.9	3.7	1.2	0.5	B	45.53 ± 4.43	
14-8y	10	0.7	5.7	0.09	3.5	3.9	6.7	9.9	4.6	2.1	B	47.11 ± 4.55	
25-3z	12	1.0	15.9	0.05	8	8.7	9.4	2.7	2.2	0.3	B	40.36 ± 2.05	
25-4z	7	1.0	34.6	0.02	9.3	6.1	0.6	0.3	1.3	0	B	36.92 ± 0.63	
26-4	14	0.9	18.4	0.04	2.7	3.5	10.2	16.6	1.1	1.7	B	47.22 ± 2.05	
26-5w	12	0.9	13.6	0.06	2.5	2.4	2.3	3.1	1.9	0.5	A	42.66 ± 2.57	
26-6w	7	0.9	11	0.03	1.1	0.6	9.2	11.6	0.8	0	B	40.88 ± 1.45	
Site mean												9	45.42 ± 6.28
Ceboruco lava flow: CB8, 9, 11, 16													
8-12z	8	0.4	5.8	0.05	1.4	1.5	0.5	0.7	16.3	4.2	B	57.34 ± 3.05	
11-3x	10	0.8	23.3	0.03	2.2	2.1	3.3	5.3	4.8	1.7	A	52.87 ± 1.57	
11-14x	6	0.6	13.5	0.03	1.9	2.8	6.1	1.1	1.3	3.8	A	51.75 ± 1.73	
16-3x	6	0.8	15.8	0.04	1.9	2.2	1.7	2.9	3.1	N	A	62.45 ± 2.61	
16-6w	9	0.9	18.7	0.04	2.8	2.3	6.6	8.3	6.7	0.8	B	64.39 ± 2.53	
16-9y	6	0.9	29.5	0.02	1.5	0.9	1.5	2.3	0.9	5.3	B	64.97 ± 1.32	
Site mean												6	58.96 ± 5.82

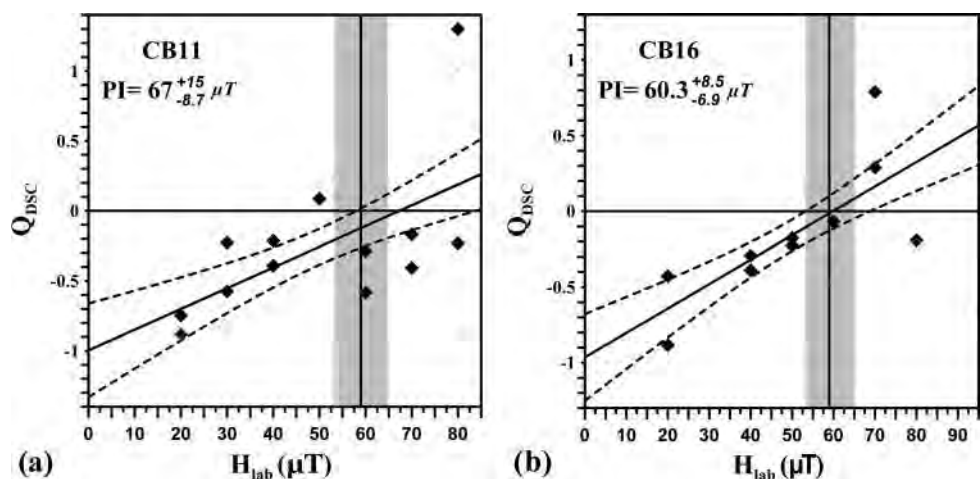


Figure 10. MSP-DSC palaeointensity results, for sites (a) CB11 and (b) CB16 of Ceboruco lava flow. Continuous black lines represent the best fit to the data shown as black diamonds, with 68 per cent confidence limits shown as dashed line. White diamonds are located outside the 95 per cent confidence limits and rejected (CB11), or were not used because of non-linearity at the 90 μT field step (CB16). The vertical lines represent the site-mean Thellier-type PI results with its standard deviations (grey-shaded area).

indistinguishable. This result is acceptable and the coincidence with the TTC result suggests that these PI data are reliable. Nevertheless, because of the difficulty to calculate a weighted mean PI from both methods, we will use only the TTC PI data for palaeomagnetic dating. Using the MSP-DSC PI would produce a very similar result.

5.4 Palaeomagnetic dating of the 1870 and Ceboruco lava flows

The palaeomagnetic dating was carried out with the Matlab tool *archaeo_dating* (Pavón-Carrasco *et al.* 2011) which uses PSV curves covering the last few millennia. Currently, there is not a well-constrained regional PSV curve for Mesoamerica for the last few millennia. For this reason, we used the recent global model SHA.DIF.14k (Pavón-Carrasco *et al.* 2014), which was developed by using only archaeomagnetic and lava flow data distributed all around the World, also including data from Central America, Mexico and the USA. For the last 400 yr, the directional model (i.e. declination and inclination) was constrained by the GUFM1 model (Jackson *et al.* 2000), which is based on historic field measurements. SHA.DIF.14k allows us to obtain a PSV curve with its uncertainty at any point over the Earth's surface and thus at the Ceboruco coordinates. We constrained the time interval of dating to the period 1000–1900 AD, as both lava flows were emplaced later than 1005 AD.

We already know the eruption age of the 1870 lava flow from historical accounts, and we will use the palaeodirection and intensity listed in Tables 1 and 4 to see if the archaeomagnetic dating method works. As noted above, there is an historical declination reported for the area of the Ceboruco volcano at 1875 (9.6° ; Iglesias *et al.* 1877), but no information about the historical inclination and intensity is provided. For this reason, we use the full-vector (declination, inclination and intensity) palaeomagnetic information to infer a possible age for this lava flow. We use the mean directions based on all individual cores of a flow, which provides a well-constrained dating due to the low value of the α_{95} (3.1°) (Fig. 11a; here only the combined PDF is shown; for

details, see Supporting Information). Within the age range 1000–1900 AD, there is only one time interval in which the SHA.DIF.14k model coincides with the palaeomagnetic direction obtained from the 1870 lava flow at a 95 per cent of confidence level: 1755–1871 AD.

The same procedure was applied to date the Ceboruco lava flow using the palaeomagnetic information of Tables 2 and 3 (Fig. 11b) providing a single interval from 1000 to 1134 AD as the most probable date of the Ceboruco flow eruption.

6 DISCUSSION

Bulk magnetic properties are different for the two lava flows, with the magnetic susceptibility 1.4 times larger and the NRM intensity 6.2 times large for the Ceboruco flow compared to the 1870 flow. This difference may be the consequence of the changed magma composition from andesitic to dacitic, with an accompanying reduction of the magnetic mineral concentration and maybe their grain sizes. More single-domain grain sizes would result in a higher NRM intensity than multidomain grains. As the difference in NRM is larger than in magnetic susceptibility, the Königsberger factor Q is much larger for the Ceboruco flow compared to the 1870 flow. A similar trend is shown by the magnetic hysteresis data and in particular the saturation remanent magnetization M_{rs} , which is 2.1 times larger for the Ceboruco than for the 1870 flow. This difference is much smaller for the saturation magnetization M_s , 1.28. MDF values are much higher for the Ceboruco than for the 1870 lava flow, suggesting a much larger contribution of single-domain grains to the NRM. Therefore, the observed difference in NRM intensity seems to be the result of variations in magnetic mineral concentration and/or grain sizes, together with stronger magnetic field intensity during the Ceboruco flow eruption than in 1870, producing a stronger TRM.

ChRM directions for the 1870 flow are variable, depending on the site location. Site CB7 close to the flow tip apparently was affected by relative block movement blocks after remanence acquisition, with coherent ChRM directions only from one large block with extension larger than 30 m. Sites CB13 (vent plug or dyke remnant,

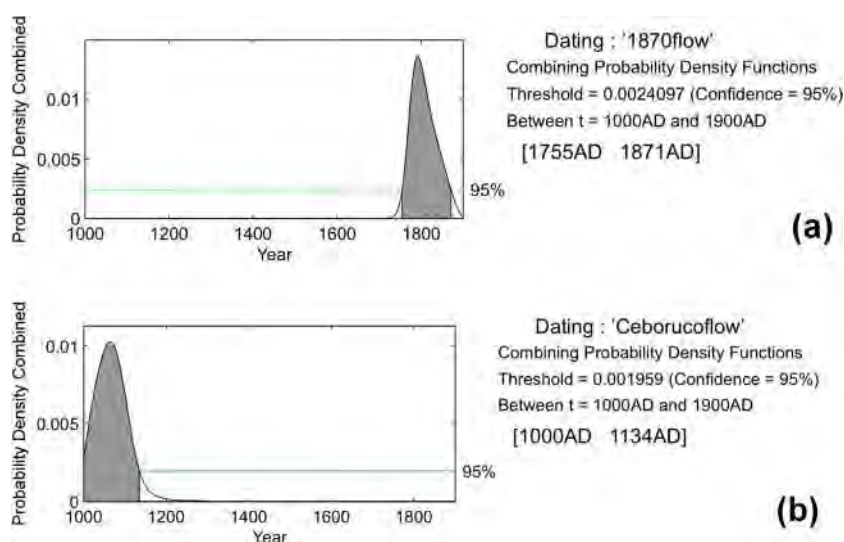


Figure 11. Palaeomagnetic dating of (a) the 1870 lava flow and (b) the Ceboruco lava flow. The combined probability density derived from the declination, inclination and palaeointensity data are shown as shaded peaks with the minimum 95 per cent confidence level by horizontal green lines. For more details, see Supporting Information.

and nearby central dome or plug) and CB15 (levee) according to our field observations seemed not to be affected by such processes, and we expected to obtain useful ChRM directions from them. Nevertheless, directions in these sites are highly dispersed and we may only speculate that this was caused by movement of already cooled parts by later injected magma. Sites CB14, CB25 and CB26 are from the massive inner and outer wall of the 1870 vent and provide consistent ChRM directions (Fig. 8). All these observations strongly suggest sampling multiple sites to be able to recognize unreliable results and finally to recover a reliable flow-mean direction which then may be used for an accurate palaeomagnetic dating.

The outcrop situation was less complex in the case of the Ceboruco lava flow. While this flow also exhibits a very blocky surface, the interior is very well exposed by road and rail-road cuts. Contrary to our expectations this flow, situated at a much lower elevation than the 1870 vent area, was more affected by lightning strikes. Here, 12 specimens showed strong overprints, but nevertheless stable ChRM directions were obtained after demagnetization experiments. Only one specimen from the 1870 lava flow was characterized by a strong secondary magnetization component.

As listed in Tables 1 and 2, overall mean directions are available as based on individual specimens as well as based on four site-mean directions. Knowing the membership of each site to a specific flow and considering the variable number of drill cores, here we use overall flow-mean directions based on individual drill cores for palaeomagnetic dating.

In case of the 1870 lava flow, the dating results in an age range of 1755–1871 AD (Fig. 11a), which includes the historic eruption age. As SHA.DIF.14k is a global model, we consider this result as a reasonable validation of the palaeomagnetic dating method for this region. While for the period 1590–1900 AD, the directional part of the SHA.DIF.14k was constricted by the model GUFM1 (Jackson *et al.* 2000), the SHA.DIF.14k also includes numerous archaeomagnetic and lava flow data from the region within a radius of 1500 km around Ceboruco volcano for pre-historic times, and this allows its application to older rocks. Dating the Ceboruco lava flow results in an age range of 1000–1134 AD (Fig. 11b), confirming the previous assumption of being older than 1528 AD (Sieron & Siebe 2008). But this result also suggests that the Ceboruco lava flow was already emplaced shortly after the big plinian Jala eruption that happened around 1005 AD, and not several hundred years later as tentatively proposed by Sieron & Siebe (2008) on the basis of the youthful appearance of this flow and its stratigraphic relation with other lava flows from Ceboruco volcano. It thus appears that all Ceboruco lava flows except the 1870 flow were emplaced shortly after 1005 AD despite of the considerable morphologic differences and the distinct vegetation cover, and then the volcano remained inactive for at least 720 yr. This scenario looks quite different to the suggested high and sustained volcanic activity for up to 500 yr after the 1005 AD plinian eruption, as originally proposed by Sieron & Siebe (2008), and will have to be taken into account for future hazard studies of Ceboruco volcano. Further on, as stratigraphically the Ceboruco lava flow may be the youngest pre-1870 flow, this much restricted age range would also have important consequences for the Ceboruco magma evolution, as it will have to allow the more or less simultaneous eruption of rocks with dacitic to basaltic andesite composition. Recently, it was reported that another Mexican volcano of similar age (El Metate, 1250 AD) emplaced about 9 km³ of lava within a very short time span of possibly no more than 39 yr (Chevrel *et al.* 2016). Ceboruco volcano emplaced about 4 km³ of lava, but this was preceded by another 3–4 km³ of tephra during the plinian Jala eruption, all this in a similar short period of activity.

7 CONCLUSIONS

Two lava flows from Ceboruco volcano in western Mexico were studied in detail: the 1870 lava flow and the Ceboruco lava flow emplaced before 1528 AD but after ~1005 AD. Samples were recovered from four or more independent sites, to analyse the variability of the palaeomagnetic record, which indeed exhibits significant variations, associated to different processes. In case of the 1870 flow, which partly (or at final emplacement stages) was emplaced by inflation, post-cooling block movement produced important dispersion of observed remanence directions in two sites within the Ceboruco crater, which lead to their rejection. Four other sites provided well-clustered directions and an overall site-mean direction at $D = 7.5^\circ$, $I = 42.3^\circ$, $\alpha_{95} = 3.1^\circ$ and $n = 25$. The Ceboruco lava flow was studied in four well-suited sites which provide a mean direction of $D = 347.1^\circ$, $I = 36.2^\circ$, $\alpha_{95} = 2.4^\circ$ and $n = 51$. For both lava flows, individual site-mean directions may deviate significantly from the overall mean direction, which we consider to be the best approximation of the palaeofield during the cooling of the lava flows. Palaeointensities were obtained by the Thellier–Coe method and the multiple specimen method. Here, we use the data from the Thellier–Coe method, resulting in flow-mean palaeointensities of $45.4 \pm 6.3 \mu\text{T}$, $N = 9$ (1870 flow) and $59.0 \pm 5.8 \mu\text{T}$, $N = 6$ (Ceboruco flow). Multispecimen palaeointensities are indistinguishable from this value, with a similar uncertainty in one site, but a large uncertainty in the other. The agreement of palaeointensities obtained with different methods supports that these data are correct.

The palaeomagnetic dating of the 1870 flow results in an age range of 1755–1871 AD, which includes the real emplacement age of 1870. In case of the Ceboruco lava flow, considered to be the youngest flow of the volcano apart of the 1870 flow, the dating resulted in an age range between 1000 and 1134 AD, which is close to the plinian Jala eruption of ~1005 AD. This result restricts the eruption of all seven post-plinian lava flows from Ceboruco volcano to a short period of ≤ 140 yr after this plinian event, and defines a much longer period of volcanic inactivity than suggested previously. Accordingly, Ceboruco volcano was inactive for at least 720 yr, until the 1870 eruption, with implications for future volcanic hazard analysis. The short time span available for lava flow emplacement has also to be considered in modelling the magma evolution of Ceboruco volcano, in order to explain the almost simultaneous occurrence of basaltic andesites to dacitic rocks.

ACKNOWLEDGEMENTS

The authors thank F. Speranza, P. Roperch and P. Camps for their revisions which helped to improve this manuscript, as well as the editorial handling by E. Petrovsky. Ing. J. Escalante supported studies with the MicroMag AGFM and the Curie balance, and E. Nava warranted the functionality of the laboratory computers and the network. This work was supported by UNAM project IN 112712 (HB and FJPC) and Conacyt grant no. 180032 (HB and ANM). FJPC has received funding from the European Union's Horizon 2020 research and innovation programme under the Marie Skłodowska-Curie grant agreement no. 659901.

REFERENCES

- Arrighi, S., Tanguy, J.-C. & Rosi, M., 2006. Eruptions of the last 2200 years at Vulcano and Vulcanello (Aeolian Islands, Italy) dated by high-accuracy archaeomagnetism, *Phys. Earth planet. Inter.*, **159**, 225–233.

- Coe, R.S., 1967. Paleo-intensities of the Earth's magnetic field determined from Tertiary and Quaternary rocks, *J. geophys. Res.*, **72**(12), 3247–3262.
- Chevrel, M.O., Guilbaud, M.-N. & Siebe, C., 2016. The ~AD 1250 effusive eruption of El Metate shield volcano (Michoacán, Mexico): magma source, crustal storage, eruptive dynamics, and lava rheology, *Bull. Volcanol.* **78**, 32, doi:10.1007/s00445-016-1020-9.
- Day, R., Fuller, M. & Schmidt, V.A., 1977. Hysteresis properties of titanomagnetites: grain-size and compositional dependence, *Phys. Earth planet. Inter.*, **13**, 260–267.
- de Ciudad Real, A., 1976. Tratado curioso y docto de las grandezas de la Nueva España, 2nd edn, Vol. 2, 484 pp., Universidad Nacional Autónoma de México (originally published 1872, Madrid).
- Dekkers, M.J. & Böhnell, H.N., 2006. Reliable absolute paleointensities independent of magnetic domain state, *Earth planet. Sci. Lett.*, **248**, 508–517.
- Dunlop, D.J., 2002. Theory and application of the Day plot (M_{rs}/M_s versus H_{cr}/H_c) 1. Theoretical curves and tests using titanomagnetite data, *J. geophys. Res.*, **107**(B3), 2056, doi:10.1029/2001JB000486.
- Fabian, K. & Leonhardt, R., 2010. Multiple-specimen absolute paleointensity determination: an optimal protocol including pTRM normalization, domain-state correction, and alteration test, *Earth planet. Sci. Lett.*, **297**(1), 84–94.
- Fisher, R.A., 1953. Dispersion on a sphere, *Proc. R. Soc. London*, **A-127**, 205–305.
- Frey, H.M., Lange, R.A., Hall, C.M. & Delgado-Granados, H., 2004. Magma eruption rates constrained by $^{40}\text{Ar}/^{39}\text{Ar}$ chronology and GIS for the Ceboruco–San Pedro volcanic field, western Mexico, *Bull. geol. Soc. Am.*, **116**, 259–276.
- Gallet, Y., Genevey, A. & Le Goff, M., 2002. Three millennia of directional variations of the Earth's magnetic field in western Europe as revealed by archaeological artefacts, *Phys. Earth planet. Inter.*, **131**, 81–89.
- García, S., 1875. Viaje al ceboruco, in *Informe y Colección de Artículos Relativos a Los Fenómenos Geológicos Verificados en Jalisco en el Presente Año y en Épocas Anteriores*, pp. 36–184, ed. García, S., Escuela de Artes y Oficios Guadalajara.
- Gardner, J.E. & Tait, S., 2000. The caldera-forming eruption of Volcán Ceboruco, Mexico, *Bull. Volcanol.*, **62**, 20–33.
- Gómez-Paccard, M., Chauvin, A., Lanos, P., McIntosh, G., Osete, M.L., Catanzariti, G., Ruiz-Martínez, V.C. & Núñez, J.I., 2006. First archaeomagnetic secular variation curve for the Iberian Peninsula: comparison with other data from western Europe and with global geomagnetic field models, *Geochem. Geophys. Geosyst.*, **7**, Q12001, doi:10.1029/2006GC001476.
- Hagstrum, J.T. & Blinman, E., 2010. Archeomagnetic dating in western North America: an updated reference curve based on paleomagnetic and archeomagnetic data sets, *Geochem. Geophys. Geosyst.*, **11**, Q06009, doi:10.1029/2009GC002979.
- Hagstrum, J.T. & Champion, D.E., 1994. Paleomagnetic correlation of Late Quaternary lava flows in the lower east rift zone of Kilauea Volcano, Hawaii, *J. geophys. Res.*, **99**, 21 679–21 690.
- Iglesias, M., Bárcena, M. & Matute, J.I., 1877. Informe sobre los temblores de Jalisco y la erupción del Volcán “Ceboruco”, *An. Minist. de Fom. de México*, **1**, 115–196.
- Jackson, A., Jonkers, A.R. & Walker, M.R., 2000. Four centuries of geomagnetic secular variation from historical records, *Phil. Trans. R. Soc. A: Math. Phys. Eng. Sci.*, **358**(1768), 957–990.
- Kirschvink, J.L., 1980. The least-squares line and plane and analysis of palaeomagnetic data, *Geophys. J. R. astr. Soc.*, **62**, 699–718.
- Kovacheva, M., Boyadziev, Y., Kostadinova-Avramova, M., Jordanova, N. & Donadini, F., 2009. Updated archeomagnetic data set of the past 8 millennia from the Sofia laboratory, Bulgaria, *Geochem. Geophys. Geosyst.*, **10**(5), doi:10.1029/2008GC002347.
- Krásá, D., Heunemann, C., Leonhardt, R. & Petersen, N., 2003. Experimental procedure to detect multidomain remanence during Thellier–Thellier experiments, *Phys. Chem. Earth, A/B/C*, **28**(16), 681–687.
- Lanza, R., Meloni, A. & Tema, E., 2005. Historical measurements of the Earth's magnetic field compared with remanence directions from lava flows in Italy over the last four centuries, *Phys. Earth planet. Inter.*, **148**(1), 97–107.
- Leonhardt, R., Heunemann, C. & Krásá, D., 2004. Analyzing absolute paleointensity determinations: acceptance criteria and the software ThellierTool4.0, *Geochem. Geophys. Geosyst.*, **5**(12), Q12016, doi:10.1029/2004GC000807.
- McIntosh, G. & Catanzariti, G., 2006. An introduction to archaeomagnetic dating, *Geochronometria*, **25**, 11–18.
- Michalk, D.M., Muxworthy, A.R., Böhnell, H.N., MacLennan, J. & Nowaczyk, N., 2008. Evaluation of the multispecimen parallel differential pTRM method: a test on historical lavas from Iceland and Mexico, *Geophys. J. Int.*, **173**, 409–420.
- Monster, M.W.L., de Groot, L.V. & Dekkers, M.J., 2015. MSP-Tool: a VBA-based software tool for the analysis of multispecimen paleointensity data, *Front. Earth Sci.*, **3**, 86, doi:10.3389/feart.2015.00086.
- Mota y Padilla, M.A. de la, 1973. *Historia del Reino de Nueva Galicia en la América Septentrional (1742)*, Colección Histórica de Obras Facsimilares, Vol. 3, INAH-Universidad de Guadalajara, 626 pp.
- Nelson, S.A., 1980. Geology and Petrology of Volcan Ceboruco, Nayarit, Mexico, *Bull. geol. Soc. Am.*, **91**, 2290–3243.
- Paterson, G.A., Tauxe, L., Biggin, A.J., Shaar, R. & Jonestrask, L.C., 2014. On improving the selection of Thellier-type paleointensity data, *Geochem. Geophys. Geosyst.*, **15**(4), 1180–1192.
- Pavón-Carrasco, F.J., Rodríguez-González, J., Osete, M.L. & Torta, J.M., 2011. A Matlab tool for archaeomagnetic dating, *J. Archaeol. Sci.*, **38**, 408–419.
- Pavón-Carrasco, F.J., Osete, M.L., Torta, J.M. & De Santis, A., 2014. A geomagnetic field model for the Holocene based on archaeomagnetic and lava flow data, *Earth planet. Sci. Lett.*, **388**, 98–109.
- Riisager, P. & Riisager, J., 2001. Detecting multidomain magnetic grains in Thellier palaeointensity experiments, *Phys. Earth planet. Inter.*, **125**(1), 111–117.
- Roperch, P., Chauvin, A., Lara, L.E. & Moreno, H., 2015. Secular variation of the Earth's magnetic field and application to paleomagnetic dating of historical lava flows in Chile, *Phys. Earth planet. Inter.*, **242**, 65–78.
- Siebe, C., Rodriguz-Lara, V., Schaaf, P. & Abrams, M., 2004. Radiocarbon ages of Holocene Pelado, Guespalapa, and Chichinautzin scoria cones, south of Mexico City: implications for archeology and future hazards, *Bull. Volcanol.*, **66**, 203–225.
- Sieron, K., 2009. Historia eruptiva, volúmenes emitidos y composición geoquímica e isotópica (sistemas Nd, Sr y Pb) del Volcán Ceboruco y edificios monogenéticos contiguos, Estado de Nayarit, México, *PhD thesis*, Posgrado en Ciencias de la Tierra, UNAM, Mexico, 152 pp.
- Sieron, K. & Siebe, C., 2008. Revised stratigraphy and eruption rates of Ceboruco stratovolcano and surrounding monogenetic vents (Nayarit, Mexico) from historical documents and new radiocarbon dates, *J. Volcanol. Geotherm. Res.*, **176**, 241–264.
- Speranza, F., Branca, S., Coltelli, M., D'Ajello Caracciolo, F. & Vigliotti, L., 2006. How accurate is “paleomagnetic dating”? New evidence from historical lavas from Mount Etna, *J. geophys. Res.*, **111**(B12), doi:10.1029/2006JB004496.
- Speranza, F., Pompilio, M., D'Ajello Caracciolo, F. & Sagnotti, L., 2008. Holocene eruptive history of the Stromboli volcano: constraints from paleomagnetic dating, *J. geophys. Res.*, **113**(B9), doi:10.1029/2007JB005139.
- Tanguy, J.C., Le Goff, M., Principe, C., Arrighi, S., Chillemi, V., Paiotti, A., La Delfa, S. & Patane, G., 2003. Archeomagnetic dating of Mediterranean volcanics of the last 2100 years: validity and limits, *Earth planet. Sci. Lett.*, **211**, 111–124.
- Tello, A.F., 1968. *Crónica miscelánea de la Sancta Provincia de Xalisco: libro segundo*, Vol. 1, pp. 1–374, Gobierno del Estado/Universidad de Guadalajara, IJAH/INAH.
- Thellier, E., 1959. Sur l'intensité du champ magnétique terrestre dans le passé historique et géologique, *Ann. Geophys.*, **15**, 285–378.
- Thorpe, R.S. & Francis, P.W., 1975. Volcan Ceboruco: a major composite volcano in the Mexican Volcanic Belt, *Bull. Volcanol.* **54**, 201–213.

SUPPORTING INFORMATION

Additional Supporting Information may be found in the online version of this paper:

Figure S1. Overall view of the orienting device with digital inclinometer, Sun compass and magnetic compass with ocular reading.

Figure S2. Sun compass scale with 0.5° subdivisions and its use on the orienting device. Note that according to the positioning on the platform an angle has to be added, here 90° . The size of the compass is about $11 \times 11 \text{ cm}^2$. Under favourable conditions, the shadow angle may be estimated with a $1/4^\circ$ of resolution.

Figure S3. Alternatively, a thick rod with a narrow slot may be employed. This produces a wide shadow with a narrow bright line in the middle. The rod has to be turned around its long axis to optimize the width of the bright line. View of the digital inclinometer.

Figure S4. Palaeomagnetic dating of the 1870 lava flow and the Ceboruco lava flow. Horizontal blue lines are defined by the measured declination and inclination values, with 95 per cent confidence limits shown in green. Expected declination and inclination values with their 95 per cent confidence limits according to the SHA.DIF.14k global field model are shown as red curves. Below the declination, inclination and intensity curves, the probability density is shown as shaded peaks, with the minimum 95 per cent confidence level by green lines. The combined probability density derived from these data is shown at the bottom.

(<http://gji.oxfordjournals.org/lookup/suppl/doi:10.1093/gji/ggw310/-/DC1>).

Please note: Oxford University Press is not responsible for the content or functionality of any supporting materials supplied by the authors. Any queries (other than missing material) should be directed to the corresponding author for the paper.

8. Conclusions

In this thesis project, three main themes were addressed: (1) paleomagnetic dating of several Holocene volcanic eruptions located within the Trans-Mexican volcanic belt (TMVB), (2) constraining the nature of eruption of the AD 1250 El Metate shield volcano, Michoacán-Guanajuato volcanic field, and (3) enhancing the Late-Quaternary paleomagnetic secular variation database for Mexico by using lavas and archeological artefacts, and build secular variation curves with the data. In order to deal with these themes, during several field trips 56 lavas were sampled and 64 archeological pieces obtained. Paleomagnetic directions were obtained by stepwise alternating field demagnetization, and paleointensities were determined using the double heating Thellier experiments. In selected cases, rock magnetic experiments represented by thermomagnetic curves and hysteresis analyses were performed.

Important key aspects were discussed in this thesis and from the obtained results the following conclusions are outlined:

- Our paleomagnetic analyses on El Metate shield volcano indicate that all sampled lava flows gave concordant paleodirections and paleointensities which emphasize that they were erupted in a single eruptive period pointing to the monogenetic origin. The paleomagnetic dating performed on these flows shows that they were erupted in an age range between 1150 and 1290 AD which thus supports the previous hypothesis of Chevrel et al. (2016), especially if restricting the age further by the older ^{14}C age. Our results thus indicate that such a huge volcano ($\approx 9.2 \text{ km}^3$) with thirteen lava flows should have had an important impact on the population and environment around El Metate. Nevertheless, absence of written archeological sources hinder against evaluating directly El Metate's impact.
- Paleomagnetic dating was tested for the first time in Mexico on two lava flows sampled from Ceboruco, western Mexico. In order to validate the method, it was to the historical

flow erupted in 1870 AD. Our dating for the 1870 yr flow resulted in an age range between 1755 and 1871 AD which interestingly includes the real emplacement age and thus boosts credibility to the method. The Ceboruco flow was dated between 1000 and 1134 AD implying that Ceboruco volcano was inactive for at least 736 years until the 1870 eruption. This period is much longer than was previously suggested and thus should be considered in the modeling of the magma evolution in this area and estimations of volcanic risk.

- Paleomagnetic constraints on the ages of four Holocene lava flow eruptions located in the western Zacapu, Michoacán have been performed to investigate the impact of the Holocene volcanic eruption on the Pre-Hispanic civilizations (the Chupícuaro and Tarascan), which occupied this area, building extended living and ceremonial structures on top of these lava flows. Only the oldest flow, El Infiernillo, was radiocarbon-dated at 3200 ± 30 yr BP (cal 1525–1420 BC), and our paleomagnetic dating gave a concordant age range of 1500–1370 BC. The three younger flows were dated at 1340–940 BC (Malpaís Las Víboras), 200–80 BC (Capaxtiro), and 830–960 AD (Malpaís Prieto). Archeological records through recent excavations indicate that the lava flows area were occupied starting around 100 BC, just after the Capaxtiro eruption, and abandonment around AD 900 which based on our results could be attributed to the eruption of Malpaís Prieto. Noteworthy, this work shows that future volcanic hazard mitigation efforts could benefit combining geophysical, volcanological and archeological studies.
- Four monogenetic Holocene vents namely La Tinaja, La Palma, Mesa La Muerta, and Malpaís de Cutzaróndiro (in chronological order according to stratigraphic relations) that form a small cluster located within the Tacámbaro-Puruarán area in Michoacán were dated by the paleomagnetic dating procedure. The La Tinaja flow was previously radiocarbon-dated at 5115 ± 130 years BP (cal 4184–3655 BC) by Guilbaud et al. (2012) and paleomagnetic dating yielded several possible ages ranges, with the range 3650–3480 BCE being closest to the radiometric date. The remaining flows were dated at 3220–2880 BC (La Palma), 2240–2070 BCE and 760–630 BC (Mesa La Muerta), and 420–320 BC (Cutzaróndiro), and thus indicate

that these occurred separated in time with varying recurrence intervals ranging between ~300 and ~2300 years, although they are closely clustered in space. The identification of such small clusters with several young volcanoes that erupted in periods of hundreds to thousands of years opens several key aspects regarding to future volcanic hazard assessments in the volcanically active Michoacán-Guanajuato volcanic field, and also should be considered when constraining the nature of the magmatic plumbing system. From the provided results several questions can be asked: Will the cluster near Tacámbaro described here reactivate again with the emergence of a new vent? How long are such clusters active? Will the next monogenetic eruption in the MGVF be a single short-lived isolated eruption, or the beginning of a cluster? Furthermore, is it possible that the historic eruptions of Jorullo and Parícutin represent each the beginning of a cluster and should a new eruption in their close vicinity be expected in the future?

- The paleointensity secular variation curve for the last 3600 years has been constructed for the first time for Mexico. This curve was calculated through the combination of 44 high-quality new archeointensity data points obtained in this work; 27 selected data of previous studies from a total of 99; the past four centuries the curve is constrained by the GUFM1 model (Jackson et al., 2000). Important features of the Earth's magnetic field intensity highs and lows could be captured from the new curve. Among these features is a large intensity peak documented for the first time for Mexico at around 250 BC, which is comparable to the Levant paleointensity spike. Comparing these findings with the data from other regions indicates that over the last 3600 years the Earth's magnetic field was driven by the emergence of strong and rapidly fluctuating nondipole components superimposing the dominating dipole field.
- Full vector secular variation curves have been constructed for Mexico for the Late Quaternary for Mexico. This work provides 32 new high quality paleomagnetic directions and 21 high fidelity paleointensities retrieved from 33 volcanic structures located within the Trans-Mexican volcanic belt. The new data are essential for enhancing the global geomagnetic field models covering the past 10,000-14,000

years [ARCH10k.1 (Constable et al., 2016, CALS10k.1b (Korte et al., 2011), SHA.DIF.14k (Pavón-Carrasco et al., 2014)]. This in turn will enhance the paleomagnetic dating approach for Mexico. The new curves were calculated for two periods: 2,000 AD–2,200 BC and 2,200 BC–45,000 BC, due to the uneven distribution of the data. During the entire period, numerous features of the Earth's magnetic field are noted where the directions abruptly changed accompanied by extremely high intensities or sudden intensity drops. Moreover, abnormal low inclinations accompanied by marked westerly declinations and very low intensities were observed between 26,000 and 24,000 BC. These anomalous behaviors could be attributed to geomagnetic jerks and/or an excursion firstly documented for Mexico for the Late Quaternary. Comparing with other regions, this anomaly may be related to the Mono Lake excursion.

References

- Aitken, M.J., Allsop, A.L., Bussell, G.D., Winter, M.B., 1988: Determination of the intensity of the Earth's magnetic field during archeological times: reliability of the Thellier technique. *Reviews of Geophysics* 26, 3–12
- Arrighi, S., Tanguy, J.-C. & Rosi, M., 2006. Eruptions of the last 2200 years at Vulcano and Vulcanello (Aeolian Islands, Italy) dated by high-accuracy archaeomagnetism, *Phys. Earth planet. Inter.*, 159, 225–233.
- Ben-Yosef, E., Tauxe, L., Levy, T.E., Shaar, R., Ron, H., Najjar, M., 2009. Geomagnetic intensity spike recorded in high resolution slag deposit in Southern Jordan. *Earth Planet. Sci. Lett.* 287 (3–4), 529–539.
- Blatter, D.L., Hammersley, L., 2010. Impact of the Orozco fracture zone on the central Mexican Volcanic Belt. *J. Volcanol. Geotherm. Res.* 197 (1), 67–84.
- Böhnell, H., Molina-Garza, R., 2002. Secular variation in Mexico during the last 40,000 years, *Phys. Earth Planet. Inter.*, 133, 99–109.
- Brown, M. C., Donadini, F., Korte, M., Nilsson, A., Korhonen, K., Lodge, A., et al., 2015. GEOMAGIA50.v3: 1. general structure and modifications to the archeological and volcanic database. *Earth Planets Space* 67, 83. doi: 10.1186/s40623-015-0232-0
- Cai S. et al., 2017. Recent Advances in Chinese Archeomagnetism. *Front Earth Sci* 5, doi: 10.3389/feart.2017.00092.
- Carmichael, I.S.E., 2002. The andesite aqueduct: perspectives on the evolution of intermediate magmatism in west-central (105–99° W) Mexico. *Contrib. Mineral. Petrol.* 143 (6), 641–663.
- Chevrel, M.O., Siebe, C., Guilbaud, M.N., Salinas, S., 2016a. The AD 1250 El Metate shield (Michoacán): Mexico's most voluminous Holocene eruption and its significance for archaeology and hazards. *The Holocene* 26 (3):471–488. <http://dx.doi.org/10.1177/0959683615609757>.
- Chevrel, M.O., Guilbaud, M.N., Siebe, C., 2016b. The AD 1250 effusive eruption of El Metate shield volcano (Michoacán, Mexico): magma source, crustal storage, eruptive dynamics, and lava rheology. *Bull. Volcanol.* 78 (4):32. <http://dx.doi.org/10.1007/s00445-016-1020-9>.

- Coe, R. S., 1967: Palaeointensities of the Earth's magnetic field determined from Tertiary and Quaternary rocks, *J. Geophys. Res.*, 72, 3247–3262.
- Constable, C., Korte, M., and Panovska, S., 2016. Persistent high paleosecular variation activity in southern hemisphere for at least 10 000 years. *Earth Planet. Sci. Lett.* 453, 78–86. doi: 10.1016/j.epsl.2016.08.015.
- Dekkers, M.J. & Böhnell, H.N., 2006: Reliable absolute palaeointensities independent of magnetic domain state, *Earth Planet. Sci. Lett.*, 248, 507-516.
- Demant, A., 1978. Características del Eje Neovolcánico Transmexicano y sus problemas de interpretación. *Rev. Mex. Cienc. Geol.* 2 (2), 172–187.
- Dunlop, D.G., 2011. Physical basis of the Thellier–Thellier and related paleointensity methods *Phys. Earth Planet. Inter.*, 187 (3–4), 118-138
- Dunlop, D. J., and K. S. Argyle, 1997: Thermoremanence, anhysteretic remanence and susceptibility of submicron magnetites: Nonlinear field dependence and variation with grain size, *J. Geophys. Res.*, 102, 20,199–20,210, doi:10.1029/97JB00957.
- Dunlop and Özdemir, 1997: *Cambridge Studies in Magnetism: Rock Magnetism: Fundamentals and Frontiers* Cambridge University Press, Cambridge, UK (1997).
- Elsasser, W.M., 1956. Hydrodynamic Dynamo Theory, *Rev. Mod. Phys.*, 28 (2), 135-163.
- Enkin, R., 2005. PMGSC 4.2. Geological survey of Canada, Sidney, British Columbia, Canada.
- Fabian, K and Leonhardt, R, 2010: Multiple-specimen absolute paleointensity determination: an optimal protocol including pTRM normalization, domain-state correction, and alteration test *Earth Planet. Sci. Lett.*, 297 (2010), pp. 84–94 <http://dx.doi.org/10.1016/j.epsl.2010.06.006>.
- Ferk A. Leonhardt R., 2009. The Laschamp geomagnetic field excursion recorded in Icelandic lavas, *Phys. Earth planet. Inter.*, 177, 19–30.
- Ferrari, L., Orozco-Esquivel, T., Manea, V., Manea, M., 2012. The dynamic history of the Trans-Mexican Volcanic Belt and the Mexico subduction zone. *Tectonophysics* 522, 122–149.
- Fisher, R.A., 1953. Dispersion on a sphere. *Proc. R. Soc. Lond. A* 127, 295–305.
- Folgheraiter, G., 1899: Sur les variations seculaire de l'inclinaison magnetique dans l'antiquite, *Arch. Sci.*

Gallet, Y., Genevey, A., Courtillot, V., 2003. On the possible occurrence of archaeomagnetic jerks in the geomagnetic field over the past three millennia. *Earth Planet. Sci. Lett.* 214, 237–242.

Genevey, A., Gallet, Y., 2002. Intensity of the geomagnetic field in western Europe over the past 2000 years: new data from ancient French pottery. *J. Geophys. Res.* 107. <http://dx.doi.org/10.1029/2001JB000701>.

Glatzmaier, G.A., Coe, R.S., Hongre, L., and Roberts, P.H. 1999. The role of the Earth's mantle in controlling the frequency of geomagnetic reversals, *Nature*, 401, 805-810.

Gómez-Paccard, M., Lanos, Ph., Chauvin, A., McInstosh, G., Osete, M.L., Catanzariti, G., Ruiz-Martínez, V.C., Núñez, J.I., 2006. The first archaeomagnetic secular variation curve for the Iberian Peninsula. Comparison with other data from Western Europe and with global geomagnetic field models *Geochem. Geophys. Geosyst.*, 7 (Q12001, 10.1029/2006GC001476).

Gómez-Tuena, A., LaGatta, A.B., Langmuir, C.H., Goldstein, S.L., Ortega-Gutiérrez, F., Carrasco- Núñez, G., 2003. Temporal control of subduction magmatism in the eastern Trans-Mexican Volcanic Belt: mantle sources, slab contributions, and crustal contamination. *Geochem. Geophys. Geosyst.* 4 (8). <http://dx.doi.org/10.1029/2003GC000524>.

Gómez-Tuena, A., Orozco-Esquivel, M.T., Ferrari, L., 2005. Petrogénesis ígnea de la Faja Volcánica Transmexicana. Volumen conmemorativo del centenario. *Temas Selectos de la Geología Mexicana. Boletín de la Sociedad Geológica Mexicana* 57(3): 227-283.

Gonzales, S., Pastrana A., Siebe, C., Duller, G., 2000. Timing of the prehistoric eruption of Xitle Volcano and the abandonment of Cuicuilco Pyramid, Southern Basin of Mexico. *Geol Soc London Sp Pub* 171:205-224.

Guilbaud, M.N., Siebe, C., Lauer, P., Salinas, S., 2012. Reconstruction of the volcanic history of the Tacámbaro-Puruarán area (Michoacán, México) reveals high frequency of Holocene monogenetic eruptions. *Bull. Volcanol.* 74, 1187–1211.

Hagstrum, J.T., Champion, D.E., 2002. Holocene paleosecular variation record from 14C-dated volcanic rocks in western north America. *J. Geophys. Res.* 107, 10.1029/2001 JB 000524.

Hagstrum, J.T. & Blinman, E., 2010. Archeomagnetic dating in western North America: an updated reference curve based on paleomagnetic and archeomagnetic data sets, *Geochem. Geophys. Geosyst.*, 11, Q06009, doi: 10.1029/2009GC002979.

- Heider, F., Dunlop, D.J., Soffel, H.C., 1992: Low-temperature and alternating field demagnetization of saturation remanence and thermoremanence in magnetite grains (0.037 m to 5 mm). *J. Geophys. Res. B* 97, 9371–9381.
- Hill M.J. Shaw J., 1999. Palaeointensity results for historic lavas from Mt. Etna using microwave demagnetization/remagnetization in a modified Thellier type experiment, *Geophys. J. Int.*, 139, 583–590.
- Hulot, G., Eymin, C., Langlais, B., Manda, M., Olsen, N., 2002. Small-scale structure of the geodynamo inferred from Oersted and Magsat satellite data. *Nature*, 416 (2002), pp. 620-623.
- Jackson, A., Jonkers, A.R., and Walker, M.R., 2000. Four centuries of geomagnetic secular variation from historical records, *Phil. Trans. R. Soc. A*, 358(1768), 957–990.
- Kim, Y., Miller, M.S., Pearce, F., Clayton, R.W., 2012. Seismic imaging of the Cocos plate subduction zone system in central Mexico. *Geochem. Geophys. Geosyst.* 13 (7). <http://dx.doi.org/10.1029/2012GC004033>
- Kirschvink, J.L., 1980. The least-squares line and plane and analysis of palaeomagnetic data. *Geophys. J. R. Astron. Soc.* 62, 699–718.
- Kissel, C., Rodriguez-Gonzalez, A., Laj, C., Perez-Torrado, F., Carracedo, J.C., Wandres, C., Guillou, H., 2015a. Paleosecular variation of the earth magnetic field at the Canary Islands over the last 15 ka. *Earth Planet. Sci. Lett.* 412, 52–60.
- Kissel, C., Laj, C., Rodriguez-Gonzalez, Perez torrado, A F., Carracedo, J.C., Wandres, C., 2015b. Holocene geomagnetic field intensity variations: contribution from the low latitude Canary Islands site *Earth Planet. Sci. Lett.*, 430 (2015), pp. 178-19.
- Koenigsberger, J.G., 1938: Natural residual magnetism of eruptive rocks. *Terr. Magn. Atmos. Elect.* 43, 299 320.
- Kok, Y.S. and Tauxe, L., 1996. Saw-toothed pattern of relative paleointensity records and cumulative viscous remanence, *Earth Planet. Sci. Lett.*, 137, 95-99.
- Korte, M., Constable, C., Donadini, F., and Holme, R., 2011. Reconstructing the holocene geomagnetic field. *Earth Planet. Sci. Lett.* 312, 497–505. doi: 10.1016/j.epsl.2011.10.031.
- Kovacheva, M., Kostadinova-Avramova, M., Jordanova, N., Lanos, P., and Boyadzhiev, Y., 2014. Extended and revised archaeomagnetic database and secular variation curves from Bulgaria for the last eight millennia. *Phys. Earth Planet. Inter.* 236, 79–94. doi: 10.1016/j.pepi.2014.07.002.

Krása, D., C. Heunemann, R. Leonhardt, and N. Petersen (2003), Experimental procedure to detect multidomain remanence during Thellier-Thellier experiments, *Phys. Chem. Earth*, 28, 681-687.

Laj, C., Kissel, C., 2014. Dynamics of the earth magnetic field in the 10–75kyr period comprising the Laschamp and Mono Lake Excursions: new results from the French Chaine des Puy in a global perspective. *Earth Planet. Sci. Lett.* 387, 184–197.

Lanos, Ph., 2004. Bayesian inference of calibration curves: application to archaeomagnetism. In: Buck, C., Millard, A. (Eds.), *Tools for Constructing Chronologies: Crossing Disciplinary Boundaries*. Springer-Verlag, London, pp. 43-82. vol. 177.

Leonhardt, R., Heunemann, C., Krása, D., 2004. Analyzing absolute paleointensity determinations: acceptance criteria and the software ThellierTool4.0. *Geochem. Geophys. Geosyst.* 5 (12).

Merrill, R.T., McElhinny, M.E., and McFadden, P.L., 1996. The magnetic field of the Earth — palaeomagnetism, the core, and the deep mantle, *Acad. Press Geophys. Ser.*, 63, 531 pp.

Michalk, D.M., Biggin, A.J., Knudsen, M.F., Böhnell, H.N., Nowaczyk, N., Ownby, S., Lopez-Martinez, M., 2010. Application of the multispecimen palaeointensity method to Pleistocene lava flows from the Trans-Mexican Volcanic Belt *Physics of the Earth and Planetary Interiors*, 179, pp. 139-156.

Mochizuki, N., Tsunakawa, H., Oishi, Y., Wakai, S., Wakabayashi, K., Yamamoto, Y., 2004: Palaeointensity study of the Oshima 1986 lava in Japan: implications for the reliability of the Thellier and LTD-DHT Shaw method. *Phys. Earth Planet. Int.* 146, 395–416.

Monster, M.W.L., de Groot, L.V. & Dekkers, M.J., 2015. MSP-Tool: a VBA based software tool for the analysis of multispecimen paleointensity data, *Front. Earth Sci.*, 3, 86, doi:10.3389/feart.2015.00086.

Néel, L. (1949), Théorie du traînage magnétique des ferromagnétiques en grains fins avec applications aux terres cuites, *Ann. Géophys.*, 5, 99-136.

Néel, L. (1955), Some theoretical aspects of rock-magnetism, *Advances in Physics*, 14, 191-243.

Oishi, Y., Tsunakawa, H., Mochizuki, N., Yamamoto, Y., Wakabayashi, K. & Shibuya, H., 2005. Validity of the LTD-DHT Shaw and Thellier paleointensity methods: a case study of the Kilauea 1970 lava, *Phys. Earth planet. Inter.*, 149, 243–257.

- Ozima, M., Ozima, M. & Akimoto, S., 1964. Low temperature characteristics of remanent magnetization of magnetite—self-reversal and recovery phenomena of remanent magnetization, *J. Geomag. Geoelectr.*, 16, 165–177.
- Pardo, M., Suárez, G., 1995. Shape of the subducted Rivera and Cocos plates in southern Mexico: seismic and tectonic implications. *J. Geophys. Res.* 100 (B7), 12357–12373
- Pasquaré, G., Ferrari, L., Garduño, V. H., Tibaldi, A., Vezzoli, L., 1991. Geology of the central sector of the Mexican Volcanic Belt, States of Guanajuato and Michoacán. Geological Society of America, Maps and Chart Series MCH072, scale 1:300000, 1 sheet, 22 p text.
- Paterson, G.A., Tauxe, L., Biggin, A.J., Shaar, R., Jonestrask, L.C., 2014. On improving the selection of Thellier-type paleointensity data. *Geochem. Geophys. Geosyst.* 15, 1180–1192.
- Pavón-Carrasco, F.J., Rodríguez-González, J., Osete, M.L. & Torta, J.M., 2011. A Matlab tool for archaeomagnetic dating, *J Archaeol. Sci.*, 38(2), 408–419.
- Pavón-Carrasco, F.J., Osete, M.L., Torta, J.M., De Santis, A., 2014. A geomagnetic field model for the Holocene based on archaeomagnetic and lava flow data. *Earth Planet. Sci. Lett.* 388, 98–109.
- Riisager, P., Riisager, J., 2001: Detecting multidomain magnetic grains in Thellier palaeointensity experiments. *Physics of the Earth and Planetary Interiors* 125 (1–4), 111–117.
- Roperch, P., Chauvin, A., Lara, L.E. & Moreno, H., 2015. Secular variation of the Earth's magnetic field and application to paleomagnetic dating of historical lava flows in Chile, *Phys. Earth planet. Inter.*, 242, 65–78.
- Schnepp, E., Lanos, P., 2005. Archaeomagnetic secular variation in Germany during the past 2500 years, *Geophys. J. Int.*, 163, 479–490, doi: arXiv: astro-ph/10.1111/j.1365-246X.2005.02734.x.
- Schnepp, E., Lanos, P., 2006. A preliminary secular variation reference curve for archaeomagnetic dating in Austria, *Geophys. J. Int.*, 166, 91–96.
- Shaar, R., and L. Tauxe (2013), Thellier_GUI: An integrated tool for analyzing paleointensity data from Thellier-type experiments, *Geochem. Geophys. Geosyst.*, 14, 677–692, doi:10.1002/ggge.20062.

- Shaw, J.: 1974: A new method of determining the magnitude of the paleomagnetic field: Application to five historic lavas and five archaeological samples, *Geophys. J. R. Astron. Soc.*, 76, 637 – 651.
- Siebe, C., 2000. Age and archaeological implications of Xitle volcano, southwestern Basin of Mexico-City. *J Volcanol Geotherm Res* 104: 45-64
- Smirnov, A., Tarduno, J., and Pisakin, B., 2003. Palaeointensity of the early geodynamo (2.45 Ga) as recorded in Korelia: a single crystal approach, *Geology*, 31 (5), 415-418.
- Speranza, F., Branca, S., Coltelli, M., D’Ajello Caracciolo, F. & Vigliotti, L., 2006. How accurate is “paleomagnetic dating”? New evidence from historical lavas from Mount Etna, *J. geophys. Res.*, 111(B12), doi: 10.1029/2006JB004496.
- Speranza, F., Pompilio, M., D’Ajello Caracciolo, F. & Sagnotti, L., 2008. Holocene eruptive history of the Stromboli volcano: constraints from paleomagnetic dating, *J. geophys. Res.*, 113(B9), doi: 10.1029/2007JB005139.
- Tanguy, J.C., Le Goff, M., Principe, C., Arrighi, S., Chillemi, V., Paiotti, A., La Delfa, S. & Patane, G., 2003. Archeomagnetic dating of Mediterranean volcanics of the last 2100 years: validity and limits, *Earth planet. Sci. Lett.* 211, 111–124.
- Tauxe, L., 1993. Sedimentary records of relative paleointensity of the geomagnetic field: Theory and practice, *Rev. Geophys.*, 31, 319-354.
- Tauxe, L., 2010. *Essentials of paleomagnetism*, University of California Press.
- Tauxe, L., Staudigel, H., 2004: Strength of the geomagnetic field in the Cretaceous Normal Superchron: new data from submarine basaltic glass of the Troodos Ophiolite. *Geochemistry Geophysics Geosystems* 5 (Art. No. Q02H06).
- Tema, E., Hedley, I., Lanos, Ph., 2006. Archaeomagnetism in Italy: a compilation of data including new results and a preliminary Italian secular variation curve *Geophys. J. Int.*, 167 (2006), pp. 1160-1171.
- Tema, E., Herrero-Bervera, E., Lanos, Ph., 2017. Geomagnetic field secular variation in Pacific Ocean: A Bayesian reference curve based on Holocene Hawaiian lava flows. *Earth Planet Sci Lett* 478:58-65.
- Thellier, E., Thellier, O., 1959: Sur l’intensité du champ magnétique terrestre dans la passé historique et géologique. *Annales de Geophysique* 15, 285–376.

Tsunakawa, H., Shaw, J., 1994: The Shaw method of palaeointensity determinations and its application to recent volcanic rocks. *Geophys. J. Int.* 118, 781–787.

Tsunakawa H. Shimura K. Yamamoto Y., 1997. Application of double heating technique of the Shaw method to the Brunhes epoch volcanic rocks (abstract)8th Scientific Assembly IAGA, Uppsala .

Walton, D., Snape, S., Rolph, T., Shaw, J., Share, J., 1996. Application of ferrimagnetic resonance heating to palaeointensity determinations 94, 183–186.

Yamamoto Y, Tsunakawa H, Shibuya H, 2003: Paleointensity study of the Hawaiian 1960 lava: implications for possible causes of erroneously high intensities. *Geophys J Int* 153:263-276.

Zijderveld, J.D.A., 1967. AC demagnetization of rocks: analysis of results. In: Runcorn, S.K., Creer, K.M., Collinson, D.W. (Eds.), *Methods in Paleomagnetism*. Elsevier, Amsterdam, pp. 254–286.

SUPPLEMENTARY MATERIALS

Supplementary Material I

Manuscript 5

A 3600 years paleointensity secular variation curve for Mexico

Ahmed Nasser Mahgoub^{1,*}, Harald Böhnel¹, Linda Manzanilla², Ann Cyphers², and Erick Juárez-Arriaga¹

¹Centro de Geociencias, Universidad Nacional Autónoma de México, Blvd. Juriquilla
3001, Querétaro 76230, Mexico

²Instituto de Investigaciones Antropológicas, Universidad Nacional Autónoma de
México, Delegación Coyoacán 04510 D.F., Mexico

To be submitted to the journal of the Physics of the Earth and Planetary Interiors.

Individual contributions of the authors:

- i. **Ahmed Nasser Mahgoub:** designing the project, sampling preparation, performing archeointensity experiments, analyzing and interpreting of data, writing the article.
- ii. **Harald Böhnel:** designing the project, participating in the interpretation of data and revising the article, financing for the project.
- iii. **Linda Manzanilla:** providing archeological samples, providing age data.
 - i. **Ann Cyphers:** providing archeological samples, providing age data.
 - ii. **Erick Juárez-Arriaga:** constructing the archeointensity secular variation model.

A 3600 years paleointensity secular variation curve for Mexico

Ahmed Nasser Mahgoub^{1,*}, Erick Juárez-Arriaga¹, Harald Böhnell¹, Linda Manzanilla², and Ann Cyphers²,

¹Centro de Geociencias, Universidad Nacional Autónoma de México, Blvd. Juriquilla 3001, Querétaro 76230, Mexico

²Instituto de Investigaciones Antropológicas, Universidad Nacional Autónoma de México, Delegación Coyoacán 04510 D.F., Mexico

Abstract

Our knowledge of the earth's magnetic field intensity changes over the past few thousand years is still limited because of the irregular spatial and temporal distribution of data, which also includes the Americas. The present study reports 44 new archeointensity data covering the past 3600 years which, together with 27 previously published data of similar quality, are used to construct a paleointensity secular variation curve for Central Mexico. This new data is an important contribution to the global intensity database and will also improve the application of paleomagnetic dating in Mexico, which is important because of the many Holocene monogenetic volcanoes within the Trans-Mexican Volcanic Belt. The most conspicuous feature of the new intensity curve is the rapid increase between 400 and 250 BC, from about 42 to 65 μT . Comparable intensity highs were observed in other low-latitude regions (15-30°N) like the Canary Islands, Senegal, Mali, and Hawaii. In the Levant, a paleointensity spike (LS) was found ~980 BC and has been proposed to have occurred during similar periods also in China, South Korea, Turkey, and Texas, all located within the 30-40°N latitude band. For this period, unfortunately, our intensity curve is undefined because no data are available. The Mexican intensity high is younger and may thus point to waxing-waning regional anomalies that additionally may have migrated laterally, similar to the South Atlantic Anomaly over the last centuries, rather than to representing globally coinciding intensity changes. Other relative intensity highs of $\approx 45\text{-}55$ μT were found around 1600 BC, 350 AD, 1200 AD and 1750 AD and relative intensity lows of $\approx 30\text{-}35$ μT around 1350 BC and 700 AD and may also reflect regional non-dipole intensity variations.

Keywords: Archeomagnetism; Mexico; paleointensity secular variation curves; TransMexican Volcanic Belt; paleomagnetic dating; Levant paleointensity Spike

1. Introduction

Deciphering the secular variation (SV) of the Earth's magnetic field (EMF) would provide important experimental data to be incorporated in dynamo models, which describe the physical processes occurring in the outer core (Biggin et al., 2012). Secular variation further has recently been used for archeomagnetic dating (Pavón-Carrasco et al., 2011). The use of these applications is limited by factors such as (i) the inaccuracy in the age data of analyzed materials (lavas, archeological artifacts, and especially sediments), (ii) the difficulty to determine reliable paleointensity records, and (iii) the uneven distribution of the SV data in time and space. For instance, plenty paleointensity data are available in several areas such as Europe (e.g. Ertepinar et al., 2012) and the Levant (e.g. Ben-Yosef et al., 2009), but this presents a bias for global SV curves (Korte et al., 2009; Korte and Constable, 2011; Nilsson et al., 2014; Pavón-Carrasco et al., 2014). In consequence, during recent years efforts have been undertaken in other regions to enhance this situation, just like in eastern China (Cai et al., 2017). The most intriguing event in the EMF that occurred during the past 3600 years is known as the Levantine intensity spike, which in the near-east Arabian suggests intensity around 980 BC about two times higher than today. Spatially, the Levantine spike (LS) has been observed in the Levant (Ben-Yosef et al., 2009; Shaar et al., 2011; Shaar et al., 2016) at ≈ 980 BC and proposed for Turkey (Ertepinar et al., 2012) at ≈ 1050 BC, Eastern Asia (Cai et al., 2017) at ≈ 1300 BC, and in North America (Bourne et al., 2016) at ≈ 1000 BC. Moreover, comparable intensity peaks were recorded in some European data including Bulgaria, Greece, and the Canary Island at around 500 BC (Kissel et al., 2015) and in Hawaiian data at ≈ 150 BC (Tema et al., 2017). Documenting such features for more regions over the world is required to decide about the spatial and temporal coincidence. At this moment the LS cannot be explained by current geodynamo theories (Nilsson et al., 2014), and thus leaves open the reasons for this phenomenon (Davies and Constable, 2017). This clearly reflects the need for reliable paleointensity (PI) data from the North America which may help us to give a more comprehensive explanation of this phenomenon and its temporal and spatial variation. Mexico as part of North America is ideally suited for obtaining PI because of the abundance of archeological sites and of

volcanic rocks, and the thermoremanent magnetization (TRM) of these records may provide us with high-quality PI data. Unexpectedly, so far Mexico suffers from a severe lack of paleointensity data even over the past few thousand years. For the past 3600 years, only 99 intensity data are reported by the GEOMAGIA50.v3 database (Brown et al., 2015), which are plotted in supplementary Fig. S1a (all data were recalculated to Mexico City, 19.43°N - 99.13°W). From Fig. S1a, Mexican PI data (MPD) show large scatter, which could be attributed to age data errors, but also to unreliable intensity data itself. Below we will demonstrate that many of these data may be classified as of low quality, lacking many of the reliability standards used today (Paterson et al., 2014). The present study aims to provide new quality intensity data which indeed fulfill such standards, with ages between 1600 BC and 1900 AD, and also to select previously published MPD in this age range fulfilling similar quality criteria. Taken into account the age and paleointensity uncertainties, a set of curves produced from a bootstrap algorithm combined with cubic P-Splines results in an intensity master curve with a 2σ uncertainty error (e.g. Thébaud and Gallet, 2010).

2. Archeological background and sampling

Archeological artifacts used in this study were collected from four locations within Central and Eastern Mexico, namely, Teotihuacan, Olmec sites, Xitle reheated pottery fragments, and the colonial temple of Santa Rosa de Viterbo (Fig. 1a). The materials from the first three locations are pottery sherds and from the last one are bricks (Figs. 1b and c), with a total of 60 pieces. Additionally, seven dated lava flows within the Trans-Mexican Volcanic Belt (TMVB) have been sampled (Fig. 1a). Below we are giving an outline of each studied archeological location and lava flows, and Table 1 lists the sites name, latitudes and longitudes, ages, the number of the archeological pieces or drill cores used from each site and the number of specimens studied from each site.

2.1. Teotihuacán

Teotihuacán (19.69°N, 98.84°W) is an ancient Mesoamerican city located in the State of Mexico 40 kilometers northeast of modern-day Mexico City, known today as the site of many of the most architecturally significant Mesoamerican pyramids built in the pre-Columbian Americas. In this location, 34 Pottery sherds were collected from 11 sites which have ^{14}C ages ranging between ~240 BC and 1435 CE (Table 1). The sherds from Cuanalan, Teopancazco, Cueva del Pirul, and Cueva de las Varillas come from extensive

excavations headed by Linda R. Manzanilla: Cuanalan is a Late and Terminal Formative village located to the south of the Teotihuacan Valley; Teopancazco is a multiethnic neighborhood center of the Classic period in Teotihuacan; Cueva del Pirul and Cueva de las Varillas are two quarry tunnels located to the east of the Pyramid of the Sun in Teotihuacan, with post-Teotihuacan occupations (Epiclassic and Late Postclassic).

2.2. San Lorenzo, Veracruz, and satellite centers (Olmec culture).

San Lorenzo is the earliest Olmec capital which is located in the coastal plains of the southeast portion of the Mexican state of Veracruz (17.75°N, 94.76°W). The secondary center of Loma del Zapote is located immediately south of the capital, and the site complex of El Bajío-El Remolino is located 3-4 km to the north. San Lorenzo is famous for the 10 majestic colossal stone heads unearthed there and many other magnificent stone sculptures. Since 1990 the San Lorenzo Tenochtitlán Archeological Project has concentrated on investigating the ancient environment and subsistence as well as documenting and explaining diachronic settlement patterns at the site and regional level. Its objectives include the excavation of diverse areas within the capital of San Lorenzo in order to understand the differential use of space over time. 18 independent pottery fragments collected in the present study (Table 1) come from whole and partial vessels found on occupation floors within sealed excavation contexts at the capital and satellite centers. These contexts vary in function with the representation of domestic, ceremonial and administrative areas. Their temporal placement is supported by ¹⁴C dates and relative dating by ceramic attributes as demonstrated in the supplementary material Fig. S2 and listed in Table S1.

2.3. Xitle reheated pottery fragments.

Xitle (19.32°N, 99.18°W) is located within the Sierra del Chichinautzin volcanic field located south of Mexico City and extending from Popocatepetel to Toluca. Xitle is considered the youngest monogenetic volcano of the SCVF as it has a C¹⁴ age of ≈1530-1630 BP (Siebe, 2000; Gonzales et al., 2000) which had direct impact on the pre-Hispanic population in this area, as observed at the archeological site of Copilco (Siebe, 2002). Several paleomagnetic analyses have been performed in Xitle (e.g. Böhnelt et al., 2003) and undesirably large discrepancies in the paleointensities were obtained (for more details see section 6.1). Böhnelt et al. (2003) have performed paleointensity experiments using the microwave technique on baked sediments and pottery fragments proved to be reheated by

the Xitle lavas and accordingly acquired a TRM of the same age as Xitle (1530-1630 BP). In order to reduce the dispersion of the paleointensity data published for Xitle, 4 pottery fragments were collected beneath the Xitle lava flow, which were subdivided into 17 specimens.

2.4. Santa Rosa de Viterbo bricks.

The Temple and Convent of Saint Rose of Viterbo (Santa Rosa de Viterbo; 20.59°N, 100.40°W) is located in the city of Queretaro, Mexico, representing the greatest expression of Queretaro Baroque in the eighteenth century and one of the most representatives building with its architecture and elaborate altar pieces. For the present study, a number of four un-oriented brick fragments (Fig. 1c) were obtained which come from the foundation of the constructions started in 1798 AD.

2.5. Lava Flows.

Seven lava flows distributed along the TMVB (Fig. 1a) were sampled during the course of several field trips in order to get insight to intensity variation in Mexico. Paleomagnetic sampling was done on two independent sites on four flows from Coacoatzintla, Nealtican, Puntigudo, Toaxtlacoaya, and Jumento volcanoes, while in both of San Martin volcano and one flow not associated to a specific vent “Non-associated flow” only one site per each was sampled. In total, 70 paleomagnetic specimens were available for the present study. Their ages are historical (San Martin) or were determined by the ^{14}C method. Age calibration was done applying the CALIB Computer Program of version 7.1 using the IntCal13 calibration curve (Reimer et al. 2013) and reported here with their 95% or 2σ uncertainty range.

3. Rock magnetic properties

Thermomagnetic measurements and hysteresis analyses were done on selected samples in order to define the magneto-mineralogy and its thermal stability and also to characterize the domain size of the enclosed magnetic minerals.

Thermomagnetic curves. 40 pieces of archeological and lava samples were milled be used in a horizontal translation Curie balance built in the laboratory, in a field of 500 mT at temperatures up to 600°C. Representative thermomagnetic curves are shown in Figure 2. Curie temperatures (T_c) were calculated using the methods of Moskowitz (1981) and the second derivative approach with the aid of the RockMag Analyzer (Leonhardt et al., 2006), and are listed in the supplementary Table S2. Almostly 60% of the investigated samples

(Table S2) are characterized by a single T_c of 520-580°C (Fig. 2 a, b), which is characteristic for titanium-poor titanomagnetite or magnetite as a prime remanence carrier. Beside a similar dominant Curie point, some other samples showed another T_c around 220–310 °C (Fig. 2 c, d), revealing that most probably Ti-rich titanomagnetite coexisted with the main magnetic mineral(s). Most of the investigated samples (27 out of 36) showed reversible heating-cooling curves with <10% decrease (Fig. 2, d) or increase (Fig. 2c) in magnetization after cooling to room temperature. On the other hand, 9 samples had an irreversible behavior with a decrease in magnetization after cooling of 10-30% which manifests the oxidation of the titanomagnetite/magnetite minerals during heating. It should be mentioned that samples containing two magnetic minerals were predominantly characterized by excellent reversibility, reflecting a high thermal stability.

Hysteresis analyses. Small chips of 30-50 mg from 40 archeological samples were used for hysteresis analyses with a MicroMag 2900 alternating gradient force magnetometer, in a maximum field of ± 1.0 T. After correction for paramagnetic and diamagnetic contributions and measuring the isothermal remanent magnetization (IRM) acquisition and backfield curves, saturation magnetization (M_s), saturation remanence (M_{rs}), coercivity force (H_c), and coercivity of remanence (H_{cr}) were determined and used to construct the Day Plot (Day et al., 1977, Dunlop, 2002) to quantify the bulk magnetic domain states of the samples. All samples are located within the pseudo-single domain (PSD) grain size field (Fig. 3d, Table S1). Three hysteresis curve shapes were observed (Fig. 3a-c), with some showing restricted loops suggesting multidomain (MD) type behavior (Fig. 3a) and lying in the lowermost part of the Day plot and slightly to the right of the theoretical single domain- multidomain (SD-MD) mixing lines (Fig. 3d). Such samples are also characterized by low H_{cr} values ranging from 13 to 21 mT. some other samples (e.g. sample TEX-68241 in Fig. 3b) exhibited a SD-like behavior lying in the uppermost part of the SD-MD mixing lines (Fig. 3d) and exhibiting a pot-bellied curve shape (Fig. 3b) and a H_{cr} of 31 mT. Four samples showed wasp-waisted shapes (Fig. 3c) which is indicative either for the presence of several magnetic phases with different coercivities or to the presence of both SD and superparamagnetic (SP) domain size particles (Tauxe et al., 1996). These samples had higher remanence coercivities in the range 45–74 mT and they are located in the Day Plot to the right of the theoretical SD-MD mixing lines (Fig. 3d).

4. Archeointensity methodology

From each archeological artefact (=pottery fragment), at least 4 specimens were processed for the intensity experiments. In order to obtain standard size paleomagnetic specimen, samples were cut and packed into salt pellets or in a non-magnetic cement (Fig. 1b). From four brick samples available from Santa Rosa de Viterbo, 25 cylindrical specimens of 25 mm diameter were drilled (RV1-RV4) (Fig. 1c). Similarly, 5 to 8 standard cylindrical specimens were used from each of the 6 investigated lava flows. Altogether, 358 specimens were subjected to the intensity experiments following the in-field, zero-field, zero-fielded, in-field “IZZI” protocol (Tauxe and Staudigel, 2004) with partial thermal remanent magnetization “pTRM” checks (Coe et al., 1978). Heatings were accomplished by using an ASC Scientific TD48 furnace with temperature reproducibility of 2°C. Heating steps were carried out at 100, 200, 250, 300, 340, 370, 400, 430, 460, 490, 510, 530, 560, and 580 °C, and pTRM checks implemented after every other temperature step at 100, 250, 340, 400, 460, 510, and 560 °C. Data were analyzed using the TellierTool 4.2 software (Leonhardt et al., 2004). In order to ensure high quality intensity data we used a stringent set of selection criteria which is listed in Table 2 together with their chosen upper limits. These selection criteria are: the number of the points included in the linear fit (N); the ratio of standard error of the slope of the selected segment in the Arai plot to the absolute value of the slope (β parameter); The fraction parameter (f); the quality factor (q); the anchored maximum angular deviation (MAD_{anc}); the angular difference between the anchored and free-floating vectors of the best fit direction (α); the relative check error (δCK) which is the maximum difference produced by a pTRM check normalized by the TRM; the cumulative pTRM check failure (δ_{pal}) quantified after the correction method of Valet et al. (1996) by calculating the difference between the slope of the non-corrected intensity estimate and slope of the check corrected intensity estimate normalized by the uncorrected slope; the absolute value of curvature of the data points used for determining the best-fit line ($|K'|$) (Paterson, 2011). At sample level (= independent archeological piece or lava flow), three classes A, B, and C were defined (Table 2) based on the minimum number of accepted specimens to calculate the sample-mean intensity and its standard deviation σ . Archeological samples of class A require that their mean intensity are calculated from at least three accepted specimens and must have a standard deviation (σ) less than 3 μT . Class B is similar except that $3 < \sigma < 5 \mu T$, while for Class C two accepted specimens must be available to calculate the sample-mean intensity with $\sigma < 5 \mu T$. The same applies for lava flow samples (Table 2), but with a standard deviation of $\sigma < 5$, $5 < \sigma < 10$, and $\sigma < 10 \mu T$

for classes A, B, and C, respectively. Higher dispersion for lava samples is allowed as these exhibit less thermal stability and contain larger magnetic particles than archeological objects, making them less suitable for paleointensity experiments.

Due to manufacturing processes, pottery and to a lesser degree also bricks (Mitra et al., 2013) are often characterized by a strong magnetic anisotropy (e.g. Rogers et al., 1979). Commonly, for the archeointensity corrections one needs to determine the anisotropy tensor (Veitch et al., 1984), which involves multiple TRM acquisition experiments. Alternatively, the laboratory field may be imparted parallel to the TRM (Aitken et al., 1981; Veitch et al., 1984; Chauvin et al., 2000; Ertepinar et al., 2012, 2016; Poletti et al., 2016), which renders unnecessary this correction. In this study, the NRM was always oriented parallel to the laboratory field (50 and 60 μT) using a special orientation tray (supplementary material, Fig. S3). No anisotropy correction was applied to lavas specimens, as these are of very low anisotropy, and the orientation of their NRM relative to the oven field was random. Dodson and McClelland-Brown (1980), Halgedahl et al. (1980), (Fox and Aitken, 1980), and (Perrin, 1998) have shown that there is a relationship between the TRM cooling rate and the intensity recorded: the slower the cooling rate the higher the magnetization, if it is carried by SD particles, whereas in MD particles the opposite may be true. In case of the TRM carried by pseudo single domain PSD particles, the effect of the cooling time is not clear, but probably negligible (Biggin et al., 2013). Therefore, cooling rate (CR) corrections are crucial for archeological artifacts, as its TRM often is carried by SD like particles. The CR correction for such materials was done following the experimental procedure of Chauvin et al. (2000) and Genevey and Gallet (2002). This involves three additional pTRM acquisition steps, at temperatures carefully selected so as at least a 60% fraction of the specimen's NRM was used. The first and the last experiments were performed with a rapid cooling time of 30 min and are named $\text{TRM}_{\text{fast1}}$ and $\text{TRM}_{\text{fast2}}$, respectively. The experiment in between (TRM_{slow}) was done with a slow cooling time ≈ 10 h, and for this purpose the oven cooling fan was turned off. The difference between $\text{TRM}_{\text{fast1}}$ and $\text{TRM}_{\text{fast2}}$ was used to detect alteration (cutoff value $< 5\%$). The cooling rate correction factor was calculated by dividing the average of the two TRM_{fast} steps by the TRM_{slow} step. Unlike in archeological artifacts, the TRM of lavas resides in larger PSD grain size particles (see above) which means there is no need for a CR correction.

5. Archeointensity results

142 out of 358 specimens provided acceptable paleointensity estimates resulting in an overall success rate of 40%. Specimens from Santa Rosa de Viterbo bricks and Olmec potteries had the highest (52%) and lowest (21%) success rates, respectively. At the sample level, 44 out of a total of 67 were accepted (37 archeological pieces and 7 lavas). Based on the aforementioned categories (Table 2), 18 samples belong to class A, 16 to class B and 10 to class C. Fig. 4a-e shows representative examples of five accepted paleointensity (or Arai) plots. Mean intensities at fragment and lava flow level are reported in Table 3, and the paleointensity estimates for all accepted specimen together with the selection parameters are listed in the supplementary Table S3. Intensity values were calculated over different temperature intervals which range from a minimum of 0-400°C to a maximum of 400-580°C. Best-fit lines for accepted specimens data are characterized by: 1) an NRM fraction (f) ranging between 50 and 96%; 2) an anchored maximum angular deviation (MAD_{anc}) ranging from 0.77° to 9.41°; (c) alteration monitoring parameters as the relative check error (δCK) between 0.74 and 9.81%, and the cumulative check difference (δpal) between 0.05 and 9.97%. The curvature parameter ($|K'|$) range from 0.0 to 0.16 with noting that it is larger in the lava than the archeological treated specimens. The large majority (68%) of the accepted specimens are characterized by f -values ≥ 0.6 , 83% have $MAD_{anc} < 5.0^\circ$, 79% have $\delta CK < 6.0\%$, 61% have $\delta pal < 6.0\%$, and 60% have ($|K'| \leq 0.10$), and thus fulfill even stricter acceptance criteria. Regarding rejected specimens, these altered during the experiment as indicated by failed pTRM checks (Fig. 2f-g), or because of zigzagging or concave PI curves in the Arai plots (Fig. 2h), an indication for an important contribution of MD particles. In some cases, samples were rejected because of the presence of large secondary overprints as indicated by the orthogonal vector plot (Fig. 2h). For accepted archeological specimens, the cooling rate correction factor was mostly between 0.79-1 (Fig. 5a), pointing to the presence of single domain magnetic grains (Dodson and McClelland-Brown, 1980; Halgedahl et al., 1980). Only for very few specimens, correction factors of 1-1.06 were noticed (Fig. 5a). Alteration of all accepted specimens after the cooling rate correction was between 0.11 and 4.70% (Fig. 5b). Finally, we mention here that no clear relation was found between the magnetic properties and paleointensity success rate. Most of the samples that gave irreversible thermomagnetic curves (Table S1) were indeed suitable for the paleointensity experiments belonging to classes A and B, while unacceptable Arai plots were sometimes related to reversible heating-cooling curves. Also,

some specimens located close to the MD size field in the Day plot gave acceptable intensity estimates.

6. Discussion and Conclusions

6.1. Selection of previously published Mexican paleointensity data

For the sake of comparison with our new results, previous PI data were revised regarding their reliability and internal consistency. The credibility of the associated age data is not addressed in this study, as not enough information is available. But we note here that some ages of volcanic rocks used in published paleomagnetic data are now known to be too old (See Mahgoub et al., 2017), which is one possible reason for the observed PI data dispersion. In the context of this study we specifically mention the monogenetic Xitle volcano, which is the most studied Mexican lava flow and probably of the entire world. Many early studies of Xitle used an age around 2000 BP (e.g., Urrutia-Fucugauchi, 1996), while recent and stratigraphically very well constrained younger ages were reported by Siebe (2000) (1675 ± 40 BP) and by Gonzales et al. (2000) (1675 ± 65 BP). We will use the latter ones, corresponding to a calibrated 2σ age range of 373 ± 56 AD, and apply it also to all previously published Xitle PI data that used other ages. Most previous PI studies used the double heating Thellier-Thellier and less often the Microwave and the multispecimen PI methods. Because of their similarities in the laboratory procedures and also the data analyses, both the Thellier-Thellier and Microwave PI data were evaluated using the same reliability criteria as for our own data. A detailed explanation of our criteria is listed in supplementary Table S4 and we resume the most important of these as following: (1) Monitoring of thermal alteration by means of the pTRM check criterions (δ_{CK} - δ_{pal}) must have been included for accepted specimens or, at least, mentioned in general in the text; (2) the stability of the NRM directions of the treated specimen during the paleointensity experiments (MAD_{anc} , α , and/or DANG) must have been evaluated; (3) both anisotropy and cooling rate corrections must have been investigated in the case of archeological artifacts; and (4) at least two specimens must have been used to compute mean intensities for archeological pieces and lavas, and their standard deviation must be ≤ 5 μ T and ≤ 10 μ T, respectively. For the multispecimen method (MSP) (Dekkers and Böhnel, 2006), set criteria are listed in Table S4, and here we note the main conditions: (1) for selection of the set temperature, thermomagnetic experiments for analysis of thermal

alteration is considered as necessary; (2) the correction method of Fabian and Leonhardt (Fabian and Leonhardt, 2010) (MSP-DSC) is required for accepting MSP data.

Accordingly, only 24 out of 99 PI data published for Mexico meet our criteria. These data and three recently published intensity results (see references in supplementary material S3) are plotted in Figure S1b, together with the 75 rejected data. It is clear that rejected PI are much more scattered than accepted data suggesting they are affected by experimental errors.

6.2. Mexican paleointensity SV curve for the last 3600 years.

In the present study, 44 robust paleointensity data covering the last 3.6 kyr were obtained which in comparison to the selected Mexican PI data representing 160%. After relocating them to Mexico City (19.43°N, 99.13°W), the obtained intensity values range from 16.3 to 76.8 μT , and the virtual axial dipole moments (VADM) range from 3.7 to 17.2×10^{22} Am^2 (Table 3). Intensity values of archeological pieces and lava flows of similar age are consistent within 10% over most of the period covered, as demonstrated in Fig. 6. Also, our new intensity data are reasonably consistent with the 27 selected previously published archeomagnetic data. This in general lends credibility to these intensity values and their age. However, in some cases significant dispersion of PI was observed between different fragments belonging to the same archeological site, as for example in the 5 accepted fragments from site Teotihuacán-Cueva Pirul (CPT) which was ^{14}C dated at 750 AD and provided intensities in the range of 16 to 40 μT . Such a large spread in the PI data may be attributed to undetected age error and/or to errors in the intensity determinations like undetected wrong cooling rate corrections. On the other hand, a large intensity spread was also observed between fragments of different archeological locations pertaining to the short period between 250 and 500 AD, where the intensity ranges from 27 to 63 μT . Such large variations could indicate a fast secular intensity change during this period but also be also related to age uncertainties. More data are needed for such periods in order to explain the observed large intensity scatter.

A paleointensity secular variation curve for Mexico was constructed from this data set. For this purpose, the bootstrap method was used (Thébaud and Gallet, 2010) with 1000 times random sampling of the data including their time and intensity uncertainties, combined with a third-order spline fit with a 50 years time window, and covering the period from 1600 BC to 1900 AD. For the past four centuries, the curve is constrained by historical data compiled from the *gufm1* model (Jackson et al., 2000) which were queried from the HISTMAG

database (Arneitz et al., 2017), and those reported by the geomagnetic observatory Teoloyucan (Mexico City) for the period 1923-1985 AD (Urrutia-Fucugauchi and Campos-Enrique, 1993). The data of our model with its 95% uncertainty limits are listed in supplementary Table S5 and plotted in Figure 6 together with curves derived from global field models. This new data serves as an addition to the global archeointensity database which in turn will improve our understanding of the global geomagnetic field behaviour, and will thus greatly contribute to better paleomagnetic dating. The latter is important for regions of active volcanism like the Trans-Mexican Volcanic Belt, where age dating is a challenge for estimating the volcanic hazard (e.g. Mahgoub et al., 2017b). The new curve is well constrained between 1600 to 1100 BC and from CE 250 to 1100, while for the period between 1100 BC and 400 BC the curve uncertainty bounds are large because there is no PI data. For the time periods 400 BC-250 AD and 1100-1750 AD, additional data may refine the intensity curve. Nevertheless, some interesting features of the geomagnetic field intensity in Mexico can be figured out from this curve. The intensity decreased sharply from 52 to 35 μT between 1600 and 1350 BC and then remained almost constant for nearly 350 years until 1100 BC. For the period between 1100 and 400 BC, where there is no available data, the curve is largely undefined. Then after, the intensity value doubled from 42 to 65 μT between 400 and 250 BC which corresponds to a noteworthy intensity change rate of about 15 $\mu\text{T}/\text{century}$. It should be noted though that this rapid rate depends on a single volcanic site PI at 400 BC, and additional data, particularly for the period 500-350 BC, are needed in order to be prove this fast change. Intensities then dropped to $\sim 40\mu\text{T}$ at 200 AD, close to the present day value, and rose to a slightly higher value of $\sim 52\mu\text{T}$ at 400 AD. A pronounced minimum is observed between 400 and 1000 AD, with an intensity drop to $\sim 30\mu\text{T}$ at 700 AD. This is followed by two small intensity highs of $\sim 50\mu\text{T}$ at 1200 and 1700 AD, separated by an intensity low of $\sim 40\mu\text{T}$ at 1450 AD. Finally, the curve decreases smoothly until reaching the present day intensity of $\sim 42\mu\text{T}$. Compared to global models, our archeointensity curve deviates notably from the CALS3k.4 (Korte and Constable, 2011) model for almost the entire period, showing much stronger intensity variations. There is much better agreement with both ARCH3k.1 (Korte et al., 2009) and SHA.DIF.14K (Pavón-Carrasco et al., 2014). However, it should be noted that the well-defined intensity peaks and lows are not that well expressed in these models, probably because of the inclusion of less reliable and more dispersed PI data, which clearly reflects the importance of the present study for contributing data to the global databases used for such models. Of

course, this also requires that less reliable data as detected in this work have to be marked as such in the global databases, to caution against their use.

6.3. Comparison with regional and global archeointensity data sets

Our results are compared with regions north and south of Mexico, located at a maximum distance of ~2500 km from Mexico City, corresponding to the Southern United States (data set S.USA corresponding to Southern California, Arizona, Utah, New Mexico, and Texas) and Mesoamerica. For Mesoamerica only from Guatemala archeointensity data could be found. Datasets were compiled from the GEOMAGIA50.v3 data base (Brown et al., 2015) and also by referring to the original publications. In order to ensure a comparable quality of archeointensity data, we applied the same selection criteria as in the present study (supplementary material S3), and the data selected this way and the corresponding references are listed in Supplementary table S6. For comparison with the Mexican data, these data are plotted in Fig. 7, as well as relative-intensity data reported by Bourne et al. (2016) from sediments of Hall's Cave, Texas. Also demonstrated the S.USA paleointensity SV curve constructed from 37 selected data (Table S6) and using the procedure of Thébault and Gallet (2010), as we used in the present study. From Fig. 7, it is evident that not only Mexico but also the S-USA continent as a whole and Central America regions suffer from a shortage of PI data and thus must be enriched. Between 100-1250 AD, PI data from S.USA and Mexico are similar but afterwards the S.USA VADM rose to a much higher value of $\sim 14.0 \times 10^{22} \text{ Am}^2$ around 1750 AD and dropped to much lower values around 1900 AD. The S-USA constructed curve has good compatibility with our curve with the absence of some intensity details simply because few number of the S-USA data are available (Fig. 7). For Guatemala, only six intensity were found to be reliable are available between 800 BC and 100 BC, limiting the comparison with Mexican data. However, as a preliminary result we point out that two Guatemala data with ages between 800 BC and 400 BC fall within the Mexican curve uncertainty limits (Fig. 7), while four data from the period between 200 BC and 100 BC have much lower PI values than the corresponding Mexican data. For the Hall's Cave record, a reasonable fit with our data exists for the period between 1600 BC and 950 BC, followed by a strong difference until 500 AD, and afterwards they are again fairly similar. During the historical times between 1700 AD and 1900 AD, the Hall's Cave record shows a pronounced intensity low which is markedly different from the Mexican, nearby S.USA and historic intensity data. It is important to mention that around 1000 BC the Hall's Cave record gave an extreme VADM value of $\sim 40 \times 10^{22} \text{ Am}^2$ (inset in Fig. 7),

which is almost five times larger than the today's value and has so far never been observed elsewhere. Bourne et al. (2016) have related this peak to the Levantine intensity spike (LS) which was proposed in the Near East around ~980 BC (Ben-Yosef et al., 2009; Shaar et al., 2011; Shaar et al., 2016), thereby suggesting that the LS may be a global geomagnetic event. As we have no data around 1000 BC, we can not evaluate to this hypothesis. For comparison with more distant regions we use PI datasets from Eastern Asia (China, Japan and South Korea), the Levant (Syria, Jordan, Israel, Egypt, Cyprus, and South Turkey), the Iberian Peninsula and Azores islands, the Canary Islands and Western Africa, and finally the Hawaii Islands. Data selection and references of each region is provided in detail in the Supplementary Table S7. All of these data come from lava rocks or archeological artifacts with at least two specimens and a mean-PI with a $SD \leq 10 \mu\text{T}$ or $\leq 5 \mu\text{T}$, respectively. For each region, a paleointensity curve was constructed applying the same methods as for the Mexican data. To avoid the effect of a latitudinal gradient (Mitra et al., 2013), an upper latitude was set to 40°N in each region. For the purpose of comparison, we have plotted the PI data retrieved from mid-latitude regions ($30\text{--}40^\circ\text{N}$) in Fig. 8 a-d while data from the latitude band $15\text{--}30^\circ\text{N}$ are given in Fig. 8 e-g. Firstly, it is evident from Fig. 8 that low latitudes still lack many data and their curves, similar to Mexico, are characterized by periods with none or few PI data which increments the uncertainty of the SV curves. This limited number of available data is the main obstacle against evaluation of the global trends of intensity variations, however, some key observations can be extracted. For instance, the LS was clearly observed only around ~1000 BC in the Levant (Ben-Yosef et al., 2009; Shaar et al., 2011) and Texas (Bourne et al., 2016) which are located at similar latitudes ($\sim 30^\circ\text{N}$) but separated by $\sim 134^\circ$ in longitude. It should be further noted that in the Levant another intensity peak was obtained at ~700 BC (Shaar et al., 2016). Intensity highs comparable to those obtained in the Levant were retrieved from Eastern Asia archeological pieces at ~1300 BC (Cai et al., 2017), and the Iberian Peninsula and the Azores islands at ~800 BC. Similar to the Levant, in the latter another intensity peak was observed at 450 BC. For low latitude regions (Fig. 8 e-g), comparable peaks were observed in the Canary Islands and Western Africa around 600 BC, whereas in Mexico two independent locations gave intensity highs at ~250 BC, and finally an intensity peak was observed in the Hawaiian islands at ~150 BC. The timing and distribution of these intensity peaks and the unavailability of additional intensity curves for locations in between makes it impossible for the time being to interpret them as the result of drifting (Dumberry and Finlay, 2007)

and/or waxing flux patches as recently occurring with the South Atlantic Anomaly (Tarduno et al., 2018). The most we could argue is that the observed intercity spike in the Hall's Cave sediment record from Texas (Bourne et al., 2016) should have been recorded in other near-by regions as Mexico or Arizona, if the sources of this anomaly were located at the core-mantle boundary or even deeper (Davies and Constable, 2017). Unfortunately, no independent data are available yet to support or refuse this hypothesis of an North American spike.

Acknowledgments

Field and laboratory costs of A.N.M. and H.B. were defrayed by Consejo Nacional de Ciencia y Tecnología (CONACyT-180032) and the Dirección General de Asuntos del Personal Académico (UNAM-DGAPA IN-111915) granted to H. Böhnell. Ing. J. Escalante supported studies with the Curie balance and Ing. E. Nava maintained the computer network and servers. Hysteresis analyses were partly done at GFZ, Potsdam-Germany.

References (they are numbered to see how man are the refe)

- Aitken MJ, Alcock P, Bussell GD, Shaw C (1981) Archaeomagnetic determination of the past geomagnetic intensity using ancient ceramics: Allowance for anisotropy. *Arch* 23: 53–64.
- Arneitz P et al. (2017) The HISTMAG database: combining historical, archaeomagnetic and volcanic data. *Geophys J Int* 210(3): 1347–1359.
- Ben-Yosef E, et al. (2009) Geomagnetic intensity spike recorded in high resolution slag deposit in Southern Jordan. *Earth Planet Sci Lett* 287(3-4):529–539.
- Biggin A, et al. (2012) Possible links between long-term geomagnetic variations and whole-mantle convection processes. *Nat Geosci* 5:526–533.
- Böhnell, H., Biggin, A.J., Walton, D., Shaw, J., Share, J.A., 2003. Microwave palaeointensities from a recent Mexican lava flow, baked sediments and reheated pottery. *Earth Planet. Sci. Lett.* 214 (1–2), 221–236.
- Bourne MD, et al. (2016) High-intensity geomagnetic field “spike” observed at ca. 3000 cal BP in Texas, USA. *Earth Planet Sci Lett* 442:80–92.

Brown MC, et al. (2015) GEOMAGIA50.v3: 1. General structure and modifications to the archeological and volcanic database. *Earth Planets Space* 67:83.

Cai S. et al. (2017) Archaeointensity results spanning the past 6 kiloyears from eastern China and implications for extreme behaviors of the geomagnetic field. *Proc Natl Acad Sci* 114: 39–44, doi: 10.1073/pnas.1616976114.

Chauvin A, Garcia Y, Lanos P, Laubenheimer F (2000) Paleointensity of the geomagnetic field recovered on archaeomagnetic sites from France. *Phys Earth Planet Inter* 120(1-2):111–136.

Coe RS, Grommé S, Mankinen EA (1978) Geomagnetic paleointensities from radiocarbon dated lava flows on Hawaii and the question of the Pacific nondipole low. *J Geophys Res Solid Earth* 83(B4):1740–1756.

Day R, Fuller M, Schmidt VA (1977) Hysteresis properties of titanomagnetites: grain-size and compositional dependence. *Phys Earth planet Inter* 13: 260–267.

Davies C, Constable C (2017) Geomagnetic spikes on the core-mantle boundary. *Nat Commun* doi: 10.1038/ncomms15593.

Dekkers MJ, Bönhel HN (2006) Reliable absolute palaeointensities independent of magnetic domain state *Earth Planet Sci Lett* 284: 508–517.

Dodson MH, McClelland-Brown E (1980) Magnetic blocking temperatures of single-domain grains during slow cooling *J Geophys Res* 85: 2625–2637.

Dumberry M, Finlay CC (2007) Eastward and westward drift of the Earth's magnetic field for the last three millennia. *Earth Planet Sci Lett* 254 146–157.

Dunlop DJ (2002) Theory and application of the Day plot (Mrs/Ms versus Hcr/Hc) 1. Theoretical curves and tests using titanomagnetite data. *J geophys. Res* 107(B3) 2056, doi: 10.1029/2001JB000486.

Ertepinar P, et al. (2012) Archaeomagnetic study of five mounds from Upper Mesopotamia between 2500 and 700 BCE: Further evidence for an extremely strong geomagnetic field ca. 3000 years ago. *Earth Planet Sci Lett* 357-358:84–98.

Fabian K, Leonhardt R (2010) Multiple-specimen absolute paleointensity determination: An optimal protocol including pTRM normalization, domain-state correction, and alteration test. *Earth Planet Sci Lett* 297: 84–94.

Genevey A, Gallet Y (2002) Intensity of the geomagnetic field in Western Europe over the past 2000 years: New data from French ancient pottery. *J Geophys Res* 107(B11): 2285.

Gonzales S, Pastrana A, Siebe C, Duller G (2000) Timing of the prehistoric eruption of Xitle Volcano and the abandonment of Cuicuilco Pyramid, Southern Basin of Mexico. *Geol Soc London Sp Pub* 171:205-224.

Halgedhal S, Day R, Fuller M (1980) The effect of the cooling rate on the intensity of weak field TRM in single domain magnetite. *J Geophys Res* 85: 3690–3698.

Jackson A, Jonkers, ART, Walker MR (2000) Four centuries of geomagnetic secular variation from historical records. *Phil Trans R Soc Lond A358*: 957–990.

Kissel C, et al. (2015) Holocene geomagnetic field intensity variations: Contribution from the low latitude Canary Islands site. *Earth Planet Sci Lett* 430:178–190.

Korte M, Donadini F, Constable CG (2009) Geomagnetic field for 0–3 ka: 2. A new series of time-varying global models. *Geochem Geophys Geosyst* 10(6):Q06008.

Korte M, Constable C (2011) Improving geomagnetic field reconstructions for 0-3 ka. *Phys Earth Planet Inter* 188(3-4):247–259.

Leonhardt R, Heunemann C, Krása D (2004) Analyzing absolute paleointensity determinations: acceptance criteria and the software ThellierTool4.0. *Geochem Geophys Geosyst* 5 (12).

Leonhardt, R. (2006), Analyzing rock magnetic measurements: The RockMagAnalyzer 1.0 software, *Comput. Geosci.*, 32, 1420 – 1431.

Mahgoub, A.N., Böhnell, H., Siebe, C., Chevrel, M.O., 2017. Paleomagnetic study of el Metate shield volcano (Michoacán, Mexico) confirms its monogenetic nature and young age (~1250 CE). *J Volcanol Geotherm Res* 336:209–218. <https://doi.org/10.1016/j.jvolgeores.2017.02.024>.

Mitra R, Tauxe L, Keech McIntosh S (2013) Two thousand years of archeointensity from West Africa. *Earth Planet Sci Lett* 364:123–133.

Moskowitz, B. M., Methods for estimating Curie temperatures of titanomaghemites from experimental Js-T data, *Earth Planet. Sci.Lett.*, 53, 84-88, 198.

Nilsson A, Holme R, Korte M, Suttie N, Hill M (2014) Reconstructing Holocene geomagnetic field variation: New methods, models and implications. *Geophys J Int* 198(1):229–248.

Paterson, G. A. (2011), A simple test for the presence of multidomain behaviour during paleointensity experiments, *J. Geophys. Res.*, 116, B10104, doi:10.1029/2011JB008369.

- Paterson GA, Tauxe L, Biggin AJ, Shaar R, Jonestrask LC (2014) On improving the selection of Thellier-type paleointensity data. *Geochem Geophys Geosyst* 15(4): 1180–1192.
- Pavón-Carrasco, F. J., J. Rodríguez-González, M. L. Osete, and J. M. Torta (2011), A Matlab tool for archaeomagnetic dating, *J. Archaeol. Sci.* 38, 408–419.
- Pavón-Carrasco FJ, et al. (2014) A geomagnetic field model for the Holocene based on archaeomagnetic and lava flow data. *Earth Planet Sci Lett* 388: 98–109.
- Poletti W, Trindade RI, Hartmann GA, Damiani N, Rech RM (2016) Archeomagnetism of Jesuit Missions in South Brazil (1657–1706 AD) and assessment of the South American database. *Earth Planet Sci Lett* 445: 36-47.
- Rogers J, Fox JMW, Aitken MJ (1979) Magnetic anisotropy in ancient pottery. *Nat* 277: 644–646.
- Reimer, P. J. et al., 2013. IntCal13 and marine13 radiocarbon age calibration curves 0–50,000 years cal bp. *Radiocarbon* 55, 1869–1887
- Siebe C (2000) Age and archaeological implications of Xitle volcano, southwestern Basin of Mexico-City. *J Volcanol Geotherm Res* 104: 45-64.
- Shaar R, et al. (2011) Geomagnetic field intensity: How high can it get? How fast can it change? Constraints from Iron Age copper slag. *Earth Planet Sci Lett* 301(1-2): 297–306.
- Shaar R, et al. (2016) Large geomagnetic field anomalies revealed in Bronze to Iron Age archeomagnetic data from Tel Megiddo and Tel Hazor, Israel. *Earth Planet Sci Lett* 442:173–185.
- Tauxe L, Mullender TAT, Pick T (1996) Potbellies, wasp-waists, and superparamagnetism in magnetic hysteresis. *J Geophys Res* 101: 571–583.
- Tauxe L, Staudigel H (2004) Strength of the geomagnetic field in the Cretaceous Normal Superchron: New data from submarine basaltic glass of the Troodos Ophiolite. *Geochem Geophys Geosyst* 5(2):Q02H06.
- Tarduno, J.A., Watkeys, M.K., Huffman, T.N., Cottrell, R.D., Blackman, E.G., Wendt, A., Scribner, C.A. & Wagner, C.L., 2015. Antiquity of the South Atlantic anomaly and evidence for top-down control on the geodynamo, *Nat. Commun.*, 6, 7865, doi:7810.1038/ncomms8865
- Tema E, Herrero-Bervera E, Lanos Ph (2017) Geomagnetic field secular variation in Pacific Ocean: A Bayesian reference curve based on Holocene Hawaiian lava flows. *Earth Planet Sci Lett* 478:58-65.
- Thébault E, Gallet Y (2010) A bootstrap algorithm for deriving the archeomagnetic field intensity variation curve in the Middle East over the past 4 millennia BC. *Geophys Res Lett* 37: L22303, 10.1029/2010GL044788.

Urrutia-Fucugauchi J (1996) Paleomagnetic study of the Xitle-Pedregal de San Angel lava flow, southern basin of Mexico. *Phys Earth Planet Inter* 97: 177–196.

Urrutia-Fucugauchi, J. and Campos-Enriquez, J.O., 1993. Geomagnetic secular variation in central Mexico since 1923 AD and comparison with 1945-1990 IGRF models. *J. Geomag. Geoelectr.*, 45: 243-249.

Valet, J.P., Brassart, J., Le Meur, I., Soler, V., Quidelleur, X., Tric, E. and Gillot, P.Y., 1996, Absolute paleointensity and magnetomineralogical changes: *Journal of Geophysical Research: Solid Earth*, v. 101, p. 25029–25044, doi:10.1029/96JB02115.

Veitch RJ, Hedley IG, Wagner JJ (1984) An investigation of the intensity of the geomagnetic field during Roman times using magnetically anisotropic brick sand tiles. *Arch Sci* 37: 359–373.

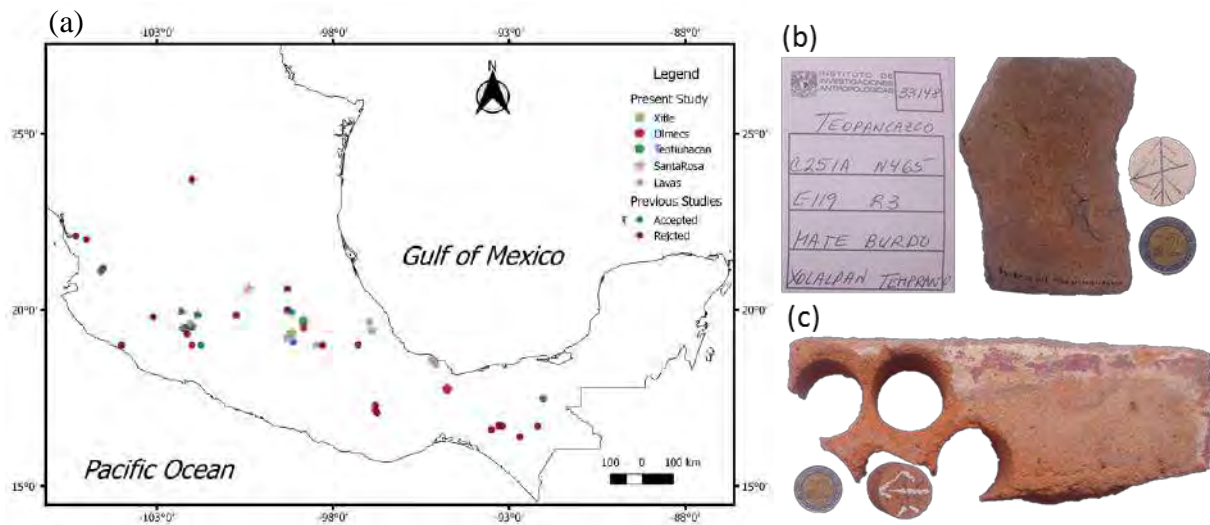


Fig. 1. (a) Location map showing the distribution of the archeological sites and lava flows studied in the present study. Teotihuacan, green triangles; Olmec sites, black crosses; Xitle reheated potteries, black squares; Santa Rosa de Viterbo temple, pink star; Lavas, green circles. previously published archeomagnetic data as compiled from the Geomagia50 database are shown as blue diamonds and red circles for those accepted and rejected ones based on the evaluation assessment done in this study (for data selection criteria see the text and Table S4). (b) representative archeological artefact and registration label from Teopancasco, piece 33148, and standard size specimens prepared from them. (c) Santa Rosa de Viterbo foundation wall brick. The diameter of standard size specimens is 2.5 cm, and a Mexican one Peso coin is also shown for scale.

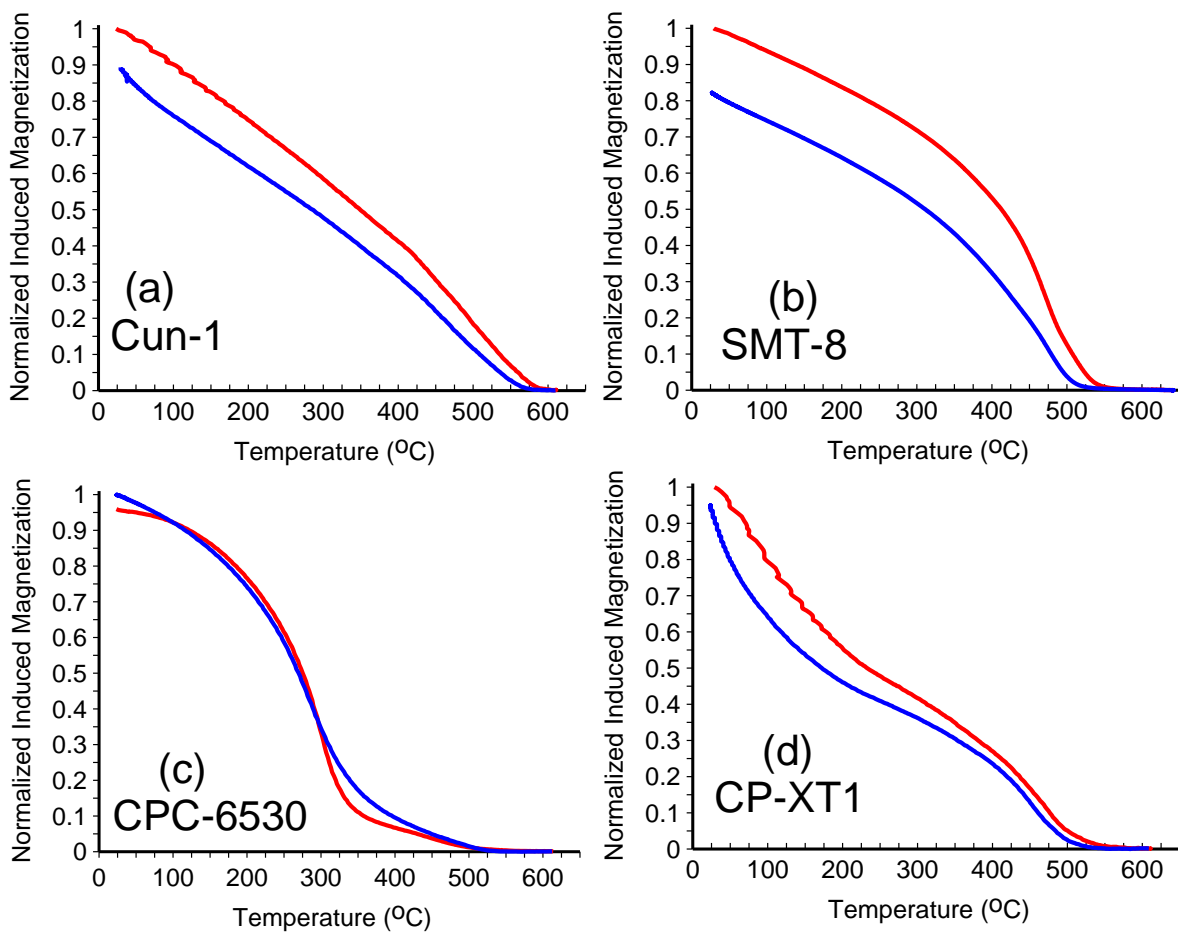


Fig. 2. Variation of high-field induced magnetization with temperature for representative samples. Red and blue lines indicate the heating and cooling curves, respectively.

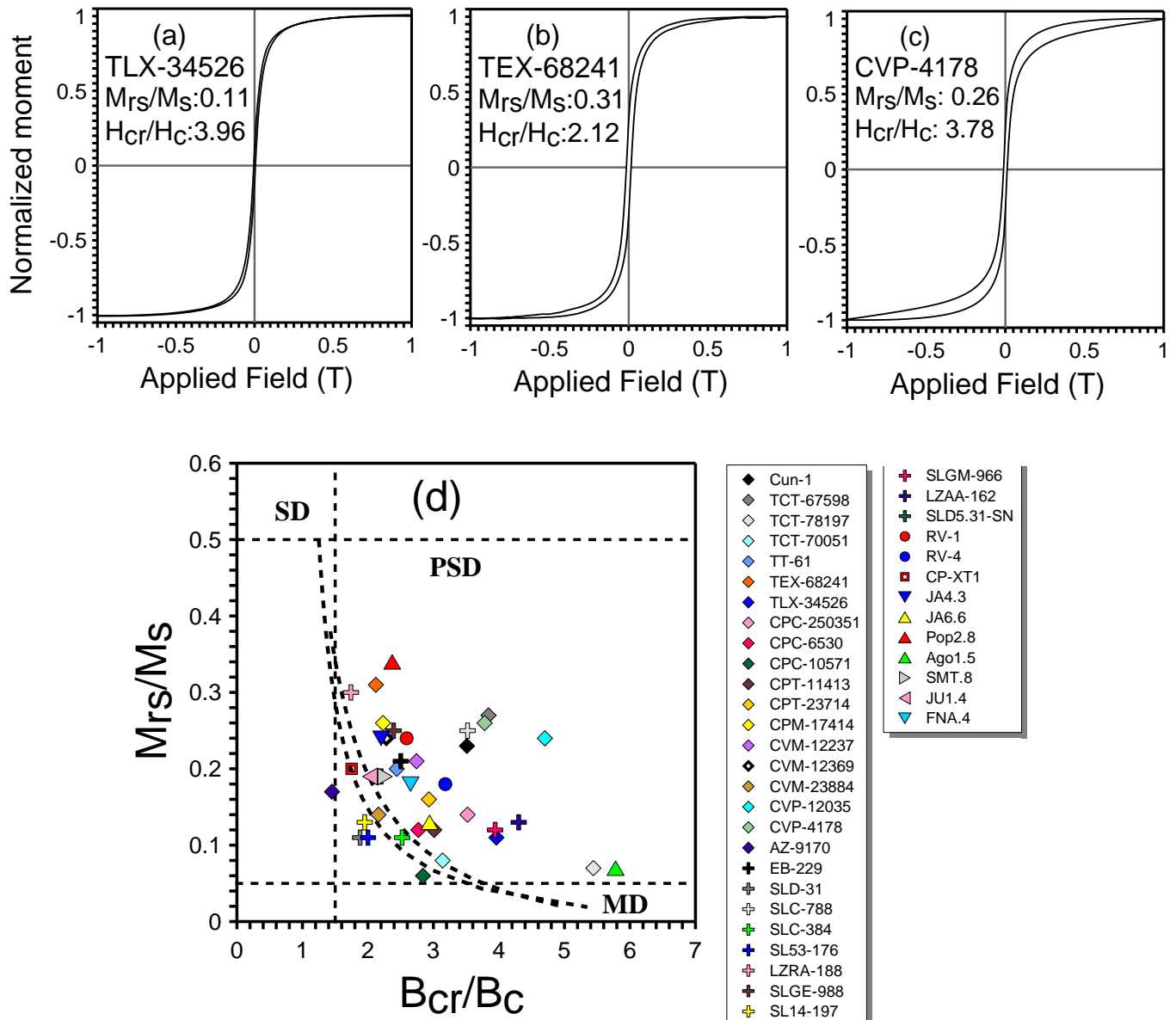


Fig. 3. (a-b-c) Examples of hysteresis loops obtained from archeological specimens (for codes see Table S1). M_{rs}/M_s : remanent saturation magnetization/saturation magnetization; H_{cr}/H_c : remanence coercivity/coercivity. (d) Day plot (Day et al., 1977). The threshold values for single domain (SD), pseudo-single domain (PSD), and multidomain (MD) fields are shown as straight dashed lines. Interrupted curved lines represent SD-MD theoretical mixing curves for magnetite after Dunlop (2002).

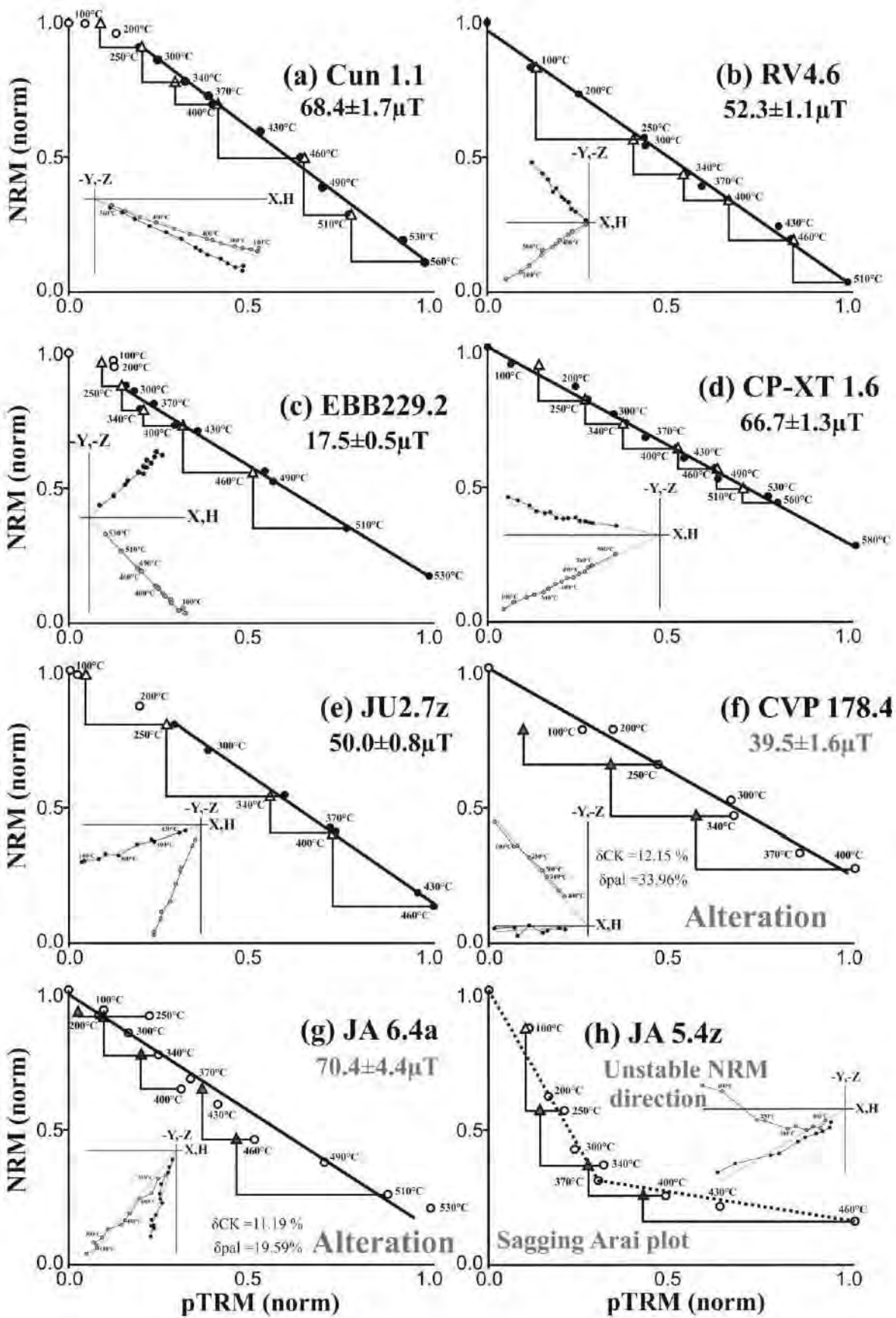


Fig. 4. Examples of typical IZZI-Thellier results and orthogonal vector plots (inset) of accepted (a-e) and rejected (f-h) specimens. NRM and pTRM data are normalized. Black (white) circles represent the accepted (rejected) NRM vs. pTRM data that were used to calculate the best-fit lines marked as black lines. Positive pTRM checks are shown as white triangles and red triangles (f-h) represent data affected by significant thermal alteration. Selected temperature steps are indicated as labels aside the symbols. Zijdeveld diagrams for each specimen are shown as insets, where the black (grey) circles are projections onto the horizontal (vertical) planes. Paleointensities were obtained by the ThellierTool program.

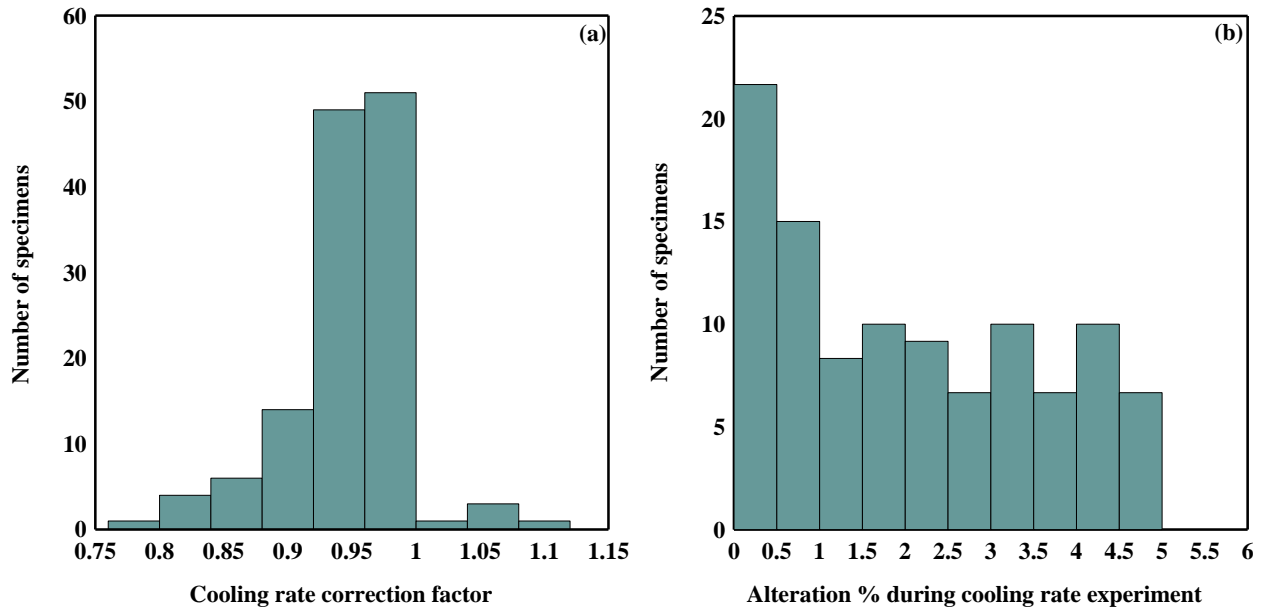


Fig 5. (a) The cooling rate correction factor calculated for each specimen by dividing the average of the two fast steps ($TRM_{fast1,2}$) over the TRM_{slow} step, (b) percentage of alteration during the cooling rate correction experiment calculated as the percentile difference between the first (TRM_{fast1}) and the third (TRM_{fast2}) heating.

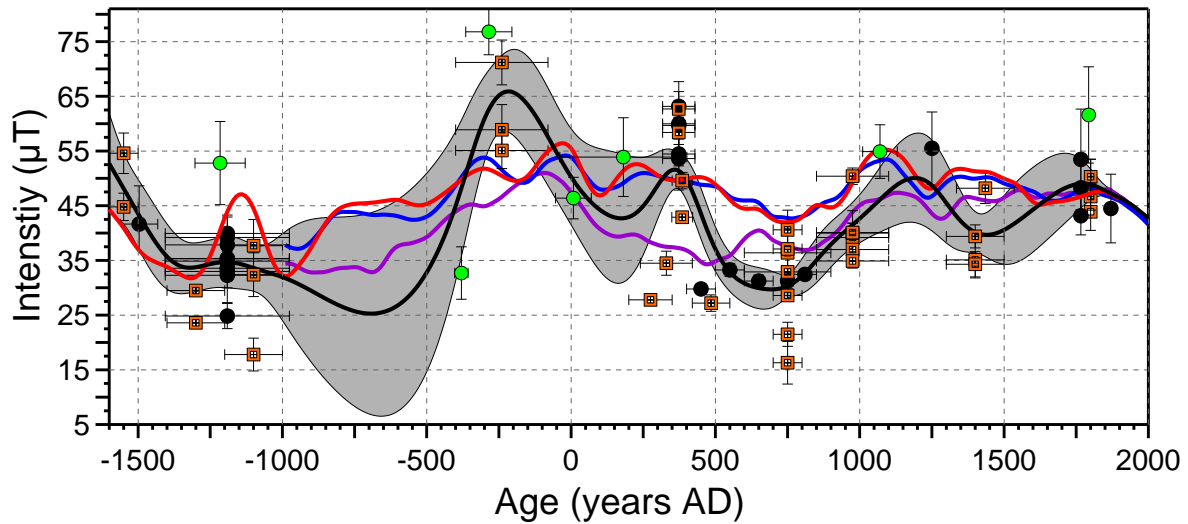


Fig. 6. Paleointensity results obtained in this study for archeological pieces (orange squares) and lava flows (green dots) together with selected previously published data (black dots). The archeointensity secular variation curve is shown as a black line with its 95% confidence limits marked in shaded grey. Curves derived from global geomagnetic models are shown in blue (ARCH3K.1), violet (CAL3K.4), and red (SHADIF.14K). Errors in ages and PI values are shown as error bars.

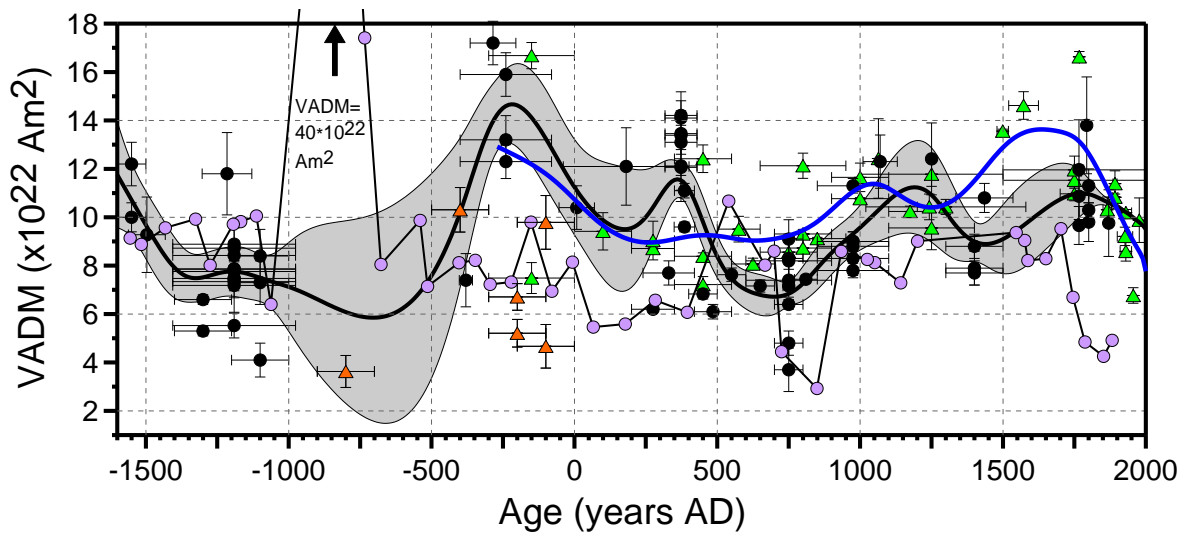


Fig. 7. North America and Guatemala virtual axial dipole moment (VADM) data compared to the Mexican data. Mexican data are shown as black dots, and the Mexican VADM curve with its 95% confidence limits as the solid thick line and grey shaded area, respectively. Southern United States archeointensity data are shown as green triangles, and relative intensity data from Hall's Cave, Texas, as violet dots. The Southern United States VADM curve is shown in thick blue line. Six selected intensity data from Guatemala are shown by orange triangles. Errors in ages and VADM values are shown as error bars.

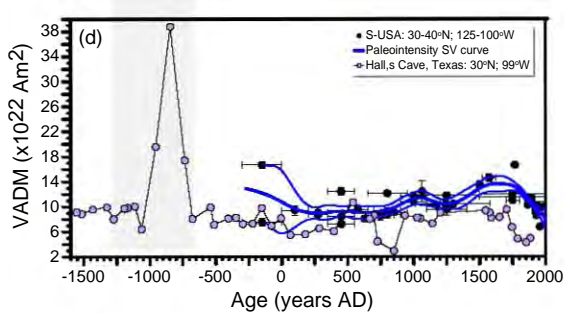
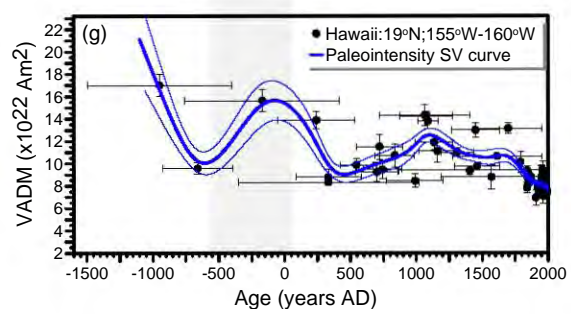
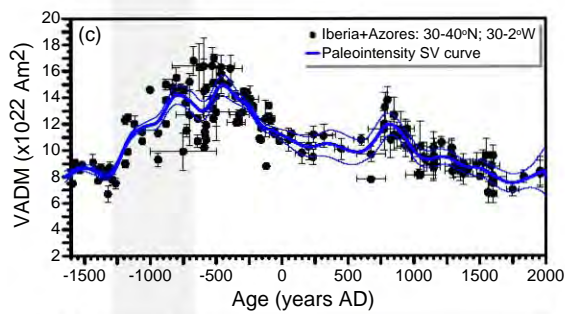
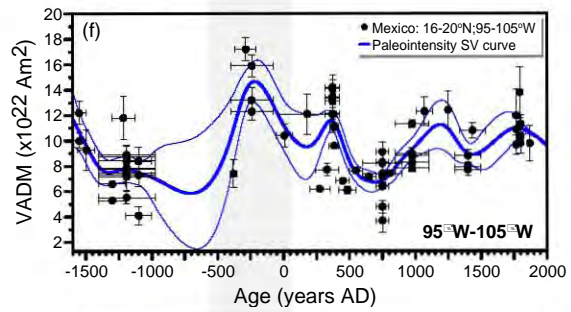
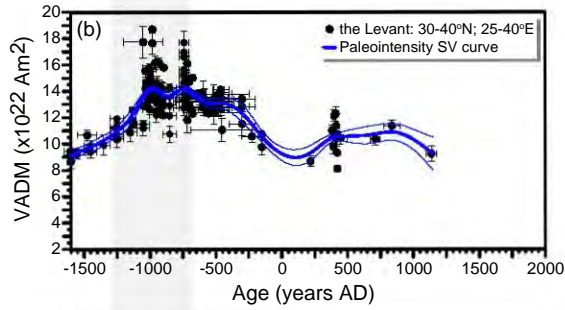
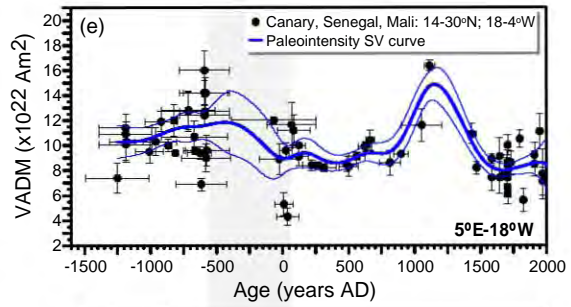
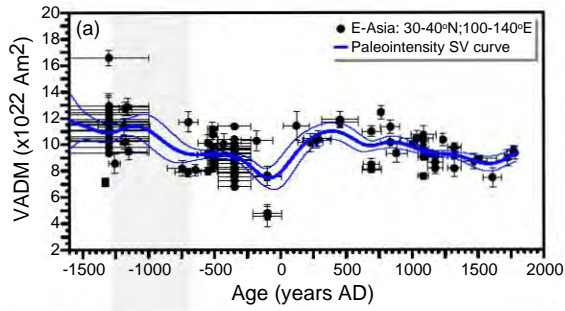


Fig. 8. VADM curves for the last 3600 years for (a) Eastern Asia, (b) the Levant, (c) the Iberian Peninsula and Azores islands, (d) the Southern United State (S-USA), (e) the Canary Islands and Western Africa (Senegal and Mali), (f) Mexico, and (g) Hawaii Islands. Data selection and references of each region are described in detail in the [Supplementary Table S7](#). All data are from lava rocks or archeological artifacts with at least two specimens and a mean-PI with a standard deviations $\leq 10 \mu\text{T}$ or $\leq 5 \mu\text{T}$, respectively. Paleointensity SV curves were calculated for each region and are shown as thick blue lines together with their 95% confidence limits as thin blue lines. Shaded vertical bars denote two periods where intensity peaks were observed at locations at latitudes of 30-40° (a to d) and latitudes $< 30^\circ$ (e-f).

Table 1: Archaeological artifacts and lava flows samples analyzed in this study.

Archeological location	site (Code)	(Age)	Age constrain	Age reference	Lat°N	Lon °W	N _i /n _i	N _a /n _a
1. Archeological samples								
Teotihuacan	Cuanalan (Cun)	400-80 BC	¹⁴ C	This study	19.69	98.84	4/19	3/12
	Teopancazco (TCT)	200-350 AD	¹⁴ C	This study	19.69	98.84	3/15	1/3
	Teopancazco (TT)	240-420 AD	¹⁴ C	This study	19.69	98.84	2/9	1/3
	Teopancazco (TEX)	350-420 AD	¹⁴ C	This study	19.69	98.84	3/14	2/5
	Teopancazco (TLX)	420-550 AD	¹⁴ C	This study	19.69	98.84	2/9	1/3
	Cueva pirul (CPC)	600-900 AD	¹⁴ C	This study	19.69	98.84	3/14	2/7
	Cueva pirul (CPT)	700-800 AD	¹⁴ C	This study	19.69	98.84	5/22	5/15
	Cueva pirul (CPM)	850-1100 AD	¹⁴ C	This study	19.69	98.84	1/7	1/3
	Cueva Varillas (CVM)	850-1100 AD	¹⁴ C	This study	19.69	98.84	6/25	5/17
	Cueva Varillas (CVP)	1300-1500 AD	¹⁴ C	This study	19.69	98.84	4/19	3/9
Aztec (AZ)	1350-1520 AD	¹⁴ C	This study	19.69	98.84	1/6	1/5	
Olmecs	El Bajío (EB-229)	1200-1000 BC	¹⁴ C+archo	This study	17.75	94.76	1/8	1/4
	San Lorenzo group D (SL D)	1200-1000 BC	¹⁴ C+archo	This study	17.75	94.76	1/6	1/3
	San Lorenzo group D (SL D)	1400-1200 BC	¹⁴ C+archo	This study	17.75	94.76	1/7	1/2
	San Lorenzo group C (SL C)	1600-1500 BC	¹⁴ C+archo	This study	17.75	94.76	1/7	1/3
	San Lorenzo group C (SL C)	1200-1000 BC	¹⁴ C+archo	This study	17.75	94.76	1/5	1/2
	San Lorenzo SL.53 (SL 53)	1600-1500 BC	¹⁴ C+archo	This study	17.75	94.76	1/6	1/2
	San Lorenzo SL.C5-6 (SL C56)	1200-1000 BC	¹⁴ C+archo	This study	17.75	94.76	1/6	0/0
	San Lorenzo SL.D4-22 (SL D4-22)	1200-1000 BC	¹⁴ C+archo	This study	17.75	94.76	1/7	0/0
	Loma del Zapote Represa Azuzul (LZ RA)	1400-1200 BC	¹⁴ C+archo	This study	17.75	94.76	1/6	0/0
	San Lorenzo B. GOBO EHG (SL GE)	1200-1000 BC	¹⁴ C+archo	This study	17.75	94.76	1/7	0/0
	San Lorenzo SL.14 (SL 14)	1200-1000 BC	¹⁴ C+archo	This study	17.75	94.76	3/20	0/0
	San Lorenzo B. GOBO MVG (SL GM)	1500-1400 BC	¹⁴ C+archo	This study	17.75	94.76	2/15	0/0
	Loma del Zapote Acrop Azuzul (LZ AA)	1200-1000 BC	¹⁴ C+archo	This study	17.75	94.76	1/6	0/0
	San Lorenzo D5-31 (SL D5-31)	1400-1200 BC	¹⁴ C+archo	This study	17.75	94.76	1/8	1/4
	Xitle reheated pottery fragments	CEPE-UNAM (CP-XT)	373±56 AD	¹⁴ C	Siebe, 2000	19.33	99.19	4/17
Santa Rosa de Viterbo Temple	Santa Rosa de Viterbo (RV)	1800 AD	Historical	Historical	20.59	100.40	4/25	3/13
Lat/Lon: latitude/longitude; N _i /n _i : is the total number of the analyzed independent fragments per each archaeological site/total number of the analyzed specimens; N _a /n _a : is the number of the accepted fragments /number of the accepted specimens.								
2. Lavas samples								
volcanic unit	Sites code	Age	Age constrain	Age reference	Lat °N	Lon °W	N _i /n _i	N _a /n _a
Coacoatzintla	JA4+JA5	1216±87 BC	¹⁴ C	Siebert and Carrasco-Nuñez , 2002	19.65	96.96	2/8	2/2
Nealtican	Pop2+Pop3+Pop4	285±80 BC	¹⁴ C	Panfil et al., 1991	19.00	98.48	2/7	2/2
Puntiagudo	Ago1+Ago2+Ago4	181±222 AD	¹⁴ C	Nelson and González-Caver, 1992	18.45	95.10	3/10	2/3
Toaxtlacoaya	JA1+JA6	1070±60 AD	¹⁴ C	Siebert and Carrasco-Nuñez , 2002	19.40	96.90	2/9	2/2
San Martin	SMT	1793 AD	Historical	Historical	18.58	95.19	1/8	1/3
Jumento	JU1+JU2	8±62 AD	¹⁴ C	Arce et al., 2015	19.18	99.31	2/18	2/5
Flujo no asociado	FNA	380±23 BC	¹⁴ C	this study	19.61	102.07	1/10	1/5
N _i /n _i : is the total number of the analyzed flow sites per each lava flow/total number of the analyzed specimens; N _a /n _a , is the number of the accepted lava flow sites / number of the accepted specimens.								

Table 2. List of the selection criteria applied on the archeological samples and the lava flows and their threshold values.

Archeological samples																	
at specimen level										at sample level							
Arai diagram and the orthogonal demagnetization plot										cooling rate alteration		class A		class B		class C	
N	β	f	q	MAD _{anc}	α	δ CK	δ pal	\rightarrow K'	(TRM _{fast1} -TRM _{fast2}) / TRM _{fast1} * 100	N _{min}	SD	N _{min}	SD	N _{min}	SD		
≥ 5	≤ 0.1	≥ 0.5	≥ 5	$\leq 10^\circ$	$\leq 10^\circ$	≤ 10	≤ 10	≤ 0.164	$< 5\%$	≥ 3	$\leq 3\mu\text{T}$	≥ 3	3-5 μT	2	$\leq 5\mu\text{T}$		
Lava flows																	
at specimen level										at flow level							
Arai diagram and the orthogonal demagnetization plot										cooling rate alteration		class A		class B		class C	
N	β	f	q	MAD _{anc}	α	δ CK	δ pal	\rightarrow K'	No cooling correction was done on lavas	N _{min}	SD	N _{min}	SD	N _{min}	SD		
≥ 5	≤ 0.1	≥ 0.5	≥ 5	$\leq 10^\circ$	$\leq 10^\circ$	≤ 10	≤ 10	≤ 0.164		≥ 3	$\leq 5\mu\text{T}$	≥ 3	5-10 μT	2	$\leq 10\mu\text{T}$		

N, number of the points used for the linear fit; β , standard error of the slope of this best fit line; f, fraction parameter; q, quality factor; MAD_{anc}, anchored maximum angular deviation; α , angular difference between the anchored and free-floating vectors of the best fit direction; δ CK, relative check error; δ pal, cumulative check difference; (|K'|): is the absolute value of curvature of the data points used for determining the best-fit line.

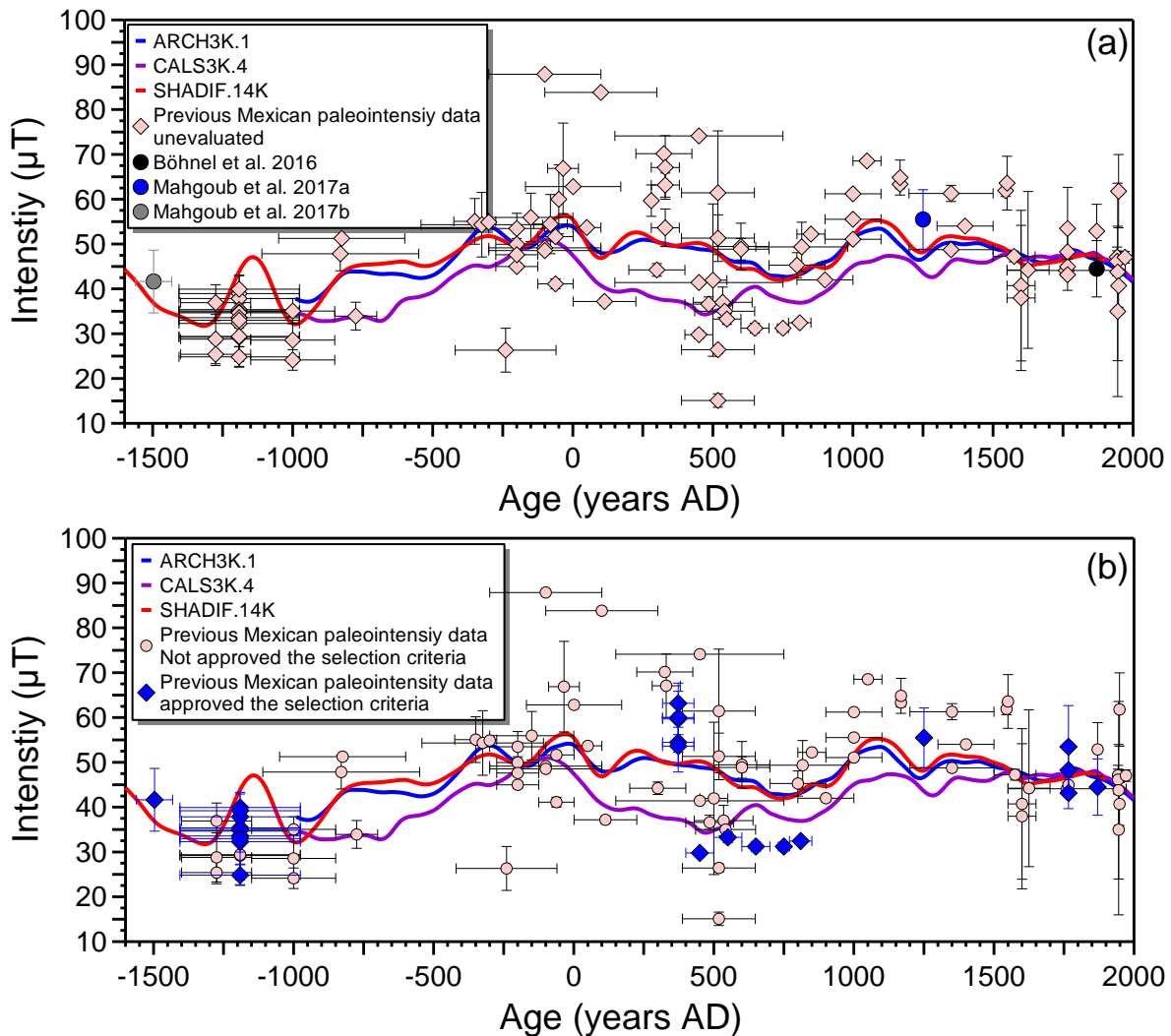
Cooling rate correction experiment (done only on the archeological pieces): TRM_{fast1} and TRM_{fast2} heating steps were done in an ordinary laboratory time of 30 min, and the intermediate TRM_{slow} step in an extended cooling time of 10 hours. The difference between TRM_{fast1} and TRM_{fast2} is used to detect alterations (cutoff value $< 5\%$).

At sample level three classes A, B, and C were defined based on the minimum number of accepted specimens to calculate the sample-mean intensity and its standard deviation. For the archeological samples: Class A rated PI are based on at least 3 accepted specimens and have an σ (μT) $\leq 3\mu\text{T}$. For class B, at least 3 accepted specimens must be included to calculate the sample-mean intensity with σ between 3-5 μT . If a sample has two accepted specimens with an σ (μT) $\leq 5\mu\text{T}$ then class C will be assigned. 20 out of 37 accepted samples belong to class A, 11 are of class B and 6 of class C.

For the lava flows: Class A rated PI are based on at least three accepted specimens and have an $\sigma \leq 5\mu\text{T}$. Class B PI are based on at least three accepted specimens with a σ between 5-10 μT . Four out of six accepted lava flow PI belong to class A and two to class B

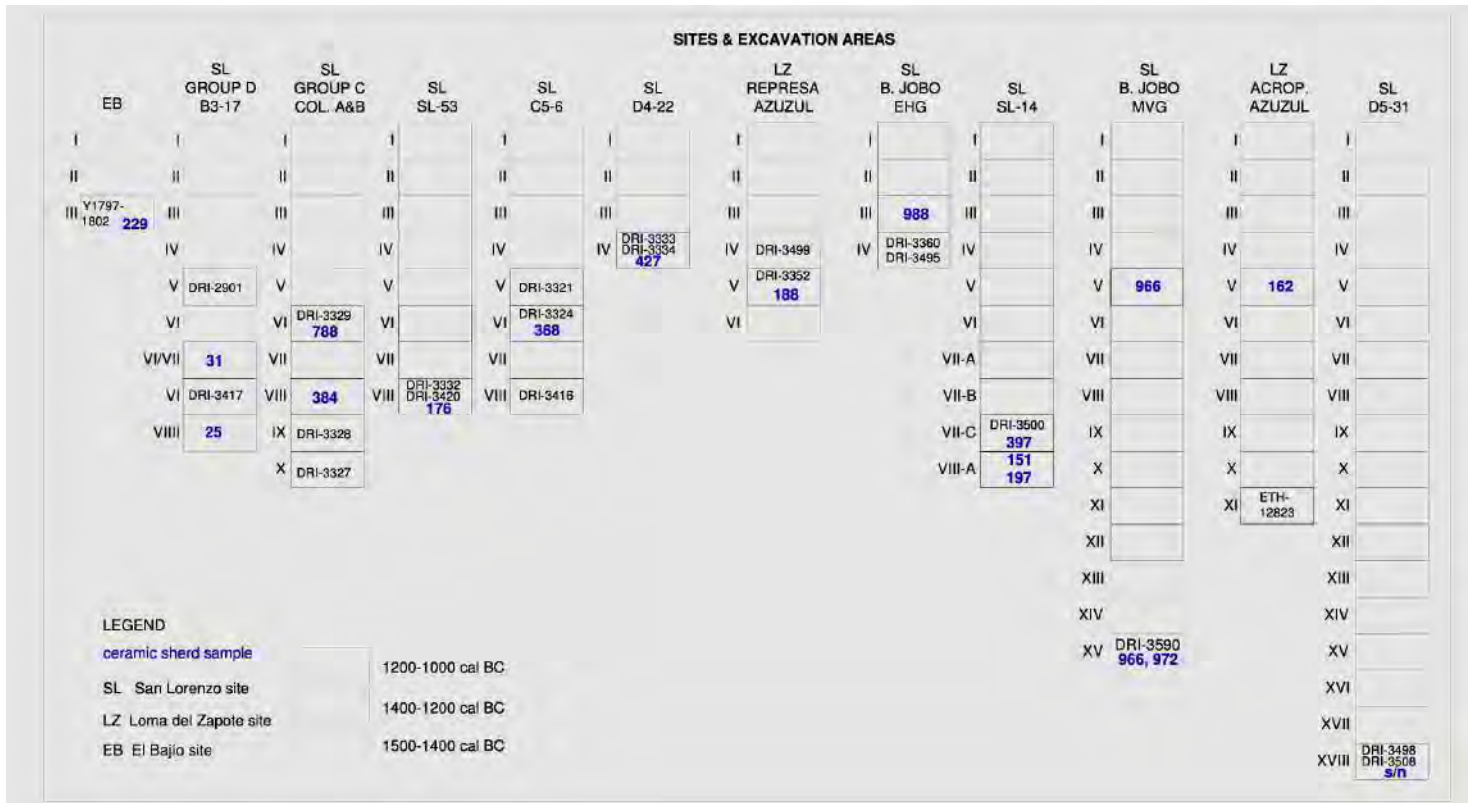
Table 3: Geomagnetic intensity results at the archeological sample/lava flow level.						
archeological sample/lava flow	Age (AD)	n_a	$H \pm SD (\mu T)$	Sample/flow Class	$H_{19.43^{\circ}N, 99.13^{\circ}W} (\mu T)$	$VADM \pm \sigma_{VADM} (x10^{22} Am^2)$
<u>Teotihuacan</u>						
Cun-1	-240±160	5	71.4±4.1	B	71.2	15.9±0.9
Cun-2	-240±160	3	55.3±3.3	B	55.1	12.3±0.7
Cun-3	-240±160	4	59.1±4.6	B	58.9	13.2±1.0
TCT-70051	275±75	3	27.9±0.6	A	27.8	6.2±0.1
TT-61	330±90	3	34.6±2.2	A	34.5	7.7±0.5
TEX-68241	385±35	2	43.0±1.0	C	42.9	9.6±0.2
TEX-33148	385±35	3	49.8±1.5	A	49.6	11.1±0.3
TLX-34526	485±65	3	27.3±1.5	A	27.2	6.1±0.3
CPC-10571	750±150	4	33.0±3.1	B	32.9	7.4±0.7
CPC-6530	750±150	3	36.5±4.5	B	36.4	8.2±1.0
CPT-23714	750±50	3	37.2±4.4	B	37.1	8.3±1.0
CPT-25159	750±50	2	21.6±2.2	C	21.5	4.8±0.5
CPT-25313	750±50	4	40.7±3.6	B	40.6	9.1±0.8
CPT-25340	750±50	3	16.4±3.9	B	16.3	3.7±0.9
CPT-11413	750±50	3	28.7±0.7	A	28.6	6.4±0.2
CPM-17414	975±125	3	39.3±2.6	A	39.2	8.8±0.6
CVM-12369	975±125	4	50.6±1.5	A	50.4	11.3±0.3
CVM-23884	975±125	3	40.1±1.8	A	40.0	9.0±0.4
CVM-10835	975±125	3	40.2±4.0	B	40.1	9.0±0.9
CVM-24759	975±125	5	37.1±2.9	A	37.0	8.3±0.7
CVM-17640	975±125	2	35.0±1.3	C	34.9	7.8±0.3
CVP-4178	1400±100	4	39.5±2.1	A	39.4	8.8±0.5
CVP-35II	1400±100	3	35.2±3.3	B	35.1	7.9±0.7
CVP-35III	1400±100	2	34.4±2.3	C	34.3	7.7±0.5
AZ-9170	1435±100	5	48.4±2.8	A	48.2	10.8±0.6
<u>Olmeccs</u>						
EB-229	-1100±100	4	17.8±3.0	A	18.2	4.1±0.7
SLD-31	-1100±100	3	31.7±4.0	B	32.4	7.3±0.9
SLC-384	-1100±100	2	36.9±4.8	C	37.7	8.4±1.1
SLD5.31-SN	-1300±100	4	23.1±0.8	A	23.6	5.3±0.2
SLA 25	-1300±100	2	28.9±0.9	C	29.5	6.6±0.2
SLC-788	-1550±50	3	43.9±2.5	A	44.8	10.0±0.6
SL53-176	-1550±50	2	53.5±3.7	C	54.6	12.2±0.9
<u>Xitle heated pottery fragments</u>						
CP-XT 1	373±56	3	62.7±1.5	A	62.8	14.1±0.3
CP-XT 2	373±56	2	58.4±1.2	B	58.5	13.1±0.3
<u>Santa Rosa de Viterbo Temple</u>						
RV 1	1800	7	51.0±3.2	B	50.3	11.3±0.7
RV 2	1800	3	44.5±3.4	B	43.9	9.8±0.8
RV 4	1800	3	46.7±2.5	A	46.0	10.3±0.6
<u>Lava Flows</u>						
JA4,5	-1216±87	2	52.9±7.6	C	52.8	11.8±1.7
Pop2,3,4	-285±80	2	76.4±4.2	C	76.8	17.2±0.9
AGO1,2,3	181±222	3	53.3±7.2	B	53.9	12.1±1.6
JA1,6	1070±60	2	54.9±4.9	C	54.9	12.3±1.1
SMT	1793	3	61.0±8.8	B	61.6	13.8±2.0
JU	8±62	5	46.3±3.8	A	46.4	10.4±0.9
FNA	-380±23	5	32.8±4.8	A	32.7	7.4±1.1

n_a , is the number of the accepted specimens; H (μT), average archeointensity with standard deviation (SD) after cooling rate correction (the asterisk* in the lava sites indicate that no cooling correction was performed); $H_{19.43^{\circ}N, 260.87^{\circ}E}$ (μT), average archeointensity relocated to $19.43^{\circ}N, 260.87^{\circ}E$; $VADM$, is the Virtual Axial Dipole Moment with standard deviation (σ_{VADM}).



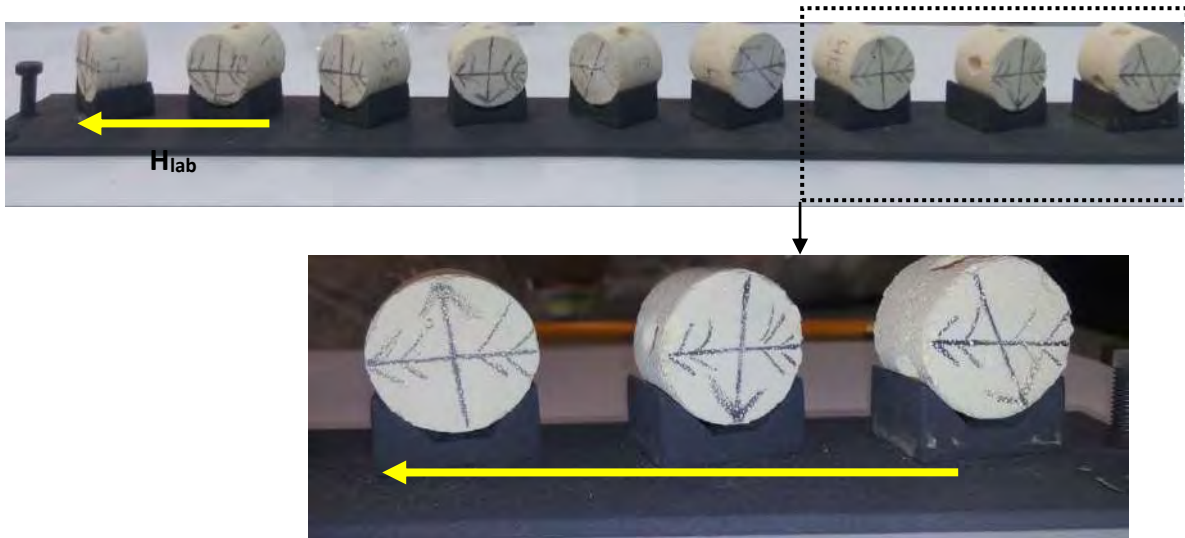
Supplementary Figure S1

Fig. S1. (a) Published 99 paleointensity data for Mexico (faded pink diamond) compiled from Geomagia50.v3 database (Brown et al., 2015) for the last 3600 years. Also plotted are recently published paleointensity data of Böhnel et al. (2016) (black circle), Mahgoub et al. (2017a) (blue circle), and Mahgoub et al. (2017b) (grey circle), which are not yet included in the Geomagia database. (b) Assessment of the previous paleointensity data (See Table S2). Pink circles represent studies with low quality paleointensity data which therefore deleted while those that have been considered reliable and of high quality data are marked as blue diamonds. The colour lines are predictions from global models of ARCH3k.1 (blue), CALS3.k.4 (violet), and SHA.DIF.14K (red).



Supplementary Figure S2

Fig. S2. Schematic cross-section drawing showing the stratigraphic position of the 14C dates and ceramic samples. Both absolute and relative dating techniques were used to be defined temporality.



Supplementary Figure S3

Fig. S3. An orientation brass plate was used in this study in order to orient individually archeomagnetic specimen thermal remanent magnetization (TRM) parallel to the magnetic field in the laboratory oven. Yellow arrows point in the direction of the oven laboratory field (H_{lab}). The capacity of the oriental trail is just for 9 specimens so as to allow free rotation of each specimen about the vertical and horizontal axis. More details can be seen in Böhnel et al. (2009).

Supplementary Table S1:

List of ceramic samples with provenience information

CERAMIC SAMPLE	SITE-EXCAVATION AREA	STRATUM
25	SL-GRUPO D: B3-17	VIII
31	SL-GRUPO D: B3-17	VI/VII
151	SL-SL-14	VIII-A
162	LZ-ACROPOLIS AZUZUL	V
176	SL-SL-53	IX
188	LZ-REPRESA AZUZUL	V
197	SL-SL-14	VIII-A
229	EB-Corte NW	IV
368	SL-C5-6	VI
384	SL-GRUPO C: COL. A	VIII
397	SL-SL-14	VII-C
427	SL-D4-22	IV
788	SL-GRUPO C: COL. B	VI
908	SL-SL-53	VI
966	SL-B. JOBO MVG	XV
972	SL-B. JOBO MVG	XV
988	SL-B. JOBO EHG	III
s/n	SL-D5-31	XVIII

Supplementary Table S2:

Rock magnetic parameters for studied samples: listed are the thermomagnetic hysteresis analyses that performed on some representative sample: the Curie temperature (T_c) for heating and cooling curves are calculated using the RockMag Analyzer program, and the remanence carriers are proposed based on the Curie Points Mag: magnetite, Ti-TM: Titanomagnetite; H_{cr}/H_c is remanent coercivity / coercivity; M_{rs}/M_s is the remanent saturation magnetization/ saturation magnetization. Relation between the rock magnetic properties and the success rate of the paleointensity experiments is demonstrated also, *for more details about the sample classes classification after intensity experiments see Table 2*

Sample	Thermomagnetic analyses		Reversibility	Remanence Carriers	Hysteresis analyses		Accepted paleointensity estimates? If yes Sample class?	Sample	Thermomagnetic analyses		Reversibility	Remanence Carriers	Hysteresis analyses		Accepted paleointensity estimates? If yes Sample class?
	Heating T_c (°C)	Cooling T_c (°C)			H_{cr}/H_c	M_{rs}/M_s			Heating T_c (°C)	Cooling T_c (°C)			H_{cr}/H_c	M_{rs}/M_s	
Cun-1	560	550	reversible	Mag	3.51	0.23	Yes-class B	SL53-176	560	550	reversible	Mag	1.89	0.11	Yes-class C
TCT-67598	230, 530	200, 500	reversible	High Ti-TM or goethite, low Ti-TM	3.84	0.27	no	LZRA-188	540	530	reversible	Low Ti-TM, Mag	1.74	0.30	no
TCT-78197	410, 530	400, 510	reversible	Low Ti-TM, Mag	5.44	0.07	no	SLGE-988	580	520	irreversible	Low Ti-TM, Mag	2.39	0.25	no
TCT-70051	250, 520	230, 510	reversible	High Ti-TM or goethite, low Ti-TM	3.14	0.08	Yes-class A	SL14-197	530	510	reversible	Low Ti-TM, Mag	1.95	0.13	no
TT-61	550	540	reversible	Low Ti-TM, Mag	2.44	0.20	Yes-class A	SLGM-966	560	540	reversible	Mag	3.94	0.12	no
TEX-68241	540	520	reversible	Mag	2.12	0.31	Yes-class C	LZAA-162	210, 500	180, 4850	reversible	High Ti-TM or goethite, low Ti-TM	4.30	0.13	no
TLX-34526	425, 530	415, 520	reversible	High Ti-TM, low Ti-TM	3.96	0.11	Yes-class A	SLD5.31-SN	550	510	irreversible	Low Ti-TM, Mag	2.20	0.19	Yes-class A
CPC-250351	250, 530	220, 510	reversible	High Ti-TM or goethite, low Ti-TM	3.52	0.14	no	RV-1	530	500	irreversible	Low Ti-TM, Mag	2.59	0.24	Yes-class B
CPC-6530	310, 500	320, 500	reversible	High Ti-TM, Mag	2.77	0.12	Yes-class B	RV-4	525	500	reversible	Low Ti-TM, Mag	3.18	0.18	Yes-class A
CPC-10571	230, 520	200, 510	reversible	High Ti-TM or goethite, low Ti-TM	2.84	0.06	Yes-class B	CP-XT1	220, 520	230, 500	reversible	High Ti-TM, low Ti-TM	1.75	0.20	Yes-class A
CPT-11413	530	510	reversible	Low Ti-TM	2.77	0.12	Yes-class A	JA4.3	545	535	reversible	Low Ti-TM, Mag	2.20	0.24	no
CPT-23714	220, 500	190, 498	reversible	High Ti-TM or goethite, low Ti-TM	2.93	0.16	Yes-class B	JA6.6	250, 580	280, 560	irreversible	High Ti-TM, low Ti-TM, Mag	2.94	0.13	no
CPM-17414	560	550	reversible	Mag	2.23	0.26	Yes-class A	Pop2.8	330, 546	560	reversible	High Ti-TM, low Ti-TM, Mag	2.37	0.34	Yes-class C
CVM-12237	420, 530	400, 510	reversible	High Ti-TM, low Ti-TM	2.74	0.21	no	Ago1.5	537	533	reversible	Low Ti-TM, Mag	5.78	0.07	Yes-class B
CVM-12369	540	520	reversible	Low Ti-TM	2.28	0.24	Yes-class A	SMT.8	530	510	irreversible	Low Ti-TM, Mag	2.26	0.19	Yes-class B
CVM-23884	250, 550	230, 530	irreversible	High Ti-TM or goethite, low Ti-TM	2.16	0.14	Yes-class A	JU1.4	550	530	reversible	Low Ti-TM, Mag	2.03	0.19	Yes-class A
CVP-12035	535	515	reversible	Low Ti-TM	4.70	0.24	no	FNA.4	530	510	irreversible	Low Ti-TM, Mag	2.65	0.18	Yes-class A
CVP-4178	220, 520	190, 490	reversible	High Ti-TM or goethite, low Ti-TM	3.78	0.26	Yes-class A								
AZ-9170	560	550	reversible	Mag	1.45	0.17	Yes-class A								
EB-229	550	520	irreversible	Low Ti-TM, Mag	2.50	0.21	Yes-class A								
SLD-31	400, 560	520	irreversible	Low Ti-TM, Mag	1.88	0.11	Yes-class B								
SLC-788	580	570	reversible	Low Ti-TM, Mag	3.52	0.25	no								
SLC-384	570	565	reversible	Low Ti-TM, Mag	2.52	0.11	Yes-class C								

Supplementary Table S3

Paleointensity results at specimen level.

Specimen	N	T _{min} - T _{max} (°C)	β	f	q	MAD _{anc} (°)	α (°)	δ CK	δ pal	\rightarrow K'	H _{raw} ± σ_B (μ T)	H (μ T)
1. Teotihuacan												
Cun 1.1	11	250-560	0.03	0.52	13.13	1.41	2.36	4.36	6.65	-0.16	79.0±2.7	75.7
Cun 1.2	11	250-560	0.03	0.69	17.96	2.56	6.33	1.94	4.15	-0.15	77.5±2.5	75.0
Cun 1.3	9	250-510	0.06	0.55	7.23	3.42	9.72	3.80	4.04	-0.06	73.7±4.7	71.7
Cun 1.4	13	100-560	0.03	0.85	26.59	1.38	1.84	4.13	0.61	-0.14	68.7±2.0	66.5
Cun 1.5	11	250-560	0.02	0.72	26.49	0.99	1.26	3.63	3.29	-0.10	68.4±1.7	68.2
Cun 2.1	11	250-560	0.03	0.61	14.4	1.56	0.31	4.44	6.44	-0.07	60.8±2.2	58.4
Cun 2.2	12	100-530	0.02	0.59	23.31	3.82	7.81	9.81	5.48	-0.14	59.7±1.4	55.6
Cun 2.4	11	100-510	0.02	0.55	22.91	3.34	9.25	4.37	2.75	-0.10	54.9±1.1	51.8
Cun 3.1	13	100-560	0.05	0.53	8.88	3.09	6.45	2.62	6.93	0.02	62.8±3.3	57.8
Cun 3.2	14	0-560	0.03	0.66	21.78	5.53	4.86	1.09	4.69	-0.07	59.3±1.6	54.5
Cun 3.3	9	340-560	0.06	0.53	7.23	6.04	9.22	5.02	4.92	0.09	71.1±4.3	65.4
Cun 3.4	11	0-490	0.04	0.84	16.16	1.93	2.36	4.95	9.97	-0.16	63.9±2.7	58.8
TCT 70051.1	12	100-530	0.04	0.77	17.88	3.14	3.63	5.34	3.21	-0.16	29.7±1.1	28.3
TCT 70051.2	12	100-530	0.03	0.78	22.23	3.65	6.86	3.07	4.75	0.10	29.6±0.9	28.3
TCT 70051.3	12	100-530	0.03	0.71	23.36	4.60	6.58	4.77	5.80	0.09	28.5±0.8	27.2
TT 61.2	8	370-560	0.02	0.52	18.04	2.48	1.82	6.53	2.28	0.00	37.9±0.8	36.9
TT 61.3	12	200-560	0.06	0.73	7.17	4.60	3.50	7.17	9.85	0.05	33.8±2.1	32.6
TT 61.4	13	100-560	0.03	0.82	17.38	4.45	3.92	9.69	7.72	0.01	36.6±1.3	34.3
TEX 68241.3	8	250-490	0.03	0.50	13.89	3.29	3.56	2.19	3.77	-0.15	45.9±1.4	42.3
TEX 68241.4	10	100-490	0.05	0.77	12.17	6.49	5.44	3.10	4.39	-0.12	47.0±2.4	43.7
TEX 33148.1	7	100-400	0.01	0.69	40.04	7.09	9.60	5.51	0.05	-0.16	59.7±0.8	49.8
TEX 33148.2	7	100-400	0.05	0.70	7.00	7.15	9.78	4.27	0.09	-0.11	61.5±3.2	51.3
TEX 33148.4	8	0-400	0.03	0.62	18.33	2.70	0.4	3.64	3.54	0.08	55.5±1.5	48.3
TLX 34526.1	5	300-490	0.02	0.68	16.5	4.77	4.54	3.08	6.08	-0.09	28.7±0.7	28.3
TLX 34526.3	7	200-490	0.04	0.72	11.2	3.71	4.4	3.16	4.97	-0.15	28.4±1.3	28.1
TLX 34526.4	8	100-430	0.02	0.63	23.77	2.71	4.50	1.12	0.13	-0.01	26.5±0.6	25.6
CPC 10571.1	9	0-430	0.03	0.59	16.3	5.77	7.98	1.51	4.33	0.08	38.1±1.1	32.4
CPC 10571.2	9	0-430	0.07	0.64	7.76	4.95	7.48	0.37	0.08	0.14	47.8±3.2	37.3
CPC 10571.3	9	0-430	0.06	0.53	7.89	3.11	3.6	1.57	3.39	-0.11	33.9±1.9	29.9
CPC 10571.4	9	0-430	0.04	0.61	11.1	2.85	6.01	3.93	7.42	-0.01	35.2±1.6	32.4
CPC 6530.1	10	0-460	0.05	0.50	7.41	3.52	2.57	3.45	6.46	-0.01	42.6±2.3	35.8
CPC 6530.3	11	0-490	0.03	0.71	23.73	4.29	5.25	6.66	8.03	0.04	36.7±1.0	32.5
CPC 6530.4	11	0-490	0.04	0.70	14.9	3.72	4.07	8.79	8.34	-0.15	45.5±1.9	41.4
CPT 23714.1	5	0-300	0.06	0.55	6.40	3.85	5.24	5.55	6.33	-0.07	33.5±2.0	33.2
CPT 23714.3	8	0-400	0.04	0.52	8.48	3.75	6.32	2.91	2	-0.01	42.4±1.9	42.0

CPT 23714.4	9	0-430	0.04	0.77	14.35	3.23	4.45	5.35	6.05	0.02	37.3±1.7	36.6
CPT 25159.1	11	100-510	0.05	0.63	10.33	4.60	6.49	3.58	1.98	0.11	20.8±1.0	20.0
CPT 25159.2	12	0-510	0.04	0.71	14.14	5.28	8.78	2.49	0.91	0.09	24.5±1.1	23.1
CPT 25313.1	12	0-510	0.03	0.57	16.18	1.90	0.09	4.51	1.52	0.12	43.9±1.4	42.1
CPT 25313.2	11	0-490	0.02	0.50	24.03	1.60	1.64	4.96	3.35	0.05	37.4±0.7	35.9
CPT 25313.3	10	0-460	0.04	0.54	11.28	1.89	3.44	2.28	2.02	0.15	47.2±1.9	44.4
CPT 25313.4	10	0-460	0.03	0.55	13.52	2.59	4.16	3.15	7.49	0.00	42.9±1.4	40.3
CPT 25340.1	11	0-510	0.05	0.57	10.72	5.87	9.36	2.22	0.74	0.03	14.0±0.7	12.3
CPT 25340.2	10	100-490	0.04	0.68	16.24	9.14	8.91	3.99	3.86	-0.05	22.8±0.9	20.1
CPT 25340.3	11	0-430	0.06	0.72	10.43	5.95	1.4	5.79	6.91	0.09	18.9±1.1	16.8
CPT 11413.2	9	200-490	0.04	0.59	13.68	3.65	8.22	2.66	1.06	-0.07	29.3±1.1	29.0
CPT 11413.3	7	0-400	0.05	0.50	7.32	4.41	8.97	5.16	7.79	-0.16	29.8±1.6	29.3
CPT 11413.5	8	0-460	0.06	0.66	8.56	2.41	5.97	5.92	9.74	0.10	28.3±1.7	27.9
CPM 17414.3	11	250-560	0.04	0.74	14.87	3.21	0.47	2.87	9.59	0.10	43.0±1.8	42.1
CPM 17414.4	7	400-560	0.04	0.52	10.53	3.41	2.14	6.43	0.13	-0.12	38.4±1.5	37.2
CPM 17414.5	14	560	0.05	0.86	13.08	5.94	8.92	6.72	5.45	-0.16	39.7±2.2	38.4
CVM 12369.2	10	200-510	0.02	0.75	24.25	1.50	0.39	3.08	5.33	0.08	54.0±1.4	52.1
CVM 12369.3	10	200-510	0.02	0.78	32.13	1.49	0.41	3.19	2.53	-0.03	50.7±1.0	49.5
CVM 12369.4	10	200-510	0.02	0.76	33.27	1.79	0.79	6.49	4.24	0.06	52.1±1.0	51.7
CVM 12369.5	10	200-510	0.02	0.66	26.34	1.38	1.00	3.22	4.09	0.07	50.4±1.1	49.1
CVM 23884.1	11	0-490	0.03	0.79	23.24	4.19	6.04	5.54	2.81	0.09	38.9±1.2	38.1
CVM 23884.3	8	0-400	0.04	0.55	12.50	3.67	7.27	4.75	9.9	0.11	41.7±1.6	41.0
CVM 23884.5	10	0-460	0.04	0.71	14.19	2.56	1.96	5.57	4.35	0.03	42.6±1.8	41.4
CVM 10835.1	7	400-560	0.02	0.51	15.76	1.36	1.55	4.41	5.69	0.06	43.9±0.9	42.8
CVM 10835.3	13	0-530	0.02	0.63	20.49	4.84	4.44	2.92	5.18	-0.16	43.3±1.1	42.2
CVM 10835.4	7	400-560	0.03	0.64	14.64	4.31	4.14	8.08	9.21	0.02	36.4±1.3	35.7
CVM 24759.1	12	0-510	0.04	0.76	17.50	3.22	5.82	1.85	6.98	0.08	45.0±1.7	42.1
CVM 24759.2	9	250-510	0.02	0.71	23.52	1.42	1.26	2.74	0.27	0.12	39.6±1.0	36.5
CVM 24759.3	10	100-510	0.01	0.87	52.00	1.77	0.76	3.40	6.68	0.04	38.0±0.5	36.5
CVM 24759.5	12	0-510	0.04	0.76	16.10	2.60	2.88	5.84	6.35	-0.09	36.0±1.4	35.1
CVM 24759.7	12	0-510	0.05	0.74	11.40	2.41	2.41	2.58	4.32	0.07	36.5±2.0	35.3
CVM 17640.1	6	0-340	0.02	0.54	18.40	2.96	4.45	0.82	1.93	0.03	39.2±0.8	35.9
CVM 17640.4	6	0-290	0.02	0.56	17.30	3.91	3.67	0.87	2.41	0.05	38.4±0.9	34.1
CVP 4178.1	8	0-400	0.05	0.80	11.60	4.70	5.45	2.01	0.38	0.07	40.6±2.2	38.7
CVP 4178.2	7	100-400	0.03	0.71	18.13	4.13	3.80	5.80	8.19	0.12	40.0±1.2	37.9
CVP 4178.5	8	0-400	0.04	0.81	13.20	4.32	1.11	1.73	4.56	-0.13	42.0±1.7	38.9
CVP 4178.7	8	0-400	0.08	0.74	6.18	5.30	4.83	2.77	2.56	0.11	45.7±3.8	42.6
CVP 35II.1	9	100-460	0.05	0.84	12.00	9.41	9.46	3.63	8.01	0.09	38.8±1.8	36.0
CVP 35II.4	7	0-370	0.06	0.83	10.04	4.38	1.20	6.07	7.12	0.16	36.4±2.2	32.7
CVP 35III.2	11	250-560	0.04	0.51	12.22	3.92	4.29	2.05	7.77	0.03	38.6±1.4	37.3

CVP 35III.5	11	250-560	0.04	0.51	11.08	3.99	3.88	6.003	3.81	-0.03	34.1±1.4	31.5
CVP 35III.6	11	250-560	0.04	0.51	11.51	3.90	2.06	3.93	7.98	-0.07	40.7±1.6	37.0
AZ 9170.1	10	100-490	0.03	0.67	19.32	1.20	1.71	5.48	5.93	0.05	53.9±1.5	52.3
AZ 9170.2	10	100-490	0.05	0.79	14.15	1.68	1.84	3.54	8.10	0.16	48.4±2.3	47.7
AZ 9170.6	9	200-490	0.03	0.71	17.61	1.71	1.17	5.46	9.48	0.09	47.7±1.6	46.8
AZ 9170.7	8	0-400	0.05	0.56	8.22	1.98	3.38	5.76	3.79	0.16	50.5±2.6	50.3
AZ 9170.9	8	0-400	0.05	0.56	8.08	1.94	3.58	3.98	5.88	0.16	46.0±2.4	45.2
2. Olmecs												
SL 788.2	10	0-460	0.07	0.76	8.84	5.22	8.4	7.16	1.71	-0.14	47.8±3.6	44.6
SL 788.3	10	0-460	0.08	0.92	9.70	6.53	9.23	6.75	1.37	0.15	49.3±4.0	46.0
SL 788.6	10	0-460	0.08	0.76	7.74	4.41	5.83	9.07	5.31	-0.08	44.1±3.8	41.1
SL 176.1	10	0-460	0.06	0.7	9.74	4.56	9.18	3.59	1.25	-0.01	51.4±3.2	50.9
SL 176.3	10	0-460	0.09	0.81	7.59	4.51	7.65	4.55	0.13	0.15	58.1±5.3	56.1
SLA s/n.1	10	0-460	0.05	0.52	8.63	3.02	6.08	1.02	0.65	-0.02	28.0±1.5	22.9
SLA s/n.2	10	0-460	0.05	0.56	10.23	3.31	5.08	2.65	6.79	-0.01	26.0±1.3	22.5
SLA s/n.5	10	0-460	0.05	0.56	10.23	3.31	5.08	2.65	6.79	0.07	23.8±0.9	22.8
SLA s/n.7	8	0-400	0.04	0.57	10.40	3.12	4.12	2.77	1.63	0.09	27.4±1.3	24.3
SLA 25.1	9	100-460	0.04	0.63	12.52	6.46	9.67	2.90	6.88	-0.07	29.4±1.2	28.2
SLA 25.2	9	100-460	0.09	0.77	6.95	5.31	7.88	5.59	4.39	0.07	30.4±2.7	29.5
SLB 31.1	9	0-430	0.06	0.68	9.05	5.55	9.14	3.35	5.81	-0.09	36.6±2.3	35.9
SLB 31.3	7	100-400	0.06	0.5	6.93	6.04	8.48	4.35	9.12	-0.14	31.6±1.8	31.3
SLB 31.4	7	0-370	0.05	0.66	10.70	5.94	7.32	3.3	9.16	-0.11	29.3±1.5	27.9
SLB 384.1	5	0-300	0.04	0.58	9.54	5.66	6.86	1.11	1.38	0.11	41.2±1.8	40.3
SLB 384.4	7	0-400	0.05	0.88	12.40	5.64	5.06	1.16	1.7	0.16	37.4±1.8	33.5
EBB 229.2	10	250-530	0.02	0.71	21.91	1.01	0.26	2.67	1.02	0.10	17.5±0.5	15.1
EBB 229.5	8	300-510	0.06	0.50	5.16	3.63	9.44	5.02	8.93	0.09	25.4±1.6	22.1
EBB 229.6	12	100-530	0.04	0.80	17.41	3.14	3.24	2.13	7.54	0.06	19.5±0.7	17.2
EBB 229.8	9	250-510	0.07	0.60	7.01	4.92	4.85	6.82	7.8	-0.09	18.3±1.3	16.5
3. Xitle heated pottery fragments												
CP-XT 1.1	12	0-510	0.06	0.52	7.88	3.55	8.08	3.16	5.87	0.13	62.6±3.6	61.6
CP-XT 1.3	12	0-510	0.07	0.51	6.57	3.58	8.38	3.24	3.42	0.10	63.9±4.3	62.1
CP-XT 1.6	15	0-580	0.02	0.72	33.48	1.54	3.07	5.41	3.61	-0.06	66.7±1.3	64.4
CP-XT 2.1	12	250-580	0.03	0.51	17.85	2.72	2.80	4.57	3.26	0.11	61.3±1.4	59.2
CP-XT 2.4	15	0-580	0.07	0.95	10.49	1.50	1.56	7.69	9.16	0.10	64.3±2.0	57.5
4. Santa Rosa de Viterbo Temple												
RV 1.3	13	0-560	0.03	0.78	22.70	1.88	0.63	2.53	6.76	-0.10	55.7±1.7	52.6
RV 1.5	6	430-560	0.06	0.51	5.92	1.50	0.98	4.33	6.59	0.13	55.7±3.6	52.7
RV 1.6	10	0-510	0.07	0.63	7.17	4.93	8.05	8.00	1.38	-0.05	58.9±4.3	55.7
RV 1.8	11	0-510	0.03	0.73	23.40	1.54	1.53	2.66	8.17	-0.11	52.3±1.4	49.5
RV 1.10	9	370-560	0.02	0.51	19.50	0.77	0.47	5.15	8.26	-0.12	53.7±1.2	50.8

RV 1.12	10	0-510	0.05	0.8	14.22	1.54	2.1	2.59	4.83	0.04	52.9±2.5	50.0
RV 1.14	11	0-530	0.09	0.83	6.55	3.13	2.09	6.91	7.57	-0.11	48.2±4.7	45.5
RV 2.2	9	200-530	0.03	0.53	14.70	2.28	0.91	0.74	5.55	0.12	50.6±1.9	48.3
RV 2.3	7	0-400	0.04	0.52	8.95	3.44	1.63	2.13	5.31	0.04	45.4±1.9	43.2
RV 2.5	7	0-400	0.05	0.54	6.90	2.00	4.77	5.27	6.51	0.05	44.0±2.1	41.9
RV 4.1	8	0-430	0.05	0.83	11.40	3.80	1.66	6.67	5.6	0.03	47.2±2.2	44.6
RV 4.4	7	0-400	0.04	0.85	13.60	2.65	2.09	2.26	2.33	0.12	48.9±1.9	46.2
RV 4.6	11	0-510	0.02	0.96	39.77	2.46	2.47	3.09	5.45	0.10	52.3±1.1	49.4
5. Lava Flows												
JA 4-3a	7	340-510	0.03	0.64	15.82	2.54	0.60	9.50	5.94	0.14	58.3±1.9	na
JA 4-4a	7	340-510	0.03	0.70	18.07	4.20	5.47	9.66	9.82	0.15	47.5±1.4	na
Pop 2.11c	5	460-560	0.04	0.67	12.08	1.35	0.50	6.27	7.45	0.11	79.3±3.1	na
Pop 4.12b	13	100-560	0.05	0.63	7.41	1.47	1.9	6.54	1.56	-0.14	73.4±2.4	na
AGO 1-10b	6	400-530	0.02	0.61	20.34	3.40	1.11	6.29	4.14	0.15	55.5±1.3	na
AGO 1-11a	8	400-460	0.02	0.77	25.88	3.30	3.07	3.78	9.69	0.02	45.2±1.1	na
AGO 3-3b	9	100-460	0.03	0.53	12.93	5.36	3.43	8.35	3.33	0.12	59.1±2.0	na
JA 6.2z	12	0-510	0.06	0.74	11.10	4.59	9.48	5.31	1.3	0.12	58.4±3.4	na
JA 6.6a	9	250-510	0.05	0.74	11.37	3.49	5.35	5.67	5.28	0.13	51.5±2.8	na
SMT 8b	9	100-460	0.05	0.81	12.45	1.37	1.39	7.39	5.81	0.14	65.5±3.6	na
SMT 14z	10	250-540	0.04	0.94	20.54	1.49	0.70	1.96	6.36	0.12	50.9±1.9	na
SMT 16a	8	0-400	0.03	0.75	19.80	3.61	6.08	3.04	4.48	0.01	66.7±2.0	na
JU1.5a	12	0-510	0.04	0.62	12.40	2.11	3.96	5.69	4.2	0.09	41.4±1.7	na
JU1.16a	12	0-510	0.03	0.78	19.40	2.62	3.05	7.33	7.07	-0.12	43.2±1.5	na
JU2.1z	11	100-510	0.01	0.81	54.37	1.71	1.80	4.64	6.60	0.04	49.4±0.6	na
JU2.6a	8	0-400	0.03	0.69	17.50	1.32	1.99	3.72	4.41	0.05	47.3±1.3	na
JU2.7z	7	250-460	0.02	0.62	28.10	1.82	0.92	3.69	8.46	0.12	50.0±0.8	na
FNA-1y	6	300-460	0.04	0.82	13.80	1.87	0.74	3.60	2.44	0.06	34.7±1.4	na
FNA-3y	10	0-460	0.04	0.82	15.80	2.22	1.22	6.20	3.44	0.05	35.8±1.4	na
FNA-4z	5	340-460	0.04	0.74	13.27	1.83	1.26	8.12	7.57	0.07	38.1±1.6	na
FNA-7x	8	0-400	0.08	0.95	9.31	4.37	4.28	2.74	4.31	0.12	28.0±2.2	na
FNA-8x	8	0-400	0.04	0.88	18.01	6.27	2.91	5.46	8.49	0.14	27.3±1.1	na

N: number of points included in the linear best-fit; T_{\min} - T_{\max} : minimum and maximum temperature used to determine the paleointensity; β : ratio of the standard error of the slope of the selected segment in the Arai plot to absolute value of the slope; f: NRM fraction used for the best-fit; q: quality factor; MAD_{anc} : anchored maximum angular deviation; α : angular difference between anchored and non-anchored best fit; δCK : relative check error; δpal : cumulative check difference; $|K'|$: is the absolute value of curvature of the data points used

for determining the best-fit line; $H_{\text{raw}} \pm \sigma_B$: average paleointensity of a specimen before any correction; H: average paleointensity of a specimen after cooling rate correction; na, no cooling correction was applied to lava flow specimens.

Supplementary Table S4:

Evaluation of previous Mexican archeointensity data

A) Thellier- Thellier + Microwave experiments

Ordinarily, retrieving accurate paleointensity values from naturally occurring materials received great attention over recent decades (e.g. Coe et al., 1978; Aitken et al., 1988; Selkin and Tauxe, 2000; Valet, 2010; Genevey et al., 2008; Biggin, 2010; Shaar and Tauxe 2013). Nevertheless, the reliability of paleointensity estimates given by Thellier-Thellier and/or Microwave methods may be tested using a set of quality parameters (Coe et al., 1978; Selkin and Tauxe, 2000; Kissel and Laj, 2004; Leonhardt et al., 2004, Tauxe and Staudigel, 2004; Biggin et al., 2007; Shaar and Tauxe, 2013; Paterson et al., 2014). Up to this moment, there is no consensus on which parameter set quantifies best the reliability of paleointensity estimates without rejecting too many data (Paterson et al., 2014). However, selection criteria have been proposed that have been used widely in recent works, which are also the basis for the present study. In the following we summarize these criteria, which are used for our own data and also for evaluating previously published Mexican paleointensity data for the last 3600 years.

1. Arai diagrams and orthogonal demagnetization plots

To start with, Coe et al. (1978) proposed the fraction (f), gab (g), and quality factors (q), which are ordinarily reported in any paleointensity work. Also, Coe et al. (1978) and Tauxe and Staudigel (2004) introduced the scatter parameter (β) which is a measure of the relative scatter around the best-fit line in an Arai plot. Thermal alteration during paleointensity estimates could be monitored by using two parameters: $\delta(CK)$ (Leonhardt et al., 2004) and DRAT (Selkin and Tauxe, 2000). Both parameters quantified the difference between the two pTRM acquisitions at specific temperature normalized either to the TRM ($\delta(CK)$) or to the length of the selected NRM-TRM segment (DRAT). Three important angles have been proposed to illustrate both the scattering and stability of the NRM directions provided during the zero-field steps of a paleointensity experiment. These are the anchored maximum angular deviation (MAD_{anc} ; Kirschvink, 1980) of the selected NRM component and the (α) angle which is the angular difference between the anchored and the non-anchored best-fit line. More recently, Selkin Tauxe and Staudigel (2004) proposed the DANG parameter which is the deviation angle between the best-fit line and the line determined by the center of mass and the origin. These criteria are for example but not limited to, but they are often used in the literature to judge the credibility of the PI data. Threshold values for these criteria have been defined by some authors and accordingly a number of criteria sets suggested, for example, PICRIT03 (Kissel and Laj, 2004), SELCRIT2 (Biggin et al., 2007), ThellierTool A and B (Leonhardt et al., 2004) and the modified sets TTA and TTB (Paterson et al., 2014). Having considering these sets, our intensity determinations were analyzed with the criteria listed in Table S2. In a similar manner, we re-examined all previously obtained PI data in the light of these criteria sets. Careful revision of these 99 PI data points was done using the original publication besides the GEOMAGIA50.v3 database (Brown et al., 2015), to avoid any error resulting from data capture (Tema and Kondopoulou, 2011). Accordingly, we note that most of the published paleointensity studies for the last 3,600 years have focused on the three Coe's criterions: the fraction (f), gab (g), and quality (q) parameters. The values of these parameters in general are larger than the threshold values proposed by Paterson et al. (2014), but all other criterions were not available in these studies. Except the recent work of Fanjat et al. (2013), all of these previous studies did not present the thermal alteration monitoring parameters and not even the NRM directional stability criterions for their accepted specimens. Some PI studies that were done several decades ago (Nagata et al., 1965, Bucha et al., 1970, and Lee, 1975) and did not include any of the above mentioned parameters at all. Based on the above, we have set a condition of the inclusion of these previously mentioned criteria for each accepted specimen (higher quality data) or, at least, must be presented as general in the literature. We point out that the work of Fanjat et al. (2013) typically contained all of these required sets and therefore the

Reference ID	Material ID	PI Method	Thermal alteration monitoring pTRM check	Stability of NRM directions MAD	Anisotropy	Cooling rate	meets quality criteria?	Notes
--------------	-------------	-----------	--	---------------------------------	------------	--------------	-------------------------	-------

provided PI data are considered of the highest quality. At this step, 39 out of the total 99 intensity data points were discarded (~39%).

2. Cooling rate correction (only for the archeological artifacts)

Dodson and McClelland-Brown (1980) and Halgedahl et al. (1980) pointed out the strong relationship between the thermal remanent magnetization (TRM) intensity and the cooling time: the slower the cooling time the higher the TRM intensity, if it is carried by single domain (SD) particles (Fox and Aitken, 1980), whereas in multidomain (MD) particles the opposite may be true (Perrin, 1998). In case of the TRM carried by pseudo single domain (PSD) particles, the effect of the cooling time is not clear, but probably negligible (Biggin et al., 2013). Therefore, cooling rate (CR) correction is crucial for archeological artifacts, as its TRM often is carried by SD particles. Unlike the archeological artifacts, the TRM of the lavas resides in larger grain sizes of PSD and/or MD particles which means there is no need to carry out a CR correction. CR correction involves three additional partial TRM (pTRM) acquisition steps at a temperature selected so that at least 60% of the specimen's TRM was used. More details on the CR correction can be found in Chauvin et al. (2000) and Genevey and Gallet (2002). For the 78 published Mexican archeointensity data, 44 were not corrected for the CR (Nagata et al., 1965; Bucha et al., 1970; and Lee, 1975; Aitkin et al., 1991; Böhnell et al., 2003) and thus deleted.

3. Anisotropy correction (only for the archeological artifacts)

Due to manufacturing processes, pottery, ceramics (to a lesser degree, Mitra et al., 2013) and also bricks are often characterized by a strong magnetic anisotropy (e.g. Rogers et al., 1979). Commonly, the anisotropy tensor has to be determined (Veitch et al., 1984) to correct the effect of anisotropy. Another method to evade the requirement for a correction of the anisotropy is imparting the laboratory field along the ancient field direction (Aitken et al., 1981; Veitch et al., 1984; Poletti et al., 2016). This method was used in the present study. Morales et al. (2009) suggested an anisotropy correction based on the TRM of six sub-specimens oriented orthogonally in six different directions (+X, -X, +Y, -Y, +Z, -Z) and averaging their PI. While this procedure with a single heating reduces thermal alteration effects, Poletti et al. (2016) demonstrated that this approach indeed does not correct for the TRM anisotropy effect (for details see Poletti et al., 2016). Therefore, data corrected with this method (Morales et al., 2009; Petronille et al., 2012; Aguilar-Reyes et al., 2013) will not be considered. From other previously reported PI data, 38 were not corrected at all for anisotropy (Nagata et al., 1965; Bucha et al., 1970; Lee, 1975) and considered as unreliable.

4. The minimum number of specimens to calculate the mean and their consistency (archeological artifacts + lavas)

Archeological sample mean intensities must be based on at least two specimens and have a standard deviation $<5 \mu\text{T}$, resulting in the deletion of 28 PI data. The PI mean calculated from a volcanic material must be based on at least two specimens and have a standard deviation $<10 \mu\text{T}$ and 4 out of 21 PI data were deleted because they do not meet this condition.

A summary of the above mentioned criteria used in this study is listed below:

Archeological Pieces								
5	1	TT	no	No	no	no	no	
13	1, 2, 4, 5	TT	no	no	no	no	no	
99	5	TC	yes	no	yes	yes	no	Cooling rate guessed
435	8	TC	yes	yes	no	yes	no	unreliable anisotropy correction
442	8	TC	yes	no	yes	yes	no	
500	5	TC	yes	yes	yes	yes	yes	
523	8	TC	Yes; < 15%	Yes	no	yes	no	unreliable anisotropy correction
524	8	TT	DRAT < 10%	yes	yes	yes	yes	
532	5	TC	< 10%	yes	no	yes	no	unreliable anisotropy correction
136	5	MW	no	no	yes	no	no	Sample TRM parallel to laboratory field
Lava rocks								
15	4	TT	no	no	no	no	no	
86	4	TC	< 15%	yes	-	-	yes	Xitle; age corrected to 373±56 CE
110	4	TC	no	no	-	-	no	standard deviation of the PI-mean >10μT
137	4	TC	< 15%	Yes	-	-	yes	Xitle; age corrected to 373±56 CE
143	4	TC	yes	yes	-	-	yes	Xitle; age corrected to 373±56 CE
382	4	TC	yes	yes	-	-	yes	Xitle; age corrected to 373±56 CE
191	4	TC	yes	yes	-	-	yes	
377	4	TC	< 15%	yes	-	-	yes	
387	4	TC	< 15%	yes	-	-	no	standard deviation of the PI-mean >10μT
136	4	MW	< 10%	< 15°	-	-	yes	Xitle; correct age used
191	4	MW	< 10%	yes	-	-	yes	
400	4	MW	no	no	-	-	no	standard deviation of the PI-mean >10μT
<p>Reference ID (as in geomagia50v3): 5, Bucha et al., 1970; 13, Lee, 1975; 15, Nagata et al., 1965; 99, Aitken et al., 1991; 86, Alva-Valdivia, 2005; 110, Gonzalez et al., 1997; 136, Böhnell et al., 2003; 137, Böhnell et al., 1997; 143, Morales et al., 2001; 191, Gratton et al., 2005; 382, Morales et al., 2006; 377, Conte-Fasano et al., 2006; 387, Urrutia-Fucugauchi et al., 2004; 400, Goguitchaichvili et al., 2005; 435, Morales et al., 2009; 442, Rodríguez-Ceja et al., 2009; 500, Duran et al., 2010; 523, Aguilar-Reyes et al., 2013; 524, Fanjat et al., 2013; 532, Petronille et al., 2012.</p> <p>Material ID (as in geomagia50v3): 1, Brick; 2, Baked clay; 4, lava; 5, Pottery; 8, Ceramic</p> <p>PI Method (as in geomagia50v3): TT, Original Thellier method (Thellier and Thellier 1959); TC, Thellier-Coe method (Coe et al., 1967); MW, Microwave single heating method.</p>								
<p>B) Multispecimen method</p> <p>Dekkers and Böhnell (2006) proposed a new method designed specially to avoid the undesirable MD effects and also to reduce the risk of thermal alteration. It is called “multispecimen parallel differential pTRM method (MSP-DB)”. Instead of step-wise increasing the temperature and applying a constant magnetic field in the furnace as in Thellier-style experiment, they proposed to apply different magnetic fields to several</p>								

samples heated all to the same temperature. The basic idea here is that if a pTRM is induced parallel to the original TRM in a laboratory field smaller than the paleofield, the result will be a lower magnetization than the original TRM due to partial demagnetization. If the pTRM is induced in a stronger field, the result will be a higher magnetization than the original TRM due to a partial remagnetization. If the field is the same as the paleofield, no change in remanence will occur. To reduce thermal alteration and history effects, an intermediate temperature is set for all specimens, and every specimen is heated only once. For this, the set-temperature to be used for a site has to be selected carefully. It has to be sufficient high to unblock a significant fraction of the NRM, and low enough to avoid thermo-chemical alterations, and this temperature can be best determined by previous rock-magnetic experiments. Two steps are needed to perform the MSP-DB experiment, (a) Measurement of the NRM (m_0), and (b) Acquisition of a partial thermoremanence pTRM (m_1) parallel to the sample NRM (TRM) by heating them in a laboratory field H_{lab} to the set temperature. Field values H_{lab} are different from one specimen to another, although several specimens may be used for each field step. The DB ratio ($QDB = (m_1 - m_0)/m_0$) is plotted against the lab field H_{lab} and a best fit applied to the data, which also provides 95% confidence limits. The PI is given by the value of this best fit at $QDB = 0$. Several advantages found in this method compared to Thellier-Thellier-type experiments:

- It is not limited to SD particles, but all magnetic domain states from SD to MD particles may be processed (as originally claimed!).
- The heating or set temperature can be chosen according to the pTRM change wanted, but avoiding alteration of magnetic minerals.
- By using this technique, one can ensure that all specimens experience the same magnetic history.
- High-temperatures tails, a phenomena characteristic of MD particles, are reduced by the parallel alignment of the laboratory pTRM parallel to the specimens' NRM.
- Finally, much less steps are required in this method which significantly decreases the total time needed to process a rock unit (Dekkers and Böhnel, 2006).

This method ideally requires that the NRM is composed uniquely by the original TRM. Small secondary viscous magnetization components which are common may be eliminated by a zero-field demagnetization at a temperature T_v smaller than the set temperature, and this has to be applied at all steps. Fabian and Leonhardt (2010) demonstrated that the original claim of domain-state independence by Dekkers and Böhnel (2006) was not entirely correct. Furthermore, the classical MSP-DB protocol suffers from tail-effects associated with imparting a pTRM. These effects give rise to overestimation of the paleointensity values calculated from the MSP-DB protocol. Based on experiments on magnetic minerals of well controlled grain sizes, Fabian and Leonhardt (2010) proposed the MSP-DSC protocol, where DSC is an abbreviation of "domain-state corrected". This modification requires three additional steps to the original MSP protocol (m_0 and m_1 represent the NRM and original single-step MSP-DB protocol).

- Step 2 (m_2): heating and cooling in a field antiparallel to the NRM : this step is used to determine a slope or fraction correction; $\beta = (m_1 + m_2)/2$.
- Step 3 (m_3): heating in zero field, cooling in parallel DC field: this step is used to estimate the domain state effect; $\mu_{DS} = (m_1 - m_3)/2$.
- Step 4 (m_4): repetition of step 1: subtracting m_4 from m_1 quantifies thermo-chemical alterations occurring

between these steps.

This extended protocol is further referred to as MSP-DSC. The α -parameter in the MSP-DSC analyses was set to 0.5 as suggested by Fabian and Leonhardt (2010). Based on all above, two important criteria were set in order to accept the PI results derived from the multispecimen method:

1. Conducting one of the Curie temperature determination experiments is vital and necessary where accordingly the set temperature could be defined (Dekkers and Böhnelt, 2006)
2. The correction of Fabian and Leonhardt (2010) (MSP-DSC) is a prerequisite for accepting the MSP data. Three criterions have emerged from this correction (see Monster et al. 2015), a) the thermal-induced alteration criterion $|\epsilon_{alt}|$, b) the directional criterion, and c) the intersection criterion (Δb).

Reference ID	Material ID	Conduct thermomagnetic analyses	Fabian & Leonhardt (2010) (MSP-DSC)			meets the present set of quality criteria	Notes
			$ \epsilon_{alt} $	Directional criterion	Δb		
379	4	yes	no	no	no	no	These two studies were done before the correction of Fabian and Leonhardt (2010)
421	4	yes	no	no	no	no	

Reference ID: 379, Dekkers and Böhnelt, 2006; 421, Michalk et al., 2008

A summary of the above mentioned criteria used in this study are listed below

Supplementary Table S4 References

Aitken MJ, Alcock P, Bussell GD, Shaw C (1981) Archeomagnetic determination of the past geomagnetic intensity using ancient ceramics: Allowance for anisotropy. *Arch* 23: 53–64.

Aitken MJ, Pesonen LJ, Leino M (1991) The Thellier paleointensity technique: Minisamples versus standard size. *J Geomagn Geoelectr* 43: 325–331.

Arce JL, Munoz-Salinas E, Castillo M, Salinas I (2015) The ~2000 yr BP Jumento volcano, one of the youngest edifices of the Chichinautzin Volcanic Field, Central Mexico. *J Volcanol Geotherm Res* 308: 30–38.

Alva-Valdivia LM (2005) Comprehensive paleomagnetic study on a succession of Holocene olivine-basalt flow: Xitle volcano (Mexico) revisited. *Earth Planets Space* 57: 839–853.

Biggin AJ, Perrin M, Dekkers MJ (2007) A reliable absolute paleointensity determination obtained from a non-ideal recorder. *Earth Planet Sci Lett* 257: 545–563 doi:10.1016/j.epsl.2007.03.017.

Biggin AJ (2010) Are systematic differences between thermal and microwave Thellier-type paleointensity estimates a consequence of multidomain bias in the thermal results?, *Phys Earth Planet Inter* 180: 16–40 doi:10.1016/j.pepi.2010.03.005.

Biggin AJ et al (2013) The effect of cooling-rate on the intensity of thermoremanent magnetization (TRM) acquired by assemblages of pseudo-single domain, multi domain, and interacting single domain grains. *Geophys J Int* 193: 1239–1249.

Böhnelt H et al (1997) Variation of Rock Magnetic Parameters and Paleointensities over a Single Holocene Lava Flow. *J Geomag Geoelectr* 49: 523–542.

Böhnelt H, Biggin AJ, Walton D, Shaw J, Share JA (2003) Microwave paleointensities from a recent Mexican lava flow, baked sediments and reheated pottery *Earth Planet Sci Lett* 214 (1–2): 221–236.

Böhnelt HN, Dekkers MJ, Delgado-Argote LA, Gratton MN (2009) Comparison between the microwave and multispecimen parallel difference pTRM paleointensity methods. *Geophys J Int* 177:383–394

Böhnelt H, Pavón-Carrasco FJ, Sieron K, Mahgoub AN (2016) Paleomagnetic dating of two recent lava flows from Ceboruco volcano, western Mexico. *Geophys J Int* 207 (2):1203–1215.

- Brown MC, et al. (2015) GEOMAGIA50.v3: 1. General structure and modifications to the archeological and volcanic database. *Earth Planets Space* 67:83.
- Bucha V, Taylor R, Berger R, Haury E (1970) Geomagnetic intensity: changes during the past 3000 years in the western hemisphere. *Science* 168:111–114.
- Conte-Fasano G, Urrutia-Fucugauchi J, Goguitchaichvili A, Morales-Contreras J (2006) Low-latitude paleosecular variation and the time-averaged field during the late Pliocene and Quaternary—paleomagnetic study of the Michoacan-Guanajuato volcanic field, Central Mexico. *Earth Planets Space* 58(10):1359–1371.
- Chauvin A, Garcia Y, Lanos P, Laubenheimer F (2000) Paleointensity of the geomagnetic field recovered on archeomagnetic sites from France. *Phys Earth Planet Inter* 120(1-2):111–136.
- Coe RS (1967) Paleo-intensities of the Earth's magnetic field determined from Tertiary and Quaternary rocks. *J geophys Res* 72(12): 3247–3262.
- Coe RS, Gromme S, Mankinen EA (1978) Geomagnetic paleointensities from radiocarbon-dated lava flows on Hawaii and the question of the Pacific nondipole low. *J Geophys Res* 83:1740–1756.
- Day R, Fuller M, Schmidt VA (1977) Hysteresis properties of titanomagnetites: grain-size and compositional dependence. *Phys Earth planet Inter* 13: 260–267.
- Dekkers MJ, Bönhel HN (2006) Reliable absolute paleointensities independent of magnetic domain state *Earth Planet Sci Lett* 284: 508-517.
- Dodson MH, McClelland-Brown E (1980) Magnetic blocking temperatures of single-domain grains during slow cooling *J Geophys Res* 85: 2625–2637.
- Dunlop DJ (2002) Theory and application of the Day plot (Mrs/Ms versus Hcr/Hc) 1. Theoretical curves and tests using titanomagnetite data. *J geophys. Res* 107(B3) 2056, doi: 10.1029/2001JB000486.
- Dunlop DJ (2002b) Theory and application of the Day plot (Mrs/Ms versus Hcr/Hc): 2. Application to data for rocks, sediments, and soils. *J Geophys Res* 107(B3) 2057, doi: 10.1029/2001JB000487.
- Duran MP (2010) Magnetic properties and Archeointensity of Earth's magnetic field recovered from El Opeño, earliest funeral architecture known in Western Mesoamerica *Stud. Geophys Geod* 54: 575-593.
- Ertepinar P, et al. (2012) Archeomagnetic study of five mounds from Upper Mesopotamia between 2500 and 700 BCE: Further evidence for an extremely strong geomagnetic field ca. 3000 years ago. *Earth Planet Sci Lett* 357-358:84–98.
- Ertepinar P, et al. (2016) Full vector archeomagnetic records from Anatolia between 2400 and 1350 BCE: Implications for geomagnetic field models and the dating of fires in antiquity. *Earth Planet Sci Lett* 434:171–186.
- Fabian K, Leonhardt R (2010) Multiple-specimen absolute paleointensity determination: An optimal protocol including pTRM normalization, domain-state correction, and alteration test. *Earth Planet Sci Lett* 297: 84–94.
- Fanjat G et al. (2013) First archeointensity determinations on Maya incense burners from Palenque temples, Mexico: new data to constrain the Mesoamerica secular variation curve. *Earth Planet Sci Lett* 363: 168–180.
- Fox JMW, Aitken MJ (1980) Cooling-rate dependence of thermoremanent magnetization. *Nature* 283: 462–463.
- Genevey A, Gallet Y (2002) Intensity of the geomagnetic field in Western Europe over the past 2000 years: New data from French ancient pottery. *J Geophys Res* 107(B11): 2285.
- Genevey A, Gallet Y, Constable C, Korte M, Hulot G (2008) ArcheoInt: An upgraded compilation of geomagnetic field intensity data for the past ten millennia and its application to the recovery of the past dipole moment. *Geochem Geophys Geosyst* 9, Q04038, doi:10.1029/2007GC001881.
- Gonzalez S, Sherwood GJ, Boehnel H, Schnepf E (1997), Paleosecular variation in central Mexico over the last 30,000 years: The record from lavas. *Geophys J Int* 130: 201–219.
- Gratton MN, Goguitchaichvili A, Conte G, Shaw J, Urrutia-Fucugauchi J (2005) Microwave paleointensity study of the Jorullo volcano (Central Mexico) *Geophys J Int* 161: 627–634.
- Goguitchaichvili A et al (2005) Microwave paleointensity analysis of historic lavas from Paricutin volcano, Mexico. *Geofisica Internacional* 44: 231–240.
- Halgedhal S, Day R, Fuller M (1980) The effect of the cooling rate on the intensity of weak field TRM in single domain magnetite. *J Geophys Res* 85: 3690–3698.

- Kirschvink JL (1980) The least squares line and plane and the analysis of paleomagnetic data. *Geophys J R Astron Soc* 62: 699-718.
- Kissel C, Laj C (2004) Improvements in procedure and paleointensity selection criteria (PICRIT-03) for Thellier and Thellier determinations: Application to Hawaiian basaltic long cores. *Phys Earth Planet Inter* 147: 155–169 doi:10.1016/j.pepi.2004.06.010.
- Lee SS (1975) Secular variation of the intensity of the geomagnetic field during the past 3,000 years in North, Central and South America. Ph.D. thesis University of Oklahoma, Norman.
- Leonhardt R, Heunemann C, Krása D (2004) Analyzing absolute paleointensity determinations: acceptance criteria and the software ThellierTool4.0. *Geochem Geophys Geosyst* 5 (12).
- Mahgoub, A.N., Böhnell, H., Siebe, C., Chevrel, M.O., 2017a. Paleomagnetic study of el Metate shield volcano (Michoacán, Mexico) confirms its monogenetic nature and young age (~1250 CE). *J Volcanol Geotherm Res* 336:209–218. <https://doi.org/10.1016/j.jvolgeores.2017.02.024>.
- Mahgoub AN, Reyes-Guzman N, Böhnell H, Siebe C, Pereira G, Dorison A (2017b) Paleomagnetic constraints on the ages of the Holocene Malpaís de Zacapu lava flow eruptions, Michoacán (Mexico): Implications for archeology and volcanic hazards. *The Holocene* <https://doi.org/10.1177/0959683617721323>.
- Mitra R, Tauxe L, Keech McIntosh S (2013) Two thousand years of archeointensity from West Africa. *Earth Planet Sci Lett* 364:123–133.
- Monster MWL, de Groot LV, Dekkers MJ (2015) MSP-Tool: a VBA-based software tool for the analysis of multispecimen paleointensity data *Front. Earth Sci.* 3 86 doi:10.3389/fearth.2015.00086.
- Nagata T, Kobayashi K, Schwarz E (1965) Archeomagnetic intensity studies of south and central America. *J Geomagn Geoelectr* 17: 399–405.
- Morales J, Goguitchaichvili A, Urrutia-Fucugauchi J (2001) A rock-magnetic and paleointensity study of some Mexican volcanic lava flows during the Latest Pleistocene to the Holocene. *Earth Planets Space* 53(9): 893–902.
- Morales J, Alva-Valdivia LM, Goguitchaichvili A, Urrutia-Fucugauchi J (2006) Cooling rate corrected paleointensities from the Xitle lava flow: Evaluation of within-site scatter for single spot-reading cooling units. *Earth Planets Space* 58: 1341–1347.
- Morales J et al (2009) Magnetic properties and archeointensity determination on pre-Columbian pottery from Chiapas, Mesoamerica. *EPS Spec Iss* 61: 83–91.
- Nelson SA, Gonzalez-Caver E (1992) Geology and K-Ar dating of the Tuxtla Volcanic Field, Veracruz, Mexico *Bull Volcanol* 55: 85-96.
- Panfil MS, Gardner TW, Hirth KG (1999) Late Holocene stratigraphy of the Tetimpa archeological sites, northeast flank of Popocatepetl volcano, central Mexico. *Geol Soc Am Bull* 111: 204–218.
- Paterson GA, Tauxe L, Biggin AJ, Shaar R, Jonestrask LC (2014) On improving the selection of Thellier-type paleointensity data. *Geochem Geophys Geosyst* 15(4): 1180–1192.
- Pétronille M, Goguitchaichvili A, Morales J, Carvallo C, Hueda-Tanabe Y (2012) Absolute geomagnetic intensity determinations on Formative potsherds (1400–700 BC) from the Oaxaca Valley, Southwestern Mexico. *Quat Res* 78: 442-453 [10.1016/j.yqres.2012.07.011](https://doi.org/10.1016/j.yqres.2012.07.011).
- Perrin M (1998) Paleointensity determination, magnetic domain structure, and selection criteria. *J Geophys Res* 103: 30591-30600.
- Poletti W, Trindade RI, Hartmann GA, Damiani N, Rech RM (2016) Archeomagnetism of Jesuit Missions in South Brazil (1657–1706 AD) and assessment of the South American database. *Earth Planet Sci Lett* 445: 36-47.
- Pollard JPJ (1999). Paleomagnetism of late Cenozoic volcanics from east-central Mexico—implications for regional tectonic evolution. PhD thesis Liverpool John–Moores University p. 268.
- Reyes A et al (2013) An integrated archeomagnetic and C14 study on pre-Columbian potsherds and associated charcoals intercalated between Holocene lacustrine sediments in Western Mexico: Geomagnetic implications. *J Geophys Res* 118: 2753-2763 [10.1002/jgrb.50196](https://doi.org/10.1002/jgrb.50196).
- Rodriguez-Ceja M et al (2009) An integrated magnetic and Raman spectroscopy study on some pre-Columbian potteries from cuanalan (a formative village in the valley of Teotihuacan) in Mesoamerica. *J Geophys Res* 114 B04103 [10.1029/2008JB006106](https://doi.org/10.1029/2008JB006106).

- Selkin PA, Tauxe L (2000) Long-term variations in paleointensity. *Philos. Trans R Soc London Ser A Philos Trans Math. Phys Eng Sci* 358:1065–1088.
- Shaar R, Tauxe L (2013) Thellier GUI: an integrated tool for analyzing paleointensity data from Thellier-type experiments. *Geochem Geophys Geosyst* 14: 677–692 doi: 10.1002/ggge.20062.
- Siebert L, Carrasco-Nuñez G (2002) Late Pleistocene to pre-Columbian behind-the-arc mafic volcanism in the eastern Mexican volcanic belt: implications for future hazards. *J Volcan Geotherm Res* 115: 179–205.
- Tauxe L, Mullender TAT, Pick T (1996) Potbellies, wasp-waists, and superparamagnetism in magnetic hysteresis. *J Geophys Res* 101: 571–583.
- Tauxe L, Staudigel H (2004) Strength of the geomagnetic field in the Cretaceous Normal Superchron: New data from submarine basaltic glass of the Troodos Ophiolite. *Geochem Geophys Geosyst* 5(2):Q02H06.
- Tema E, Kondopoulou D (2011) Secular variation of the Earth's magnetic field in the Balkan region during the last eight millennia based on archeomagnetic data. *Geophys J Int* 186(2): 603–614. doi:10.1111/j.1365-246X.2011.05088.x.
- Thellier E, Thellier O (1959) Sur l'intensité du champ magnétique terrestre dans le passé historique et géologique. *Ann Géophys* 15: 285–376.
- Urrutia-Fucugauchi J, Alva-Valdivia L, Goguitchaichvili A, M. Rivas ML, Morales J (2004) Paleomagnetic, rock-magnetic and microscopy studies of historic lava flows from Parícutin volcano, Mexico: Implications for the deflection of paleomagnetic measurements, *Geophys J Int* 156: 431–442.
- Yu YJ, Tauxe L (2005). Testing the IZZI protocol of geomagnetic field intensity determination. *Geochem Geophys Geosyst.*, 6, Q05H17, doi:10.1029/2004GC000840.
- Valet JP, Herrero-Bervera E, Carlot J, Kondopoulou D (2010) A selective procedure for absolute paleointensity in lava flows, *Geophys. Res. Lett.*, 37, L16308, doi: 10.1029/2010GL044100.
- Veitch RJ, Hedley IG, Wagner JJ (1984) An investigation of the intensity of the geomagnetic field during Roman times using magnetically anisotropic brick sand tiles. *Arch Sci* 37: 359–373.

Supplementary Table S5

The Mexican paleointensity secular variation curve data

Age CE	PI _{mean} (μ T)	PI _{upper} (μ T)	PI _{lower} (μ T)
-1600	52.7	61.9	43.6
-1590	51.8	60.3	43.4
-1580	50.9	58.7	43.1
-1570	50.0	57.2	42.7
-1560	49.1	55.9	42.2
-1550	48.1	54.6	41.6
-1540	47.2	53.5	40.9
-1530	46.3	52.5	40.1
-1520	45.4	51.6	39.2
-1510	44.5	50.7	38.3
-1500	43.6	49.8	37.3
-1490	42.6	49.0	36.3
-1480	41.8	48.2	35.3
-1470	40.9	47.4	34.4
-1460	40.0	46.5	33.5
-1450	39.2	45.7	32.7
-1440	38.4	44.8	31.9
-1430	37.6	44.0	31.3
-1420	36.9	43.2	30.7
-1410	36.3	42.4	30.2
-1400	35.7	41.7	29.8
-1390	35.2	41.0	29.4
-1380	34.8	40.3	29.2
-1370	34.4	39.8	29.0
-1360	34.1	39.3	28.9
-1350	33.9	38.9	28.9
-1340	33.8	38.6	28.9
-1330	33.7	38.4	29.0
-1320	33.7	38.2	29.1
-1310	33.7	38.2	29.2
-1300	33.8	38.2	29.3
-1290	33.9	38.3	29.4
-1280	34.0	38.4	29.6
-1270	34.1	38.5	29.7
-1260	34.2	38.6	29.8
-1250	34.3	38.7	29.9
-1240	34.4	38.9	30.0
-1230	34.5	39.0	30.0
-1220	34.6	39.1	30.1
-1210	34.6	39.2	30.1
-1200	34.7	39.3	30.0
-1190	34.7	39.3	30.0
-1180	34.6	39.3	29.9
-1170	34.6	39.3	29.9
-1160	34.5	39.2	29.8
-1150	34.4	39.0	29.8
-1140	34.3	38.8	29.7
-1130	34.1	38.6	29.7
-1120	34.0	38.3	29.6
-1110	33.8	38.1	29.5
-1100	33.6	37.9	29.4
-1090	33.5	37.7	29.2
-1080	33.3	37.7	28.9
-1070	33.1	37.7	28.6
-1060	33.0	37.8	28.1
-1050	32.8	38.0	27.6
-1040	32.6	38.3	27.0
-1030	32.5	38.7	26.3
-1020	32.3	39.1	25.6
-1010	32.1	39.5	24.8
-1000	32.0	39.9	24.0
-990	31.8	40.3	23.2
-980	31.5	40.7	22.4
-970	31.3	41.0	21.6
-960	31.1	41.3	20.8
-950	30.8	41.6	20.0
-940	30.6	41.8	19.3

-930	30.3	42.1	18.5
-920	30.0	42.2	17.8
-910	29.7	42.4	17.1
-900	29.4	42.5	16.4
-890	29.2	42.6	15.7
-880	28.9	42.7	15.0
-870	28.6	42.8	14.4
-860	28.3	42.8	13.8
-850	28.0	42.8	13.2
-840	27.7	42.9	12.6
-830	27.5	42.9	12.0
-820	27.2	42.9	11.5
-810	26.9	42.9	11.0
-800	26.7	42.9	10.5
-790	26.5	43.0	10.0
-780	26.3	43.0	9.5
-770	26.1	43.0	9.1
-760	25.9	43.1	8.7
-750	25.7	43.1	8.3
-740	25.6	43.2	8.0
-730	25.5	43.3	7.7
-720	25.4	43.4	7.4
-710	25.3	43.5	7.1
-700	25.3	43.6	6.9
-690	25.3	43.8	6.8
-680	25.3	43.9	6.6
-670	25.3	44.1	6.6
-660	25.4	44.4	6.5
-650	25.6	44.6	6.5
-640	25.7	44.9	6.6
-630	25.9	45.1	6.7
-620	26.2	45.4	6.9
-610	26.5	45.8	7.1
-600	26.8	46.1	7.4
-590	27.2	46.5	7.8
-580	27.6	46.9	8.3
-570	28.0	47.3	8.8
-560	28.6	47.8	9.4
-550	29.1	48.2	10.0
-540	29.8	48.7	10.8
-530	30.4	49.3	11.6
-520	31.2	49.8	12.5
-510	32.0	50.4	13.6
-500	32.8	51.0	14.7
-490	33.7	51.6	15.9
-480	34.7	52.2	17.2
-470	35.7	52.9	18.6
-460	36.8	53.6	20.1
-450	38.0	54.3	21.7
-440	39.3	55.1	23.4
-430	40.6	55.9	25.2
-420	41.9	56.7	27.1
-410	43.4	57.6	29.2
-400	44.9	58.6	31.3
-390	46.5	59.6	33.5
-380	48.2	60.6	35.7
-370	49.9	61.7	38.0
-360	51.6	62.9	40.4
-350	53.3	64.0	42.7
-340	55.0	65.0	45.0
-330	56.6	66.0	47.2
-320	58.2	67.0	49.4
-310	59.6	67.9	51.3
-300	60.9	68.7	53.1
-290	62.1	69.4	54.7
-280	63.1	70.1	56.0
-270	63.9	70.8	57.0
-260	64.6	71.4	57.8
-250	65.2	72.0	58.3
-240	65.5	72.5	58.6
-230	65.8	72.9	58.6
-220	65.9	73.3	58.5
-210	65.9	73.5	58.2
-200	65.7	73.6	57.8
-190	65.5	73.6	57.3
-180	65.1	73.4	56.8
-170	64.6	73.1	56.1
-160	64.1	72.8	55.4
-150	63.5	72.3	54.6

-140	62.8	71.7	53.9
-130	62.0	71.0	53.0
-120	61.2	70.2	52.2
-110	60.4	69.4	51.3
-100	59.5	68.5	50.5
-90	58.5	67.5	49.6
-80	57.6	66.5	48.7
-70	56.6	65.5	47.8
-60	55.7	64.5	46.9
-50	54.7	63.5	46.0
-40	53.8	62.5	45.1
-30	52.9	61.6	44.2
-20	52.0	60.7	43.3
-10	51.1	59.8	42.4
0	50.3	59.1	41.5
10	49.5	58.4	40.6
20	48.8	57.8	39.7
30	48.0	57.3	38.8
40	47.4	56.9	37.9
50	46.7	56.5	37.0
60	46.2	56.2	36.1
70	45.6	56.0	35.3
80	45.1	55.8	34.5
90	44.7	55.6	33.7
100	44.2	55.4	33.1
110	43.9	55.3	32.4
120	43.6	55.2	31.9
130	43.3	55.1	31.5
140	43.0	54.9	31.1
150	42.9	54.8	30.9
160	42.8	54.7	30.8
170	42.7	54.5	30.8
180	42.7	54.4	31.0
190	42.8	54.3	31.3
200	42.9	54.1	31.7
210	43.2	54.0	32.3
220	43.5	53.9	33.0
230	43.9	53.8	33.9
240	44.4	53.8	34.9
250	44.9	53.8	36.0
260	45.6	53.9	37.3
270	46.3	54.1	38.5
280	47.1	54.3	39.9
290	47.9	54.5	41.2
300	48.7	54.8	42.6
310	49.5	55.0	43.9
320	50.2	55.2	45.1
330	50.8	55.4	46.2
340	51.2	55.4	47.1
350	51.5	55.3	47.8
360	51.6	55.1	48.1
370	51.5	54.8	48.2
380	51.1	54.5	47.8
390	50.5	54.0	47.0
400	49.7	53.5	46.0
410	48.8	52.8	44.7
420	47.6	51.9	43.3
430	46.3	50.8	41.8
440	45.0	49.5	40.4
450	43.5	48.2	38.9
460	42.1	46.7	37.5
470	40.8	45.3	36.3
480	39.4	43.8	35.1
490	38.2	42.4	34.0
500	37.1	41.2	33.0
510	36.0	40.0	32.1
520	35.1	38.9	31.3
530	34.3	37.9	30.6
540	33.5	37.1	29.9
550	32.9	36.4	29.3
560	32.3	35.9	28.8
570	31.9	35.4	28.3
580	31.5	35.0	27.9
590	31.1	34.7	27.5
600	30.8	34.4	27.2
610	30.6	34.2	26.9
620	30.4	34.1	26.7
630	30.2	33.9	26.5
640	30.1	33.8	26.3

650	29.9	33.7	26.2
660	29.8	33.6	26.1
670	29.8	33.5	26.1
680	29.7	33.3	26.1
690	29.7	33.1	26.3
700	29.7	32.9	26.5
710	29.7	32.7	26.8
720	29.8	32.5	27.1
730	29.9	32.4	27.5
740	30.1	32.4	27.8
750	30.3	32.5	28.1
760	30.6	32.8	28.3
770	30.9	33.3	28.5
780	31.3	33.9	28.6
790	31.7	34.6	28.8
800	32.2	35.3	29.0
810	32.7	36.1	29.2
820	33.2	36.9	29.6
830	33.8	37.6	30.0
840	34.4	38.4	30.4
850	35.0	39.1	30.9
860	35.6	39.7	31.5
870	36.2	40.4	32.0
880	36.8	41.0	32.6
890	37.4	41.5	33.2
900	37.9	42.0	33.8
910	38.4	42.5	34.3
920	38.9	43.0	34.9
930	39.4	43.4	35.4
940	39.9	43.9	35.9
950	40.4	44.4	36.4
960	40.8	44.8	36.8
970	41.3	45.4	37.2
980	41.7	45.9	37.6
990	42.2	46.5	37.9
1000	42.7	47.1	38.2
1010	43.1	47.7	38.6
1020	43.6	48.4	38.9
1030	44.1	49.0	39.2
1040	44.6	49.8	39.4
1050	45.1	50.5	39.7
1060	45.6	51.3	39.9
1070	46.1	52.0	40.2
1080	46.6	52.8	40.4
1090	47.1	53.5	40.7
1100	47.6	54.2	40.9
1110	48.0	54.9	41.1
1120	48.5	55.6	41.4
1130	48.8	56.1	41.6
1140	49.2	56.6	41.7
1150	49.5	57.1	41.9
1160	49.7	57.5	42.0
1170	49.9	57.8	42.0
1180	50.0	58.1	42.0
1190	50.1	58.2	41.9
1200	50.1	58.3	41.8
1210	50.0	58.3	41.6
1220	49.8	58.1	41.4
1230	49.5	57.9	41.1
1240	49.1	57.5	40.8
1250	48.7	57.0	40.4
1260	48.2	56.4	40.0
1270	47.6	55.6	39.6
1280	46.9	54.8	39.1
1290	46.2	53.8	38.6
1300	45.5	52.8	38.2
1310	44.8	51.8	37.8
1320	44.1	50.7	37.4
1330	43.4	49.7	37.1
1340	42.8	48.6	36.9
1350	42.2	47.6	36.7
1360	41.7	46.7	36.6
1370	41.2	45.8	36.6
1380	40.8	45.0	36.5
1390	40.4	44.4	36.5
1400	40.2	43.9	36.4
1410	39.9	43.6	36.3
1420	39.8	43.5	36.1
1430	39.7	43.6	35.8

1440	39.7	43.8	35.6
1450	39.7	44.1	35.3
1460	39.8	44.6	35.0
1470	39.9	45.1	34.7
1480	40.1	45.7	34.5
1490	40.3	46.3	34.4
1500	40.6	46.9	34.3
1510	40.9	47.5	34.3
1520	41.2	48.1	34.3
1530	41.5	48.6	34.4
1540	41.9	49.2	34.6
1550	42.3	49.7	34.8
1560	42.6	50.2	35.1
1570	43.0	50.7	35.4
1580	43.4	51.2	35.7
1590	43.9	51.6	36.1
1600	44.3	52.0	36.5
1610	44.7	52.4	37.0
1620	45.1	52.8	37.4
1630	45.5	53.1	37.9
1640	45.9	53.4	38.4
1650	46.3	53.7	38.8
1660	46.6	53.9	39.3
1670	47.0	54.2	39.8
1680	47.3	54.3	40.3
1690	47.6	54.5	40.8
1700	47.9	54.6	41.3
1710	48.2	54.6	41.8
1720	48.4	54.6	42.3
1730	48.6	54.5	42.8
1740	48.8	54.3	43.3
1750	48.9	54.1	43.8
1760	49.0	53.7	44.3
1770	49.1	53.3	44.8
1780	49.1	52.9	45.3
1790	49.0	52.3	45.7
1800	48.9	51.7	46.1
1810	48.7	51.1	46.4
1820	48.5	50.4	46.6
1830	48.3	49.8	46.8
1840	48.0	49.2	46.9
1850	47.8	48.7	46.8
1860	47.5	48.3	46.7
1870	47.2	48.0	46.5
1880	47.0	47.7	46.3
1890	46.7	47.4	46.1
1900	46.5	47.0	45.9
1910	46.2	46.7	45.7
1920	45.9	46.3	45.5
1930	45.6	45.8	45.3
1940	45.2	45.4	45.0
1950	44.8	44.9	44.8
1960	44.4	44.5	44.4
1970	44.0	44.1	43.9
1980	43.6	43.7	43.4
1990	43.1	43.4	42.9
2000	42.4	42.7	42.2

Supplementary Table S6

Paleointensity data (represented in VADM formula) for the Northern American database located at a maximum distance of 2500 KM from Mexico City

Reference	Age (yr.AD)	Sigma (yr.AD)	VADM (10^{22} Am ²)	Sigma VADM (10^{22} Am ²)	Lat (°N)	Long (°W)	Material
1. Southern United States (Southern California, Arizona, Utah, New Mexico, and Texas)							
Bowles et al., 2002	800	150	12.1	0.5	32.76	114.72	Archeo
Bowles et al., 2002	1250	250	11.8	0.5	33.12	115.36	Archeo
Bowles et al., 2002	1750	250	11.5	0.3	32.26	115.79	Archeo
Bowles et al., 2002	1750	250	12.0	0.6	33.02	116.28	Archeo
Sternberg, 1989	-150	150	7.5	0.6	33.19	111.92	Archeo
Sternberg, 1989	-150	150	16.7	0.5	33.19	111.92	Archeo
Sternberg, 1989	100	100	9.4	0.8	33.19	111.92	Archeo
Sternberg, 1989	275	75	8.7	0.0	33.19	111.92	Archeo
Sternberg, 1989	275	75	9.0	0.8	33.19	111.92	Archeo
Sternberg, 1989	450	100	8.4	0.1	33.19	111.92	Archeo
Sternberg, 1989	450	100	12.4	0.6	33.19	111.92	Archeo
Sternberg, 1989	450	100	7.2	0.3	33.19	111.92	Archeo
Sternberg, 1989	575	75	9.5	0.5	33.19	111.92	Archeo
Sternberg, 1989	625	75	8.1	0.2	33.19	111.92	Archeo
Sternberg, 1989	750	100	8.6	0.7	33.19	111.92	Archeo
Sternberg, 1989	800	100	8.7	0.6	33.19	111.92	Archeo
Sternberg, 1989	800	100	9.3	0.2	33.19	111.92	Archeo
Sternberg, 1989	850	100	9.1	0.1	33.19	111.92	Archeo
Sternberg, 1989	1000	100	10.8	0.0	33.19	111.92	Archeo
Sternberg, 1989	1000	100	11.7	0.6	33.19	111.92	Archeo
Sternberg, 1989	1175	75	10.2	0.2	32.06	110.99	Archeo
Sternberg, 1989	1250	150	9.6	0.9	33.47	112.11	Archeo
Sternberg, 1989	1750	50	11.0	0.3	35.83	110.4	Archeo
Sternberg, 1989	1865	15	10.3	0.5	35.83	110.4	Archeo
Sternberg, 1989	1892	10	10.8	0.1	32.6	112.04	Archeo
Sternberg, 1989	1892	7	11.4	0.5	35.83	110.4	Archeo
Sternberg, 1989	1927	27	9.2	0.4	35.83	110.4	Archeo
Sternberg, 1989	1956	0	6.8	0.3	32.36	112.5	Archeo
Champion, 1980	1064	0	12.4	1.6	35.38	111.52	Volcanic
Sternberg, 1989	1242	42	10.4	0.5	37.17	108.54	Archeo
Sternberg, 1989	1499	20	13.6	0.1	35.64	106.33	Archeo
Sternberg, 1989	1572	52	14.6	0.6	35.64	106.33	Archeo
Sternberg, 1989	1767	4	16.6	0.2	35.06	106.46	Archeo
Sternberg, 1989	1930	20	10.2	0.1	35.5	106.71	Archeo
Sternberg, 1989	1930	20	8.6	0.4	35.5	106.71	Archeo
Sternberg, 1989	1977	0	9.9	0.9	27.75	107.63	Archeo
Champion, 1980	1300	280	10.4	0.3	38.93	112.51	Volcanic
2. Guatemala							
Alva-Valdivia et al., 2010	-800	100	3.6	0.7	14.61	269.47	Archeo
Alva-Valdivia et al., 2010	-400	100	10.3	0.9	14.61	269.47	Archeo
Alva-Valdivia et al., 2010	-200	100	5.2	0.6	14.61	269.47	Archeo
Alva-Valdivia et al., 2010	-200	100	6.7	0.6	14.61	269.47	Archeo
Alva-Valdivia et al., 2010	-100	100	4.7	0.9	14.61	269.47	Archeo
Alva-Valdivia et al., 2010	-100	100	9.8	1.1	14.61	269.47	Archeo

Supplementary Table S6 References

L.M. Alva-Valdivia, J. Morales, A. Goguitchaivili, M. Popenoe de Hatch, F. Hernandez-Bernal Absolute geomagnetic intensity data from preclassic Guatemalan pottery. *Phys. Earth Planet. Inter.*, 180 (1–2) (2010), pp. 41-51

Bowles, J, J. Gee, J. Hildebrand, and L. Tauxe (2002): Archeomagnetic intensity results from California and Ecuador: Evaluation of regional data. *Earth Planet. Sci. Lett.*, 203, 967–981.

Sternberg, R. S. (1989), Archeomagnetic paleointensity in the American Southwest during the past 2000 years, *Phys. Earth Planet. Inter.*, 56, 1–17.

Champion, D. E. (1980), Holocene geomagnetic secular variation in the western United States: Implications for the global geomagnetic field, U.S. Geophys. Res. Open File Rep., OF 80-824.

Supplementary Table S7

Global archeointensity Database:

for the purpose of comparison, we have recalled the global AI datasets including

- 1) Eastern Asia (China, Japan and South Korea),
- 2) The Levant (Syria, Jordan, Israel, Egypt, Cyprus, and South Turkey),
- 3) The Iberian Peninsula and the Azores islands,
- 4) The Northern American database (*See supplementary Table S6*)
- 5) The Canary Islands and the Western Africa,
- 6) The Hawaii Islands.

For Eastern Asia, we only use recently published data (Cai et al., 2014; 2016; Yu, 2012; Hong et al., 2013) providing a number of 115 PIs. In the Levant we use the Geomagia (Brown et al., 2015) database for compiling the intensity database for latitudes between 30 and 40 °N and longitudes between 25 and 40 °E. Also listed the recent works of Shaar et al. (2016), Ben-Yosef et al. (2017), and Ertepinar et al. (2012), summing up to a total of 156 data. Kissel et al. (2015) provided new PIs retrieved from lavas located on Canary Islands, and they also compiled previous data from W-Africa including Senegal and Mali. Recently published additional data from Canary Islands (de Groot et al., 2015) was also included, and in total 68 data points were obtained. For Iberia and Azores, we also used the Kissel et al. (2015) compilation together with the recent study of Gómez-Paccard et al (2016) on Murcia and 141 data are available. Tema et al. (2017) constructed Bayesian Holocene full vector SV curves for Hawaii based solely on lava flow studies, from which 59 PI data points are available. All of these global data were from lava rocks or archaeological artifacts with at least two specimens and a mean-PI with a $SD \leq 10 \mu T$ or $\leq 5 \mu T$, respectively.

Below is a list of the global AI datasets:

1. Eastern Asia: 30-40 °N; 100-140°E

<u>Reference</u>	<u>Age[yr.AD]</u>	<u>Sigma-ve[yr.]</u>	<u>VADM (10^{22} Am^2)</u>	<u>Sigma VADM (10^{22} Am^2)</u>	<u>Lat (°N)</u>	<u>Lon (°W)</u>
Cai et al., 2017	-1328	28	7.1	0.3	36.71	117.11
Cai et al., 2017	-1256	44	8.6	0.7	36.71	117.11
Cai et al., 2017	-1182	30	10.2	0.5	36.71	117.11
Cai et al., 2017	-99	107	7.5	0.3	36.01	120.15
Cai et al., 2017	-99	107	7.6	0.7	36.01	120.15
Cai et al., 2017	-99	107	4.8	0.5	37.63	117.10
Cai et al., 2017	-99	107	4.6	0.8	37.63	117.10
Cai et al., 2017	1506	138	8.9	0.3	36.78	115.78
Cai et al., 2017	1320	49	9.7	0.1	41.33	117.74
Cai et al., 2017	1320	49	9.1	0.1	41.33	117.74
Cai et al., 2017	1320	49	9.8	0.1	41.33	117.74
Cai et al., 2017	691	73	11.0	0.4	30.63	120.07
Cai et al., 2017	-348	127	11.4	0.2	30.61	121.02
Cai et al., 2017	-513	37	8.3	0.2	30.63	120.01
Cai et al., 2017	-1300	300	9.3	0.0	30.72	120.05
Cai et al., 2017	-1300	300	16.6	0.6	30.72	120.05
Cai et al., 2014	-550	74	9.2	0.3	30.62	120.02
Cai et al., 2014	-550	74	8.0	0.3	30.62	120.02
Cai et al., 2014	-550	74	10.1	0.6	30.62	120.02

Cai et al., 2014	123	98	11.4	1.1	30.51	120.00
Cai et al., 2014	691	73	8.1	0.2	30.63	120.07
Cai et al., 2014	691	73	8.1	0.1	30.63	120.07
Cai et al., 2014	453	136	11.7	0.4	30.36	120.02
Cai et al., 2014	453	136	11.9	0.6	30.36	120.02
Cai et al., 2014	-697	74	11.7	0.8	30.59	120.01
Cai et al., 2014	-348	127	6.8	0.1	30.62	120.02
Cai et al., 2014	-348	127	7.3	0.1	30.62	120.02
Cai et al., 2014	-348	127	8.3	0.3	30.62	120.02
Cai et al., 2014	-348	127	8.6	0.2	30.62	120.02
Cai et al., 2014	-348	127	7.8	0.5	30.62	120.02
Cai et al., 2014	-348	127	9.6	0.6	30.62	120.02
Cai et al., 2014	-348	127	9.3	0.7	30.62	120.02
Cai et al., 2014	-348	127	8.1	0.4	30.62	120.02
Cai et al., 2014	-348	127	9.1	0.3	30.62	120.02
Cai et al., 2014	-348	127	8.9	0.1	30.62	120.02
Cai et al., 2014	-348	127	9.3	0.1	30.62	120.02
Cai et al., 2014	-348	127	7.9	0.1	30.62	120.02
Cai et al., 2014	-348	127	10.1	0.2	30.62	120.02
Cai et al., 2014	-348	127	9.6	0.7	30.62	120.02
Cai et al., 2014	-348	127	8.9	0.3	30.62	120.02
Cai et al., 2014	-348	127	7.6	0.1	30.62	120.02
Cai et al., 2014	-348	127	9.4	0.3	30.62	120.02
Cai et al., 2014	-348	127	9.9	0.3	30.62	120.02
Cai et al., 2014	-348	127	10.4	0.2	30.62	120.02
Cai et al., 2014	-348	127	9.7	0.5	30.62	120.02
Cai et al., 2014	-348	127	9.7	0.5	30.62	120.02
Cai et al., 2014	-348	127	8.8	0.3	30.62	120.02
Cai et al., 2014	-348	127	9.1	0.4	30.62	120.02
Cai et al., 2014	-513	37	9.2	0.3	30.63	120.01
Cai et al., 2014	-513	37	9.8	0.6	30.63	120.01
Cai et al., 2014	-513	37	9.3	0.4	30.63	120.01
Cai et al., 2014	-513	37	8.8	0.3	30.63	120.01
Cai et al., 2014	-513	37	9.2	0.6	30.63	120.01
Cai et al., 2014	-513	37	8.5	0.6	30.63	120.01
Cai et al., 2014	-513	37	9.0	0.1	30.63	120.01
Cai et al., 2014	-513	37	9.8	0.3	30.63	120.01
Cai et al., 2014	-513	37	10.8	1.0	30.63	120.01
Cai et al., 2014	-513	37	11.2	0.3	30.63	120.01
Cai et al., 2014	-1300	300	11.7	0.3	30.72	120.05
Cai et al., 2014	-1300	300	12.9	0.9	30.72	120.05
Cai et al., 2014	-1300	300	11.0	0.8	30.72	120.05
Cai et al., 2014	-1300	300	12.9	0.8	30.72	120.05
Cai et al., 2014	-1300	300	10.3	0.3	30.72	120.05
Cai et al., 2014	-1300	300	12.3	0.6	30.72	120.05
Cai et al., 2014	-1300	300	11.8	0.7	30.72	120.05
Cai et al., 2014	-1300	300	12.6	1.0	30.72	120.05
Cai et al., 2014	-1300	300	10.6	0.4	30.72	120.05
Cai et al., 2014	-1300	300	11.1	0.9	30.72	120.05
Cai et al., 2014	-1300	300	9.8	0.6	30.72	120.05
Cai et al., 2014	-1300	300	12.5	0.4	30.72	120.05
Cai et al., 2014	-1300	300	10.2	0.6	30.72	120.05

Cai et al., 2014	-1300	300	11.9	1.2	30.72	120.05
Cai et al., 2014	-1300	300	10.5	0.3	30.72	120.05
Cai et al., 2014	-1300	300	10.5	0.8	30.72	120.05
Cai et al., 2014	-1300	300	11.5	0.2	30.72	120.05
Cai et al., 2014	-1300	300	11.6	0.7	30.72	120.05
Cai et al., 2014	1320	49	9.8	0.4	38.80	114.70
Cai et al., 2014	1085	42	10.3	0.4	38.80	114.70
Cai et al., 2014	835	72	10.2	0.5	38.80	114.70
Cai et al., 2014	835	72	11.3	0.5	38.80	114.70
Cai et al., 2014	1085	42	7.6	0.3	38.80	114.70
Cai et al., 2014	1002	42	10.0	0.3	38.80	114.70
Cai et al., 2014	1175	60	9.1	0.1	38.80	114.70
Cai et al., 2014	1175	60	9.2	0.3	38.80	114.70
Cai et al., 2014	1175	60	8.6	0.1	38.80	114.70
Cai et al., 2014	1175	60	8.2	0.4	38.80	114.70
Cai et al., 2014	1085	42	9.7	0.3	38.80	114.70
Cai et al., 2014	1139	96	9.3	0.2	38.80	114.70
Cai et al., 2014	1320	49	8.2	0.7	38.80	114.70
Cai et al., 2014	1085	42	9.0	0.3	38.80	114.70
Yu, 2012	-700	100	7.9	0.3	32.99	131.08
Yu, 2012	765	5	12.4	0.5	31.58	130.69
Yu, 2012	1235	5	10.4	0.5	31.88	130.90
Yu, 2012	1768	5	9.5	0.4	31.95	130.85
Yu, 2012	1779	5	9.3	0.5	31.55	130.66
Hong et al., 2013	-1185	195	11.4	0.6	36.30	126.85
Hong et al., 2013	-1175	45	12.7	0.5	36.65	126.56
Hong et al., 2013	-1160	160	12.8	0.7	36.80	127.15
Hong et al., 2013	-1150	140	9.5	0.6	36.82	127.06
Hong et al., 2013	-745	115	8.2	0.6	36.05	126.68
Hong et al., 2013	-645	125	8.1	0.5	36.02	126.74
Hong et al., 2013	-550	80	9.2	0.9	36.09	126.69
Hong et al., 2013	-520	80	9.4	0.7	35.19	126.84
Hong et al., 2013	-430	90	10.0	0.8	36.10	126.69
Hong et al., 2013	-180	120	10.3	0.8	37.22	127.09
Hong et al., 2013	225	95	10.1	0.7	36.80	127.06
Hong et al., 2013	275	105	10.3	0.6	37.20	127.10
Hong et al., 2013	285	105	10.5	0.6	36.62	127.84
Hong et al., 2013	690	60	8.5	0.5	35.88	128.49
Hong et al., 2013	880	80	9.3	0.7	36.34	127.34
Hong et al., 2013	1035	125	10.5	0.5	36.78	127.13
Hong et al., 2013	1085	95	10.7	0.7	37.15	126.92
Hong et al., 2013	1470	100	8.7	0.6	37.17	127.09
Hong et al., 2013	1610	70	7.5	0.7	36.25	128.30
Hong et al., 2013	1725	25	9.0	0.6	36.06	126.69
2. The Levant: 30-40 °N; 25-40°E						
Liritzis and Thomas, 1980	-1353	27	9.89	0.88	35.10	26.26
Aitken, 1984	-1025	25	12.94	0.72	34.70	32.59
Ben-Yosef et al., 2009	-899	83	14.16	0.89	30.68	35.44
Ben-Yosef et al., 2009	-899	83	14.57	0.45	30.68	35.44
Ben-Yosef et al., 2009	-899	83	12.17	0.87	30.68	35.44
Ben-Yosef et al., 2009	-899	83	11.57	0.25	30.68	35.44
Ben-Yosef et al., 2009	-899	83	11.04	0.83	30.68	35.44

Ben-Yosef et al., 2009	-899	83	14.22	0.54	30.68	35.44
Ben-Yosef et al., 2009	-899	83	13.02	0.87	30.68	35.44
Nachasova et al., 2007	-525	25	13.77	0.18	38.80	29.80
Nachasova et al., 2007	-520	30	15.54	0.51	38.80	29.80
Nachasova et al., 2007	-513	13	14.61	0.14	38.80	29.80
Nachasova et al., 2007	-500	10	14.72	0.49	38.80	29.80
Nachasova et al., 2007	-487	13	14.86	0.32	38.80	29.80
Nachasova et al., 2007	-482	8	13.72	0.53	38.80	29.80
Nachasova et al., 2007	-450	50	15.31	0.07	38.80	29.80
Nachasova et al., 2007	-450	50	12.77	0.28	38.80	29.80
Nachasova et al., 2007	-425	25	13.6	0.18	38.80	29.80
Nachasova et al., 2007	-400	10	12.55	0.42	38.80	29.80
Nachasova et al., 2007	-350	50	12.37	0.39	38.80	29.80
Nachasova et al., 2007	-350	50	12.97	0.72	38.80	29.80
Nachasova et al., 2007	-300	100	13.51	0.26	38.80	29.80
Nachasova et al., 2007	-265	10	12.41	0.44	38.80	29.80
Nachasova et al., 2007	-250	100	11.6	0.3	38.80	29.80
Nachasova et al., 2008	-215	5	11.32	0.12	38.80	29.80
Nachasova et al., 2007	-150	50	11.2	0.19	38.80	29.80
Nachasova et al., 2007	-120	30	10.65	0.21	38.80	29.80
Nachasova et al., 2007	-100	100	11.42	0.3	38.80	29.80
Nachasova et al., 2007	-100	100	10.81	0.18	38.80	29.80
Nachasova et al., 2007	-63	5	10.9	0.11	38.80	29.80
Nachasova et al., 2007	-50	50	11.37	0.3	38.80	29.80
Nachasova et al., 2007	-40	60	10.27	0.11	38.80	29.80
Nachasova et al., 2007	-25	25	10.2	0.39	38.80	29.80
Nachasova et al., 2007	0	25	10.15	0.75	38.80	29.80
De Marco et al., 2008	0	100	10.3	0.89	37.08	25.15
Nachasova et al., 2007	0	100	11.39	0.05	38.80	29.80
Nachasova et al., 2007	40	35	10.39	0.25	38.80	29.80
Nachasova et al., 2007	100	10	11.14	0.18	38.80	29.80
Nachasova et al., 2007	162	38	10.57	0.07	38.80	29.80
Genevey et al., 2003	450	50	10.44	0.47	32.70	36.60
Ben-Yosef et al., 2008	1250	50	8.26	0.29	30.68	35.45
Hussain, 1987	1795	50	8.41	0.84	30.00	31.00
Aitken, 1988	1950	30	8.09	0.42	35.20	25.10
Odah et al., 1995	1990		7.62	0.07	30.60	31.20
Spasov et al., 2010	726	10	8.69	1.35	36.40	25.38
Spasov et al., 2010	726	10	8.71	0.49	36.40	25.38
Spasov et al., 2010	1570	5	5.09	1.14	36.40	25.38
Spasov et al., 2010	1570	5	7.92	0.5	36.40	25.38
Spasov et al., 2010	1707	5	8.1	1.05	36.40	25.38
Spasov et al., 2010	1707	5	7.65	0.29	36.40	25.38
Spasov et al., 2010	1925	1	8.35	1.82	36.40	25.38
Spasov et al., 2010	1925	1	7.5	1.51	36.40	25.38
Spasov et al., 2010	1940	1	5.63	0.29	36.40	25.38
Spasov et al., 2010	1940	1	7.77	0.29	36.40	25.38
Spasov et al., 2010	1941	1	7.74	0.5	36.40	25.38
Spasov et al., 2010	1941	1	7.3	0.4	36.40	25.38
Spasov et al., 2010	1941	1	6.76	0.25	36.40	25.38
Spasov et al., 2010	1950	1	5.77	1.68	36.40	25.38
Spasov et al., 2010	1950	1	6.4	0.25	36.40	25.38

Shaar et al., 2016	-1550	100	9.4	0.0	33.02	35.57
Shaar et al., 2016	-1550	100	9.2	0.3	33.02	35.57
Shaar et al., 2016	-1450	50	9.4	0.1	32.59	35.18
Shaar et al., 2016	-1450	50	9.5	0.5	32.59	35.18
Shaar et al., 2016	-1450	50	9.9	0.4	32.59	35.18
Shaar et al., 2016	-1350	50	9.9	0.8	32.59	35.18
Shaar et al., 2016	-1250	50	11.3	0.3	32.59	35.18
Shaar et al., 2016	-1250	50	10.4	0.2	32.59	35.18
Shaar et al., 2016	-1250	50	11.3	0.1	32.59	35.18
Shaar et al., 2016	-1250	50	10.7	0.0	32.59	35.18
Shaar et al., 2016	-1250	50	11.1	0.1	33.02	35.57
Shaar et al., 2016	-1250	50	11.2	0.7	33.02	35.57
Shaar et al., 2016	-1250	50	11.9	0.1	33.02	35.57
Shaar et al., 2016	-1250	50	10.5	0.2	33.02	35.57
Shaar et al., 2016	-1130	25	12.6	0.2	32.59	35.18
Shaar et al., 2016	-1130	25	11.8	0.6	32.59	35.18
Shaar et al., 2016	-1130	25	11.8	0.5	32.59	35.18
Shaar et al., 2016	-1130	25	11.5	0.1	32.59	35.18
Shaar et al., 2016	-1125	25	11.5	0.1	32.59	35.18
Shaar et al., 2016	-1050	50	12.9	0.0	33.02	35.57
Shaar et al., 2016	-1050	50	11.5	0.0	33.02	35.57
Shaar et al., 2016	-1050	50	11.2	0.6	33.02	35.57
Shaar et al., 2016	-1000	50	12.6	0.1	32.59	35.18
Shaar et al., 2016	-1000	50	13.9	0.0	32.59	35.18
Shaar et al., 2016	-1000	50	15.7	0.0	32.59	35.18
Shaar et al., 2016	-1000	50	15.8	0.1	32.59	35.18
Shaar et al., 2016	-1000	50	12.7	0.5	32.59	35.18
Shaar et al., 2016	-950	50	12.5	0.3	33.02	35.57
Shaar et al., 2016	-950	50	14.5	0.0	33.02	35.57
Shaar et al., 2016	-950	50	12.2	0.5	33.02	35.57
Shaar et al., 2016	-950	50	12.4	0.2	33.02	35.57
Shaar et al., 2016	-900	50	14.1	0.5	32.59	35.18
Shaar et al., 2016	-900	50	12.8	0.5	32.59	35.18
Shaar et al., 2016	-900	50	13.0	0.1	32.59	35.18
Shaar et al., 2016	-900	50	12.1	0.2	32.59	35.18
Shaar et al., 2016	-850	50	12.1	0.0	33.02	35.57
Shaar et al., 2016	-850	50	13.6	0.1	33.02	35.57
Shaar et al., 2016	-850	50	10.7	0.6	33.02	35.57
Shaar et al., 2016	-850	50	12.9	0.5	33.02	35.57
Shaar et al., 2016	-850	50	14.3	0.3	33.02	35.57
Shaar et al., 2016	-740	34	16.6	0.1	33.02	35.57
Shaar et al., 2016	-740	34	14.2	0.9	33.02	35.57
Shaar et al., 2016	-740	34	15.6	0.1	33.02	35.57
Shaar et al., 2016	-740	34	12.7	0.1	33.02	35.57
Shaar et al., 2016	-740	34	15.3	0.4	33.02	35.57
Shaar et al., 2016	-740	34	13.8	0.3	33.02	35.57
Shaar et al., 2016	-740	34	12.8	0.6	33.02	35.57
Shaar et al., 2016	-740	34	13.3	0.1	33.02	35.57
Shaar et al., 2016	-740	34	14.6	0.0	33.02	35.57
Shaar et al., 2016	-740	34	14.2	0.5	33.02	35.57
Shaar et al., 2016	-740	34	15.2	0.5	33.02	35.57
Shaar et al., 2016	-740	34	17.7	0.9	33.02	35.57

Shaar et al., 2016	-740	34	14.4	0.6	33.02	35.57
Shaar et al., 2016	-740	34	15.1	0.2	33.02	35.57
Shaar et al., 2016	-740	34	17.0	0.1	33.02	35.57
Gallet et al., 2014	-1600	25	9.3	0.4	35.7	36.7
Gallet et al., 2014	-1600	25	8.7	0.5	35.7	36.7
Gallet et al., 2014	-1475	75	10.7	0.4	35.7	36.7
Gallet and Le-Golf, 2006	-1250	50	10.4	0.7	35.8	40.9
Gallet et al., 2006	-1150	50	10.9	0.7	34.9	40.6
Gallet et al., 2006	-725	25	13.1	0.5	35	40.6
Gallet and Le-Golf, 2006	-725	25	13.5	0.5	35	40.6
Gallet and Le-Golf, 2006	-650	50	13.7	0.4	35	40.6
Gallet and Le-Golf, 2006	-575	25	12.7	0.2	35.8	40.9
Genevey et al., 2003	-225	75	10.6	0.5	34.8	40.8
Genevey et al., 2003	220	15	8.7	0.4	34.8	40.8
Genevey et al., 2003	450	50	10.4	0.5	32.7	36.6
Genevey et al., 2003	712	37	10.3	0.5	35.2	40.3
Genevey et al., 2003	837	62	11.4	0.4	35.2	40.3
Genevey et al., 2003	1137	37	9.2	0.6	35.2	40.3
Ertipinar et al., 2012	-1050	150	17.7	1.2	38.38	38.36
Ben Yousef et al., 2017	-716.5	15.5	11.8	0.9	31.68	34.98
Ben Yousef et al., 2017	-716.5	15.5	16.1	0.6	31.68	34.98
Ben Yousef et al., 2017	-716.5	15.5	14.9	0.5	31.68	34.98
Ben Yousef et al., 2017	-716.5	15.5	13.7	0.5	31.68	34.98
Ben Yousef et al., 2017	-675.5	25.5	12.3	0.0	31.68	34.98
Ben Yousef et al., 2017	-675.5	25.5	13.7	0.3	31.68	34.98
Ben Yousef et al., 2017	-675.5	25.5	15.0	0.2	31.68	34.98
Ben Yousef et al., 2017	-702.5	1.5	14.7	0.2	31.68	34.98
Ben Yousef et al., 2017	-702.5	1.5	14.0	0.5	31.68	34.98
Ben Yousef et al., 2017	-702.5	1.5	13.0	0.6	31.68	34.98
Ben Yousef et al., 2017	-690	60	12.6	0.3	31.68	34.98
Ben Yousef et al., 2017	-608	22	13.8	0.0	31.68	34.98
Ben Yousef et al., 2017	-608	22	13.7	0.0	31.68	34.98
Ben Yousef et al., 2017	-553	33	13.0	0.2	31.68	34.98
Ben Yousef et al., 2017	-553	33	12.4	0.0	31.68	34.98
Ben Yousef et al., 2017	-553	33	12.3	0.2	31.68	34.98
Ben Yousef et al., 2017	-460	60	14.1	0.2	31.68	34.98
Ben Yousef et al., 2017	-460	60	13.9	0.3	31.68	34.98
Ben Yousef et al., 2017	-460	60	13.4	0.2	31.68	34.98
Ben Yousef et al., 2017	-460	60	12.6	0.5	31.68	34.98
Ben Yousef et al., 2017	-300	100	13.4	0.0	31.68	34.98
Ben Yousef et al., 2017	-300	100	12.8	0.0	31.68	34.98
Ben Yousef et al., 2017	-300	100	11.5	0.9	31.68	34.98
Ben Yousef et al., 2017	-150	10	10.7	0.0	31.68	34.98
Ben Yousef et al., 2017	-150	10	10.7	0.0	31.68	34.98
Ben Yousef et al., 2017	-150	10	9.7	0.6	31.68	34.98
3. Iberian Peninsula and the Azores islands: 30-40 °N; 30-2°W						
Burakov et al., 2005	-1263	--	7.5	0.4	39.00	-3.50
Burakov et al., 2005	-1288	--	7.8	0.4	39.00	-3.50
Burakov et al., 2005	-1308	--	8.7	0.4	39.00	-3.50
Burakov et al., 2005	-1322	--	6.7	0.6	39.00	-3.50
Burakov et al., 2005	-1339	--	8.0	0.1	39.00	-3.50
Burakov et al., 2005	-1355	--	8.5	0.1	39.00	-3.50

Burakov et al., 2005	-1375	--	8.7	0.3	39.00	-3.50
Burakov et al., 2005	-1395	--	7.7	0.1	39.00	-3.50
Burakov et al., 2005	-1415	--	8.6	0.4	39.00	-3.50
Burakov et al., 2005	-1435	--	9.1	0.6	39.00	-3.50
Burakov et al., 2005	-1517	--	8.9	0.2	39.00	-3.50
Burakov et al., 2005	-1536	--	8.5	0.2	39.00	-3.50
Burakov et al., 2005	-1555	--	8.7	0.0	39.00	-3.50
Burakov et al., 2005	-1572	--	9.1	0.2	39.00	-3.50
Burakov et al., 2005	-1589	--	7.5	0.2	39.00	-3.50
Burakov et al., 2005	1959	1	8.2	1.0	40.10	-5.70
Catanzariti et al., 2012	601	55	10.8	0.4	39.90	-4.00
Catanzariti et al., 2012	316	67	11.1	0.9	39.90	-4.00
Gómez-Paccard et al., 2006b	1150	50	9.6	0.9	38.00	-1.10
Gómez-Paccard et al., 2006b	1150	50	9.3	1.6	38.00	-1.10
Gómez-Paccard et al., 2006b	1150	50	9.0	0.6	38.00	-1.10
Gómez-Paccard et al., 2006b	1150	50	8.7	0.6	38.00	-1.10
Gómez-Paccard et al., 2006b	1150	50	8.9	1.1	38.00	-1.10
Gómez-Paccard et al., 2006b	1150	50	10.2	1.2	38.00	-1.10
Gómez-Paccard et al., 2006b	1150	50	9.6	1.0	38.00	-1.10
Gómez-Paccard et al., 2008	1959	0	8.4	1.1	40.10	-5.70
Gómez-Paccard et al., 2008	1287	12	10.2	0.5	39.00	-3.80
Gómez-Paccard et al., 2008	1287	12	9.5	0.7	39.00	-3.80
Gómez-Paccard et al., 2008	1287	12	9.7	1.2	39.00	-3.80
Gómez-Paccard et al., 2008	1410	10	8.5	0.5	39.00	-3.80
Gómez-Paccard et al., 2008	1050	50	10.3	1.9	38.00	-1.10
Gómez-Paccard et al., 2008	1835	10	8.0	0.5	40.60	-3.20
Gómez-Paccard et al., 2008	235	15	9.5	0.6	38.90	0.00
Gómez-Paccard et al., 2008	1525	75	9.1	0.9	39.50	-0.40
Gómez-Paccard et al., 2008	1475	25	8.9	0.9	39.50	-0.40
Gómez-Paccard et al., 2008	1587	62	8.8	0.7	39.50	-0.40
Gómez-Paccard et al., 2008	1520	91	9.1	0.7	39.50	-0.40
Gómez-Paccard et al., 2008	1294	56	8.4	0.5	39.50	-0.40
Gómez-Paccard et al., 2008	1319	81	8.8	0.4	39.50	-0.40
Gómez-Paccard et al., 2008	1375	75	9.0	0.7	39.50	-0.40
Gómez-Paccard et al., 2008	1375	75	8.2	0.8	39.50	-0.40
Gómez-Paccard et al., 2008	1600	25	9.6	0.8	39.50	-0.40
Gómez-Paccard et al., 2012b	850	25	12.7	1.3	38.50	-1.60
Gómez-Paccard et al., 2012b	782	12	13.3	1.1	38.50	-1.60
Gómez-Paccard et al., 2012b	775	25	12.0	1.0	38.50	-1.60
Nochasova et al., 2007b	-700	100	12.7	2.3	39.70	-2.00
Nochasova et al., 2007b	-500	100	12.9	2.2	39.70	-1.40
Nochasova et al., 2007b	-500	100	14.1	2.3	39.70	-1.40
Nochasova et al., 2007b	-300	100	12.9	0.9	39.70	-1.40
Nochasova et al., 2007b	-125	75	12.4	1.4	39.70	-2.00
Nochasova et al., 2007b	825	75	10.8	1.4	39.70	-1.40
Nochasova et al., 2007b	900	100	11.6	1.3	39.70	-1.40
Nochasova et al., 2007b	-670	20	16.8	1.1	39.50	-0.40
Nochasova et al., 2007b	-625	25	16.3	1.8	39.50	-0.40
Nochasova et al., 2007b	-590	10	14.5	2.4	39.50	-0.40
Nochasova et al., 2007b	-530	50	16.4	1.4	39.50	-0.40
Nochasova et al., 2007b	-390	90	16.2	1.0	39.50	-0.40
Nochasova et al., 2007b	-240	60	13.9	1.0	39.50	-0.40

Casas et al., 2008	1595	7	8.1	0.7	31.00	-8.00
Gómez-Paccard et al., 2012a	1350	60	8.5	0.8	34.30	-357.00
Kovacheva et al., 2009	50	50	10.8	0.9	34.10	-357.00
Kovacheva et al., 2009	450	50	10.1	0.8	34.10	-357.00
Kovacheva et al., 2009	200	50	10.3	1.0	35.50	-6.00
Kovacheva et al., 2009	-50	50	11.2	0.2	35.50	-325.00
Kovacheva et al., 2009	150	50	9.8	0.8	35.50	-325.00
Di Chiara et al., 2014	1563	0	6.8	0.8	37.80	-25.60
Di Chiara et al., 2014	1500	200	8.0	0.2	37.70	-25.60
Di Chiara et al., 2014	1300	0	9.4	0.7	37.80	-25.60
Di Chiara et al., 2014	1209	54	10.6	0.4	37.90	-25.60
Di Chiara et al., 2014	1073	90	9.5	1.1	37.80	-25.60
Di Chiara et al., 2014	1048	113	8.1	0.2	37.80	-25.60
Di Chiara et al., 2014	800	0	13.8	1.0	37.70	-25.60
Di Chiara et al., 2014	775	124	11.6	1.6	37.70	-25.60
Di Chiara et al., 2014	675	107	7.8	0.2	37.80	-25.60
Di Chiara et al., 2014	675	107	9.7	0.6	37.80	-25.60
Di Chiara et al., 2014	240	168	11.2	0.6	37.80	-15.50
Di Chiara et al., 2014	-593	236	16.4	2.1	37.80	-25.70
Di Chiara et al., 2014	-750	250	9.9	1.4	37.80	-25.60
Hartmann et al., 2009	1550	30	9.6	1.3	38.70	-9.10
Hartmann et al., 2009	1600	30	6.7	0.7	38.70	-9.10
Hartmann et al., 2009	1600	30	7.5	1.5	38.70	-9.10
Hartmann et al., 2009	1600	30	7.9	1.1	38.70	-9.10
Hartmann et al., 2009	1750	50	7.0	0.5	38.70	-9.10
Nochasove et al., 2009	-1170	--	9.9	0.1	38.40	-10.00
Nochasove et al., 2009	-1170	--	12.5	0.3	38.40	-10.00
Nochasove et al., 2009	-1190	--	9.0	0.3	38.40	-10.00
Nochasove et al., 2009	-1190	--	12.3	0.3	38.40	-10.00
Nochasove et al., 2009	-1120	--	12.0	0.6	38.50	-10.00
Nochasove et al., 2009	-1060	--	11.4	0.0	38.40	-10.00
Nochasove et al., 2009	-1060	--	10.7	0.1	38.40	-10.00
Nochasove et al., 2009	-1000	--	14.6	0.1	38.40	-10.00
Nochasove et al., 2009	-940	--	11.3	0.2	38.50	-10.00
Nochasove et al., 2009	-940	--	9.3	0.5	38.50	-10.00
Nochasove et al., 2009	-880	--	15.0	0.4	38.50	-10.00
Nochasove et al., 2009	-880	--	12.0	0.2	38.50	-10.00
Nochasove et al., 2009	-880	--	13.8	0.2	38.50	-10.00
Nochasove et al., 2009	-820	--	14.4	0.0	38.50	-10.00
Nochasove et al., 2009	-830	--	14.8	0.6	38.50	-10.00
Nochasove et al., 2009	-725	--	11.5	0.5	38.50	-10.00
Nochasove et al., 2009	-730	--	13.6	0.9	38.50	-10.00
Nochasove et al., 2009	-740	--	14.6	0.3	38.50	-10.00
Nochasove et al., 2009	-765	--	14.7	0.3	38.50	-10.00
Nochasove et al., 2009	-800	--	15.5	0.8	38.50	-10.00
Nochasove et al., 2009	-700	--	15.2	0.6	38.50	-10.00
Nochasove et al., 2009	-640	--	10.7	0.5	38.50	-10.00
Nochasove et al., 2009	-640	--	12.4	0.1	38.50	-10.00
Nochasove et al., 2009	-575	--	10.8	0.1	38.60	-10.00
Nochasove et al., 2009	-575	--	11.9	0.7	38.60	-10.00
Nochasove et al., 2009	-575	--	14.7	0.3	38.60	-10.00
Nochasove et al., 2009	-580	--	11.0	0.8	38.60	-10.00

Nochasove et al., 2009	-585	--	11.4	0.5	38.60	-10.00
Nochasove et al., 2009	-590	--	10.2	0.3	38.60	-10.00
Nochasove et al., 2009	-515	--	17.0	0.3	38.50	-10.00
Nochasove et al., 2009	-520	--	15.1	0.3	38.50	-10.00
Nochasove et al., 2009	-520	--	12.4	0.2	38.50	-10.00
Nochasove et al., 2009	-525	--	13.9	0.1	38.50	-10.00
Nochasove et al., 2009	-525	--	13.2	0.5	38.50	-10.00
Nochasove et al., 2009	-460	--	16.3	0.9	38.40	-10.00
Nochasove et al., 2009	-460	--	15.2	0.9	38.40	-10.00
Nochasove et al., 2009	-460	--	15.8	0.7	38.40	-10.00
Nochasove et al., 2009	-400	--	15.1	0.1	38.40	-10.00
Nochasove et al., 2009	-325	--	12.3	0.4	38.50	-10.00
Nochasove et al., 2009	-325	72.5	12.7	0.4	38.50	-10.00
Nochasove et al., 2009	-345	69	12.1	0.3	38.50	-10.00
Nochasove et al., 2009	-355	--	14.1	0.4	38.50	-10.00
Nochasove et al., 2009	-265	--	14.4	0.2	38.40	-10.00
Nochasove et al., 2009	-280	--	13.7	0.2	38.40	-10.00
Nochasove et al., 2009	-280	--	14.1	0.2	38.40	-10.00
Nochasove et al., 2009	-290	--	14.5	0.2	38.40	-10.00
Nochasove et al., 2009	-220	--	13.4	0.1	38.20	-10.00
Nochasove et al., 2009	-220	--	13.1	0.2	38.20	-10.00
Nochasove et al., 2009	-160	--	11.7	0.0	38.10	-10.00
Nochasove et al., 2009	-160	--	10.8	0.1	38.10	-10.00
Nochasove et al., 2009	-85	--	12.3	0.3	38.70	-10.00
Nochasove et al., 2009	-100	--	13.4	0.1	38.70	-10.00
Nochasove et al., 2009	-100	--	12.6	0.1	38.70	-10.00
Nochasove et al., 2009	-120	--	8.8	0.1	38.70	-10.00
Nochasove et al., 2009	70	--	11.3	0.2	38.80	-10.00
Nochasove et al., 2009	-20	--	10.7	0.0	38.80	-10.00
Nochasove et al., 2009	-60	--	11.4	0.3	38.80	-10.00
Nochasove et al., 2009	-170	--	10.9	0.1	38.80	-10.00
Gómez-Paccard et al., 2016	850	25	11.2	1.1	38.00	-1.13
Gómez-Paccard et al., 2016	875	25	11.1	1.0	38.00	-1.13
Gómez-Paccard et al., 2016	937.5	37.5	11.5	0.7	38.00	-1.13
Gómez-Paccard et al., 2016	937.5	37.5	10.3	0.9	38.00	-1.13
Gómez-Paccard et al., 2016	937.5	37.5	11.1	1.2	38.00	-1.13
Gómez-Paccard et al., 2016	937.5	37.5	11.0	0.6	38.00	-1.13
Gómez-Paccard et al., 2016	950	25	11.6	0.6	38.00	-1.13
Gómez-Paccard et al., 2016	987.5	37.5	10.1	1.0	38.00	-1.13
Gómez-Paccard et al., 2016	987.5	37.5	10.1	0.3	38.00	-1.13
Gómez-Paccard et al., 2016	1037.5	37.5	8.2	0.4	38.00	-1.13
Gómez-Paccard et al., 2016	1087.5	37.5	9.3	0.4	38.00	-1.13
4. the Canary Islands and the Western Africa: 14-30° N; 18-4° W						
Sherwood, 1991	1470	--	8.2	0.5	28.60	-16.00
Sherwood, 1991	1704	--	8.6	1.0	28.30	-16.00
Sherwood, 1991	1705	--	7.4	1.6	28.30	-16.00
Sherwood, 1991	1909	--	8.5	1.0	28.30	-16.00
Tulloch, 1992	1971	5	7.1	1.1	28.60	-17.90
Tulloch, 1992	1971	5	7.7	2.0	28.60	-17.90
Tulloch, 1992	1949	5	11.1	1.4	28.60	-17.90
Tulloch, 1992	1909	5	9.2	1.0	28.30	-16.60
Tulloch, 1992	1824	5	5.6	0.9	29.00	-13.60

Tulloch, 1992	1798	5	10.5	0.7	28.30	-16.60
Tulloch, 1992	1730	5	8.6	0.9	29.00	-13.60
Tulloch, 1992	1712	5	8.3	0.4	28.60	-17.90
Tulloch, 1992	1706	5	6.1	0.8	28.30	-16.60
Tulloch, 1992	1705	5	8.4	1.2	28.30	-16.60
Tulloch, 1992	1704	5	6.6	0.6	28.30	-16.60
Tulloch, 1992	1677	5	7.6	0.4	28.60	-17.90
Tulloch, 1992	1646	5	7.4	1.3	28.60	-17.90
Tulloch, 1992	1646	5	9.1	1.5	28.60	-17.90
Tulloch, 1992	1585	5	7.4	1.0	28.60	-17.90
Tulloch, 1992	1585	5	8.9	0.4	28.60	-17.90
Tulloch, 1992	1435	35	10.9	0.8	28.30	-16.60
De Groot et al., 2015	1706	0	7.9	0.1	28.27	-16.60
De Groot et al., 2015	1115	39	16.3	0.4	28.27	-16.60
De Groot et al., 2015	69.5	184.5	11.6	1.8	28.27	-16.60
De Groot et al., 2015	-64.5	320.5	12.0	0.3	28.27	-16.60
De Groot et al., 2015	-711.5	202.5	12.7	1.6	28.27	-16.60
De Groot et al., 2015	-711.5	202.5	12.8	1.5	28.27	-16.60
De Groot et al., 2015	-820	23	12.0	1.3	28.27	-16.60
De Groot et al., 2015	-1187	200	10.9	0.6	28.27	-16.60
De Groot et al., 2015	-1187	200	11.4	1.1	28.27	-16.60
De Groot et al., 2015	-1187	200	10.1	1.3	28.27	-16.60
Kissel et al., 2015	1706	0	10.0	0.8	28.36	-16.76
Kissel et al., 2015	1055	155	11.6	1.3	28.27	-16.73
Kissel et al., 2015	85	124	11.2	1.2	28.24	-16.72
Kissel et al., 2015	-25	148	8.9	1.2	28.38	-16.71
Kissel et al., 2015	-579	185	9.0	1.1	28.32	-16.68
Kissel et al., 2015	-667	250	10.7	1.3	28.31	-16.79
Kissel et al., 2015	38	85	4.3	0.7	28.04	-15.46
Kissel et al., 2015	10	70	5.3	0.9	27.95	-15.53
Kissel et al., 2015	-575	175	9.6	1.2	28.08	-15.58
Kissel et al., 2015	-580	168	14.2	1.2	28.05	-15.47
Kissel et al., 2015	-590	190	12.4	0.9	28.02	-15.43
Kissel et al., 2015	-590	190	16.0	1.6	28.02	-15.42
Kissel et al., 2015	-590	190	12.7	1.2	28.03	-15.42
Kissel et al., 2015	-590	190	14.2	1.0	28.03	-15.43
Kissel et al., 2015	-615	195	6.9	0.5	28.04	-15.42
Kissel et al., 2015	-920	120	11.9	0.8	28.08	-15.66
Kissel et al., 2015	-960	160	10.3	1.1	28.07	-15.65
Kissel et al., 2015	-1008	102	9.5	0.9	28.04	-15.62
Kissel et al., 2015	-1183	126	10.3	1.6	28.03	-15.62
Kissel et al., 2015	-1250	240	7.4	1.2	28.05	-15.64
Mitra et al., 2013	899	56	9.3	0.2	15.30	-5.40
Mitra et al., 2013	815	81	8.6	1.0	15.80	-13.30
Mitra et al., 2013	664	31	10.4	0.8	13.70	-4.50
Mitra et al., 2013	624	52	9.9	0.4	15.80	-13.30
Mitra et al., 2013	563	61	9.1	0.3	15.80	-13.30
Mitra et al., 2013	502	72	8.3	0.8	15.80	-13.30
Mitra et al., 2013	485	75	8.5	0.6	16.00	-13.60
Mitra et al., 2013	315	95	8.2	0.3	16.00	-13.60
Mitra et al., 2013	271	58	8.4	0.3	15.30	-5.50
Mitra et al., 2013	221	70	8.4	0.4	16.00	-13.60

Mitra et al., 2013	125	48	10.0	0.1	13.70	-4.50
Mitra et al., 2013	124	73	9.1	0.7	16.00	-13.60
Mitra et al., 2013	27	47	9.6	0.6	13.70	-4.50
Mitra et al., 2013	-628	92	9.4	0.5	16.50	-14.30
Mitra et al., 2013	-662	72	9.6	0.3	15.40	-5.50
Mitra et al., 2013	-812	12	9.4	0.2	15.40	-5.50
Mitra et al., 2013	-865	25	10.0	0.5	15.40	-5.50
5.Mexico: 19° N; 155-160° W						
Duran et al., 2010	-1191	215	8.89	0.67	19.95	-102.30
Duran et al., 2010	-1191	215	8.42	0.56	19.95	-102.30
Duran et al., 2010	-1191	215	7.19	0.22	19.95	-102.30
Duran et al., 2010	-1191	215	7.87	0.36	19.95	-102.30
Duran et al., 2010	-1191	215	7.86	1.78	19.95	-102.30
Duran et al., 2010	-1191	215	7.47	0.38	19.95	-102.30
Duran et al., 2010	-1191	215	7.76	0.40	19.95	-102.30
Duran et al., 2010	-1191	215	7.47	1.07	19.95	-102.30
Duran et al., 2010	-1191	215	5.53	0.51	19.95	-102.30
Duran et al., 2010	-1191	215	8.72	0.31	19.95	-102.30
Duran et al., 2010	-1191	215	7.34	0.67	19.95	-102.30
Morales et al., 2006	373	56	13.39	0.79	19.30	-99.20
Morales et al., 2001	373	56	12.12	1.47	19.93	-99.18
Alva-Valdivia et al., 2005	373	56	13.46	1.73	19.30	-99.18
Böhnel et al., 1997	373	56	14.21	0.61	19.08	-99.13
Böhnel et al., 2003	373	56	12.06	0.94	19.08	-99.13
Fanjat et al., 2011	450	50	6.83	0.21	17.48	-92.04
Fanjat et al., 2011	550	50	7.63	0.28	17.48	-92.04
Fanjat et al., 2011	650	50	7.16	0.25	17.48	-92.04
Fanjat et al., 2011	750	20	7.16	0.14	17.48	-92.04
Fanjat et al., 2011	810	40	7.44	0.16	17.48	-92.04
Gratton et al., 2006	1766	7	9.66	0.78	19.48	-102.25
Conte-Fasano et al., 2006	1766	7	10.87	1.29	19.00	-101.75
Gratton et al., 2006	1766	7	11.97	2.06	19.48	-102.25
Böhnel et al., 2016	1870	--	9.8	1.4	21.10	-104.58
Mahgoub et al., 2017a	1250	0	12.4	1.5	19.54	-101.99
Mahgoub et al., 2017b	-1496.5	64.5	9.3	1.6	19.86	-101.84
<i>This Study</i>	-240	160	15.90	0.90	19.69	-98.84
<i>This Study</i>	-240	160	12.30	0.70	19.69	-98.84
<i>This Study</i>	-240	160	13.20	1.00	19.69	-98.84
<i>This Study</i>	275	75	6.20	0.10	19.69	-98.84
<i>This Study</i>	330	90	7.70	0.50	19.69	-98.84
<i>This Study</i>	385	36	9.60	0.20	19.69	-98.84
<i>This Study</i>	385	35	11.10	0.30	19.69	-98.84
<i>This Study</i>	485	65	6.10	0.30	19.69	-98.84
<i>This Study</i>	750	150	7.40	0.70	19.69	-98.84
<i>This Study</i>	750	150	8.20	1.00	19.69	-98.84
<i>This Study</i>	750	50	8.30	1.00	19.69	-98.84
<i>This Study</i>	750	50	4.80	0.50	19.69	-98.84
<i>This Study</i>	750	50	9.10	0.80	19.69	-98.84
<i>This Study</i>	750	50	3.70	0.90	19.69	-98.84
<i>This Study</i>	750	50	6.40	0.20	19.69	-98.84
<i>This Study</i>	975	125	8.80	0.60	19.69	-98.84
<i>This Study</i>	975	125	11.30	0.30	19.69	-98.84

<i>This Study</i>	975	125	9.00	0.40	19.69	-98.84	
<i>This Study</i>	975	125	9.00	0.90	19.69	-98.84	
<i>This Study</i>	975	125	8.30	0.70	19.69	-98.84	
<i>This Study</i>	975	125	7.80	0.30	19.69	-98.84	
<i>This Study</i>	1400	100	8.80	0.50	19.69	-98.84	
<i>This Study</i>	1400	100	7.90	0.70	19.69	-98.84	
<i>This Study</i>	1400	100	7.70	0.50	19.69	-98.84	
<i>This Study</i>	1435	100	10.80	0.60	19.69	-98.84	
<i>This Study</i>	-1550	50	10.00	0.60	17.75	-94.76	
<i>This Study</i>	-1550	50	12.20	0.90	17.75	-94.76	
<i>This Study</i>	-1300	100	5.30	0.20	17.75	-94.76	
<i>This Study</i>	-1300	100	6.60	0.20	17.75	-94.76	
<i>This Study</i>	-1100	100	7.30	0.90	17.75	-94.76	
<i>This Study</i>	-1100	100	8.40	1.10	17.75	-94.76	
<i>This Study</i>	-1100	100	4.10	0.70	17.75	-94.76	
<i>This Study</i>	373	56	14.10	0.30	19.33	-99.19	
<i>This Study</i>	373	56	13.10	0.30	19.33	-99.19	
<i>This Study</i>	1800	0	11.30	0.70	20.59	-100.40	
<i>This Study</i>	1800	0	9.80	0.80	20.59	-100.40	
<i>This Study</i>	1800	0	10.30	0.60	20.59	-100.40	
<i>This Study</i>	-1216	87	11.80	1.70	19.65	-96.96	
<i>This Study</i>	-285	80	17.20	0.90	19.00	-98.48	
<i>This Study</i>	181	220	12.10	1.60	18.45	-95.10	
<i>This Study</i>	1070	60	12.30	1.10	19.40	-96.90	
<i>This Study</i>	1793	0	13.80	2.00	18.58	-95.19	
<i>This Study</i>	8	62	10.40	0.90	19.18	-99.31	
<i>This Study</i>	-380	23	7.4	1.1	19.61	-102.07	
6.Hawaii Islands: 19° N; 155-160° W							
De Groot et al., 2013	1990	--	7.5	0.7	19.37	-154.96	
Cromwell et al., 2015	1990	--	7.3	0.3	19.36	-154.97	
Chauvin et al., 2005	1982	--	8.1	0.4	19.50	-155.00	
Chauvin et al., 2005	1977	--	8.6	0.3	19.50	-155.00	
Chauvin et al., 2005	1972	--	7.6	0.8	19.50	-155.00	
De Groot et al., 2013	1960	--	8.3	0.4	19.51	-154.80	
Herrero-Bervera and Valet, 2009	1960	--	8.2	0.4	19.50	-155.00	
Hill and Shaw, 2000	1960	--	7.1	0.7	19.50	-155.00	
Cromwell et al., 2015	1960	--	8.1	0.7	19.52	-154.81	
Tanaka and Kono, 1991	1960	--	8.3	0.9	19.51	-155.84	
Hagstrum and Champion, 1995	1960	--	8.3	0.9	19.51	-154.84	
Tanaka et al., 1995	1960	--	9.2	1.0	19.50	-155.00	
Chauvin et al., 2005	1960	--	7.5	1.1	19.50	-155.00	
Herrero-Bervera and Valet, 2009	1955	--	7.7	0.3	19.50	-155.00	
Herrero-Bervera and Valet, 2009	1955	--	9.4	0.4	19.50	-155.00	
Shaw, 1974	1955	--	8.8	0.8	19.50	-155.00	
Chauvin et al., 2005	1955	--	8.3	0.9	19.40	-154.92	
De Groot et al., 2013	1950	--	8.3	0.2	19.27	-155.87	
Cromwell et al., 2015	1950	--	7.8	0.7	19.26	-155.87	
Chauvin et al., 2005	1950	--	8.8	1.0	19.50	-155.00	
De Groot et al., 2013	1935	--	7.7	0.4	19.63	-155.50	
Cromwell et al., 2015	1935	--	7.9	0.5	19.69	-155.46	
De Groot et al., 2013	1926	--	8.1	0.1	19.19	-155.90	
Shaw, 1974	1926	--	7.6	0.4	19.50	-155.00	

De Groot et al., 2013	1919	--	7.9	0.1	19.23	-155.90
Shaw, 1974	1907	--	6.9	0.7	19.50	-155.00
De Groot et al., 2013	1868	--	8.8	0.6	19.05	-155.70
Cromwell et al., 2015	1859	--	8.7	0.4	19.86	-155.91
De Groot et al., 2013	1855	--	8.2	0.2	19.58	-155.50
De Groot et al., 2013	1843	--	9.3	0.4	19.63	-155.50
Cromwell et al., 2015	1843	--	8.8	0.5	19.64	-155.51
Tanaka and Kono, 1991	1840	--	7.8	0.4	19.56	-154.88
Hagstrum and Champion, 1995	1840	--	7.8	0.4	19.56	-154.88
De Groot et al., 2013	1790	--	10.1	0.9	19.45	-154.80
Tanaka and Kono, 1991	1697	253	13.1	0.5	19.60	-155.02
Mankinen and Champion, 1993	1613	337	10.6	0.1	19.55	-155.30
De Groot et al., 2013	1570	380	8.8	1.1	19.35	-155.40
De Groot et al., 2013	1462	173	9.8	0.4	19.45	-154.50
Hagstrum and Champion, 1995	1449	182	13.0	0.6	19.43	-155.26
De Groot et al., 2013	1407	543	9.4	0.4	19.50	-155.10
De Groot et al., 2013	1311	121	11.0	0.4	19.23	-155.45
Tanaka and Kono, 1991	1159	139	11.1	1.0	19.46	-155.29
De Groot et al., 2013	1135	141	11.9	0.7	19.13	-155.55
Pressling et al., 2006	1088	76	13.8	0.7	19.42	-155.39
De Groot et al., 2013	1075	200	14.3	0.4	19.18	-155.55
Pressling et al., 2006	1064	343	14.3	0.9	19.33	-155.28
Pressling et al., 2006	990	215	8.4	0.6	19.39	-155.52
Pressling et al., 2006	836	150	10.7	1.0	19.30	-155.31
Pressling et al., 2006	700	163	9.2	0.9	19.67	-155.81
De Groot et al., 2013	742	145	9.5	0.8	19.56	-155.34
Pressling et al., 2006	720	173	11.5	1.1	19.19	-155.34
De Groot et al., 2013	545	125	9.9	0.6	19.63	-155.00
Mankinen and Champion, 1993	333	247	8.8	0.7	19.53	-155.35
De Groot et al., 2013	332	685	8.3	0.2	19.53	-155.80
Tanaka and Kono, 1991	241	294	13.9	0.8	19.19	-155.49
Pressling et al., 2006	-169	586	15.6	1.0	19.39	-155.78
Mankinen and Champion, 1993	-660	264	9.6	0.5	19.54	-155.34
Pressling et al., 2006	-949	547	17.0	1.0	19.45	-155.24

Table S7 References

Cai, S., Tauxe, L., Deng, C., Pan, Y., Jin, G., Zheng, J., et al. (2014). Geomagnetic intensity variations for the past 8 kyr: new archaeointensity results from eastern China. *Earth Planet. Sci. Lett.* 392, 217–229. doi: 10.1016/j.epsl.2014.02.030.

Cai, S. et al. Archaeointensity results spanning the past 6 kiloyears from eastern China and implications for extreme behaviors of the geomagnetic field. *Proc. Natl. Acad. Sci.* 114, 39–44, doi: 10.1073/pnas.1616976114 (2017).

Yu, Y., (2012) High-fidelity paleointensity determination from historic volcanoes in Japan. *J. Geophys. Res.* 117, B08101.

Hong, H., Yu, Y., Lee, C. H., Kim, R. H., Park, J., Doh, S.-J., et al. (2013). Globally strong geomagnetic field intensity circa 3000 years ago. *Earth Planet. Sci. Lett.* 383, 142–152. doi: 10.1016/j.epsl.2013.09.043.

Liritzis, Y., and R. Thomas (1980), Palaeointensity and thermoluminescence measurements on Cretan kilns from 1300 to 2000 bc, *Nature*, 282, 54–55.

- Aitken, M.J., Allsop, A.L., Bussell, G.D., Winter, M.B., 1984. Geomagnetic Intensity in Egypt and Western Asia during the 2nd Millennium Bc. *Nature* 310, 305-306.
- Ben-Yosef, E., Tauxe, L., Levy, T.E., Shaar, R., Ron, H., Najjar, M., 2009. Geomagnetic intensity spike recorded in high resolution slag deposit in Southern Jordan. *Earth Planet Sc Lett* 287, 529-539.
- Ben-Yosef, E., Tauxe, L., Ron, H., Agnon, A., Avner, U., Najjar, M., Levy, T.E., 2008. A new approach for geomagnetic archaeointensity research: insights on ancient metallurgy in the Southern Levant. *J Archaeol Sci* 35, 2863-2879.
- Nachasova IE, Burakov KS, Molina F, Cámara JA (2007) Archaeomagnetic study of ceramics from the Neolithic Los Castillejos multilayer monument (Montefrío, Spain). *Izv Phys Solid Earth* 43:170–176.
- De Marco, E., Spatharas, V., Gómez-Paccard, M., Chauvin, A., Kondopoulou, D., 2008. New archaeointensity results from archaeological sites and variation of the geomagnetic field intensity for the last 7 millennia in Greece. *Phys. Chem. Earth* 33, 578e595.
- Genevey, A., Y. Gallet, and J. Margueron (2003), Eight thousand years of geomagnetic field intensity variations in the eastern Mediterranean, *J. Geophys. Res.*, 108(B5), 2228, doi:10.1029/2001JB001612.
- Ben-Yosef, E., Tauxe, L., Ron, H., Agnon, A., Avner, U., Najjar, M., Levy, T.E., 2008. A new approach for geomagnetic archaeointensity research: insights on ancient metallurgy in the Southern Levant. *J Archaeol Sci* 35, 2863-2879.
- Hussain, A.G., 1987. The Secular Variation of the Geomagnetic-Field in Egypt in the Last 5000 Years. *Pure Appl Geophys* 125, 67-90.
- Odah, H., Heider, F., Hussain, A.G., Hoffmann, V., Soffel, H., Elgamili, M., 1995. Paleointensity of the Geomagnetic-Field in Egypt from 4000bc to 150ad Using the Thellier Method. *J Geomagn Geoelectr* 47, 41-58.
- Spasov S. Valet J.P. Kondopoulou D. Zananiri I. Casas L. Le Goff M., 2010. Rock magnetic property and paleointensity determination on historical Santorini lava flows, *Geochem. Geophys. Geosyst.*, 11, Q07006, doi:10.1029/2009GC003006.
- Shaar, R., L. Tauxe, H. Ron, Y. Ebert, S. Zuckerman, I. Finkelstein, and A. Agnon (2016), Large geomagnetic field anomalies revealed in Bronze to Iron Age archeomagnetic data from Tel Megiddo and Tel Hazor, Israel, *Earth Planet. Sci. Lett.*, 442, 173–185.
- Gallet, Y., Genevey, A., Le Goff, M., Fluteau, F., Ali Eshraghi, S., 2006. Possible impact of the Earth's magnetic field on the history of ancient civilizations. *Earth Planet Sc Lett* 246, 17-26.
- Gallet, Y., and M. Le Goff (2006), High-temperature archeointensity measurements from Mesopotamia, *Earth Planet. Sci. Lett.*, 241, 159–173.
- Genevey, A.S., Gallet, Y., Margueron, J.C., 2003. Eight thousand years of geomagnetic field intensity variations in the eastern Mediterranean. *J Geophys Res-Sol Ea* 108.
- Ertepinar, P., C. G. Langereis, A. J. Biggin, M. Frangipane, T. Matney, T. Okse, and A. Engin (2012), Archaeomagnetic study of five mounds from Upper Mesopotamia between 2500 and 700 BCE: Further evidence for an extremely strong geomagnetic field ca. 3000 years ago, *Earth Planet. Sci. Lett.*, 357, 84–98.
- Ben-Yosef, E., M. Milman, R. Shaar, L. Tauxe, and O. Lipschits (2017), Seven centuries of geomagnetic intensity variations recorded by royal Judean stamped jar handles, *Proc. Natl. Acad. Sci. U.S.A.*, 114(9), 2160–2165.
- Burakov. K. S., Nachasova I. E., Najera T., Molina F., and Camara H. A., 2005. Geomagnetic intensity in Spain in the second millennium BC. *Phys. Solid Earth. Engl. Transl.*, 41. 622–623

Catanzariti. G., Gómez-Paccard. M., McIntosh. G., Pavón-Carrasco. F.J., Chauvin. A., Osete. M.L., 2012. New archaeomagnetic data recovered from the study of Roman and Visigothic remains from central Spain (3rd–7th centuries). *Geophys. J. Int.* 188. 979–993.

Gomez-Paccard. M., Catanzariti. G., Ruiz-Martinez. V.C., McIntosh. G., Nunez. J.I., Osete. M.L., Chauvin. A., Lanos. Ph., Tarling. D.H., Bernal-Casasola. D., Thiriot J., and 'Archaeological Working Group'. 2006b. A catalogue of Spanish archaeomagnetic data. *Geophys. J. Int.*, 166. 1125 – 1143. doi:10.1111/j.1365-246X.2006.03020.x.

Gomez-Paccard. M., Chauvin. A., Lanos. P., and Thiriot J., 2008. New archeointensity data from Spain and the geomagnetic dipole moment in western Europe over the past 2000 years. *J. Geophys. Res.*, 113. B09103. doi:10.1029/2008JB005582.

Gómez-Paccard. M., Chauvin. A., Lanos. P., Dufresne. P., Kovacheva. M., Hill. M.J., Beamud. E., Blain. S., Bouvier. A., Guibert. P., and Archaeological Working Team. 2012b. Improving our knowledge of the rapid geomagnetic intensity variation observed in Europe around 800 AD: new archeointensity data from Western Europe. *Earth Planet. Sci. Lett.* 355–356. 131–143.

Nachasova. I. E., Burakov. K. S. and Bernabeu J., 2002. Geomagnetic field intensity variation in Spain. *Phys. Solid Earth. Engl. Transl.*, 38. 371–376.

Casas L., Brioso J.L., Alvarez A., Benzzi K., Shaw J., 2008. *Phys. Chem. Earth* 33. 474–480.

Gómez-Paccard. M., McIntosh. G., Chauvin. A., Beamud. E., Pavón-Carrasco. F.J., Thiriot. J., 2012a. Archaeomagnetic and rock magnetic study of six kilns from North Africa (Tunisia and Morocco). *Geophys. J. Int.* 189. 169–186. <http://dx.doi.org/10.1111/j.1365-246X.2011.05335.x>.

Kovacheva. M., Boyadziev. Y., Kostadinova-Avramova. M., Jordanova. N., Donadini. F., 2009. Updated archeomagnetic data set of the past 8 millennia from the Sofia laboratory. Bulgaria. *Geochem. Geophys. Geosyst.* 10. Q05002. <http://dx.doi.org/10.1029/2008GC002347>.

Di Chiara. A., Tauxe. L., Speranza. F., 2014. Paleointensity determination from São Miguel (Azores Archipelago) over the last 3 ka. *Physics Earth Planet. Int.* 234. 1–13.

Hartmann. G. A., Trindade R. I. F., Goguitchaichvili. A., Etchevarne. C., Morales. J. and Marisa C. Afonso. M. C., 2009. First archeointensity results from Portuguese potteries (1550–1750 AD). *Earth Planets Space* 61. 93–100.

Nachasova. I.E., and Burakov. K.S., 2009. Variation of the intensity of the Earth's magnetic field in Portugal in the 1st Millennium BC. *Phys. Solid Earth* 45 (7). 595–603.

Gómez-Paccard, M., Osete, M.L., Chauvin, A., Pavón-Carrasco, F.J., Pérez-Asensio, M., Jiménez, P., Lanos, P., 2016. New constraints on the most significant paleointensity change in Western Europe over the last two millennia. A nondipolar origin? *Earth Planet. Sci. Lett.* 454, 55–64.

Sherwood, G.J., 1991. Evaluation of a multi-specimen approach to palaeointensity determination, *J. Geomagn. Geoelect.*, 43, 341–349.

Tulloch A.M, 1992. A study of Recent secular variation of the geomagnetic field as recorded by lavas from Mount Vesuvius and the Canary Islands. Ph.D. Thesis; University of Liverpool, Liverpool, U.K., 368pp.

de Groot, L.V., Beguin, A., Kosters, M.E., van Rijsingen, E.M., Struijk, E.L.M., Biggin, A.J., Hurst, E.A., Langereis, C.G., Dekkers, M.J., 2015. High paleointensities for the Canary Islands constrain the Levant geomagnetic high. *Earth Planet. Sci. Lett.* 419, 154–167.

Kissel, C. et al. Holocene geomagnetic field intensity variations: Contribution from the low latitude Canary Islands site. *Earth Planet. Sci. Lett.* 430, 178–190, doi: 10.1016/j.epsl.2015.08.005 (2015).

Mitra, R., Tauxe, L., Mcintosh, S.K. 2013. Two thousand years of archeointensity from West Africa. *Earth Planet. Sci. Lett.* 364, 123–133.

Alva-Valdivia LM (2005) Comprehensive paleomagnetic study on a succession of Holocene olivine-basalt flow: Xitle volcano (Mexico) revisited. *Earth Planets Space* 57: 839-853.

Böhm H et al (1997) Variation of Rock Magnetic Parameters and Paleointensities over a Single Holocene Lava Flow. *J Geomag Geoelectr* 49: 523–542.

Böhm H, Biggin AJ, Walton D, Shaw J, Share JA (2003) Microwave palaeointensities from a recent Mexican lava flow, baked sediments and reheated pottery *Earth Planet Sci Lett* 214 (1–2): 221–236.

Böhm H, Pavón-Carrasco FJ, Sieron K, Mahgoub AN (2016) Palaeomagnetic dating of two recent lava flows from Ceboruco volcano, western Mexico. *Geophys J Int* 207 (2):1203–1215.

Duran MP (2010) Magnetic properties and Archeointensity of Earth's magnetic field recovered from El Opeño, earliest funeral architecture known in Western Mesoamerica *Stud. Geophys Geod* 54: 575-593.

Fanjat G et al. (2013) First archaeointensity determinations on Maya incense burners from Palenque temples, Mexico: new data to constrain the Mesoamerica secular variation curve. *Earth Planet Sci Lett* 363: 168–180.

Gratton MN, Goguitchaichvili A, Conte G, Shaw J, Urrutia-Fucugauchi J (2005) Microwave palaeointensity study of the Jorullo volcano (Central Mexico) *Geophys J Int* 161: 627–634.

Mahgoub, A.N., Böhm, H., Siebe, C., Chevrel, M.O., 2017a. Paleomagnetic study of el Metate shield volcano (Michoacán, Mexico) confirms its monogenetic nature and young age (~1250 CE). *J Volcanol Geotherm Res* 336:209–218. <https://doi.org/10.1016/j.jvolgeores.2017.02.024>.

Mahgoub A.N, Böhm, H, Siebe C, Salinas S, Guilbaud M-N (2017) Paleomagnetically inferred ages of a cluster of Holocene monogenetic eruptions in the Tacámbaro-Puruarán area (Michoacán, México): implications for volcanic hazards. *J Volcanol Geotherm Res* 347:360–370. <https://doi.org/10.1016/j.jvolgeores.2017.10.004>.

Morales J, Goguitchaichvili A, Urrutia-Fucugauchi J (2001) A rock-magnetic and paleointensity study of some Mexican volcanic lava flows during the Latest Pleistocene to the Holocene. *Earth Planets Space* 53(9): 893–902.

Morales J, Alva-Valdivia LM, Goguitchaichvili A, Urrutia-Fucugauchi J (2006) Cooling rate corrected paleointensities from the Xitle lava flow: Evaluation of within-site scatter for single spot-reading cooling units. *Earth Planets Space* 58: 1341–1347.

Conte-Fasano G, Urrutia-Fucugauchi J, Goguitchaichvili A, Morales-Contreras J (2006) Low-latitude paleosecular variation and the time-averaged field during the late Pliocene and Quaternary—paleomagnetic study of the Michoacan-Guanajuato volcanic field, Central Mexico. *Earth Planets Space* 58(10):1359–1371.

de Groot, L.V., Biggin, A.J., Dekkers, M.J., Langereis, C.G., Herrero-Bervera, E., 2013. Rapid regional perturbations to the recent global geomagnetic decay revealed by a new Hawaiian record. *Nature Communications*, doi: 10.1038/ncomms3727.

- Cromwell, G., Tauxe, L., Staudigel, H., Ron, H., 2015. Paleointensity estimates from historic and modern Hawaiian lava flows using glassy basalt as a primary source material. *Physics of Earth and Planetary Interiors*, doi: <http://dx.doi.org/10.1016/j.pepi.2014.12.007>.
- Chauvin, A., Roperch, P., Levi, S., 2005. Reliability of geomagnetic paleointensity data: effects of the NRM fraction and concave-up behavior on paleointensity determinations by the Thellier method. *Physics of the Earth and Planetary Interiors*, 150, 265-286.
- Herrero-Bervera, E., Valet, J.P., 2009. Testing determinations of absolute paleointensity from the 1955 and 1960 Hawaiian flows. *Earth Planetary Science Letters*, 287, 420-433.
- Hill, M.J., Shaw, J., 2000. Magnetic field intensity study of the 1960 Kilauea lava flow, Hawaii, using the microwave palaeointensity technique. *Geophys. J. Int.*, 142, 487-504.
- Tanaka, H., Kono, M., 1991. Preliminary results and reliability of palaeointensity studies on historical and ¹⁴C dated Hawaiian lavas. *J. Geomag. Geoelectr.*, 43, 375-388.
- Hagstrum, J.T., Champion, D.E., 1995. Late Quaternary geomagnetic secular variation from historical and ¹⁴C-dated lava flows on Hawaii. *Journal of Geophysical Research*, 100, No B12, 24393-24403.
- Tanaka, H., Athanassopoulos, J.D.E., Dunn, J.R., Fuller, M., 1995. Paleointensity determinations with measurements at high temperature. *J. Geomag. Geoelectr.*, 47, 103-113.
- Shaw, J., 1974. A new method of determining the magnitude of the palaeomagnetic field. Application to five historic lavas and five archaeological samples. *Geophys. J. R. astr. Soc.*, 39, 133-141.
- Pressling, N., Laj, C., Kissel, C., Champion, D., Gubbins, D., 2006. Palaeomagnetic intensities from ¹⁴C-dated lava flows on the Big Island, Hawaii: 0-21 kyr. *Earth and Planetary Science Letters*, 247, 26-40.
- Mankinen, E.A., Champion, D.E., 1993. Broad trends in geomagnetic paleointensity on Hawaii during Holocene time. *Journal of Geophysical Research*, 98, No B5, 7959-7976.

Supplementary Material II

Manuscript 6

Late-Quaternary secular variation data from Mexican volcanoes

Ahmed Nasser Mahgoub^{1*}, Erick Juárez-Arriaga¹ Harald Böhnell¹, Claus Siebe²,
Francisco Javier Pavón-Carrasco³

¹Centro de Geociencias, Universidad Nacional Autónoma de México, Blvd. Juriquilla 3001, Querétaro 76230, Mexico

²Departamento de Vulcanología, Instituto de Geofísica, Universidad Nacional Autónoma de México, Coyoacán, C.P. 04510, México D.F., México

³Departamento Física de la Tierra I, Facultad de Ciencias Físicas, Universidad Complutense, 28040 Madrid, Spain

Submitted to the journal of the *earth and planetary science letters*.

Individual contributions of the authors:

- i. **Ahmed Nasser Mahgoub:** designing the project and field work, laboratory measurements, analyzing and interpreting of data, writing the article.
- i. **Erick Juárez-Arriaga:** constructing the full-vector secular variation model.
- ii. **Harald Böhnell:** designing the project, field work, participating in the interpretation of data and revising the article, financing for the project.
- iii. **Claus Siebe:** field work, participating in the interpretation of data and revising the article.
- i. **Francisco Javier Pavón-Carrasco:** constructing the full-vector secular variation model, participating in the interpretation of data and revising the article.

Manuscript Number:

Title: Late-Quaternary secular variation data from Mexican volcanoes

Article Type: Letters

Keywords: Paleomagnetic secular variation; Late Quaternary; Trans-Mexican volcanic belt; Mexico; Short-term geomagnetic field variations

Corresponding Author: Mr. Ahmed Nasser Mahgoub,

Corresponding Author's Institution: Universidad Nacional Autonoma de Mexico

First Author: Ahmed Nasser Mahgoub

Order of Authors: Ahmed Nasser Mahgoub; Erick Juárez-Arriaga; Harald Böhnel; Claus Siebe; Francisco Javier Pavón-Carrasco

Abstract: We present 32 new paleomagnetic directions and 21 absolute paleomagnetic intensities (PI) from 33 volcanoes, sampled at 66 sites and covering the last 46 ka. Of these, 29 were radiocarbon-dated, 3 by thermo-luminescence, and one is of historical age (AD 1793). Rock magnetic experiments show that the dominant minerals are magnetite and titanomagnetite of low to intermediate titanium content, and of pseudo single domain size. Paleodirections were determined using stepwise demagnetization protocols, and PI by the IZZI or Thellier-Coe protocols, and strict selection criteria were applied to ensure the reliability of the data. Previously published data were evaluated to fulfill similar quality criteria as our data and 65 directions and 77 intensities were found acceptable. All accepted data come from a region within an 860 km radius around Mexico City. Paleosecular variation (PSV) curves of the past geomagnetic full-vector were established by using the bootstrap-resampling algorithm combined with cubic P-Splines for smoothing and interpolation. Because of the uneven time distribution of the data, this was done for two successive periods, between AD 2000 - 2200 BC and 2200 BC - 44000 BC. The full-vector PSV curves are unique for the American continents because of their temporal extension and because they include both, directions and absolute PI. The recent PSV curve is well defined, with only small data gaps, which then increment the uncertainty. The older PSV curves are well defined only within some periods and otherwise only define general PSV trends. Several intensity peaks with values up to 65 μT (VADM 15 μT) were observed around 250 BC, 12000 BC, 15000 BC and 27000 BC, and intensity lows around AD 700, 1200 BC, 24000-17000 BC, and 34000 BC. Abnormal directions were found around 26000 BC, with negative inclinations down to about -30° , which may be related to the Mono Lake event. A comparison with other PSV curves is complicated by the large distance to Europe and the Hawaii islands, with longitude differences of 99° and 57° , respectively. Lake sediment data from southern Texas show more differences than agreements, suggesting that either of the data may be affected by systematic errors.

Suggested Reviewers: Luis Manuel Alva Valdivia

lalva@geofisica.unam.mx

Evdokia Tema
evdokia.tema@unito.it

Emilio Herrero-Bervera
herrero@soest.hawaii.edu

Lennart de Groot
L.V.deGroot@uu.nl

Mark Dekkers
M.J.Dekkers@uu.nl

Opposed Reviewers:



Centro de Geociencias
Universidad Nacional Autónoma de México (UNAM)

Blvd. Juriquilla No. 3001, Querétaro, 76230, México

Tel. (52-442)492-8149

Ahmed Nasser Mahgoub

PhD student

June 6, 2018

Earth and Planetary Science Letters

Dear Editor

We wish to submit a new manuscript entitled "Late-Quaternary secular variation data from Mexican volcanoes" for consideration by the EPSL. We confirm that this work is original and has not been published elsewhere nor is it currently under consideration for publication elsewhere. In this manuscript we have presented new directions and intensities gathered from 33 volcanoes with ages range from 47 ka up to AD 1793.

After careful assessment of the previous data and inserting the new data, we have constructed a full vector paleosecular variation curves for Mexico. These curves are unique for the American continents because of their temporal extension end because they include both, directions and absolute PI. The new curves have indicated several interesting features of the geomagnetic field that was clearly discussed in the manuscript. Of most notably, the presence of several intensity highs and lows were obtained during the entire period which were directly compared to the global intensity field models. Also, abnormal directions and intensities were obtained around 28 ka which may be related to the Mono Lake geomagnetic excursion, which is reported here for the first time in Mexico.

We hope this work is of interest to the readers of your journal and look forward to hear about your opinion!

Sincerely,

Ahmed Nasser Mahgoub

Highlights

- 32 new paleomagnetic directions and 21 paleointensities were obtained in this study.
- Previous paleomagnetic data were carefully assessed.
- Full-vector secular variation curves were established for Mexico between 46 ka to the present.
- Several intensity highs and lows were obtained during the Late-Quaternary.
- Abnormal directions were found around 28 ka which may be related to the Mono Lake excursion.

1 Late-Quaternary secular variation data from Mexican volcanoes

2 Ahmed Nasser Mahgoub^{1*}, Erick Juárez-Arriaga¹, Harald Böhnel¹, Claus Siebe², Francisco Javier
3 Pavón-Carrasco³

4 ¹Centro de Geociencias, Universidad Nacional Autónoma de México, Blvd. Juriquilla 3001,
5 Querétaro 76230, Mexico

6 ²Departamento de Vulcanología, Instituto de Geofísica, Universidad Nacional Autónoma de
7 México, Coyoacán, C.P. 04510, México D.F., México

8 ³Departamento Física de la Tierra y Astrofísica, Facultad de Ciencias Físicas, Universidad
9 Complutense, 28040 Madrid, Spain

10

11 ***Corresponding author: ahmednasser@geociencias.unam.mx**

12

13 **Abstract**

14 We present 32 new paleomagnetic directions and 21 absolute paleomagnetic intensities (PI)
15 from 33 volcanoes, sampled at 66 sites and covering the last 46 ka. Of these, 29 were
16 radiocarbon-dated, 3 by thermo-luminescence, and one is of historical age (AD 1793).
17 Rock magnetic experiments show that the dominant minerals are magnetite and
18 titanomagnetite of low to intermediate titanium content, and of pseudo single domain size.
19 Paleodirections were determined using stepwise demagnetization protocols, and PI by the
20 IZZI or Thellier-Coe protocols, and strict selection criteria were applied to ensure the
21 reliability of the data. Previously published data were evaluated to fulfill similar quality
22 criteria as our data and 65 directions and 77 intensities were found acceptable. All accepted
23 data come from a region within an 860 km radius around Mexico City. Paleosecular
24 variation (PSV) curves of the past geomagnetic full-vector were established by using the

25 bootstrap-resampling algorithm combined with cubic P-Splines for smoothing and
26 interpolation. Because of the uneven time distribution of the data, this was done for two
27 successive periods, between AD 2000 - 2200 BC and 2200 BC - 44000 BC. The full-vector
28 PSV curves are unique for the American continents because of their temporal extension end
29 because they include both, directions and absolute PI. The recent PSV curve is well
30 defined, with only small data gaps, which then increment the uncertainty. The older PSV
31 curves are well defined only within some periods and otherwise only define general PSV
32 trends. Several intensity peaks with values up to $65 \mu\text{T}$ ($\text{VADM } 15 \cdot 10^{22} \text{ Am}^2$) were
33 observed around 250 BC, 12000 BC, 15000 BC and 27000 BC, and intensity lows around
34 AD 700 , 1200 BC, 24000-17000 BC, and 34000 BC. Abnormal directions were found
35 around 26000 BC, with negative inclinations down to about -30° , which may be related to
36 the Mono Lake event. A comparison with other PSV curves is complicated by the large
37 distance to Europe and the Hawaii islands, with longitude differences of 99° and 57° ,
38 respectively. Lake sediment data from southern Texas show more differences than
39 agreements, suggesting that either of the data may be affected by systematic errors.

40 **Keywords:** Paleomagnetic secular variation; Late Quaternary; Trans-Mexican volcanic
41 belt; Mexico; Short-term geomagnetic field variations

42

43 **1. Introduction**

44 Reconstructing the spatial and temporal evolution of the past Earth's magnetic field
45 (paleosecular variation; PSV) during the Late Quaternary has extensive applications in
46 many sub-disciplines, including the understanding of the behavior of the geodynamo in the
47 Earth's deep interior (e.g. Biggin et al., 2012) or for undertaken plate tectonic

48 reconstructions (e.g. Torsvik et al., 2012). A more recent application is in paleomagnetic
49 dating (e.g. Aitken, 1990), which can be achieved by comparing the thermal remanent
50 magnetization (TRM) direction and/or paleointensity (PI) retained by fired archeological
51 artifacts or volcanic materials with either a local PSV reference curve or with curves
52 derived from global field models (e.g., CALS10k.2 and ARCH10k.1, Constable et al.,
53 2016; SHA.DIF.14k, Pavón-Carrasco et al., 2014). Large efforts have been undertaken for
54 constructing full vector PSV reference curves, and over the last decade we have seen the
55 emergence of such curves in several regions including Bulgaria (Kovacheva et al., 2014)
56 for the last 8 ka, Canary and Azores Islands (Kissel et al., 2015) and Hawaii Islands (Tema
57 et al., 2017) for the Holocene, and China for the last 6 ka (Cai et al., 2017). No comparable
58 curves have so far been established for Mexico in spite of the large number of Quaternary
59 volcanoes concentrated along the Trans-Mexican volcanic belt (TMVB). Gonzales et al.
60 (1997) and Böhnell and Molina (2002) have reported the available full vector PSV data for
61 Mexico, and recently, Goguitchaichvili et al. (2018) have constructed a 3,000 years secular
62 variation curve of the magnetic field intensity for the Mesoamerica and southern United
63 States regions based entirely on previously published data. According to the
64 GEOMAGIA50.v3 database (Brown et al., 2015), 116 directions and 165 paleointensities
65 have been published for Mexico for the Late Quaternary (0-50 ka), and they are plotted in
66 supplementary Fig. S1. This supplement also includes data that have not yet been included
67 into this database (see Fig. S1). As Fig. S1 shows, that there is a lack of data particularly
68 for older periods: pre-Holocene directional and intensity data represent only 14% and 9%
69 of the total, respectively. Data are also dispersed, which could be attributed to unreliable
70 paleomagnetic and paleointensity data (Mahgoub et al., submitted), but also to errors in the
71 ages assigned. Based on the above, the present study aims to:

- 72 1. Enrich the Late-Quaternary Mexican paleosecular variation database by providing
73 new directions and intensities compiled from 33 volcanoes distributed along the
74 TMVB.
- 75 2. Evaluate previously published data for rejecting the unreliable ones, due to age and
76 paleomagnetic/PI errors.
- 77 3. Establish regional full-vector paleosecular variation reference curves for Mexico for
78 the Late Quaternary. The new curves are developed using the bootstrap algorithm
79 and running average procedure as proposed by Thébault and Gallet (2010).

80

81 **2. Geological background and field work**

82 Late-Quaternary volcanism in Mexico is mainly concentrated in the TMVB which is an
83 active volcanic arc crossing central Mexico in E-W direction for 1200 km, formed as the
84 result of the subduction of the oceanic Cocos and Rivera Plates underneath the continental
85 North America Plate (e.g., Nixon et al., 1987). Based on low-resolution topographic maps
86 and satellite images, Hasenaka and Carmichael (1985) estimated a minimum number of
87 around 8,000 volcanic structures, most of them younger than 2 Ma.

88 Paleomagnetic sampling was done on 33 volcanic units in lavas and/or bombs, from three
89 regions along the TMVB: 15 from the Michoacán-Guanajuato volcanic field (MGVF), 10
90 from the Sierra de Chichinautzin Volcanic Field (SCVF) south of Mexico City, and 8 from
91 the Eastern-TMVB (Fig. 1 and Table 1). These units were drilled in 66 paleomagnetic sites
92 for obtaining well-averaged paleomagnetic mean directions and intensities. 29 of the
93 volcanic eruptions have been radiocarbon dated (^{14}C) and ages were calibrated to calendar
94 years with the CALIB 7.1 software (Stuiver and Reimer, 1993) and IntCal13 (Reimer et al.,
95 2013). Another 3 flows were dated by the thermo luminescence (TL) method and one is of

96 historical age (San Martin-SMT, AD 1793). All ages are listed in Table 1 together with
97 their 68% confidence limits (one-sigma level; 1σ). Consequently, our sampling units range
98 in age from 44 kyr BC to 1793 AD, but almost one third of them are from the last 4200
99 years (Table 1).

100 Sampling was done with a portable gasoline-powered drill, and in-situ orientation with a
101 magnetic compass and inclinometer and a sun compass. For the purpose of getting reliable
102 paleo-directions, outcrops of large lateral extension were chosen wherever possible, where
103 the inner parts were exposed for instance along road cuts or in large quarries. Sometimes,
104 only natural outcrops were available. In such cases we sampled two sites or more from each
105 lava flow in order to detect unreliable directions due to undetected tilting after TRM
106 acquisition. At some cinder cones 6 to 10 volcanic bombs of ≈ 40 cm diameter were
107 sampled in quarries, where they were clearly seen to be in situ. Most sampling sites belong
108 to lava flows, but in the case of few volcanoes, both, lava flows and bombs could be
109 sampled (see Table 1).

110

111 **3. Laboratory experiments**

112 From each site, 7-15 widely distributed 25-mm-diameter cores were recovered. Each core
113 provided at least 3 standard-sized specimens. Hysteresis analyses were carried out using a
114 MicroMag 2900 alternating gradient force magnetometer in a maximum field of 1.0 T.
115 Thermomagnetic measurements were performed with a horizontal balance in an inducing
116 field of 0.5 T and in air atmosphere. Two cores per flow (in total 66) were used in order to
117 characterize the domain state of the conserved magnetic minerals and also its magneto-
118 mineralogy content and thermal stability. Natural remanent magnetization (NRM) vectors
119 of specimens were measured with a JR5 spinner magnetometer, and the characteristic

120 remanent magnetization (ChRM) direction was isolated by means of alternating field (AF)
121 demagnetization. Ten AF steps from 5 to 80 mT peak field were applied using an AGICO
122 LDA-3 equipment, and the demagnetization data were plotted as orthogonal vector
123 diagrams (Zijderveld, 1967). ChRM components were calculated by principal components
124 analysis (Kirschvink, 1980), and site mean directions by using the Fisher-statistic tool
125 (Fisher, 1953).

126 Paleointensity experiments were done mainly using the double heating IZZI-Thellier
127 experiments (Tauxe and Staudigel, 2004) and, in few cases, the ZI-Coe protocol (Coe et al.,
128 1967) was applied. Heatings were accomplished by using an ASC Scientific TD48 furnace
129 with temperature reproducibility within 2°C, and a field of 50 or 60 μ T was applied along
130 the specimen's z-axis. Partial thermoremanent magnetization (pTRM) checks (Coe et al.,
131 1978) were carried out in order to evaluate thermally induced alterations, and pTRM tail
132 checks (Riisager and Riisager, 2001) were executed only during ZI-Coe experiments for
133 detecting multidomain effects. PI data were analyzed using the TellierTool 4.2 software
134 (Leonhardt et al., 2004) and results displayed on NRM vs. pTRM (Arai) plots (Nagata et
135 al., 1965). In order to evaluate the reliability of the results obtained, a set of selection
136 criteria were used: the number of data points included in the linear fit, $N > 5$; the ratio of
137 the standard error of the slope of the selected segment in the Arai plot to the absolute value
138 of the slope, $\beta \leq 0.1$; the NRM-fraction, $f \geq 0.5$; the quality factor, $q \geq 5$; the maximum
139 angular deviation angle which measures the scatter of demagnetization points along the
140 best-fit line, $MAD_{anc} \leq 10^\circ$; the angular difference between the anchored and the free-
141 floating best-fit directions, $\alpha \leq 10^\circ$; the maximum difference produced by a pTRM check
142 normalized by the total TRM, $\delta CK \leq 10\%$; the cumulative pTRM check determined after
143 Valet et al. (1996) by calculating the difference between the slope of the non-corrected

144 intensity estimate and slope of the check-corrected intensity estimate normalized by the
145 uncorrected slope, $\delta_{pal} \leq 10\%$; the tail check criterion (applied only for specimens treated
146 with the Coe protocol) quantified after Leonhardt et al. (2004) by calculating the maximum
147 difference between the zero-field and the tail-check steps normalized by the NRM after
148 correction for angular dependence, $\delta_{t^*} \leq 99\%$. To ensure consistency, a flow mean PI must
149 be based on at least two specimens and the standard deviation should not exceed 20% or
150 $10\mu\text{T}$.

151

152 **4. Results**

153 **4.1. Rock magnetic properties**

154 From hysteresis curves the parameters saturation magnetization (M_s), saturation remanence
155 (M_{rs}), coercivity forces (H_c), and the coercivity of remanence (H_{cr}) were obtained for two
156 cores per volcanic unit. These parameters are used to construct the Day plot (Day et al.,
157 1977) where the bulk magnetic domain state of a sample can be figured out: single domain
158 (SD), pseudo-single domain (PSD), multidomain (MD), superparamagnetic (SP). The Day
159 plot together with the SD-MD mixing lines of Dunlop (2002) are shown in Fig. 2a, and the
160 M_{rs}/M_s and H_{cr}/H_c ratios are listed in supplementary Table S1. The majority of the samples
161 lies within the PSD grain size field (Fig. 2a) and is located either along the SD-MD line or
162 shifted to the right, indicating most likely the presence of a mixture of SD and MD particles
163 in different percentages. Representative hysteresis curves of these samples are shown in
164 Figs. 2b-e, which demonstrates that their loops are constricted to different degrees. Three
165 samples out of 66 have near ideal SD like curves, and are located in the Day plot within or
166 very close to the SD field (Fig. 2d). Two samples have H_{cr}/H_c ratios around 5 and are thus
167 clearly shifted to the right of the SD-MD mixing lines. These loops have distinct wasp-

168 waisted shapes (Fig. 2e), which could point to the presence of two magnetic phases with
169 strongly different coercivities (Tauxe et al., 1996).

170 Representative thermomagnetic curves are shown in Figs. 2f–i and the Curie temperatures
171 (T_C) derived from their heating and cooling branches are listed in Supplementary Table S1.
172 The results are classified into two groups. High temperature group (HT; Figs. 2f and 2g)
173 samples have a single T_C of 470-580°C suggesting that titanium (Ti)-poor titanomagnetite
174 (TM) or magnetites are the main magnetic carriers. The second group (LH; Figs. 2h and 2i)
175 is characterized by a component of low T_C of 150-358°C, which always occurs together
176 with the aforementioned high Curie temperature component, revealing that Ti-rich TM
177 coexists with Ti-poor TM or magnetite.

178 Thermomagnetic curves are considered as reversible when magnetization showed a <10%
179 change in magnetization after cooling (Figs. 2f and 2h), and otherwise as irreversible (Figs.
180 2g and 2i). According to these classifications, 45 samples out of 66 belong to the HT group
181 and 50 thermomagnetic curves are reversible (Table S1), indicating stability of the
182 magnetic minerals against thermal alteration.

183

184 **4.2. Paleomagnetic directions**

185 Representative Zijderveld diagrams are shown in Fig. 3. In most cases, linear
186 demagnetization curves are directed toward the origin (Figs. 3a, b), indicating the presence
187 of a single TRM component. In such cases, the ChRM direction could be calculated from 7
188 to 10 vector end points and is characterized by maximum angular deviation (MAD) values
189 of $\sim 1.5^\circ$ on average. In few cases, stronger secondary components of probably isothermal
190 remanence magnetization (IRM) origin were observed (Fig. 3d), and then ChRM directions
191 could still be calculated from the higher AF steps (30-80 mT). Finally, in some samples, a

192 small secondary component of probably viscous origin (Fig. 3c) was easily removed at the
193 first demagnetization steps. Flow mean directions are provided in Table 1 together with the
194 precision parameter (k) and the 95% confidence level (α_{95}). Only flow FNA gave dispersed
195 ChRM directions, most probably due to block movements after TRM acquisition (this site
196 was sampled several years ago and has not been revisited since then). At least 6 specimens
197 were used to calculate the flow mean directions, which are characterized by relatively high
198 k -values (27 to 1066, with an average of 196) and small uncertainties α_{95} (1.7° to 8.5° , in
199 average 4.0°) (see Table 1); 19 flows have $k > 100$ and only 7 flows have $\alpha_{95} > 5^\circ$. The
200 paleodirections vary between -26.1° and 19.9° in declination, and -28.6° to 59.6° in
201 inclination. The historical flow SMT (AD 1793) has a mean direction of $D = 9.9^\circ$, $I =$
202 42.2° , $\alpha_{95} = 5.2^\circ$, which agrees with the global field model (GUFM1, Jackson et al., 2000)
203 prediction ($D = 7.0^\circ$, $I = 40.0^\circ$). The overall mean direction calculated for the Late
204 Quaternary based on 33 flows is: $D = -4.0^\circ$, $I = 35.2^\circ$, $k = 15.46$, $\alpha_{95} = 6.7^\circ$, which corresponds
205 to a paleopole position at Lat. = 85.7°N , Long. = 185.9°E , $K = 23.74$, $A_{95} = 5.3^\circ$. This
206 direction and paleopole is consistent with the geocentric axial dipole (GAD) field direction
207 expected for Central Mexico ($D = 0^\circ$; $I = 32^\circ$), indicating that the present dataset averages out
208 the paleosecular variation. Mean directions are scattered around the GAD direction, with
209 the exception of two flows (Las Cabras, Tochimilco; Table 1), which have negative
210 inclinations (see Table 1). Excluding these flows, the virtual geomagnetic pole (VGP)
211 scatter gives an angular standard deviation of $s = 14.2^\circ$, which coincides perfectly with the
212 McElhinny and McFadden (1997) value for the last 5 Ma of $s \approx 13.5^\circ$. The anomalous
213 inclinations will be discussed below in the light of their possible relation to geomagnetic
214 excursions or events.

215

216 4.3. Paleointensities

217 The IZZI-PI experiments were done on 166 specimens from 26 volcanic units, which were
218 selected to have a single TRM or only minor secondary remanence components. The
219 remaining 6 lava flows (SMT, JA1&6, AGO, JU, POP2, FNA, JA4&5) were previously
220 studied by Mahgoub et al. (2018, submitted) and their PI are marked in Table 1. PI values
221 fulfilling the selection criteria mentioned above were obtained from 76 specimens
222 belonging to 21 volcanoes, resulting in an overall success rate of 46% at the specimen and
223 78% at the flow-level (see Table S2). Mean paleointensities of the studied units are listed in
224 Table 1 and Fig. 4 shows paleointensity-Arai plots of four accepted and two rejected
225 samples, together with the corresponding orthogonal vector plots defined by the
226 demagnetizations steps. The best-fit lines of the accepted Arai plots (Figs. 4a-d) at the
227 specimen-level are characterized by: N-values ranging from 5 to 14, 79% have $N \geq 7$; the
228 scatter parameter β ranges between 0.01 and 0.09, with 55% ≤ 0.05 ; fraction factor f ranges
229 between 50 and 100%, and 68% of the accepted specimens have $f \geq 70\%$; q varies from 5
230 to 56, and 49% have $q \geq 10$; MAD_{anc} has values between 1.5° and 9.1° , and in 68% of the
231 samples is $\leq 5^\circ$; α ranges from 0.2° to 9.8° and 59% have $\alpha \leq 5^\circ$; finally, the alteration
232 monitoring parameters δCK and δpal range between 0.3 and 8.7%, and 0.1 and 9.9%,
233 respectively, and 92% / 72% of the accepted specimens have δCK and $\delta pal \leq 7\%$. These
234 values indicate that the obtained paleointensity values are of good to excellent quality. On
235 the other hand, IZZI-PI results were rejected for 5 flows (see Table 1), which is related to
236 problems often encountered in volcanic rocks: multidomain effects seen as zigzagging or
237 concave-PI curves in Arai plots (Fig. 4e); magneto-mineralogical alterations (Fig. 4f); large
238 secondary components of VRM or IRM origin overprinting the primary TRM (Fig. 4f).
239 From 3 to 6 accepted specimens were used to calculate flow-mean PI, which vary from

240 14.7 μT (PUB) to 71.2 μT (ALE), with standard deviations (σ_{PI}) from 0.6 μT to 9.1 μT .
241 Notably, 12 volcanoes out of 21 have $\sigma_{\text{PI}} \leq 5.0 \mu\text{T}$ indicating high internal consistencies. PI
242 obtained from bombs show no tendency for lower σ_{PI} values compared to lava flows,
243 suggesting that despite a much faster cooling than for lava flows, no cooling rate effect
244 seems to have affected the PI recovered from these volcanic materials, most probably
245 because their TRM is carried by pseudo single domain particles (Biggin et al., 2013).
246 Referring to a possible relation between the paleointensity success rate and the magnetic
247 properties we note that no clear relation was found: some samples that are located close to
248 the MD grain size field in the Day plot provided acceptable paleointensities, while other
249 samples located close to the SD field had to be rejected (Fig. 2a). Moreover, we have
250 obtained acceptable PI from some samples that have irreversible thermomagnetic curves
251 (Table S1), which may be explained by an onset of alteration at higher temperatures than
252 those used for PI analysis.

253

254 **4.4. Evaluation of the Mexican paleomagnetic database (50 ka to AD 1900)**

255 First radiometrically dated PSV-directions for Mexico were obtained by Latham et al.
256 (1986) from a stalagmite and by Wolfman (1990) from archeological materials.
257 Paleointensity experiments on archeological artifacts were first carried out by Nagata et al.
258 (1965) and Bucha et al. (1970). These were followed by PSV studies of Gonzales et al.
259 (1997) and Böhnelt and Molina (2002) as first attempts in constructing a full-vector curve
260 for Mexico, based on directions and intensities retrieved from volcanic rocks. Numerous
261 studies have been conducted over the past two decades (e.g. Morales et al., 2001; Conte-
262 Fasano et al., 2006; Michalk et al., 2010; and references therein). Data from all these
263 studies were recovered from the GEOMAGIA50.v3 database (Brown et al., 2015), together

264 with recently published results (Fig. S1). All paleomagnetic data were evaluated in terms of
265 their reliability and internal consistency, and if possible, examined in regard to the trust
266 worthiness of the age data. In order to avoid errors during transfer between databases, we
267 referred always to the original publications, and ^{14}C ages were revised and calibrated when
268 necessary (Stuiver and Reimer, 1993).

269 Here we will accept only PSV data retrieved from volcanic and archeological materials and
270 not from lake sediments and cave-deposit archives (Latham et al., 1986), as these may
271 include unknown but potentially large and systematic errors in age and/or because of the
272 remanence acquisition processes involved. For accepting a mean direction, at least 5
273 specimens must have been used to calculate the mean, with an $\alpha_{95} \leq 10^\circ$. In regard to the
274 ages, we accept the ^{14}C and thermo-luminescence methods as reliable dating techniques.
275 Archeological ages are acceptable, particularly if they are corroborated with radiocarbon
276 data. However, we note here that the ^{14}C method may provide precise but not necessarily
277 exact ages: it yields too old ages when paleosols are sampled at depths $> 2\text{-}3$ cm below a
278 volcanic product (generally a tephra layer), or are completely wrong if the tephra layer
279 belongs to a volcano different from the studied one. Both type of errors have been
280 encountered in the case of El Metate monogenetic volcano (Chevrel et al., 2016), and
281 recent ^{14}C age determinations have shown that previously published ^{14}C ages (e.g.
282 Hasenaka and Carmichael, 1985) are occasionally too old by up to several thousand years
283 (Siebe, personal communication). In this context we also mention the Xitle volcano close to
284 Mexico City, which has often been assigned an age of around 2000 BP (e.g. Cordova et al.,
285 1994; Urrutia-Fucugauchi, 1996), while later stratigraphically much better constrained ages
286 of $\sim 1530\text{-}1630$ BP were reported (Siebe, 2000; Gonzales et al., 2000). We use these
287 younger ages and therefore apply them also to all previously published data for Xitle lavas.

288 For evaluation of previously published paleointensity data we will use the same quality
289 parameters as described in Mahgoub et al. (submitted) who demonstrated that 75% of the
290 available archeointensity data are of questionable quality.

291 Methods used are the double heating Thellier-type (Thellier and Thellier, 1959), the
292 microwave (Walton et al., 1992), the multispecimen (Dekkers and Böhnell, 2006), and the
293 Shaw (Shaw, 1974) methods. Shaw method data lack stringent quality control criteria,
294 multispecimen results were not corrected for domain-state effects and alteration tests
295 (Fabian and Leonhard, 2010), and thus both were rejected. Thellier-type and microwave PI
296 results must meet the following conditions to be accepted: thermal alteration monitoring by
297 conducting the pTRM checks (Coe et al., 1978) must be included; the stability of the NRM
298 directions of the treated specimen during the paleointensity experiments must be indicated;
299 the anisotropy and cooling rate corrections must be investigated in the case of
300 archaeological artifacts; the PI-mean must be based on at least two specimens, with a
301 standard deviation (σ_{PI}) $\leq 5 \mu\text{T}$ for archeological and $\leq 10 \mu\text{T}$ for volcanic materials.
302 Further, in the case of three flows (Pelado, El Pueblito, and Juanyan) which have been
303 studied before (Gonzales et al., 1997; Morales et al., 2001; Conte-Fasano et al., 2006) we
304 use these older data only if the directions differ less than 15° and the intensities less than
305 $15\mu\text{T}$.

306 Based on these criteria, 65 directions of 116 and 77 intensities of 165 are accepted and
307 plotted together with the rejected ones in supplement Fig. S2. The rejected data are listed in
308 Table S3 so that they may be tagged correspondingly in the paleomagnetic data bases. As a
309 result of the evaluation process it is clear that scattering is much higher for the rejected than
310 for the accepted data. Abnormal Holocene directions were also rejected this way,

311 suggesting that such discrepancies observed in the Mexican data are most likely due to
312 systematic errors and indeed do not represent the behaviour of the Earth's magnetic field.

313

314 **4.5. Full-vector paleosecular variation of the Earth's magnetic field in Mexico**

315 We combine our results with the selected previous data in order to construct a reference
316 curve for the past geomagnetic field direction and intensity for Mexico based on volcanic
317 materials and archeological artifacts. Directions were relocated to Mexico City (19.43°N,
318 99.13°W) using the Noel and Batt (1990) virtual geomagnetic pole relocation method
319 assuming a dipolar field nature, and obtained intensities were relocated to the same point by
320 the Virtual Axial Dipole Moment (VADM) method (Creer et al., 1983) in order to reduce
321 the latitude effect. The new reference curves were calculated by using the bootstrap
322 algorithm taking into account the uncertainties of the input data (e.g. Thébault and Gallet,
323 2010). Since we have information of the geomagnetic full-vector, i.e. declination,
324 inclination and intensity data, we used a unique generalized inversion to fit all the three
325 geomagnetic elements together. To do that, we applied an iterative approach to linearize the
326 relation between the geomagnetic elements (declination, inclination and intensity) and the
327 Cartesian components of a dipolar full-vector located at the reference coordinates. Because
328 the present dataset is unevenly distributed over the past 46 kyr, we decided to construct
329 curves for two successive periods outlined below. Both periods of curves were modeled in
330 the temporal part with cubic penalized b-splines of third order, orthogonal and normalized.
331 The resultant PSV curves together with their 68% uncertainty limits are listed in
332 supplementary Tables S4 and S5.

333

334 **4.5.1. Paleosecular variation from AD 2000 to 2200 BC**

335 For this period, a number of 63 directions and 73 intensities are available (Fig. 5). They are
336 mostly distributed over last two thousand years, with data gaps between 1000 BC and 400
337 BC, and before 1600 BC. As demonstrated in Fig. 5, there is a good agreement between our
338 present and the selected previous data, which validates their technical quality and the
339 accuracy of their ages. Generally, the agreement is much better for directions than for
340 intensities, probably because of the much larger uncertainties of PI. Nevertheless, we note
341 that the intensity data are consistent within 10%, which is acceptable. Declinations scatter
342 around 0° during this period and vary between 18°W and 13°E ; one abnormal declination
343 value of 37°W was found at 1175 AD. Inclinations range from 15° to 55° , and intensities
344 from 15 to $76\ \mu\text{T}$. Directions scatter around the GAD field values of $D=0^\circ$ and $I=35^\circ$, and
345 PI around the present day value of $36\ \mu\text{T}$.

346 PSV curves for this period are presented in Fig. 5, and they were also constrained for the
347 past four centuries by historical data compiled from the *gufm1* model of Jackson et al.
348 (2000) (HISTMAG database, Arneitz et al., 2017), and those reported by the Teoloyucan
349 geomagnetic observatory (Mexico City) for the period AD 1923-1985 (Urrutia-Fucugauchi
350 and Campos-Enriquez, 1993). The directional curves (Figs. 5a and b) are well constrained
351 between 300 BC and AD 1200 and from AD 1600 to present, while for time periods 2200-
352 300 BC and AD 1200-1600 additional data are needed in order to reduce the uncertainty
353 limits. The intensity curve is well constrained between 1600 to 1100 BC, while between
354 2200-1600 BC and 1100-300 BC the curve uncertainty bounds are large (Fig. 5c).

355 Amplitudes and frequency of declination and inclination curves are variable over this
356 period, and may be described by the angular variation of the field vector per time unit (Fig.
357 5d). Accordingly, the field vector changes between about $0.01\text{-}0.216^\circ/100\ \text{yrs}$. Two periods
358 of fast PSV change centered on AD 700 and AD 900 are separated by a period of much

359 slower PSV. PI shows rapid changes around 400 BC (about 10 $\mu\text{T}/100$ yrs) and AD 1000
360 (about 9 $\mu\text{T}/100$ yrs) and in both periods coincides with fast directional changes, which
361 may point mainly to variations in the dipole component of the field.

362 **4.5.2. Paleosecular variation from 2200 BC to 44000 BC**

363 The present study increments significantly the number of paleomagnetic data for this
364 period, representing 64% of the directions and 76% of the intensities. From Fig. 5 it is
365 evident that they are concentrated between 30000 and 5000 BC, and scarce between 30000-
366 44000 BC and 5000-2500 BC. Declinations vary between 26°W and 20°E, inclinations
367 from -26° to 64°, and intensities from 15 to 76 μT , and similarly to the recent period scatter
368 around the GAD field values. PSV curves have reasonable uncertainty limits only back to
369 about 15000 BC, and around 25000 BC. Due to the larger time span and the smaller
370 number of data per time unit than for the recent period, field variations are only resolved at
371 longer periods, with directional changes mostly $<0.02^\circ/100$ yrs and PI changes <2 $\mu\text{T}/100$
372 yrs.

373 The fastest directional change occurred between 28000 BC to 25000 BC and is
374 characterized by negative inclinations of -10.5° and -28.6° around 26000 BC (28 ka BP),
375 accompanied by declinations around 25°W. PI was high (≈ 75 μT) shortly before this
376 period, although defined only by a single data point, and decreased rapidly to ≈ 15 μT until
377 24500 BC. Another two well-defined intensity peaks of ≈ 65 μT occurred at 15000 and
378 12000 BC.

379

380 **5. Discussion**

381 The obtained PSV curves with their errors bands at 1σ are shown in Fig. 5 together with
382 those derived from global models and the recently calculated intensity curve of
383 Goguitchaichvili et al. (2018) which altogether allow the following interpretations.
384 Between 200 BC and today our new declination and inclination curves generally agree
385 within uncertainty limits with curves derived from the global models SHA.DIF.14k (Pavón-
386 Carrasco et al., 2014); ARCH10k.1 and CALS10k.2 (Constable et al., 2016). Intensities
387 show similar trends, but our curve shows a deeper minimum around AD 750 and a higher
388 maximum around 250 BC than the global models. Before this period, our curves are
389 smoother and diverge, due to the reduced number of data used for their construction.
390 Nevertheless, they still show similar trends of directional changes that are similar to those
391 of the global model curves.

392 Between 1000 BC and AD 300, our curve is distinctly different from the intensity curve of
393 Goguitchaichvili et al. (2018), and afterwards they show a similar trend between AD 300
394 and 750. Subsequently the two curves disagree again. It must be emphasized here that our
395 intensity curve was built mainly from our own results (Mahgoub et al., submitted; see
396 Table S3) and previous data where it is concluded that only 24% of the previous Mexican
397 data meet the acceptance criteria applied to our own data (see section 5). On the other hand,
398 the Goguitchaichvili et al. (2018) curve was constructed using only the previous data where
399 they selected them based on the number of provided specimens and the cooling rate and
400 anisotropy corrections, without any mention of the thermal alteration and NRM stability
401 directions of the treated specimen during the intensity experiments. Moreover, regarding
402 the anisotropy correction, Goguitchaichvili et al. (2018) accepted data that used the
403 anisotropy correction method of Goguitchaichvili et al. (2012), which has been recently

404 demonstrated to be insufficient (Poletti et al., 2016). Finally, they included data from the
405 United States, at a distance >2,000 km, which may affect secular variation at smaller scales.
406 These arguments may explain the differences between the two intensity curves and show
407 the great importance of the current results.

408 Our results do not show intensity peaks as reported for the Levantine (Shaar et al., 2016)
409 between 1000-700 BC and neither do so the data of Goguitchaichvili et al. (2012). Close to
410 Mexico, in lake sediments from Texas (Bourne et al., 2016), extremely high relative PI
411 have been proposed around 1000 BC and were related to the Levantine intensity spike.
412 Unfortunately, in our data set a gap exists between 1,100 BC - 400 BC, which renders it
413 impossible to make a meaningful comparison.

414 A major feature expressed by our data is the sudden drop of the inclination around 26000
415 BC to values between -10° and -29° (Fig. 5b1), accompanied by a declination change from
416 25° W to 0° . Remarkably, intensity was very high about 1000 years earlier (ca. $70 \mu\text{T}$ at
417 27000 BC; Fig. 5c1) and decreased rapidly, reaching values of about $15 \mu\text{T}$ around 24000
418 BC. This inclination drop is defined by two independent volcanoes (Tochimilco and Las
419 Cabras, Table 1), suggesting that this indeed corresponds to a real behavior of the
420 geomagnetic field. The corresponding VGP have latitudes of ≈ 47.5 and 55° N, suggesting
421 that these records may be related to a geomagnetic excursion. According to the ages, this
422 could only be related to the Mono Lake excursion, recently dated by Laj and Kissel (2014)
423 at 34.2 ± 1.2 ka; other age data for this excursion vary by several thousand years and go up
424 to about 27 ka (Nowaczyk and Antonow, 1997). Based on the above, we propose that the
425 anomalous geomagnetic field found in Mexico around ~ 28 ka may indeed be related to the
426 Mono Lake excursion, which hence is being reported here for the first time from sites in
427 Mexico. Precision age dating of the lava flows is needed to unravel this situation. 2000

428 years later, directions returned to their normal values (Fig. 5a1 and b1) but intensities were
429 still very low, around 15 μT , and only increase to values $> 20 \mu\text{T}$ until 18,000 BC (Fig. 5c).
430 Regarding intensities, most of our data display clearly higher values than those in the
431 mentioned model data covering the Holocene. This is also true when comparing to the
432 models established by Knudsen et al. (2008) and Channell et al. (2009) (PISO1500) (Fig.
433 5c1), which show lower intensities for most of the period except between about 25,000 BC-
434 17,000 BC. As these models represent mainly the dipole component of the field, our data
435 correspond to the total field in Mexico, which includes also non-dipole terms. The
436 dominantly higher than expected intensities were already noted by Michalk et al. (2010),
437 using a much smaller data set. In that work, the high intensities were interpreted to be
438 produced by the used multi specimen PI method. It is notable then, that the use of the
439 Thellier-type PI methods in the present work also produced such high intensities.

440 Our new PSV curves show larger amplitude but smaller frequency variations than those
441 from global models. This may reflect the use of unreliable data in these models, averaging
442 out amplitudes and incrementing the frequency content. Additionally, the incorporation of
443 data from locations far away ($>2,000$ km) from Mexico to calculate local PSV curves may
444 have contributed to such an effect. Whatever such rapid PSV changes are real will only be
445 resolved by the gathering of more data. Additional data will probably increment the
446 frequency content of the current PSV curves, which were constructed using cubic splines
447 fits resulting for smoothing and interpolation.

448 Comparison with the global full vector models shows that the new directional curves agree
449 reasonably well for the last 4000 years but are different at least for some parts of the Early
450 Holocene. Intensities show even larger differences and are mainly higher than in global
451 models. This implies that conducting paleomagnetic dating for rocks older than 4000 years

452 can give unfaithful results, e.g. when using the SHA.DIF.14k model, which is based on the
453 GEOMAGIA50.v3 database. It is therefore important to update the current paleomagnetic
454 databases by including the new data presented here and excluding unreliable data published
455 previously.

456

457 **6. Conclusions**

458 Thirty-two new paleomagnetic field directions and 21 paleointensities were determined for
459 Mexico, based on 66 sites from volcanic units. Regarding previously published data, 65 of
460 116 directions and 77 of 165 paleointensities are considered to be reliable, providing a total
461 of 97 directions and 98 intensities for constructing secular variation curves. These data
462 come from an area within an 860 km radius around Mexico City and were relocated to be
463 comparable. PSV curves were determined by using the bootstrap algorithm combined with
464 cubic P-Spline smoothing and interpolation for two successive periods, 2000 AD-2200 BC
465 and 2200-44000 BC, as dictated by the density of the available data. During the younger
466 period, directions vary within typical limits of PSV, but intensity shows a pronounced peak
467 around 250 BC, with $PI \approx 65 \mu T (15 \cdot 10^{22} Am^2)$. No data are available between 1,100 BC -
468 400 BC, which makes it impossible to establish the occurrence of the Levantine intensity
469 spike in Mexico during this period. For older times, intensity peaks are seen around 12000
470 BC, 15000, and 27000 BC, and also intensity lows around 24000 BC - 17000 BC, and
471 34000 BC. More important though are two abnormal inclination values of -10° to -29°
472 around 26000 BC, which correspond to excursions and according to their age
473 may be related to the Mono Lake excursion. These low inclinations are concurrent with a
474 fast intensity decrease following the intensity peak around 27000 BC. More

475 geochronological and paleomagnetic data are needed to pin down this excursion, which is
476 reported here for the first time in Mexico.

477

478 **Acknowledgments**

479 Field and laboratory costs of A.N.M. and H.B. were defrayed by Consejo Nacional de
480 Ciencia y Tecnología (CONACyT-180032) and the Dirección General de Asuntos del
481 Personal Académico (UNAM-DGAPA IN-111915). A.N.M. and E.J.A received
482 CONACYT scholarships. Work of C.S. was supported by UNAM-DGAPA IN-103618.

483

484

485 **References**

- 486 Agustín-Flores J., Siebe, C., Guilbaud, M.N., 2011. Geology and geochemistry of
487 Pelagatos, Cerro del Agua, and Dos Cerros monogenetic volcanoes in the Sierra
488 Chichinautzin volcanic field, south of México City. *J. Volcanol. Geoth. Res.* 201(1),
489 143–162. <https://doi.org/10.1016/j.jvolgeores.2010.08.010>.
- 490 Aitken, M.J., 1990. *Science-Based Dating in Archaeology*. Longman, London & New
491 York, 267 pp.
- 492 Arce, J.L., Muñoz-Salinas, E., Castillo, M., Salinas, I., 2015. The ~2000 yr BP Jumento
493 volcano, one of the youngest edifices of the Chichinautzin Volcanic Field, Central
494 Mexico. *J. Volcanol. Geoth. Res.* 308, 30-38.
- 495 Arneitz, P., Leonhardt, R., Schnepf, E., Heilig, B., Mayrhofer, F., Kovacs, P., Hejda, P.,
496 Valach, F., Vadasz, G., Hammerl, C., Egli, R., Fabian, K., Kompein, N., 2017. The
497 HISTMAG database: combining historical, archaeomagnetic and volcanic data.
498 *Geophys. J. Int.* 210(3), 1347–1359.

499 Biggin, A.J., Steinberger, B., Aubert, J., Suttie, N., Holme, R., Torsvik, T.H., van der Meer,
500 D.G., van Hinsbergen, D.J.J., 2012. Possible links between long-term geomagnetic
501 variations and whole-mantle convection processes. *Nature Geosci.* 5, 526–533.
502 [doi:10.1038/ngeo1521](https://doi.org/10.1038/ngeo1521)

503 Biggin, A.J., Badejo, S., Hodgson, E., Muxworthy, A.R., Shaw, J., Dekkers, M.J., 2013.
504 The effect of cooling-rate on the intensity of thermoremanent magnetization (TRM)
505 acquired by assemblages of pseudo-single domain, multi domain, and interacting
506 single domain grains. *Geophys. J. Int.* 193 (3), 1239-1249.
507 <https://doi.org/10.1093/gji/ggt078>

508 Bloomfield, K., 1975. A Late Quaternary monogenetic volcano field in central Mexico,
509 *Geol. Rundsch.*, 64, 476-497.

510 Böhnel, H., Molina-Garza, R., 2002. Secular variation in Mexico during the last 40,000
511 years, *Phys. Earth Planet. Int.*, 133, 99–109.

512 Bourne, M.D., Feinberg, J.M., Stafford, T.W., Waters, M.R., Lundelius, E. and Forman,
513 S.L., 2016. High-intensity geomagnetic field “spike” observed at ca. 3000 cal BP in
514 Texas, USA. *Earth Planet. Sci. Lett.* 442, 80-92.

515 Bucha, V., Taylor, R., Berger, R., Haury, E., 1970. Geomagnetic intensity: changes during
516 the past 3000 years in the western hemisphere. *Science* 168, 111–114.

517 Brown, M.C., Donadini, F., Korte, M., Nilsson, A., Korhonen, K., Lodge, A., Lengyel,
518 S.N., Constable, C.G., 2015. GEOMAGIA50.v3: 1. general structure and
519 modifications to the archeological and volcanic database. *Earth Planets Space* 67, 83.
520 [doi: 10.1186/s40623-015-0232-0](https://doi.org/10.1186/s40623-015-0232-0).

521 Cai, S., Tauxe, L., Paterson, G.A., Deng, C., Pan, Y., Qin, H., Zhu, R., 2017. Recent
522 advances in Chinese archeomagnetism. *Front Earth Sci.* 5.
523 <https://doi.org/10.3389/feart.2017.00092>

524 Carmichael, I.S.E., 2002. The andesite aqueduct: perspectives on the evolution of
525 intermediate magmatism in west-central (105–99° W) Mexico. *Contrib. Mineral.
526 Petrol.* 143 (6), 641–663.

527 Channell, J.E.T., Xuan, C., Hodell, D.A., 2009. Stacking paleointensity and oxygen isotope
528 data for the last 1.5 Myr (PISO-1500). *Earth Planet. Sci. Lett.* 283, 14–23.
529 [doi:10.1016/j.epsl.2009.03.012](https://doi.org/10.1016/j.epsl.2009.03.012).

530 Chevrel, M.O., Siebe, C., Guilbaud, M.N., Salinas, S., 2016. The AD 1250 El Metate shield
531 (Michoacán): Mexico’s most voluminous Holocene eruption and its significance for
532 archaeology and hazards. *The Holocene* 26(3), 471–488.
533 [DOI:10.1177/0959683615609757](https://doi.org/10.1177/0959683615609757).

534 Coe, R.S., 1967. Paleo-intensities of the Earth's magnetic field determined from Tertiary
535 and Quaternary rocks. *J. Geophys. Res.* 72 (12), 3247–3262.

536 Coe, R.S., Gromme, S., Mankinen, E.A., 1978. Geomagnetic paleointensities from
537 radiocarbon-dated lava flows on Hawaii and the question of the Pacific nondipole
538 low. *J. Geophys. Res.* 83, 1740–1756.

539 Constable, C., Korte, M., Panovska, S., 2016. Persistent high paleosecular variation activity
540 in southern hemisphere for at least 10 000 years. *Earth Planet. Sci. Lett.* 453, 78–86.
541 [doi:10.1016/j.epsl.2016.08.015](https://doi.org/10.1016/j.epsl.2016.08.015).

542 Conte-Fasano, G., Urrutia-Fucugauchi, J., Goguitchaichvili, A., Morales-Contreras, J.,
543 2006. Low-latitude paleosecular variation and the time-averaged field during the late

544 Pliocene and Quaternary—paleomagnetic study of the Michoacan-Guanajuato
545 volcanic field, Central Mexico. *Earth Planets Space* 58(10), 1359–1371.

546 Cordova, C., Martin, A.L., López, J., 1994. Palaeolandforms and volcanic impact on the
547 environment of prehistoric Cuicuilco, southern Basin of Mexico. *J. Arch. Sci.* 21,
548 585–596.

549 Creer, K. M., Tucholka, P., Barton, C.E., 1983. *Geomagnetism of Baked Clays and Recent*
550 *Sediments*. Elsevier, Amsterdam, 324 pp.

551 Day, R., Fuller, M., Schmidt, V.A., 1977. Hysteresis properties of titanomagnetites: grain-
552 size and compositional dependence. *Phys. Earth Planet. Inter.* 13, 260–267.

553 Demant, A., 1978. Características del Eje Neovolcánico Transmexicano y sus problemas de
554 interpretación. *Revista Mexicana de Ciencias Geológicas* 2 (2), 172–187.

555 Dekkers, M.J., Böhnell, H.N., 2006. Reliable absolute palaeointensities independent of
556 magnetic domain state. *Earth Planet. Sci. Lett.* 284, 508-517.

557 Dunlop, D.J., 2002. Theory and application of the Day plot (Mrs/Ms versus Hcr/Hc) 1.
558 Theoretical curves and tests using titanomagnetite data. *J. Geophys. Res* 107(B3)
559 2056. doi:10.1029/2001JB000486.

560 Fabian, K., Leonhardt, R., 2010. Multiple-specimen absolute paleointensity determination:
561 An optimal protocol including pTRM normalization, domain-state correction, and
562 alteration test. *Earth Planet. Sci. Lett.* 297, 84–94.

563 Fisher, R.A., 1953. Dispersion on a sphere. *Proc. R. Soc. Lond. A* 127, 295–305.

564 Goguitchaichvili, A., Loponte, D., Morales, J., Acosta, A., 2012. The archaeointensity of
565 the Earth's magnetic field retrieved from Pampean ceramics (South America).
566 *Archaeometry* 54 (2), 388–400. <http://dx.doi.org/10.1111/j.1475-4754.2011.00620.x>.

567 Goguitchaichvilia, A., García Ruiza, R., Pavón-Carrasco, F.J., Morales, J., Soler
568 Arechaldea, A.M., Urrutia-Fucugauchia, J., 2018. Last three millennia Earth's
569 Magnetic field strength in Mesoamerica and southern United States: Implications in
570 geomagnetism and archaeology. *Phys. Earth Planet. Inter.* 279, 79–91.
571 <https://doi.org/10.1016/j.pepi.2018.04.003>

572 González, S., Sherwood, G., Böhnell, H., Schnepf, E., 1997. Paleosecular variation in
573 central Mexico over the last 30,000 years: the record from lavas. *Geophys. J. Int.* 130,
574 201–219.

575 González, S., Pastrana, A., Siebe, C., Duller, G., 2000. Timing of the prehistoric eruption of
576 Xitle volcano and the abandonment of Cuicuilco pyramid, southern Basin of Mexico.
577 *Geol. Soc. London Sp. Pub.* 171, 205-224.
578 <https://doi.org/10.1144/GSL.SP.2000.171.01.17>.

579 Guilbaud, M.N., Arana-Salinas, L., Siebe, C., Barba-Pingarrón, L.A., Ortiz, A., 2015.
580 Volcanic stratigraphy of a high-altitude *Mammuthus columbi* (Tlacotenco, Sierra
581 Chichinautzin), Central México *Bull. Volcanol.* 77, 17.
582 <https://doi.org/10.1007/s00445-015-0903-5>.

583 Hasenaka, T., Carmichael, I.S.E., 1985. The cinder cones of Michoacán-Guanajuato,
584 central Mexico: their age, volume and distribution, and magma discharge rate. *J.*
585 *Volcanol. Geotherm. Res.* 25, 105–124.

586 Jackson, A., Jonkers, A.R., Walker, M.R., 2000. Four centuries of geomagnetic secular
587 variation from historical records. *Phil. Trans. R. Soc. A-358 (1768)*, 957–990.

588 Kirschvink, J.L., 1980. The least-squares line and plane and analysis of palaeomagnetic
589 data. *Geophys. J. R. Astron. Soc.* 62, 699–718.

590 Knudsen, M. F., Riisager, P., Donadini, F., Snowball, I., Muscheler, R., Korhonen, K.,
591 Pesonen, L.J., Jacobsen, B.H., 2008. Variations in the geomagnetic dipole moment
592 during the Holocene and the past 50 kyr. *Earth Planet. Sci. Lett.* 272, 319 – 329.

593 Kshirsagar, P., Siebe, C., Guilbaud, M.N., Salinas, S., Layer, P., 2015. Late Pleistocene
594 Alberca de Guadalupe maar volcano (Zacapu basin, Michoacán): stratigraphy,
595 tectonic setting, and paleo-hydrogeological environment. *J. Volcanol. Geotherm. Res.*
596 304, 214–236. <https://doi.org/10.1016/j.jvolgeores.2015.09.003>.

597 Kshirsagar, P., Siebe, C., Guilbaud, M.N., Salinas, S., 2016. Geological and environmental
598 controls on the change of eruptive style (phreatomagmatic to Strombolian-effusive)
599 of Late Pleistocene El Caracol tuff cone and its comparison with adjacent volcanoes
600 around the Zacapu basin (Michoacán, México). *J. Volcanol. Geotherm. Res.* 318,
601 114–133. <https://doi.org/10.1016/j.jvolgeores.2016.03.015>.

602 Kissel, C., Laj, C., Rodríguez-González, A., Perez-Torrado, F., Carracedo, J.C., Wandres,
603 C., 2015. Holocene geomagnetic field intensity variations: Contribution from the low
604 latitude Canary Islands site. *Earth Planet. Sci. Lett.* 430, 178-190.

605 Kovacheva, M., Kostadinova-Avramova, M., Jordanova, N., Lanos, P., Boyadzhiev, Y.,
606 2014. Extended and revised archaeomagnetic database and secular variation curves
607 from Bulgaria for the last eight millennia. *Phys. Earth Planet. Inter.* 236, 79–94.
608 [doi:10.1016/j.pepi.2014.07.002](https://doi.org/10.1016/j.pepi.2014.07.002).

609 Laj, C., Kissel, C., 2014. Dynamics of the Earth's magnetic field in the 10–75 kyr period
610 comprising the Laschamp and Mono Lake Excursions: new results from the French
611 Chaîne des Puys in a global perspective. *Earth Planet. Sci. Lett.* 387, 184–197.

612 Latham, A.G., Schwarcz, H.P., Ford, D.C., 1986. The paleomagnetism and U–Th dating of
613 Mexican stalagmite, DAS2. *Earth Planet. Sci. Lett.* 79, 195–207.

614 Leonhardt, R., Heunemann, C., Krása, D., 2004. Analyzing absolute paleointensity
615 determinations: acceptance criteria and the software ThellierTool4.0. *Geochem.*
616 *Geophys. Geosyst.* 5 (12).

617 Mahgoub, A.N., Juárez-Arriaga, E., Böhnell, H., Manzanilla, L.R., Cyphers, A.,
618 (submitted). A 3600 years paleointensity secular variation curve for Mexico. *Earth*
619 *Planet. Sci. Lett.*

620 McElhinny, M.W., McFadden, P.L., 1997. Paleosecular variation over the past 5 Myr based
621 on a new generalized database. *Geophys. J. Int.* 131, 240–252.

622 Michalk, D.M., Biggin, A.J., Knudsen, M.F., Böhnell, H.N., Nowaczyk, N., Ownby, S.,
623 López-Martínez, M., 2010. Application of the multispecimen palaeointensity method
624 to Pleistocene lava flows from the Trans-Mexican Volcanic Belt. *Phys. Earth Planet.*
625 *Int.* 179, 139-156.

626 Morales, J., Goguitchaichvili, A., Urrutia-Fucugauchi, J., 2001. A rock-magnetic and
627 paleointensity study of some Mexican volcanic lava flows during the Latest
628 Pleistocene to the Holocene. *Earth Planets Space* 53(9), 893–902.

629 Nagata, T., Kobayashi, K., Schwarz, E. J., 1965. Archeomagnetic intensity studies of South
630 and Central America. *J. Geomagn. Geoelectr.* 17, 399–405.

631 Nelson, S.A., González-Caver, E., 1992. Geology and K-Ar dating of the Tuxtla Volcanic
632 Field, Veracruz, Mexico. *Bull. Volcanol* 55, 85-96.

633 Nixon, G.T., Demant, A., Armstrong, R.L., Harakal, J.E., 1987. K-Ar and geologic data
634 bearing on the age and evolution of the Trans-Mexican Volcanic Belt. *Geofísica*
635 *Internacional*, 26(1), 109-158.

636 Noel, M., Batt, C.M., 1990. A method for correcting geographically separated remanence
637 directions for the purpose of archaeomagnetic dating. *Geophys. J. Int.* 102, 753–756.
638 [doi:10.1111/j.1365-246X.1990.tb04594.x](https://doi.org/10.1111/j.1365-246X.1990.tb04594.x)

639 Nowaczyk, N. R., Antonow, M., 1997. High-resolution magnetostratigraphy of four
640 sediment cores from the Greenland Sea: I. Identification of the Mono Lake excursion,
641 Laschamp and Biwa I/JAMAica geomagnetic polarity events, *Geophys. J. Int.* 131,
642 310–324.

643 Panfil, M.S., Gardner, T.W., Hirth, K.G., 1999. Late Holocene stratigraphy of the Tetimpa
644 archeological sites, northeast flank of Popocatepetl volcano, central Mexico. *Geol.*
645 *Soc. Am. Bull.* 111, 204–218.

646 Pavón-Carrasco, F.J., Osete, M.L., Torta, J.M., De Santis, A., 2014. A geomagnetic field
647 model for the Holocene based on archaeomagnetic and lava flow data. *Earth Planet.*
648 *Sci. Lett.* 388, 98–109.

649 Poletti W, Trindade RI, Hartmann GA, Damiani N, Rech RM (2016) Archeomagnetism of
650 Jesuit Missions in South Brazil (1657–1706 AD) and assessment of the South
651 American database. *Earth Planet Sci Lett* 445: 36-47.

652 Ramírez-Urbe, I., 2017. Geología y aspectos arqueológicos del volcán monogénico
653 Rancho Seco y estructuras volcánicas vecinas (Michoacán, México). Facultad de
654 Ingeniería. Universidad Nacional Autónoma de México, México, 108 pp.

655 Reimer, P.J., Bard, E., Bayliss, A., Beck, J.W., Blackwell, P.G., Bronk Ramsey, C., Buck,
656 C.E., Cheng, H., Edwards, R.L., Friedrich, M., Grootes, P.M., Guilderson, T.P.,
657 Haflidason, H., Hajdas, I., Hatté, C., Heaton, T.J., Hogg, A.G., Hughen, K.A., Kaiser,
658 K.F., Kromer, B., Manning, S.W., Niu, M., Reimer, R.W., Richards, D.A., Scott,
659 E.M., Southon, J.R., Turney, C.S.M., van der Plicht, J., 2013. *IntCal13 and*

660 MARINE13 radiocarbon age calibration curves 0-50,000 years cal BP. Radiocarbon
661 55(4), 1869-1887.

662 Reyes-Guzmán, N., Siebe, C., Chevrel, M.O., Guilbaud, M.N., Salinas, S., Layer, P., ,
663 2018. Geology and radiometric dating of Quaternary monogenetic volcanism in the
664 western Zacapu lacustrine basin (Michoacán, México): implications for archeology
665 and future hazard evaluations. Bull. Volcanol. 80 (2), 18.
666 <https://doi.org/10.1007/s00445-018-1193-5>.

667 Riisager, P., Riisager, J., 2001. Detecting multidomain magnetic grains in Thellier
668 palaeointensity experiments. Phys. Earth Planet. Int. 125(1), 111–117.

669 Shaar, R., Tauxe, L., Ron, H., Ebert, Y., Zuckerman, S., Finkelstein, I., Agnon, A., 2016.
670 Large geomagnetic field anomalies revealed in Bronze to Iron Age archeomagnetic
671 data from Tel Megiddo and Tel Hazor, Israel. Earth Planet. Sci. Lett., 442, 173-185.
672 <https://doi.org/10.1016/j.epsl.2016.02.038>

673 Shaw, J., 1974. A new method of determining the magnitude of the palaeomagnetic field:
674 application to five historic lavas and five archaeological samples. Geophys. J. R.
675 Astr. Soc. 39, 133-141.

676 Siebe, C., 2000. Age and archaeological implications of Xitle volcano, southwestern Basin
677 of Mexico-City. J. Volcanol. Geotherm. Res. 104, 45-64.
678 [https://doi.org/10.1016/S0377-0273\(00\)00199-2](https://doi.org/10.1016/S0377-0273(00)00199-2).

679 Siebe, C., Rodríguez-Lara, V., Schaaf, P., Abrams, M., 2004. Radiocarbon ages of
680 Holocene Pelado, Guespalapa, and Chichinautzin scoria cones, south of Mexico City:
681 implications for archeology and future hazards. Bull. Volcanol. 66, 203–225.
682 <https://doi.org/10.1007/s00445-003-0304-z>.

683 Siebe, C., Guilbaud, M.-N., Salinas, S., Chedeville-Monzo, C., 2012. Eruption of Alberca
684 de los Espinos tuff cone causes transgression of Zacapu lake ca. 25,000 yr BP in
685 Michoacán, Mexico. In: 4IMC Conference, Auckland, New Zealand (20-24 February,
686 2012), Geoscience Society of New Zealand Miscellaneous Publication 131A, 74–75
687 (Abstract volume).

688 Siebe, C., Salinas, S., Arana-Salinas, L., Macías, J.L., Gardner, J., Bonasia, R., 2017. The
689 ~23,500 y 14C BP White Pumice Plinian eruption and associated debris avalanche
690 and Tochimilco lava flow of Popocatepetl volcano, México. *J. Volcanol. Geotherm.*
691 *Res.* 333-334, 66-95. <https://doi.org/10.1016/j.jvolgeores.2017.01.011>.

692 Siebert, L., Carrasco-Nuñez, G., 2002. Late Pleistocene to pre-Columbian behind-the-arc
693 mafic volcanism in the eastern Mexican volcanic belt: implications for future hazards.
694 *J. Volcanol. Geotherm. Res.* 115, 179–205.

695 Stuiver, M., Reimer, P.J., 1993. Extended 14C database and revised CALIB radiocarbon
696 calibration program. *Radiocarbon* 35, 215–230.

697 Tauxe, L., Mullender, T.A.T., Pick, T., 1996. Potbellies, wasp-waists, and
698 superparamagnetism in magnetic hysteresis. *J. Geophys. Res.* 101, 571–583.

699 Tauxe, L., Staudigel, H., 2004. Strength of the geomagnetic field in the Cretaceous Normal
700 Superchron: new data from submarine basaltic glass of the Troodos Ophiolite.
701 *Geochem. Geophys. Geosyst.* 5 (Q02H06).

702 Tema, E., Herrero-Bervera, E., Lanos, Ph., 2017. Geomagnetic field secular variation in
703 Pacific Ocean: A Bayesian reference curve based on Holocene Hawaiian lava flows.
704 *Earth Planet. Sci. Lett.* 478, 58-65.

705 Thellier, E., Thellier, O., 1959. Sur l'intensité du champ magnétique terrestre dans le passé
706 historique et géologique. *Ann. Géophys.* 15, 285–376.

707 Thébault, E., Gallet, Y., 2010. A bootstrap algorithm for deriving the archeomagnetic field
708 intensity variation curve in the Middle East over the past 4 millennia BC. *Geophys.*
709 *Res. Lett.* 37, L22303. [10.1029/2010GL044788](https://doi.org/10.1029/2010GL044788).

710 Torsvik, T.H., van der Voo, R., Preeden, U., Mac Niocaill, C., Steinberger, B., Doubrovine,
711 P. V., van Hinsbergen, D.J., Domeier, M., Gaina, C., Tohver, E., Meert, J.G., 2012.
712 Phanerozoic polar wander, palaeogeography and dynamics: *Earth Sci. Rev.* 114, 325–
713 368. [doi:10.1016/j.earscirev.2012.06.002](https://doi.org/10.1016/j.earscirev.2012.06.002).

714 Urrutia-Fucugauchi, J., 1996. Paleomagnetic study of the Xitle-Pedregal de San Angel lava
715 flow, southern basin of Mexico. *Phys. Earth Planet. Int.* 97, 177–196.

716 Urrutia-Fucugauchi, J., Campos-Enriquez, J.O., 1993. Geomagnetic secular variation in
717 central Mexico since 1923 AD and comparison with 1945-1990 IGRF models. *J.*
718 *Geomag. Geoelectr.* 45, 243-249.

719 Valet, J.-P., Brassart, J., Meur, I.L., Soler, V., Quidelleur, X., Tric, E., Gillot, P.Y., 1996.
720 Absolute paleointensity and magnetomineralogical changes, *J. Geophys. Res.*
721 101(B11), 25029–25044.

722 Walton, D., Shaw, J., Share, J.A, Hakes, J., 1992. Microwave demagnetization. *J. Appl.*
723 *Phys.* 71, 1549-1551.

724 Wolfman, D., 1990. Mesoamerican chronology and archaeomagnetic dating, AD 1–1200.
725 In: Eighmy, J.L.S., Sternberg, R.S. (Eds.), *Archaeomagnetic Dating*. University of
726 Arizona Press, Tucson, pp. 261–308.

727 Zijdeveld, J.D.A., 1967. AC demagnetization of rocks: analysis of results. In: Runcorn,
728 S.K., Creer, K.M., Collinson, D.W. (Eds.), *Methods in Paleomagnetism*. Elsevier,
729 Amsterdam, pp. 254–286.

730

731 **List of Figures**

732 **Figure 1** Location map showing the distribution of the sampled lavas studied in the present
733 study shown as blue squares. Paleomagnetic data from Geomagica50 database are shown as
734 turquoise (accepted) and pink diamonds (rejected). For data selection criteria see the text
735 and supplementary Table S3.

736 **Figure 2** Rock magnetic properties. (a) Day plot (Day et al., 1977). The threshold values
737 for single domain (SD), pseudo-single domain (PSD), and multidomain (MD) fields are
738 shown as straight black dashed lines. Grey curved lines represent theoretical SD-MD
739 mixing curves for magnetite (after Dunlop, 2002). (b-e) Examples of representative
740 hysteresis loops obtained from the studied lavas. M_{rs}/M_s : remanent saturation
741 magnetization/saturation magnetization; H_{cr}/H_c : remanence coercivity/coercivity. (f-i)
742 variation of high-field induced magnetization with temperature for representative samples.
743 Red and blue lines indicate the heating and cooling curves, respectively.

744 **Figure 3** Representative demagnetization diagrams for the studied flows showing (a, b)
745 univectorial magnetization, (c) small secondary overprint, and (d) large secondary overprint
746 most probably produced by lightning strike. Red circles and blue squares represent the
747 projection of the magnetic vectors on the horizontal and vertical plane, respectively. Labels
748 along curves denote the maximum AF amplitude applied during the demagnetization steps.

749 **Figure 4** Examples of typical IZZI-Thellier paleointensity results and orthogonal vector
750 plots shown as insets of accepted (a-d) and rejected (e, f) specimens. NRM and pTRM data
751 are normalized. NRM vs. pTRM data are shown as circles, with best-fit lines marked in
752 black solid (a-d) and dashed grey (e, f) for the accepted and the rejected specimens,
753 respectively. pTRM checks are shown as triangles. Some temperature steps are also
754 indicated. Paleointensity analyses were done using ThellierTool.

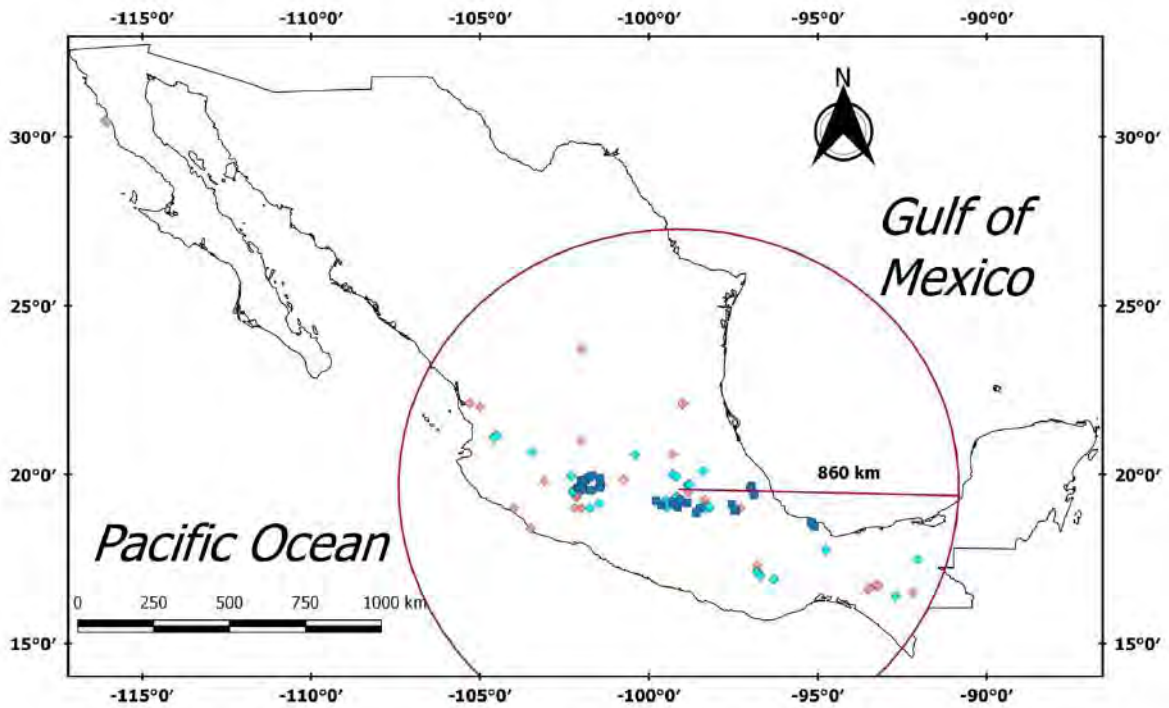
755 **Figure 5** Paleosecular variation curves for Mexico for the last 47 kyr. Declinations (a, a1),
756 inclinations (b, b1), and intensities (c, c1) obtained in the present study (purple squares) are
757 plotted together with selected previous results (turquoise crosses). The new paleosecular
758 variation curves are plotted as thick black lines together with their 95% confidence limits as
759 thin black lines. Red/blue/green lines represent the SHA.DIF.14k (Pavón-Carrasco et al.,
760 2014), CALS10k.2 and ARCH10k.1 (Constable et al., 2016) global geomagnetic model
761 predictions for the coordinates of Mexico City. The brown line in c represent the intensity
762 curve of Goguitchaichvilia et al., (2018). The orange and the light blue lines in c1 represent
763 the reconstruction model of Knudsen et al. (2008) and the PISO1500 stack of Channell et
764 al. (2009), respectively. The dashed lines are the GAD field direction and today's field
765 intensity.

766

767 **List of Tables**

768 **Table 1** Paleomagnetic directions and intensities obtained in the present study. **(1)**
769 Sampling locations including the volcanic units sampled; type of materials; region: A-
770 Michoacán-Guanajuato Volcanic Field (MGVF), B- Sierra del Chichinautzin Volcanic
771 Field (SCVF), C- Eastern-TMVB including Los Tuxtlas and Pico de Orizaba Volcanic
772 Field; site code; site latitude and longitude. **(2)** Age data given by ^{14}C and
773 thermoluminescence methods. Radiocarbon ages are calibrated to calendar years by using
774 the CALIB program version 7.1 (Stuiver and Reimer, 1993) using the latest IntCal13
775 calibration curve (Reimer et al., 2013), providing 95% confidence limits (two-sigma level;
776 2σ). **(3)** The paleomagnetic declinations (Dec) and inclinations (Inc) are listed together with
777 the precision parameter (k) and 95% confidence angle (α_{95}). Also listed is the number of
778 samples used to calculate the mean direction (n_d) and the number of used sites (N). **(4)** The

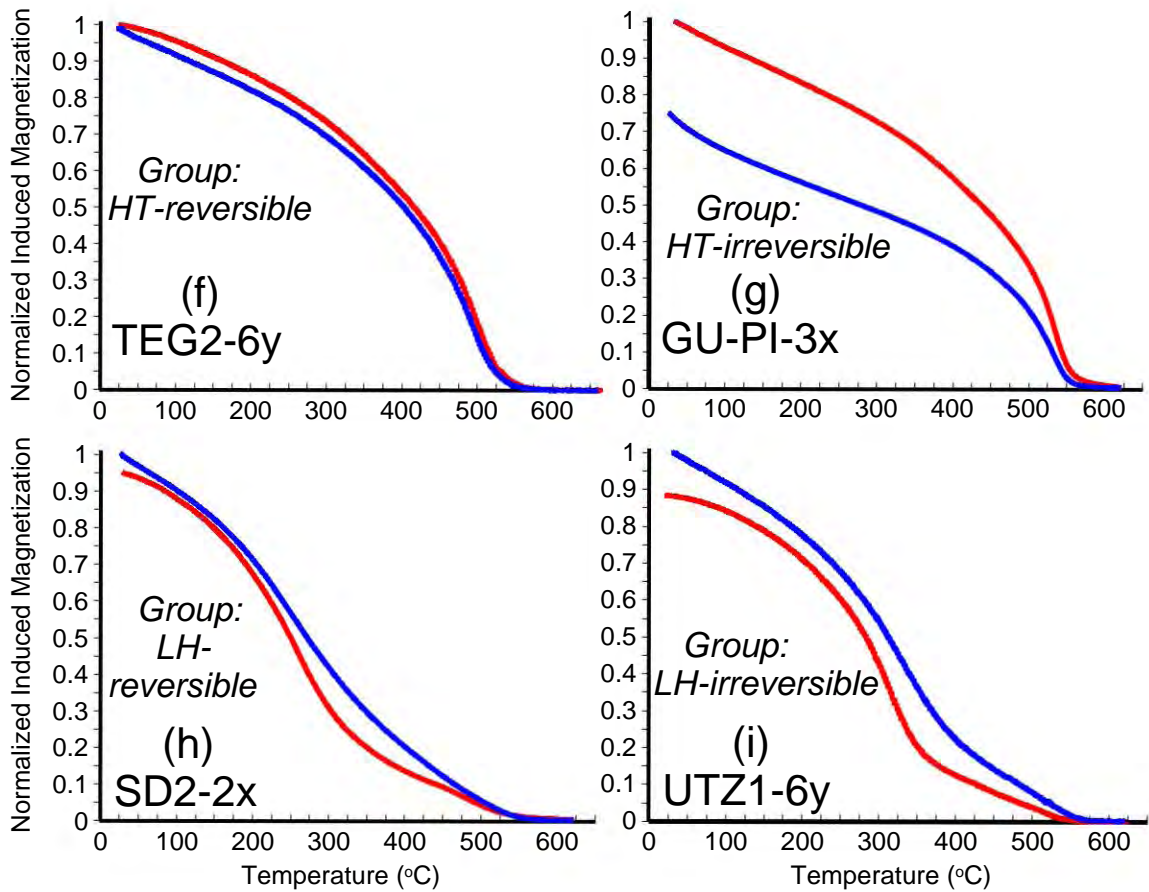
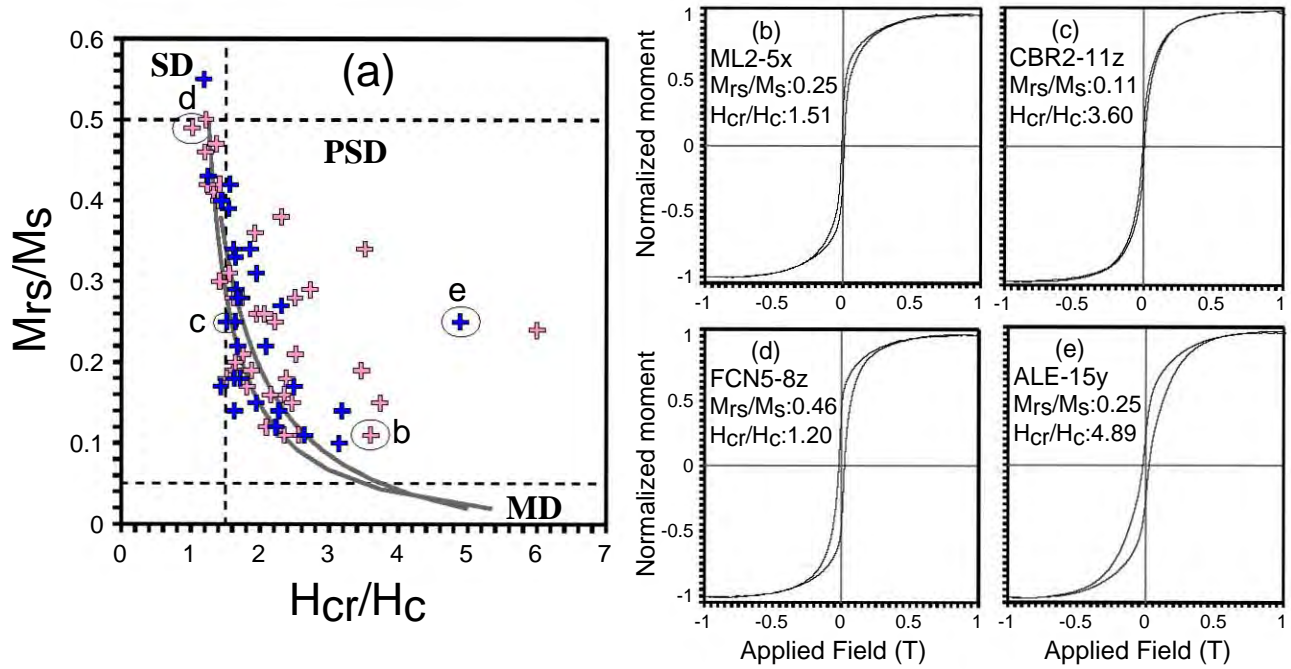
779 paleointensity results (PI) and the standard deviation of PI (σ_{PI}) in μT and the number of
780 specimens (n_P) used to calculate the mean-intensity. Also listed is the Virtual Axial Dipole
781 Moment (VADM) with standard deviation (σ_{VADM}). All directions and intensities were
782 calculated after relocating them to the coordinates of Mexico City (19.43°N, 99.13°W).
783



784

785 **Figure 1** Location map showing the distribution of the sampled lavas studied in the present
786 study shown as blue squares. Paleomagnetic data from Geomagia50 database are shown as
787 turquoise (accepted) and pink diamonds (rejected). For data selection criteria see the text
788 and supplementary Table S3.

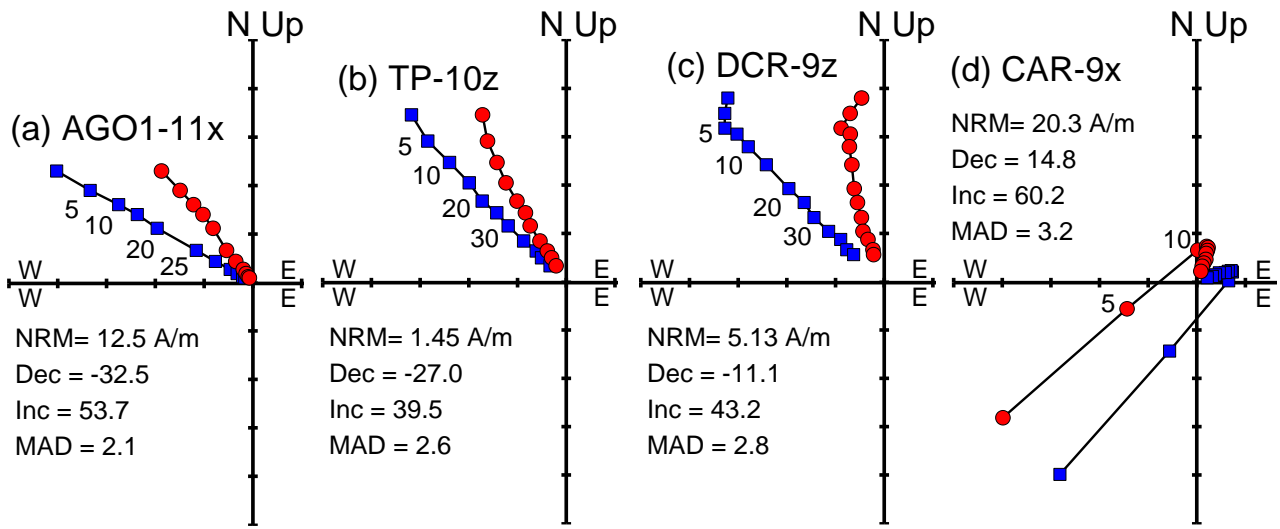
789



792 **Figure 2** Rock magnetic properties. (a) Day plot (Day et al., 1977). The threshold values
793 for single domain (SD), pseudo-single domain (PSD), and multidomain (MD) fields are
794 shown as straight black dashed lines. Grey curved lines represent theoretical SD-MD
795 mixing curves for magnetite (after Dunlop, 2002). (b-e) Examples of representative
796 hysteresis loops obtained from the studied lavas. M_r/M_s : remanent saturation
797 magnetization/saturation magnetization; H_{cr}/H_c : remanence coercivity/coercivity. (f-i)
798 variation of high-field induced magnetization with temperature for representative samples.
799 Red and blue lines indicate the heating and cooling curves, respectively.

800

801



802

803

804 **Figure 3** Representative demagnetization diagrams for the studied flows showing (a, b)
805 univectorial magnetization, (c) small secondary overprint, and (d) large secondary overprint
806 most probably produced by lightning strike. Red circles and blue squares represent the
807 projection of the magnetic vectors on the horizontal and vertical plane, respectively. Labels
808 along curves denote the maximum AF amplitude applied during the demagnetization steps.

809

810

811

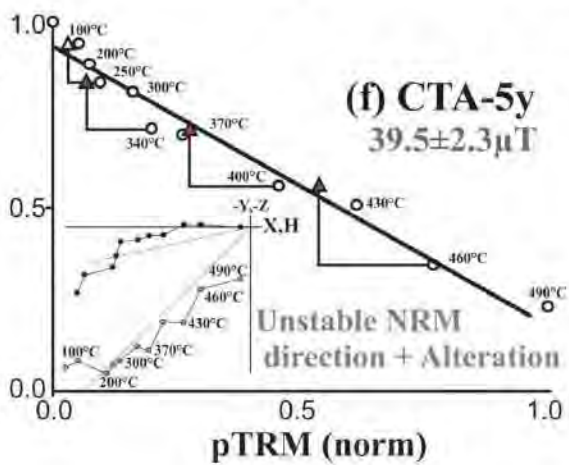
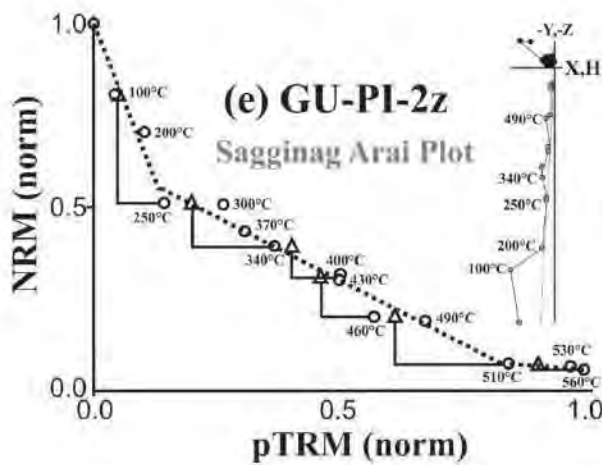
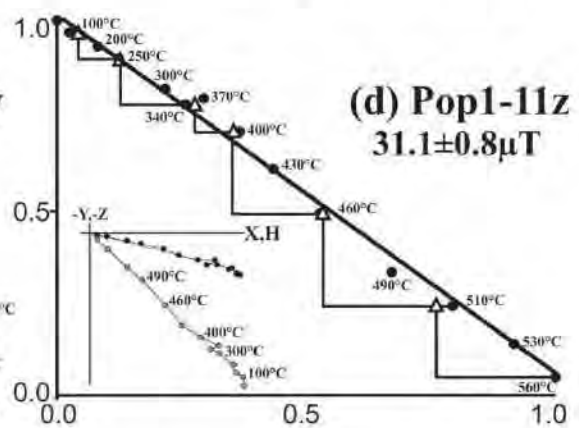
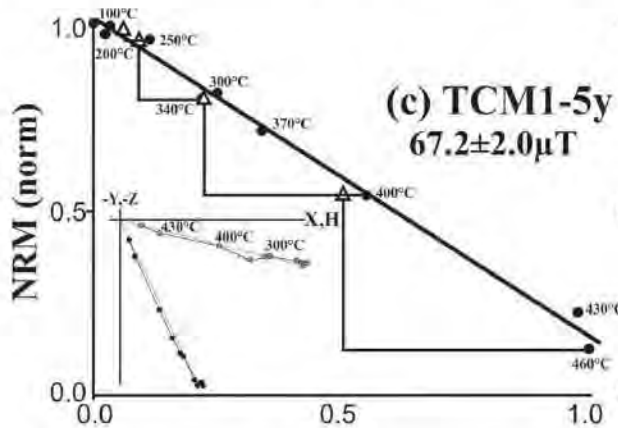
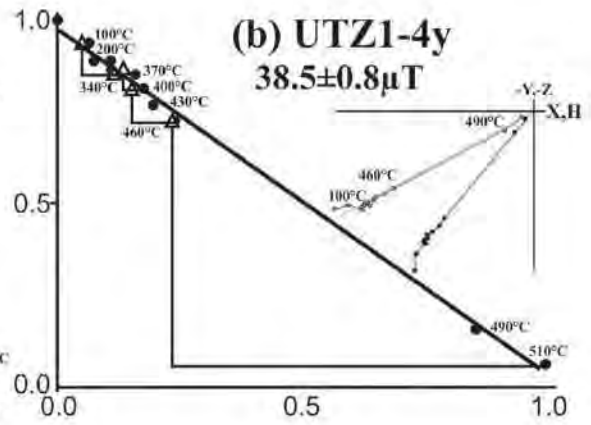
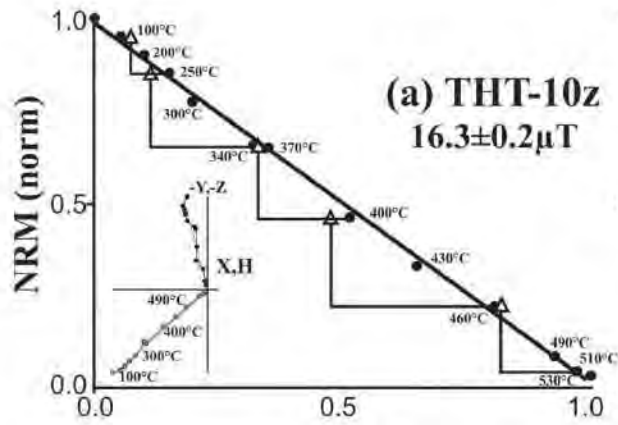
812

813

814

815

816



817

818

819

820 **Figure 4** Examples of typical IZZI-Thellier paleointensity results and orthogonal vector
821 plots shown as insets of accepted (a-d) and rejected (e, f) specimens. NRM and pTRM data
822 are normalized. NRM vs. pTRM data are shown as circles, with best-fit lines marked in
823 black solid (a-d) and dashed grey (e, f) for the accepted and the rejected specimens,
824 respectively. pTRM checks are shown as triangles. Some temperature steps are also
825 indicated. Paleointensity analyses were done using ThellierTool.

826

827

828

829

830

831

832

833

834

835

836

837

838

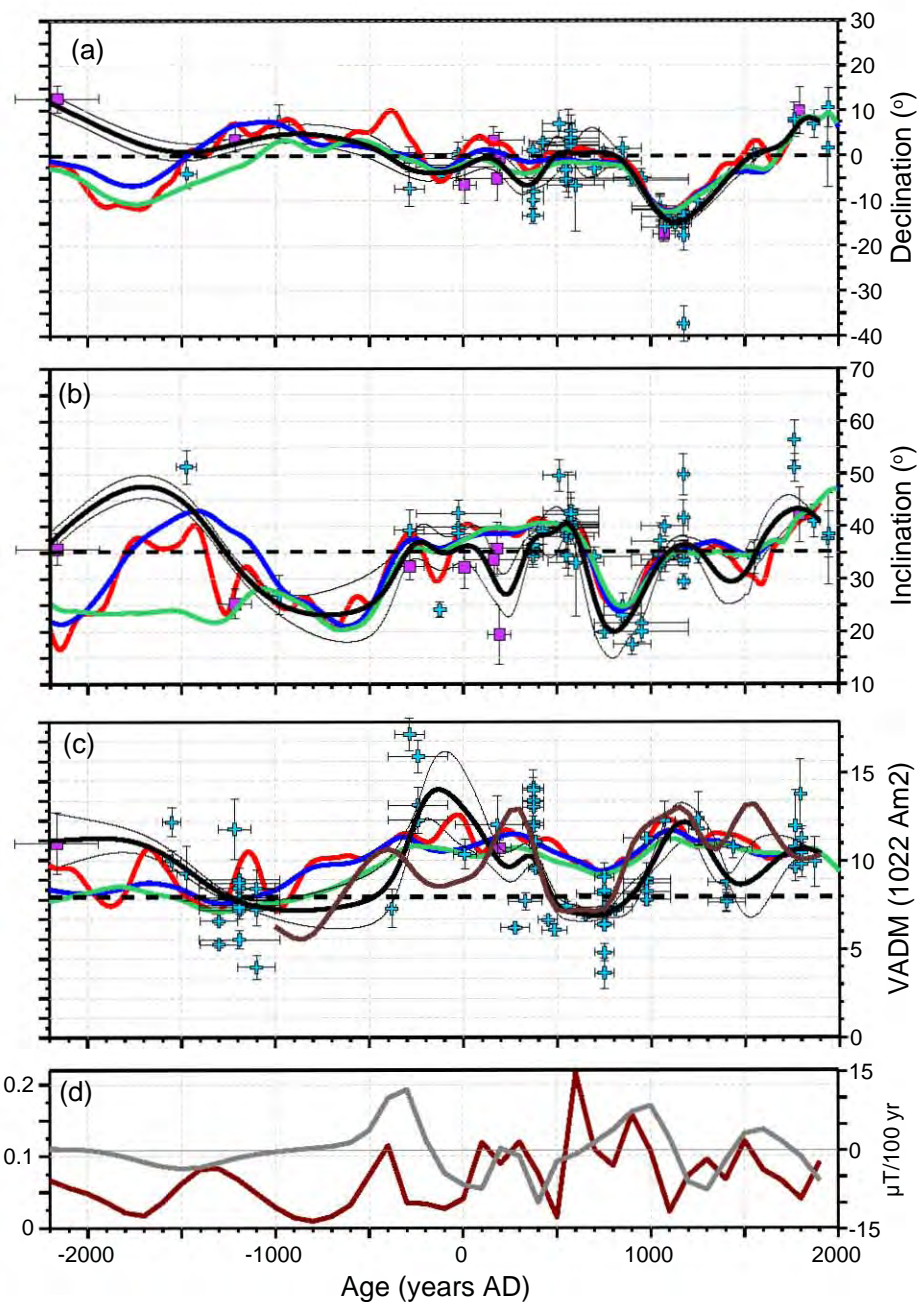
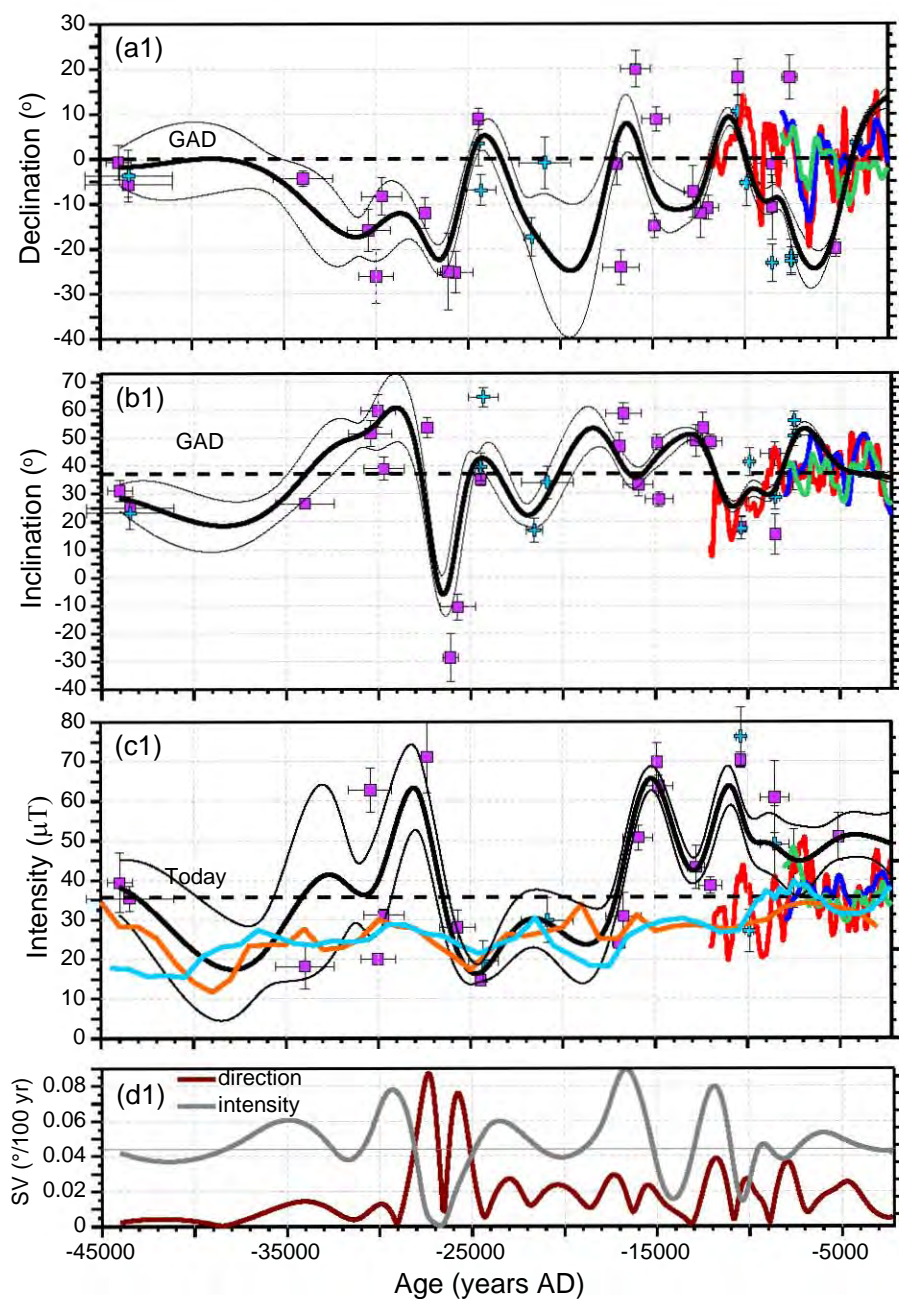


Figure 5 Paleosecular variation curves for Mexico for the last 47 kyr. Declinations (a, a1), inclinations (b, b1), and intensities (c, c1) obtained in the present study (purple squares) are plotted together with selected previous results (turquoise crosses). The new paleosecular variation curves are plotted as thick black lines together with their 68% confidence limits as thin black lines. Red/blue/green lines represent the SHA.DIF.14k (Pavón-Carrasco et al., 2014), ARCH10k.1 and CALS10k.1b (Constable et al., 2016) global geomagnetic model predictions for the coordinates of Mexico City. The brown line in c represent the intensity curve of Goguitchaichvilia et al., (2018). The orange and the light blue lines in c1 represent the reconstruction model of Knudsen et al. (2008) and the PISO1500 stack of Channell et al. (2009), respectively. The dashed lines are the GAD field direction and today's field intensity.

Table 1 Paleomagnetic directions and intensities obtained in the present study. **(1)** Sampling locations including the volcanic units sampled; type of materials; region: A- Michoacán-Guanajuato Volcanic Field (MGVF), B- Sierra del Chichinautzin Volcanic Field (SCVF), C- Eastern-TMVB including Los Tuxtlas and Pico de Orizaba Volcanic Field; site code; site latitude and longitude. **(2)** Age data given by ^{14}C and thermoluminescence methods. Radiocarbon ages are calibrated to calendar years by using the CALIB program version 7.1 (Stuiver and Reimer, 1993) using the latest IntCal13 calibration curve (Reimer et al., 2013), providing 95% confidence limits (two-sigma level; 2σ). **(3)** The paleomagnetic declinations (Dec) and inclinations (Inc) are listed together with the precision parameter (k) and 95% confidence angle (α_{95}). Also listed is the number of samples used to calculate the mean direction (n_d) and the number of used sites (N). **(4)** The paleointensity results (PI) and the standard deviation of PI (σ_{PI}) in μT and the number of specimens (n_p) used to calculate the mean-intensity. Also listed is the Virtual Axial Dipole Moment (VADM) with standard deviation (σ_{VADM}). All directions and intensities were calculated after relocating them to the coordinates of Mexico City (19.43°N , 99.13°W).

(1) <u>Sampling location</u>				(2) <u>Age data</u>			(3) <u>Paleomagnetic direction</u>					(4) <u>Paleointensity</u>		
Volcanic unit (material)-region	Code (No. Sites)	Lat (°N)	Long (°W)	Age (yrs. AD) ±2σ	Dating method	Age ref.	n _a (N:used sites)	Dec (°)	Inc (°)	k	a ₉₅ (°)	n _p	PI ±σ _{PI} (μT)	VADM ±σ _{VADM} (×10 ²² A/m)
San Martin flanco Norte (lavas - massively distributed)-C	SMT (1)	18.5811	95.1917	1793	Historical	Historical	9 (1)	9.9	42.2	100.13	5.2	3	61.6±8.8	13.8±2.0
Toaxtlacoaya (lavas - blocks)-C	JA1&6 (10)	19.4000	96.9000	1070±60	¹⁴ C	Siebert and Carrasco-Núñez , 2002	50 (10)	-17.4	34.2	1049.60	1.7	2	54.9±4.9	12.3±1.1
Cicapien (lavas - blocks)-A	FCN (2)	19.5786	102.0919	193±62	¹⁴ C	This study	25 (2)	-0.4	19.4	27.42	5.6	3	48.0±2.1	10.8±0.5
Punti-Agudo (lavas - blocks)-C	AGO (3)	18.4470	95.0995	181±220	¹⁴ C	Nelson and González-Caver, 1992	12 (3)	-5.1	35.8	79.30	4.9	3	53.9±7.2	12.1±1.6
Chichinautzin (lavas - blocks)-B	GU-PI (2)	19.0200	99.1400	164±101	¹⁴ C	Siebe et al. (2004)	23 (2)	3.4	33.7	98.40	3.1	Unsuccessful experiments; mutidomain		
El Jumento (lavas - massively distributed)-B	JU (2)	19.1867	99.3201	8±62	¹⁴ C	Arce et al. (2015)	25 (2)	-6.5	32.2	51.69	4.1	5	46.4±3.8	10.4±0.9
Nealtican (lavas - quarries)-B	POP2 (3)	18.9893	98.4820	-285±80	¹⁴ C	Panfil et al. (1999)	36 (3)	-0.5	32.4	90.43	2.5	2	76.8±4.2	17.2±0.9
Non-associated flow (lavas - blocks)-A	FNA (1)	19.6128	102.0714	-380±23	¹⁴ C	This study	No mean direction could be obtained					5	32.7±4.8	7.3±1.1
Coacoatzintla (lavas - blocks)-C	JA4&5 (2)	19.6500	96.9600	-1178±42	¹⁴ C	Siebert and Carrasco-Núñez , 2002	16 (2)	3.6	25.3	174.90	2.8	2	52.8±7.6	11.8±1.7
Urutzen (lavas - massively distributed)-A	UTZ (1)	19.5702	101.9412	-2161±222	¹⁴ C	Chevrel et al. (2016)	13 (1)	12.7	35.7	231.68	3.0	6	49.2±7.8	11.0±1.7
Tendeparacua (lavas - road cut)-A	TP (1)	19.8853	101.4502	-5070±139	¹⁴ C	Kshirsagar et al. (2015)	9 (1)	-19.9	38.4	668.73	2.0	3	50.9±6.0	11.4±1.3
Tenango1 (lavas - blocks)-B	TEG1 (1)	19.0895	99.6258	-7550±422	¹⁴ C	Bloomfield (1975)	10 (1)	18.0	36.0	98.50	4.9	Unsuccessful experiments; large overprint		
La Taza (lavas - massively distributed)-A	CTA (1)	19.5303	101.7328	-8505±222	¹⁴ C	Hasenaka & Carmichael (1985)	7 (1)	-10.8	15.3	73.70	7.1	Unsuccessful experiments; alteration; overprint		
Juanyan (bombs)-A	JUN (2)	19.6857	101.9803	-8523±800	¹⁴ C	Hasenaka & Carmichael (1985)	11 (1)	-1.2	44.1	115.50	4.3	4	60.9±9.1	13.6±2.0
Pelado (lavas - blocks)-B	PEL I-II (2)	19.1200	99.1900	-10362±256	¹⁴ C	Siebe et al. (2004)	12 (2)	18.0	17.9	115.10	4.1	3	70.3±2.0	15.7±0.4
El Melón (lavas - blocks & bombs)-A	ML (2)	19.6706	101.4287	-12000±619	¹⁴ C	Ramírez-Urbe et al., 2017	12 (1)	-10.9	48.5	261.48	2.7	3	38.6±2.0	8.6±0.4
upper Toluca pumice (lavas - massively distributed)-B	AB (1)	19.2233	99.7875	-12405±95	¹⁴ C	Bloomfield (1975)	6 (1)	-12.1	53.5	156.20	5.4	Unsuccessful experiments; large overprint		
Cerro Hueco (lavas - massively distributed)-A	CHU (1)	19.7019	101.4585	-12798±474	¹⁴ C	Kshirsagar et al. (2015)	16 (1)	-7.3	48.9	42.43	5.7	3	43.2±5.4	9.7±1.2
Tecuítlapa mar (bombs)-C	TCM (4)	19.1210	97.5440	-14800±750	TL	This study	24 (4)	8.8	27.9	132.80	2.6	4	63.8±2.6	14.3±0.6
Dos Cerros (lavas - road cut)-B	DCR (1)	19.1557	98.8684	-14900±290	¹⁴ C	Agustín-Flores et al. (2011)	15 (1)	-14.9	48.2	208.58	2.7	3	69.9±4.8	15.7±1.1
Molcayete Zipiajo (lavas - massively distributed)-A	ZP (1)	19.8127	102.0288	-15911±809	¹⁴ C	Kshirsagar et al. (2015)	13 (1)	19.9	33.2	72.07	4.0	3	50.7±3.2	11.4±0.7
Molcayete de Eréndira (lava) - blocks)-A	Molc (1)	19.8381	101.8746	-16717±978	¹⁴ C	Reyes-Guzmán et al. (2018)	13 (1)	-24.1	58.7	118.74	3.8	3	30.8±6.0	6.9±1.3
Raices-Cajete (lavas - blocks)-B	PI3 (1)	19.1058	99.2406	-16955±344	14C	This study	6 (1)	-1.1	47.0	193.80	4.8	3	24.2±0.6	5.4±0.1
El Pueblito (lavas - road cut)-A	PUB (1)	19.8204	101.9247	-24450±125	¹⁴ C	Reyes-Guzmán et al. (2018)	8 (1)	8.9	35.1	531.79	2.4	3	14.7±0.9	3.3±0.2
Tochimilco (lavas - massively distributed)-B	POP1 (1)	18.8740	98.6036	-25706±976	¹⁴ C	Siebe et al. (2017)	10 (1)	-25.2	-10.5	111.80	4.6	6	28.1±4.4	6.3±1.0
Las Cabras (lavas - road cut) & (bombs)-A	CBR (3)	19.8301	101.8983	-26110±416	¹⁴ C	Reyes-Guzmán et al. (2018)	6 (1)	-25.0	-28.6	63.22	8.5	Unsuccessful experiments; large overprint		
Alberca de los Espinos (bombs)-A	ALE (1)	19.9037	101.7729	-27344±221	¹⁴ C	Siebe et al. (2012)	18 (1)	-12.0	53.7	100.32	3.5	3	71.2±9.1	15.9±2.0
S Cd Serdan (lavas - road cut)-C	CSD (4)	18.9328	97.4357	-29700±1100	TL	This study	27 (4)	-8.3	38.9	46.60	4.1	5	31.1±1.5	7.0±0.3
Rancho Seco (lavas - road cut) & (bombs)-A	RS (2)	19.6161	101.4707	-30010±929	¹⁴ C	Ramírez-Urbe et al., 2017	11 (2)	-26.1	59.6	60.27	5.9	3	20.0±1.4	4.5±0.3
El Caracol (lavas - road cut)-A	CAR (1)	19.9624	101.6918	-30422±1179	¹⁴ C	Kshirsagar et al. (2016)	9 (1)	-15.9	51.5	121.23	4.7	3	62.8±5.5	14.1±1.2
Teuhtli (lavas - road cut)-B	THT (1)	19.2438	99.0539	-33970±1600	¹⁴ C	Guilbaud et al. (2015)	8 (1)	-4.3	26.5	1066.25	1.7	3	18.2±5.8	4.1±1.3
La Joya flow (lavas - blocks)-C	JA3-13 (2)	19.5900	96.9900	-43448±2367	¹⁴ C	Siebert and Carrasco-Núñez , 2002	10 (2)	-5.7	25.0	337.10	2.6	3	35.4±3.1	7.9±0.7
Serdan (lavas - road cut)-C	SD (4)	18.9347	97.4719	-44000±680	TL	This study	24 (4)	-0.7	31.2	62.20	3.8	6	39.4±7.5	8.8±1.7

Overall Paleodirection

[N_{lavas}= 32 , Dec= -4.0° , Inc=35.2° , k=15.46 , a₉₅= 6.7°]

Supplementary materials

The supplementary materials consist of two figures and five tables

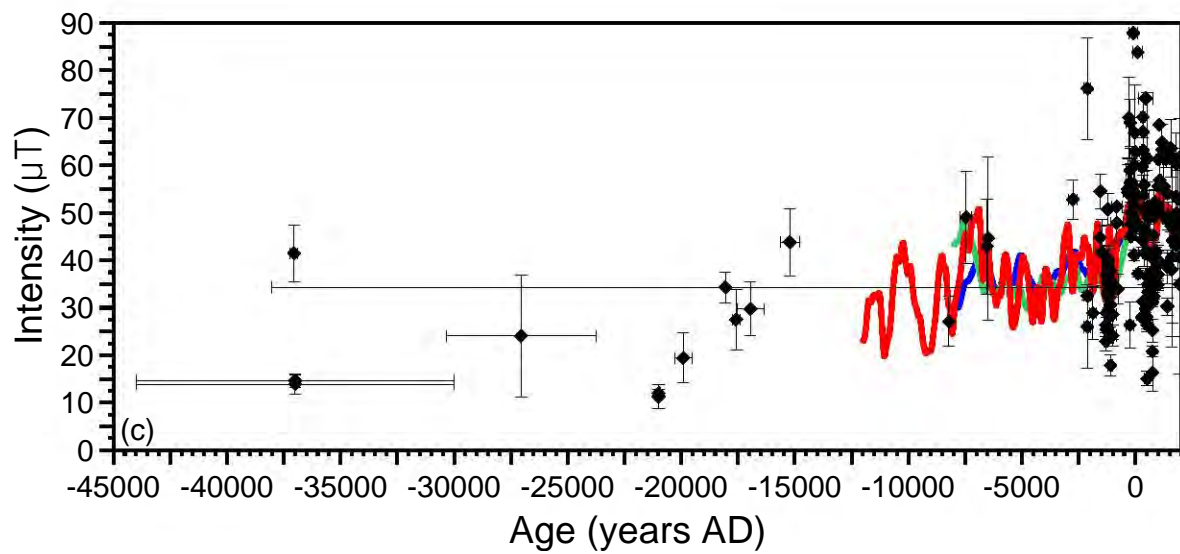
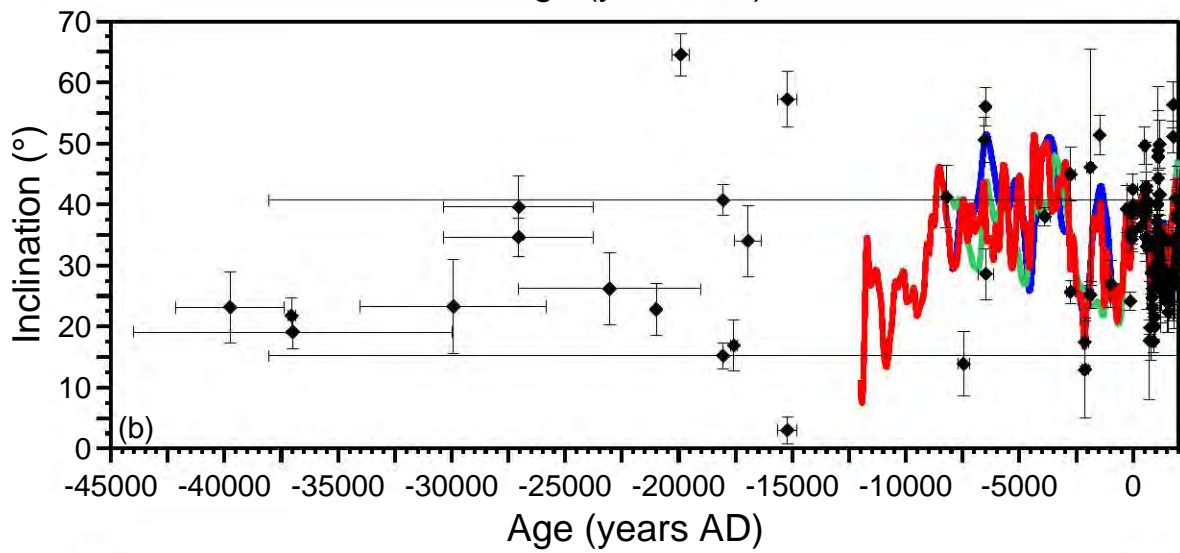
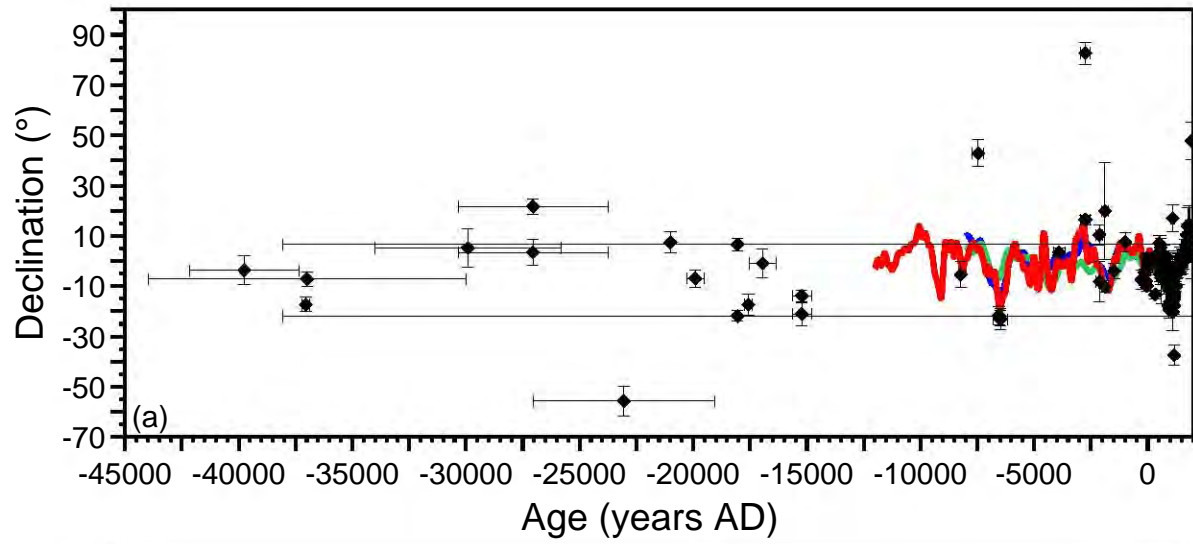


Figure S1. Late Quaternary paleomagnetic declination (a) and inclination (b) secular variation data published for Mexico, and (c) paleointensity data, compiled from the Geomag50.v3 database (Brown et al., 2015). Also included are new data from five recently published studies by Böhnel et al. (2016), Mahgoub et al. (2017a, b; 2018), and Mahgoub et al., (submitted). Colored lines are predictions from global models ARCH10k.1 (blue), CALS10k.2 (green), and SHA.DIF.14K (red).

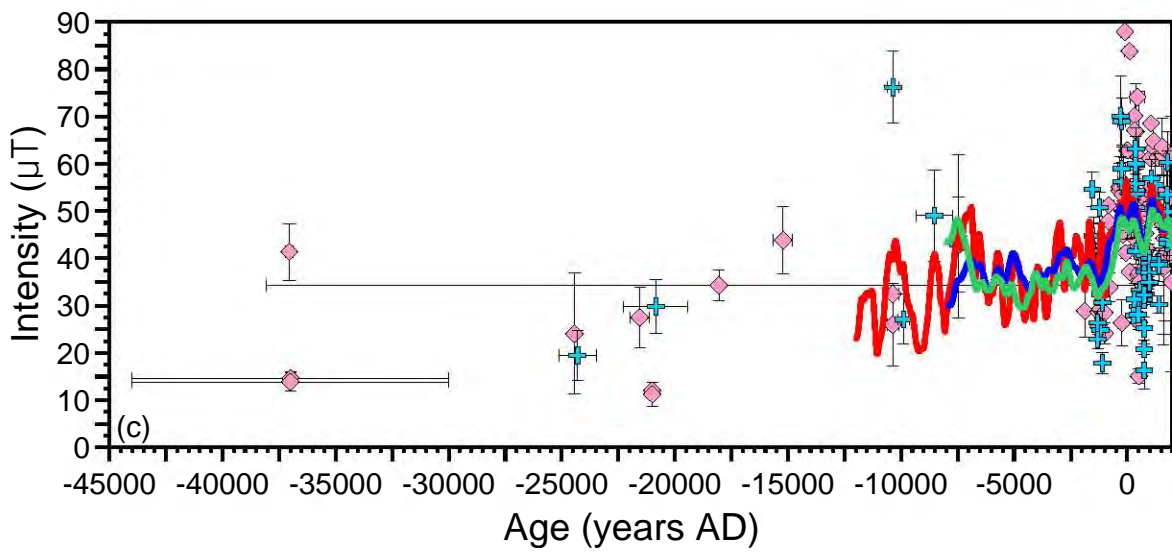
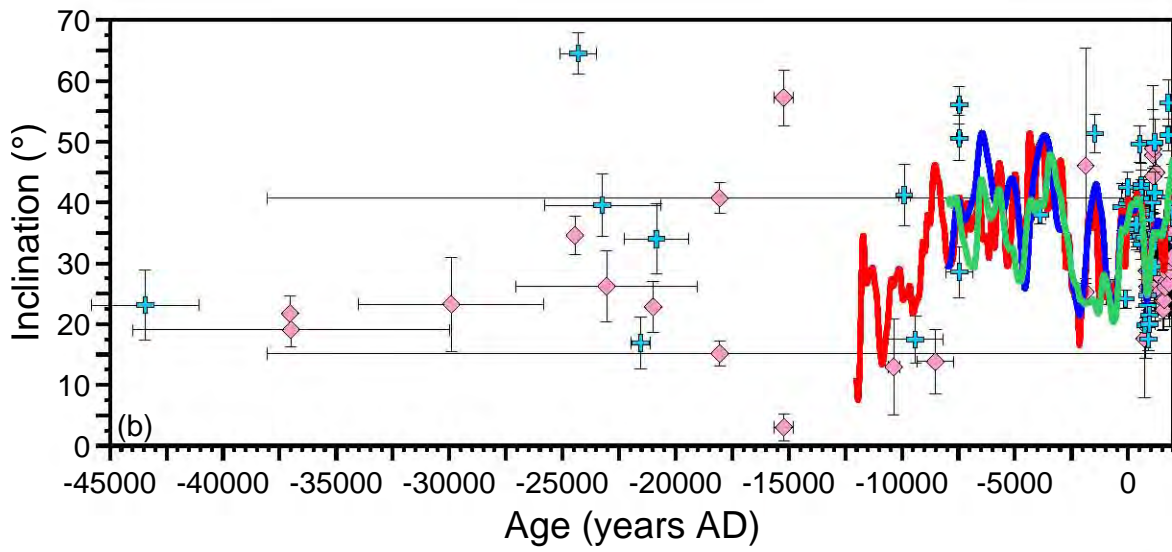
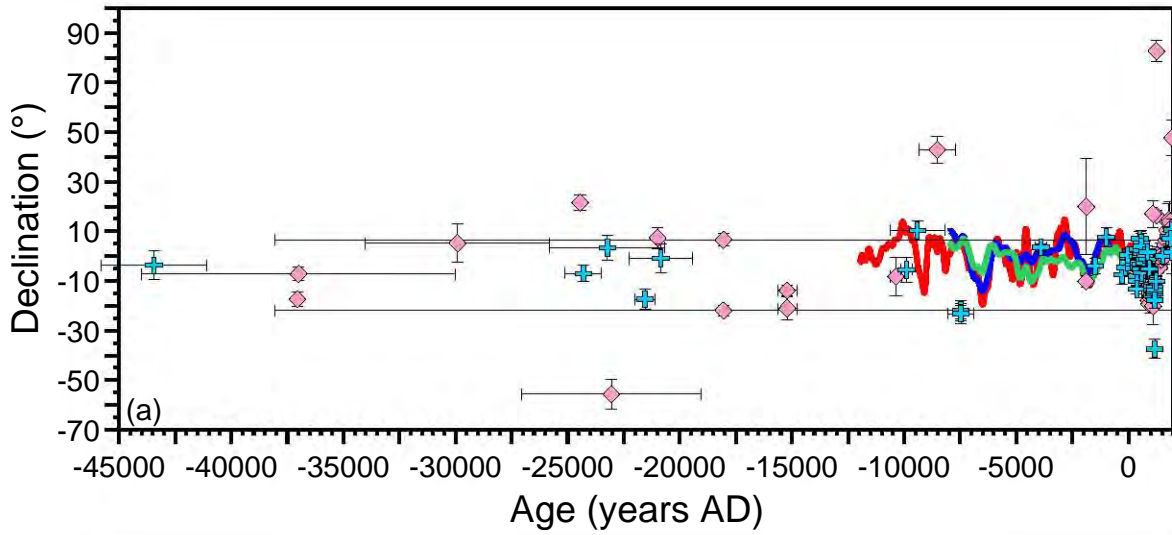


Figure S2 Selection of Late Quaternary paleomagnetic data published for Mexico. Pink diamonds are low quality paleomagnetic directions (A, B) or unreliable paleointensities (C), and light blue crosses data represent accepted data according to our assessment criteria. Unreliable age data are marked by pink diamonds. Predictions from global models are shown in blue (ARCH10k.1), green (CAL510.k.2), and red (SHA.DIF.14K).

Supplementary Table S1: Rock magnetic parameters for studied samples: listed are the thermomagnetic hysteresis analyses that performed on some representative sample: the Curie temperature (T_c) for heating and cooling curves are calculated using the RockMag Analyzer program, and the remanence carriers are proposed based on the Curie Points Mag: magnetite, Ti-TM: Titanomagnetite; H_{cr}/H_c is remanent coercivity / coercivity; M_{rs}/M_s is the remanent saturation magnetization/ saturation magnetization. Relation between the rock magnetic properties and the success rate of the paleointensity experiments is demonstrated also, *for more details about the sample classes classification after intensity experiments see Table 2.*

Sample	Thermomagnetic		Reversibility	Remanence Carriers	Hysteresis analyses		Accepted paleointensity estimates?	Sample	Thermomagnetic		Reversibility	Remanence Carriers	Hysteresis		Accepted paleointensity estimates?
	Heating T _c (°C)	Cooling T _c (°C)			H _{cr} /H _c	M _r /M _s			Heating T _c (°C)	Cooling T _c (°C)			H _{cr} /H _c	M _r /M _s	
SMT-16x	473	450	reversible	low Ti-TM	2.23	0.12	Yes	CHU1-2x	240, 550	540	irreversible	High Ti-TM, low Ti-TM	3.14	0.10	Yes
SMT-5y	470	445	reversible	low Ti-TM	2.56	0.11	No	CHU1-4z	266, 550	541	irreversible	High Ti-TM, low Ti-TM	1.01	0.49	No
JA6-6a	580	565	reversible	Mag	1.43	0.17	Yes	TCM1-5y	559	545	reversible	Low Ti-TM	1.67	0.22	Yes
JA1-3z	550	540	reversible	Low Ti-TM	2.09	0.12	No	TCM1-3z	576	554	irreversible	Mag	2.35	0.16	No
FCN5-1y	515	510	reversible	low Ti-TM	1.63	0.14	Yes	DCR-2z	280, 547	260, 530	reversible	High Ti-TM, low Ti-TM	1.71	0.28	Yes
FCN5-8z	580	560	irreversible	Mag	1.20	0.46	No	DCR-14x	540	230	reversible	Low Ti-TM	1.61	0.28	No
AGOA-11z	530	490	irreversible	low Ti-TM	2.08	0.22	Yes	ZP1-4x	150, 570	560	irreversible	High Ti-TM, Mag	1.64	0.25	Yes
AGOB-6x	560	530	irreversible	Mag	1.81	0.17	No	ZP1-7z	282, 570	560	irreversible	High Ti-TM, Mag	1.41	0.30	No
GU-PI-3x	555	540	irreversible	low Ti-TM	1.61	0.19	No	PI3-6x	580	570	reversible	Mag	1.44	0.40	Yes
GU-PI-4y	562	553	reversible	Low Ti-TM	1.51	0.18	No	PI3-2z	580	560	reversible	Mag	1.68	0.28	No
JU1-16y	515	500	irreversible	Low Ti-TM	1.54	0.39	Yes	MOLC2-	570	560	reversible	Mag	1.94	0.31	Yes
JU1-3z	540	520	irreversible	Low Ti-TM	1.75	0.21	No	MOLC2-	550	567	reversible	Mag	1.41	0.42	No
POP4-11x	570	560	reversible	Mag	1.56	0.42	Yes	PUB1-1x	580	570	reversible	Mag	1.67	0.28	Yes
POP2-3x	540	510	reversible	Low Ti-TM	2.72	0.29	No	PUB1-1x	580	566	reversible	Mag	1.87	0.19	No
FNA-7x	540	530	reversible	Low Ti-TM	1.65	0.29	Yes	POP1-4y	580	570	reversible	Mag	1.61	0.34	Yes
FNA-2y	520	515	reversible	Low Ti-TM	1.55	0.31	No	POP1-5z	580	574	reversible	Mag	1.95	0.26	No
JA6-6x	292, 525	520	reversible	High Ti-TM, low Ti-TM	1.71	0.18	Yes	CBR2-11z	358, 548	540	irreversible	High Ti-TM, low Ti-TM	3.60	0.11	No
JA6-4z	315, 507	306, 536	irreversible	High Ti-TM, low Ti-TM	2.51	0.21	No	CBR3-6z	495	458	reversible	low Ti-TM	1.36	0.47	No
UTZ1-6y	352, 550	560	irreversible	High Ti-TM, Mag	2.49	0.17	Yes	ALE-15y	560	550	reversible	Low Ti-TM, Mag	4.89	0.25	Yes
UTZ2-7x	368, 542	530	irreversible	High Ti-TM, low Ti-TM	2.38	0.18	No	ALE-1z	350, 540	530	reversible	High Ti-TM, low Ti-TM	3.46	0.19	No
TP1-2y	580	558	reversible	Mag	1.94	0.15	Yes	CSD1-7z	500	490	reversible	Low Ti-TM	2.30	0.27	Yes
TP1-12z	580	570	reversible	Mag	1.92	0.36	No	CSD1-2z	560	550	reversible	Low Ti-TM, Mag	2.21	0.25	No
CTA-5y	523	520	reversible	Low Ti-TM	1.32	0.41	No	RS1-2z	580	556	reversible	low Ti-TM, Mag	1.64	0.33	Yes
CTA-3z	510	500	reversible	Low Ti-TM	2.30	0.38	No	RS1-1z	250, 567	546	reversible	low Ti-TM, Mag	1.23	0.42	No
TEG2-4z	550	547	reversible	Low Ti-TM	6.00	0.24	No	CAR-12y	531	520	reversible	low Ti-TM	2.64	0.11	Yes
TEG2-6y	560	550	reversible	Low Ti-TM	1.73	0.28	No	CAR-11x	573	570	reversible	Mag	2.15	0.16	No
JUN1-2y	545	540	irreversible	Low Ti-TM	1.18	0.55	Yes	THT-1x	570	550	irreversible	Mag	1.85	0.34	Yes
JUN1-1z	550	530	reversible	Low Ti-TM	1.21	0.50	No	THT-14z	209, 538	200, 530	irreversible	High Ti-TM, low Ti-TM	2.06	0.26	No
PEL-14x	280, 579	558	reversible	High Ti-TM, low Ti-TM	1.24	0.43	Yes	JA3-13-6y	570	550	irreversible	Mag	1.62	0.18	Yes
PEL-15z	290, 578	557	reversible	High Ti-TM, low Ti-TM	1.39	0.40	No	JA3-13-2z	560	545	reversible	Low Ti-TM	1.64	0.20	No
ML2-5x	296, 560	556	irreversible	High Ti-TM, low Ti-TM, Mag	1.51	0.25	Yes	SD1-7y	545	530	reversible	Low Ti-TM	2.27	0.14	Yes
ML1-5z	530	543	reversible	Low Ti-TM	2.35	0.11	No	SD1-6z	550	540	reversible	Low Ti-TM	2.46	0.15	No
AB-2z	310, 550	300, 540	reversible	High Ti-TM, low Ti-TM, Mag	2.50	0.28	No	SD2-3X	560	550	reversible	Mag	3.18	0.14	Yes
AB-5y	540	530	irreversible	Low Ti-TM	3.51	0.34	No	SD2-2x	319, 515	512	reversible	High Ti-TM, low Ti-TM	3.73	0.15	No

Supplementary Table S2: Paleointensity results of the accepted specimens

Specimen	$T_{\min} - T_{\max}$ (°C)	N	β	f	q	MAD_{anc} (°)	α (°)	δCK (%)	δpal (%)	PI (μT)	σ_{PI} (μT)
Selection criteria used in the present study		≥ 5	≤ 0.1	≥ 0.5	≥ 5	$\leq 10^\circ$	$\leq 10^\circ$	$\leq 10\%$	$\leq 10\%$		$\leq 10\mu\text{T}$
1. <u>Michoacan-Guanajuato Volcanic Field (MGVF)</u>											
FCN5-1y	0-300	5	0.06	0.55	5.80	6.89	7.70	8.71	3.43	47.1	2.7
FCN5-2x	0-340	6	0.05	0.66	9.29	8.77	1.67	2.77	7.59	50.4	2.4
FCN5-3z	0-300	5	0.09	0.80	5.10	7.81	8.26	4.95	6.95	46.5	4.5
UTZ1-2z	0-500	12	0.08	0.91	7.21	3.42	3.64	5.70	3.15	53.4	4.3
UTZ1-3x	0-530	13	0.07	0.52	5.42	2.17	7.71	2.48	1.23	50.5	3.7
UTZ1-4y	0-510	12	0.02	0.95	27.31	1.64	1.12	2.41	1.35	38.5	0.8
UTZ1-6y	0-490	11	0.05	0.93	9.91	2.59	2.59	4.73	1.25	48.6	2.5
UTZ1-8y	0-530	13	0.06	0.95	11.10	2.65	3.84	4.07	5.36	60.8	3.9
UTZ1-11x	200-490	9	0.03	0.77	16.10	1.99	4.36	3.30	8.99	43.2	1.5
TP1-1z	0-460	10	0.08	0.57	5.83	3.59	9.51	6.64	0.46	57.5	4.7
TP1-2y	0-460	10	0.05	0.51	9.53	2.15	4.35	3.49	0.73	45.6	2.2
TP1-9x	0-460	10	0.06	0.52	6.92	3.30	8.21	2.19	6.32	49.7	3.1
JUN1-2y	0-430	8	0.03	0.82	20.20	1.71	0.77	3.08	4.47	65.4	2.2
JUN1-3y	0-400	8	0.05	0.93	14.40	1.72	1.27	3.84	0.05	56.7	2.8
JUN1-6x	0-480	9	0.04	0.83	16.90	1.89	1.86	3.01	4.11	71.1	2.7
JUN1-7z	0-400	8	0.05	0.98	8.50	2.03	0.90	7.50	6.04	50.6	2.4
PEL-10z	0-400	8	0.02	0.63	8.99	5.16	9.17	3.96	0.33	68.4	3.6
PEL-12x	0-400	8	0.08	0.65	6.47	5.16	9.17	4.65	6.71	70.0	5.5
PEL-14x	0-400	8	0.09	0.64	5.57	5.20	8.95	1.27	8.48	72.4	6.8
ML2-5x	0-340	6	0.07	0.70	6.71	8.30	9.42	4.45	6.40	37.2	2.8
ML2-7y	0-300	5	0.08	0.64	5.22	8.16	9.82	1.65	0.35	37.8	3.1
ML2-9x	0-300	5	0.06	0.51	5.66	5.43	8.94	4.35	5.05	40.9	2.5
CHU1-2x	0-340	6	0.05	0.94	12.42	9.08	6.67	6.41	7.65	47.4	2.3
CHU1-3z	0-340	6	0.05	0.88	8.98	3.00	1.98	5.66	8.64	37.1	2.1
CHU1-9x	0-300	5	0.05	0.56	8.30	3.82	5.53	4.96	1.92	45.0	2.1
TCM1-1y	0-460	10	0.05	0.96	14.45	2.82	3.07	5.49	7.65	64.5	3.2
TCM1-2z	0-460	10	0.04	0.92	21.16	4.73	5.78	6.39	3.85	62.3	2.3
TCM1-4y	0-460	10	0.03	0.97	21.73	2.89	2.84	5.08	0.65	61.1	2.0

TCM1-5y	0-460	10	0.03	0.86	22.41	1.49	1.56	3.94	7.93	67.1	2.0
DRC-1x	0-340	6	0.07	0.57	5.93	1.66	2.78	4.00	5.76	69.1	4.9
DRC-2z	0-430	9	0.09	0.69	5.15	4.19	6.35	3.62	3.40	75.0	7.4
DCR-5z	0-340	6	0.05	0.85	12.70	1.78	1.66	6.17	5.95	65.5	3.1
ZP1-4x	0-340	6	0.04	0.81	13.70	3.97	4.23	1.42	0.06	54.2	2.1
ZP1-12x	0-340	6	0.07	0.81	8.46	6.46	4.99	3.00	0.43	49.9	3.4
ZP1-14x	0-340	6	0.09	0.75	5.93	5.85	7.89	1.86	2.01	47.9	4.7
PI3-6x	0-490	11	0.05	0.77	8.23	3.48	5.22	1.22	3.39	24.9	1.3
PI3-9x	0-490	11	0.03	0.77	14.42	2.81	4.64	1.24	2.57	23.9	0.8
PI3-10y	250-490	8	0.03	0.79	24.58	6.35	6.04	3.24	3.76	23.9	0.6
Molc1-4x	0-460	10	0.05	0.69	10.50	5.15	9.13	3.65	7.17	26.2	1.4
Molc2-2Z	300-460	6	0.05	0.73	10.40	6.07	4.54	6.35	8.60	37.5	2.0
Molc2-4y	0-460	10	0.03	0.76	19.00	4.78	8.94	3.61	9.36	28.6	0.9
Pub1-2x	200-490	7	0.07	0.87	10.10	2.75	1.36	4.35	9.68	13.7	0.9
Pub1-4x	0-530	10	0.02	0.94	30.90	5.09	2.17	5.88	2.92	15.0	0.4
Pub1-5z	0-490	8	0.08	0.89	9.01	3.79	4.83	0.35	0.43	15.4	1.2
POP1-2z	0-560	14	0.04	0.61	13.00	2.40	3.37	2.49	0.97	31.3	1.2
Pop1-3y	0-460	14	0.03	0.66	14.00	1.48	1.51	2.42	2.52	31.3	1.1
POP1-4y	250-560	11	0.01	0.86	35.20	1.94	0.84	3.41	4.24	30.1	0.5
POP1-6x	0-560	14	0.04	0.96	23.40	4.46	2.40	4.73	9.01	22.4	0.8
POP1-8y	0-560	14	0.04	0.98	23.60	3.82	1.88	6.72	9.95	22.5	0.9
POP1-11z	0-560	14	0.03	0.93	27.60	2.77	1.26	4.79	2.61	31.1	0.8
ALE1-2y	0-530	10	0.08	0.99	9.87	1.22	0.22	5.89	3.61	80.8	6.7
ALE1-14z	0-510	7	0.08	1.00	5.22	1.43	0.62	3.74	3.34	62.7	5.3
ALE1-15y	0-460	7	0.07	0.59	5.13	1.02	1.38	5.61	3.10	70.0	5.0
CSD1-1x	0-460	10	0.09	0.82	6.06	8.72	4.51	7.46	9.31	30.1	3.0
CSD1-4z	0-460	10	0.09	0.72	6.32	6.16	6.60	2.62	6.95	30.3	2.8
CSD1-5x	0-400	8	0.09	0.76	6.04	4.60	3.06	3.96	0.75	30.5	2.8
CSD1-7z	0-460	10	0.08	0.78	7.80	7.79	8.41	2.74	0.93	30.8	2.5
CSD1-9x	0-460	10	0.09	0.63	5.20	5.49	9.86	2.85	4.80	33.8	3.2
RS1-2z	0-460	10	0.03	0.94	27.00	2.46	2.85	7.48	0.18	21.5	0.6
RS1-4z	0-460	10	0.05	0.93	15.30	2.14	1.07	5.29	1.77	19.8	0.9
RS1-6z	0-340	6	0.09	0.79	5.76	3.68	5.43	6.75	7.59	18.8	1.7
CAR1-2x	250-560	11	0.07	0.96	11.40	2.50	1.58	6.61	6.70	58.9	3.9
CAR1-3z	100-460	9	0.06	0.70	9.38	5.19	9.45	4.31	0.39	60.3	3.8
CAR1-12y	0-490	11	0.06	0.62	7.30	2.45	3.66	4.91	1.64	69.1	4.3
THT1-1x	0-530	12	0.05	0.99	15.80	6.70	2.73	1.47	0.74	13.6	0.7
THT1-10z	0-530	12	0.01	0.98	56.24	2.02	0.60	3.82	6.51	16.3	0.2
THT1-13x	0-400	9	0.05	0.77	9.89	1.38	1.52	2.99	5.95	24.8	1.3

JA3-13-4z	0-400	9	0.07	0.77	9.74	2.66	3.63	7.41	4.12	35.1	2.3
JA3-13-6y	0-400	9	0.07	0.73	8.01	2.37	3.03	8.01	2.04	38.7	2.9
JA3-13-7z	0-400	9	0.06	0.84	10.34	2.82	1.70	5.52	9.09	32.6	2.3
SD1-7y	0-460	8	0.02	0.71	24.40	5.67	8.93	3.01	1.86	48.2	0.9
SD1-8z	100-490	8	0.02	0.73	21.41	5.67	8.51	3.88	7.27	49.7	1.2
SD1-9x	0-490	7	0.08	0.58	5.03	4.33	8.01	5.03	7.70	35.0	2.7
SD2-1x	0-460	10	0.03	0.56	18.05	2.91	7.94	2.36	8.30	34.4	0.9
SD2-3x	0-460	10	0.05	0.51	7.94	3.66	8.71	5.26	9.20	35.3	1.8
SD2-4x	0-460	10	0.04	0.58	10.64	3.31	7.58	5.43	8.31	33.5	1.5

T_{\min} - T_{\max} : minimum and maximum temperature used to determine the paleointensity; N: number of points included in the linear best-fit; β : ratio of the standard error of the slope of the selected segment in the Arai plot to absolute value of the slope; f: NRM fraction used for the best-fit; q: quality factor; MAD_{anc} : anchored maximum angular deviation; α : angular difference between anchored and non-anchored best fit; δCK : relative check error; δpal : cumulative check difference; PI: paleointensity; σ_{PI} : standard deviation.

Supplementary Table S3: Mexican paleomagnetic database of accepted and rejected data according to the selection criteria set used in the present study. For every rejected data, the reason behind the deletion is indicated. New data obtained in the recent studies of Böhnel et al. (2016) and Mahgoub et al. (2017a, b; 2018) which are not yet inserted in the GEOMAGIA50.v3 database (Brown et al., 2015)

Age data		Location		Paleomagnetic direction			Paleointensity		meets quality criteria for direction and intensity	Reason for rejection	Reference
Age (AD)	σ Age (yr)	Dating method	Lat (°N)	Long (°W)	Dec (°)	Inc (°)	α_{95} (°)	PI $\pm \sigma$ PI (μ T)			
<u>The selection criteria outlines</u>											
1. We will accept the directions and intensities retrieved only from volcanic and archeological materials and abandoned the lake sediment and cave deposits archives (Latham et al., 1986).											
2. We will approve the ^{14}C and the thermoluminescence methods as a reliable dating technique. The archeological age will be accepted for the archeological artefacts particularly if they are corroborated with the radiocarbon data.											
3. The sampling sites were carefully checked and if we find sampling error we consider the results unreliable											
4. For the directional aspect, at least 5 specimens must be available to calculate the mean direction with $\alpha_{95} \leq 10^\circ$.											
5. The PI results obtained by Shaw (Shaw, 1974) and multispecimen (Dekkers and Böhnel, 2006) methods are not considered reliable because the required correction steps were not performed.											
. Paleointensity results attained by the Thellier-Thellier and Microwave techniques must meet the following											
. Thermal alteration monitoring by conducting the pTRM checks (Coe et al., 1978) should be included											
. The stability of the NRM directions during the paleointensity experiments should be notified											
. The anisotropy and cooling rate corrections must be investigated in case the archaeological artifacts treated											
. The PI-mean should be calculated from at least two specimens with a standard deviation $\leq 5 \mu\text{T}$ and $\leq 10 \mu\text{T}$, for the archaeological and volcanic materials, respectively.											

6. We put into consideration the difference between the current data and the previous only in case the same volcano was targeted which was the case for three flows, namely Pelado, El Pueblito, and Juanyan, we set an upper difference limit to $\pm 15^\circ$ for directions and $\pm 15\mu\text{T}$ for the intensities.

7. The paleomagnetic directions and intensities obtained from historical volcanoes, For example Paricutin must be within 10% of the observatory data, exceeding this value is one reason of excluding the result.

1. <u>Volcanic materials</u>												
-43448	2367	^{14}C	19.59	96.99	-3.68	23.14	5.8	not done	yes			Böhnel and Molina, 2002
<u>-37050</u>	<u>160</u>	^{14}C	19.22	99.27	-17.29	21.77	2.9	41.14 \pm 6	no		unreliable age data	Morales et al., 2001
<u>-37000</u>	<u>7000</u>	Ar-Ar + helium exp.	30.48	116.10	-7.10	19.09	2.8	<u>14.65\pm1.4</u>	no		unreliable age + MSP-method	Böhnel et al., 2009
<u>-37000</u>	<u>7000</u>	Ar-Ar + helium exp.						13.87 \pm 2.0	no		unreliable age data	Böhnel et al., 2009
-29920	4100	^{14}C	20.66	103.46	5.25	23.27	7.7	not done	yes			Böhnel and Molina, 2002
-24305	820	^{14}C	19.22	99.47	-6.95	64.53	3.4	19.45 \pm 5.3	yes			Gonzales et al., 1997
-23236	2560	^{14}C	19.82	101.92	3.44	39.58	5.1	<u>24.08\pm12.8</u>	yes only for direction		PI obtained by Shaw method	Gonzales et al., 1997
-23236	2560	^{14}C	19.82	101.92	<u>21.66</u>	<u>34.62</u>	<u>3.2</u>	not done	no		Direction exceed the threshold difference (see text for details)	Conte-Fasano et al., 2006
-23050	4000	relative chronology	19.52	101.66	-55.59	26.21	5.9	not done	no		unreliable age data	Conte-Fasano et al., 2006
-21553	435	^{14}C	19.17	99.42	-17.36	16.91	4.2	<u>27.49\pm6.4</u>	yes only for direction		PI obtained by Shaw method	Gonzales et al., 1997
<u>-21000</u>	<u>0</u>	Helium exposure age	30.46	116.04	7.37	22.8	4.2	12.05 \pm 0.8	no		unreliable age data	Böhnel et al., 2009
<u>-21000</u>	<u>0</u>	Helium exposure age						11.27 \pm 2.5	no		unreliable age data	Böhnel et al., 2009
-20842	1420	^{14}C	19.22	99.21	-0.90	34.02	5.8	29.78 \pm 5.7	yes			Gonzales et al., 1997
<u>-18050</u>	<u>20000</u>	relative chronology	19.66	102.03	6.59	40.72	2.5	34.28 \pm 3.24	no		unreliable age data	Conte-Fasano et al., 2006
<u>-18050</u>	<u>20000</u>	relative chronology	19.00	102.20	-21.89	15.18	2.1	not done	no		unreliable age data	Conte-Fasano et al., 2006
<u>-15220</u>	<u>430</u>	^{14}C	19.71	101.42	-21.05	57.25	4.6	43.89 \pm 7.1	no		unreliable age data	Gonzales et al., 1997
<u>-15220</u>	<u>430</u>	^{14}C	19.70	101.40	-13.80	3.02	2.2	not done	no		unreliable age data	Conte-Fasano et al., 2006
-9895	249	^{14}C	19.10	99.18	-5.42	41.24	5.1	27.11 \pm 5.3	yes			Gonzales et al., 1997

-9409	1208	¹⁴ C	19.18	99.17	10.41	17.47	3.9	<u>25.98±8.8</u>	yes only for direction	PI exceed the threshold difference (see text for details)	Morales et al., 2001
-9409	1208	¹⁴ C	19.14	99.17	<u>-8.20</u>	<u>12.94</u>	<u>7.9</u>	76.19±7.59	Yes	Direction exceed the threshold difference (see text for details)	Gonzales et al., 1997
-9409	1208	¹⁴ C	19.14	99.17				<u>32.49±0.76</u>	no	PI obtained by Shaw method	Gonzales et al., 1997
-8523	800	¹⁴ C	19.67	101.98	<u>42.92</u>	<u>13.87</u>	5.3	49.05±9.7	yes only for intensity	Direction exceed the threshold difference (see text for details)	Gonzales et al., 1997
-7470	119	¹⁴ C	19.01	99.50	-21.67	50.59	3.7	42.92±10	yes		Vlag et al., 2000
-7470	119	¹⁴ C	19.12	99.49	-22.80	56.05	3.1	<u>44.67±17.2</u>	yes only for direction	PI obtained by Shaw method	Gonzales et al., 1997
-7466	587	¹⁴ C	19.53	101.69	-23.16	28.58	4.2	not done	yes		Conte-Fasano et al., 2006
<u>-1880</u>	<u>150</u>	¹⁴ C	19.45	102.11	19.95	46.07	<u>19.4</u>	28.89±5.5	no	unreliable age, $\alpha_{95} > 10^\circ$, Shaw method	Gonzales et al., 1997
<u>-1880</u>	<u>150</u>	¹⁴ C	19.42	102.13	-10.17	25.23	2.2	not done	no	unreliable age data	Conte-Fasano et al., 2006
-980	55	¹⁴ C	19.65	96.96	7.59	26.97	3.8	not done	yes		Böhnel and Molina, 2002
-285	80	¹⁴ C	19.05	98.45	-7.39	39.25	3.9	not done	yes		Böhnel and Molina, 2002
373	56	¹⁴ C	19.93	99.18	-7.98	35.25	2.5	54.46±6.6	yes		Morales et al., 2001
373	56	¹⁴ C	19.30	99.18	1.10	34.3	2.1	59.99±7.7	yes		Alva Valdivia, 2005
373	56	¹⁴ C	19.32	99.18	-9.91	35.55	2	<u>66.89±10.1</u>	yes only for direction	PI-mean uncertainty > 10 μ T	Gonzales et al., 1997
373	56	¹⁴ C	19.08	99.13	-13.33	36.4	1.7	53.63±4.2	yes		Böhnel et al., 2003
373	56	¹⁴ C	19.30	99.20		not done		59.69±3.5	no		Morales et al., 2006
373	56	¹⁴ C	19.08	99.13	-13.33	36.4	1.7	63.17±2.7	yes		Böhnel et al., 1997
1130	88	¹⁴ C	19.40	96.90	-15.04	35.27	1.8	not done	yes		Böhnel and Molina, 2002
1250	50	¹⁴ C	19.57	102.01	<u>82.73</u>	<u>44.96</u>	4.4	52.81±4.2	yes only for intensity	Declination is rare	Gonzales et al., 1997
1250	50	¹⁴ C	19.57	102.20	16.44	25.69	1.9	not done	no	Sampling error encountered	Conte-Fasano et al., 2006

1550	8	Historical	21.14	104.50	0.08	34.04	3.2	not done	yes		Böhnel and Molina, 2002	
1545	5	Historical	19.01	97.29				not done	<u>61.92±1.3</u>	no	PI obtained by MSP method	Michalk et al., 2008
1550	5	Historical	21.18	104.53				not done	<u>63.59±6.0</u>	no	PI obtained by MSP method	Michalk et al., 2008
1766	7	Historical	19.00	101.75	8.00	56.36	3.8		48.28±5.71	yes		Conte-Fasano et al., 2006
1766	7	Historical	19.48	102.25					43.17±3.5			Gratton et al., 2005
1766	7	Historical	19.48	102.25	7.54	51.09	2.6		53.47±9.2	yes		Gratton et al., 2005
1766	7	Historical	19.50	102.00				not done	<u>44.96±na</u>	no	PI obtained by MSP method	Dekkers and Böhnel, 2006
1870	1	Historical	21.10	104.59				not done	<u>52.88±6.0</u>	no	PI obtained by MSP method	Michalk et al., 2008
1943	0	Historical	19.00	102.00				not done	<u>46.14±3.2</u>	no	PI obtained by MSP method	Dekkers and Böhnel, 2006
1943	1	Historical	19.32	104.12				not done	<u>47.10±1.4</u>	no	PI obtained by MSP method	Michalk et al., 2008
1944	2	Historical	19.53	102.25	47.76	30.95	7.3		not done	no	very rare direction	Conte-Fasano et al., 2006
1945	1	Historical	19.47	102.25				not done	34.98± <u>19.0</u>	no	PI-mean uncertainty>10μT	Goguitchaichvili et al., 2005
1945	5	Historical	19.47	102.25					43.78± <u>19.8</u>		PI-mean uncertainty>10μT	Urrutia-Fucugauchi et al., 2004
1945	5	Historical	19.47	102.25	1.71	37.57	8.7		34.98± <u>19.0</u>	yes only for direction	PI-mean uncertainty>10μT	Urrutia-Fucugauchi et al., 2004
1948	5	Historical	19.50	102.20	10.60	38.47	4.4		<u>40.71±4.79</u>	yes only for direction	PI obtained by Shaw method	Gonzales et al., 1997
1948	5	Historical	19.50	102.20	10.60	38.47	4.4		<u>61.80±8.17</u>	yes only for direction	Observatory data gave ~45 μT	Gonzales et al., 1997
2. Archeological materials												
-1191	215	¹⁴ C	19.95	102.3				not done	39.94±3.0	yes		Duran et al., 2010
-1191	215	¹⁴ C	19.95	102.3				not done	37.85±2.5	yes		Duran et al., 2010
-1191	215	¹⁴ C	19.95	102.3				not done	32.29±1.0	yes		Duran et al., 2010
-1191	215	¹⁴ C	19.95	102.3				not done	35.37±1.6	yes		Duran et al., 2010
-1191	215	¹⁴ C	19.95	102.3				not done	33.58±1.7	yes		Duran et al., 2010
-1191	215	¹⁴ C	19.95	102.3				not done	34.87±1.8	yes		Duran et al., 2010
-1191	215	¹⁴ C	19.95	102.3				not done	33.58±4.8	yes		Duran et al., 2010

-1191	215	¹⁴ C	19.95	102.3	not done	24.84±2.3	yes		Duran et al., 2010
-1191	215	¹⁴ C	19.95	102.3	not done	39.2±1.4	yes		Duran et al., 2010
-1191	215	¹⁴ C	19.95	102.3	not done	32.99±3.0	yes		Duran et al., 2010
-1191	215	¹⁴ C	19.95	102.3	not done	35.3± 8.0	no	PI-uncertainty>5μT	Duran et al., 2010
-1191	215	¹⁴ C	19.95	102.3	not done	29.21± 6.5	no	PI-uncertainty>5μT	Duran et al., 2010
-1191	215	¹⁴ C	19.95	102.3	not done	34.67± 5.7	no	PI-uncertainty>5μT	Duran et al., 2010
-1191	215	¹⁴ C	19.95	102.3	not done	29.41± 5.6	no	PI-uncertainty>5μT	Duran et al., 2010
-1275	125	Archeological age	17.08	96.75	not done	36.93 ±4.0	no	unreliable anisotropy correction	Petronille et al., 2012
-1275	125	Archeological age	17.08	96.75	not done	25.41 ±2.5	no	unreliable anisotropy correction	Petronille et al., 2012
-1275	125	Archeological age	17.08	96.75	not done	28.8 ± 5.5	no	unreliable anisotropy; uncertainty>5μT	Petronille et al., 2012
-1000	150	Archeological age	17.15	96.80	not done	28.57 ± 5.3	no	unreliable anisotropy; uncertainty>5μT	Petronille et al., 2012
-1000	150	Archeological age	17.15	96.80	not done	24.15 ±2.3	no	unreliable anisotropy correction	Petronille et al., 2012
-1000	150	Archeological age	17.15	96.80	not done	35.05 ±2.3	no	unreliable anisotropy correction	Petronille et al., 2012
-830	280	¹⁴ C	19.00	104.00	not done	47.85 ± 3.8	no	Not including any PI-criteria	Bucha et al., 1970
-825	225	¹⁴ C	19.00	104.00	not done	51.27 ± 0.3	no	Not including any PI-criteria	Bucha et al., 1970
-775	75	Archeological age	17.15	96.80	not done	33.92 ±3.1	no	unreliable anisotropy correction	Petronille et al., 2012
-350	75	Archeological age	16.70	93.20	not done	55.07 ± 5.1	no	Not including any PI-criteria	Lee, 1975
-325	217	Archeological age + ¹⁴ C	16.73	93.26	not done	54.33 ± 7.2	no	unreliable anisotropy; uncertainty>5μT	Morales et al., 2009
-300	0	Archeological age	19.60	92.70	not done	54.88 +na	no	Not including any PI-criteria	Lee, 1975
-240	180	¹⁴ C	19.48	98.83	not done	26.33 ±4.9	no	exceeded the MADanc and α- angles threshold value	Rodríguez-Ceja et al., 2009

-200	75	Archeological age	16.60	93.50				not done	<u>49.96±1.3</u>	no	Not including any PI-criteria	Lee, 1975
-200	75	Archeological age	16.60	93.50				not done	<u>45.00±0.7</u>	no	Not including any PI-criteria	Lee, 1975
-200	75	Archeological age	16.70	93.30				not done	<u>47.63±na</u>	no	Not including any PI-criteria	Lee, 1975
-200	100	Archeological age	19.00	104.00				not done	<u>53.48±3.4</u>	no	Not including any PI-criteria	Bucha et al., 1970
-150	150	Archeological age	19.35	99.16				not done	<u>55.95±5.4</u>	no	Not including any PI-criteria	Nagata et al., 1965
-125	0	Archeological age + ¹⁴ C	16.40	92.70	-4.55	24.15	1.5	not done		yes		Eighmy and Sternberg, 1990
-100	200	Archeological age	19.00	104.00				not done	<u>49.16±na</u>	no	Not including any PI-criteria	Bucha et al., 1970
-100	200	Archeological age	18.40	103.80				not done	<u>87.90±na</u>	no	Not including any PI-criteria	Bucha et al., 1970
-100	200	Archeological age	19.00	104.00				not done	<u>48.55±na</u>	no	Not including any PI-criteria	Bucha et al., 1970
-62	63	Archeological age	16.70	93.20				not done	<u>41.12±1.1</u>	no	Not including any PI-criteria	Lee, 1975
-62	63	Archeological age	16.70	93.20				not done	<u>51.66±na</u>	no	Not including any PI-criteria	Lee, 1975
-25	225	Archeological age + ¹⁴ C	16.90	96.30	-2.58	39.8	2.9	not done		yes		Eighmy and Sternberg, 1990
-25	225	Archeological age + ¹⁴ C	17.00	96.70	-0.50	38.68	1.7	not done		yes		Eighmy and Sternberg, 1990
-25	225	Archeological age + ¹⁴ C	17.00	96.70	0.44	42.48	2.5	not done		yes		Eighmy and Sternberg, 1990
1	170	Archeological age	19.00	104.00				not done	<u>62.83±na</u>	no	Not including any PI-criteria	Bucha et al., 1970
50	50	Archeological age	19.00	104.00				not done	<u>53.68±na</u>	no	Not including any PI-criteria	Bucha et al., 1970
100	200	¹⁴ C	19.00	104.00				not done	<u>83.84±0.2</u>	no	Not including any PI-criteria	Bucha et al., 1970
113	112	Archeological age	16.70	93.20				not done	<u>37.19±0.8</u>	no	Not including any PI-criteria	Lee, 1975
300	100	Archeological age	15.00	92.20				not done	<u>44.23±1.4</u>	no	Not including any PI-criteria	Lee, 1975
325	100	¹⁴ C	19.00	104.00				not done	<u>70.17±na</u>	no	Not including any PI-criteria	Bucha et al., 1970
373	56	¹⁴ C	19.08	99.13				not done	67.09± <u>7.1</u>	no	PI-uncertainty>5μT	Böhnel et al., 2003
450	300	Archeological age	19.00	104.00				not done	<u>41.42±na</u>	no	Not including any PI-criteria	Bucha et al., 1970
450	300	Archeological age	18.40	103.80				not done	<u>74.13±na</u>	no	Not including any PI-criteria	Bucha et al., 1970
450	50	Archeological age	17.48	92.04				not done	29.79±0.9	yes		Fanjat et al., 2013

485	85	Archeological age + ¹⁴ C	19.85	100.75	not done	<u>36.61</u>±1.6	no	unreliable anisotropy correction	Aguilar-Reyes et al., 2013
535	105	Archeological age + ¹⁴ C	19.85	100.75	not done	<u>37.01</u>±3.4	no	unreliable anisotropy correction	Aguilar-Reyes et al., 2013
542	107	Archeological age + ¹⁴ C	19.85	100.75	not done	<u>35.02</u>±1.3	no	unreliable anisotropy correction	Aguilar-Reyes et al., 2013
<u>500</u>	<u>50</u>	Unknown	17.00	102.00	not done	<u>41.96</u>±17	no	lack PI-criteria, uncertainty>5μT	Aitken et al., 1991
518	130	Archeological age + ¹⁴ C	16.73	93.26	not done	61.45± <u>13.8</u>	no	unreliable anisotropy; uncertainty>5μT	Morales et al., 2009
518	130	Archeological age + ¹⁴ C	16.73	93.26	not done	<u>15.1</u>±1.5	no	unreliable anisotropy correction	Morales et al., 2009
518	130	Archeological age + ¹⁴ C	16.73	93.26	not done	<u>51.33</u>±5.2	no	unreliable anisotropy; uncertainty>5μT	Morales et al., 2009
518	130	Archeological age + ¹⁴ C	16.73	93.26	not done	<u>26.44</u>±0.9	no	unreliable anisotropy correction	Morales et al., 2009
550	50	Archeological age	17.48	92.04	not done	33.27±1.2	yes		Fanjat et al., 2013
600	100	Archeological age	19.00	104.00	not done	<u>49.46</u>±5.2	no	Not including any PI-criteria	Bucha et al., 1970
600	100	Archeological age	19.00	104.00	not done	<u>48.86</u>±2.4	no	Not including any PI-criteria	Bucha et al., 1970
650	50	Archeological age	17.48	92.04	not done	31.23±1.1	yes		Fanjat et al., 2013
750	20	Archeological age	17.48	92.04	not done	31.23±0.6	yes		Fanjat et al., 2013
800	100	Archeological age	15.00	92.20	not done	<u>45.28</u>±2.8	no	Not including any PI-criteria	Lee, 1975
810	40	Archeological age	17.48	92.04	not done	32.45±0.7	yes		Fanjat et al., 2013
817	164	Archeological age + ¹⁴ C	16.73	93.26	not done	<u>49.37</u>±5.5	no	unreliable anisotropy; uncertainty>5μT	Morales et al., 2009
850	50	Archeological age	20.60	99.30	not done	<u>52.23</u>±0.1	no	Not including any PI-criteria	Bucha et al., 1970
900	100	Archeological age	16.40	92.70	not done	<u>42.00</u>±0.7	no	Not including any PI-criteria	Lee, 1975
1000	100	Archeological age	19.80	103.10	not done	<u>55.54</u>±0.2	no	Not including any PI-criteria	Bucha et al., 1970
1000	100	Archeological age	19.80	103.10	not done	<u>61.22</u>±na	no	Not including any PI-criteria	Bucha et al., 1970

1000	100	Archeological age	15.00	92.20	not done				<u>51.08±0.7</u>	no	Not including any PI-criteria	Lee, 1975
1050	50	Archeological age	22.10	105.30	not done				<u>68.55±na</u>	no	Not including any PI-criteria	Bucha et al., 1970
1168	0	Archeological age	20.00	99.30	not done				<u>63.35±1.0</u>	no	Not including any PI-criteria	Lee, 1975
1168	0	Archeological age	20.00	99.30	not done				<u>64.84±3.9</u>	no	Not including any PI-criteria	Lee, 1975
1350	150	Archeological age	22.10	105.30	not done				<u>61.30±1.8</u>	no	Not including any PI-criteria	Bucha et al., 1970
1350	150	Archeological age	19.00	98.30	not done				<u>48.76±0.7</u>	no	Not including any PI-criteria	Lee, 1975
1400	100	Archeological age	22.00	105.00	not done				<u>54.02±na</u>	no	Not including any PI-criteria	Bucha et al., 1970
1575	75	Archeological age	19.00	98.30	not done				<u>47.25±1.2</u>	no	Not including any PI-criteria	Lee, 1975
<u>1600</u>	<u>50</u>	<u>Unknown</u>	16.80	102.00	not done				<u>40.73±16.8</u>	no	lack PI-criteria, uncertainty>5μT	Aitken et al., 1991
<u>1600</u>	<u>50</u>	<u>Unknown</u>	16.20	102.00	not done				<u>37.98±16.2</u>	no	lack PI-criteria, uncertainty>5μT	Aitken et al., 1991
<u>1625</u>	<u>75</u>	<u>Unknown</u>	17.50	102.00	not done				<u>44.23±17.5</u>	no	lack PI-criteria, uncertainty>5μT	Aitken et al., 1991
1761	211	Archeological age	17.30	96.80	not done				<u>44.12±1.4</u>	no	Not including any PI-criteria	Lee, 1975
1971	0	Archeological age	19.00	98.30	not done				<u>47.05±1.3</u>	no	Not including any PI-criteria	Lee, 1975
<u>1100</u>	<u>100</u>	paleomagnetic dating	19.04	98.2	16.96	44.25	5.3	not done		no	unreliable age data	Goguitchaichvili et al., 2004
<u>1100</u>	<u>100</u>	paleomagnetic dating	19.06	98.31	-20.14	47.83	7.5	not done		no	unreliable age data	Goguitchaichvili et al., 2004
<u>1100</u>	<u>100</u>	paleomagnetic dating	19.06	98.31	-8.07	48.85	<u>10.4</u>	not done		no	unreliable age data, $\alpha_{95} > 10^\circ$	Goguitchaichvili et al., 2004
<u>1100</u>	<u>100</u>	paleomagnetic dating	19.24	98.34	-11.32	35.60	10	not done		no	unreliable age data	Goguitchaichvili et al., 2004
425	75	Archeological age + ¹⁴ C	19.00	98.20	2.86	39.54	0.8	not done		yes		Eighmy and Sternberg, 1990
425	75	Archeological age + ¹⁴ C	19.00	98.20	-0.15	39.11	2.6	not done		yes		Eighmy and Sternberg, 1990
512	87	Archeological age + ¹⁴ C	19.70	98.80	7.05	49.65	3	not done		yes		Eighmy and Sternberg, 1990
550	150	Archeological age + ¹⁴ C	17.00	96.70	-5.50	34.53	2.6	not done		yes		Eighmy and Sternberg, 1990

550	150	Archeological age + ¹⁴ C	17.00	96.70	-5.10	38.08	3	not done	yes	Eighmy and Sternberg, 1990
550	25	Archeological age	19.04	98.20	-3.16	39.12	3.6	not done	yes	Soler et al.,2006
562	12	Archeological age	19.04	98.20	0.46	40.43	9.8	not done	yes	Soler et al.,2006
575	150	Archeological age + ¹⁴ C	19.70	98.80	3.00	38.7	0.6	not done	yes	Eighmy and Sternberg, 1990
575	150	Archeological age + ¹⁴ C	19.70	98.80	2.22	40.21	0.9	not done	yes	Eighmy and Sternberg, 1990
575	150	Archeological age + ¹⁴ C	19.70	98.80	1.02	39.62	1	not done	yes	Eighmy and Sternberg, 1990
575	150	Archeological age + ¹⁴ C	19.70	98.80	2.42	40.41	1.6	not done	yes	Eighmy and Sternberg, 1990
575	150	Archeological age + ¹⁴ C	19.70	98.80	5.42	42.91	3.6	not done	yes	Eighmy and Sternberg, 1990
575	150	Archeological age + ¹⁴ C	19.70	98.80	2.43	42.32	3	not done	yes	Eighmy and Sternberg, 1990
575	150	Archeological age + ¹⁴ C	19.70	98.80	2.12	40.72	3.1	not done	yes	Eighmy and Sternberg, 1990
575	150	Archeological age + ¹⁴ C	19.70	98.80	3.91	39.8	3.3	not done	yes	Eighmy and Sternberg, 1990
600	150	Archeological age	19.20	99.56	-6.60	33.08	10.25	not done	yes	Lopez-Delgado et al., 2010
700	200	Archeological age + ¹⁴ C	19.00	98.30	-2.81	34.21	1.9	not done	yes	Eighmy and Sternberg, 1990
750	50	Archeological age + ¹⁴ C	16.90	96.30	0.55	19.84	1.2	not done	yes	Eighmy and Sternberg, 1990
850	100	Archeological age + ¹⁴ C	20.10	98.40	-1.29	23.05	1.9	not done	yes	Eighmy and Sternberg, 1990
850	100	Archeological age + ¹⁴ C	20.10	98.40	1.61	24.71	2.5	not done	yes	Eighmy and Sternberg, 1990
900	100	Archeological age + ¹⁴ C	16.40	92.70	-4.93	17.54	1.9	not done	yes	Eighmy and Sternberg, 1990
950	250	Archeological age + ¹⁴ C	17.10	96.80	-5.58	21.54	1.9	not done	yes	Eighmy and Sternberg, 1990
950	250	Archeological age + ¹⁴ C	17.10	96.80	-5.01	19.97	2.1	not done	yes	Eighmy and Sternberg, 1990
1050	150	Archeological age + ¹⁴ C	16.90	96.30	-11.92	34.56	2.7	not done	yes	Eighmy and Sternberg, 1990
1050	150	Archeological age + ¹⁴ C	16.90	96.30	-11.36	32.57	2.9	not done	yes	Eighmy and Sternberg, 1990
1050	150	Archeological age + ¹⁴ C	16.90	96.30	-12.15	37.18	3.4	not done	yes	Eighmy and Sternberg, 1990
1075	125	Archeological age + ¹⁴ C	20.00	99.30	-13.55	39.99	1.9	not done	yes	Eighmy and Sternberg, 1990
1075	125	Archeological age + ¹⁴ C	20.00	99.30	-15.84	33.70	2.4	not done	yes	Eighmy and Sternberg, 1990

1175	25	Archeological age + ¹⁴ C	20.00	99.30	-12.65	35.22	1.1	not done	yes	Eighmy and Sternberg, 1990
1175	25	Archeological age + ¹⁴ C	20.00	99.30	-14.95	33.49	1.2	not done	yes	Eighmy and Sternberg, 1990
1175	25	Archeological age + ¹⁴ C	20.00	99.30	-14.45	29.44	1.5	not done	yes	Eighmy and Sternberg, 1990
1175	25	Archeological age + ¹⁴ C	20.00	99.30	-13.55	34.81	2.5	not done	yes	Eighmy and Sternberg, 1990
1175	25	Archeological age + ¹⁴ C	20.00	99.30	-17.73	41.61	3.4	not done	yes	Eighmy and Sternberg, 1990
1175	25	Archeological age + ¹⁴ C	20.00	99.30	-37.41	49.89	3.9	not done	yes	Eighmy and Sternberg, 1990

3. Stalagmite

726	50	U-Th method	22.09	99.00	-3.50	19.88	5.5	not done	no	unaccepted material stalagmite	Latham et al., 1986
770	50	U-Th method	22.09	99.00	-6.91	28.79	5	not done	no	unaccepted material stalagmite	Latham et al., 1986
815	50	U-Th method	22.09	99.00	-10.38	26.19	2.6	not done	no	unaccepted material stalagmite	Latham et al., 1986
855	50	U-Th method	22.09	99.00	-17.77	29.01	1.6	not done	no	unaccepted material stalagmite	Latham et al., 1986
900	50	U-Th method	22.09	99.00	-19.24	29.58	3.5	not done	no	unaccepted material stalagmite	Latham et al., 1986
945	50	U-Th method	22.09	99.00	-16.77	30.04	3.6	not done	no	unaccepted material stalagmite	Latham et al., 1986
990	50	U-Th method	22.09	99.00	-15.79	28.96	4.1	not done	no	unaccepted material stalagmite	Latham et al., 1986
1030	50	U-Th method	22.09	99.00	-13.33	28.90	3.5	not done	no	unaccepted material stalagmite	Latham et al., 1986
1075	50	U-Th method	22.09	99.00	-3.50	19.88	5.5	not done	no	unaccepted material stalagmite	Latham et al., 1986
1120	50	U-Th method	22.09	99.00	-7.89	29.87	5.2	not done	no	unaccepted material stalagmite	Latham et al., 1986
1160	50	U-Th method	22.09	99.00	-5.93	28.25	5.9	not done	no	unaccepted material stalagmite	Latham et al., 1986
1205	50	U-Th method	22.09	99.00	-3.47	27.16	6.6	not done	no	unaccepted material stalagmite	Latham et al., 1986
1250	50	U-Th method	22.09	99.00	-3.46	28.22	5.5	not done	no	unaccepted material stalagmite	Latham et al., 1986
1290	50	U-Th method	22.09	99.00	-1.49	29.27	5.4	not done	no	unaccepted material stalagmite	Latham et al., 1986
1340	50	U-Th method	22.09	99.00	-1.98	28.74	4.8	not done	no	unaccepted material stalagmite	Latham et al., 1986
1380	50	U-Th method	22.09	99.00	-4.45	29.29	5	not done	no	unaccepted material stalagmite	Latham et al., 1986
1425	50	U-Th method	22.09	99.00	1.47	25.54	4	not done	no	unaccepted material stalagmite	Latham et al., 1986

1470	50	U-Th method	22.09	99.00	-1.49	27.68	4	not done	no	unaccepted material stalagmite	Latham et al., 1986
1515	50	U-Th method	22.09	99.00	-0.02	23.96	5	not done	no	unaccepted material stalagmite	Latham et al., 1986
1555	50	U-Th method	22.09	99.00	0.97	22.38	3.3	not done	no	unaccepted material stalagmite	Latham et al., 1986
1600	50	U-Th method	22.09	99.00	-0.02	23.96	3.1	not done	no	unaccepted material stalagmite	Latham et al., 1986
1640	50	U-Th method	22.09	99.00	4.43	26.08	4.1	not done	no	unaccepted material stalagmite	Latham et al., 1986
1690	50	U-Th method	22.09	99.00	6.40	27.14	4.5	not done	no	unaccepted material stalagmite	Latham et al., 1986
1730	50	U-Th method	22.09	99.00	10.35	28.77	4.5	not done	no	unaccepted material stalagmite	Latham et al., 1986
1775	50	U-Th method	22.09	99.00	13.80	28.28	7.4	not done	no	unaccepted material stalagmite	Latham et al., 1986
1820	50	U-Th method	22.09	99.00	14.80	26.71	7.1	not done	no	unaccepted material stalagmite	Latham et al., 1986
1860	50	U-Th method	22.09	99.00	13.80	28.81	7.4	not done	no	unaccepted material stalagmite	Latham et al., 1986
1905	50	U-Th method	22.09	99.00	11.30	34.64	5	not done	no	unaccepted material stalagmite	Latham et al., 1986

Paleomagnetic data not included in Geomagia

-3901	246	¹⁴ C	19.13	101.48	3.53	38.03	1.5	62.97± 21.96	Yes for only direction	PI-uncertainty>10μT	Mahgoub et al., 2017b
-1472	52	¹⁴ C	19.85	101.84	-3.98	51.37	3.2	41.65±6.99	yes		Mahgoub et al., 2018
1250	5	¹⁴ C	19.54	101.99	-10.08	34.83	1.9	55.50±6.64	yes		Mahgoub et al., 2017a
1870	0	Historical	21.0	104.58	7.04	40.96	3.1	44.48±6.28	yes		Böhnel et al., 2016
-240	160	14C	19.69	98.84				71.2±4.1	yes		Mahgoub et al., Submitted
-240	160	14C	19.69	98.84				55.1±3.3	yes		Mahgoub et al., Submitted
-240	160	14C	19.69	98.84				58.9±4.6	yes		Mahgoub et al., Submitted
275	75	14C	19.69	98.84				27.8±0.6	yes		Mahgoub et al., Submitted
330	90	14C	19.69	98.84				34.5±2.2	yes		Mahgoub et al., Submitted
385	36	14C	19.69	98.84				42.9±1.0	yes		Mahgoub et al., Submitted
385	35	14C	19.69	98.84				49.6±1.5	yes		Mahgoub et al., Submitted

485	65	14C	19.69	98.84	not done	27.2±1.5	yes	Mahgoub et al., Submitted
750	150	14C	19.69	98.84	not done	32.9±3.1	yes	Mahgoub et al., Submitted
750	150	14C	19.69	98.84	not done	36.4±4.5	yes	Mahgoub et al., Submitted
750	50	14C	19.69	98.84	not done	37.1±4.4	yes	Mahgoub et al., Submitted
750	50	14C	19.69	98.84	not done	21.5±2.2	yes	Mahgoub et al., Submitted
750	50	14C	19.69	98.84	not done	40.6±3.6	yes	Mahgoub et al., Submitted
750	50	14C	19.69	98.84	not done	16.3±3.9	yes	Mahgoub et al., Submitted
750	50	14C	19.69	98.84	not done	28.6±0.7	yes	Mahgoub et al., Submitted
975	125	14C	19.69	98.84	not done	39.2±2.6	yes	Mahgoub et al., Submitted
975	125	14C	19.69	98.84	not done	50.4±1.5	yes	Mahgoub et al., Submitted
975	125	14C	19.69	98.84	not done	40.0±1.8	yes	Mahgoub et al., Submitted
975	125	14C	19.69	98.84	not done	40.1±4.0	yes	Mahgoub et al., Submitted
975	125	14C	19.69	98.84	not done	37.0±2.9	yes	Mahgoub et al., Submitted
975	125	14C	19.69	98.84	not done	34.9±1.3	yes	Mahgoub et al., Submitted
1400	100	14C	19.69	98.84	not done	39.4±2.1	yes	Mahgoub et al., Submitted
1400	100	14C	19.69	98.84	not done	35.1±3.3	yes	Mahgoub et al., Submitted
1400	100	14C	19.69	98.84	not done	34.3±2.3	yes	Mahgoub et al., Submitted
1435	100	14C	19.69	98.84	not done	48.2±2.8	yes	Mahgoub et al., Submitted
-1550	50	14C+Archeological age	17.75	94.76	not done	18.2±3.0	yes	Mahgoub et al., Submitted
-1550	50	14C+Archeological age	17.75	94.76	not done	32.4±4.0	yes	Mahgoub et al., Submitted
-1300	100	14C+Archeological age	17.75	94.76	not done	37.7±4.8	yes	Mahgoub et al., Submitted
-1300	100	14C+Archeological age	17.75	94.76	not done	23.6±0.8	yes	Mahgoub et al., Submitted
-1100	100	14C+Archeological age	17.75	94.76	not done	29.5±0.9	yes	Mahgoub et al., Submitted
-1100	100	14C+Archeological age	17.75	94.76	not done	44.8±2.5	yes	Mahgoub et al., Submitted

-1100	100	14C+Archeological age	17.75	94.76	not done	54.6±3.7	yes	Mahgoub et al., Submitted
373	56	14C	19.33	99.19	not done	62.8±1.5	yes	Mahgoub et al., Submitted
373	56	14C	19.33	99.19	not done	58.5±1.2	yes	Mahgoub et al., Submitted
1800	0	Historical	20.59	100.40	not done	50.3±3.2	yes	Mahgoub et al., Submitted
1800	0	Historical	20.59	100.40	not done	43.9±3.4	yes	Mahgoub et al., Submitted
1800	0	Historical	20.59	100.40	not done	46.0±2.5	yes	Mahgoub et al., Submitted
-1216	87	14C	19.65	96.96	not done	52.8±7.6	yes	Mahgoub et al., Submitted
-285	80	14C	19.00	98.48	not done	76.8±4.2	yes	Mahgoub et al., Submitted
181	220	14C	18.45	95.10	not done	53.9±7.2	yes	Mahgoub et al., Submitted
1070	60	14C	19.40	96.90	not done	54.9±4.9	yes	Mahgoub et al., Submitted
1793	0	Historical	18.58	95.19	not done	61.6±8.8	yes	Mahgoub et al., Submitted
8	62	14C	19.18	99.31	not done	46.4±3.8	yes	Mahgoub et al., Submitted
-380	23	14C	19.61	102.07	not done	32.7±4.8	yes	Mahgoub et al., Submitted

Supplementary Table S3 references

- Reyes, A., Goguitchaichvili, B.A., Morales, J., Garduño, V.H., Pineda, M., Carvallo, C., Moran, T.G., Israde, I., Rathert, M.C., 2013. An integrated archeomagnetic and C14 study on pre-Columbian potsherds and associated charcoals intercalated between Holocene lacustrine sediments in Western Mexico: Geomagnetic implications. *J. Geophys. Res.* 118, 2753–2763, <http://dx.doi.org/10.1002/jgrb.50196>.
- Aitken MJ, Pesonen LJ, Leino M (1991) The Thellier paleointensity technique: Minisamples versus standard size. *J Geomagn Geoelectr* 43: 325–331.
- Alva-Valdivia LM (2005) Comprehensive paleomagnetic study on a succession of Holocene olivine-basalt flow: Xitle volcano (Mexico) revisited. *Earth Planets Space* 57: 839-853.
- Böhm H et al (1997) Variation of Rock Magnetic Parameters and Paleointensities over a Single Holocene Lava Flow. *J Geomag Geoelectr* 49: 523–542.
- Böhm, H., Molina-Garza, 2002. Secular variation in Mexico during the last 40,000 years, *Phys. Earth Planet. Inter.*, 133, 99–109.
- Böhm H, Biggin AJ, Walton D, Shaw J, Share JA (2003) Microwave paleointensities from a recent Mexican lava flow, baked sediments and reheated pottery *Earth Planet Sci Lett* 214 (1–2): 221–236.
- Böhm HN, Dekkers MJ, Delgado-Argote LA, Gratton MN (2009) Comparison between the microwave and multispecimen parallel difference pTRM paleointensity methods. *Geophys J Int* 177:383-394.
- Böhm, H., Pavón-Carrasco, F.J., Sieron, K., Mahgoub, A.N., 2016. Palaeomagnetic dating of two recent lava flows from Ceboruco volcano, western Mexico. *Geophys. J. Int.* 207 (2), 1203–1215.

- Bucha V, Taylor R, Berger R, Haury E (1970) Geomagnetic intensity: changes during the past 3000 years in the western hemisphere. *Science* 168:111–114.
- Conte-Fasano G, Urrutia-Fucugauchi J, Goguitchaichvili A, Morales-Contreras J (2006) Low-latitude paleosecular variation and the time-averaged field during the late Pliocene and Quaternary—paleomagnetic study of the Michoacan-Guanajuato volcanic field, Central Mexico. *Earth Planets Space* 58(10):1359–1371.
- Duran, M.P., Goguitchaichvili, A., Morales, J., Reyes, B.A., Valdivia, L.M.A., Oliveros Morales, A., Calvo-Rathert, M., Moran, T.G., Robles-Camacho, J., 2010. Magnetic properties and Archeointensity of Earth's magnetic field recovered from El Opeño, earliest funeral architecture known in Western Mesoamerica. *Stud. Geophys. Geod.* 54, 575–593
- Eighmy, J. L., and R. S. Sternberg (Eds.) (1990), *Archaeomagnetic Dating*, 367–393 pp., Univ. of Ariz. Press, Tucson.
- Fanjat, G., Camps, P., Valdivia, L.A., Sougrati, M.T., Cuevas-Garcia, M., Perrin, M., 2013. First archeointensity determinations on Maya incense burners from Palenque temples, Mexico: New data to constrain the Mesoamerica secular variation curve. *Earth Planet. Sci. Lett.* 363, 168–180.
- Goguitchaivili, A. Soler, E. Zanella, G. Chiari, R. Lanza, J. Urrutia-Fucugauchi, T. Gonzalez, Pre-Columbian mural paintings from Mesoamerica as geomagnetic field recorders, *Geophys. Res. Lett.* 31 (2004) L12607, doi:10.1029/2004GL020065.
- Goguitchaichvili A., Conte G., Urrutia-Fucugauchi J., Alva-Valdivia L., Morales J. and González Moran T., 2005. Microwave paleointensity analysis of historic lavas from Paricutin volcano, Mexico. *Geofisica Internacional*, 44, 231–240

- Gonzalez S, Sherwood GJ, Boehnel H, Schnepf E (1997), Paleosecular variation in central Mexico over the last 30,000 years: The record from lavas. *Geophys J Int* 130: 201–219.
- Gratton MN, Goguitchaichvili A, Conte G, Shaw J, Urrutia-Fucugauchi J (2005) Microwave paleointensity study of the Jorullo volcano (Central Mexico) *Geophys J Int* 161: 627–634.
- Latham, A.G., Schwarcz, H.P., Ford, D.C., 1986. The paleomagnetism and U–Th dating of Mexican stalagmite, DAS2. *Earth Planet. Sci. Lett.* 79, 195–207.
- Lee SS (1975) Secular variation of the intensity of the geomagnetic field during the past 3,000 years in North, Central and South America. Ph.D. thesis University of Oklahoma, Norman.
- López-Delgado, V., Soler-Arechalde, A.M., Espinosa-Rodriguez, G., Goguitchaichvili, A., 2010. Rock-magnetic and Archeomagnetic survey from some Classical settlements at Chapultepec archeological site (western Mesoamerica). *Stud. Geophys. Geod.* 55, 329–342.
- Mahgoub, A.N., Böhnel, H., Siebe, C., Chevrel, M.O., 2017a. Paleomagnetic study of el Metate shield volcano (Michoacán, Mexico) confirms its monogenetic nature and young age (~1250 CE). *J. Volcanol. Geotherm. Res.* 336:209–218. <https://doi.org/10.1016/j.jvolgeores.2017.02.024>.
- Mahgoub A.N, Böhnel, H, Siebe C, Salinas S, Guilbaud M-N., 2017b. Paleomagnetically inferred ages of a cluster of Holocene monogenetic eruptions in the Tacámbaro-Puruarán area (Michoacán, México): implications for volcanic hazards. *J Volcanol Geotherm Res* 347:360–370. <https://doi.org/10.1016/j.jvolgeores.2017.10.004>.

- Mahgoub, A.N., Reyes-Guzman, N., Böhnell, H., Siebe, C., Pereira, G., Dorison, A., 2018. Paleomagnetic constraints on the ages of the Holocene Malpaís de Zacapu lava flow eruptions, Michoacán (Mexico): Implications for archeology and volcanic hazards. *The Holocene* 28(2):229-245 <https://doi.org/10.1177/0959683617721323>.
- Mahgoub, AN, Juárez-Arriaga, E, Böhnell, H, Manzanilla, L.R, Cyphers, A., Submitted. A 3600 years paleointensity secular variation curve for Mexico, submitted to the *Earth and Planetary Science Letters*.
- Michalk, D.M., Muxworthy, A.R., Böhnell, H.N., MacLennan, J., Nowaczyk, N., 2008. Evaluation of the multispecimen parallel differential pTRM method: a test on historical lavas from Iceland and Mexico. *Geophys. J. Int.* 173 (2), 409–420.
- Michalk, D.M., Biggin, A.J., Knudsen, M.F., Böhnell, H.N., Nowaczyk, N., Ownby, S., Lopez-Martinez, M., 2010. Application of the multispecimen palaeointensity method to Pleistocene lava flows from the Trans-Mexican Volcanic Belt *Physics of the Earth and Planetary Interiors*, 179, pp. 139-156.
- Morales J, Goguitchaichvili A, Urrutia-Fucugauchi J (2001) A rock-magnetic and paleointensity study of some Mexican volcanic lava flows during the Latest Pleistocene to the Holocene. *Earth Planets Space* 53(9): 893–902.
- Morales J, Alva-Valdivia LM, Goguitchaichvili A, Urrutia-Fucugauchi J (2006) Cooling rate corrected paleointensities from the Xitle lava flow: Evaluation of within-site scatter for single spot-reading cooling units. *Earth Planets Space* 58: 1341–1347.
- Morales, J., Goguitchaichvili, A., Acosta, G., González-Morán, T., Alva-Valdivia, L., Robles-Camacho J., and Hernández-Bernal, M., 2009, Magnetic properties and archeointensity determination on Pre-Columbian pottery from Chiapas, Mesoamerica,

Earth Planets & Space, special issue on 'Magnetism of volcanic materials, tribute to works of Michel Prévot', doi:10.19EPS2364.10.29.

Nagata T, Kobayashi K, Schwarz E (1965) Archeomagnetic intensity studies of south and central America. *J Geomagn Geoelectr* 17: 399–405.

Pétronille M, Goguitchaichvili A, Morales J, Carvallo C, Hueda-Tanabe Y (2012) Absolute geomagnetic intensity determinations on Formative potsherds (1400–700 BC) from the Oaxaca Valley, Southwestern Mexico. *Quat Res* 78: 442-453
10.1016/j.yqres.2012.07.011.

Rodriguez-Ceja, M., Goguitchaichvili, A., Chauvin, A., Morales, J., Ostroumov, M., Manzanilla, L. R., Aguilar Reyes B., Urrutia-Fucugauchi, J., 2009. An Integrated Magnetic and Raman Spectroscopy Study on Some Pre-Columbian Potteries From Cuanalan (A Formative Village in the Valley of Teotihuacan) in Mesoamerica. *J. Geophys. Res.*, 114, B04103, doi:10.1029/2008JB006106

A. Soler-Arechalde, F. Sanchez, M. Rodriguez, C. Caballero-Miranda, A. Goguitchaishvili, J. Urrutia-Fucugauchi, D. Tarling, Archeomagnetic investigation of oriented pre-Columbian lime-plasters from Teotihuacan, Mesoamerica, *Earth Planets Space* 58 (2006) 1433–1439

Urrutia-Fucugauchi J, Alva-Valdivia L, Goguitchaichvili A, M. Rivas ML, Morales J (2004) Paleomagnetic, rock-magnetic and microscopy studies of historic lava flows from Paricutin volcano, Mexico: Implications for the deflection of paleomagnetic measurements, *Geophys J Int* 156: 431–442.

Vlag P. Alva-Valdivia L. de Boer C.B. Gonzalez S. Urrutia-Fucugauchi J., 2000. A rock- and paleomagnetic study of a Holocene lava flow in Central Mexico, *Phys. Earth planet. Inter.*, 118, 259–272.

Supplementary Table S4: Full vector PSV curve data calculated for Mexico from AD

2000 to AD -2200. Data provided every 100 years.

Age (AD)	D (°)	D max(°)	D min(°)	I (°)	I max(°)	I min(°)	Int (μT)	Int max(μT)	Int min(μT)
-2200	11.88	14.08	9.69	36.79	38.95	34.63	49.89	57.24	-49.89
-2190	11.67	13.83	9.50	37.18	39.25	35.11	49.92	57.13	-49.92
-2180	11.45	13.59	9.32	37.56	39.56	35.57	49.95	57.03	-49.95
-2170	11.24	13.35	9.14	37.93	39.86	36.00	49.98	56.92	-49.98
-2160	11.04	13.11	8.96	38.29	40.16	36.41	50.01	56.82	-50.01
-2150	10.83	12.88	8.78	38.63	40.46	36.81	50.04	56.73	-50.04
-2140	10.63	12.66	8.60	38.97	40.76	37.18	50.07	56.63	-50.07
-2130	10.43	12.43	8.42	39.30	41.06	37.54	50.10	56.54	-50.10
-2120	10.23	12.22	8.24	39.62	41.36	37.89	50.13	56.45	-50.13
-2110	10.03	12.00	8.06	39.94	41.66	38.21	50.16	56.35	-50.16
-2100	9.83	11.79	7.88	40.25	41.96	38.53	50.19	56.27	-50.19
-2090	9.64	11.57	7.70	40.55	42.26	38.84	50.22	56.18	-50.22
-2080	9.44	11.36	7.52	40.85	42.56	39.13	50.24	56.09	-50.24
-2070	9.24	11.16	7.33	41.14	42.86	39.42	50.27	56.00	-50.27
-2060	9.05	10.95	7.14	41.43	43.16	39.70	50.30	55.91	-50.30
-2050	8.85	10.74	6.95	41.72	43.45	39.98	50.33	55.82	-50.33
-2040	8.65	10.53	6.76	42.00	43.75	40.24	50.36	55.74	-50.36
-2030	8.44	10.32	6.57	42.28	44.05	40.51	50.38	55.65	-50.38
-2020	8.24	10.12	6.37	42.55	44.34	40.76	50.41	55.56	-50.41
-2010	8.04	9.91	6.17	42.82	44.63	41.01	50.43	55.47	-50.43

-2000	7.84	9.71	5.97	43.09	44.92	41.26	50.45	55.38	-50.45
-1990	7.63	9.50	5.77	43.35	45.21	41.50	50.47	55.29	-50.47
-1980	7.43	9.30	5.56	43.61	45.49	41.73	50.49	55.20	-50.49
-1970	7.23	9.10	5.36	43.86	45.76	41.96	50.51	55.11	-50.51
-1960	7.02	8.90	5.15	44.10	46.03	42.18	50.52	55.01	-50.52
-1950	6.82	8.70	4.95	44.34	46.29	42.39	50.53	54.92	-50.53
-1940	6.62	8.50	4.74	44.57	46.54	42.60	50.53	54.82	-50.53
-1930	6.42	8.30	4.53	44.80	46.79	42.81	50.54	54.72	-50.54
-1920	6.22	8.11	4.32	45.02	47.03	43.01	50.54	54.62	-50.54
-1910	6.02	7.92	4.12	45.23	47.26	43.20	50.53	54.52	-50.53
-1900	5.82	7.73	3.91	45.43	47.49	43.38	50.52	54.41	-50.52
-1890	5.62	7.54	3.71	45.63	47.70	43.56	50.50	54.31	-50.50
-1880	5.43	7.35	3.51	45.82	47.90	43.73	50.48	54.20	-50.48
-1870	5.24	7.17	3.30	46.00	48.10	43.90	50.46	54.08	-50.46
-1860	5.05	6.99	3.10	46.17	48.29	44.06	50.43	53.97	-50.43
-1850	4.86	6.81	2.91	46.33	48.46	44.21	50.39	53.85	-50.39
-1840	4.67	6.63	2.71	46.49	48.63	44.35	50.34	53.72	-50.34
-1830	4.49	6.46	2.52	46.63	48.78	44.49	50.29	53.60	-50.29
-1820	4.31	6.29	2.33	46.77	48.93	44.61	50.23	53.46	-50.23
-1810	4.13	6.12	2.14	46.90	49.06	44.73	50.17	53.33	-50.17
-1800	3.96	5.96	1.96	47.01	49.18	44.84	50.09	53.19	-50.09
-1790	3.79	5.80	1.78	47.12	49.30	44.95	50.01	53.04	-50.01
-1780	3.62	5.64	1.60	47.22	49.40	45.04	49.92	52.89	-49.92
-1770	3.45	5.48	1.43	47.31	49.49	45.13	49.83	52.73	-49.83

-1760	3.29	5.33	1.26	47.39	49.56	45.21	49.72	52.57	-49.72
-1750	3.14	5.18	1.09	47.45	49.63	45.27	49.61	52.40	-49.61
-1740	2.98	5.03	0.93	47.51	49.68	45.33	49.48	52.22	-49.48
-1730	2.83	4.89	0.78	47.55	49.72	45.38	49.35	52.04	-49.35
-1720	2.69	4.75	0.63	47.59	49.75	45.42	49.20	51.85	-49.20
-1710	2.55	4.61	0.48	47.61	49.77	45.45	49.05	51.65	-49.05
-1700	2.41	4.48	0.34	47.62	49.77	45.47	48.89	51.44	-48.89
-1690	2.28	4.35	0.20	47.62	49.76	45.47	48.72	51.23	-48.72
-1680	2.15	4.23	0.07	47.60	49.73	45.47	48.53	51.01	-48.53
-1670	2.03	4.11	-0.05	47.57	49.69	45.45	48.34	50.77	-48.34
-1660	1.91	3.99	-0.17	47.53	49.64	45.42	48.13	50.53	-48.13
-1650	1.80	3.88	-0.28	47.48	49.57	45.38	47.91	50.29	-47.91
-1640	1.69	3.77	-0.39	47.41	49.49	45.33	47.69	50.03	-47.69
-1630	1.59	3.67	-0.49	47.33	49.39	45.26	47.45	49.76	-47.45
-1620	1.50	3.57	-0.58	47.23	49.27	45.18	47.20	49.49	-47.20
-1610	1.41	3.48	-0.67	47.12	49.14	45.09	46.94	49.20	-46.94
-1600	1.32	3.39	-0.75	46.99	49.00	44.99	46.68	48.91	-46.68
-1590	1.24	3.31	-0.82	46.86	48.84	44.87	46.40	48.61	-46.40
-1580	1.17	3.23	-0.88	46.70	48.67	44.74	46.12	48.30	-46.12
-1570	1.11	3.15	-0.94	46.54	48.48	44.60	45.83	47.99	-45.83
-1560	1.05	3.09	-0.99	46.36	48.27	44.44	45.53	47.67	-45.53
-1550	0.99	3.02	-1.04	46.16	48.05	44.27	45.22	47.34	-45.22
-1540	0.94	2.96	-1.07	45.95	47.82	44.08	44.91	47.00	-44.91
-1530	0.90	2.91	-1.10	45.73	47.57	43.88	44.59	46.66	-44.59

-1520	0.87	2.86	-1.12	45.49	47.30	43.67	44.26	46.32	-44.26
-1510	0.84	2.82	-1.14	45.23	47.02	43.44	43.93	45.96	-43.93
-1500	0.82	2.78	-1.14	44.96	46.73	43.20	43.60	45.61	-43.60
-1490	0.81	2.75	-1.14	44.68	46.42	42.94	43.26	45.24	-43.26
-1480	0.80	2.73	-1.13	44.38	46.09	42.67	42.92	44.87	-42.92
-1470	0.80	2.71	-1.12	44.06	45.75	42.38	42.57	44.50	-42.57
-1460	0.81	2.70	-1.09	43.73	45.39	42.07	42.23	44.12	-42.23
-1450	0.82	2.69	-1.06	43.39	45.02	41.75	41.88	43.74	-41.88
-1440	0.84	2.70	-1.01	43.02	44.63	41.42	41.53	43.36	-41.53
-1430	0.87	2.70	-0.97	42.65	44.23	41.07	41.17	42.97	-41.17
-1420	0.90	2.71	-0.91	42.26	43.81	40.70	40.82	42.58	-40.82
-1410	0.94	2.73	-0.85	41.85	43.38	40.32	40.47	42.20	-40.47
-1400	0.99	2.76	-0.78	41.43	42.94	39.92	40.12	41.81	-40.12
-1390	1.04	2.79	-0.70	41.00	42.49	39.52	39.78	41.42	-39.78
-1380	1.10	2.82	-0.62	40.56	42.03	39.10	39.44	41.04	-39.44
-1370	1.16	2.86	-0.54	40.11	41.56	38.67	39.10	40.66	-39.10
-1360	1.23	2.91	-0.44	39.66	41.09	38.22	38.77	40.28	-38.77
-1350	1.31	2.96	-0.35	39.19	40.60	37.77	38.44	39.91	-38.44
-1340	1.38	3.02	-0.25	38.71	40.12	37.31	38.12	39.54	-38.12
-1330	1.46	3.08	-0.15	38.23	39.62	36.84	37.81	39.18	-37.81
-1320	1.55	3.14	-0.04	37.75	39.13	36.37	37.50	38.83	-37.50
-1310	1.64	3.21	0.07	37.26	38.64	35.89	37.21	38.48	-37.21
-1300	1.73	3.28	0.18	36.77	38.14	35.41	36.92	38.14	-36.92
-1290	1.82	3.36	0.29	36.29	37.65	34.92	36.64	37.82	-36.64

-1280	1.92	3.44	0.40	35.80	37.16	34.44	36.37	37.50	-36.37
-1270	2.02	3.53	0.52	35.32	36.67	33.96	36.11	37.20	-36.11
-1260	2.12	3.62	0.63	34.84	36.19	33.48	35.86	36.91	-35.86
-1250	2.23	3.71	0.75	34.37	35.72	33.01	35.63	36.64	-35.63
-1240	2.33	3.80	0.86	33.90	35.26	32.54	35.40	36.38	-35.40
-1230	2.44	3.90	0.98	33.45	34.81	32.09	35.19	36.14	-35.19
-1220	2.55	4.00	1.09	33.00	34.36	31.63	34.98	35.92	-34.98
-1210	2.65	4.10	1.20	32.56	33.93	31.19	34.79	35.72	-34.79
-1200	2.76	4.21	1.31	32.13	33.50	30.75	34.60	35.53	-34.60
-1190	2.87	4.32	1.42	31.71	33.08	30.33	34.43	35.37	-34.43
-1180	2.98	4.42	1.53	31.29	32.68	29.91	34.26	35.22	-34.26
-1170	3.08	4.53	1.63	30.89	32.28	29.50	34.11	35.10	-34.11
-1160	3.19	4.64	1.73	30.50	31.90	29.09	33.96	34.99	-33.96
-1150	3.29	4.76	1.83	30.12	31.53	28.70	33.82	34.90	-33.82
-1140	3.40	4.87	1.92	29.74	31.17	28.31	33.68	34.82	-33.68
-1130	3.50	4.98	2.01	29.38	30.83	27.94	33.56	34.76	-33.56
-1120	3.60	5.09	2.10	29.03	30.50	27.57	33.44	34.71	-33.44
-1110	3.69	5.20	2.19	28.69	30.18	27.21	33.33	34.67	-33.33
-1100	3.79	5.31	2.26	28.36	29.87	26.85	33.23	34.65	-33.23
-1090	3.88	5.42	2.34	28.05	29.58	26.51	33.13	34.63	-33.13
-1080	3.97	5.53	2.41	27.74	29.31	26.17	33.04	34.63	-33.04
-1070	4.05	5.63	2.48	27.45	29.05	25.84	32.95	34.63	-32.95
-1060	4.14	5.73	2.54	27.16	28.80	25.53	32.87	34.64	-32.87
-1050	4.21	5.83	2.59	26.89	28.57	25.21	32.80	34.66	-32.80

-1040	4.29	5.93	2.64	26.63	28.35	24.91	32.73	34.68	-32.73
-1030	4.35	6.02	2.69	26.38	28.15	24.61	32.66	34.71	-32.66
-1020	4.42	6.11	2.73	26.14	27.97	24.32	32.60	34.75	-32.60
-1010	4.48	6.20	2.77	25.92	27.79	24.04	32.55	34.79	-32.55
-1000	4.54	6.28	2.80	25.70	27.64	23.77	32.50	34.83	-32.50
-990	4.59	6.36	2.82	25.50	27.50	23.50	32.45	34.89	-32.45
-980	4.64	6.43	2.85	25.30	27.37	23.23	32.41	34.94	-32.41
-970	4.68	6.50	2.86	25.12	27.26	22.98	32.38	35.01	-32.38
-960	4.72	6.56	2.87	24.94	27.16	22.72	32.34	35.07	-32.34
-950	4.75	6.63	2.88	24.78	27.08	22.48	32.32	35.14	-32.32
-940	4.78	6.68	2.88	24.62	27.01	22.24	32.29	35.22	-32.29
-930	4.81	6.74	2.88	24.48	26.95	22.00	32.27	35.30	-32.27
-920	4.83	6.78	2.87	24.34	26.91	21.78	32.26	35.38	-32.26
-910	4.84	6.83	2.86	24.21	26.87	21.55	32.24	35.47	-32.24
-900	4.85	6.86	2.85	24.09	26.85	21.33	32.23	35.56	-32.23
-890	4.86	6.90	2.82	23.98	26.84	21.12	32.23	35.65	-32.23
-880	4.86	6.92	2.80	23.88	26.84	20.92	32.23	35.75	-32.23
-870	4.86	6.95	2.77	23.78	26.85	20.72	32.23	35.85	-32.23
-860	4.85	6.96	2.74	23.69	26.86	20.52	32.24	35.95	-32.24
-850	4.84	6.97	2.70	23.61	26.89	20.33	32.25	36.05	-32.25
-840	4.82	6.98	2.65	23.53	26.92	20.15	32.26	36.16	-32.26
-830	4.80	6.98	2.61	23.47	26.96	19.97	32.27	36.27	-32.27
-820	4.77	6.98	2.56	23.40	27.01	19.80	32.29	36.38	-32.29
-810	4.74	6.97	2.50	23.35	27.06	19.64	32.31	36.49	-32.31

-800	4.70	6.96	2.45	23.30	27.12	19.48	32.34	36.61	-32.34
-790	4.66	6.94	2.39	23.26	27.19	19.33	32.37	36.73	-32.37
-780	4.62	6.92	2.32	23.22	27.27	19.18	32.40	36.85	-32.40
-770	4.57	6.89	2.26	23.20	27.34	19.05	32.43	36.97	-32.43
-760	4.52	6.86	2.19	23.17	27.43	18.92	32.47	37.09	-32.47
-750	4.47	6.83	2.11	23.16	27.52	18.80	32.51	37.22	-32.51
-740	4.42	6.79	2.04	23.15	27.61	18.69	32.56	37.35	-32.56
-730	4.36	6.75	1.96	23.15	27.70	18.59	32.60	37.48	-32.60
-720	4.29	6.70	1.88	23.15	27.81	18.49	32.66	37.61	-32.66
-710	4.23	6.66	1.80	23.16	27.91	18.40	32.71	37.74	-32.71
-700	4.16	6.60	1.72	23.17	28.02	18.32	32.77	37.88	-32.77
-690	4.09	6.55	1.63	23.19	28.13	18.25	32.83	38.01	-32.83
-680	4.02	6.49	1.55	23.22	28.24	18.19	32.89	38.15	-32.89
-670	3.94	6.43	1.46	23.25	28.36	18.14	32.96	38.29	-32.96
-660	3.86	6.36	1.37	23.29	28.48	18.09	33.03	38.43	-33.03
-650	3.78	6.29	1.27	23.33	28.60	18.06	33.10	38.58	-33.10
-640	3.70	6.22	1.18	23.38	28.73	18.03	33.18	38.73	-33.18
-630	3.61	6.14	1.08	23.44	28.86	18.02	33.26	38.88	-33.26
-620	3.52	6.06	0.98	23.50	28.99	18.01	33.35	39.03	-33.35
-610	3.42	5.97	0.87	23.57	29.13	18.02	33.44	39.19	-33.44
-600	3.33	5.88	0.77	23.65	29.27	18.03	33.54	39.36	-33.54
-590	3.22	5.79	0.66	23.74	29.42	18.06	33.64	39.53	-33.64
-580	3.12	5.69	0.54	23.83	29.57	18.10	33.75	39.70	-33.75
-570	3.01	5.58	0.43	23.94	29.72	18.16	33.87	39.88	-33.87

-560	2.89	5.47	0.30	24.05	29.88	18.23	34.00	40.07	-34.00
-550	2.77	5.35	0.18	24.18	30.05	18.31	34.14	40.27	-34.14
-540	2.64	5.23	0.04	24.32	30.22	18.42	34.28	40.47	-34.28
-530	2.50	5.09	-0.09	24.48	30.41	18.55	34.44	40.69	-34.44
-520	2.36	4.95	-0.24	24.65	30.60	18.71	34.62	40.92	-34.62
-510	2.20	4.79	-0.39	24.84	30.79	18.89	34.81	41.17	-34.81
-500	2.04	4.63	-0.55	25.05	31.00	19.10	35.02	41.42	-35.02
-490	1.87	4.45	-0.71	25.28	31.22	19.35	35.25	41.70	-35.25
-480	1.69	4.26	-0.88	25.54	31.44	19.64	35.50	41.99	-35.50
-470	1.49	4.05	-1.06	25.83	31.68	19.98	35.78	42.30	-35.78
-460	1.29	3.83	-1.25	26.14	31.92	20.37	36.10	42.64	-36.10
-450	1.08	3.60	-1.45	26.49	32.17	20.81	36.44	42.99	-36.44
-440	0.85	3.35	-1.65	26.88	32.44	21.32	36.83	43.38	-36.83
-430	0.61	3.08	-1.85	27.30	32.71	21.88	37.25	43.79	-37.25
-420	0.37	2.80	-2.07	27.75	32.99	22.51	37.73	44.23	-37.73
-410	0.11	2.50	-2.28	28.24	33.28	23.21	38.26	44.71	-38.26
-400	-0.16	2.19	-2.50	28.77	33.57	23.98	38.85	45.22	-38.85
-390	-0.43	1.86	-2.72	29.34	33.87	24.81	39.50	45.77	-39.50
-380	-0.70	1.53	-2.93	29.94	34.18	25.69	40.23	46.36	-40.23
-370	-0.98	1.19	-3.14	30.57	34.50	26.63	41.03	46.99	-41.03
-360	-1.25	0.85	-3.35	31.22	34.83	27.61	41.91	47.67	-41.91
-350	-1.52	0.51	-3.54	31.88	35.16	28.60	42.88	48.39	-42.88
-340	-1.78	0.17	-3.73	32.55	35.52	29.58	43.92	49.16	-43.92
-330	-2.03	-0.15	-3.92	33.20	35.90	30.51	45.04	49.96	-45.04

-320	-2.27	-0.44	-4.09	33.84	36.31	31.37	46.23	50.79	-46.23
-310	-2.49	-0.72	-4.27	34.43	36.76	32.11	47.47	51.65	-47.47
-300	-2.70	-0.96	-4.43	34.99	37.24	32.73	48.76	52.53	-48.76
-290	-2.88	-1.16	-4.60	35.48	37.76	33.20	50.08	53.45	-50.08
-280	-3.05	-1.34	-4.76	35.92	38.30	33.53	51.42	54.40	-51.42
-270	-3.19	-1.48	-4.91	36.28	38.82	33.75	52.75	55.43	-52.75
-260	-3.32	-1.58	-5.06	36.58	39.30	33.86	54.06	56.57	-54.06
-250	-3.43	-1.67	-5.20	36.80	39.71	33.89	55.32	57.86	-55.32
-240	-3.53	-1.73	-5.32	36.94	40.04	33.84	56.52	59.29	-56.52
-230	-3.60	-1.78	-5.42	37.00	40.27	33.74	57.64	60.81	-57.64
-220	-3.66	-1.82	-5.50	37.00	40.42	33.58	58.66	62.35	-58.66
-210	-3.71	-1.86	-5.57	36.93	40.47	33.39	59.59	63.87	-59.59
-200	-3.75	-1.90	-5.61	36.80	40.43	33.17	60.40	65.31	-60.40
-190	-3.78	-1.93	-5.63	36.62	40.31	32.93	61.08	66.64	-61.08
-180	-3.80	-1.97	-5.62	36.39	40.11	32.67	61.65	67.84	-61.65
-170	-3.81	-2.02	-5.61	36.14	39.86	32.42	62.09	68.91	-62.09
-160	-3.81	-2.06	-5.57	35.88	39.57	32.18	62.42	69.84	-62.42
-150	-3.81	-2.10	-5.53	35.63	39.28	31.97	62.65	70.63	-62.65
-140	-3.80	-2.13	-5.47	35.40	38.99	31.81	62.78	71.28	-62.78
-130	-3.79	-2.16	-5.42	35.20	38.72	31.69	62.82	71.79	-62.82
-120	-3.76	-2.17	-5.35	35.05	38.49	31.62	62.77	72.16	-62.77
-110	-3.73	-2.17	-5.29	34.95	38.29	31.60	62.65	72.40	-62.65
-100	-3.69	-2.16	-5.23	34.89	38.14	31.64	62.46	72.50	-62.46
-90	-3.64	-2.12	-5.16	34.89	38.05	31.73	62.21	72.48	-62.21

-80	-3.58	-2.06	-5.10	34.94	38.00	31.87	61.90	72.35	-61.90
-70	-3.51	-1.99	-5.04	35.03	38.00	32.06	61.54	72.10	-61.54
-60	-3.43	-1.88	-4.97	35.16	38.04	32.27	61.14	71.74	-61.14
-50	-3.33	-1.76	-4.90	35.31	38.11	32.51	60.71	71.29	-60.71
-40	-3.22	-1.61	-4.82	35.48	38.22	32.74	60.24	70.75	-60.24
-30	-3.08	-1.44	-4.72	35.66	38.36	32.95	59.75	70.13	-59.75
-20	-2.93	-1.25	-4.62	35.83	38.55	33.11	59.23	69.44	-59.23
-10	-2.77	-1.04	-4.50	35.99	38.77	33.21	58.69	68.68	-58.69
0	-2.59	-0.81	-4.37	36.13	39.02	33.24	58.14	67.87	-58.14
10	-2.39	-0.56	-4.23	36.23	39.28	33.18	57.57	67.01	-57.57
20	-2.18	-0.30	-4.07	36.30	39.55	33.04	56.99	66.12	-56.99
30	-1.97	-0.02	-3.91	36.31	39.79	32.82	56.39	65.18	-56.39
40	-1.75	0.25	-3.75	36.26	40.00	32.53	55.78	64.21	-55.78
50	-1.53	0.52	-3.59	36.15	40.14	32.16	55.14	63.21	-55.14
60	-1.32	0.78	-3.42	35.96	40.19	31.73	54.48	62.17	-54.48
70	-1.13	1.02	-3.27	35.70	40.14	31.26	53.79	61.10	-53.79
80	-0.95	1.23	-3.13	35.36	39.98	30.74	53.08	60.00	-53.08
90	-0.79	1.42	-3.01	34.95	39.70	30.19	52.35	58.87	-52.35
100	-0.67	1.57	-2.91	34.45	39.28	29.62	51.58	57.70	-51.58
110	-0.58	1.68	-2.84	33.88	38.73	29.03	50.79	56.51	-50.79
120	-0.53	1.74	-2.81	33.24	38.03	28.44	49.98	55.30	-49.98
130	-0.53	1.76	-2.82	32.54	37.23	27.86	49.17	54.10	-49.17
140	-0.57	1.73	-2.87	31.81	36.33	27.29	48.36	52.93	-48.36
150	-0.66	1.66	-2.98	31.05	35.35	26.75	47.56	51.80	-47.56

160	-0.80	1.53	-3.14	30.29	34.34	26.24	46.79	50.74	-46.79
170	-1.00	1.36	-3.35	29.54	33.34	25.74	46.06	49.79	-46.06
180	-1.24	1.14	-3.62	28.84	32.44	25.24	45.39	48.95	-45.39
190	-1.53	0.89	-3.94	28.21	31.71	24.72	44.79	48.26	-44.79
200	-1.86	0.59	-4.32	27.69	31.19	24.19	44.28	47.72	-44.28
210	-2.24	0.27	-4.74	27.31	30.93	23.68	43.86	47.33	-43.86
220	-2.65	-0.09	-5.20	27.08	30.92	23.24	43.54	47.08	-43.54
230	-3.08	-0.48	-5.68	27.02	31.12	22.92	43.34	46.96	-43.34
240	-3.53	-0.88	-6.18	27.14	31.51	22.78	43.24	46.97	-43.24
250	-3.99	-1.31	-6.67	27.46	32.04	22.89	43.25	47.09	-43.25
260	-4.44	-1.74	-7.14	27.98	32.68	23.27	43.38	47.31	-43.38
270	-4.88	-2.18	-7.58	28.66	33.39	23.93	43.60	47.59	-43.60
280	-5.29	-2.63	-7.96	29.47	34.14	24.81	43.91	47.92	-43.91
290	-5.66	-3.06	-8.27	30.38	34.89	25.88	44.27	48.26	-44.27
300	-5.98	-3.48	-8.49	31.36	35.61	27.11	44.66	48.57	-44.66
310	-6.24	-3.87	-8.62	32.36	36.28	28.44	45.06	48.81	-45.06
320	-6.44	-4.24	-8.64	33.36	36.87	29.84	45.43	48.96	-45.43
330	-6.56	-4.55	-8.57	34.31	37.39	31.23	45.74	48.99	-45.74
340	-6.61	-4.81	-8.40	35.19	37.82	32.56	45.94	48.86	-45.94
350	-6.57	-4.97	-8.16	35.97	38.16	33.78	45.99	48.57	-45.99
360	-6.44	-5.01	-7.87	36.63	38.43	34.83	45.85	48.10	-45.85
370	-6.23	-4.87	-7.58	37.18	38.72	35.64	45.54	47.51	-45.54
380	-5.93	-4.51	-7.36	37.61	39.11	36.11	45.04	46.86	-45.04
390	-5.56	-3.92	-7.20	37.95	39.65	36.25	44.37	46.18	-44.37

400	-5.12	-3.16	-7.08	38.19	40.25	36.12	43.54	45.46	-43.54
410	-4.61	-2.27	-6.94	38.33	40.84	35.83	42.56	44.64	-42.56
420	-4.04	-1.29	-6.78	38.41	41.39	35.43	41.47	43.70	-41.47
430	-3.42	-0.28	-6.57	38.45	41.90	35.00	40.32	42.68	-40.32
440	-2.79	0.73	-6.32	38.47	42.34	34.60	39.15	41.60	-39.15
450	-2.16	1.69	-6.01	38.51	42.73	34.28	38.01	40.50	-38.01
460	-1.57	2.52	-5.66	38.59	43.06	34.11	36.93	39.42	-36.93
470	-1.02	3.23	-5.27	38.71	43.33	34.10	35.94	38.40	-35.94
480	-0.53	3.77	-4.84	38.89	43.52	34.26	35.04	37.46	-35.04
490	-0.12	4.13	-4.37	39.11	43.64	34.58	34.25	36.61	-34.25
500	0.22	4.29	-3.86	39.38	43.67	35.09	33.59	35.89	-33.59
510	0.45	4.22	-3.32	39.68	43.58	35.77	33.05	35.29	-33.05
520	0.60	3.96	-2.76	39.98	43.39	36.56	32.63	34.81	-32.63
530	0.68	3.55	-2.19	40.24	43.10	37.37	32.31	34.44	-32.31
540	0.70	3.05	-1.65	40.42	42.73	38.12	32.07	34.18	-32.07
550	0.69	2.53	-1.16	40.50	42.31	38.69	31.91	33.99	-31.91
560	0.65	2.11	-0.81	40.43	41.91	38.96	31.78	33.85	-31.78
570	0.60	2.00	-0.79	40.21	41.68	38.75	31.69	33.76	-31.69
580	0.55	2.25	-1.15	39.84	41.64	38.03	31.62	33.68	-31.62
590	0.51	2.72	-1.71	39.29	41.64	36.95	31.56	33.61	-31.56
600	0.47	3.26	-2.32	38.58	41.54	35.63	31.49	33.51	-31.49
610	0.45	3.80	-2.91	37.70	41.28	34.12	31.41	33.38	-31.41
620	0.44	4.33	-3.45	36.67	40.86	32.48	31.32	33.21	-31.32
630	0.44	4.81	-3.93	35.51	40.29	30.73	31.22	33.02	-31.22

640	0.46	5.24	-4.32	34.26	39.58	28.94	31.12	32.82	-31.12
650	0.48	5.60	-4.63	32.93	38.71	27.15	31.02	32.62	-31.02
660	0.52	5.87	-4.83	31.56	37.70	25.42	30.93	32.43	-30.93
670	0.57	6.06	-4.93	30.17	36.56	23.79	30.84	32.24	-30.84
680	0.61	6.16	-4.94	28.80	35.32	22.28	30.77	32.08	-30.77
690	0.66	6.18	-4.87	27.46	34.01	20.91	30.72	31.95	-30.72
700	0.69	6.11	-4.72	26.20	32.67	19.72	30.70	31.84	-30.70
710	0.72	5.95	-4.50	25.03	31.32	18.73	30.70	31.76	-30.70
720	0.74	5.70	-4.22	23.96	30.03	17.90	30.73	31.72	-30.73
730	0.75	5.39	-3.90	23.02	28.83	17.21	30.80	31.73	-30.80
740	0.73	5.04	-3.57	22.19	27.77	16.62	30.90	31.80	-30.90
750	0.70	4.64	-3.24	21.50	26.89	16.12	31.03	31.96	-31.03
760	0.65	4.22	-2.92	20.95	26.21	15.69	31.20	32.21	-31.20
770	0.57	3.78	-2.64	20.53	25.72	15.33	31.41	32.55	-31.41
780	0.46	3.33	-2.41	20.23	25.40	15.06	31.64	32.98	-31.64
790	0.33	2.89	-2.24	20.04	25.20	14.88	31.90	33.46	-31.90
800	0.16	2.46	-2.15	19.96	25.07	14.85	32.17	34.00	-32.17
810	-0.05	2.04	-2.14	19.97	24.97	14.97	32.47	34.56	-32.47
820	-0.29	1.63	-2.22	20.07	24.89	15.25	32.78	35.14	-32.78
830	-0.57	1.23	-2.38	20.25	24.83	15.67	33.11	35.73	-33.11
840	-0.90	0.83	-2.62	20.51	24.81	16.21	33.45	36.32	-33.45
850	-1.26	0.41	-2.94	20.84	24.84	16.85	33.82	36.88	-33.82
860	-1.67	-0.03	-3.31	21.24	24.96	17.53	34.21	37.42	-34.21
870	-2.12	-0.49	-3.75	21.70	25.24	18.17	34.63	37.93	-34.63

880	-2.61	-0.98	-4.23	22.21	25.72	18.70	35.08	38.42	-35.08
890	-3.14	-1.51	-4.77	22.76	26.41	19.12	35.56	38.88	-35.56
900	-3.71	-2.06	-5.35	23.35	27.22	19.49	36.09	39.31	-36.09
910	-4.31	-2.66	-5.96	23.97	28.08	19.87	36.65	39.72	-36.65
920	-4.94	-3.29	-6.59	24.62	28.95	20.29	37.25	40.12	-37.25
930	-5.60	-3.95	-7.24	25.29	29.79	20.79	37.90	40.51	-37.90
940	-6.27	-4.64	-7.90	25.98	30.58	21.38	38.58	40.92	-38.58
950	-6.95	-5.35	-8.56	26.68	31.29	22.07	39.30	41.35	-39.30
960	-7.65	-6.09	-9.20	27.40	31.92	22.87	40.06	41.83	-40.06
970	-8.34	-6.85	-9.83	28.12	32.47	23.77	40.86	42.40	-40.86
980	-9.02	-7.61	-10.43	28.83	32.94	24.73	41.70	43.13	-41.70
990	-9.69	-8.37	-11.01	29.54	33.33	25.74	42.56	44.07	-42.56
1000	-10.33	-9.11	-11.55	30.23	33.67	26.79	43.45	45.20	-43.45
1010	-10.95	-9.83	-12.06	30.90	33.94	27.85	44.36	46.46	-44.36
1020	-11.53	-10.52	-12.53	31.54	34.17	28.90	45.28	47.80	-45.28
1030	-12.07	-11.17	-12.97	32.14	34.39	29.89	46.21	49.17	-46.21
1040	-12.57	-11.75	-13.38	32.71	34.63	30.79	47.13	50.52	-47.13
1050	-13.02	-12.27	-13.77	33.23	34.91	31.55	48.03	51.84	-48.03
1060	-13.42	-12.72	-14.13	33.71	35.25	32.16	48.91	53.09	-48.91
1070	-13.77	-13.08	-14.46	34.14	35.66	32.62	49.75	54.26	-49.75
1080	-14.07	-13.38	-14.76	34.53	36.11	32.96	50.54	55.33	-50.54
1090	-14.32	-13.60	-15.03	34.89	36.56	33.21	51.28	56.30	-51.28
1100	-14.51	-13.77	-15.25	35.20	36.97	33.43	51.96	57.14	-51.96
1110	-14.65	-13.88	-15.42	35.48	37.31	33.65	52.56	57.84	-52.56

1120	-14.74	-13.94	-15.54	35.72	37.58	33.86	53.09	58.41	-53.09
1130	-14.78	-13.96	-15.60	35.93	37.77	34.08	53.54	58.85	-53.54
1140	-14.77	-13.93	-15.61	36.10	37.91	34.28	53.91	59.15	-53.91
1150	-14.72	-13.86	-15.57	36.23	37.99	34.47	54.20	59.34	-54.20
1160	-14.62	-13.75	-15.49	36.33	38.03	34.64	54.39	59.41	-54.39
1170	-14.48	-13.60	-15.36	36.40	38.02	34.78	54.50	59.38	-54.50
1180	-14.30	-13.40	-15.19	36.43	37.99	34.86	54.51	59.25	-54.51
1190	-14.08	-13.17	-15.00	36.41	37.95	34.88	54.44	59.04	-54.44
1200	-13.83	-12.90	-14.77	36.36	37.89	34.83	54.27	58.76	-54.27
1210	-13.55	-12.60	-14.51	36.27	37.82	34.72	54.01	58.42	-54.01
1220	-13.25	-12.26	-14.23	36.13	37.73	34.54	53.66	58.03	-53.66
1230	-12.92	-11.91	-13.93	35.95	37.62	34.29	53.22	57.60	-53.22
1240	-12.57	-11.53	-13.61	35.73	37.50	33.96	52.70	57.13	-52.70
1250	-12.21	-11.14	-13.28	35.45	37.36	33.54	52.09	56.63	-52.09
1260	-11.84	-10.73	-12.94	35.13	37.22	33.04	51.42	56.09	-51.42
1270	-11.45	-10.31	-12.59	34.76	37.06	32.46	50.67	55.52	-50.67
1280	-11.06	-9.89	-12.22	34.35	36.89	31.80	49.88	54.90	-49.88
1290	-10.65	-9.45	-11.85	33.90	36.72	31.09	49.06	54.23	-49.06
1300	-10.23	-9.00	-11.46	33.44	36.53	30.34	48.21	53.51	-48.21
1310	-9.80	-8.54	-11.06	32.96	36.34	29.58	47.36	52.72	-47.36
1320	-9.35	-8.06	-10.65	32.47	36.13	28.82	46.51	51.86	-46.51
1330	-8.90	-7.58	-10.23	32.00	35.91	28.09	45.67	50.92	-45.67
1340	-8.44	-7.08	-9.80	31.54	35.67	27.41	44.85	49.90	-44.85
1350	-7.97	-6.57	-9.37	31.11	35.42	26.81	44.06	48.79	-44.06

1360	-7.50	-6.05	-8.94	30.73	35.16	26.30	43.31	47.59	-43.31
1370	-7.02	-5.53	-8.51	30.39	34.89	25.89	42.59	46.33	-42.59
1380	-6.54	-5.00	-8.08	30.10	34.63	25.58	41.92	45.03	-41.92
1390	-6.06	-4.46	-7.65	29.87	34.38	25.36	41.30	43.75	-41.30
1400	-5.58	-3.93	-7.22	29.69	34.14	25.23	40.74	42.57	-40.74
1410	-5.11	-3.41	-6.80	29.56	33.93	25.19	40.24	41.74	-40.24
1420	-4.64	-2.90	-6.38	29.49	33.77	25.20	39.80	41.55	-39.80
1430	-4.19	-2.40	-5.97	29.46	33.66	25.26	39.44	41.86	-39.44
1440	-3.74	-1.92	-5.56	29.49	33.64	25.35	39.14	42.43	-39.14
1450	-3.31	-1.46	-5.16	29.58	33.69	25.46	38.92	43.12	-38.92
1460	-2.89	-1.01	-4.77	29.72	33.84	25.61	38.78	43.86	-38.78
1470	-2.49	-0.57	-4.41	29.93	34.06	25.81	38.71	44.63	-38.71
1480	-2.11	-0.07	-4.14	30.20	34.34	26.07	38.71	45.41	-38.71
1490	-1.75	0.74	-4.25	30.54	34.65	26.42	38.77	46.16	-38.77
1500	-1.32	0.76	-3.41	30.92	34.93	26.91	38.88	46.88	-38.88
1510	-1.03	0.78	-2.84	31.31	35.73	26.90	39.05	47.55	-39.05
1520	-0.72	1.01	-2.46	31.85	36.56	27.13	39.27	48.15	-39.27
1530	-0.41	1.19	-2.01	32.48	36.96	28.00	39.52	48.71	-39.52
1540	-0.14	1.21	-1.50	33.20	36.86	29.55	39.81	49.21	-39.81
1550	0.10	1.30	-1.10	34.00	36.84	31.15	40.13	49.64	-40.13
1560	0.31	1.40	-0.77	34.80	37.34	32.25	40.48	50.01	-40.48
1570	0.50	1.47	-0.48	35.58	38.14	33.01	40.85	50.31	-40.85
1580	0.65	1.52	-0.22	36.32	39.41	33.22	41.24	50.56	-41.24
1590	0.79	1.53	0.04	36.99	40.38	33.61	41.64	50.76	-41.64

1600	0.90	1.54	0.25	37.62	41.06	34.18	42.06	50.91	-42.06
1610	1.00	1.54	0.46	38.21	41.69	34.73	42.49	51.03	-42.49
1620	1.09	1.55	0.64	38.77	42.30	35.23	42.91	51.11	-42.91
1630	1.19	1.57	0.82	39.29	42.87	35.71	43.34	51.16	-43.34
1640	1.30	1.61	0.99	39.78	43.39	36.16	43.77	51.18	-43.77
1650	1.42	1.69	1.16	40.23	43.87	36.60	44.19	51.18	-44.19
1660	1.57	1.79	1.34	40.66	44.30	37.02	44.59	51.16	-44.59
1670	1.75	1.94	1.55	41.05	44.67	37.43	44.99	51.12	-44.99
1680	1.96	2.13	1.79	41.41	45.00	37.83	45.36	51.07	-45.36
1690	2.22	2.37	2.06	41.75	45.28	38.22	45.72	51.01	-45.72
1700	2.52	2.66	2.38	42.05	45.50	38.59	46.05	50.93	-46.05
1710	2.88	3.00	2.76	42.32	45.67	38.96	46.35	50.84	-46.35
1720	3.28	3.38	3.18	42.56	45.79	39.32	46.63	50.72	-46.63
1730	3.73	3.82	3.65	42.76	45.85	39.67	46.88	50.59	-46.88
1740	4.23	4.29	4.16	42.94	45.86	40.01	47.09	50.44	-47.09
1750	4.75	4.80	4.71	43.07	45.81	40.34	47.27	50.26	-47.27
1760	5.31	5.33	5.29	43.18	45.70	40.66	47.42	50.05	-47.42
1770	5.87	5.88	5.86	43.24	45.54	40.95	47.53	49.81	-47.53
1780	6.41	6.44	6.39	43.28	45.33	41.22	47.62	49.56	-47.62
1790	6.91	6.96	6.87	43.27	45.09	41.46	47.68	49.29	-47.68
1800	7.35	7.42	7.28	43.24	44.82	41.67	47.71	49.03	-47.71
1810	7.70	7.80	7.60	43.18	44.51	41.84	47.72	48.76	-47.72
1820	7.96	8.09	7.84	43.09	44.19	41.98	47.71	48.50	-47.71
1830	8.15	8.30	8.00	42.96	43.84	42.08	47.66	48.24	-47.66

1840	8.25	8.40	8.09	42.79	43.46	42.12	47.59	47.99	-47.59
1850	8.27	8.41	8.13	42.58	43.07	42.10	47.48	47.75	-47.48
1860	8.22	8.32	8.12	42.33	42.67	41.99	47.35	47.52	-47.35
1870	8.10	8.13	8.07	42.04	42.31	41.76	47.18	47.31	-47.18
1880	7.94	8.01	7.86	41.70	42.04	41.37	46.98	47.11	-46.98
1890	7.74	7.94	7.53	41.34	41.82	40.86	46.77	46.89	-46.77
1900	7.52	7.89	7.15	40.94	41.61	40.28	46.53	46.65	-46.53

Supplementary Table S5: Full vector PSV curve data calculated for Mexico from AD - 2200 to AD -45000. Data provided every 100 years.

Age (AD)	D (°)	D max(°)	D min(°)	I (°)	I max(°)	I min(°)	Int (μT)	Int max(μT)	Int min(μT)
-44000	-1.75	2.27	-5.77	28.65	33.34	23.95	38.23	45.29	31.17
-43900	-1.75	2.49	-5.99	28.51	33.54	23.48	38.02	45.26	30.78
-43800	-1.75	2.71	-6.22	28.37	33.73	23.00	37.79	45.24	30.34
-43700	-1.75	2.95	-6.45	28.21	33.91	22.50	37.55	45.22	29.87
-43600	-1.74	3.19	-6.67	28.04	34.08	22.00	37.28	45.20	29.36
-43500	-1.73	3.43	-6.89	27.87	34.24	21.50	37.00	45.17	28.83
-43400	-1.72	3.67	-7.11	27.68	34.38	20.99	36.70	45.13	28.28
-43300	-1.70	3.91	-7.31	27.49	34.49	20.50	36.39	45.08	27.70
-43200	-1.68	4.15	-7.50	27.30	34.59	20.00	36.06	45.02	27.11
-43100	-1.65	4.38	-7.68	27.10	34.68	19.52	35.72	44.94	26.50
-43000	-1.62	4.61	-7.85	26.89	34.74	19.04	35.36	44.84	25.88
-42900	-1.59	4.83	-8.01	26.67	34.78	18.57	35.00	44.73	25.26
-42800	-1.55	5.05	-8.15	26.46	34.80	18.11	34.61	44.61	24.62
-42700	-1.51	5.26	-8.29	26.23	34.81	17.66	34.22	44.46	23.98
-42600	-1.47	5.47	-8.41	26.01	34.79	17.22	33.82	44.30	23.34
-42500	-1.43	5.66	-8.52	25.78	34.76	16.79	33.41	44.13	22.69
-42400	-1.38	5.85	-8.62	25.54	34.71	16.37	32.99	43.94	22.04
-42300	-1.33	6.04	-8.71	25.31	34.65	15.97	32.56	43.74	21.39
-42200	-1.28	6.21	-8.78	25.07	34.56	15.57	32.13	43.52	20.73
-42100	-1.23	6.38	-8.85	24.83	34.47	15.18	31.68	43.29	20.08
-42000	-1.18	6.54	-8.91	24.58	34.36	14.81	31.24	43.04	19.43

-41900	-1.13	6.70	-8.95	24.34	34.23	14.45	30.78	42.78	18.78
-41800	-1.07	6.84	-8.99	24.10	34.10	14.10	30.33	42.52	18.14
-41700	-1.02	6.98	-9.02	23.85	33.95	13.76	29.87	42.24	17.50
-41600	-0.96	7.12	-9.04	23.61	33.79	13.43	29.40	41.95	16.86
-41500	-0.90	7.24	-9.05	23.37	33.62	13.11	28.94	41.65	16.23
-41400	-0.85	7.36	-9.05	23.12	33.44	12.81	28.47	41.34	15.60
-41300	-0.79	7.47	-9.05	22.88	33.25	12.52	28.01	41.03	14.98
-41200	-0.73	7.57	-9.03	22.65	33.06	12.23	27.54	40.71	14.37
-41100	-0.68	7.67	-9.02	22.41	32.85	11.96	27.08	40.38	13.77
-41000	-0.62	7.75	-8.99	22.18	32.65	11.71	26.61	40.04	13.18
-40900	-0.56	7.83	-8.96	21.95	32.43	11.46	26.15	39.71	12.60
-40800	-0.51	7.91	-8.93	21.72	32.21	11.23	25.70	39.36	12.03
-40700	-0.46	7.97	-8.89	21.50	31.99	11.01	25.24	39.01	11.47
-40600	-0.40	8.03	-8.84	21.28	31.77	10.80	24.80	38.66	10.93
-40500	-0.35	8.08	-8.79	21.07	31.54	10.60	24.35	38.31	10.40
-40400	-0.30	8.13	-8.74	20.86	31.31	10.41	23.92	37.95	9.88
-40300	-0.26	8.17	-8.68	20.66	31.08	10.24	23.49	37.60	9.39
-40200	-0.21	8.20	-8.62	20.46	30.85	10.08	23.07	37.24	8.91
-40100	-0.17	8.22	-8.55	20.28	30.62	9.93	22.66	36.88	8.45
-40000	-0.13	8.23	-8.49	20.10	30.39	9.80	22.26	36.52	8.00
-39900	-0.09	8.24	-8.42	19.92	30.17	9.67	21.87	36.16	7.58
-39800	-0.06	8.24	-8.35	19.76	29.95	9.56	21.49	35.80	7.18
-39700	-0.02	8.23	-8.28	19.60	29.73	9.47	21.12	35.44	6.81
-39600	0.00	8.21	-8.20	19.45	29.52	9.38	20.77	35.08	6.45

-39500	0.03	8.19	-8.13	19.31	29.31	9.31	20.42	34.72	6.12
-39400	0.05	8.15	-8.05	19.18	29.11	9.26	20.10	34.37	5.82
-39300	0.07	8.11	-7.97	19.06	28.91	9.22	19.78	34.02	5.55
-39200	0.08	8.06	-7.89	18.95	28.72	9.19	19.49	33.67	5.30
-39100	0.09	8.00	-7.81	18.86	28.54	9.17	19.21	33.33	5.09
-39000	0.10	7.93	-7.74	18.77	28.37	9.17	18.94	32.99	4.90
-38900	0.10	7.86	-7.66	18.70	28.20	9.19	18.70	32.65	4.75
-38800	0.09	7.77	-7.58	18.63	28.05	9.22	18.47	32.32	4.62
-38700	0.09	7.67	-7.50	18.59	27.91	9.27	18.27	32.00	4.53
-38600	0.07	7.57	-7.43	18.55	27.77	9.33	18.08	31.68	4.48
-38500	0.05	7.45	-7.35	18.53	27.65	9.41	17.91	31.36	4.46
-38400	0.03	7.33	-7.28	18.52	27.54	9.50	17.77	31.06	4.48
-38300	0.00	7.19	-7.20	18.52	27.44	9.61	17.65	30.76	4.53
-38200	-0.04	7.05	-7.13	18.55	27.36	9.74	17.55	30.48	4.63
-38100	-0.08	6.89	-7.06	18.58	27.28	9.88	17.48	30.20	4.76
-38000	-0.13	6.73	-7.00	18.63	27.23	10.04	17.43	29.94	4.92
-37900	-0.19	6.55	-6.93	18.70	27.18	10.22	17.41	29.68	5.13
-37800	-0.25	6.36	-6.87	18.79	27.16	10.42	17.41	29.45	5.38
-37700	-0.32	6.17	-6.81	18.89	27.14	10.63	17.44	29.23	5.66
-37600	-0.40	5.96	-6.76	19.01	27.15	10.87	17.50	29.03	5.98
-37500	-0.48	5.74	-6.71	19.15	27.17	11.12	17.59	28.85	6.33
-37400	-0.57	5.51	-6.66	19.30	27.21	11.39	17.71	28.69	6.72
-37300	-0.67	5.27	-6.62	19.47	27.27	11.68	17.85	28.57	7.14
-37200	-0.78	5.02	-6.58	19.67	27.35	11.98	18.03	28.47	7.59

-37100	-0.90	4.77	-6.56	19.88	27.45	12.31	18.24	28.42	8.07
-37000	-1.02	4.50	-6.54	20.11	27.58	12.65	18.49	28.41	8.57
-36900	-1.15	4.23	-6.53	20.37	27.72	13.01	18.76	28.45	9.08
-36800	-1.29	3.95	-6.53	20.64	27.89	13.39	19.07	28.55	9.60
-36700	-1.44	3.67	-6.54	20.94	28.09	13.78	19.41	28.71	10.11
-36600	-1.60	3.38	-6.57	21.25	28.31	14.19	19.79	28.95	10.62
-36500	-1.77	3.09	-6.62	21.59	28.56	14.62	20.19	29.27	11.12
-36400	-1.94	2.80	-6.68	21.95	28.85	15.06	20.63	29.68	11.59
-36300	-2.13	2.51	-6.77	22.33	29.16	15.51	21.10	30.19	12.02
-36200	-2.32	2.23	-6.88	22.74	29.50	15.98	21.61	30.79	12.42
-36100	-2.53	1.96	-7.01	23.16	29.88	16.45	22.14	31.50	12.78
-36000	-2.74	1.69	-7.18	23.61	30.29	16.94	22.70	32.30	13.09
-35900	-2.96	1.44	-7.37	24.08	30.73	17.43	23.28	33.20	13.36
-35800	-3.20	1.20	-7.60	24.57	31.22	17.93	23.89	34.19	13.59
-35700	-3.44	0.98	-7.86	25.09	31.73	18.44	24.53	35.27	13.78
-35600	-3.69	0.77	-8.16	25.62	32.29	18.96	25.18	36.42	13.94
-35500	-3.96	0.58	-8.50	26.18	32.88	19.48	25.85	37.64	14.07
-35400	-4.23	0.40	-8.87	26.75	33.50	20.00	26.54	38.92	14.17
-35300	-4.51	0.24	-9.27	27.35	34.17	20.53	27.25	40.26	14.24
-35200	-4.81	0.09	-9.71	27.97	34.86	21.07	27.97	41.63	14.31
-35100	-5.11	-0.04	-10.18	28.60	35.60	21.61	28.69	43.03	14.35
-35000	-5.42	-0.17	-10.67	29.25	36.36	22.15	29.42	44.45	14.39
-34900	-5.74	-0.29	-11.19	29.92	37.15	22.70	30.16	45.89	14.43
-34800	-6.07	-0.41	-11.74	30.61	37.97	23.25	30.90	47.33	14.46

-34700	-6.41	-0.53	-12.30	31.31	38.82	23.80	31.63	48.76	14.50
-34600	-6.76	-0.64	-12.88	32.02	39.69	24.36	32.36	50.19	14.54
-34500	-7.11	-0.76	-13.47	32.75	40.58	24.92	33.09	51.59	14.59
-34400	-7.48	-0.88	-14.07	33.49	41.49	25.48	33.80	52.96	14.64
-34300	-7.84	-1.00	-14.68	34.23	42.41	26.05	34.50	54.29	14.71
-34200	-8.22	-1.14	-15.30	34.99	43.34	26.63	35.18	55.58	14.79
-34100	-8.60	-1.28	-15.92	35.74	44.28	27.20	35.85	56.80	14.89
-34000	-8.98	-1.43	-16.54	36.50	45.22	27.78	36.49	57.97	15.01
-33900	-9.37	-1.60	-17.15	37.26	46.16	28.36	37.11	59.06	15.15
-33800	-9.76	-1.78	-17.75	38.02	47.09	28.95	37.70	60.08	15.32
-33700	-10.16	-1.97	-18.35	38.77	48.01	29.54	38.25	61.00	15.51
-33600	-10.55	-2.17	-18.93	39.52	48.91	30.12	38.77	61.82	15.73
-33500	-10.94	-2.40	-19.49	40.25	49.79	30.72	39.26	62.54	15.98
-33400	-11.34	-2.64	-20.03	40.98	50.64	31.31	39.70	63.14	16.26
-33300	-11.73	-2.90	-20.55	41.68	51.46	31.91	40.10	63.62	16.58
-33200	-12.11	-3.18	-21.04	42.37	52.24	32.51	40.45	63.96	16.93
-33100	-12.49	-3.49	-21.50	43.04	52.97	33.12	40.75	64.17	17.33
-33000	-12.87	-3.81	-21.93	43.69	53.66	33.73	40.99	64.23	17.76
-32900	-13.24	-4.16	-22.32	44.31	54.29	34.34	41.18	64.13	18.24
-32800	-13.60	-4.54	-22.67	44.91	54.86	34.96	41.31	63.87	18.76
-32700	-13.96	-4.93	-22.98	45.47	55.36	35.58	41.38	63.44	19.32
-32600	-14.30	-5.35	-23.24	46.00	55.80	36.20	41.39	62.84	19.93
-32500	-14.63	-5.80	-23.47	46.50	56.17	36.82	41.33	62.08	20.58
-32400	-14.95	-6.26	-23.64	46.96	56.47	37.45	41.20	61.14	21.26

-32300	-15.26	-6.75	-23.77	47.39	56.70	38.07	41.01	60.04	21.99
-32200	-15.55	-7.26	-23.85	47.78	56.85	38.70	40.77	58.79	22.74
-32100	-15.83	-7.78	-23.87	48.13	56.94	39.33	40.47	57.41	23.53
-32000	-16.09	-8.33	-23.85	48.46	56.95	39.97	40.13	55.91	24.35
-31900	-16.33	-8.89	-23.77	48.76	56.89	40.62	39.75	54.32	25.18
-31800	-16.55	-9.46	-23.63	49.03	56.77	41.28	39.34	52.67	26.01
-31700	-16.74	-10.05	-23.44	49.28	56.59	41.96	38.92	51.02	26.82
-31600	-16.92	-10.64	-23.20	49.51	56.36	42.66	38.49	49.41	27.58
-31500	-17.06	-11.21	-22.91	49.73	56.09	43.36	38.08	47.90	28.25
-31400	-17.18	-11.76	-22.60	49.94	55.81	44.07	37.68	46.57	28.79
-31300	-17.27	-12.24	-22.29	50.15	55.56	44.75	37.31	45.49	29.13
-31200	-17.32	-12.64	-22.00	50.38	55.37	45.39	36.98	44.72	29.24
-31100	-17.33	-12.90	-21.77	50.62	55.30	45.93	36.71	44.30	29.11
-31000	-17.32	-12.99	-21.64	50.88	55.43	46.34	36.49	44.23	28.75
-30900	-17.26	-12.90	-21.61	51.18	55.78	46.58	36.34	44.45	28.23
-30800	-17.16	-12.62	-21.70	51.51	56.37	46.65	36.27	44.92	27.62
-30700	-17.02	-12.18	-21.86	51.88	57.19	46.58	36.29	45.58	27.00
-30600	-16.84	-11.62	-22.07	52.30	58.19	46.41	36.40	46.37	26.43
-30500	-16.63	-10.97	-22.28	52.76	59.33	46.20	36.63	47.29	25.97
-30400	-16.38	-10.27	-22.48	53.27	60.57	45.98	36.98	48.30	25.65
-30300	-16.10	-9.55	-22.64	53.83	61.87	45.80	37.47	49.42	25.52
-30200	-15.79	-8.83	-22.74	54.44	63.20	45.68	38.10	50.62	25.58
-30100	-15.46	-8.14	-22.78	55.09	64.53	45.64	38.89	51.92	25.86
-30000	-15.12	-7.49	-22.75	55.77	65.84	45.69	39.83	53.29	26.37

-29900	-14.77	-6.90	-22.65	56.47	67.10	45.84	40.92	54.73	27.11
-29800	-14.43	-6.37	-22.49	57.18	68.28	46.07	42.14	56.22	28.06
-29700	-14.09	-5.92	-22.26	57.88	69.38	46.38	43.48	57.74	29.22
-29600	-13.77	-5.55	-21.99	58.55	70.36	46.75	44.92	59.29	30.55
-29500	-13.46	-5.25	-21.67	59.18	71.21	47.14	46.43	60.84	32.03
-29400	-13.17	-5.03	-21.31	59.73	71.92	47.54	48.01	62.37	33.64
-29300	-12.91	-4.90	-20.93	60.19	72.47	47.91	49.61	63.88	35.35
-29200	-12.68	-4.83	-20.53	60.54	72.85	48.23	51.23	65.34	37.12
-29100	-12.48	-4.84	-20.12	60.75	73.04	48.46	52.84	66.75	38.92
-29000	-12.32	-4.92	-19.71	60.80	73.03	48.57	54.41	68.09	40.73
-28900	-12.19	-5.07	-19.32	60.67	72.80	48.54	55.93	69.34	42.52
-28800	-12.11	-5.28	-18.94	60.34	72.33	48.34	57.38	70.50	44.26
-28700	-12.08	-5.56	-18.60	59.78	71.61	47.95	58.73	71.55	45.91
-28600	-12.10	-5.90	-18.30	58.97	70.61	47.33	59.96	72.46	47.46
-28500	-12.18	-6.31	-18.06	57.90	69.33	46.46	61.04	73.22	48.87
-28400	-12.33	-6.78	-17.88	56.54	67.75	45.34	61.96	73.80	50.11
-28300	-12.55	-7.31	-17.78	54.88	65.84	43.92	62.67	74.19	51.16
-28200	-12.85	-7.92	-17.77	52.91	63.61	42.21	63.15	74.33	51.97
-28100	-13.22	-8.59	-17.86	50.60	61.03	40.17	63.37	74.22	52.52
-28000	-13.68	-9.33	-18.04	47.94	58.09	37.80	63.28	73.80	52.76
-27900	-14.23	-10.14	-18.32	44.91	54.78	35.05	62.86	73.05	52.66
-27800	-14.85	-11.00	-18.69	41.51	51.10	31.92	62.09	71.98	52.20
-27700	-15.53	-11.90	-19.16	37.72	47.05	28.39	60.97	70.57	51.37
-27600	-16.27	-12.84	-19.71	33.56	42.64	24.47	59.54	68.88	50.19

-27500	-17.06	-13.79	-20.33	29.05	37.90	20.20	57.82	66.96	48.69
-27400	-17.86	-14.73	-21.00	24.28	32.87	15.69	55.90	64.87	46.94
-27300	-18.68	-15.64	-21.72	19.35	27.64	11.07	53.84	62.67	45.00
-27200	-19.48	-16.51	-22.45	14.42	22.33	6.51	51.69	60.42	42.96
-27100	-20.24	-17.29	-23.19	9.67	17.13	2.21	49.49	58.13	40.85
-27000	-20.94	-17.98	-23.89	5.28	12.24	-1.69	47.26	55.81	38.71
-26900	-21.53	-18.53	-24.54	1.44	7.91	-5.04	44.99	53.42	36.55
-26800	-22.01	-18.93	-25.08	-1.72	4.37	-7.82	42.68	50.98	34.38
-26700	-22.32	-19.14	-25.50	-4.07	1.92	-10.06	40.35	48.48	32.21
-26600	-22.44	-19.14	-25.74	-5.54	0.75	-11.83	38.01	45.95	30.07
-26500	-22.34	-18.90	-25.78	-6.09	0.92	-13.10	35.71	43.42	28.00
-26400	-22.02	-18.43	-25.61	-5.72	2.35	-13.78	33.48	40.93	26.02
-26300	-21.46	-17.71	-25.22	-4.46	4.84	-13.76	31.36	38.53	24.18
-26200	-20.68	-16.77	-24.60	-2.39	8.20	-12.97	29.38	36.25	22.51
-26100	-19.70	-15.62	-23.77	0.38	12.17	-11.41	27.56	34.12	21.00
-26000	-18.53	-14.31	-22.75	3.72	16.55	-9.11	25.91	32.15	19.66
-25900	-17.21	-12.87	-21.54	7.46	21.08	-6.17	24.41	30.34	18.48
-25800	-15.75	-11.33	-20.17	11.45	25.58	-2.68	23.07	28.68	17.45
-25700	-14.18	-9.73	-18.63	15.53	29.83	1.22	21.86	27.17	16.55
-25600	-12.53	-8.09	-16.96	19.56	33.70	5.43	20.78	25.78	15.78
-25500	-10.81	-6.44	-15.18	23.43	37.07	9.80	19.82	24.52	15.13
-25400	-9.06	-4.80	-13.32	27.05	39.88	14.23	18.99	23.38	14.59
-25300	-7.30	-3.19	-11.41	30.33	42.07	18.60	18.27	22.35	14.18
-25200	-5.56	-1.65	-9.47	33.23	43.65	22.82	17.66	21.43	13.89

-25100	-3.86	-0.18	-7.55	35.71	44.63	26.80	17.16	20.62	13.70
-25000	-2.24	1.20	-5.69	37.77	45.07	30.47	16.77	19.92	13.63
-24900	-0.72	2.48	-3.92	39.41	45.06	33.76	16.50	19.35	13.65
-24800	0.66	3.64	-2.31	40.66	44.73	36.59	16.33	18.92	13.74
-24700	1.89	4.69	-0.91	41.57	44.35	38.80	16.27	18.66	13.88
-24600	2.93	5.63	0.24	42.19	44.41	39.96	16.32	18.60	14.04
-24500	3.78	6.47	1.09	42.55	45.25	39.86	16.47	18.76	14.18
-24400	4.42	7.20	1.64	42.70	46.35	39.05	16.72	19.13	14.31
-24300	4.86	7.81	1.92	42.65	47.30	38.01	17.07	19.70	14.43
-24200	5.12	8.28	1.95	42.43	47.97	36.89	17.49	20.42	14.56
-24100	5.19	8.62	1.77	42.04	48.34	35.74	17.99	21.26	14.72
-24000	5.10	8.80	1.40	41.49	48.41	34.58	18.55	22.19	14.90
-23900	4.86	8.85	0.88	40.81	48.20	33.42	19.15	23.18	15.13
-23800	4.49	8.76	0.22	40.01	47.75	32.27	19.80	24.21	15.39
-23700	3.98	8.53	-0.56	39.10	47.07	31.12	20.48	25.26	15.69
-23600	3.37	8.17	-1.43	38.09	46.19	29.99	21.17	26.31	16.03
-23500	2.65	7.68	-2.39	37.01	45.15	28.86	21.88	27.35	16.41
-23400	1.84	7.08	-3.40	35.86	43.96	27.76	22.59	28.37	16.82
-23300	0.95	6.36	-4.45	34.66	42.65	26.68	23.30	29.34	17.25
-23200	0.00	5.52	-5.53	33.43	41.24	25.62	23.99	30.28	17.70
-23100	-1.02	4.59	-6.62	32.19	39.77	24.61	24.66	31.16	18.16
-23000	-2.07	3.56	-7.71	30.94	38.24	23.64	25.31	31.98	18.64
-22900	-3.16	2.45	-8.77	29.71	36.69	22.74	25.93	32.75	19.11
-22800	-4.27	1.25	-9.80	28.52	35.13	21.90	26.52	33.46	19.58

-22700	-5.40	0.00	-10.79	27.37	33.60	21.15	27.07	34.10	20.04
-22600	-6.51	-1.29	-11.73	26.30	32.11	20.48	27.59	34.69	20.48
-22500	-7.61	-2.60	-12.62	25.32	30.71	19.92	28.06	35.21	20.91
-22400	-8.68	-3.90	-13.47	24.44	29.42	19.47	28.49	35.67	21.30
-22300	-9.72	-5.13	-14.30	23.70	28.29	19.12	28.87	36.07	21.66
-22200	-10.70	-6.25	-15.14	23.11	27.37	18.84	29.20	36.42	21.99
-22100	-11.62	-7.19	-16.05	22.67	26.71	18.63	29.49	36.71	22.27
-22000	-12.48	-7.90	-17.07	22.40	26.36	18.43	29.74	36.96	22.51
-21900	-13.28	-8.37	-18.20	22.29	26.35	18.24	29.93	37.15	22.70
-21800	-14.03	-8.61	-19.45	22.36	26.65	18.07	30.07	37.31	22.84
-21700	-14.73	-8.68	-20.77	22.58	27.23	17.94	30.17	37.42	22.92
-21600	-15.38	-8.62	-22.14	22.96	28.03	17.88	30.22	37.49	22.94
-21500	-16.00	-8.48	-23.53	23.48	29.03	17.93	30.22	37.54	22.91
-21400	-16.60	-8.30	-24.91	24.12	30.16	18.09	30.18	37.54	22.82
-21300	-17.18	-8.11	-26.26	24.88	31.39	18.36	30.10	37.53	22.67
-21200	-17.76	-7.95	-27.57	25.73	32.71	18.76	29.98	37.48	22.47
-21100	-18.33	-7.83	-28.83	26.68	34.08	19.27	29.82	37.41	22.22
-21000	-18.90	-7.75	-30.04	27.69	35.49	19.89	29.62	37.32	21.92
-20900	-19.47	-7.74	-31.20	28.78	36.93	20.62	29.40	37.22	21.57
-20800	-20.03	-7.77	-32.29	29.91	38.39	21.44	29.14	37.10	21.18
-20700	-20.59	-7.86	-33.31	31.10	39.86	22.34	28.86	36.97	20.76
-20600	-21.13	-8.00	-34.27	32.32	41.33	23.32	28.56	36.82	20.30
-20500	-21.66	-8.17	-35.16	33.58	42.79	24.36	28.24	36.67	19.82
-20400	-22.17	-8.38	-35.97	34.86	44.25	25.46	27.91	36.50	19.31

-20300	-22.66	-8.60	-36.72	36.15	45.69	26.61	27.57	36.33	18.80
-20200	-23.11	-8.83	-37.38	37.45	47.12	27.79	27.22	36.16	18.27
-20100	-23.52	-9.06	-37.97	38.75	48.51	29.00	26.86	35.98	17.75
-20000	-23.88	-9.29	-38.48	40.05	49.87	30.23	26.51	35.79	17.23
-19900	-24.20	-9.50	-38.91	41.33	51.19	31.46	26.17	35.61	16.73
-19800	-24.47	-9.69	-39.24	42.58	52.47	32.70	25.83	35.41	16.24
-19700	-24.67	-9.86	-39.48	43.81	53.68	33.93	25.50	35.22	15.78
-19600	-24.81	-10.00	-39.63	44.99	54.84	35.14	25.19	35.02	15.35
-19500	-24.88	-10.10	-39.67	46.13	55.93	36.33	24.89	34.82	14.96
-19400	-24.87	-10.15	-39.60	47.21	56.94	37.49	24.62	34.63	14.62
-19300	-24.79	-10.17	-39.41	48.23	57.86	38.61	24.38	34.43	14.33
-19200	-24.61	-10.13	-39.10	49.18	58.68	39.69	24.16	34.23	14.10
-19100	-24.35	-10.04	-38.65	50.06	59.40	40.71	23.98	34.03	13.94
-19000	-23.98	-9.90	-38.07	50.84	60.00	41.68	23.84	33.83	13.84
-18900	-23.52	-9.69	-37.34	51.54	60.48	42.59	23.74	33.64	13.83
-18800	-22.94	-9.43	-36.46	52.13	60.83	43.43	23.68	33.46	13.90
-18700	-22.26	-9.10	-35.42	52.61	61.03	44.19	23.67	33.28	14.06
-18600	-21.45	-8.70	-34.20	52.98	61.09	44.86	23.71	33.11	14.32
-18500	-20.53	-8.23	-32.82	53.22	60.99	45.45	23.81	32.95	14.67
-18400	-19.47	-7.69	-31.26	53.33	60.73	45.94	23.97	32.82	15.13
-18300	-18.30	-7.06	-29.54	53.31	60.31	46.32	24.21	32.72	15.70
-18200	-17.00	-6.36	-27.64	53.16	59.73	46.59	24.51	32.65	16.37
-18100	-15.58	-5.56	-25.60	52.87	59.00	46.73	24.90	32.64	17.16
-18000	-14.05	-4.68	-23.41	52.44	58.14	46.74	25.39	32.71	18.07

-17900	-12.41	-3.71	-21.12	51.88	57.15	46.61	25.99	32.88	19.09
-17800	-10.69	-2.63	-18.76	51.19	56.06	46.32	26.70	33.17	20.23
-17700	-8.91	-1.46	-16.36	50.38	54.90	45.87	27.55	33.62	21.48
-17600	-7.08	-0.19	-13.98	49.48	53.70	45.25	28.55	34.25	22.84
-17500	-5.25	1.20	-11.69	48.48	52.49	44.47	29.70	35.09	24.31
-17400	-3.42	2.69	-9.53	47.40	51.29	43.51	31.02	36.17	25.87
-17300	-1.64	4.29	-7.57	46.27	50.14	42.40	32.50	37.50	27.50
-17200	0.07	5.96	-5.83	45.10	49.04	41.16	34.14	39.07	29.22
-17100	1.68	7.66	-4.31	43.91	47.97	39.84	35.94	40.86	31.02
-17000	3.16	9.31	-2.99	42.72	46.93	38.50	37.87	42.83	32.91
-16900	4.48	10.80	-1.83	41.54	45.91	37.17	39.91	44.92	34.91
-16800	5.62	12.08	-0.84	40.41	44.91	35.92	42.04	47.09	37.00
-16700	6.54	13.08	0.00	39.35	43.92	34.78	44.23	49.29	39.18
-16600	7.23	13.78	0.67	38.38	42.98	33.79	46.44	51.47	41.41
-16500	7.66	14.17	1.15	37.53	42.10	32.97	48.65	53.62	43.68
-16400	7.82	14.23	1.41	36.83	41.30	32.36	50.82	55.69	45.95
-16300	7.71	13.99	1.44	36.29	40.63	31.95	52.92	57.66	48.18
-16200	7.35	13.44	1.26	35.93	40.08	31.77	54.92	59.50	50.34
-16100	6.74	12.61	0.88	35.75	39.69	31.81	56.81	61.21	52.41
-16000	5.91	11.52	0.31	35.76	39.45	32.08	58.55	62.75	54.35
-15900	4.89	10.20	-0.43	35.96	39.38	32.54	60.14	64.13	56.15
-15800	3.71	8.72	-1.30	36.32	39.47	33.16	61.56	65.34	57.78
-15700	2.41	7.11	-2.28	36.82	39.73	33.92	62.79	66.36	59.21
-15600	1.04	5.45	-3.37	37.45	40.16	34.74	63.81	67.21	60.41

-15500	-0.36	3.80	-4.53	38.17	40.76	35.58	64.63	67.88	61.38
-15400	-1.76	2.24	-5.77	38.95	41.52	36.38	65.21	68.35	62.07
-15300	-3.12	0.83	-7.07	39.76	42.43	37.10	65.56	68.63	62.49
-15200	-4.40	-0.38	-8.41	40.59	43.45	37.73	65.67	68.71	62.63
-15100	-5.58	-1.40	-9.76	41.41	44.54	38.29	65.53	68.58	62.49
-15000	-6.64	-2.22	-11.06	42.22	45.64	38.79	65.15	68.24	62.07
-14900	-7.58	-2.90	-12.26	43.00	46.70	39.29	64.55	67.70	61.40
-14800	-8.39	-3.46	-13.32	43.75	47.70	39.79	63.73	66.97	60.50
-14700	-9.08	-3.94	-14.22	44.47	48.61	40.33	62.73	66.08	59.39
-14600	-9.65	-4.35	-14.96	45.16	49.42	40.89	61.57	65.04	58.11
-14500	-10.12	-4.71	-15.53	45.81	50.14	41.49	60.28	63.87	56.68
-14400	-10.49	-5.03	-15.95	46.44	50.76	42.12	58.88	62.61	55.14
-14300	-10.78	-5.32	-16.24	47.03	51.31	42.76	57.39	61.26	53.53
-14200	-10.99	-5.57	-16.41	47.60	51.78	43.42	55.86	59.86	51.86
-14100	-11.14	-5.80	-16.48	48.12	52.17	44.08	54.29	58.41	50.18
-14000	-11.24	-6.02	-16.46	48.62	52.51	44.73	52.73	56.94	48.52
-13900	-11.30	-6.23	-16.38	49.08	52.79	45.37	51.19	55.47	46.90
-13800	-11.33	-6.43	-16.23	49.50	53.02	45.98	49.69	54.02	45.37
-13700	-11.34	-6.64	-16.04	49.89	53.20	46.57	48.28	52.59	43.96
-13600	-11.33	-6.85	-15.81	50.23	53.34	47.12	46.95	51.22	42.68
-13500	-11.31	-7.06	-15.55	50.54	53.44	47.63	45.75	49.93	41.58
-13400	-11.28	-7.27	-15.28	50.79	53.50	48.08	44.70	48.73	40.66
-13300	-11.24	-7.48	-15.00	50.99	53.51	48.47	43.81	47.67	39.94
-13200	-11.18	-7.65	-14.71	51.13	53.47	48.78	43.10	46.77	39.43

-13100	-11.09	-7.77	-14.41	51.18	53.38	48.98	42.60	46.07	39.12
-13000	-10.96	-7.81	-14.11	51.13	53.22	49.05	42.31	45.63	39.00
-12900	-10.77	-7.73	-13.80	50.97	52.98	48.95	42.26	45.48	39.04
-12800	-10.48	-7.51	-13.45	50.65	52.63	48.67	42.44	45.67	39.21
-12700	-10.07	-7.11	-13.03	50.17	52.16	48.18	42.86	46.21	39.51
-12600	-9.52	-6.52	-12.52	49.50	51.55	47.46	43.51	47.08	39.94
-12500	-8.81	-5.74	-11.87	48.63	50.76	46.51	44.38	48.25	40.52
-12400	-7.92	-4.78	-11.07	47.56	49.78	45.34	45.46	49.66	41.25
-12300	-6.88	-3.66	-10.10	46.29	48.60	43.97	46.72	51.26	42.17
-12200	-5.67	-2.39	-8.95	44.84	47.24	42.43	48.13	53.01	43.26
-12100	-4.34	-1.02	-7.66	43.24	45.72	40.75	49.68	54.84	44.51
-12000	-2.91	0.42	-6.25	41.51	44.05	38.97	51.32	56.73	45.91
-11900	-1.42	1.89	-4.74	39.70	42.28	37.12	53.02	58.62	47.42
-11800	0.10	3.37	-3.17	37.84	40.44	35.24	54.74	60.48	49.00
-11700	1.61	4.81	-1.60	35.97	38.57	33.36	56.43	62.26	50.61
-11600	3.06	6.17	-0.04	34.12	36.71	31.53	58.07	63.92	52.21
-11500	4.44	7.43	1.45	32.35	34.91	29.79	59.58	65.42	53.74
-11400	5.70	8.56	2.83	30.69	33.20	28.18	60.94	66.72	55.17
-11300	6.80	9.52	4.08	29.18	31.62	26.73	62.09	67.75	56.43
-11200	7.73	10.29	5.17	27.87	30.23	25.50	62.98	68.48	57.48
-11100	8.46	10.85	6.06	26.79	29.05	24.52	63.56	68.85	58.27
-11000	8.96	11.19	6.73	25.97	28.13	23.81	63.80	68.83	58.77
-10900	9.22	11.28	7.15	25.44	27.49	23.40	63.67	68.41	58.93
-10800	9.22	11.15	7.29	25.21	27.16	23.26	63.17	67.61	58.73

-10700	8.97	10.81	7.13	25.28	27.18	23.38	62.31	66.46	58.16
-10600	8.46	10.28	6.64	25.62	27.53	23.71	61.14	65.04	57.24
-10500	7.70	9.55	5.84	26.21	28.18	24.23	59.73	63.47	55.99
-10400	6.71	8.64	4.77	26.97	29.06	24.88	58.16	61.83	54.50
-10300	5.52	7.56	3.48	27.86	30.09	25.63	56.54	60.23	52.85
-10200	4.17	6.32	2.02	28.78	31.16	26.41	54.96	58.79	51.13
-10100	2.72	4.98	0.46	29.66	32.19	27.14	53.51	57.57	49.45
-10000	1.21	3.58	-1.16	30.44	33.10	27.77	52.25	56.62	47.88
-9900	-0.29	2.18	-2.77	31.04	33.82	28.26	51.23	55.95	46.51
-9800	-1.76	0.82	-4.34	31.45	34.31	28.58	50.45	55.53	45.37
-9700	-3.14	-0.47	-5.81	31.64	34.54	28.73	49.90	55.33	44.48
-9600	-4.42	-1.67	-7.18	31.62	34.53	28.71	49.55	55.31	43.80
-9500	-5.59	-2.77	-8.41	31.42	34.30	28.55	49.36	55.44	43.29
-9400	-6.63	-3.77	-9.49	31.08	33.89	28.28	49.29	55.66	42.92
-9300	-7.53	-4.64	-10.42	30.66	33.37	27.94	49.28	55.93	42.64
-9200	-8.28	-5.37	-11.19	30.20	32.81	27.59	49.31	56.21	42.40
-9100	-8.86	-5.96	-11.77	29.79	32.30	27.28	49.33	56.47	42.19
-9000	-9.28	-6.37	-12.19	29.48	31.91	27.06	49.32	56.67	41.98
-8900	-9.52	-6.59	-12.44	29.36	31.72	26.99	49.27	56.80	41.74
-8800	-9.59	-6.63	-12.55	29.47	31.83	27.12	49.16	56.83	41.48
-8700	-9.51	-6.49	-12.53	29.87	32.25	27.50	48.98	56.77	41.19
-8600	-9.33	-6.24	-12.42	30.58	33.00	28.16	48.74	56.62	40.87
-8500	-9.09	-5.97	-12.22	31.60	34.06	29.14	48.45	56.39	40.51
-8400	-8.87	-5.77	-11.97	32.91	35.39	30.44	48.11	56.09	40.12

-8300	-8.72	-5.74	-11.70	34.49	36.94	32.04	47.73	55.77	39.70
-8200	-8.72	-5.96	-11.48	36.27	38.66	33.87	47.33	55.43	39.24
-8100	-8.93	-6.45	-11.42	38.20	40.52	35.88	46.93	55.10	38.76
-8000	-9.39	-7.13	-11.64	40.22	42.46	37.98	46.53	54.79	38.26
-7900	-10.10	-7.93	-12.27	42.26	44.43	40.09	46.14	54.53	37.75
-7800	-11.06	-8.74	-13.38	44.25	46.36	42.13	45.80	54.32	37.27
-7700	-12.21	-9.54	-14.89	46.12	48.20	44.03	45.49	54.14	36.84
-7600	-13.51	-10.39	-16.63	47.82	49.90	45.73	45.23	54.00	36.47
-7500	-14.87	-11.28	-18.45	49.30	51.41	47.19	45.03	53.88	36.18
-7400	-16.23	-12.21	-20.24	50.55	52.70	48.40	44.88	53.78	35.99
-7300	-17.52	-13.14	-21.91	51.54	53.74	49.35	44.79	53.69	35.90
-7200	-18.73	-14.05	-23.41	52.29	54.53	50.06	44.76	53.60	35.92
-7100	-19.82	-14.92	-24.72	52.81	55.08	50.54	44.78	53.52	36.04
-7000	-20.80	-15.75	-25.85	53.10	55.38	50.81	44.85	53.44	36.27
-6900	-21.66	-16.54	-26.78	53.18	55.47	50.89	44.98	53.38	36.58
-6800	-22.41	-17.28	-27.54	53.08	55.36	50.79	45.14	53.32	36.97
-6700	-23.04	-17.97	-28.12	52.80	55.06	50.55	45.35	53.26	37.44
-6600	-23.56	-18.60	-28.53	52.38	54.60	50.17	45.59	53.22	37.97
-6500	-23.97	-19.16	-28.77	51.83	53.99	49.66	45.87	53.20	38.54
-6400	-24.25	-19.65	-28.86	51.16	53.26	49.06	46.17	53.19	39.15
-6300	-24.42	-20.05	-28.79	50.39	52.42	48.36	46.49	53.20	39.78
-6200	-24.46	-20.35	-28.56	49.55	51.50	47.59	46.82	53.23	40.42
-6100	-24.37	-20.55	-28.19	48.64	50.51	46.76	47.17	53.30	41.05
-6000	-24.15	-20.62	-27.67	47.69	49.48	45.90	47.53	53.40	41.66

-5900	-23.79	-20.57	-27.02	46.71	48.41	45.00	47.89	53.55	42.24
-5800	-23.30	-20.37	-26.22	45.72	47.34	44.10	48.25	53.73	42.77
-5700	-22.66	-20.02	-25.30	44.74	46.27	43.20	48.60	53.95	43.25
-5600	-21.88	-19.50	-24.26	43.78	45.23	42.33	48.94	54.21	43.67
-5500	-20.95	-18.80	-23.11	42.87	44.24	41.50	49.27	54.50	44.03
-5400	-19.88	-17.90	-21.85	42.02	43.30	40.73	49.57	54.81	44.34
-5300	-18.65	-16.82	-20.49	41.23	42.43	40.03	49.86	55.13	44.59
-5200	-17.30	-15.54	-19.05	40.53	41.64	39.41	50.12	55.44	44.79
-5100	-15.81	-14.09	-17.53	39.91	40.94	38.88	50.35	55.74	44.96
-5000	-14.21	-12.49	-15.93	39.38	40.33	38.42	50.56	56.02	45.11
-4900	-12.52	-10.78	-14.27	38.92	39.81	38.03	50.75	56.27	45.22
-4800	-10.77	-8.98	-12.55	38.54	39.38	37.71	50.91	56.49	45.32
-4700	-8.97	-7.13	-10.80	38.23	39.02	37.44	51.04	56.67	45.41
-4600	-7.16	-5.28	-9.04	37.97	38.73	37.22	51.15	56.81	45.48
-4500	-5.36	-3.44	-7.27	37.76	38.50	37.02	51.24	56.92	45.55
-4400	-3.60	-1.67	-5.54	37.59	38.32	36.85	51.30	57.00	45.60
-4300	-1.92	0.01	-3.85	37.44	38.18	36.69	51.35	57.05	45.64
-4200	-0.31	1.59	-2.22	37.31	38.07	36.55	51.37	57.06	45.68
-4100	1.19	3.05	-0.67	37.20	37.98	36.41	51.37	57.05	45.69
-4000	2.59	4.39	0.78	37.09	37.90	36.28	51.35	57.01	45.69
-3900	3.87	5.61	2.13	37.00	37.83	36.16	51.32	56.96	45.68
-3800	5.03	6.71	3.36	36.90	37.76	36.04	51.27	56.89	45.64
-3700	6.09	7.70	4.47	36.81	37.69	35.93	51.20	56.81	45.58
-3600	7.03	8.59	5.48	36.72	37.63	35.82	51.11	56.73	45.49

-3500	7.88	9.39	6.38	36.63	37.57	35.70	51.01	56.65	45.38
-3400	8.64	10.11	7.18	36.55	37.52	35.58	50.90	56.57	45.24
-3300	9.32	10.77	7.88	36.46	37.47	35.46	50.78	56.50	45.06
-3200	9.93	11.36	8.49	36.38	37.43	35.33	50.65	56.45	44.85
-3100	10.47	11.92	9.02	36.30	37.41	35.19	50.51	56.42	44.61
-3000	10.95	12.44	9.47	36.22	37.39	35.04	50.37	56.40	44.33
-2900	11.39	12.94	9.85	36.13	37.38	34.88	50.21	56.41	44.02
-2800	11.79	13.42	10.16	36.05	37.39	34.72	50.06	56.43	43.68
-2700	12.16	13.89	10.42	35.98	37.40	34.55	49.89	56.48	43.30
-2600	12.50	14.35	10.64	35.90	37.43	34.36	49.72	56.55	42.90
-2500	12.83	14.83	10.83	35.81	37.45	34.18	49.55	56.64	42.46
-2400	13.15	15.30	10.99	35.73	37.49	33.98	49.37	56.75	42.00
-2300	13.46	15.80	11.12	35.65	37.53	33.77	49.19	56.90	41.49
-2200	13.83	16.40	11.26	35.55	37.58	33.51	48.98	57.09	40.87

Supplementary Material III

This section represents supplementary data for the manuscript ‘‘Paleomagnetically inferred ages of a cluster of Holocene monogenetic eruptions in the Tacámbaro-Puruarán area (Michoacán, México): Implications for volcanic hazards’’ presented as chapter three in the thesis, and published in the journal of the *Volcanology and Geothermal Research*.

The supplementary data herein contains five figures and two supplementary tables. The figures are dealing with the equal area projections for the characteristic remanent directions (Fig. S1) and four paleomagnetic dating results (Fig. S2-S5). The tables listed the site mean directions results (Table S1) and the paleointensity results (Table S2).

Figure S1: Equal area projections show the dispersed characteristic remanent magnetization directions in La Tinaja2 and La Palma2 and 3. In La Muerta2 and Cutzaróndiro1, the calculated site-mean directions differ markedly from the flow-mean directions and were therefore rejected. Solid/open red diamonds are the site-mean direction with positive and negative inclination, respectively.

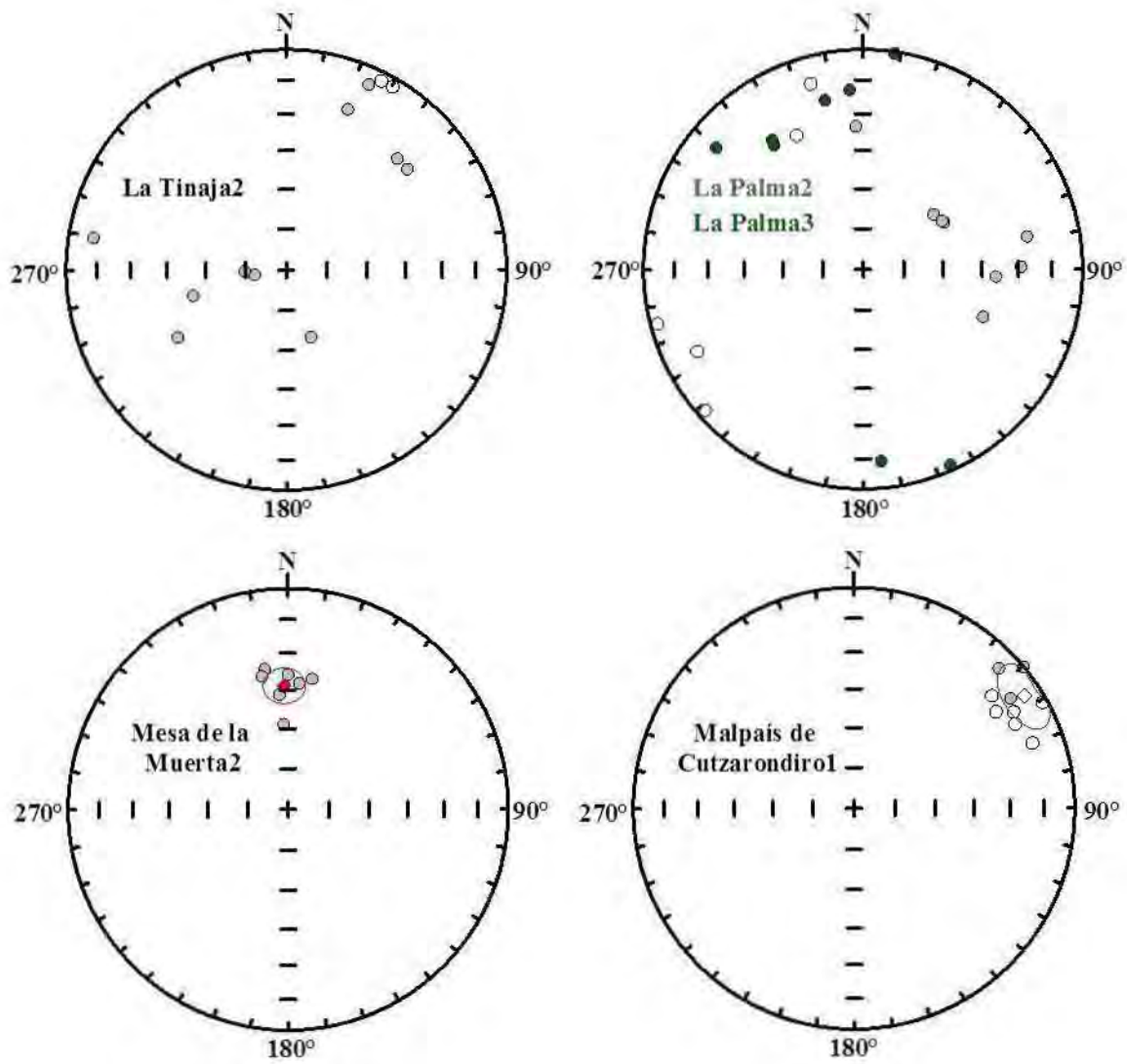


Figure S2: Paleomagnetic dating of La Tinaja flow. Red curves show the variation in time of the components of the paleomagnetic field as determined from the SHA.DIF.14k model, and blue horizontal lines are the components of the full vector direction determined for La Tinaja volcano; all curves and lines are shown with their respective 95% confidence intervals. The combined probability density derived from the declination, inclination, and paleointensity data is shown as shaded peaks and the minimum 95% confidence level by horizontal green lines.

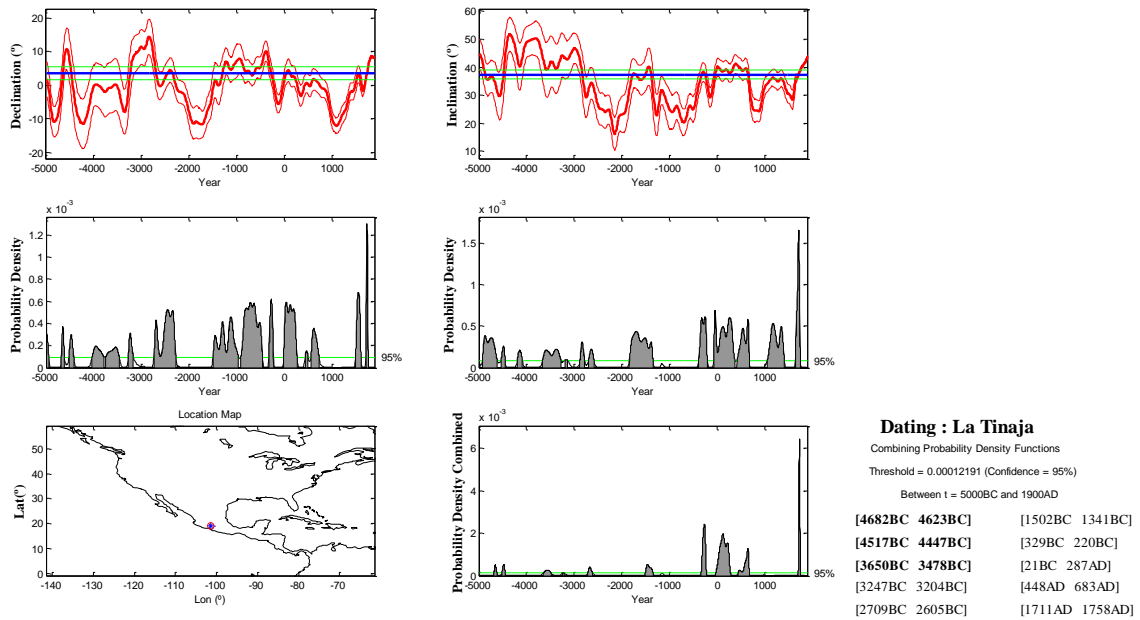


Figure S3: Paleomagnetic dating of La Palma flow. For further details see caption of Figure S2.

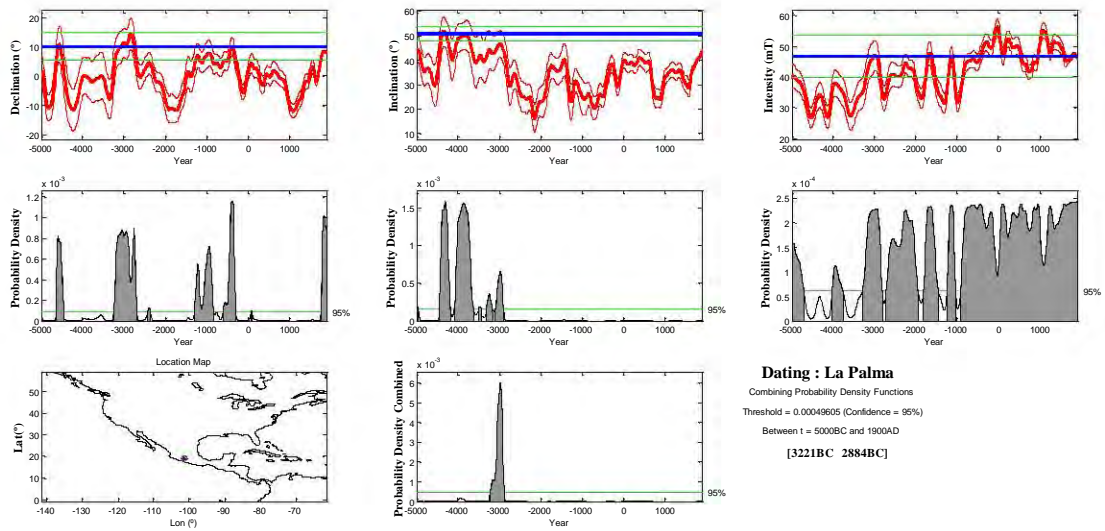


Figure S4: Paleomagnetic dating of Mesa La Muerta flow. For further details see caption of Figure S2.

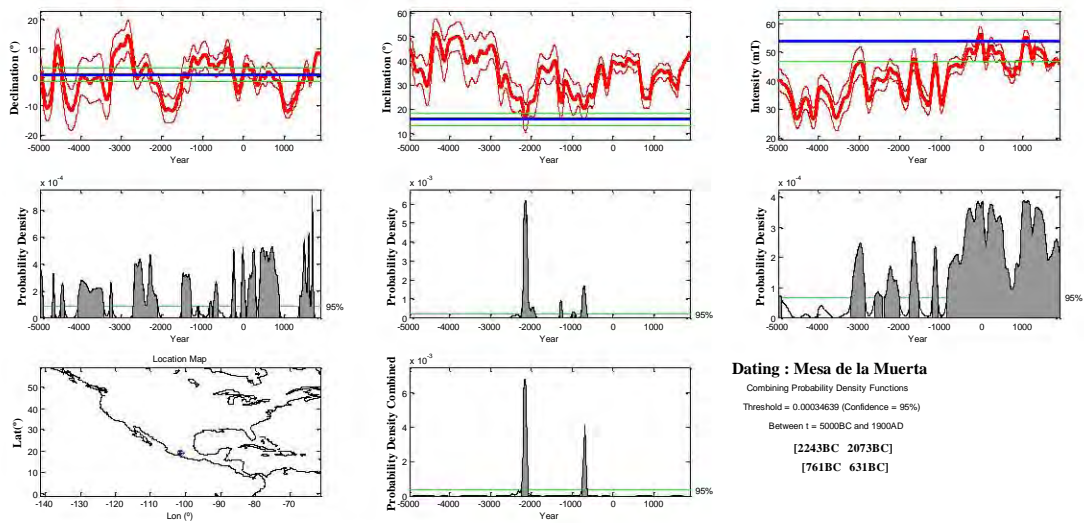


Figure S5: Paleomagnetic dating of Malpaís de Cutzaróndiro flow. For further details see caption of Figure S2.

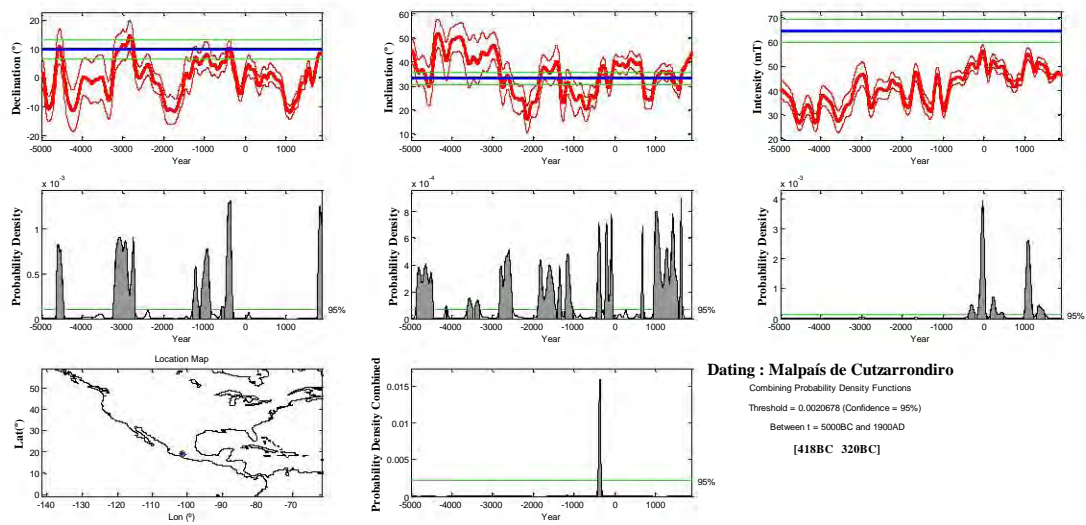


Table S1: site mean directions for the four Tacámbaro lava flows: Latitude and longitude of the sampling coordinates, n = number of samples used in the calculation of the site-mean direction, N = total number of samples measured, R= unit vector sum, k = precision parameter; α_{95} = 95% confidence angle, Dec = declination, Inc = inclination. Shaded rows mark rejected sites (see text for details). Mean-directions at site level are shaded in light blue colour.

Site	Latitude (N)	Longitude (W)	n	N	R	k	α_{95}	Dec	Inc
La Tinaja (LTJ)									
LTJ1	19° 7'54.90"	101°28'44.60"	12	12	11.94726	208.58	3.0	1.6	37.1
LTJ2	19° 7'41.30"	101°29'16.60"	No site means direction could be calculated						
LTJ3	19° 7'42.00"	101°29'13.56"	9	9	8.96640	238.07	3.3	6.3	42.5
LTJ4	19° 7'36.78"	101°29'26.34"	16	18	15.95482	332.00	2.0	4.0	37.3
LTJ5	19° 9'37.26"	101°30'46.56"	8	9	7.97734	308.97	3.2	3.0	32.4
Mean: Core level			45	48	44.76948	190.87	1.5	3.6	37.4
Mean: Site level			4	4	3.99114	338.46	5.0	3.7	37.3
Mesa La Muerta (MMU)									
MMU1	19° 8'42.30"	101°29'10.70"	9	9	8.94446	144.05	4.3	2.6	18.9
MMU2	19°10'23.40"	101°30'19.80"	7	7	6.91697	72.26	7.1	358.2	43.2
MMU3	19°10'18.47"	101°30'21.49"	8	8	7.95241	147.08	4.6	0.6	18.4
MMU4	19°10'0.37"	101°30'31.04"	7	9	6.93473	91.93	6.3	2.3	13.3
MMU5	19° 9'40.00"	101°30'0.00"	6	13	5.95310	106.61	6.5	0.1	14.4
MMU6	19° 9'56.00"	101°29'51.00"	10	10	9.84970	59.88	6.3	0.5	13.9
Mean: Core level			40	56	39.57148	91.01	2.4	0.8	15.9
Mean: Site level			5	5	4.99497	795.51	2.7	1.2	15.8
Malpaís de Cutzaróndiro (MPC)									
MPC1	19°11'18.70"	101°30'3.20"	9	9	8.70026	26.69	10.1	56.4	-8.2
MPC2	19°12'7.70"	101°30'12.50"	9	9	8.94656	149.71	4.2	14.5	34.1
MPC3	19°12'36.00"	101°29'21.30"	10	10	9.89517	85.85	5.2	4.9	28.8
MPC4	19°12'40.00"	101°29'8.00"	9	14	8.87892	66.07	6.4	10.9	34.6
MPC5	19°12'29.00"	101°28'38.00"	7	7	6.93334	90.01	6.4	9.8	36.2
Mean: Core level			35	40	34.56293	77.79	2.8	9.8	33.2
Mean: Site level			4	4	3.99018	305.48	5.3	10.0	33.5
La Palma (LPM)									
LPM1	19° 9'12.24"	101°31'43.62"	8	11	7.91801	85.38	6.0	11.2	48.8
LPM2	19° 6'15.00"	101°30'4.00"	No site means direction could be calculated						
LPM3	19° 6'27.00"	101°30'1.00"	No site means direction could be calculated						
LPM4	19° 7'13.00"	101°30'20.00"	7	7	6.89687	58.18	8.0	7.0	56.2
LPM5	19° 8'12.36"	101°30'34.68"	15	16	14.84683	91.40	4.0	11.0	49.5

Mean: Core level	30	34	29.61721	75.76	3.0	10.2	50.9
Mean: Site level	3	3	2.99429	350.55	6.6	9.9	51.5

Table S2: Paleointensity results and associated statistics for accepted specimens of the Tacámbaro studied flows: N, number of points included in the linear best-fit; T (°C) (min-max), minimum and maximum temperature used to determine the paleointensity; β , the ratio of standard error of the slope of the selected segment in the Arai plot to absolute value of the slope; f, fraction of the NRM used for best-fit; q, quality factor; MAD_{anc} , anchored maximum angular deviation; α , angular difference between anchored and non-anchored best solution; DRAT, the ratio of difference between the pTRM check and relevant TRM value at specific temperature to the length of the selected NRM-TRM segment; δCK , relative check error; δpal , cumulative check difference; PI, paleointensity; σ (μT), standard deviation.

Sample	N	T (°C) (min-max)	β	f	q	MAD_{anc}	α	DRAT	δCK	δpal	PI	σ (μT)
La Tinaja (LTJ)												
1-5a	10	0-460	0.04	0.63	12.1	2.60	2.83	5.54	4.72	9.80	54.36	2.13
1-9z	5	340-460	0.02	0.44	14.4	2.57	2.33	6.20	3.34	2.07	43.16	0.79
3-4z	9	0-430	0.07	0.50	5.86	2.58	6.32	6.59	6.45	2.74	99.65	7.07
4-15d	10	0-460	0.05	0.51	9.25	3.24	7.37	3.55	2.45	7.37	54.61	2.54
4-16b	14	0-560	0.02	0.90	37.7	1.85	0.74	2.38	3.12	7.12	63.09	1.28
Mean											62.97	21.69
La Palma (LPM)												
1-5b	14	0-560	0.03	0.98	32.1	2.58	1.08	5.95	7.47	1.49	47.22	1.27
1-6z	10	0-460	0.06	0.82	12.4	4.73	8.86	2.50	2.77	5.12	53.63	3.02
3-4 ^a	5	0-340	0.02	0.73	27.8	2.50	1.50	5.25	5.33	9.59	47.53	0.92
5-1 ^a	11	0-490	0.06	0.84	9.05	3.68	6.63	6.06	6.37	3.17	37.54	2.47
5-10z	10	250-530	0.04	0.81	15.5	3.02	1.40	8.75	9.09	5.99	40.67	1.53
5-4z	13	0-530	0.05	0.86	15.5	5.0	8.0	6.55	7.44	3.83	43.26	2.09
5-16 ^a	8	0-400	0.05	0.70	9.02	2.22	2.77	6.0	6.38	7.90	56.77	2.80
Mean											46.66	6.86
Mesa La Muerta (MMU)												
3-2 ^a	6	430-560	0.01	0.47	22.9	2.84	4.52	8.78	5.80	8.17	60.30	0.95
3-4z	14	0-560	0.04	0.80	18.6	2.03	3.03	7.64	8.99	0.46	64.74	2.46
3-8 ^a	14	0-560	0.01	0.89	51.4	1.69	1.69	2.47	2.91	6.58	52.39	0.78
4-1 ^a	14	0-560	0.02	0.98	28.9	3.52	2.08	5.47	7.01	4.02	50.63	1.25
4-3z	5	0-300	0.04	0.80	12.9	2.21	2.93	1.46	1.53	0.40	50.57	2.05
4-8z	14	0-560	0.04	0.92	19.6	2.01	0.97	8.61	9.86	4.26	44.85	1.79

Mean											53.91	7.27
Malpaís de Cutzaróndiro (MPC)												
2-1z	6	0-340	0.03	0.53	12.2	3.85	6.76	2.12	1.89	8.54	67.53	2.10
2-7b	5	0-300	0.04	0.70	10.7	1.70	1.74	4.38	5.22	0.50	69.29	3.14
3-2b	10	0-460	0.02	0.90	22.0	1.89	1.20	1.52	1.92	0.56	58.67	1.41
3-10 ^a	10	0-460	0.03	0.88	18.6	1.72	0.57	2.38	3.05	4.68	63.55	2.05
Mean											64.76	4.72

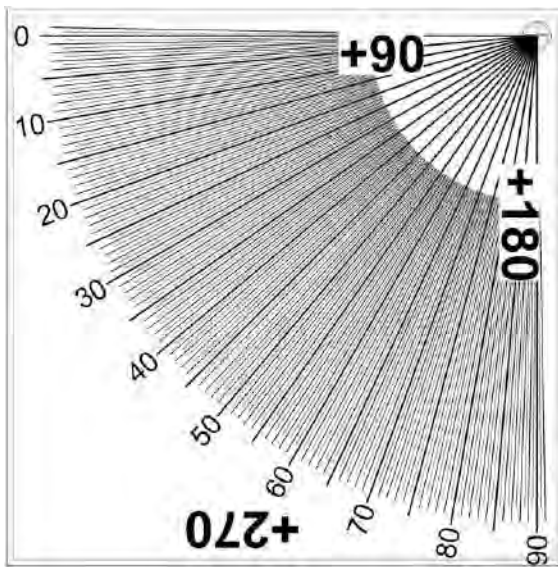
Supplementary Material IV

This section represents supplementary data for the manuscript ‘Palaeomagnetic dating of two recent lava flows from Ceboruco volcano, western Mexico’ presented as chapter five in the thesis, and published in the journal of the Geophysical Journal International.

The supplementary data herein contains five figures. The first three figures are dealing with an orienting digital device and sun compass scale. The last two figures represent paleomagnetic dating results



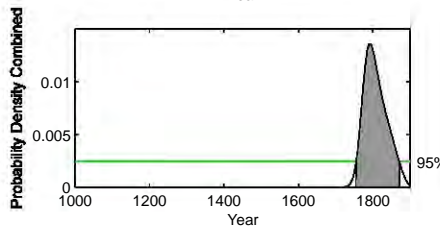
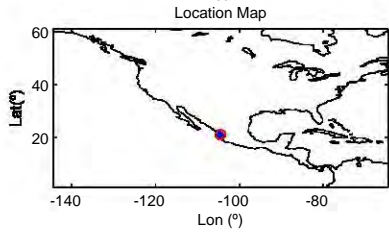
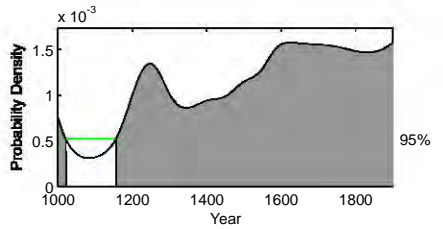
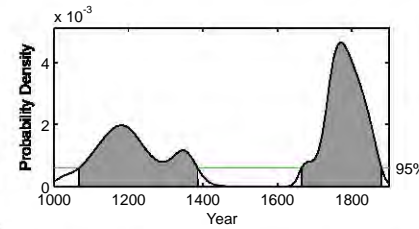
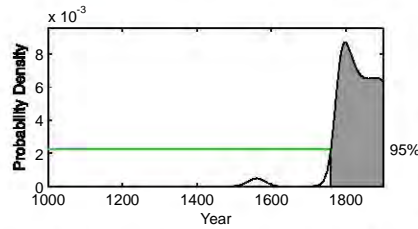
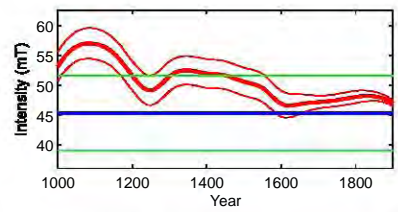
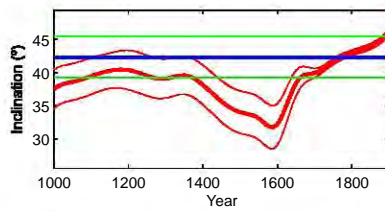
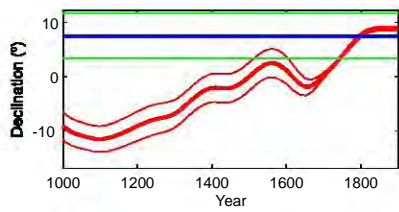
Overall view of the orienting device with digital inclinometer and Sun to magnetic compass with ocular reading.



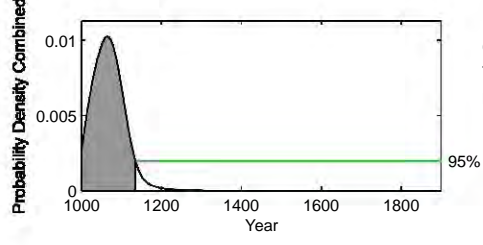
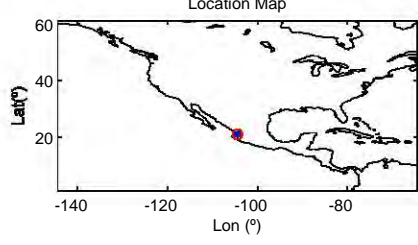
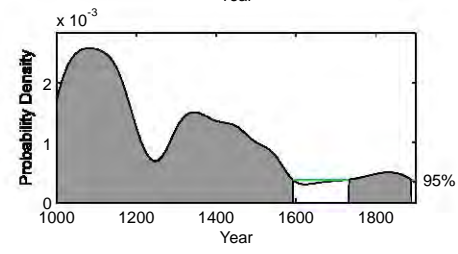
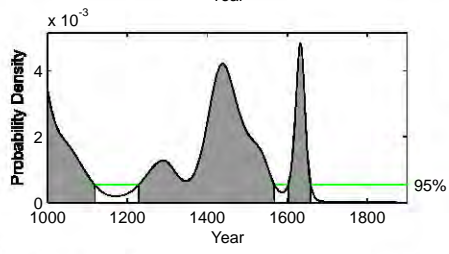
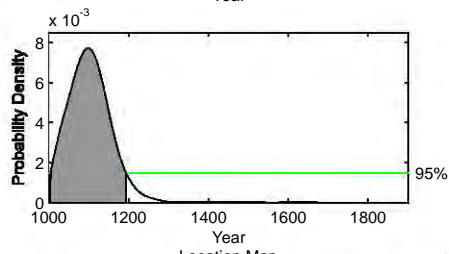
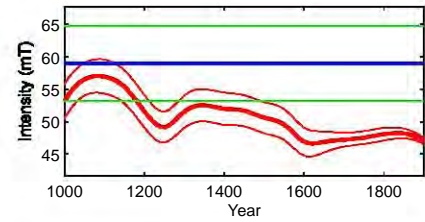
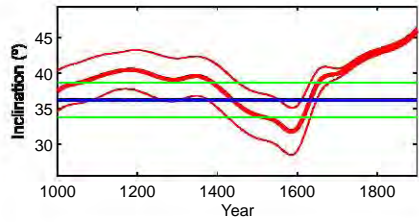
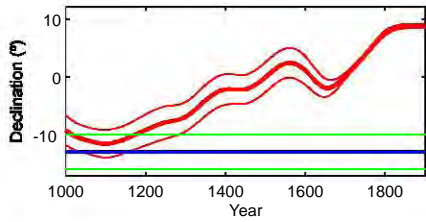
Sun compass scale with 0.5° subdivisions and its use on the orienting device. Note that according to the positioning on the platform an angle has to be added, here 90° . The size of the compass is about $11 \times 11 \text{ cm}^2$. Under favorable conditions, the shadow angle may be estimated with a $\frac{1}{4}^\circ$ of resolution.



Alternatively, a thick rod with a narrow slot may be employed. This produces a wide shadow with a narrow bright line in the middle. The rod has to be turned around its long axis to optimize the width of the bright line. View of the digital inclinometer.



Dating : '1870flow'
 Combining Probability Density Functions
 Threshold = 0.0024097 (Confidence = 95%)
 Between t = 1000AD and 1900AD
 [1755AD 1871AD]



Dating : 'Ceborucoflow'
 Combining Probability Density Functions
 Threshold = 0.001959 (Confidence = 95%)
 Between t = 1000AD and 1900AD
 [1000AD 1134AD]

Palaeomagnetic dating of the 1870 lava flow and the Ceboruco lava flow. Horizontal blue lines are defined by the measured declination and inclination values, with 95% confidence limits shown in green. Expected declination and inclination values with their 95% confidence limits according to the SHA.DIF.14k global field model are shown as red curves. Below the declination, inclination and intensity curves the probability density is shown as shaded peaks, with the minimum 95% confidence level by green lines. The combined probability density derived from these data is shown at the bottom.